Communications Research Centre

RAIN ATTENUATION STATISTICS FOR TERRESTRIAL MICROWAVE LINKS IN CANADA

by

B. SEGAL

CRC REPORT NO. 1351-E

Department of Communications
Ministère des Communications

OTTAWA, JANUARY 1982

ERRATUM

CRC Report No. 1351-E

"Rain attenuation statistics for
terrestrial microwave links in Canada"

by B. Segal

Page 2, Table 1: The latitude of the rain gauge situated at Regina Airport should read 50^{o} 26' and not 50^{o} 56' as given.

RAIN ATTENUATION STATISTICS

FOR TERRESTRIAL MICROWAVE LINKS IN CANADA

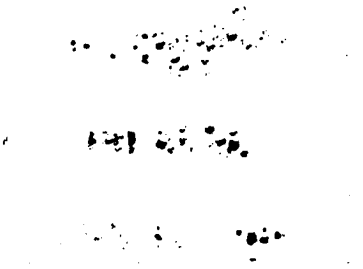

COMMUNICATIONS RESEARCH CENTRE

DEPARTMENT OF COMMUNICATIONS
CANADA

RAIN ATTENUATION STATISTICS
FOR TERRESTRIAL MICROWAVE LINKS IN CANADA

by

B. Segal

(Radar and Communications Technology Branch)

CRC REPORT NO. 1351-E

January 1982
OTTAWA

PREFACE

This report is the third in a series devoted to the exploration of climatic factors which bear heavily on the design and performance of radio systems, especially within the Canadian environment. The first of these reports was entitled "Tropospheric Refractivity Atlas for Canada" and presented long-term statistics of both the annual and seasonal behaviour of the refractive index of the atmosphere near the surface and in vertical profile (Segal and Barrington, 1977). The second report, "High-Intensity Rainfall Statistics for Canada", not only presented the statistics of intense rainfall across Canada, but also described in some detail the nature of precipitation as it relates to radio system performance (Segal, 1979).

The latter report was conceived as a companion to the present one which deals more directly with the impact of rainfall on terrestrial microwave transmission. The sizeable meteorological data base employed in the present work is the same as the one described in considerable detail in Segal (1979). Readers are therefore referred to that publication for such additional details as might be required.

Like its predecessor, this monograph contains a substantial amount of explanatory background material. This should assist the serious reader who may wish to delve more fully into the foundations, complexity and some of the implications of the computations reported here.

The main product of this report is a detailed set of cumulative distributions of rain attenuation for locations across the length and breadth of the country. For these locations, the data encompass a wide range of hop lengths and as broad a frequency spectrum as is likely to be of concern to communications specialists in the near future. There remain, of course, various aspects of this work to be treated in greater depth as time and knowledge permit. It is nonetheless hoped that the data presented here will aid in the orderly and efficient utilization of the microwave spectrum in Canada.

B. Segal

Ottawa
November 1981.

TABLE OF CONTENTS

1. INTRODUCTION

It is widely accepted that attenuation of radio waves by atmospheric precipitation represents a serious obstacle to microwave transmission at frequencies in excess of about 10 GHz. In fact, a careful examination of this generalized assertion reveals details of considerable interest to specific design situations. The frequency of onset of precipitation attenuation is found to be fairly distinct and characteristic of a given location, reflecting its particular rainfall climatology (Segal, 1978). The impact of precipitation increases rapidly for frequencies beyond this critical value. Individual climatic characteristics, however, result in differences in the growth and behaviour of the attenuation with respect to frequency, fade margin and link length.

Some of these characteristics are displayed in Figure 1. Differences in the critical frequency for these locations are immediately apparent. The distinctiveness of the western coastal station is dramatic. It is also apparent that similarities or inter-relationships which may apply among the different stations at one frequency do not necessarily apply at another. It is for this reason that attenuation predictions must be carried out independently for each location.

There is currently no unified set of attenuation data based on operational microwave experience in Canada, nor are there established prediction procedures in place for use with published rainfall statistics for different locations. This document presents a broad, comprehensive set of attenuation predictions in a useful form for terrestrial microwave system planning.

Canadian meteorological stations for which adequate rainfall data were available in a form suitable for these purposes are indicated on the map in Figure 2. Table 1 serves to identify these locations. While the duration of the precipitation records at different locations varied from less than five complete years at one particular site to as much as 20 years for some others, there was generally a 10-year sample available for analysis. The predictions derived from this data base still show certain irregularities due to insufficient data. On the other hand, it is worth noting that very few, if any, experimental programs have been able to examine a comparable climatological interval. For a more detailed description of the rainfall records themselves and the manner in which their analysis was conducted, the reader is referred to Segal (1979).

Chapter 2 discusses some of the detailed aspects of rain structure which affect the calculation of attenuation from a knowledge of the instantaneous precipitation intensities. Chapter 3 outlines the basis of the synthetic storm procedure which is used in this report to compute the rain attenuation for terrestrial links. Chapter 4 describes the range of microwave hop parameters for which attenuation prediction data are presented and examines a number of current schemes for frequency extrapolation. Also presented is a selection of contour maps giving the attenuation levels and maximum permissible hop lengths on a geographic basis. Chapter 5 looks briefly at the polarization characteristics of rain attenuation. Finally, the predicted attenuation distributions for the individual locations are presented in Figures 34 to 409, at the end of the report.

TABLE 1

List of Precipitation-recording Stations for Which Attenuation Statistics are Derived

	LOCATION	LAT		LONG	
		deg	min	deg	min
1	Calgary, ALTA.	51	06	114	01
2	Cambridge Bay, NWT.	69	06	105	07
3	Caplan, QUE.	48	06	065	39
4	Carmacks, YT.	62	06	136	18
5	Central Patricia, ONT.	51	30	090	09
6	Churchill, MAN.	58	45	094	04
7	Comox, BC.	49	43	124	54
8	Dauphin, MAN.	51	06	100	03
9	Edmonton. ALTA.	53	34	113	31
10	Fredericton, NB.	45	55	066	37
11	Gagnon, QUE.	51	57	068	08
12	Gander, NFLD.	48	57	054	34
13	Geraldton, ONT.	49	41	086	57
14	Goose Bay, NFLD.	53	19	060	25
15	Halifax, NS.	44	38	063	30
16	Hope, BC.	49	23	121	26
17	Kentville, NS.	45	04	064	29
18	Kingston, ONT.	44	14	076	29
19	London, ONT.	43	02	081	09
20	Mission, BC.	49	09	122	16
21	Montreal, QUE.	45	28	073	45
22	Moosonee, ONT.	51	16	080	39
23	Normandin, QUE.	48	51	072	32
24	North Bay, ONT.	46	22	079	25
25	Ottawa, ONT.	45	23	075	43
26	Poste de la Baleine, QUE.	55	17	077	46
27	Prince Albert, SASK.	53	13	105	41
28	Prince George, BC.	53	53	122	40
29	Quebec, QUE.	46	48	071	23
30	Regina, SASK.	50	26	104	40
31	Saint John, NB.	45	19	065	53
32	St. John's, NFLD.	47	37	052	45
33	Sault Ste. Marie, ONT.	46	29	084	30
34	Sioux Lookout, ONT.	50	07	091	54
35	Stephenville, NFLD.	48	32	058	33
36	Summerland, BC.	49	34	119	39
37	Summerside, PEI.	46	26	063	50
38	Swift Current, SASK.	50	16	107	44
39	Sydney, NS.	46	10	060	03
40	Toronto, ONT.	43	41	079	38
41	Uranium City, SASK.	59	34	108	29
42	Val d'Or, QUE.	48	03	077	47
43	Vancouver, BC.	49	11	123	10
44	Watino, ALTA.	55	43	117	37
45	Weyburn, SASK.	49	40	103	51
46	Windsor, ONT.	42	16	082	58
47	Winnipeg, MAN.	49	54	097	14

2. PARTICULATE STRUCTURE OF RAIN

2.1 ATTENUATION BY UNIFORM RAINFALL

Mie (1908) developed the theory of absorption and scattering of electromagnetic waves by dielectric particles whose dimensions are comparable with the wavelength of the incident radiation. Ryde (1946) first applied this theory to the problem of attenuation of radar signals by an ensemble of raindrops. The main features of these calculations were later verified and extended by Gunn and East (1954) who found that the attenuation rate due to rain was not directly proportional to the rainfall intensity. Their results are generally expressed in the form of a power relation, namely,

$$\Gamma = kR^{\alpha} \tag{1}$$

where R is the rainfall rate in mm/h. Γ is the rate of attenuation, frequently referred to as the specific attenuation and expressed in dB/km. The coefficients k and α are physical parameters which may depend on the wavelength of the incident radiation, the electrical characteristics of water and the size and number of raindrops along the path as well as their shape and orientation. Olsen et al. (1978) have recently examined the theoretical basis for (1). They found that the specific attenuation could be expressed as a power series jointly involving frequency and rainfall rate provided the distribution of drop sizes within the precipitation area could be represented by means of a generalized exponential function. The various distributions to be discussed in the following section all satisfy this condition. For a given set of raindrop parameters, rigorous expressions were established for both the low-frequency asymptote ($k \propto$ freq, $\alpha \approx$ const) and the high-frequency limit (k, $\alpha \approx$ const). At intermediate frequencies both k and α are frequency dependent. Their effective values are best derived by numerical integration for an appropriate assemblage of raindrops. We are thus faced with questions concerning the physical microstructure of rainfall.

2.2 DROP-SIZE DISTRIBUTIONS

Under suitable conditions water droplets may grow within the turbulent environment of certain clouds to yield precipitable drops of varying size. Even during the brief precipitation phase, modifying influences are present. Drops may collide with one another due to unequal rates of fall, giving rise to a growth in drop size by coalescence. Eventually, however, they reach unstable dimensions and, as a result of atmospheric turbulence, break up into many smaller components. Evaporation serves to reduce or completely eliminate some of the very small drops. The resultant mix of drop sizes has long been, and remains to this day, a subject of considerable interest.

The first careful and fairly complete set of observations was made by Laws and Parsons (1945) whose concern was primarily that of soil erosion. The next significant series of experimental measurements of drop size distributions was undertaken at Ottawa in the early post-war years. In analyzing these data, Marshall and Palmer (1948) proposed the functional form

$$N(D) = N_0 e^{-\Lambda D} \tag{2a}$$

as an approximation to the drop size density function. N(D) is the number of drops per unit volume having diameter D (mm), and a value of 8,000 ($m^{-3}mm^{-1}$) was suggested for N_0. The exponential coefficient Λ is itself given in terms of the rainfall rate R by an expression of the form

$$\Lambda = \beta R^{\gamma} \tag{2b}$$

It has always been recognized, of course, that the distribution of drop sizes varies with prevailing meteorological conditions. Employing electro-acoustical drop measuring techniques, Joss et al. (1968) were able to distinguish statistically among the distributions for three different situations. On average, these were found to approximate the exponential form (2) but with somewhat different values for the coefficients. Table 2 summarizes the various results for a number of measured drop size distributions.

TABLE 2

Coefficients for Drop Size Distributions

Rain Type *	Observer **	$N_0(m^{-3}mm^{-1})$	$\beta(mm^{-1})$	γ
R	MP	8,000	4.1	−0.21
L	JTW	31,000	5.7	−0.21
R	JTW	7,000	4.1	−0.21
TR	JTW	14,000	3.0	−0.21
TR	SS	$7000R^{0.37}$	3.8	−0.14

* *L = drizzle or light rain*
R = widespread rainfall
TR = thundershower

** *MP = Marshall and Palmer (1948)*
JTW = Joss, Thams and Waldvogel (1968)
SS = Sekhon and Srivastava (1971)

2.3 DISTRIBUTION NORMALIZATION

While the functional form (2) appears to provide an adequate description of the variation in drop size characteristics of rain of different intensities, etc., there are substantial errors inherent in its direct application with some of the original coefficients as given in Table 2.

The contribution by drops of diameter D to the total volume of liquid water striking unit horizontal area of the earth's surface is given by

$$\frac{1}{6}\pi\, D^3N(D)v(D)\ mm^3m^{-2}sec^{-1}mm^{-1} \tag{3}$$

where v(D) is the terminal fall velocity of the drops (e.g., Gunn and Kinzer, 1949; Best, 1950). The overall rate of rain accumulation is therefore

$$R' = 6\pi \times 10^{-4} \int D^3N(D)v(D)dD \tag{4}$$

Substituting N(D) from (2) for a given rate R, results in an actual rainfall rate R' which is generally different from the assumed value R. The inadvertent use of incorrect values for the precipitation rate would result in equivalent errors in the predicted rain attenuation. Figure 3 indicates the magnitude of these errors for the distributions summarized in Table 2. To compensate for this discrepancy, an appropriate correction factor was applied to N_0 for each rainfall rate and precipitation model.

2.4 DROP-SIZE MODELS FOR ATTENUATION CALCULATIONS

The preceding sections described several recent determinations of drop-size distributions and outlined the nature of the corrections necessary before these may be used in the computation of the coefficients for specific attenuation rates. There remains, however, the question of which of the various drop-size distributions to employ. Figure 4 indicates the nature and magnitude of the differences implicit in these different distribution forms for the same observed rainfall rate.

Differences in the computed link attenuation are not easily reconciled with the selection of one rainfall distribution or another. The use of the thunderstorm type distribution, for example, tends to yield greater

attenuations for the lower microwave frequencies. At the higher frequencies, where the influence of very large drops is less pronounced, the widespread rain distribution might yield a greater attenuation. However, inter-relationships such as those illustrated in Figure 4 are rain-rate dependent so that the overall impact of a particular choice will depend on the rainfall climate for a given location, that is on its particular mix of light, moderate and intense rain.

It is clear that the nature of rainfall is different from one event to another. Even during a single, continuous rainstorm the precipitation rates and the drop-size "signature" during the onset or final phase might be very different from conditions prevailing – perhaps only briefly – during the most intense interval. For terrestrial design applications it is usually the more severe attenuation events which are of greatest interest. It might be tempting therefore to argue in favour of a thunderstorm type distribution and for its attenuation parameters. This would be to overlook the possible application of these attenuation statistics to earth-space propagation or to applications where only modest reliability is required. The ultimate experimental verification of the methodology employed in this report would also require a complete range of attenuation statistics.

The attenuation procedure to be described in section 3.2 considers the contribution of each element of rainfall along the path. Therefore, the characteristic rain type was independently selected for each instant without regard to any other rainfall elements – including those for the immediately preceding or following minute. For this purpose, the three distributions of Joss et al. (1968) were employed and the following choices were made.

For most locations, rainfall exhibiting instantaneous rates exceeding 75 mm/h was assumed to possess a drop-size distribution best described by the thunderstorm parameters. Below 5 mm/h the predominantly small raindrop distribution of the drizzle type was applied. The so-called widespread rain type was assumed for intermediate rainfall rates.

By comparison with conditions in the rest of Canada, rain is a fairly common occurrence along the west coast. Driven by the prevailing westerly winds, moisture laden air off the Pacific is cooled adiabatically as it is forced upward by the coastal mountains. Condensation and precipitation are readily induced. Under such orographic conditions, the drop size distributions more closely resemble those described for drizzle than for other rain types (Blanchard and Spencer, 1957).

For the west coast, the Joss drizzle distribution was therefore adopted for rain rates up to 10 mm/h. Conversely, the thunderstorm distribution was assumed to hold from 50 mm/h onward since rainfall along this coast rarely attains the intensities common during thundershowers in many other parts of the country (Segal, 1978,1979).

3. PREDICTION OF MICROWAVE ATTENUATION

3.1 ATTENUATION OVER A TERRESTRIAL LINK

The basic objective of this report is the calculation of the path attenuation suffered by a microwave signal propagating through a region filled with rain. Available rainfall rate data relate to observations made at a fixed point. Because rainfall is rarely uniform over the entire area of precipitation, the variation of attenuation with respect to the length of a microwave link is not a trivial one. The total path attenuation is not obtained merely by multiplying the specific attenuation by the actual hop length.

Figure 5 illustrates the hop length dependence of attenuation exceeded for various percentages of time. For low and moderate probabilities of occurrence, the attenuation level is seen to be approximately proportional to the length involved only over a short range. In this context, "short" is of the order of ten kilometres or less and is a rough indication of the extent over which rainfall of moderate intensity might be

taking place simultaneously. Such areas have been referred to as small mesoscale areas (Austin and Houze, 1972; Segal, 1979). As the propagation distance increases, the attenuation no longer grows in direct proportion since the path now tends to include rainfall of varying intensity with the most intense region occupying only a small portion of the entire path.

Light rain (such as the case for a probability of 1×10^{-3}), almost always extends over great distances. The linear dependence of attenuation with hop length therefore also extends to greater distances than in the other examples illustrated.

One approach to the problem of calculating attenuation over a link is to employ appropriate correction factors to yield an "effective" path length. Not only are these factors dependent on frequency, path length and rainfall rate (i.e., probability) but on the regional precipitation climate. Such factors can reliably be derived only on the basis of very extensive operational experience or through some other prediction scheme. Since both of these conditions were initially lacking, it was decided to proceed with a thorough prediction program employing the most realistic attenuation model available.

3.2 SYNTHETIC-STORM CONCEPT FOR ATTENUATION PREDICTION

With very few exceptions, existing rainfall data bases result from observations taken at selected widely-spaced points. Bussey (1950) was the first to attempt an estimate of path average rainfall rates from point rainfall measurements. Reasoning that storms move with a finite velocity v, he observed good statistical agreement between the instantaneous rainfall rates integrated along a path of length L and the point rainfall rate averaged over intervals $\tau = L/v$.

Hamilton and Marshall (1961) developed this concept to correct for attenuation of radar signals by rain. Using a 3-cm radar to observe the movement of storms in the Montreal area, they were able to synthesize spatial precipitation patterns for individual events from point rainfall observations taken simultaneously. The technique has been successfully extended to the prediction of attenuation statistics over terrestrial links (Drufuca, 1972,1973; Ro, 1973).

If x is the distance along a microwave path of length x_L and R(x,t) is the instantaneous rainfall intensity at a point on the path, then the rain-induced attenuation over the hop will be

$$A_t = \int_{x_i=0}^{x_L} \Gamma(x_i,t)dx_i \tag{5}$$

where $\Gamma(x_i,t) = k\,[R(x_i,t)]^{\alpha}$

If the rainfall pattern moves along the link with speed v, then

$$\Gamma(x_i,t) = \Gamma\left(x_o, t - \frac{x_i}{v}\right) \tag{6}$$

Thus,
$$A_t = v \int_{t-\frac{x_L}{v}}^{t} \Gamma(x_o,t)dt \tag{7}$$

For rainfall records of finite resolution Δt, the integral is replaced by an equivalent summation of the form

$$A_t = v \sum_{i=n-\frac{x_L}{v\Delta t}}^{n} \Gamma(x_o,t_i)\Delta t \tag{8}$$

For the subsequent instant,

$$A_{t+\Delta t} = v \sum_{i=n-\frac{x_L}{v\Delta t}+1}^{n+1} \Gamma(x_o,t_i)\Delta t$$

$$= A_t + v\left[\Gamma(t_{n+1}) - \Gamma(t_{n-x_L/v\Delta t})\right]\Delta t \tag{9}$$

and so on until the completion of the entire rainfall record. The cumulative statistics are then obtained from the complete set of A_t values.

For all of the results presented here, Δt was nominally assumed to be one minute. In order to avoid summation errors, it was necessary that $x_L/(v\Delta t)$ be a perfect integer. To ensure this, Δt was reduced slightly from its nominal value, if necessary. For example, when considering a 40 km hop in a region where the average rain storm speed was 35 km/h, the step was automatically reduced from 60 seconds to 59.63 seconds.

A tacit assumption which is made when applying the synthetic storm method is that within a given region, rain is an ergodic process: the probability of an event occurring is the same at any point along the path as it is at the rain gauge. As a consequence, the prediction method is a statistical one requiring a suitably long data base for reliability. Nonetheless, limited experimental comparisons have shown the method to be reasonable even over relatively short periods (Drufuca, 1972; Watson et al., 1978). Mogensen and Stephansen (1978) examined a number of different prediction methods with respect to a 45 km, 14 GHz experiment in Denmark and found the method of Bussey (1950) to yield the best results overall. That method, of course, is analogous to the synthetic storm approach for a particular hop length at any given location.

One question of some importance when attempting to apply a single rain storm model and/or prediction algorithm across all of Canada is whether irregularities in the regional terrain may adversely influence the results. Drufuca (1973) had originally demonstrated the validity of the synthetic storm technique in predicting rain attenuation for a short link over a relatively flat area along the St. Lawrence valley, south of Montreal. More recently, however, Bertok et al. (1977) have obtained equally good agreement in predicting attenuation for hops up to 50 km in length in the Alpine region of northern Italy.

In concept, the synthetic storm method is appealing because it represents the closest approximation to the reality of rain storm behaviour under all conditions.

3.3 SPECIFIC ATTENUATION COEFFICIENTS

Section 2.1 presented an expression for the rate of attenuation through uniform rainfall. Section 2.4 made reference to the choice of different drop-size distributions under different geographic and meteorological circumstances. Each of these distributions yields a distinct set of values for the parameters k and α in (1).

In addition, however, these coefficients are slowly varying functions of rainfall rate as illustrated by the example in Figure 6. The sense of the variation in each one is such as to compensate partially for the variation in the other so that the computed attenuation is not unduly sensitive to which pair of values is selected. Typically, values are derived on the basis of the "best fit" over the entire range of rainfall rates (Fedi, 1979). As was the case with respect to the selection of a suitable drop-size distribution, the synthetic storm procedure

does not demand a unique choice. Independent values of the parameters k and α were therefore computed for each of the drop-size distributions. These were specifically fitted over the range of rainfall intensities for which that distribution was assumed to apply, as discussed earlier. For the continental rain model that was used for all of Canada except the west coast, the interval from 5 to 75 mm/h, was further subdivided and two sets of values were employed: one for the range 5 to 15 mm/h and another over the range 15 to 75 mm/h. Olsen et al (1978) have similarly computed independent values of the attenuation coefficients for several different drop-size distributions. However, those were fitted over three broad, overlapping ranges of rainfall rates which differed somewhat from the intervals chosen in the present study.

3.4 RAIN STORM SPEED

Heavy rain storms are generally found to contain one or more highly localized areas of intense rainfall, or cells, embedded within extended regions of much lighter precipitation. These cells move with a speed related to the contemporaneous winds in the troposphere at cloud level (Austin and Houze, 1972; Hobbs and Locatelli, 1978). Of course, storm clouds extend over a considerable range of heights and wind speeds aloft vary greatly. Large cumulus clouds typically extend from altitudes of about 1 km to 5 km, or more. A height of 3 km, corresponding to a barometric pressure of about 700 mbar (70 kPa), may therefore be considered as a typical mid-cloud level during rain events. Atmospheric wind measurements at a number of standard altitudes, including the 700 mbar level, are routinely made twice daily at rawinsonde stations around the globe.

Employing a network of rain gauges, Holland (1967) indicated the 700-mbar height as a reasonable "steering level" for rain cell movement. On average, the 700-mbar winds accurately yielded the direction of storm motion but somewhat overestimated the speed. Drufuca (1972) observed good correlation between the rain storm speeds as monitored by means of an S-band weather radar and the 700-mbar winds measured by a rawinsonde situated 190 km from the radar site. Harden, Norbury and White (1974) obtained similar results using a network of rain gauges to estimate the storm movement. MacKenzie and Allnutt (1977) found the speed and direction of motion of rain cells within a line squall to be reasonably correlated with the 600-mbar winds, while Hobbs and Locatelli (1978) concluded that rain cores move with winds below the 550-mbar level (i.e., at an altitude corresponding to a higher pressure).

The observations summarized above are by no means comprehensive or conclusive. Furthermore, for extensive and long-term application, the use of independent wind speeds for each rain event would at best be awkward; for some locations it would be impossible. Segal (1979) indicated the magnitude and direction of the seasonally averaged 700-mbar wind velocities for locations across Canada and the neighbouring United States. In applying the synthetic storm algorithm to the rainfall data for the various locations, stations were grouped regionally, as appropriate, and an average 700-mbar speed was established for each group. Figure 7 indicates the final speeds assumed for rain storm movement in different parts of the country.

Examination of the upper atmospheric data for several Canadian locations suggests that there may be an increase of perhaps 10 percent or 20 percent in wind speed averaged over days of heavy precipitation compared with the overall average for the same location. Fortunately, the synthetic storm predictions are found to be insensitive to the actual speed assumed for rain cell displacement. Rainfall of long duration is also widespread geographically. In general, such precipitation engulfs the propagation path completely. The attenuation in this case is determined primarily by the rainfall intensity and is independent of storm speed.

When the precipitation rate is rapidly varying, however, such as during storms containing short periods of intense rain, the situation is more complex. A particular rainfall rate which lasts at a point for a time δt, may be assumed to cover a segment of the propagation path of length $v\delta t$. Under such circumstances, a higher speed of translation, for example, implies that each element of rainfall (and its associated element of attenuation) is stretched in proportion and therefore contributes to an increase in the overall path attenuation. This corresponds to a positive displacement of the distribution curve along the x-axis, as indicated by the arrow (a) in Figure 8. On the other hand, the total time necessary for a given element to pass completely over the link is inversely proportional to storm speed. Thus, an increase in speed is tantamount to a reduction in the

probability of occurrence and corresponds to a negative displacement of the distribution curve along the y-axis, represented by the arrow (b) in Figure 8. The combined effect of both influences is seen to be a diagonal translation of the curve more or less parallel to itself with very little net change.

4. DATA PRESENTATION

4.1 FIXED PARAMETER SELECTION

The preceding portions of this report have outlined the basic problems and procedures in the calculation of rain attenuation statistics. A complete exposition of the results is complicated by the fact that a total of four distinct design quantities are involved: frequency, path length, attenuation level and exceedance probability.

The overall pattern of spectral allocation for different services is governed by various international agreements. In most design situations, the operating frequency will have been dictated in advance in accordance with national policy, consistent with services and users already operating within the various bands. Frequency was therefore considered as one of the "constants" for purposes of statistical data presentation, that is, distributions are presented for a fixed set of frequencies. Of course, this demands an interpolation procedure for use with frequencies which are well removed from those considered here. This matter is discussed further in section 4.3.

The variety of radio path lengths encountered in practice is greater than is the case with respect to operating frequency. For a particular application, however, the hop length may also be taken as pre-determined. Even where distances to be covered are greater than can be accomplished with a single hop, there are usually no more than two or three practical alternatives to be considered.

The remaining design parameters are the rain attenuation level and the probability of exceeding that level. For each frequency, attenuation probabilities were computed for as great a range of hop lengths as plausible. These were chosen in such a manner as to simplify the interpolation procedure. In most instances, interpolation performed directly on the relevant figures should prove adequate. Hence, the bulk of the statistical data presented here consists of cumulative attenuation distributions for each of the 47 individual locations considered. These are contained in Figures 34 to 409.

Terrestrial microwave transmissions are usually polarized in either the horizontal or vertical plane. Propagation conditions differ somewhat depending upon which of these orientations is being used. The attenuation factors presented here are idealizations based on the assumption of perfectly spherical rain drops. At any given probability level, these factors are somewhat greater than the corresponding attenuation rates for vertically polarized waves and less than (but a little closer to) those for horizontal polarization. Section 5.1 will examine this matter further.

4.1.1 Standard Frequency Selection

Selecting the set of frequencies to be used in the present study involved certain compromises among the different considerations. One hopes, for example, to cover as broad a spectral range as possible, and yet to employ as few frequencies as feasible. It was also essential that the frequencies chosen include as many of the active bands for microwave relay service as possible. Earth-space communication bands represent a logical choice for the higher frequencies. The final selection of "standard" frequencies was derived as follows. The lowest frequency was taken as f_1=8.0 GHz, a frequency of considerable importance in long-haul terrestrial communications systems, while the upper frequency was somewhat arbitrarily though conveniently set at 100 GHz. The broad range encompassed in this way was then divided into six sub-intervals by means of frequencies equally spaced on a logarithmic scale. That is, the frequencies were related to one another through the formula

$$f_N = f_{N-1}^{1.1417} \quad (10)$$

Frequency f_4 was reduced slightly from 22.1 GHz, near the peak of a water vapour absorption band, to 20 GHz which falls in a band allocated to satellite downlink communication. The following frequency, f_5, was increased slightly from 34.2 GHz to 35 GHz, within a radiolocation band. Rounding all values to the nearest integer yields the sequence 8,11,15,20,35,56,100 GHz. To this was added a single frequency between 11 and 15 GHz and equal to their geometric mean, viz., 12.8 GHz.

4.1.2 Standard Path Length Selection

The length of each microwave hop is determined by a unique mix of geography, climate, population distribution and economics. While it has been argued that the hop length may effectively be considered as a predetermined quantity in any given instance, it is not possible – in advance – to indicate the specific lengths which are likely to be used in any future application. The pre-selection of hop lengths for prediction purposes is therefore a compromise between a desire for completeness and the limitations of computational effort and expense.

For 8, 11 and 12.8 GHz, the path lengths chosen for the calculation of rain attenuation at each location started with 5 km and increased by factors of two until 80 km, with a final length of 120 km being considered. At 15 GHz and 20 GHz, shorter path lengths of 2 km and 1 km, respectively, were added to this list. For 35 GHz and beyond, the two longest hop lengths were omitted. At 56 and 100 GHz, the greatest distance considered was 30 km rather than 40 km as was used at the lower frequencies.

The intent in selecting the above pattern of hop lengths was to substantially exceed the range encountered in most practical situations. Section 3.1 has already suggested that for very short paths or for high probability levels the attenuation experienced at a fixed probability is approximately proportional to distance. For hop lengths greater than about 10 km and probabilities less than about 3×10^{-3}, interpolation with respect to the logarithm of distance would generally be appropriate. Where scaling at a fixed attenuation level is more relevant, a power law relation for probability in terms of hop length may be used.

4.2 GRAPHICAL PRESENTATIONS

4.2.1 Geographic Distribution of Rain Attenuation

In order to present an alternative, broader image of the precipitation attenuation climate across Canada, illustrations of two additional types were prepared. The first of these consists of eight maps of constant path-length contours (Figures 9 to 16). For frequencies of 11 to 20 GHz, these maps indicate the maximum propagation range possible in different parts of the country for outages of 0.01 percent and 0.003 percent and for a fixed fade margin of 40 dB. At 11 GHz only southern Ontario and Quebec warrant detailed study at the 0.01 percent level. A northward recession in the maximum allowable hop length takes place as the frequency is increased. Southern Manitoba forms the focus of an attenuation zone at 12.8 GHz, while Alberta begins to exhibit severe propagation range limiting due to rain at 15 GHz. At 20 GHz, the entire country divides into widely differing propagation zones.

The second group of maps (Figures 17 to 29) is a presentation of isoleptinsic, or constant attenuation, contours for various propagation conditions. Table 3 summarizes the different sets of values for the link parameters. While the highest levels of attenuation are seen to be concentrated along the east coast and southern Ontario, there appears to be a strong east-west continuity stretching from the Atlantic into the prairie provinces. Gradual changes in the attenuation pattern take place both with frequency and probability of occurrence. At high probabilities there is little restriction imposed by rain in the northern and western sectors. As path lengths increase there is a migration of the pattern both westward and northward, with a secondary

centre of attenuation in southern Manitoba. A reduction in probability of occurrence leads to a similar westward shift in the attenuation pattern. Features move from the Ontario-Manitoba border into southern Saskatchewan, while a centre of high attenuation develops in Alberta.

TABLE 3

Parameters Relevant to Constant Attenuation Isograms

Figure	F(GHz)	L(km)	P(%)
17	11	40	.01
18	11	80	.01
19	15	40	.1
20	15	40	.03
21	15	40	.01
22	15	40	.003
23	15	80	.1
24	15	80	.03
25	15	80	.01
26	15	80	.003
27	20	40	.1
28	20	40	.03
29	20	40	.01

While maps such as these help to identify "at a glance" regions of better or worse than average propagation conditions, caution must be exercised before applying the results to particular design situations. Statistical studies of rare events often require vast amounts of data. Despite the very large data base employed in this investigation, the statistical analysis was pursued to the point where uncertainties are sometimes in evidence. Some of these problems are addressed in the following section.

In some instances, distinct geographic characteristics may be distinguished in the sets of cumulative distributions themselves (Figures 34 to 409). These, of course, reflect differences in the rainfall regimes in different parts of the country (Segal, 1978,1980). Very intense rainfall, for example, tends to be an uncommon occurrence on the west coast. As a result, the attenuation at low frequencies is extremely small in comparison with other locations (e.g., Figures 82, 154, 370). Of particular interest, this behaviour is not observed in the eastern maritime provinces.

At the same time, the total rainfall accumulations are generally very large at coastal and near coastal locations. Since the bulk of this rainfall is of very low intensity, its influence is manifest at the higher frequencies. Thus, the predicted 100 GHz attenuations for 30 km paths lie completely outside the graph boundaries for most of these locations (see Figures 89, 161, 193, 289, 345, 377). Only slightly smaller attenuation probabilities are predicted for a number of other locations near the east coast (see Figures 129, 153, 169, 281, 313, 329).

4.2.2 Effects of Finite Sample Size

Most of the distributions in Figures 34 to 409 exhibit the characteristic behaviour expected; however, the effects of both the limited data sample and the finite resolution time become important at the 10^{-5}

probability level and beyond. To a large extent the one-minute sampling time was established as a compromise between slightly smoother sets of curves and a significant increase in the computer processing requirements. Many of the ripples in the distribution curves are the result of this limit in resolution. It is generally a trivial matter to smooth out such irregularities before use.

A more difficult set of problems, occasionally evident at the lower frequencies, is that arising out of the use of limited data samples. In the simplest of these situations, the total path attenuation for a fixed probability level may exhibit a distinct quantum jump as the hop length is increased. Figures 108 (Fredericton) and 291 (Sault Ste Marie) are examples of this type of behaviour. It is not at all difficult to extrapolate the distributions for the particular hop lengths affected in a manner consistent with those for the other lengths. In a number of cases, it was possible to circumvent this problem entirely by a very slight adjustment in the resolution time.

A somewhat more difficult situation arises when all of the distributions for a given frequency are simultaneously affected. The synthetic storm procedure employed here models the line rainfall behaviour from precipitation observations taken at a point. As a result, there is an apparent enhancement in the statistical occurrence – or absence – of rare events, with the greatest effect being manifest for long simulated hop lengths. The 8 GHz distributions for Calgary for example indicate an abrupt upper attenuation limit of 18 dB for all paths lengths between 20 km and 120 km. The fact that the rain gauge located at a fixed point at the International Airport failed to record several minutes of more intense precipitation in the course of the 10 years considered does not imply that the path attenuation is irrevocably bounded in the manner of Figure 34. The curves in question should be extended, in a fashion resembling the curves for most other locations, to attenuations of perhaps 22 to 45 dB at the 10^{-6} level, depending on path length.

The converse, and in some ways the most difficult situation, arises from an "excessive" accumulation of extreme events. Figure 98 suggests the repeated occurrence of anomalously heavy rainfall at the location of the gauge, which translates into abnormally large attenuation predictions. While the data giving rise to these results are "real", such extremes in the tail of the rainfall rate distribution are rare; decades may pass before such results are again predicted for the same location. Similar examples of extended distribution tails are found in the results for Central Patricia, Dauphin, London, Normandin and Swift Current. In all of these cases, judgement is again required for dealing with the curves below the 10^{-4} level. Of course the individual rare events could have been searched out and discarded (Drufuca, 1973); however, it was felt that such *a priori* manipulation of statistical data was unjustified. The rare occurrence is as much a statistical reality as an inordinately deficient situation – it would be unthinkable to "add" rainfall to a data sample because it was known to fall short of the long-term average! A study of the various "outliers" will be carried out as part of a more detailed analysis of the natural variability in the duration and occurrence of extreme events.

While discrepancies of the sorts outlined tend to be less prominent at higher frequencies, there may be some distortion in the isograms of Figures 9 to 29 as they were based entirely on the numerical data without detailed examination of all of the individual distributions.

4.3 FREQUENCY INTERPOLATION

In order to estimate the performance of a microwave link at a frequency other than the standard set for which results are presented, a reliable interpolation procedure is necessary. Various methods and models have been proposed for translating available results from one frequency to another. Procedures of this sort are referred to as frequency scaling. There is little unanimity at present regarding the respective merits of the different techniques. Attenuation predictions based on long-term climatological information represent a useful, self-consistent means of examining the different approaches. The following sections use the attenuation predictions for Ottawa to study – by no means exhaustively – some of the methods currently employed for frequency scaling.

4.3.1 The Method of Battesti

One of the simplest and most direct methods for frequency scaling has been proposed by Battesti (1981). The relevant expressions arise from an examination of the specific attenuation rates computed for spatially uniform rain of typical drop-size distribution. Battesti noted that the results could be approximated by means of linear relationships with respect to frequency. Thus, to relate the attenuation levels A_1 and A_2 which would occur with equal probability at respective frequencies f_1 and f_2,

$$\frac{A_2}{A_1} = \frac{f_2 - 6}{f_1 - 6} \tag{11a}$$

for f_1, $f_2 \leqslant 20$ GHz. Similarly,

$$\frac{A_2}{A_1} = \frac{f_2 - 10}{f_1 - 10} \tag{11b}$$

for f_1, $f_2 \geqslant 20$ GHz. If $f_1 < 20$ GHz and $f_2 > 20$ GHz, then one proceeds first from frequency f_1 to f_x by means of (11a), then from f_x to f_2 by means of (11b). That is, setting $f_x = 20$ GHz,

$$\frac{A_2}{A_1} = 1.4\,\frac{f_2 - 10}{f_1 - 6} \tag{11c}$$

In Figure 30 the results of scaling according to (E11) are shown for a hypothetical 40 km hop located in the Ottawa region. A "reference" frequency of 11 GHz was assumed. The scaled results appear to consistently underestimate the attenuation for large probabilities of occurrence, especially at the higher frequencies. The estimates converge rapidly to the data as the probability is reduced to levels approaching 1×10^{-4}, which are generally of greatest concern in terrestrial systems design. Results were not examined for lower probabilities.

It is, of course, equally possible to consider f_2 as the "reference" and to scale downward to a lower frequency f_1. This process is found to yield a corresponding overestimate, although by a greatly reduced amount.

The total frequency spread presented in Figure 30 is considerably greater than required for interpolation between the standard frequencies considered in this report. The broader frequency range is helpful, however, in estimating the relative accuracies of the different methods.

4.3.2 Hodge's Formulation

In contrast with the method described in the previous section, many other techniques for scaling rain attenuation attempt to take account of the fact that the precipitation rate is not constant over the entire length of the microwave link. Hodge (1977) assumed that at any given instant the point rainfall rate along the propagation path could be expressed as a Gaussian function of position. That is, the instantaneous attenuation is given by

$$A = \int_0^L kR(x)^{\alpha} dx \tag{12a}$$

where

$$R(y) = R_0 e^{-(y/l_0)^2} \tag{12b}$$

R_0 is the peak rainfall rate assumed to occur along the path of length L. The distance y is measured from the position of maximum rainfall intensity, assumed to be some distance from the terminal points, and $l_0 \ll L$ is

a measure of the cellular rain structure. Under these conditions, the attenuation ratio for frequencies f_2 and f_1 is given by the expression

$$\frac{A_2}{A_1} = \frac{k_2}{k_1}\sqrt{\frac{\alpha_1}{\alpha_2}}\left\{\frac{A_1}{k_1}\sqrt{\frac{\alpha_1}{\pi}}\right\}^{\left(\frac{\alpha_2}{\alpha_1}-1\right)} \tag{13}$$

This relationship is likewise presented in Figure 30 for $f_1 = 11$ GHz. At the lower probabilities of occurrence, the results resemble those predicted by Battesti's method and approximate reasonably well to the computed values. For $P > 1\text{x}10^{-3}$ the agreement by means of (13) is somewhat closer to the synthetic storm values; nonetheless, the deviation grows increasingly large as the design frequency increases. Similar underestimation was noted in comparison with terrestrial measurements in northern Europe (CCIR, 1980a).

4.3.3 Rue Formula

Misme and Fimbel (1975) presented a method for calculating rain attenuation statistics based on a log-normal approximation to the cumulative rainfall rate distribution. In the Misme-Fimbel model, rain is explicitly assumed to consist of an intense, compact core of constant rainfall rate surrounded by a much larger area of very light "residual" rain. Rue (1977) simplified some of the numerical procedures of the Misme-Fimbel model, and on the basis of this modification developed a formula relating the attenuation levels at two frequencies. In generalized form,

$$A_2 = k_2 R_{res}^{\alpha_2} D + k_{2d}\left\{\frac{A_1 - k_1 R_{res}^{\alpha_1} D}{k_1 d}\right\}^{\alpha_2/\alpha_1} \tag{14}$$

where d is the diameter of the idealized, cylindrical rain core (assumed to be 3.0 km), R_{res} is the residual rainfall rate of 5.0 mm/h (Rue, 1980), and D is the lesser of L-3 and 27 km.

The Misme-Fimbel concept is most clearly applicable to precipitation of high intensity, i.e., for events having a relatively low probability of occurrence. As seen in Figure 30, the Rue scaling formula yields extremely good agreement with the synthetic storm attenuation data for Ottawa. For $P < 3\text{x}10^{-4}$ the fit in Figure 30 is virtually exact. For the larger probabilities and higher frequencies, there is a slight overestimation of the attenuation levels. In order to apply (14) in the case $P = 3\text{x}10^{-3}$, however, it was necessary to reduce R_{res} slightly from its postulated value of 5.0 mm/h to 4.8 mm/h. The magnitude of the necessary correction to R_{res} increases rapidly for higher probabilities.

4.3.4 Power-law Scaling

A formula for attenuation scaling which is frequently employed is the power law relation

$$\frac{A_2}{A_1} = \left(\frac{f_2}{f_1}\right)^n \tag{15}$$

Based on a limited number of synthetic storm type calculations, Ro (1973) and Drufuca (1974) proposed $n = 1.72$ over the frequency interval 11.2 GHz to 18.7 GHz. A value of $n = 2$ is sometimes employed, especially for frequencies above about 20 GHz.

To examine the applicability of power-law scaling, the Ottawa data of Figure 30 were re-plotted on a log-log scale. Figure 31 reveals that the results may be fitted by a family of nearly parallel straight lines. Between 11 and 30 GHz the approximation is extremely good. Even over the complete range of frequencies in

Figure 31 (i.e., 8–50 GHz), the approximations are good ones and the exponent n is virtually the same as for the more restricted range.

The average value of n for the four probability levels shown is 1.98. For all intents and purposes, therefore, an f^2 scaling relation appears to apply in this instance. In fact, the gradients vary slightly from about 1.87 for $P \approx 1 \times 10^{-4}$ to 2.17 for $P \approx 3 \times 10^{-3}$. This increase in the effective value of n is the result of changes in the rainfall drop size distribution. The lower rainfall rates associated with a high probability of occurrence contain a much larger proportion of smaller drop diameters. These contribute more significantly to the attenuation at high frequencies than they do at lower ones.

It is interesting to note in the present context that the curves predicted by Hodge's formula (13), are themselves close approximations to power-law expressions. Over the range 8 to 30 GHz, Hodge's results are fitted by curves having an average value of $n = 1.88$. As in the case examined above, the magnitude of the exponent tends to increase with increasing probability.

It should also be noted that Owolabi and Ajayi (1980) have recently examined the specific attenuation rates for a Laws and Parsons drop-size distribution in the manner of Battesti (section 4.3.1). Unlike that work however, Owolabi and Ajayi find an f^2 relation to hold, approximately, at least over the range 10–20 GHz. Their work also reveals the trend of increasing n with decreasing rainfall rate (increasing probability).

4.3.5 Fixed-level Scaling

One of the difficulties with frequency scaling at constant probability arises from the fact that the atmospheric attenuation values corresponding to the reference frequency f_1 and the design frequency f_2 may differ by significant amounts. As seen in Figure 30, this effect is particularly prominent for low probabilities of occurrence. A relationship between the probability of exceeding a given fade margin at one frequency with the performance at another frequency of an otherwise identical link (i.e., frequency scaling at constant attenuation level), would be a valuable alternative to the constant probability methods discussed earlier.

Data were examined in a purely statistical manner for several locations across the country. No attempt was made at imposing any physical model to the data. Instead, a number of curve fitting procedures were attempted. The form which applied to all of the data examined was a second order polynomial in log-log coordinates, i.e.,

$$\log \xi = C_0 + C_1 \log \eta + C_2 (\log \eta)^2 \qquad (16a)$$

where, because of the very wide frequency range considered (6-100 GHz), it was found that (16a) had to be applied in two complementary ways for each data set. Thus,

$$\text{for} \qquad f \leqslant f_x \quad \xi = \text{freq} \;\; ; \;\; \eta = \text{prob} \qquad (16b)$$

$$\text{and for} \qquad f \geqslant f_x \quad \xi = \text{prob} \;\; ; \;\; \eta = \text{freq} \qquad (16c)$$

The "crossover" frequency f_x is not a critical parameter. For most locations f_x=20 GHz was appropriate; for the west coast, where the onset of significant attenuation occurs at a higher frequency, f_x=30 GHz is more suitable.

Figure 32 presents data for 20 and 80 km links at Ottawa along with the approximating curves determined by logarithmic regression. Similar results are observed for other hop lengths and fade amplitudes at each location. The curves presented earlier in Figure 1, for example, are the constant level approximations for 40 km hops at various locations from coast to coast. These were all obtained from their respective data bases in analogous fashion through the use of (16).

While the general form of the constant-level approximation appears to hold at all locations and for different hop lengths and fade depths, the application of this approach to existing operational experience is difficult because there does not appear to be a simple relationship between the numerical coefficients of (16a) and a particular geographic location. Of course, this is no constraint in the case of the data presented here since the coefficients can be determined from these data. The method may be used to interpolate fading statistics to frequencies of interest, especially at the higher frequencies where the intervals between data are numerically large.

4.3.6 Two-frequency Scaling Method

Another technique which may be employed for the interpolation of attenuation data is the two-frequency scaling method presented by Hogg (1973; Kheirallah and Olsen, 1982). If the attenuations A_1 and A_2 at a given probability level are known for frequencies f_1 and f_2, then an estimate of the equi-probable attenuation at frequency f_3 is given by the expression

$$A_3 = k_3 \left(\frac{A_1}{k_1}\right)^{\frac{\alpha_3 - \alpha_2}{\alpha_1 - \alpha_2}} \left(\frac{A_2}{k_2}\right)^{\frac{\alpha_1 - \alpha_3}{\alpha_1 - \alpha_2}} \tag{17}$$

where the different k_i and α_i are the specific attenuation coefficients for the appropriate frequency, f_i.

Using Ottawa data at 11 and 25 GHz as reference values, attenuations were then scaled by means of (17) over the range 8 to 50 GHz and compared with the synthetic storm curves of Figure 30. The result was an extremely precise fit to the synthetic storm data, not only in the interval between 11 and 25 GHz, but extending from 8 GHz to about 40 GHz. Beyond 40 GHz there was a small underestimation in the extrapolated attenuation values.

On the basis of this limited example, the two-frequency method appears to be a simple and accurate technique for the interpolation of attenuation data.

5. EFFECTS OF NON-SPHERICAL RAINDROPS

5.1 DIFFERENTIAL ATTENUATION

During the brief period of transit from cloud to surface, the forces of gravity, atmospheric drag and aerodynamic pressure combat the influence of surface tension on each rain drop. Asymmetries are produced and the falling drops acquire a generally oblate or horizontally flattened aspect (Jones, 1959; Pruppacher and Pitter, 1971). Horizontally polarized waves therefore tend to experience greater attenuation than vertically polarized ones under otherwise similar conditions.

Up to this point, all of the attenuation computations have been made with the implicit assumption of spherically symmetrical raindrops. It is therefore appropriate now to examine the nature of the attenuation variability with respect to wave polarization. To do this the precipitation data for Ottawa have been analyzed in terms of a hypothetical 40 km long hop. The CCIR (1980b) coefficients were used for waves linearly polarized parallel to the major and minor axes of the raindrops. These are euphemistically referred to as horizontal and vertical polarizations, respectively. The equi-probable attenuations for the two orthogonal polarizations were then derived from the individual cumulative distributions for a wide range of frequencies and probabilities.

Of prime interest is the ratio of the equi-probable attenuation difference to the corresponding attenuation for spherical raindrops. For this purpose we may approximate the spherical attenuation by the mean of the

values for the two orthogonal polarizations. Figure 33 presents the results of this examination for the Ottawa example. The figure shows the normalized (percentage) difference in attenuation of either polarization from the mean as a function of frequency for the range 8 to 100 GHz. A family of four curves is presented, for mean (spherical) attenuation values from 10 dB to 70 dB.

Typically, the difference in the attenuation characteristics between these orthogonal polarizations is small in comparison with the total attenuation for either one. There is a generally decreasing trend in the polarization difference with increasing frequency reflecting a similar trend in the values of α_h and α_v. Beyond 60 GHz, $\alpha_h \approx \alpha_v$ and the polarization difference becomes independent of A_o, the mean path attenuation. Conversely, there is a relatively large A_o dependence between 18 and 35 GHz due to a relative maximum in the difference between the two exponents. The sharp drop in fractional attenuation difference at 15 GHz is the result of a decrease in the fractional difference between k_h and k_v.

In the design of terrestrial systems, the difference in attenuation rates for the different polarizations does not, in itself, appear to be a matter for serious concern. For frequencies below 12 GHz the polarization differences increase from 8 percent to 14 percent of the spherical attenuation; however, rain attenuation is not usually a limiting factor at these frequencies. On the other hand, for terrestrial propagation beyond about 50 GHz there is only a modest dispersion in attenuation with respect to the wave polarization angle. Over the intermediate range some polarization correction might be required for critical applications. The results presented in Figure 33 provide an adequate means for doing this. Though derived on the basis of a 40 km hop at Ottawa, these curves are more generally applicable because they are presented here in a normalized form, i.e., as a fraction of the mean path attenuation.

It should be noted that the polarization differences discussed here represent an upper limit to what is likely to be encountered in practice. The winds which inevitably accompany a heavy rain event will tilt the raindrops relative to the wave polarization axis. Furthermore, individual drops along the length of the hop will be oriented differently from one another, with some drops deviating widely from their free-fall configuration. The effective vertical and horizontal drop dimensions will therefore be closer to the spherical approximation than the major and minor drop diameters implicitly assumed by the use of the CCIR (1980b) coefficients. It should also be noted that the attenuation predictions for spherical raindrops as presented in this report are conservative inasmuch as these are actually closer to the values for horizontal polarization than to the corresponding ones for vertically polarized waves (Oguchi, 1973).

5.2 CROSS-POLAR ISOLATION

As indicated above, atmospheric turbulence and wind shear may tilt the axis of rotational symmetry of the individual rain drops with respect to the vertical. In general, therefore, vertically and horizontally polarized waves will not be aligned with the principal axes of the raindrops. One consequence is a net rotation of the plane of polarization resulting in a received component which is orthogonal to the originally transmitted wave. Such contamination may limit the use of dual polarization at a given frequency over a single microwave link.

The ratio of received signal having the desired polarization to the orthogonally polarized signal is generally termed the cross-polar discrimination (XPD). Oguchi (1973, 1977) has developed generalized theoretical expressions for the XPD in terms of the scattering properties of raindrops as determined by their shape and orientation with respect to the propagation trajectory. Nowland et al. (1977) examined these expressions and derived a simplified relationship of the form

$$XPD = U - V \log(CPA) - W \log (R) \qquad (18)$$

where CPA is the appropriate co-polar attenuation and R is the rainfall rate having the same probability of occurrence.

In general, the second term in (18) is at least an order of magnitude greater than the one involving log(R). Near 11 or 12 GHz the latter term becomes vanishingly small. Since the two are very closely related, the direct term in log(R) is sometimes incorporated into the term in log(CPA) with a corresponding modification in the coefficient V. This allows the cross polarization statistics to be estimated on the basis of rain attenuation data.

Very few direct or indirect measurements have been made of the range and distribution of drop canting angles through different sections of a typical rain storm. It is therefore difficult to establish values for the various coefficients on a purely physical basis. Effective values of some of these coefficients have therefore been established by empirical means (Olsen and Nowland, 1978; Chu, 1980; Olsen, 1981a). The resulting relation currently accepted by the CCIR (1980c) is

$$XPD = U_0 + 30 \log(f) - 20 \log(CPA) \qquad (19)$$

for $8 \leqslant f \leqslant 20$ GHz, with $U_0 = 9$ dB as a conservative estimate. The ability to estimate the cross-polar characteristics of a microwave system during rain will likely be improved as additional meteorological and experimental data are examined.

Polarization cross-talk on microwave systems is not exclusively the result of hydrometeors along the propagation path. On long hops clear-air depolarization is frequently a more serious consideration (Olsen, 1981b). This may be brought about by imperfections in antenna design, off-axis propagation due to refractive effects, reflection from a tilted surface or atmospheric layer or by a combination of these. The subject, however, is clearly beyond the scope of this report.

6. REFERENCES

Austin, P.M. and R.A. Houze, Jr., *Analysis of the Structure of Precipitation Patterns in New England*, J. App. Meteor., 11, 926–935, (Sept. 1972).

Battesti, J., *Au sujet de la dépendance en fréquence de l'affaiblissement dû a la pluie*, Ann. des Télécomm., 36, 274–275, (Mar. – Apr. 1981).

Bertok, E., G. de Renzis, and G. Drufuca, *Estimate of Attenuation Due to Rain at 11 GHz From Raingauge Data*, Proc. URSI Comm. F Symp., (La Baule), pp. 295–300, (Apr. 1977).

Best, A.C., *The Size Distribution of Raindrops*, Quart. J. Roy. Meteor. Soc., 76, 16–36, (Jan. 1950).

Blanchard, D.C. and A.T. Spencer, *Rainfall Measurements During Project Shower*, Tellus, 9, 541–552, (Nov. 1957).

Bussey, H.E., *Microwave Attenuation Statistics Estimated From Rainfall and Water Vapour Statistics*, Proc. I.R.E., 38, 781–785, (July 1950).

CCIR, *Frequency Scaling of Rain Attenuation*, Doc. 5/78 (Sweden), Int. Telecomm. Union, Geneva, (March 1980a).

CCIR, *Attenuation by Precipitation and Other Atmospheric Particles*, Report 721–1, Conclusions of the Interim Meeting of Study Group 5, Int. Telecomm. Union, Geneva, (Aug. 1980b).

CCIR, *Propagation Data Required for Line-of-sight Radio-relay Systems*, Report 338-3, Conclusions of the Interim Meeting of Study Group 5, Int. Telecomm. Union, Geneva, (Aug. 1980c).

Chu, T.S., *Rain-induced Cross-polarization at Centimeter and Millimeter Wavelengths*, Bell Syst. Tech. J., 53, 1557–1579, (Oct. 1974).

Drufuca, G., *Rain Attenuation Statistics for Frequencies Above 10 GHz From Raingauge Records*, in: AGARD Conference Proceedings 107, NATO, (Sept. 1972).

Drufuca, G., *Rain Attenuation Studies*, Report MW-77, Stormy Weather Group. McGill University, Montreal, (Mar. 1973).

Drufuca, G., *Rain Attenuation Statistics for Frequencies Above 10 GHz From Raingauge Observations*, Jour. Rech. Atmosph., 8, 399–411, (Jan. – June 1974).

Fedi, F., *Attenuation Due to Rain on a Terrestrial Path*, Alta Freq., 66, 167–184, (Apr. 1979).

Gunn, K.L.S. and T.W.R. East, *The Microwave Properties of Precipitation Particles*, Quart. J. Roy. Meteor. Soc., 80, 522–545, (1954).

Gunn, R. and G.D. Kinzer, *The Terminal Velocity of Fall for Water Droplets in Stagnant Air*, J. Meteor., 6, 243–248, (Aug. 1949).

Hamilton, P.M. and J.S. Marshall, *Weather-radar Attenuation Estimates From Raingauge Statistics*, Report MW-32, Stormy Weather Group, McGill University, Montreal, (Jan. 1961).

Harden, B.N., J.R. Norbury and W.J.K. White, *Model of Intense Convective Rain Cells for Estimating Attenuation on Terrestrial Millimetric Radio Links*, Electron. Lett., 10, 483–484, (Nov. 1974).

Hobbs, P.V. and J.D. Locatelli, *Rainbands, Precipitation-cores and Generating Cells in a Cyclonic Storm*, J. Atmos. Sci., 35, 230–241, (Feb. 1978).

Hodge, D.B., *Frequency Scaling of Rain Attenuation*, Trans. IEEE, AP-25, 446–447, (May 1977).

Hogg, D.C., *Intensity and Extent of Rain on Earth-space Paths*, Nature, 243, 337–338, (June 1973).

Holland, D.J., *The Cardington Rainfall Experiment*, Meteor. Mag., 96, 193–202, (1967).

Jones, D.M.A., *The Shape of Raindrops*, J. Meteor., 16, 504–510, (Oct. 1959).

Joss, J., J.C. Thams and A. Waldvogel, *The Variation of Raindrop Size Distribution at Locarno*, in: Preprints of Conference on Cloud Physics (Toronto), pp. 369–373, Amer. Meteor. Soc., Boston, (Aug. 1968).

Kheirallah, H.N. and R.L. Olsen, *Comparison of a One and a Two-frequency Technique for Frequency Scaling of Rain Attenuation Statistics*, Submitted to Electron, Lett., (1982).

Laws, J.O. and D.A. Parsons, *The Relation of Raindrop-size to Intensity*, Trans. A.G.U., 24, 452–460, (April 1943).

MacKenzie, E.C. and J.E. Allnutt, *Effect of Squall-line Direction on Space-diversity Improvement Obtainable With Millimetre-wave Satellite Radiocommunication Systems*, Electron. Lett., 13, 571–573, (Sept. 1977).

Marshall, J.S. and W. McK. Palmer, *The Distribution of Raindrops With Size*, J. Meteor., 5, 165–166, (Aug. 1948).

Mie, G., *Beitäge zur Optik trüber Medien, speziell colloidaler Metallösungen*, Ann. Phys., 25, 377–445, (Mar. 1908).

Misme, P. and J. Fimbel, *Détermination théorique et experimentale de l'affaiblissement par la pluie sur un trajet radioélectrique*, Ann. des Télécomm., 30, 149–158, (May–June 1975).

Mogensen, G. and E. Stephansen, *Estimation of Methods for Prediction of Rain Induced Attenuation on L.O.S. Paths*, in: Conf. Publ. No. 169, pp. 97–101, Instn. Electr. Eng., London, (Nov. 1978).

Nowland, W.L. R.L. Olsen, and I.P. Shkarofsky, *Theoretical Relationship Between Rain Depolarization and Attenuation*, Electron. Lett., 13, 676–678, (Oct. 1977).

Oguchi, T., *Scattering Properties of Oblate Raindrops and Cross Polarization of Radio Waves Due to Rain: Calculations at 19.3 and 34.8 GHz*, J. Radio Res. Labs., 20, 79–118, (1973).

Oguchi, T., *Scattering Properties of Pruppacher-and-Pitter Form Raindrops and Cross Polarization Due to Rain: Calculations at 11, 13, 19.3, and 34.8 GHz*, Radio Science, 12, 41–51, (Jan. – Feb. 1977).

Olsen, R.L., *Cross Polarization During Precipitation on Terrestrial Links: A Review*, Radio Sci., 16, 761–779, (Sept. – Oct. 1981a).

Olsen, R.L., *Cross Polarization During Clear-air Conditions on Terrestrial Links: A Review*, Radio Sci., 16, 631–647, (Sept. – Oct. 1981b).

Olsen, R.L. and W.L. Nowland, *Semi-empirical Relations for the Prediction of Rain Depolarization Statistics: Their Theoretical and Experimental Basis*, in: Proc. Symp. Ant. Prop., (Sendai), pp. 477–480, (Aug. 1978).

Olsen, R.L., D.V. Rogers and D.B. Hodge, *The aR^b Relation in the Calculation of Rain Attenuation*, Trans. IEEE, AP-26, 318–329, (Mar. 1978).

Owolabi, I.E. and G.O. Ajayi, *Frequency Scaling Technique for Rainfall Attenuation Prediction on Terrestrial Microwave Links*, presented at: URSI Commission F Symposium (Lennoxville), (May 1980).

Pruppacher, H.R. and R.L. Pitter, *A Semi-empirical Determination of the Shape of Cloud and Rain Drops*, J. Atmos. Sci., 28, 86–94, (Jan. 1971).

Ro, C.-U., *Rain Attenuation Statistics Across Canada*, M. Sc. Thesis, Dept. of Meteor., McGill Univ., Montreal, (Mar. 1973).

Rue, O., *Effects of Rainstorms on the System Performance of Multi-hop Radio Relay Links*, in: Proc URSI Comm. F Symp. (La Baule), pp. 311–316, (April 1977).

Rue, O., *Radio Wave Propagation at Frequencies Above 10 GHz. New Formulas for Rain Attenuation*, TELE (English edition), 32(1), 11–17, (1980).

Ryde, J.W., *The Attenuation and Radar Echoes Produced at Centimetre Wavelengths by Various Meteorological Phenomena*, in: Meteorological Factors in Radio Wave Propagation, pp. 169–188, The Physical Society, London, (1946).

Segal, B., *Radio Climatological Studies*, in: DOC seminar series, Research in Radio Propagation, Communications Research Centre, Ottawa, (Sept. 1978).

Segal, B., *High-intensity Rainfall Statistics for Canada*, CRC Report 1329, Communications Research Centre, Ottawa, (Nov. 1979).

Segal, B., *A New Procedure for the Determination and Classification of Rainfall Rate Climatic Zones*, Ann. des Télécomm., 35, 411–417, (Nov. – Dec. 1980).

Segal, B. and R.E. Barrington, *Tropospheric Refractivity Atlas for Canada*, CRC Report 1315, Communications Research Centre, Ottawa, (Dec. 1977).

Sekhon, R.S. and R.C. Srivastava, *Doppler Radar Observations of Drop-size Distributions in a Thunderstorm*, J. Atmos. Sci., 28, 983–994, (Sept. 1971).

Watson, P.A., H.J. Ahmed and G. Papioannou, *Long Term Prediction of Attenuation on Terrestrial Radio Links From Rainfall Data*, in: Conf. Publ. No. 169, pp. 92–96, Instn. Electr. Eng., London, (Nov. 1978).

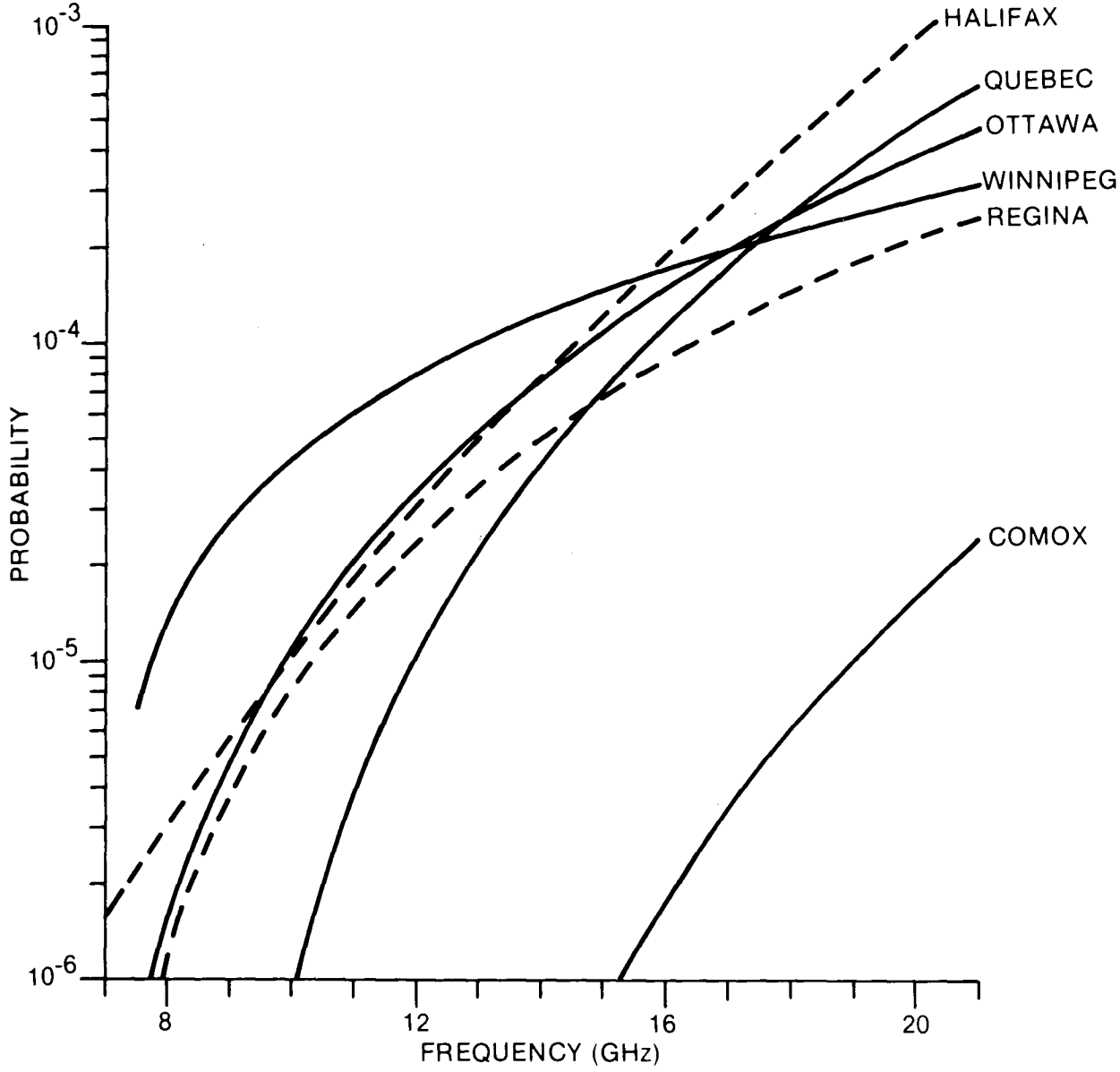

Figure 1. Probability of experiencing a 40 dB propagation fade due to rain on 40 km long hops at several randomly selected locations across Canada. Note the sharp onset of attenuation for non-coastal locations and the rapid growth in probability level with increasing frequency.

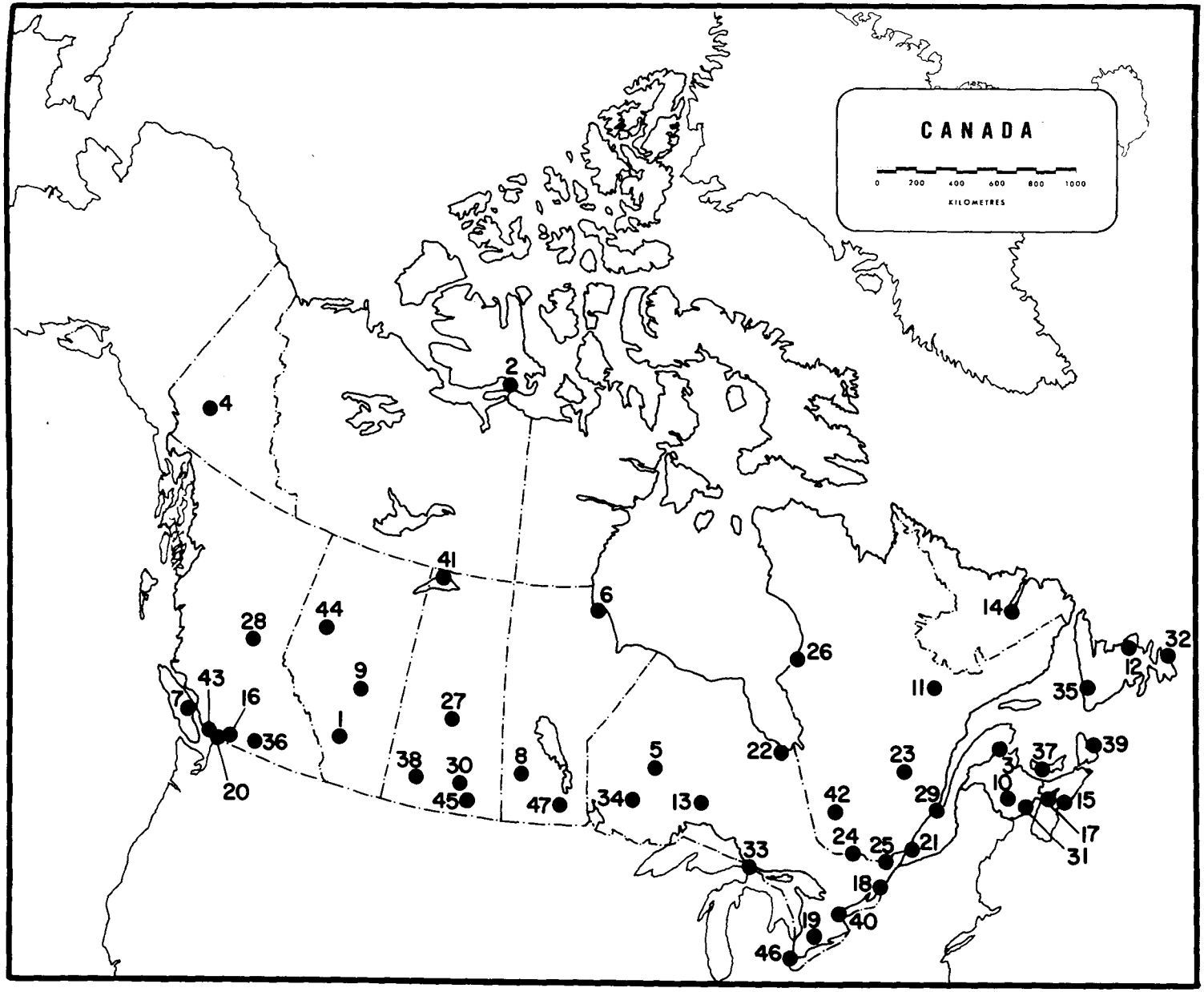

Figure 2. Location of precipitation recording stations for which attenuation characteristics are presented. The numerals correspond to the station listing in Table 1.

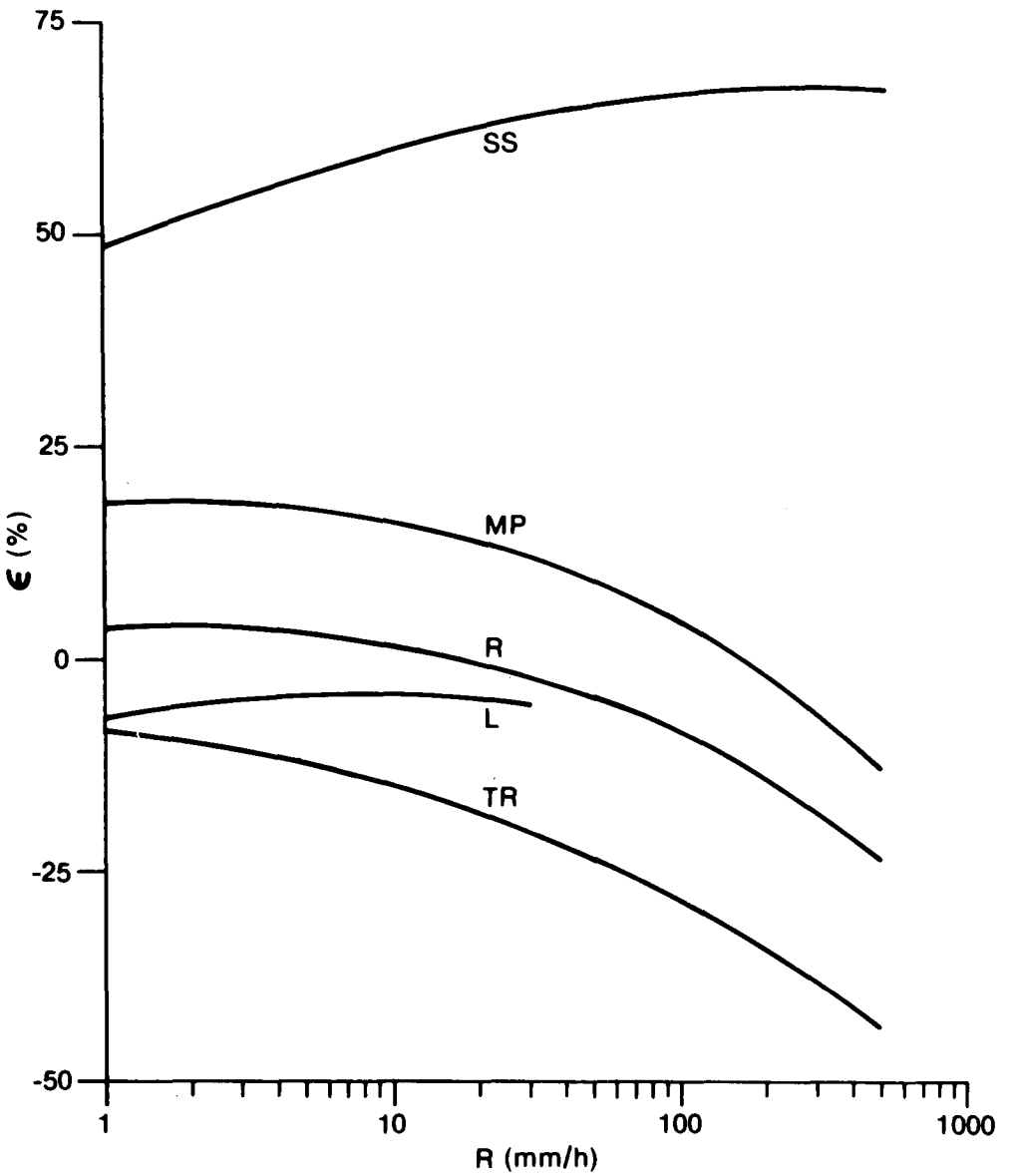

Figure 3. Potential errors from the use of un-normalized drop-size distributions, shown as a function of rainfall rate. The curves for thunderstorm (TR), drizzle (L) and continuous rain (R) relate to distributions of Joss et al. (1968); MP refers to the widespread rainfall distribution of Marshall and Palmer (1948). The curve labelled SS refers to a thunderstorm distribution proposed by Sekon and Srivastava (1971). A raindrop temperature of 10°C was assumed, with terminal velocities given by Gunn and Kinzer (1949).

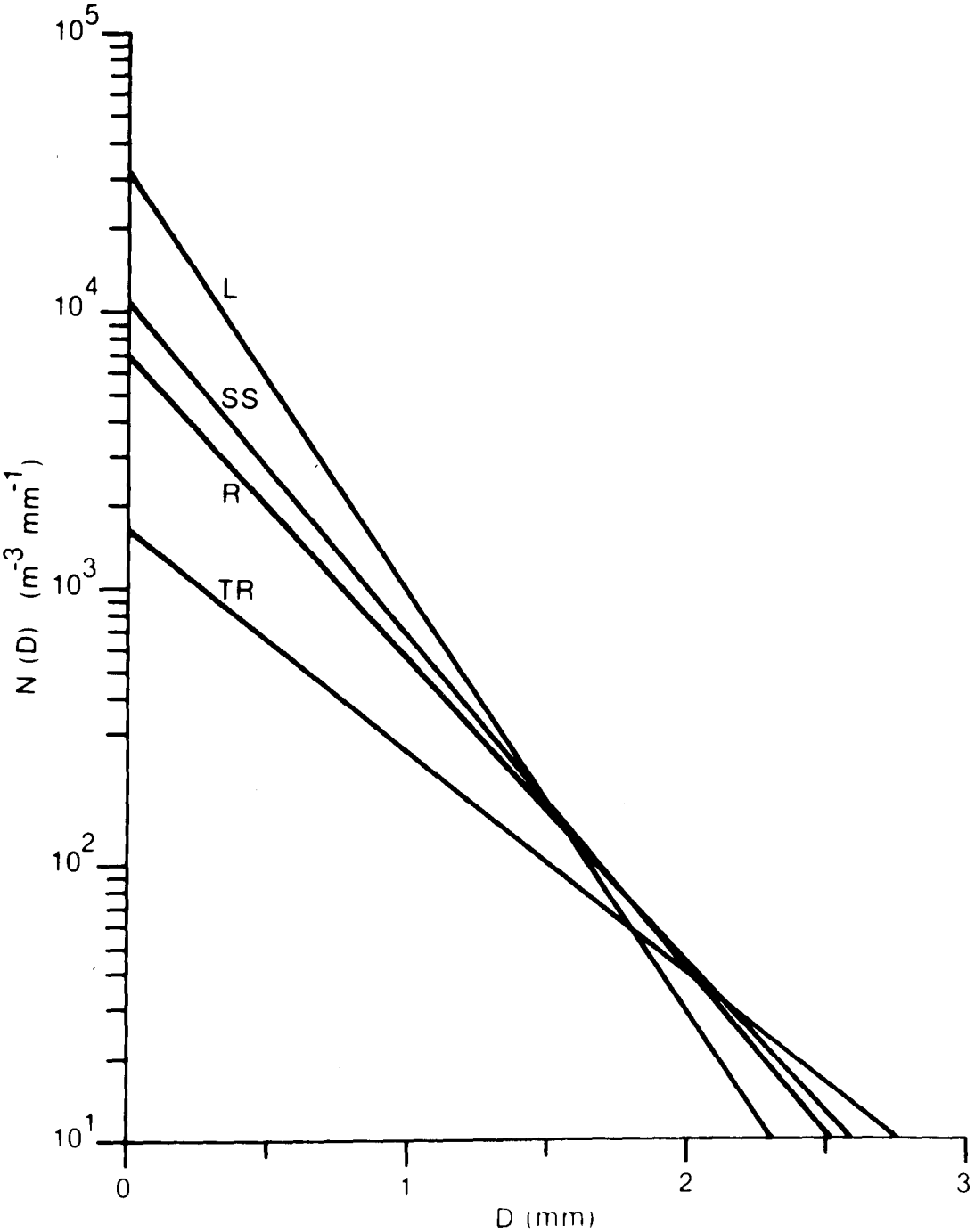

Figure 4. Several different drop-size distributions yielding identical rainfall rates of 10 mm/h. The curves are labelled as in Figure 3.

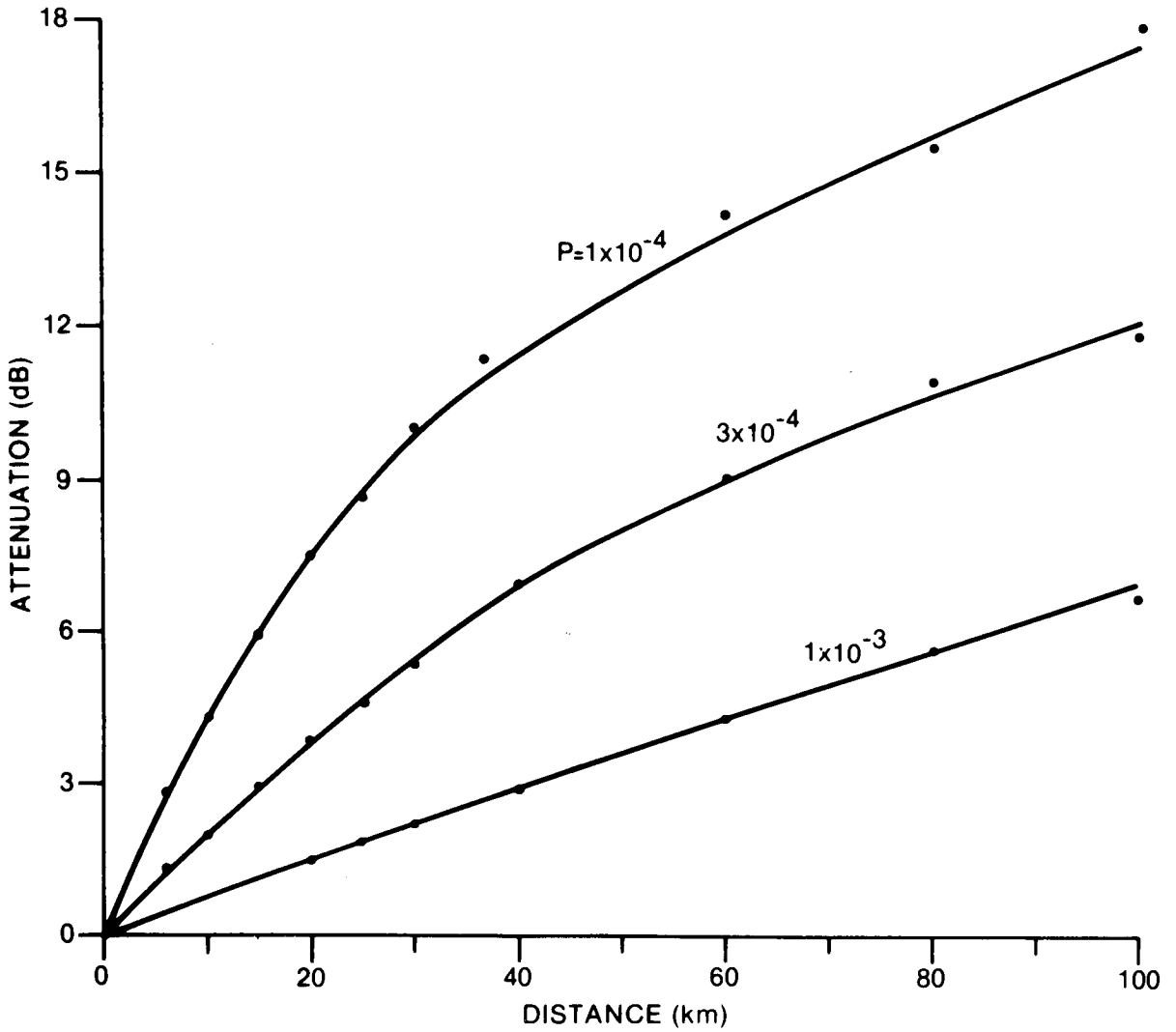

Figure 5. Hop length dependence of attenuation for 8 GHz propagation at Ottawa. Values of cumulative exceedance probability are indicated. Analogous behaviour is observed for locations in other climatic regions and/or at higher frequencies.

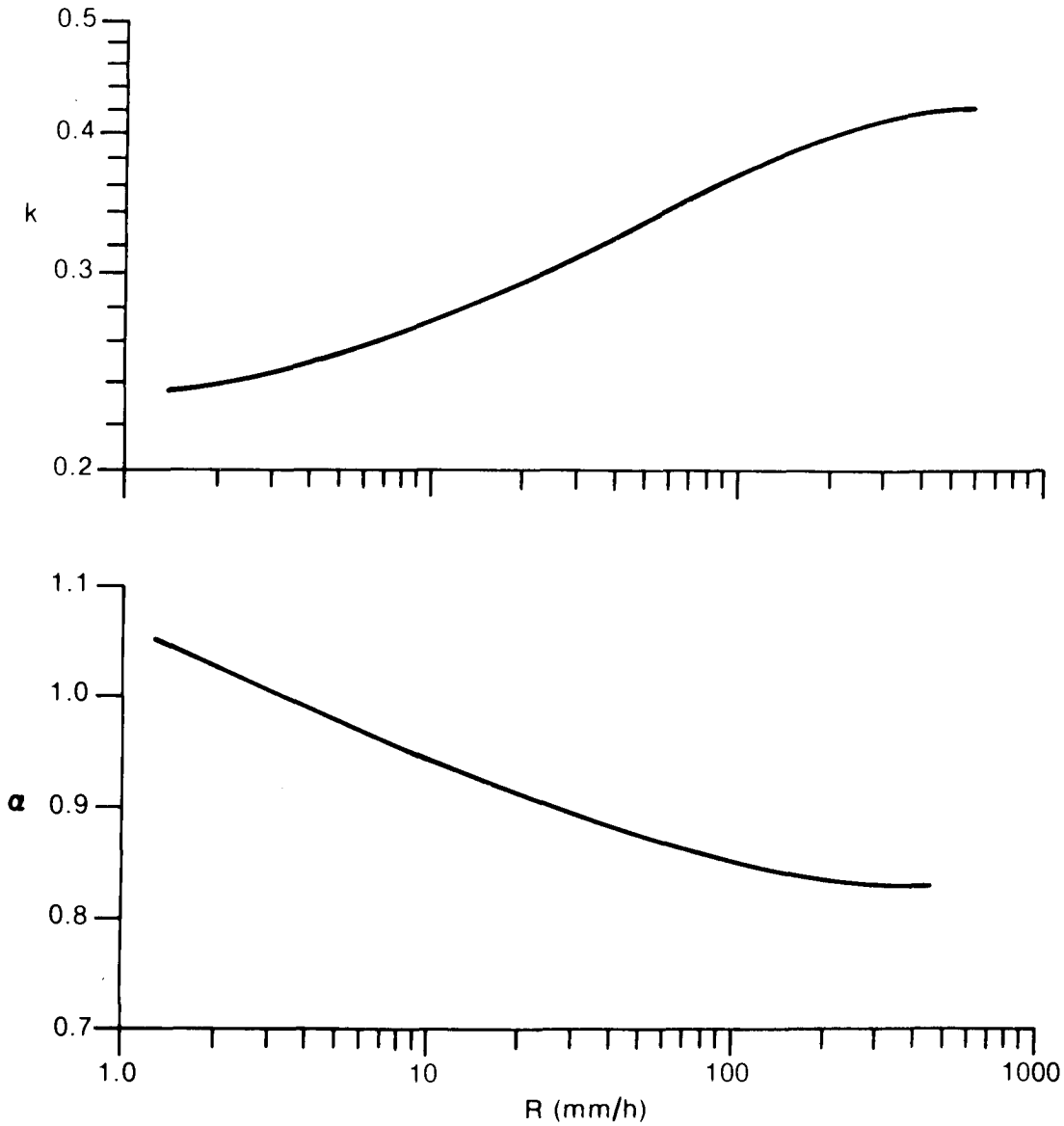

Figure 6. Variation in the specific attenuation coefficients k and α at 35 GHz as functions of rainfall rate for a thunderstorm type drop-size distribution.

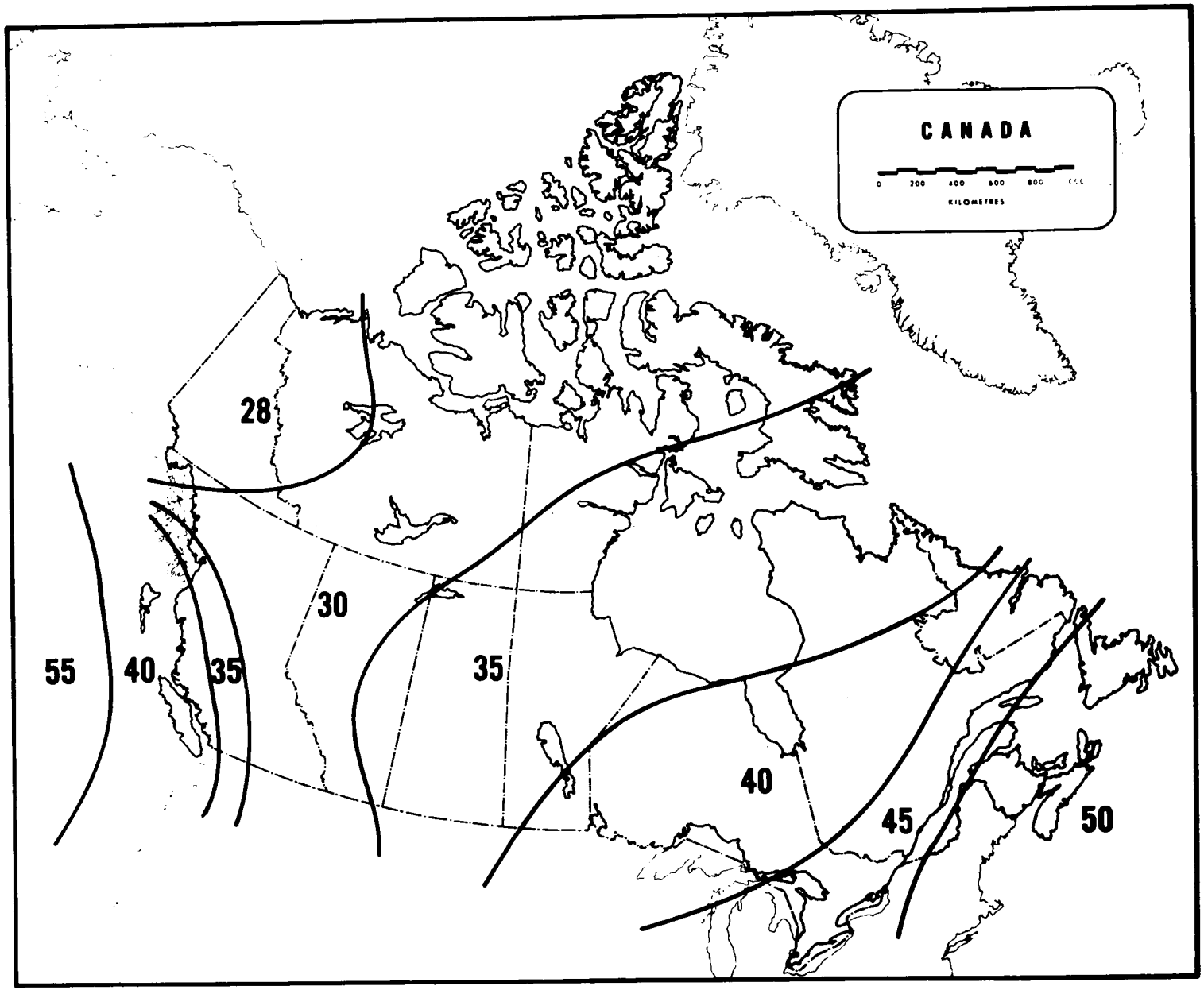

Figure 7. Assumed average speed of storm movement (km/h) in different regions of the country.

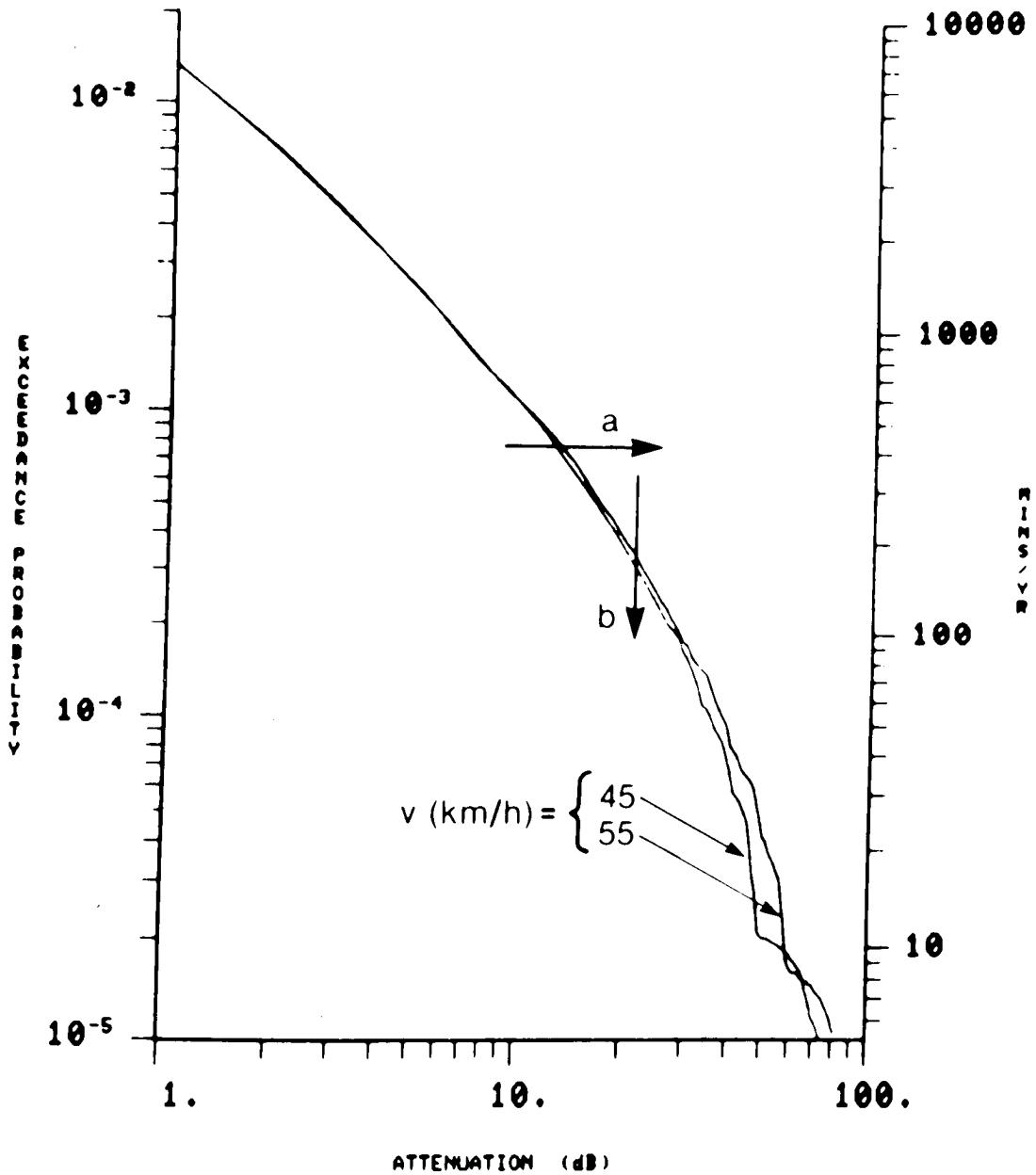

Figure 8. Influence of storm speed on predicted 15 GHz rain attenuation at Ottawa.

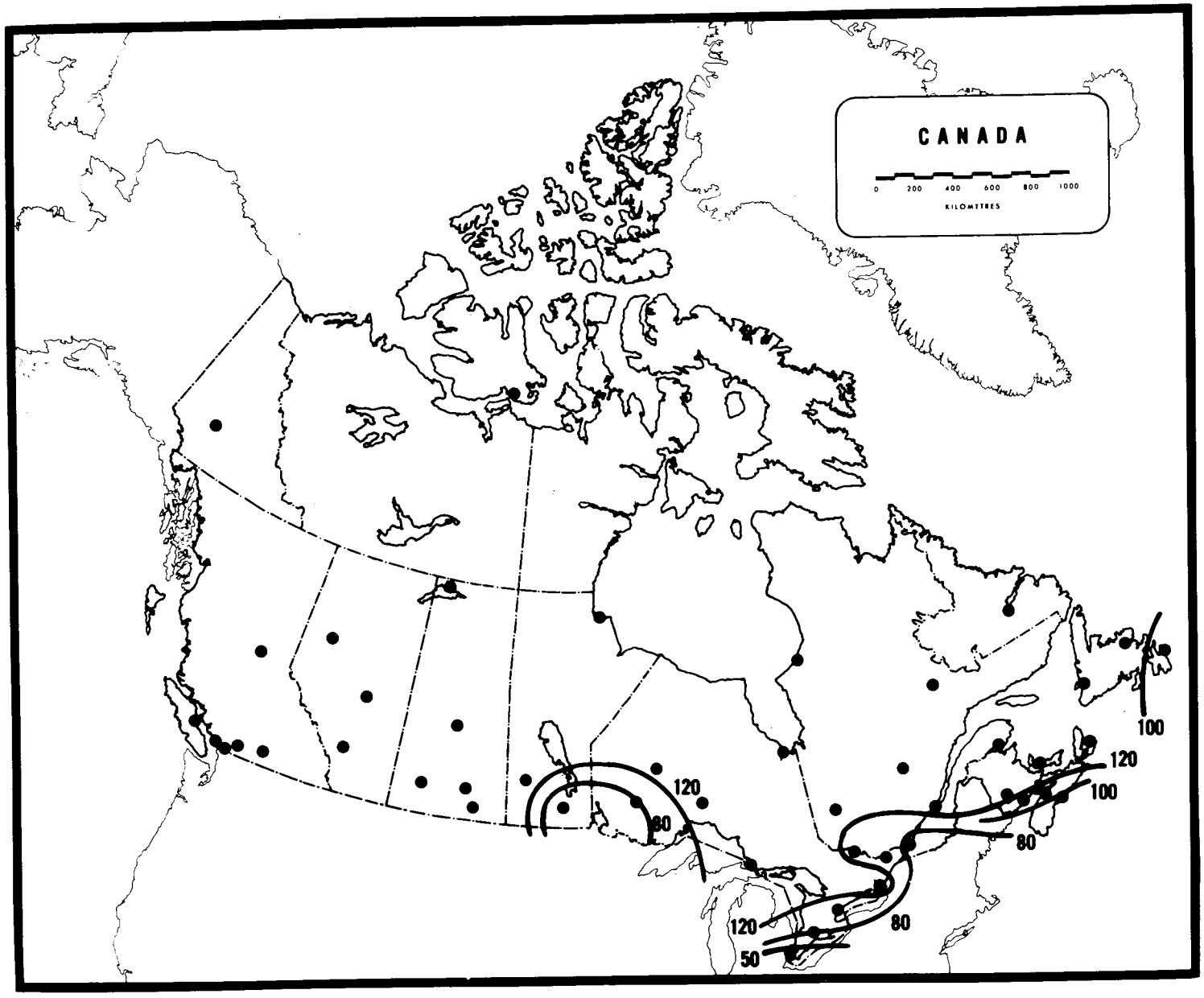

Figure 9. Maximum path length for 0.01 percent probability of exceeding a 40 dB fade due to rain attenuation at 11 GHz.

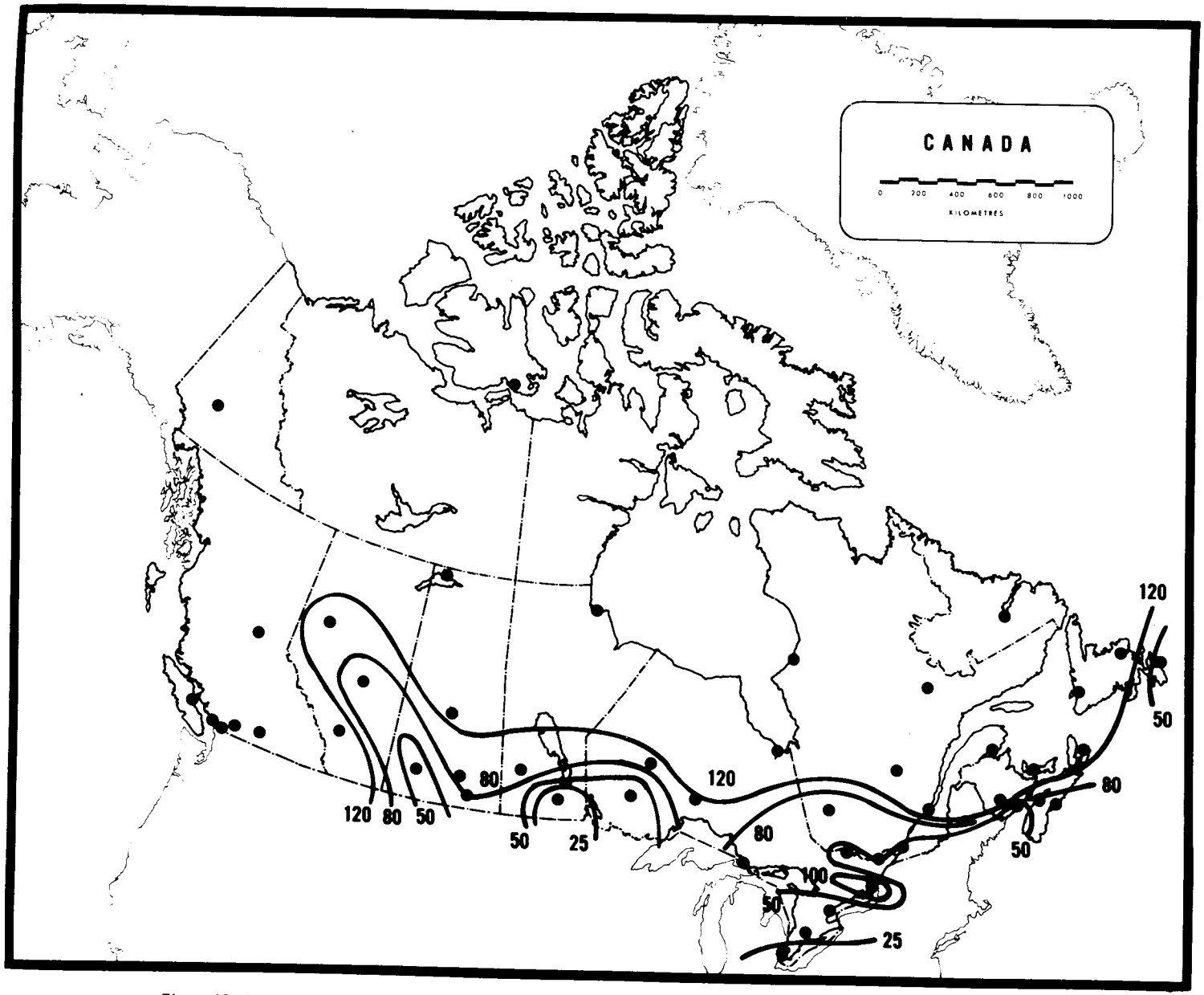

Figure 10. Maximum path length for a 0.003 percent probability of exceeding a 40 dB fade due to rain attenuation at 11 GHz.

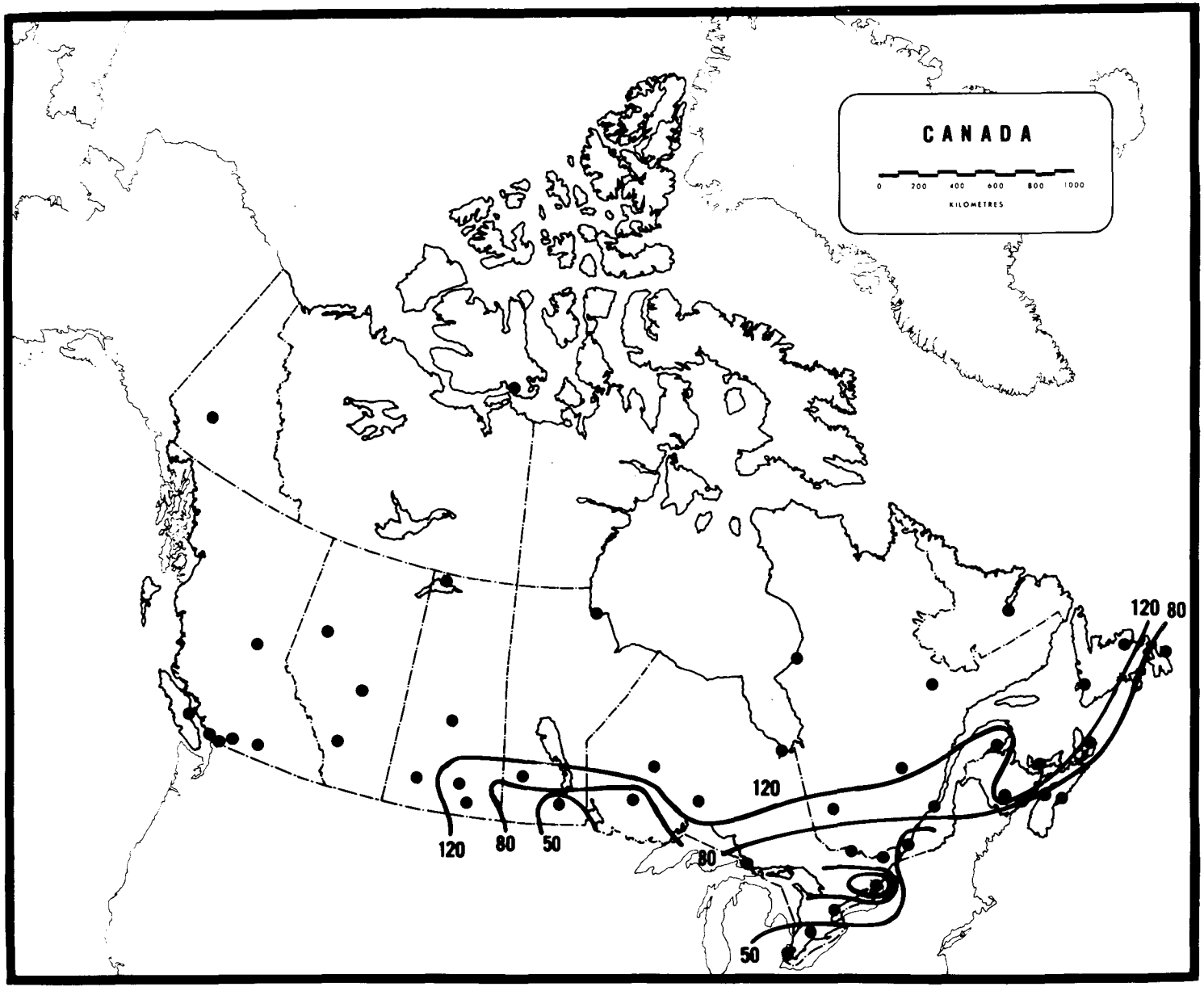

Figure 11. Maximum path length for a 0.01 percent probability of exceeding a 40 dB fade due to rain attenuation at 12.8 GHz.

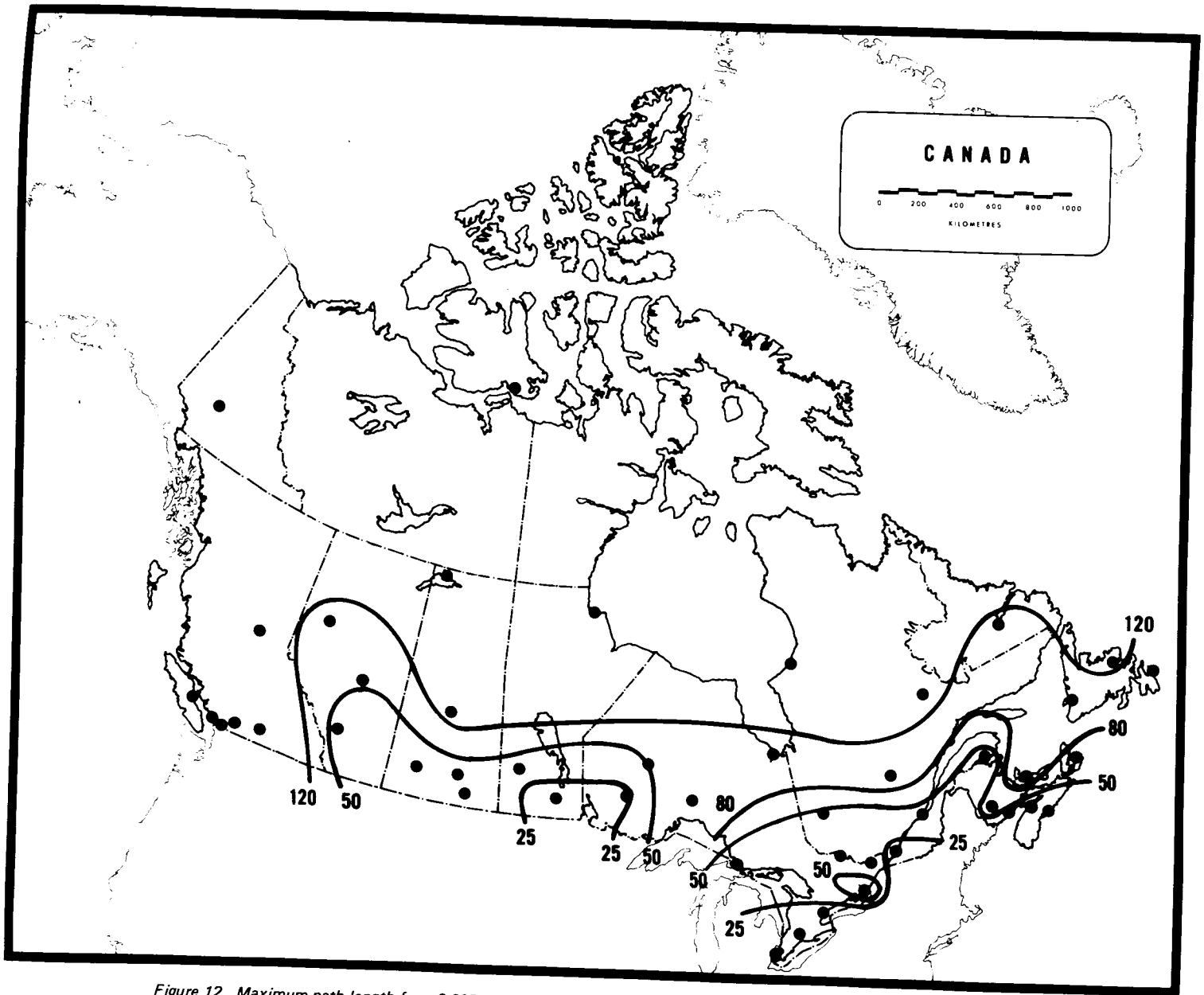

Figure 12. Maximum path length for a 0.003 percent probability of exceeding a 40 dB fade due to rain attenuation at 12.8 GHz.

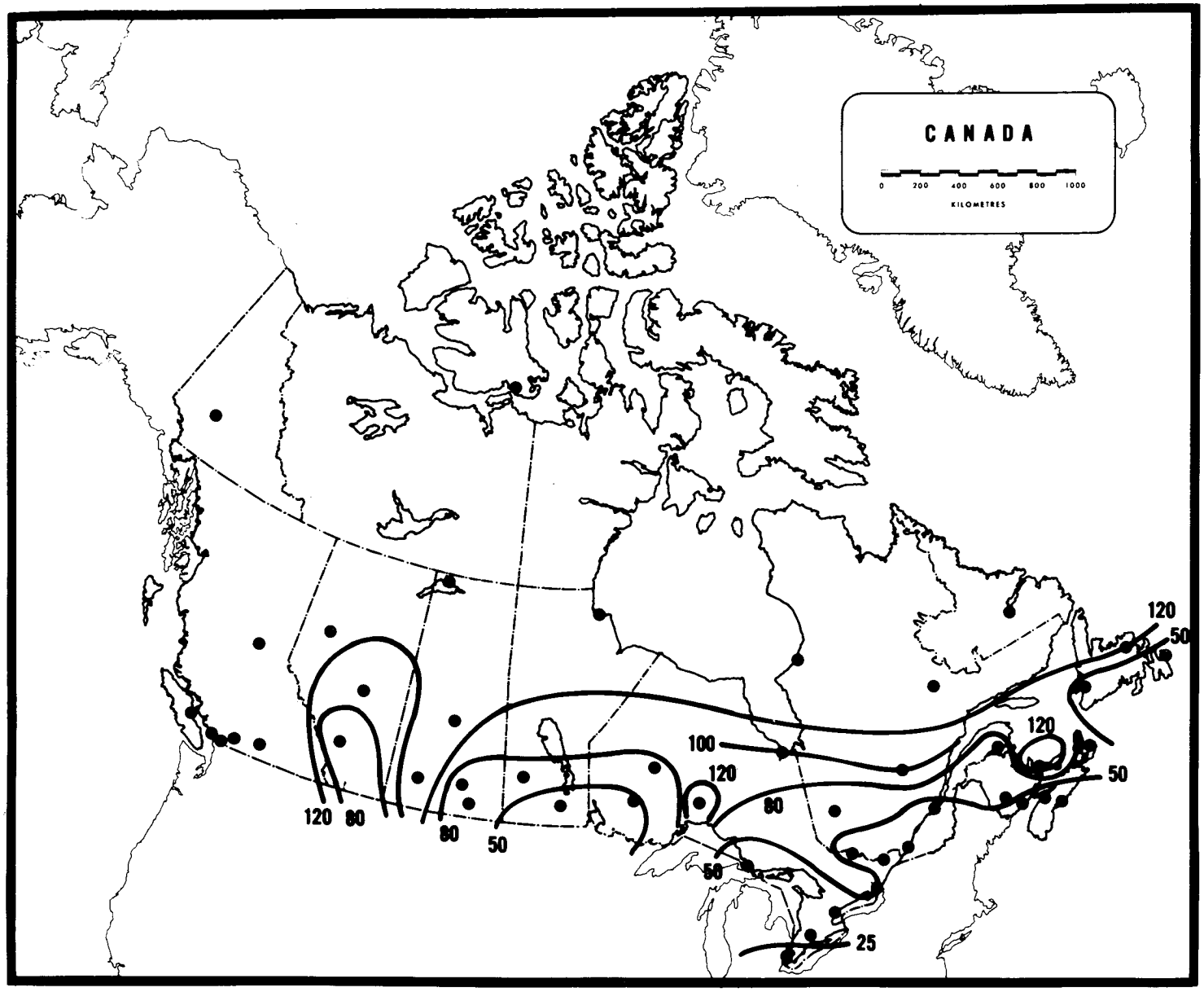

Figure 13. Maximum path length for 0.01 percent probability of exceeding a 40 dB fade due to rain attenuation at 15GHz.

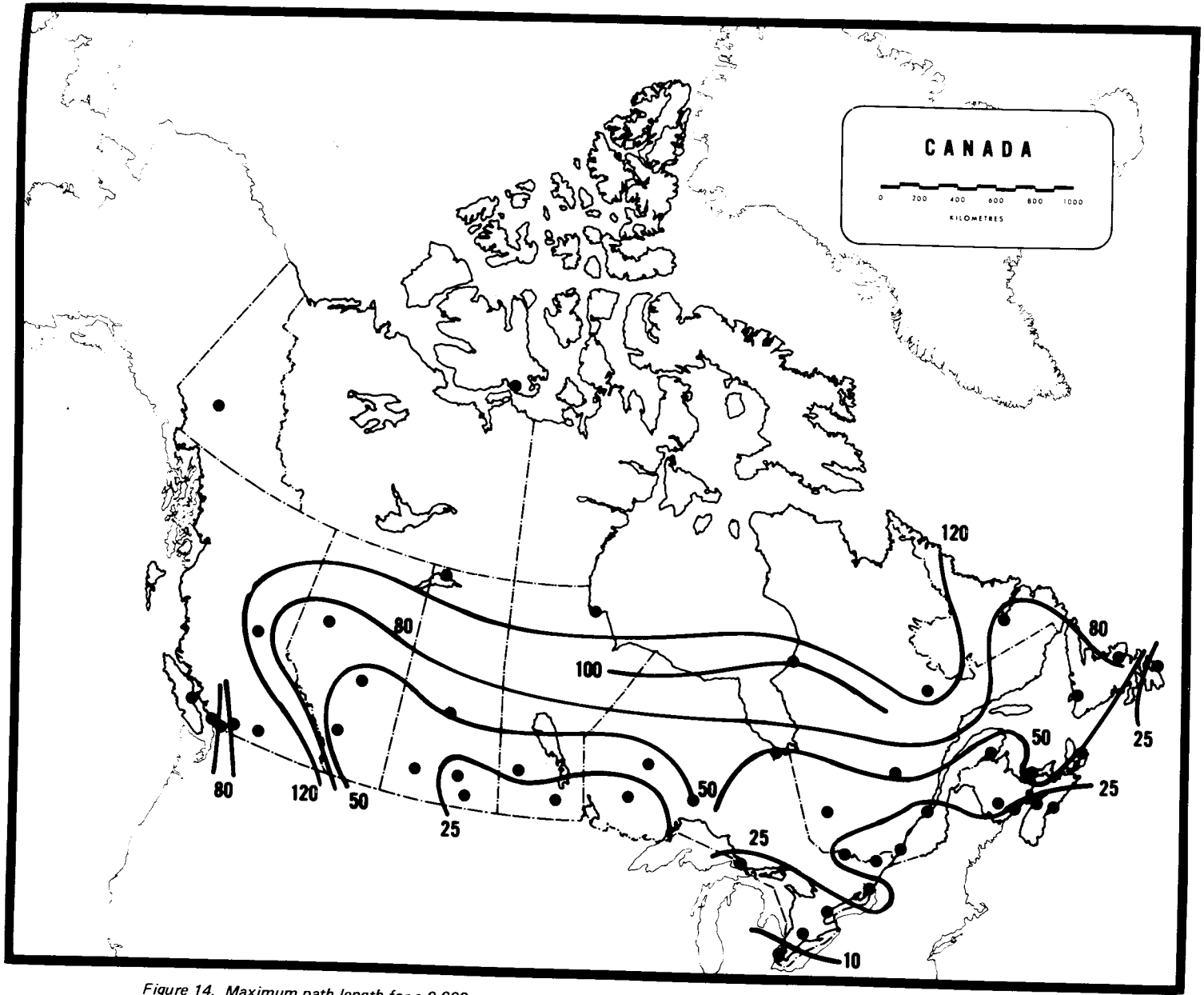

Figure 14. Maximum path length for a 0.003 percent probability of exceeding a 40 dB fade due to rain attenuation at 15 GHz.

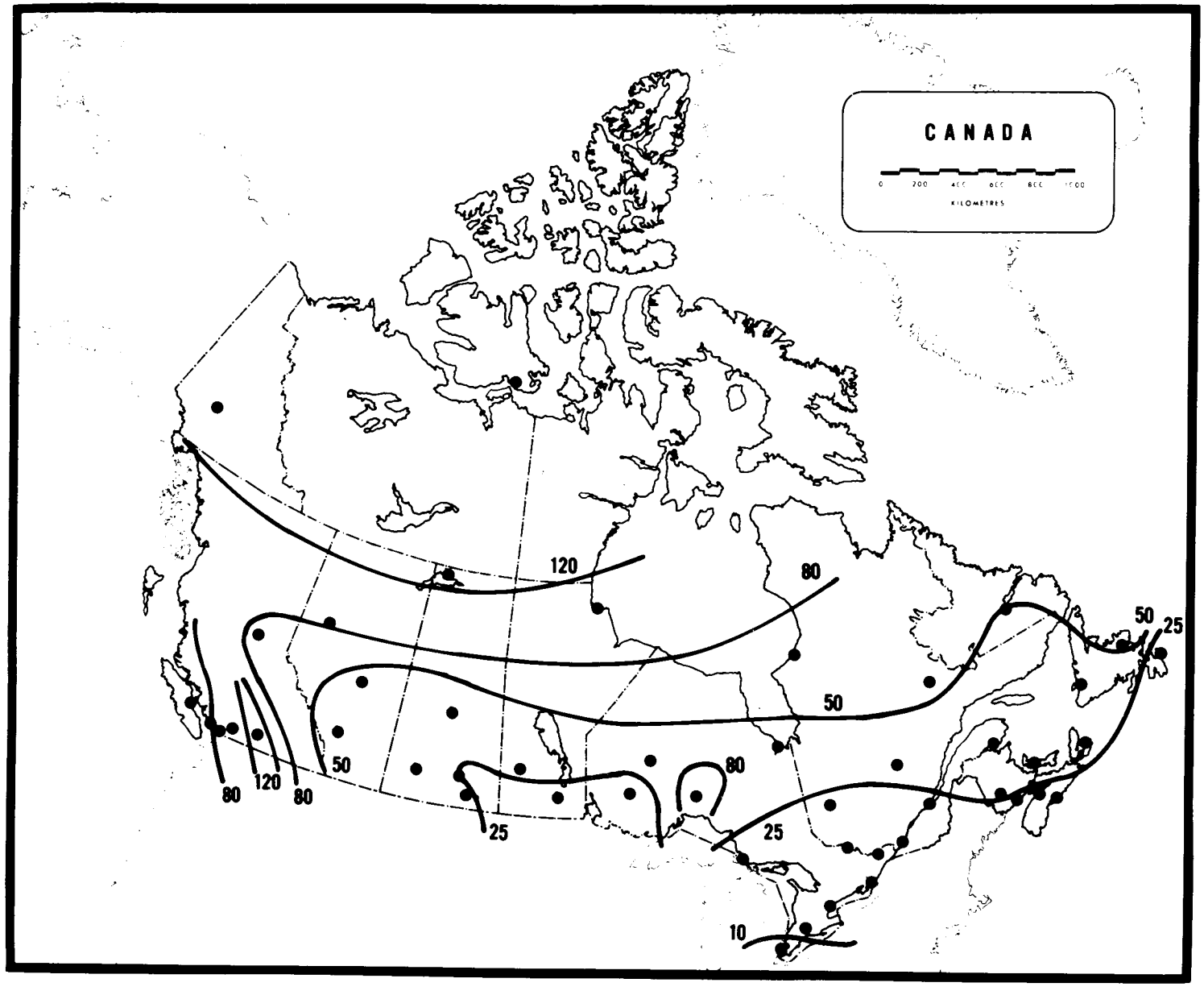

Figure 15. Maximum path length for 0.01 percent probability of exceeding a 40 dB fade due to rain attenuation at 20 GHz.

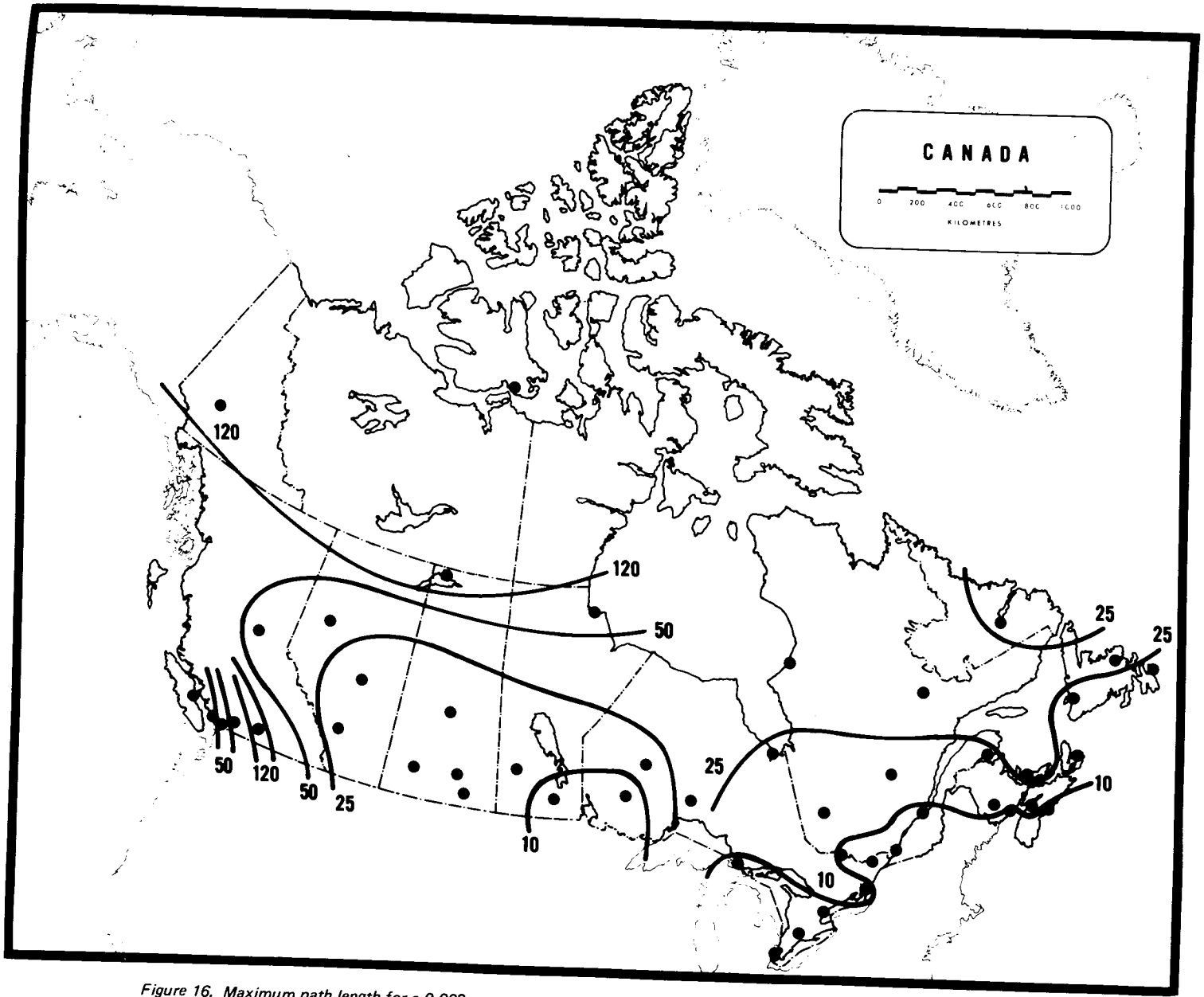

Figure 16. Maximum path length for a 0.003 percent probability of exceeding a 40 dB fade due to rain attenuation at 20 GHz.

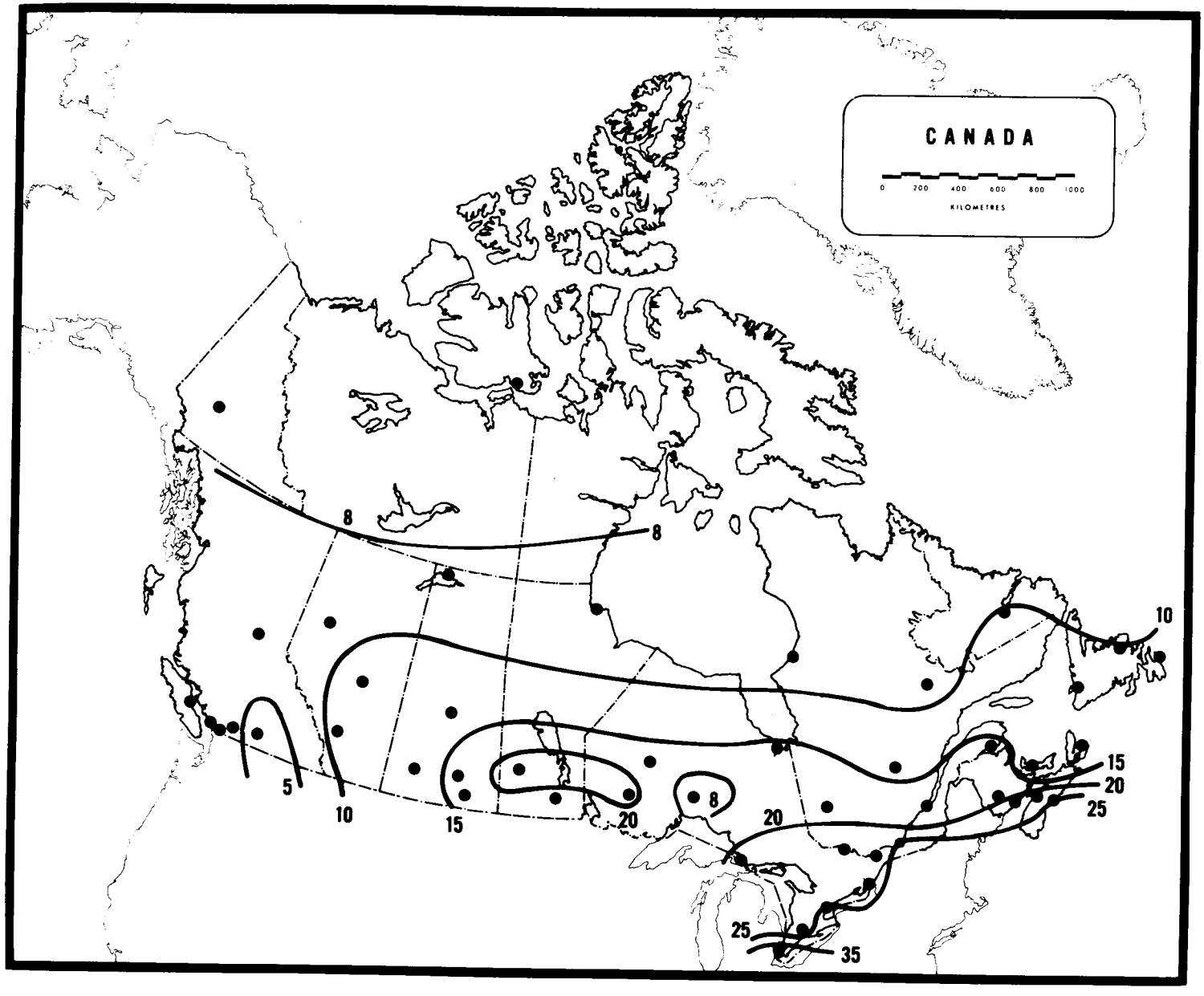

Figure 17. Contours of rain attenuation levels exceeded 0.01 percent of time over an 11 GHz, 40 km link.

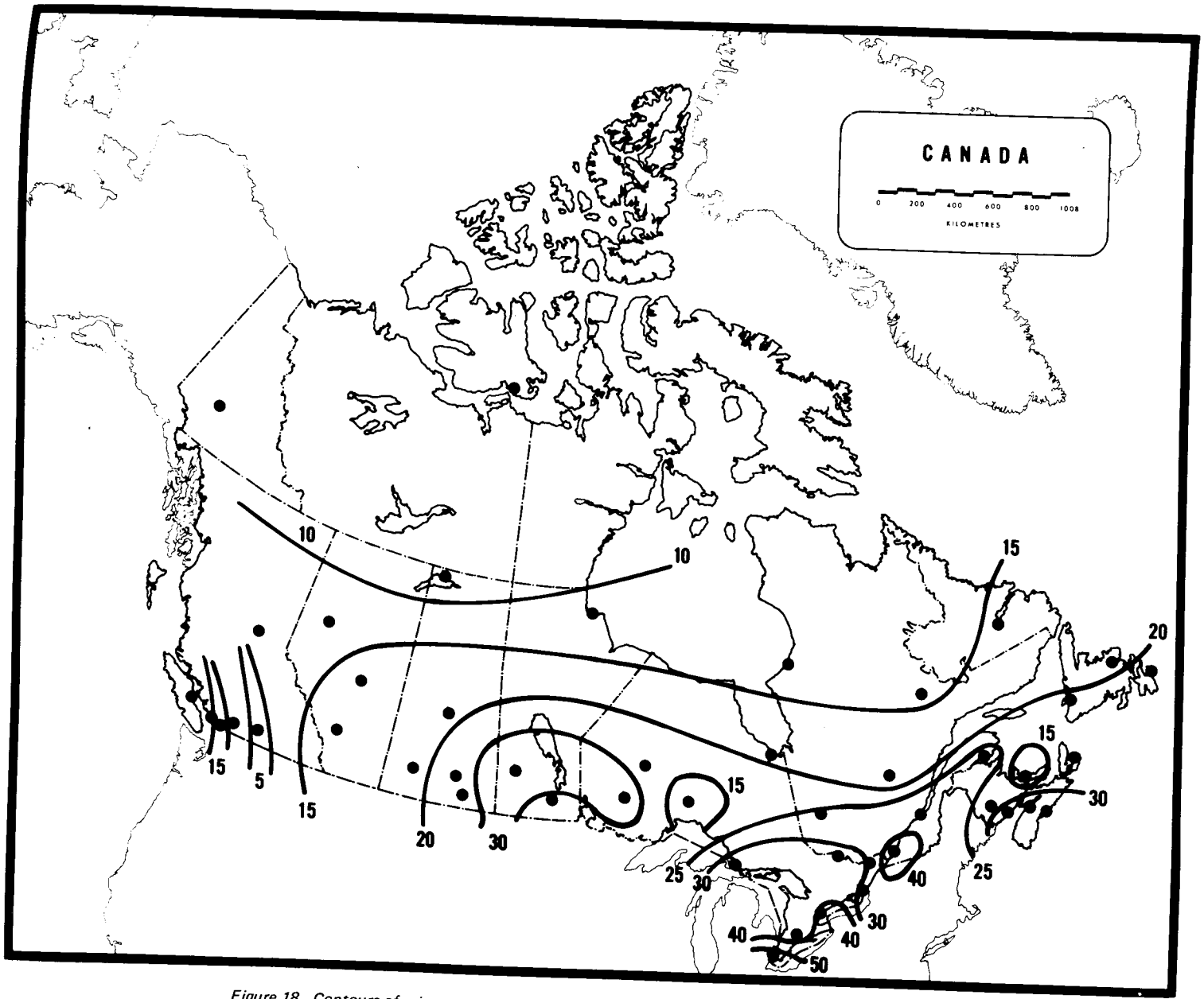

Figure 18. Contours of rain attenuation levels exceeded 0.01 percent of time over an 11 GHz, 80 km link.

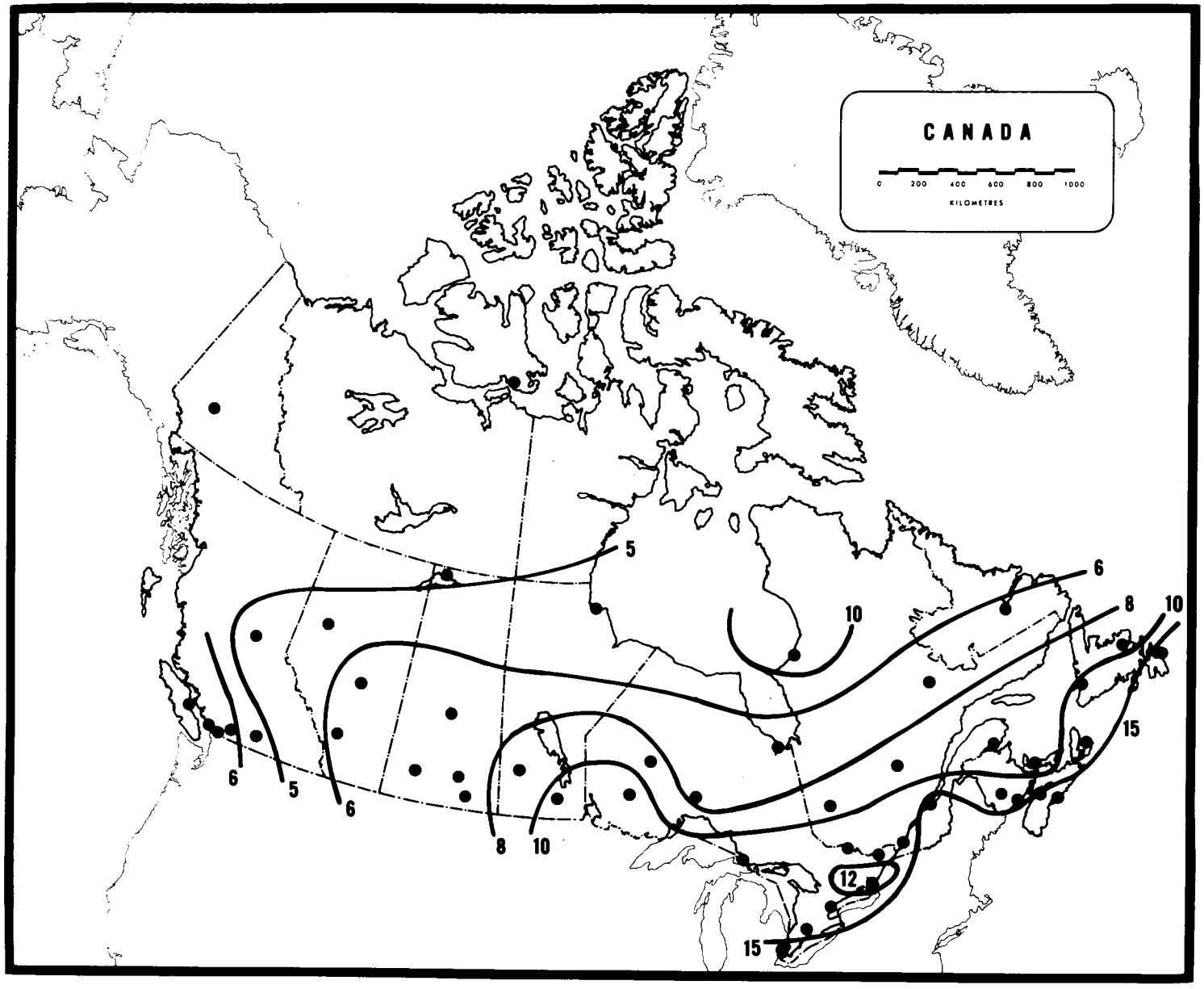

Figure 19. Contours of rain attenuation levels exceeded 0.1 percent of time over a 15 GHz, 40 km link.

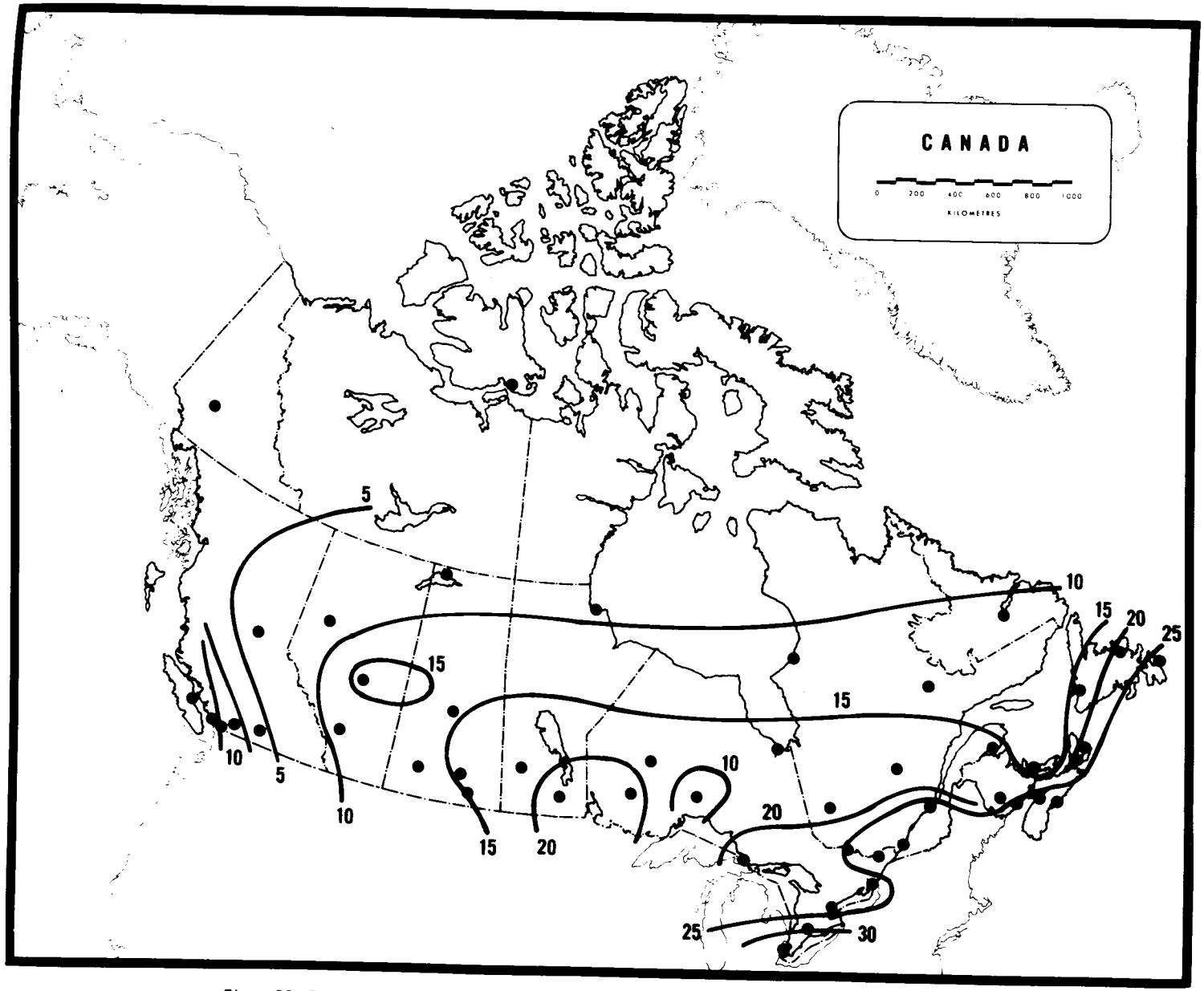

Figure 20. Contours of rain attenuation levels exceeded 0.03 percent of time over a 15 GHz, 40 km link.

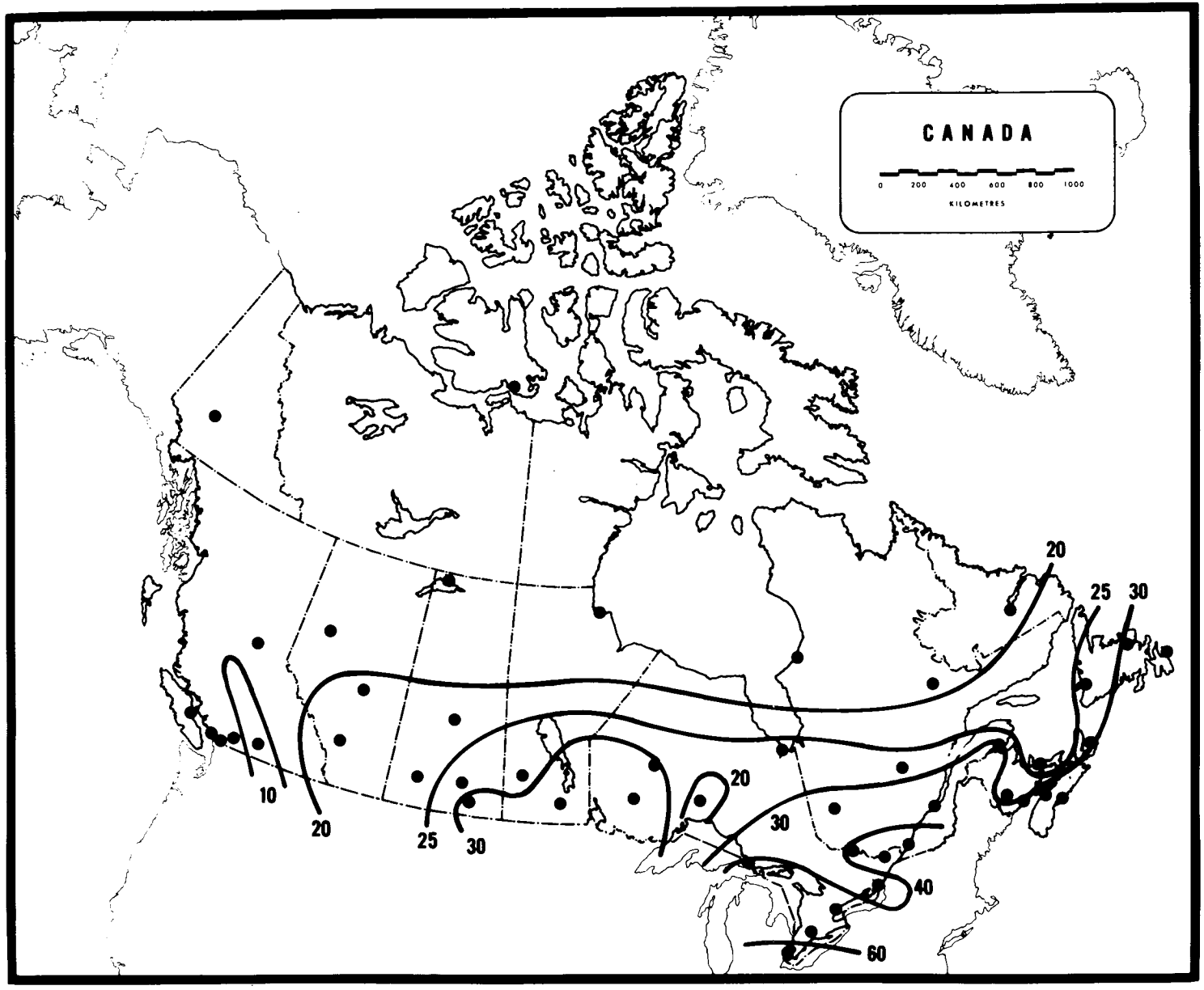

Figure 21. Contours of rain attenuation levels exceeded 0.01 percent of time over a 15 GHz, 40 km link.

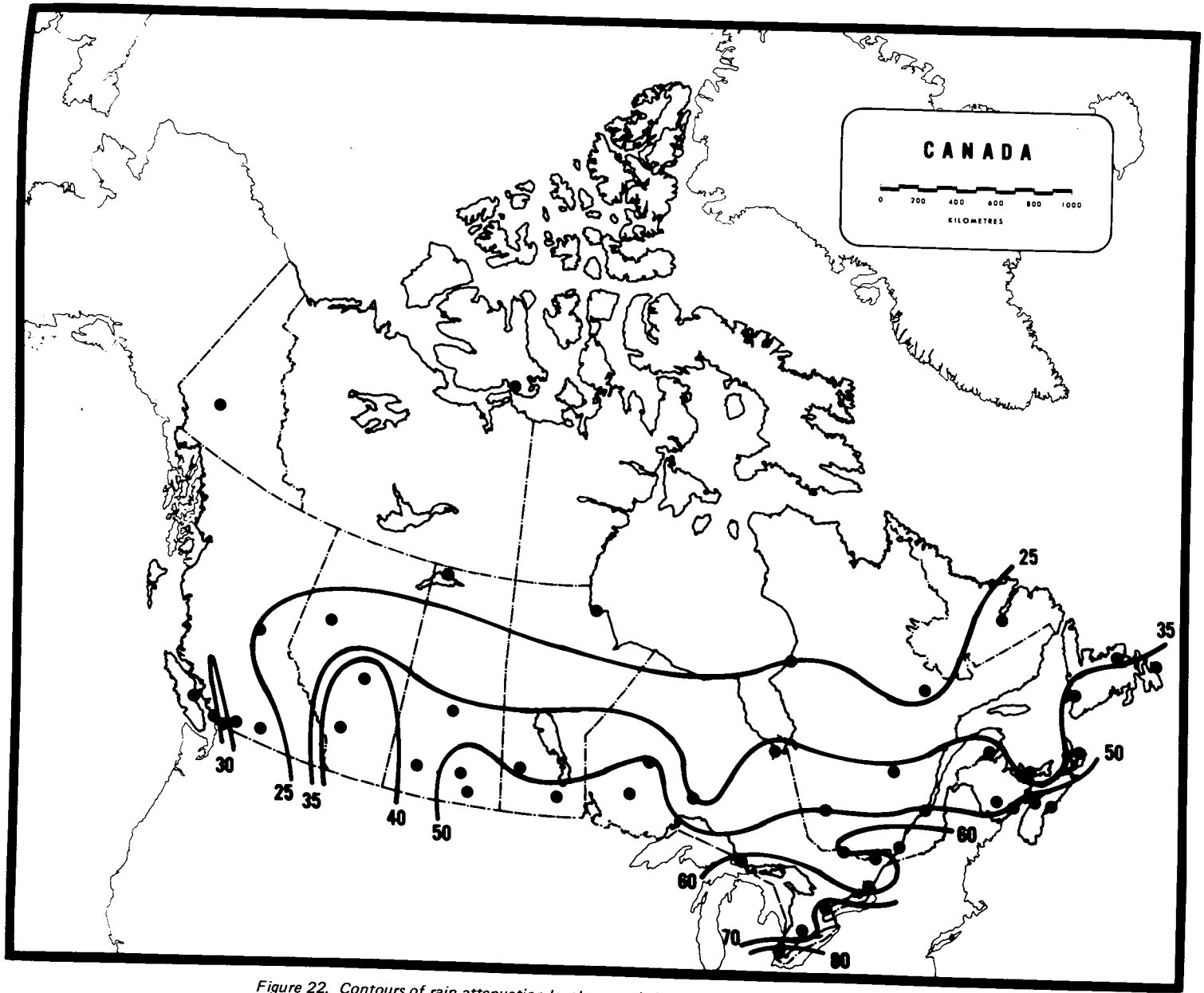

Figure 22. Contours of rain attenuation levels exceeded 0.003 percent of time over a 15 GHz, 40 km link.

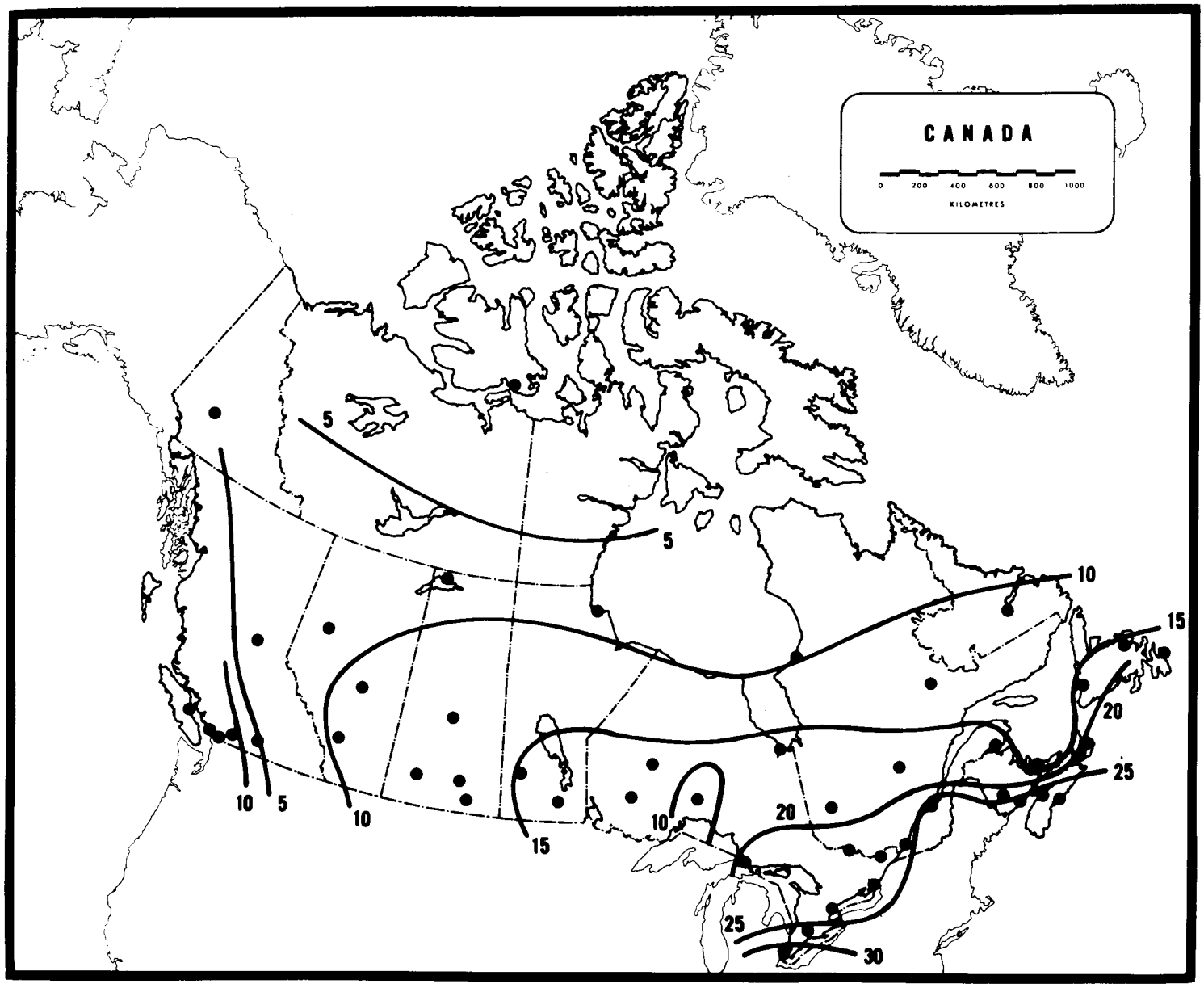

Figure 23. Contours of rain attenuation levels exceeded 0.1 percent of time over a 15 GHz, 80 km link.

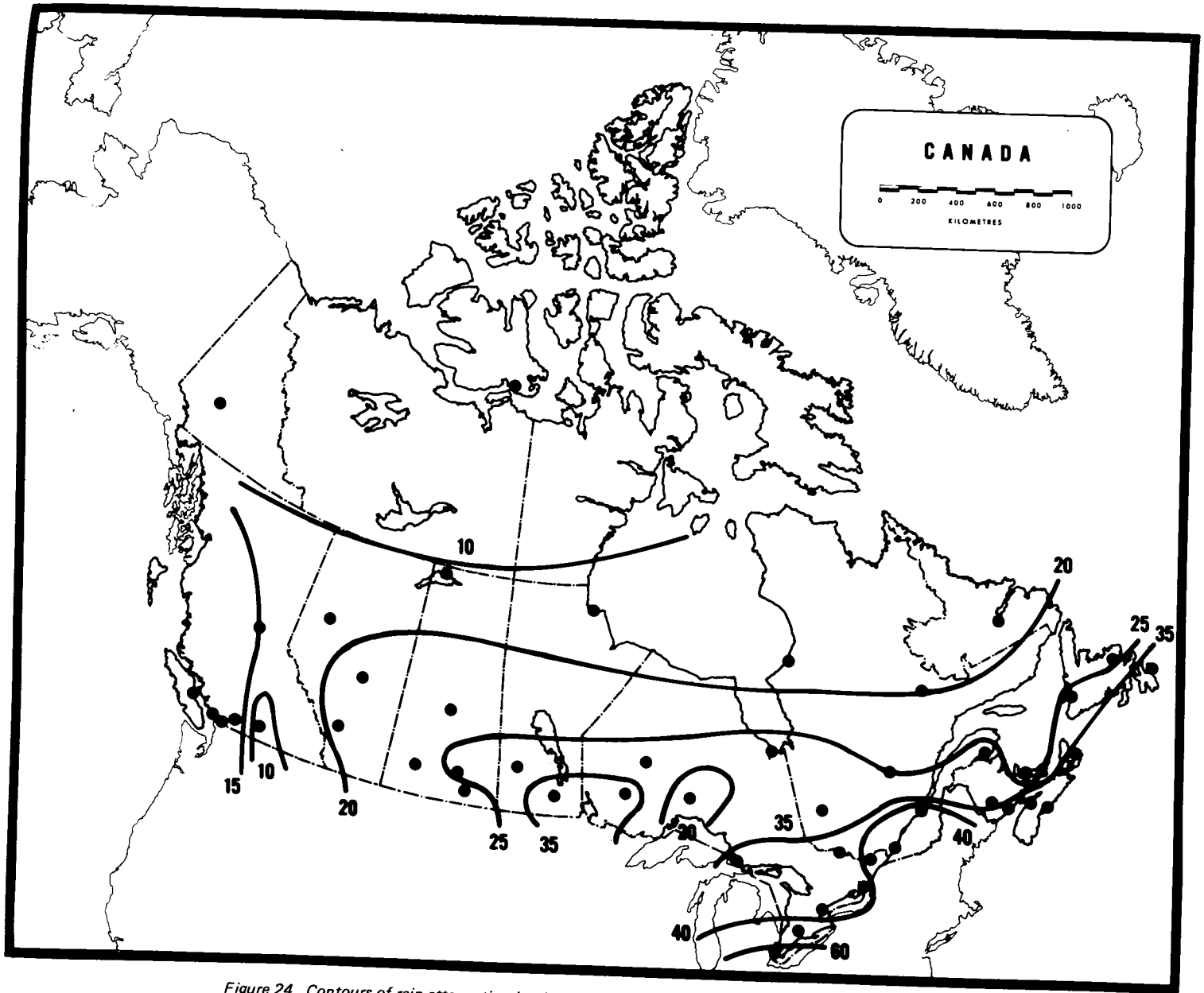

Figure 24. Contours of rain attenuation levels exceeded 0.03 percent of time over a 15 GHz, 80 km link.

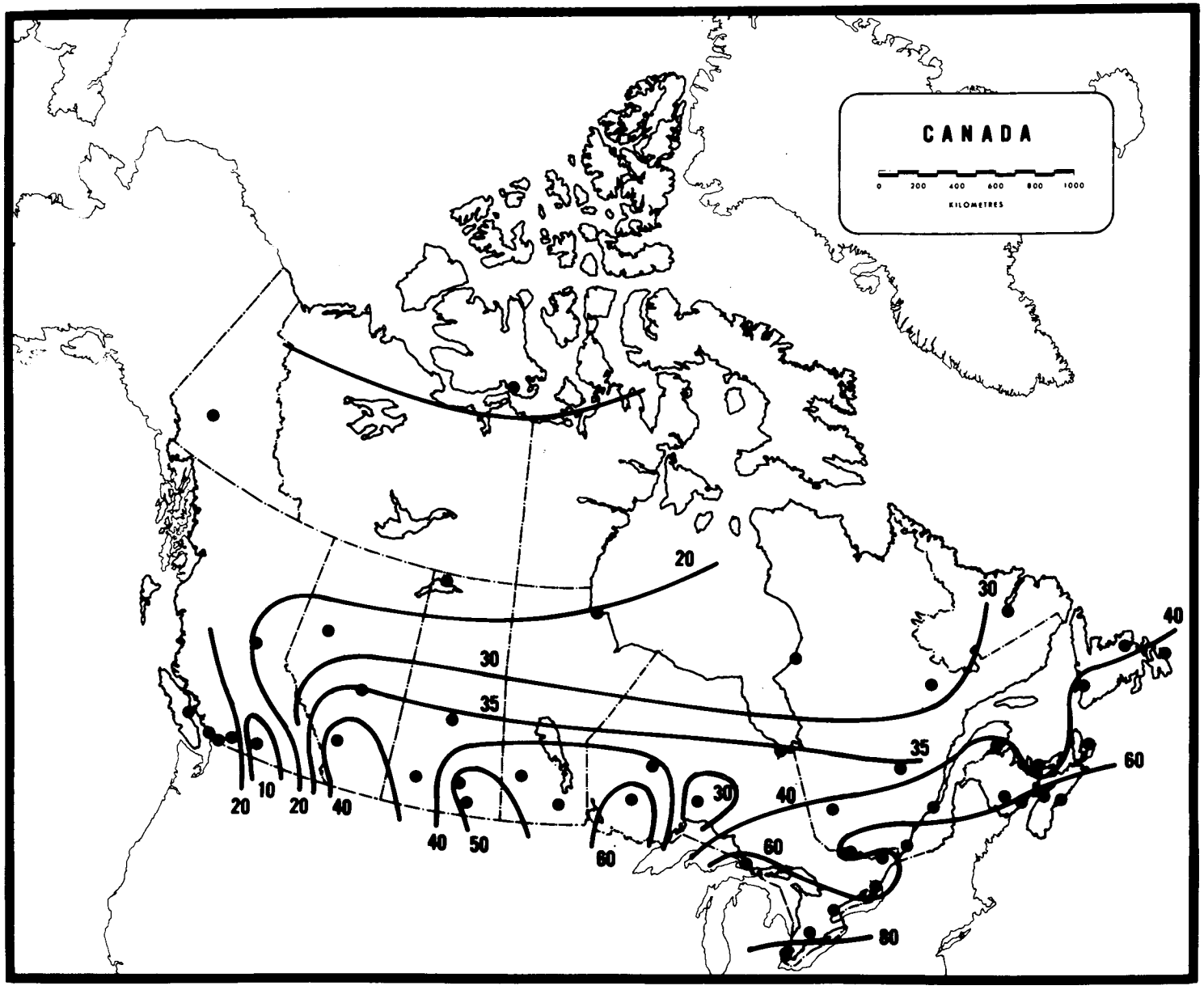

Figure 25. Contours of rain attenuation levels exceeded 0.01 percent of time over a 15 GHz, 80 km link.

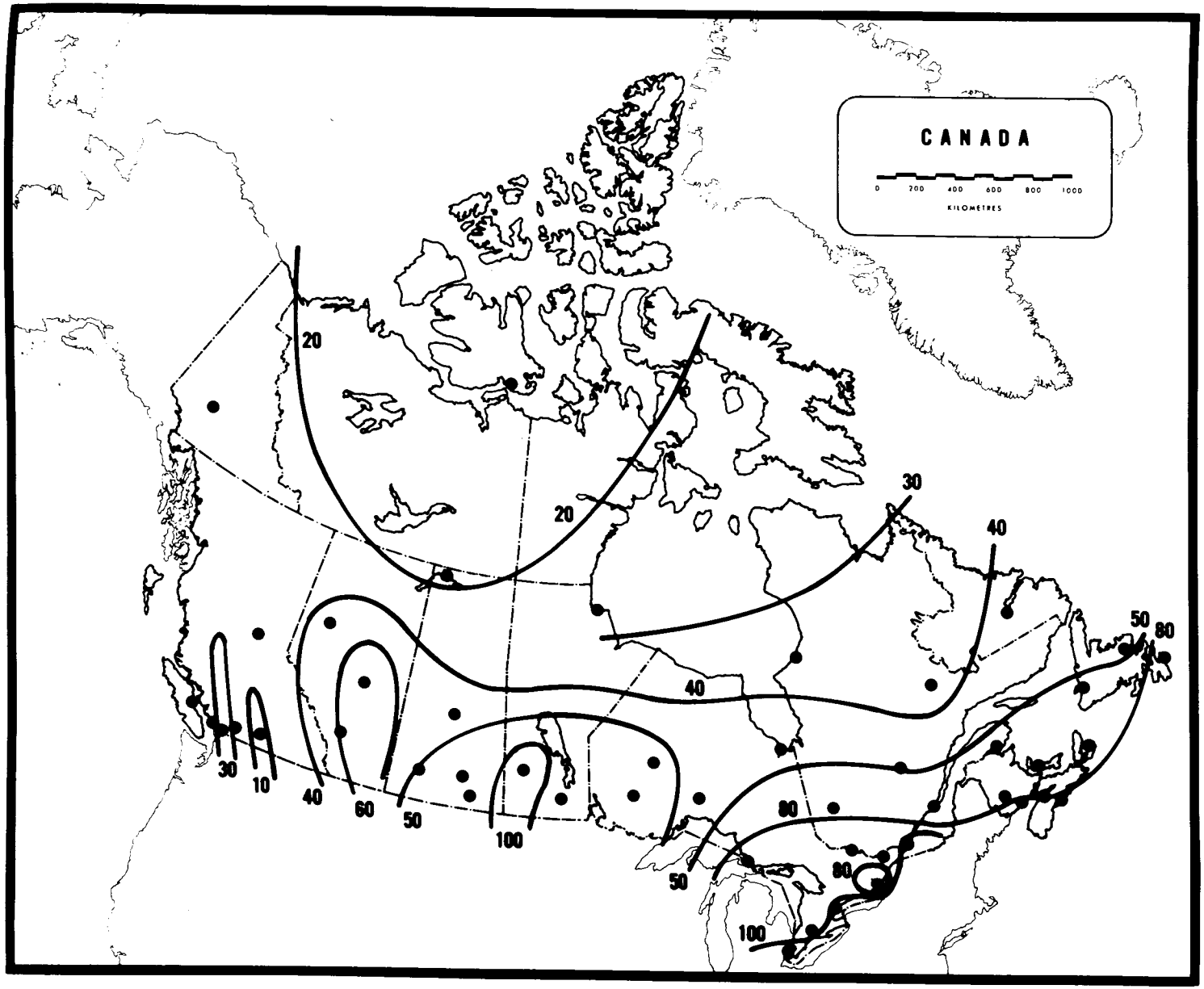

Figure 26. Contours of rain attenuation levels exceeded 0.003 percent of time over a 15 GHz, 80 km link.

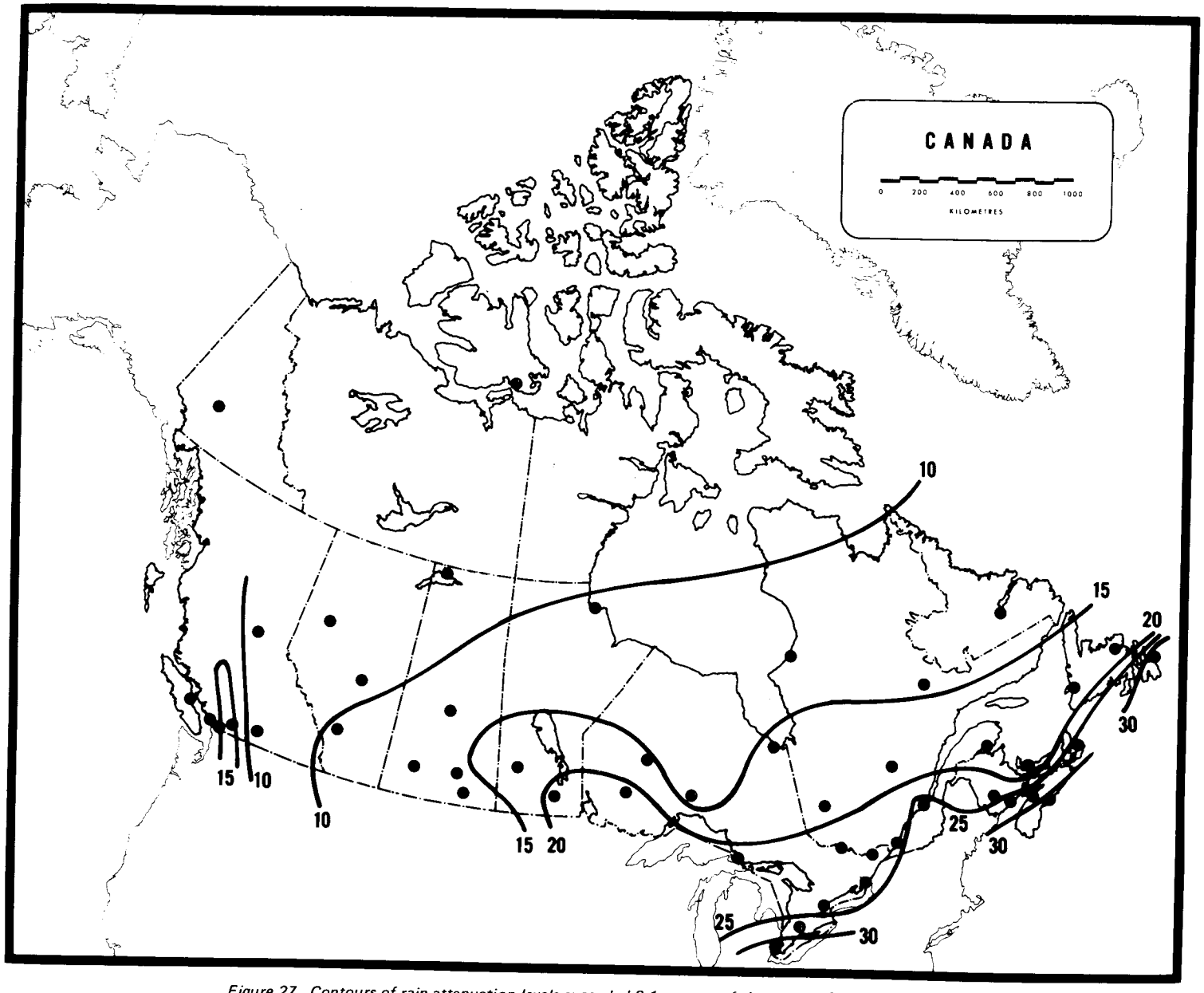

Figure 27. Contours of rain attenuation levels exceeded 0.1 percent of time over a 20 GHz, 40 km link.

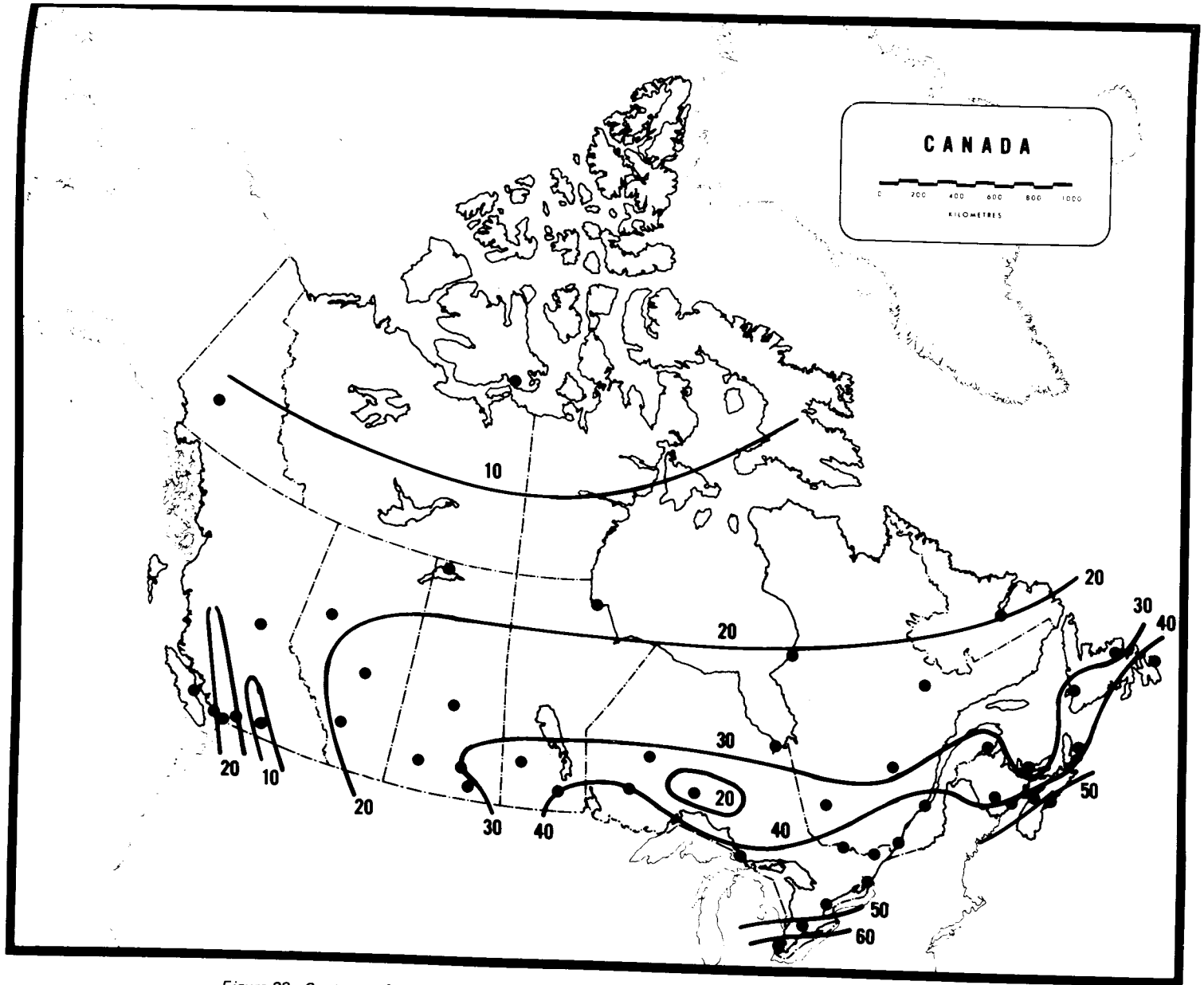

Figure 28. Contours of rain attenuation levels exceeded 0.03 percent of time over a 20 GHz, 40 km link.

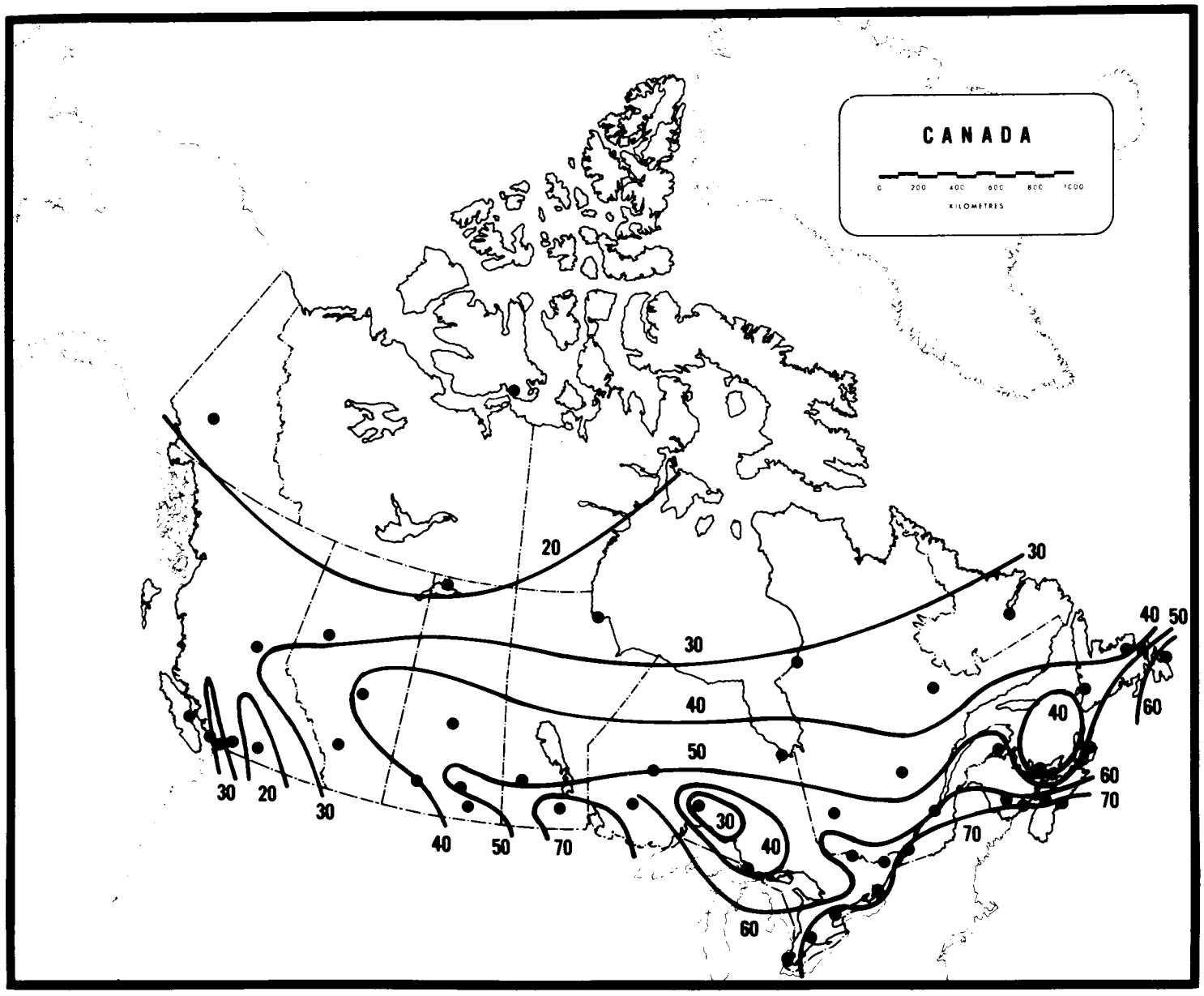

Figure 29. Contours of rain attenuation levels exceeded 0.01 percent of time over a 20 GHz, 40 km link.

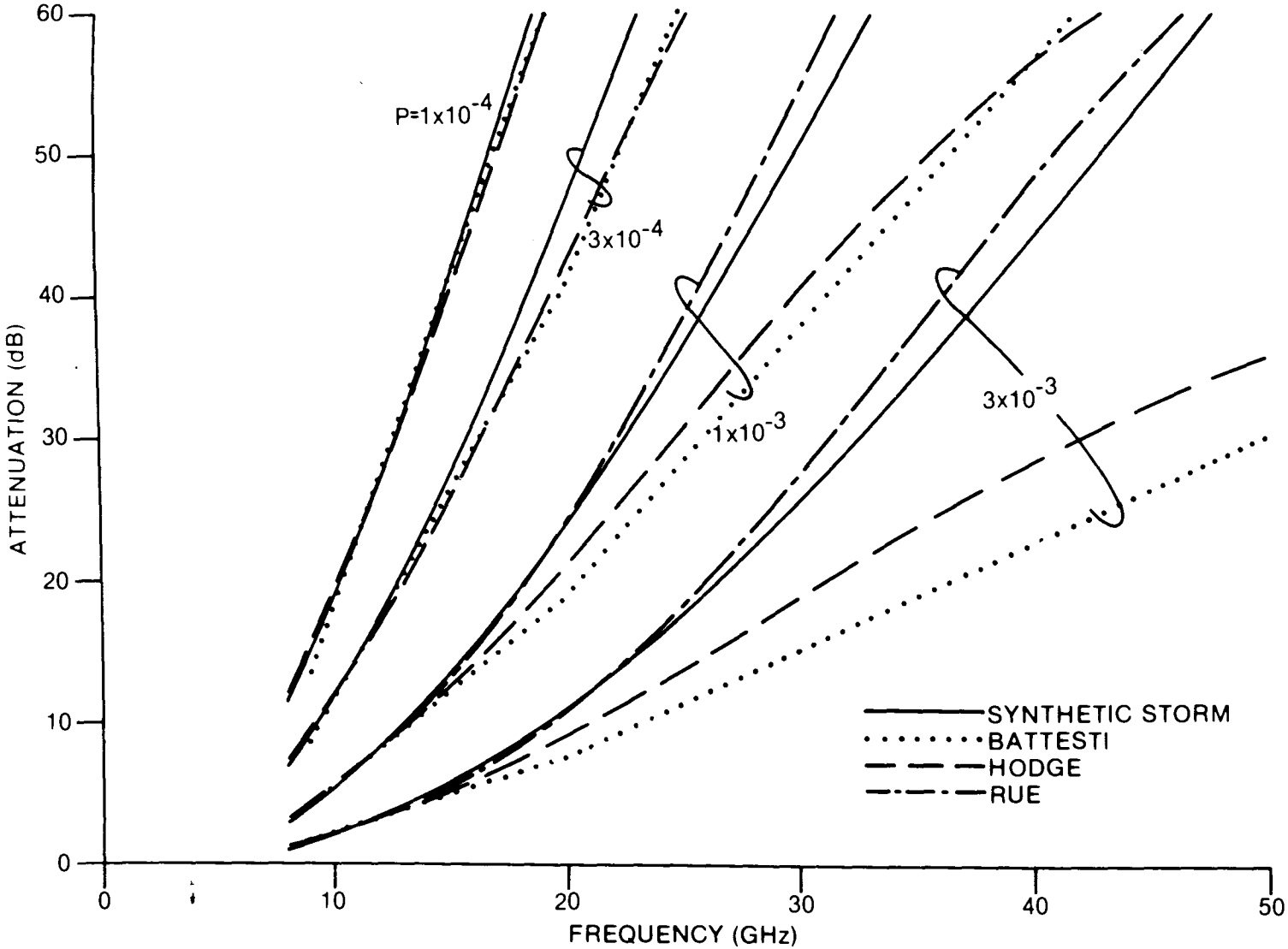

Figure 30. Attenuation levels exceeded as a function of frequency over a hypothetical 40 km path at Ottawa. Each of the four curves computed by the synthetic storm method is flanked by three approximations according to different frequency scaling formulae. The Rue approximation, not evident for the two lowest probabilities, effectively lies over the original curves.

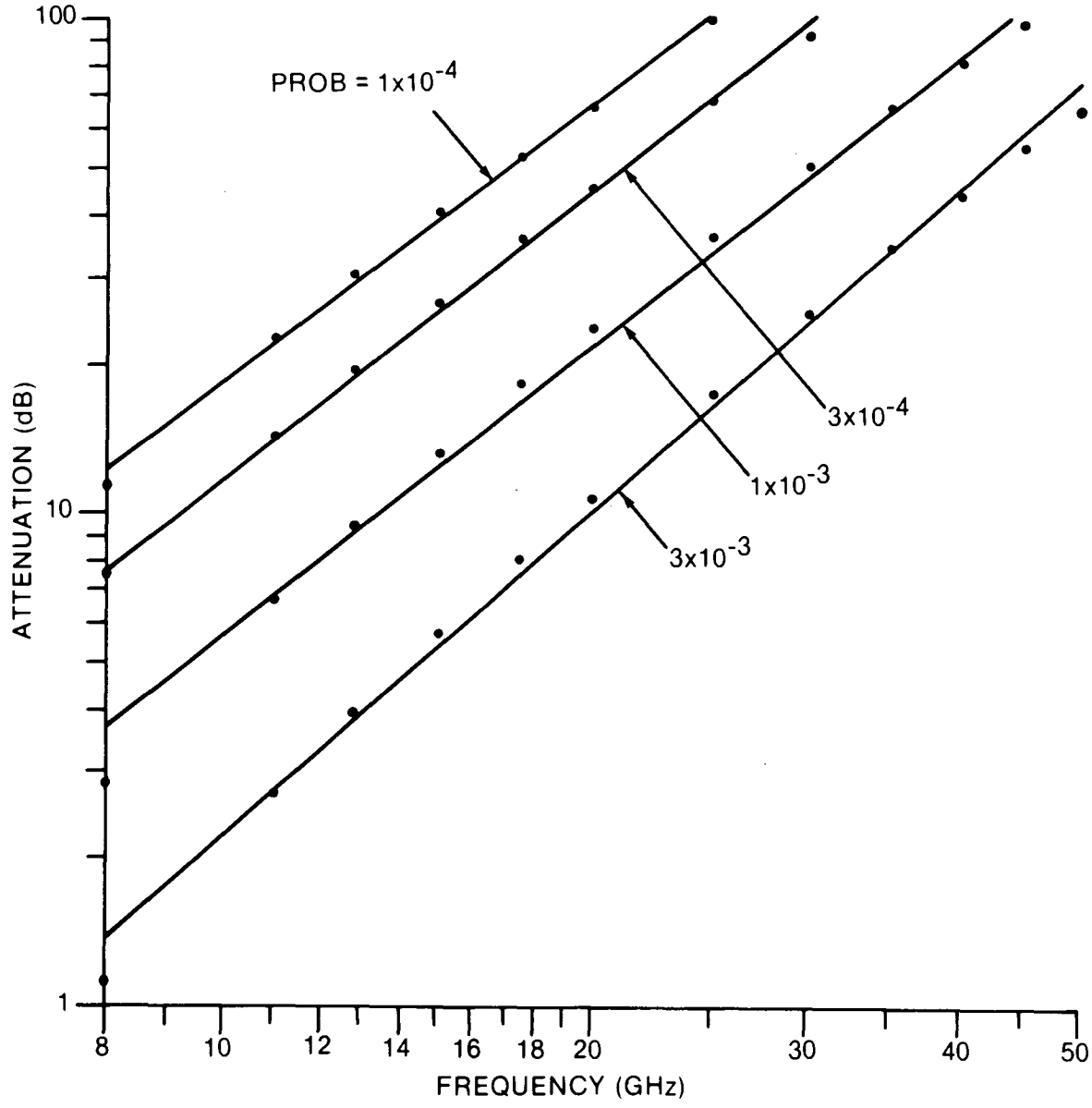

Figure 31. Attenuation versus frequency for a 40 km path at Ottawa. The straight lines represent power law approximations to the data.

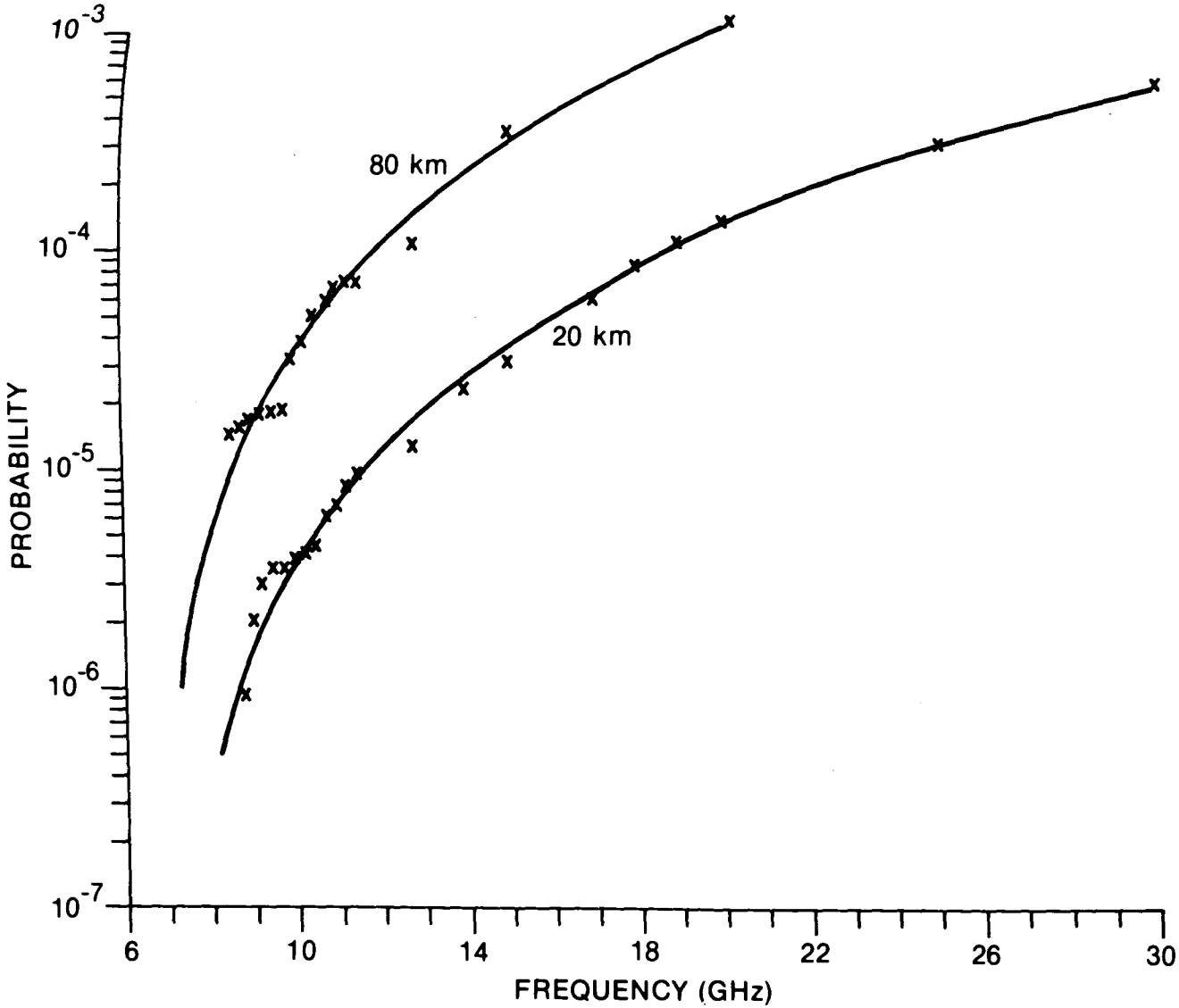

Figure 32. Approximations to constant attenuation level statistics for hypothetical links of 20 and 80 km in the Ottawa area. Data points were computed by the synthetic storm technique from 10 years' rainfall records.

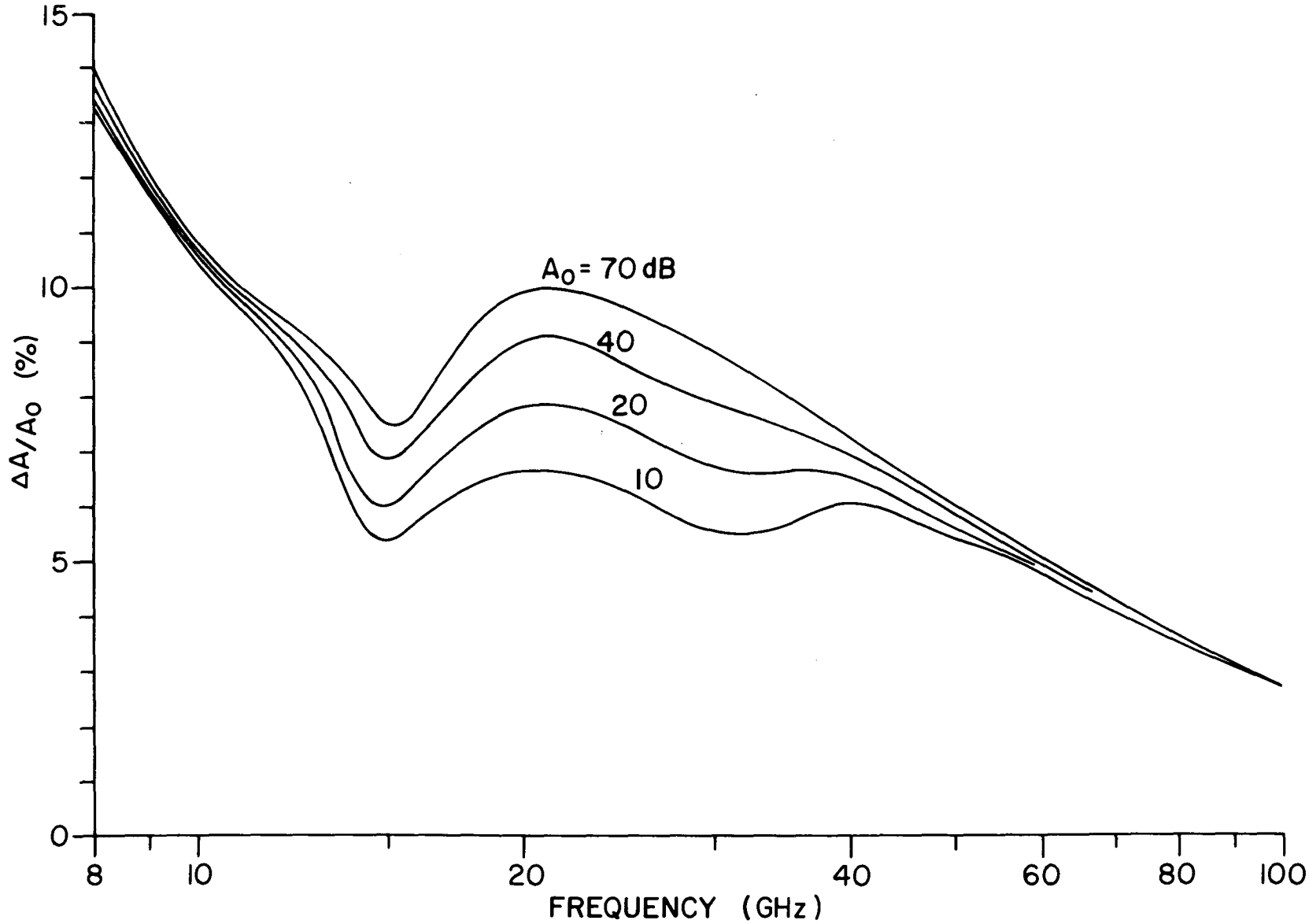

Figure 33. Fractional attenuation difference for linearly polarized waves relative to the path attenuation, A_0, for spherical raindrops. Results are for a 40 km hop at Ottawa. The propagation parameters corresponding to a Laws and Parsons distribution were employed (CCIR, 1980b). ΔA is the difference between the spherical attenuation and equi-probable attenuation for either of the two linearly polarized waves.

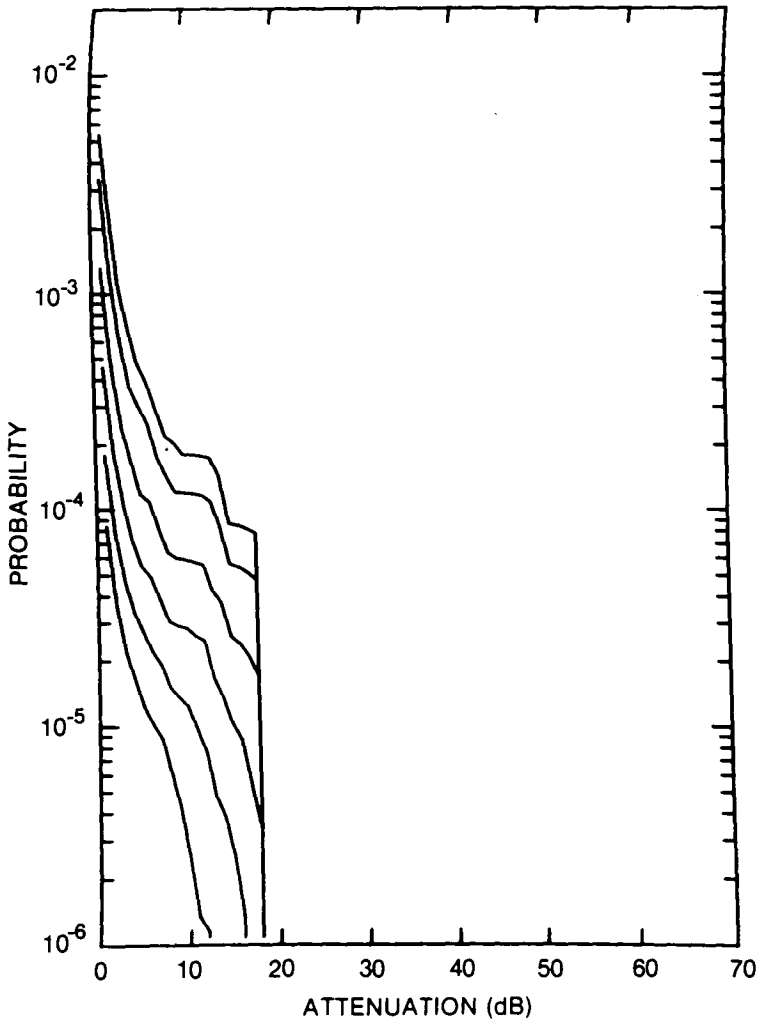

Figure 34. Cumulative distribution of rain attenuation for 8 GHz at Calgary, ALTA. Curves, moving from lowest to highest, are for hop lengths of 5, 10, 20, 40, 80 and 120 km, respectively.

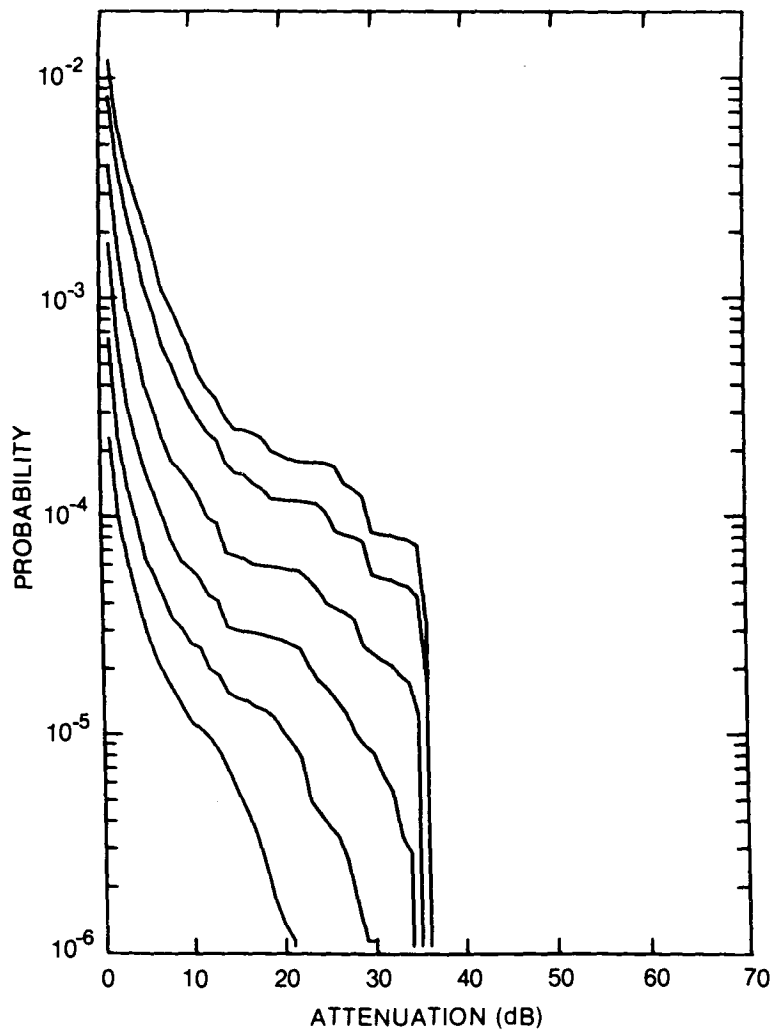

Figure 35. Cumulative distribution of rain attenuation for 11 GHz at Calgary, ALTA. Curves, moving from lowest to highest, are for hop lengths of 5, 10, 20, 40, 80 and 120 km, respectively.

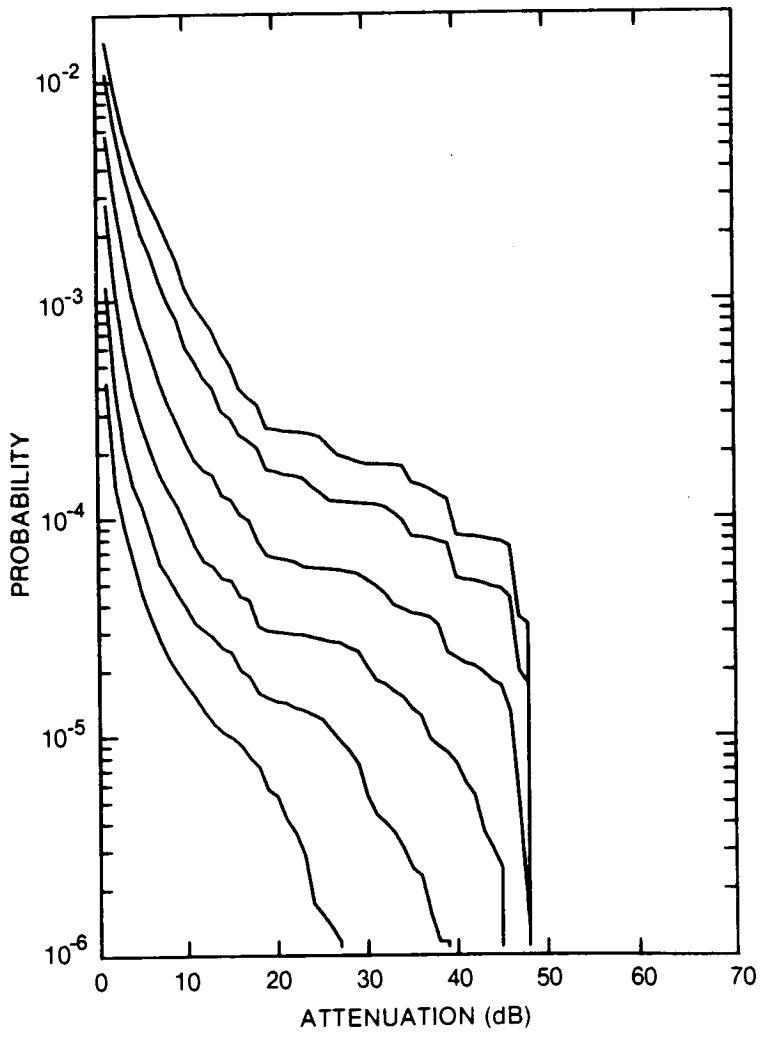

Figure 36. Cumulative distribution of rain attenuation for 12.8 GHz at Calgary, ALTA. Curves, moving from lowest to highest, are for hop lengths of 5, 10, 20, 40, 80 and 120 km, respectively.

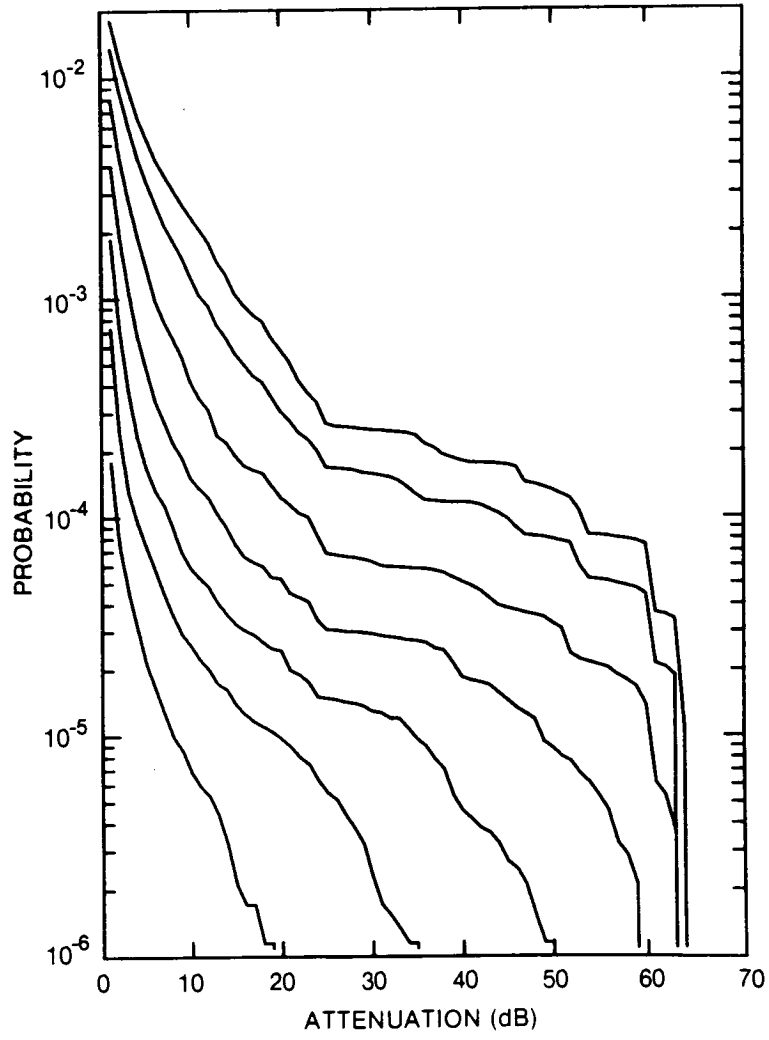

Figure 37. Cumulative distribution of rain attenuation for 15 GHz at Calgary, ALTA. Curves, moving from lowest to highest, are for hop lengths of 2, 5, 10, 20, 40, 80 and 120 km, respectively.

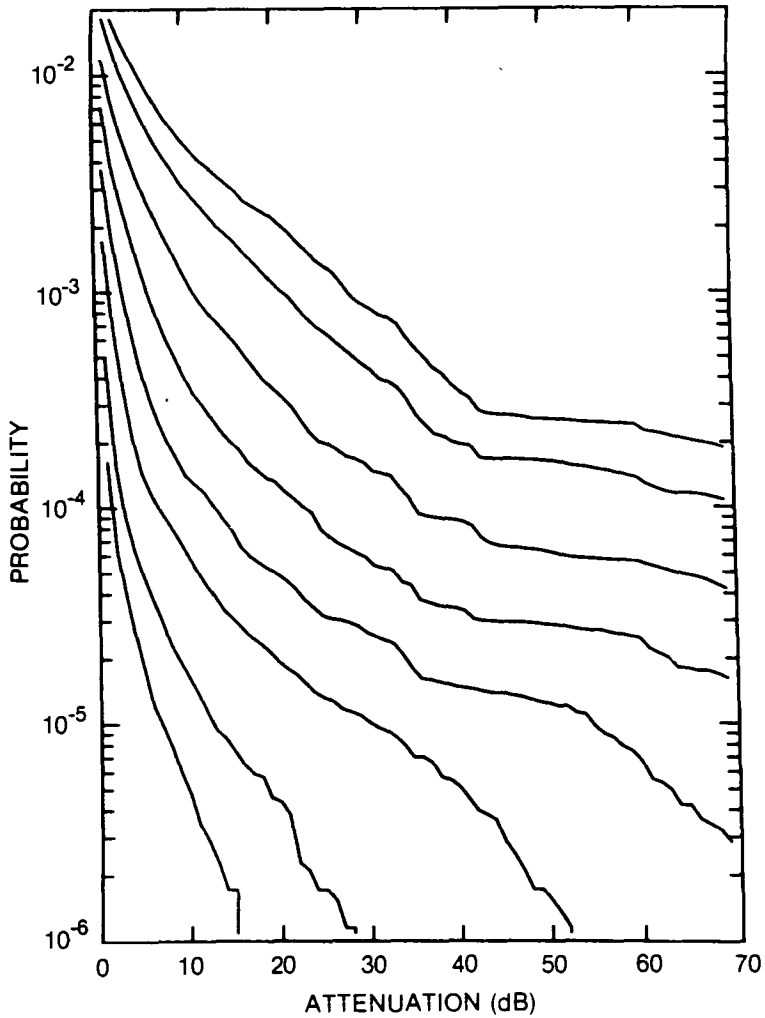

Figure 38. Cumulative distribution of rain attenuation for 20 GHz at Calgary, ALTA. Curves, moving from lowest to Highest, are for hop lengths of 1, 2, 5, 10, 20, 40, 80 and 120 km, respectively.

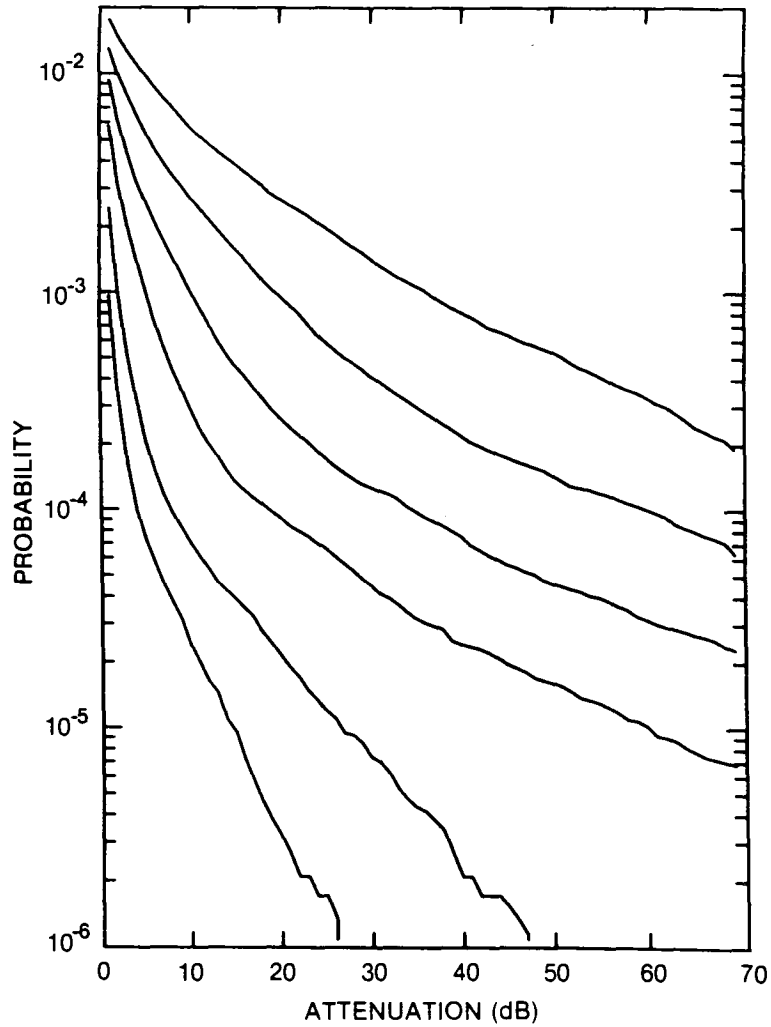

Figure 39. Cumulative distribution of rain attenuation for 35 GHz at Calgary, ALTA. Curves, moving from lowest to highest, are for hop lengths of 1, 2, 5, 10, 20, and 40 km, respectively.

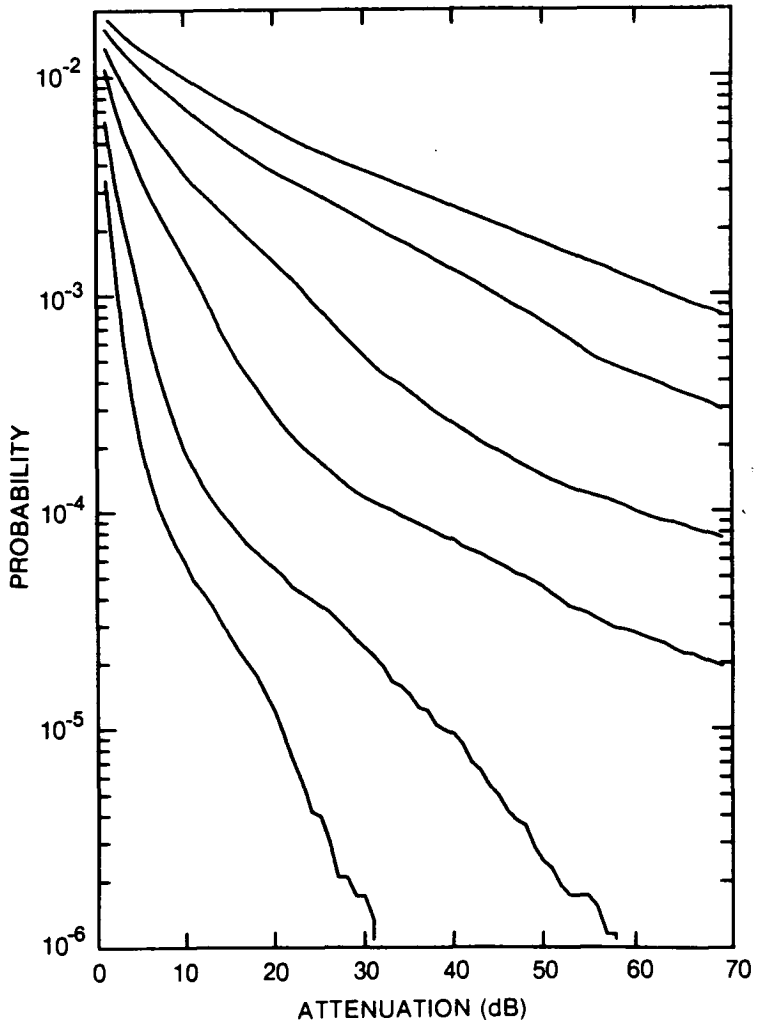

Figure 40. Cumulative distribution of rain attenuation for 56 GHz at Calgary, ALTA. Curves, moving from lowest to highest, are for hop lengths of 1, 2, 5, 10, 20 and 30 km, respectively.

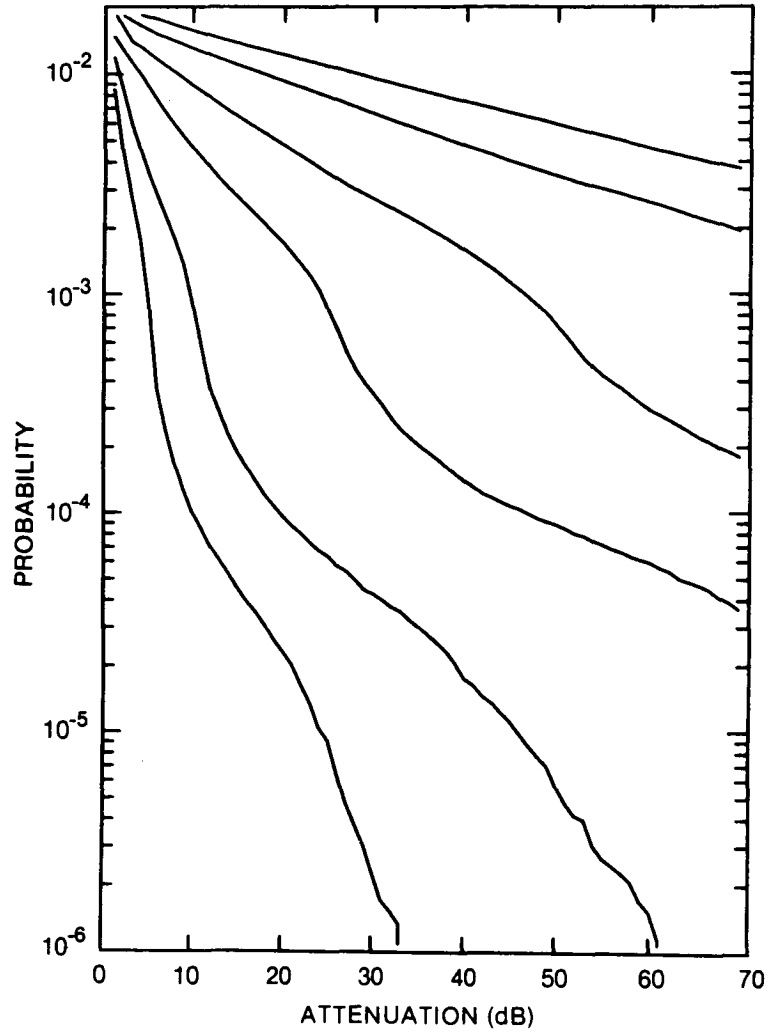

Figure 41. Cumulative distribution of rain attenuation for 100 GHz at Calgary, ALTA. Curves, moving from lowest to highest, are for hop lengths of 1, 2, 5, 10, 20 and 30 km, respectively.

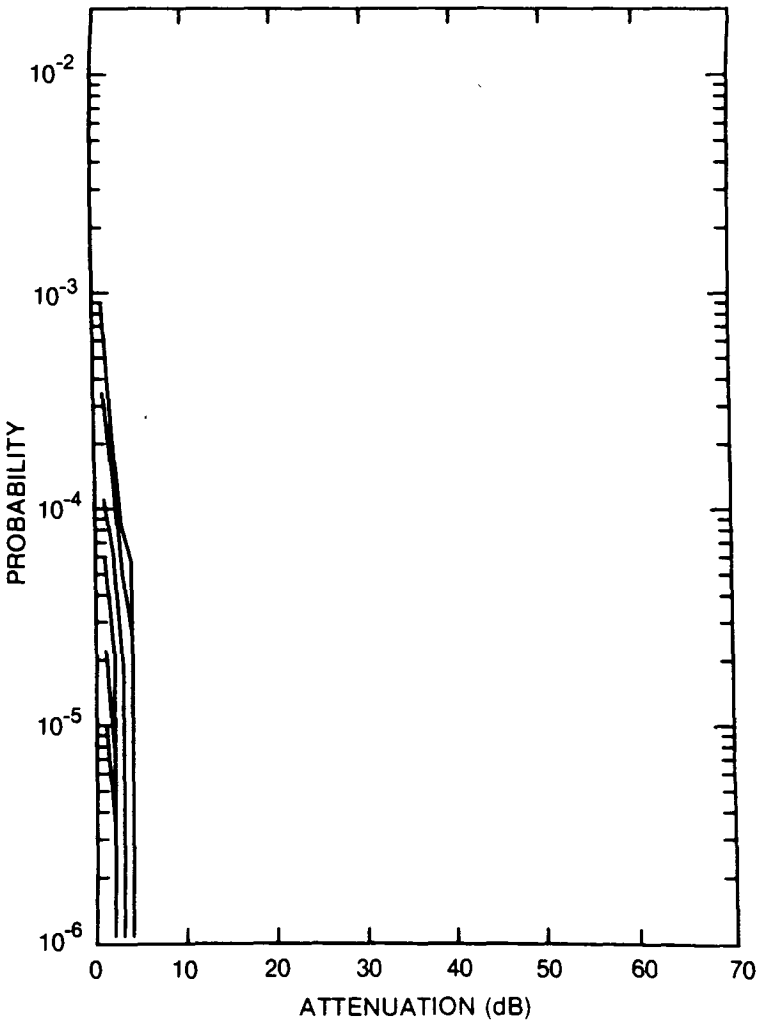

Figure 42. Cumulative distribution of rain attenuation for 8 GHz at Cambridge Bay, NWT. Curves, moving from lowest to highest, are for hop lengths of 5, 10, 20, 40, 80 and 120 km, respectively.

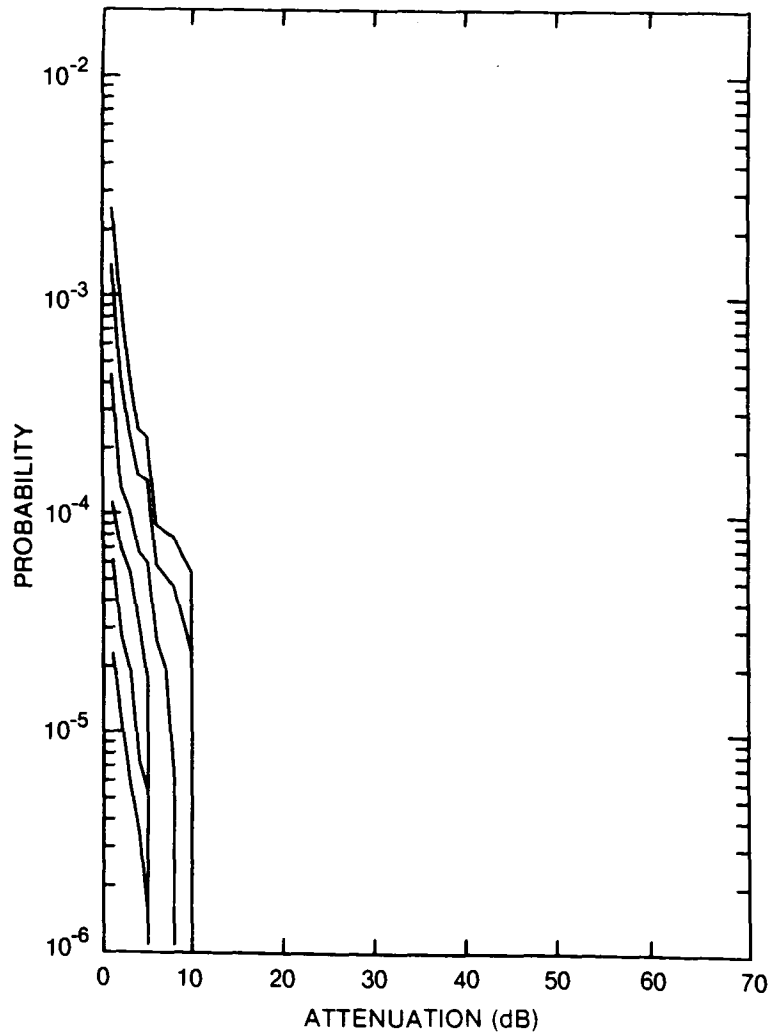

Figure 43. Cumulative distribution of rain attenuation for 11 GHz at Cambridge Bay, NWT. Curves, moving from lowest to highest, are for hop lengths of 5, 10, 20, 40, 80 and 120 km, respectively.

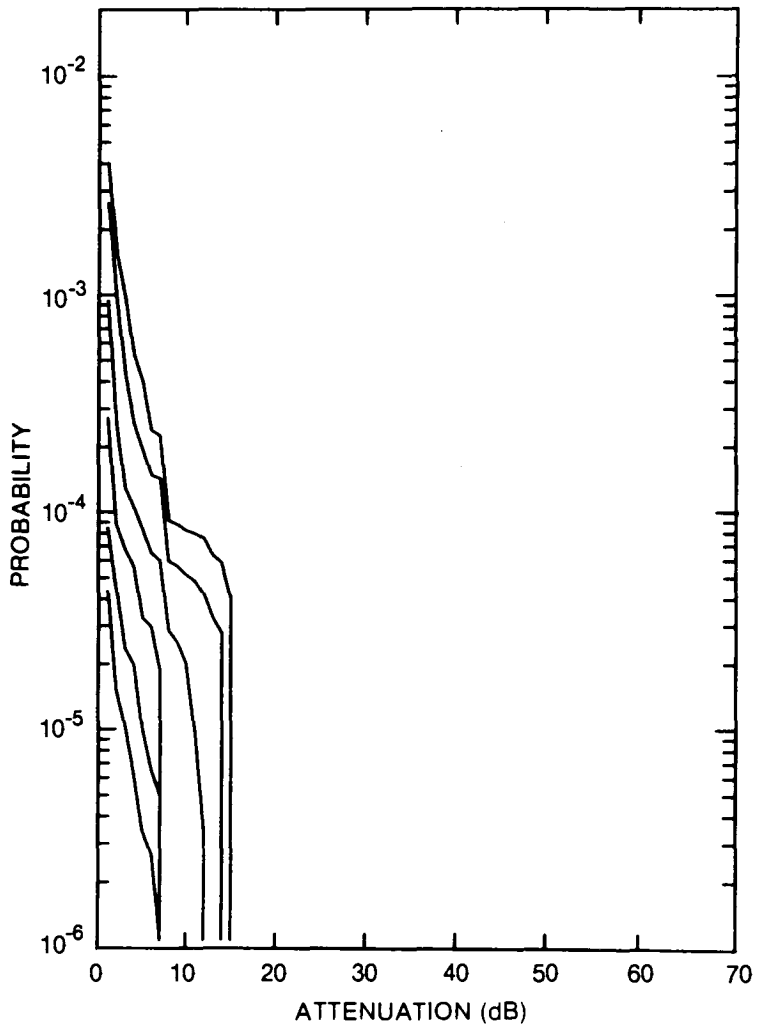

Figure 44. Cumulative distribution of rain attenuation for 12.8 GHz at Cambridge Bay, NWT. Curves, moving from lowest to highest, are for hop lengths of 5, 10, 20, 40, 80 and 120 km, respectively.

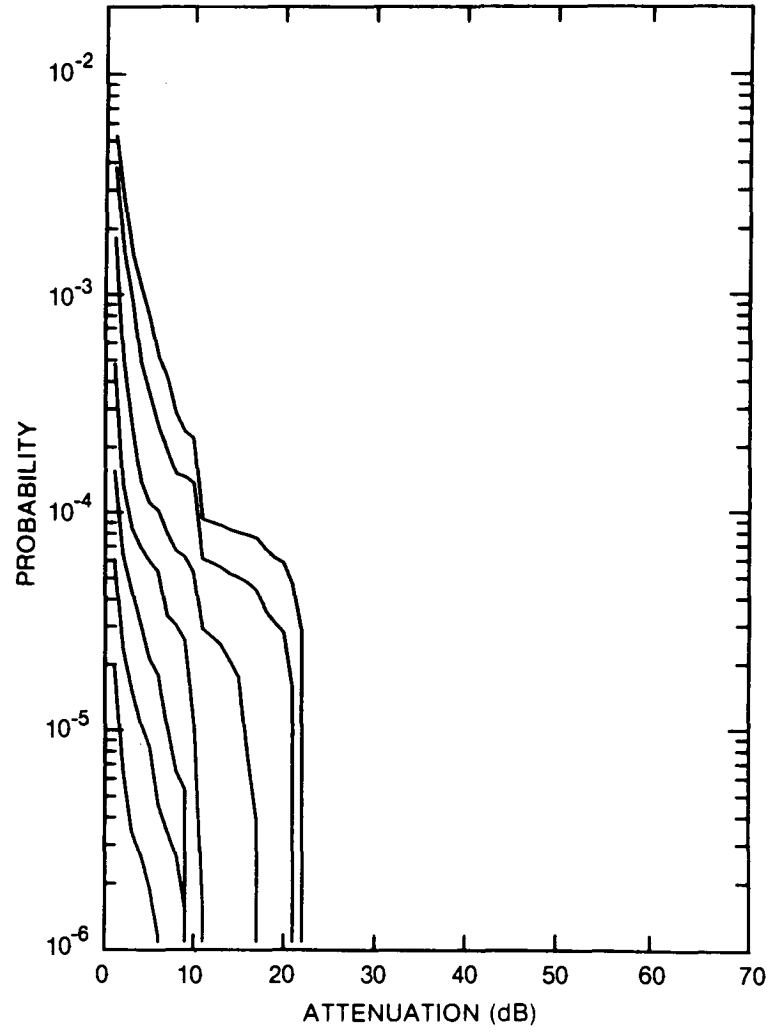

Figure 45. Cumulative distribution of rain attenuation for 15 GHz at Cambridge Bay, NWT. Curves, moving from lowest to highest, are for hop lengths of 2, 5, 10, 20, 40, 80 and 120 km, respectively.

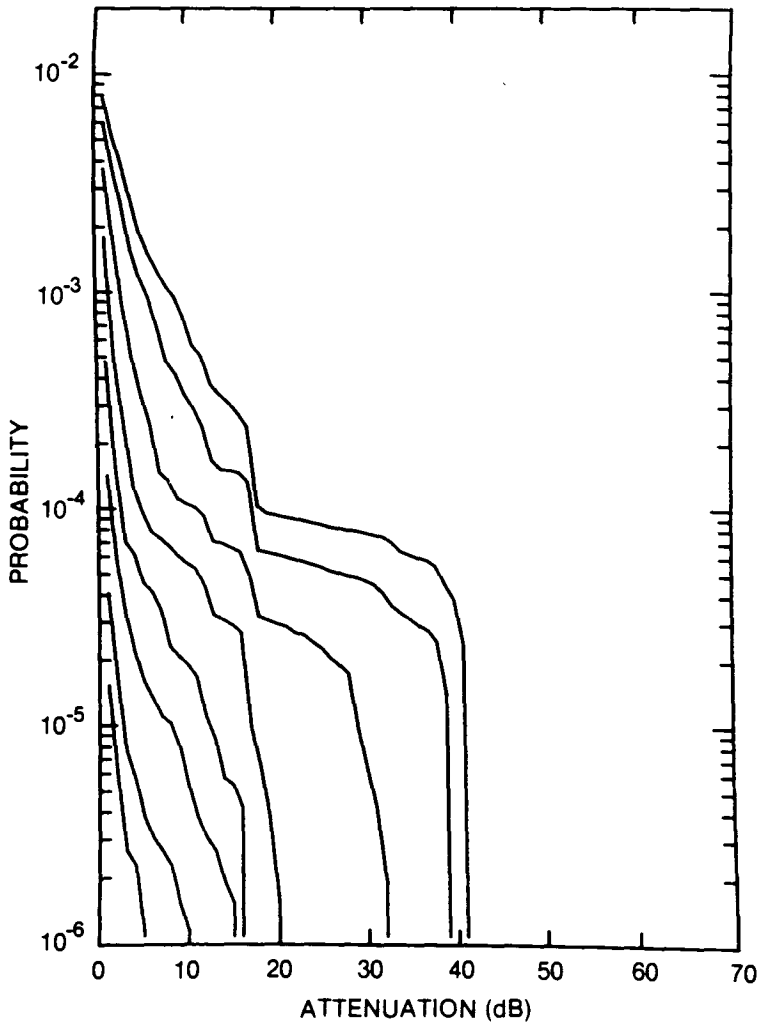

Figure 46. Cumulative distribution of rain attenuation for 20 GHz at Cambridge Bay, NWT. Curves, moving from lowest to highest, are for hop lengths of 1, 2, 5, 10, 20, 40, 80 and 120 km, respectively.

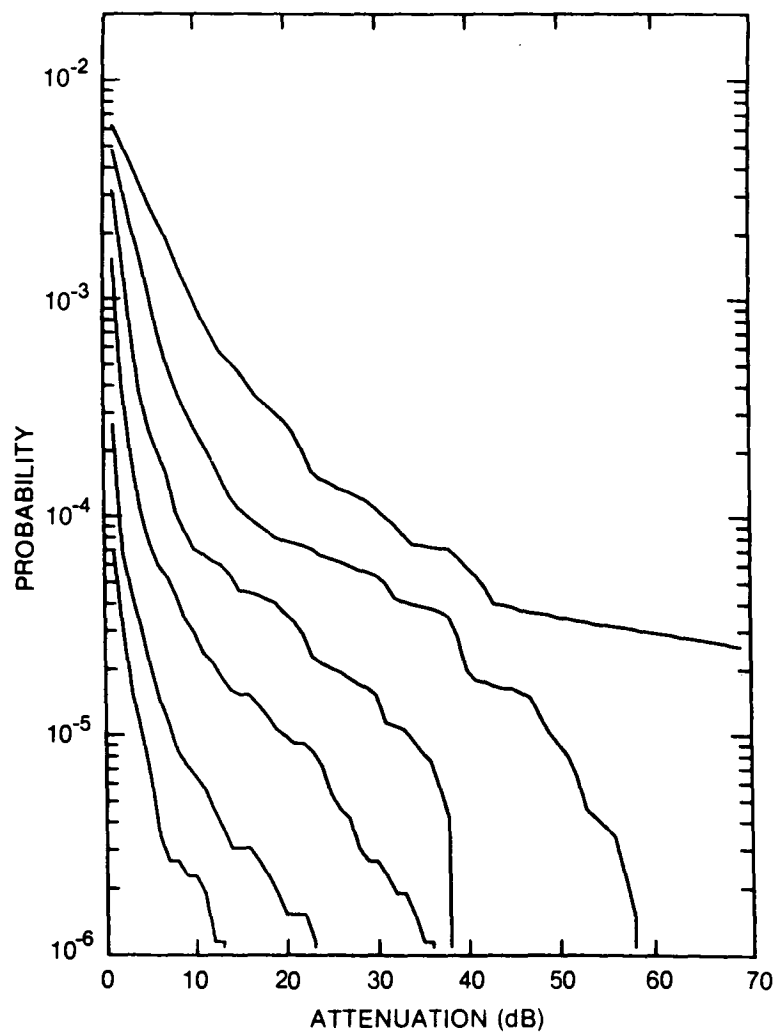

Figure 47. Cumulative distribution of rain attenuation for 35 GHz at Cambridge Bay, NWT. Curves, moving from lowest to highest, are for hop lengths of 1, 2, 5, 10, 20 and 40 km, respectively.

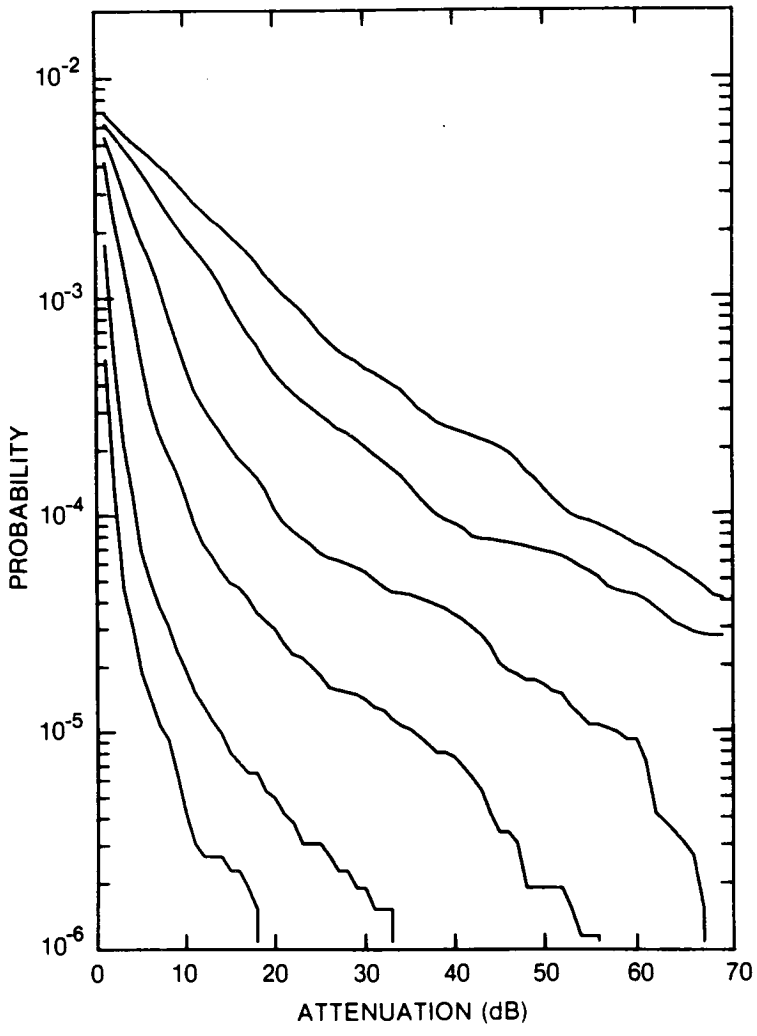

Figure 48. Cumulative distribution of rain attenuation for 56 GHz at Cambridge Bay, NWT. Curves, moving from lowest to highest, are for hop lengths of 1, 2, 5, 10, 20 and 30 km, respectively.

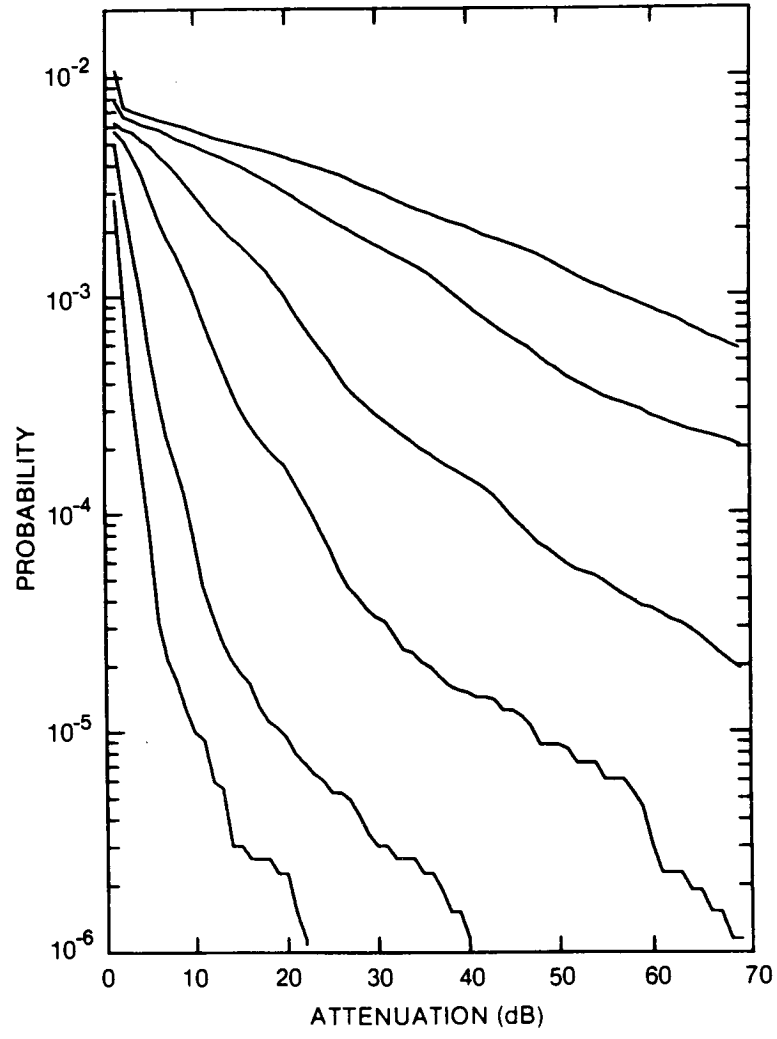

Figure 49. Cumulative distribution of rain attenuation for 100 GHz at Cambridge Bay, NWT. Curves, moving from lowest to highest, are for hop lengths of 1, 2, 5, 10, 20 and 30 km, respectively.

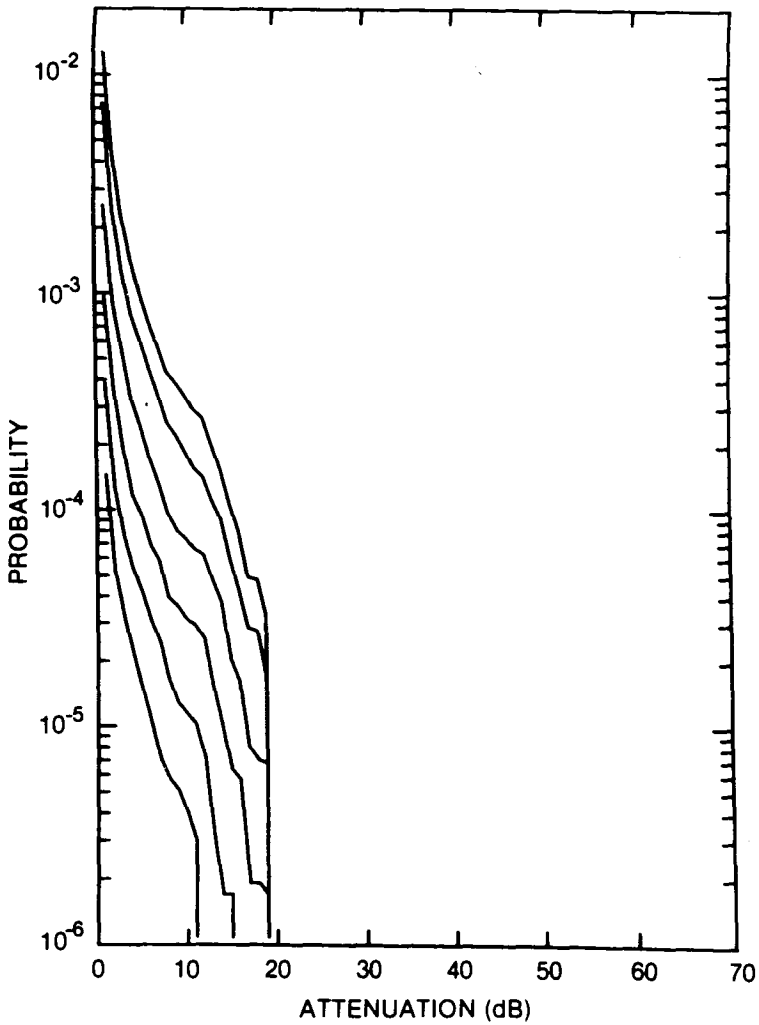

Figure 50. Cumulative distribution of rain attenuation for 8 GHz at Caplan, QUE. Curves, moving from lowest to highest, are for hop lengths of 5, 10, 20, 40, 80 and 120 km, respectively.

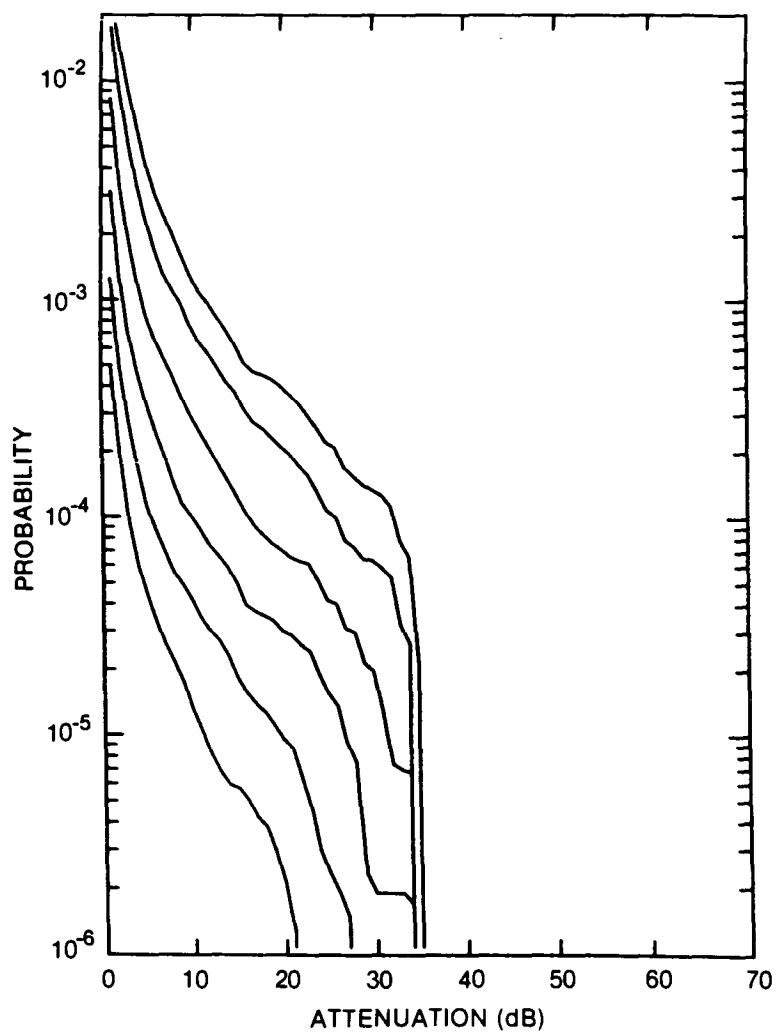

Figure 51. Cumulative distribution of rain attenuation for 11 GHz at Caplan, QUE. Curves, moving from lowest to highest, are for hop lengths of 5, 10, 20, 40, 80 and 120 km, respectively.

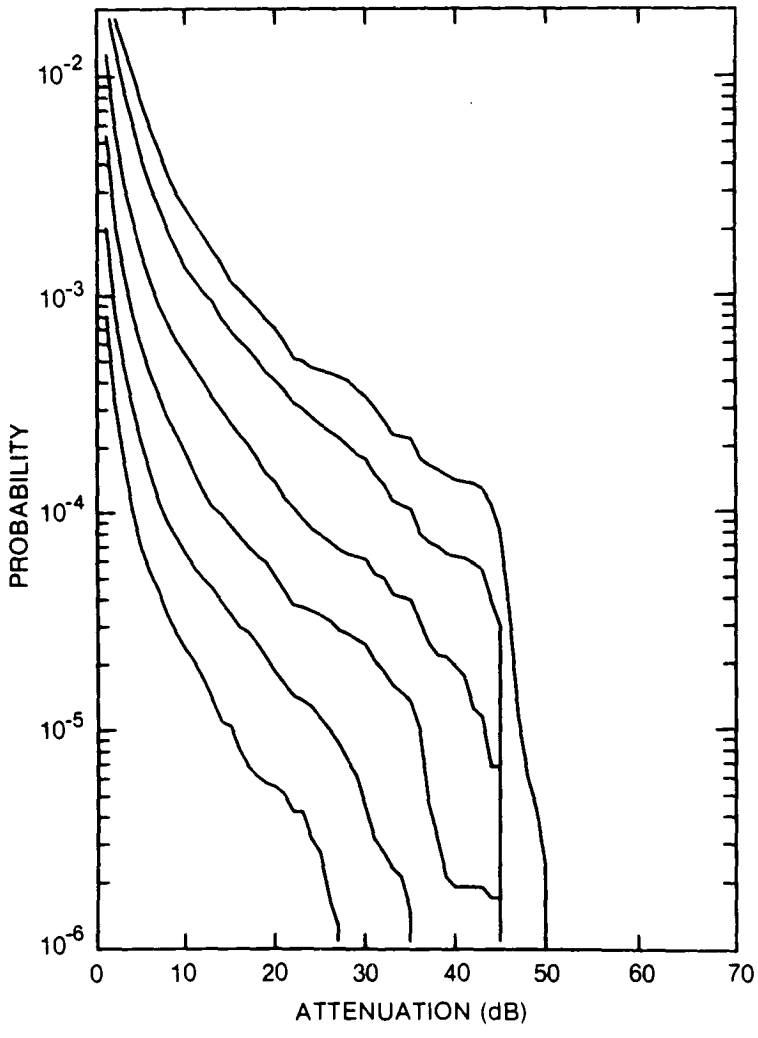

Figure 52. Cumulative distribution of rain attenuation for 12.8 GHz at Caplan, QUE. Curves, moving from lowest to highest, are for hop lengths of 5, 10, 20, 40, 80 and 120 km, respectively.

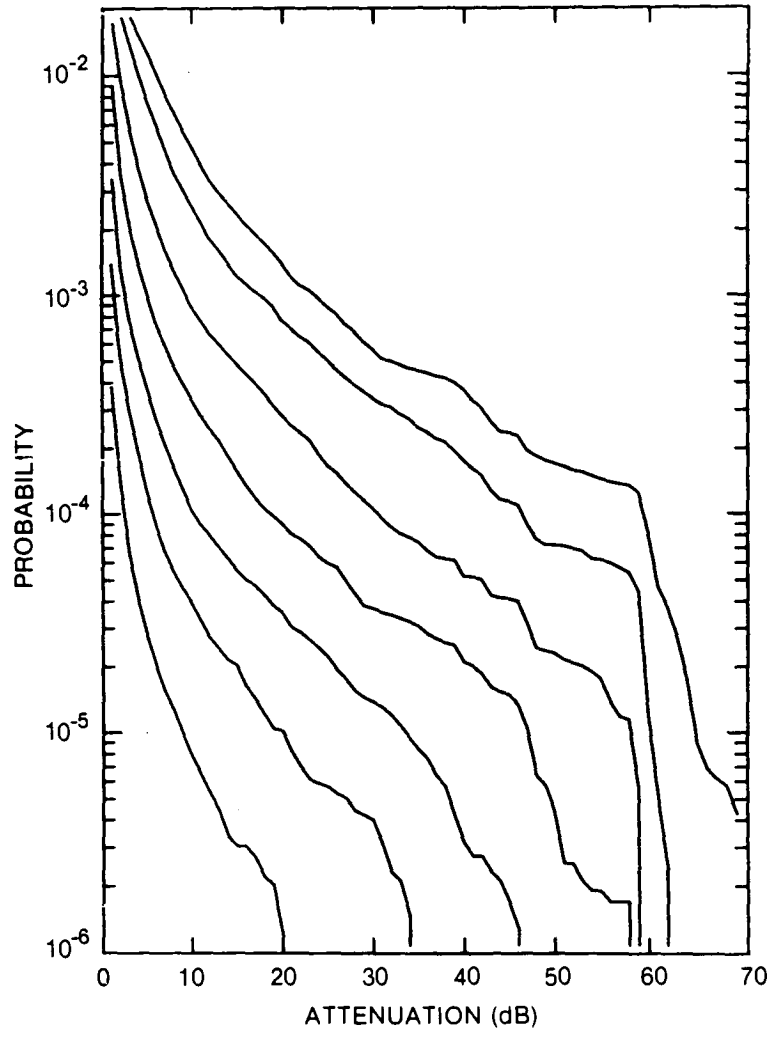

Figure 53. Cumulative distribution of rain attenuation for 15 GHz at Caplan, QUE. Curves, moving from lowest to highest, are for hop lengths of 2, 5, 10, 20, 40, 80 and 120 km, respectively.

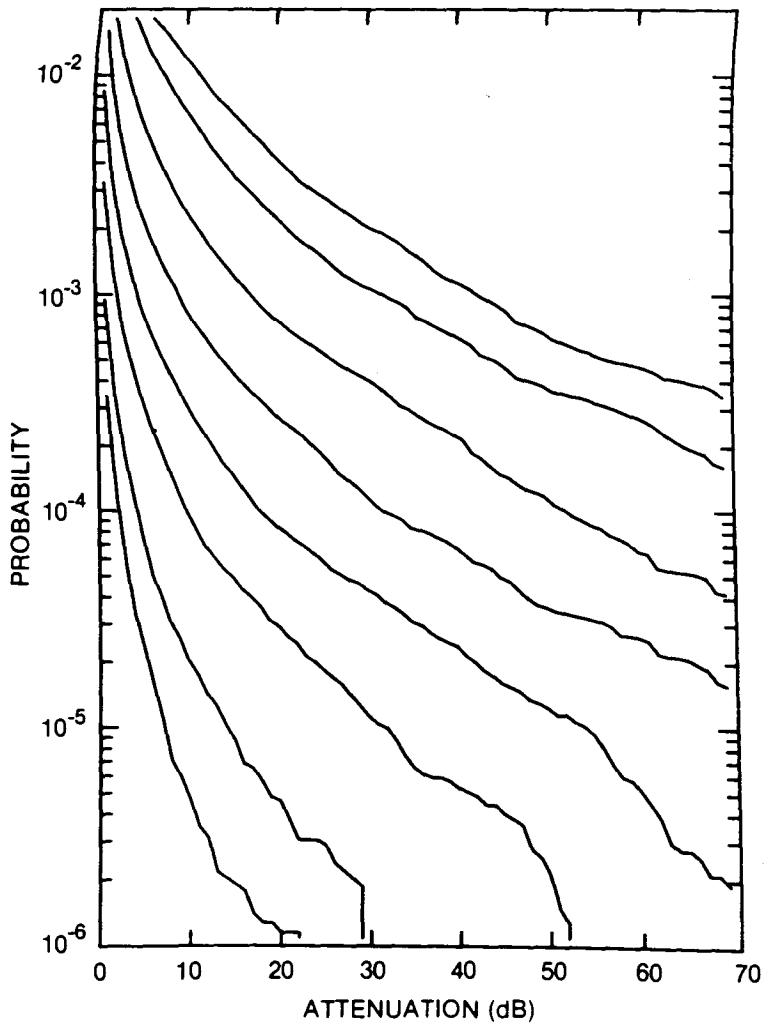

Figure 54. Cumulative distribution of rain attenuation for 20 GHz at Caplan, QUE. Curves, moving from lowest to highest, are for hop lengths of 1, 2, 5, 10, 20, 40, 80 and 120 km, respectively.

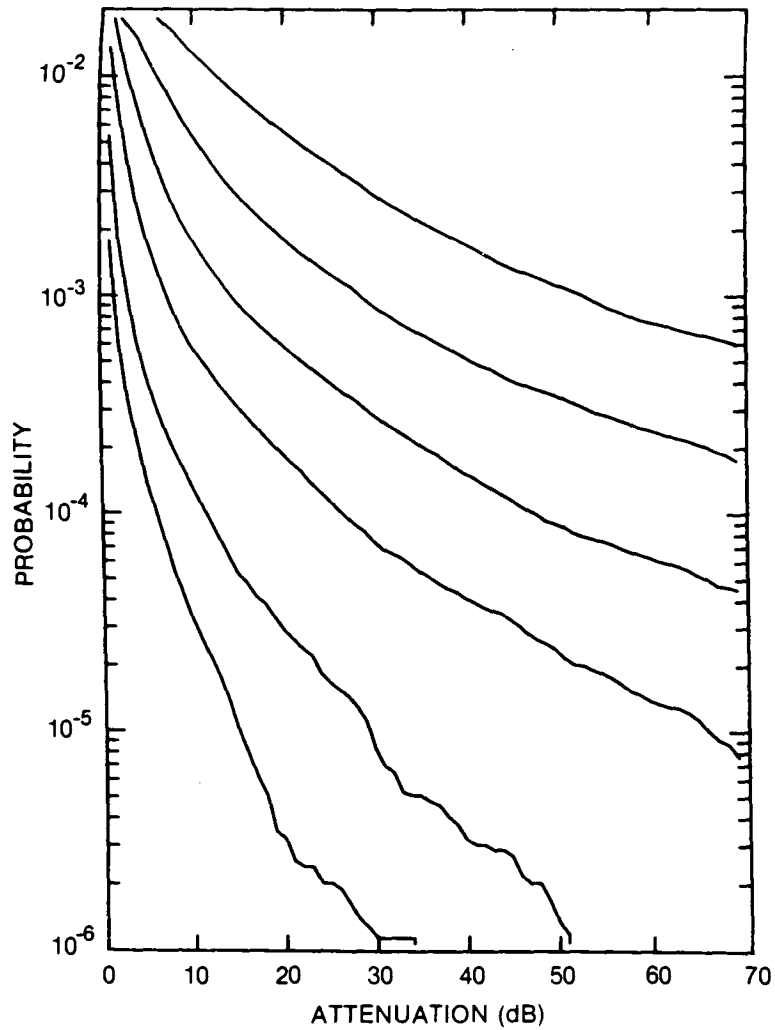

Figure 55. Cumulative distribution of rain attenuation for 35 GHz at Caplan, QUE. Curves, moving from lowest to highest, are for hop lengths of 1, 2, 5, 10, 20 and 40 km, respectively.

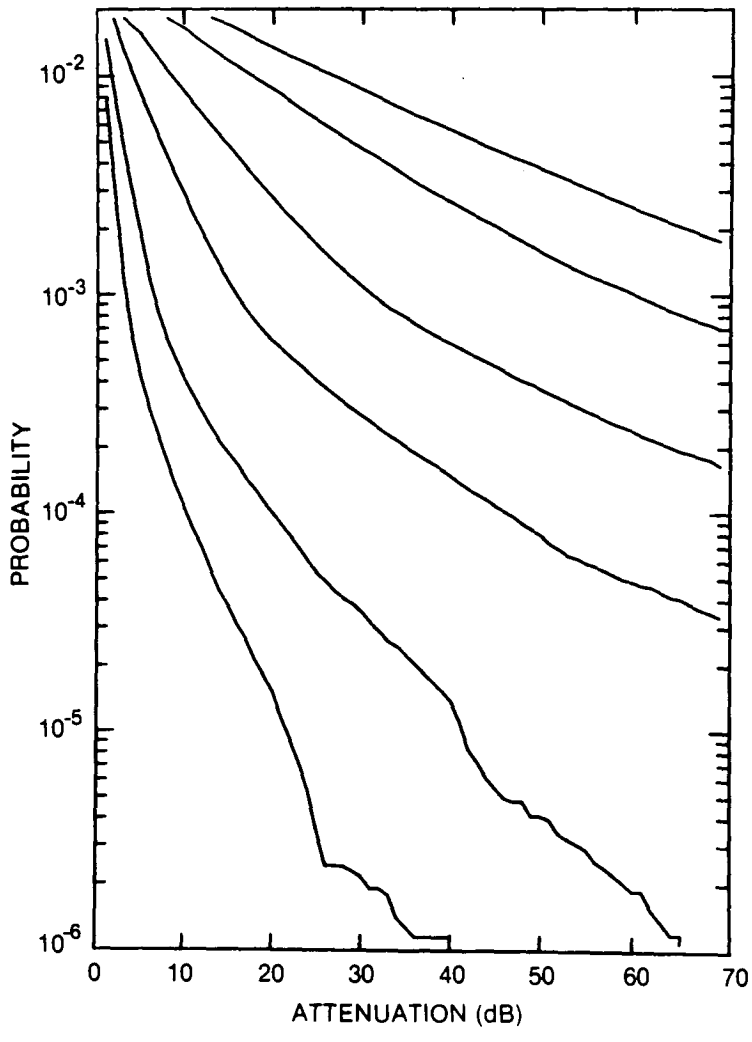

Figure 56. Cumulative distribution of rain attenuation for 56 GHz at Caplan, QUE. Curves, moving from lowest to highest, are for hop lengths of 1, 2, 5, 10, 20 and 30 km, respectively.

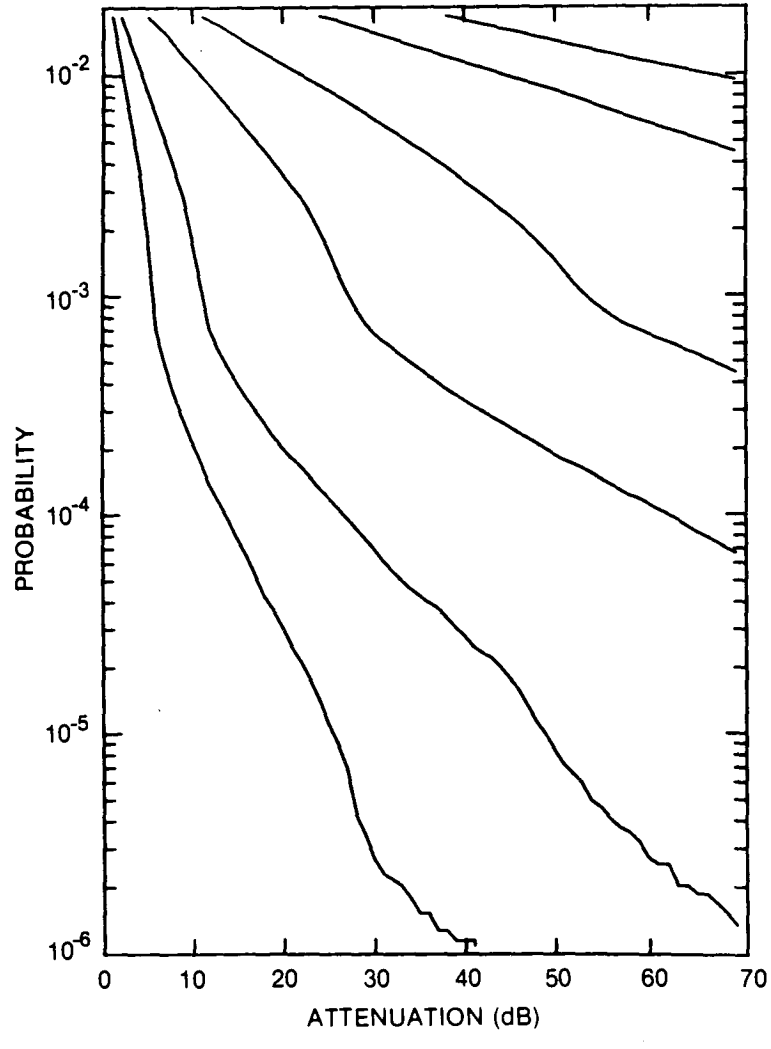

Figure 57. Cumulative distribution of rain attenuation for 100 GHz at Caplan, QUE. Curves, moving from lowest to highest, are for hop lengths of 1, 2, 5, 10, 20 and 30 km, respectively.

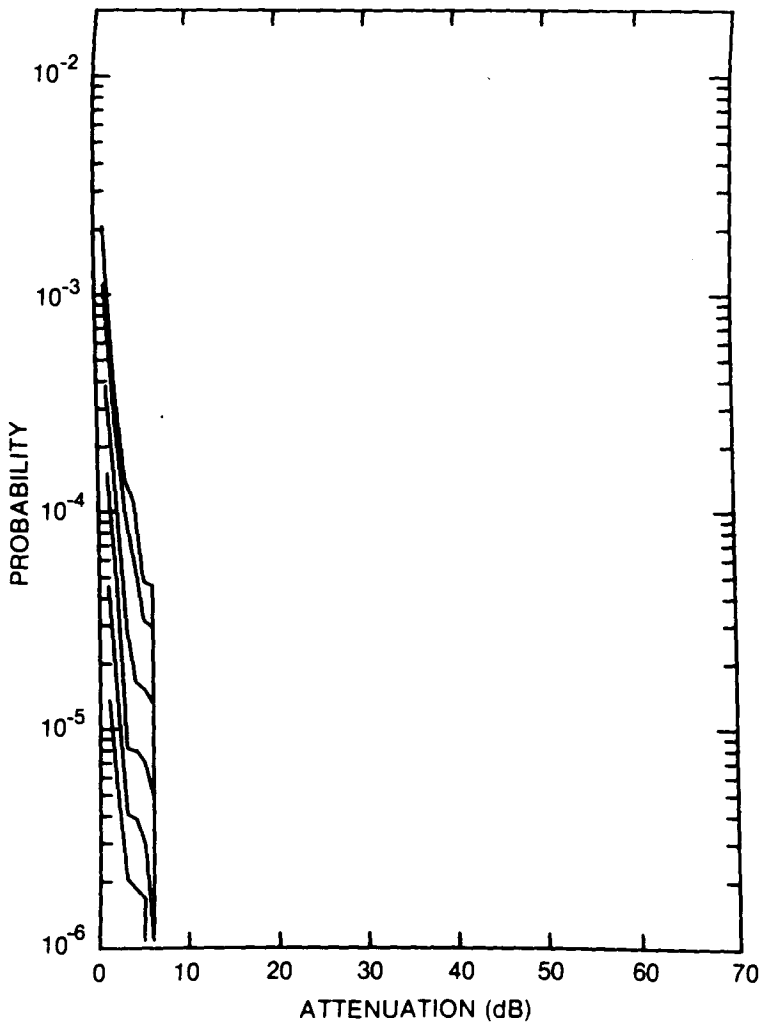

Figure 58. Cumulative distribution of rain attenuation for 8 GHz at Carmacks, YT. Curves, moving from lowest to highest, are for hop lengths of 5, 10, 20, 40, 80 and 120 km, respectively.

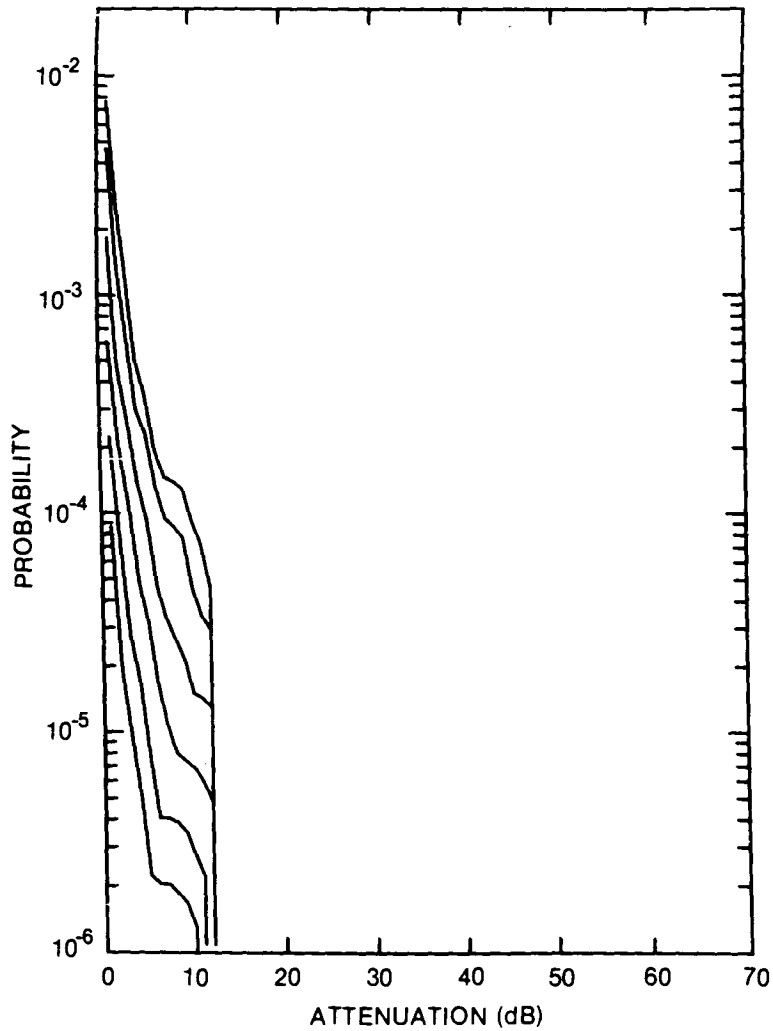

Figure 59. Cumulative distribution of rain attenuation for 11 GHz at Carmacks, YT. Curves, moving from lowest to highest, are for hop lengths of 5, 10, 20, 40, 80 and 120 km, respectively.

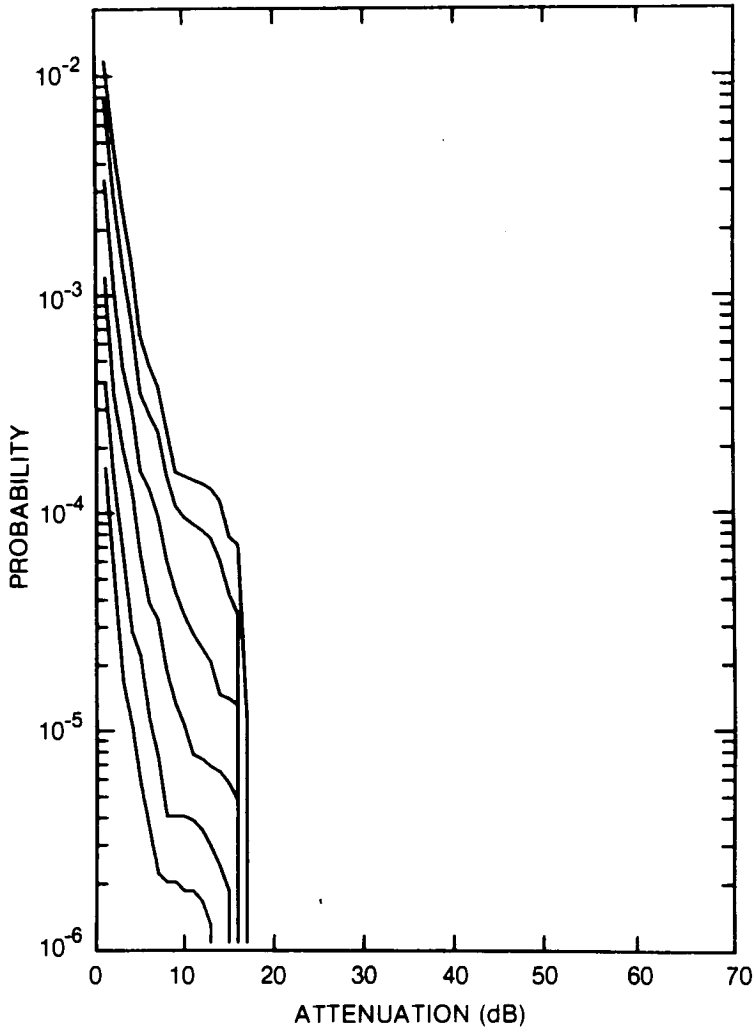

Figure 60. Cumulative distribution of rain attenuation for 12.8 GHz at Carmacks, YT. Curves, moving from lowest to highest, are for hop lengths of 5, 10, 20, 40, 80 and 120 km, respectively.

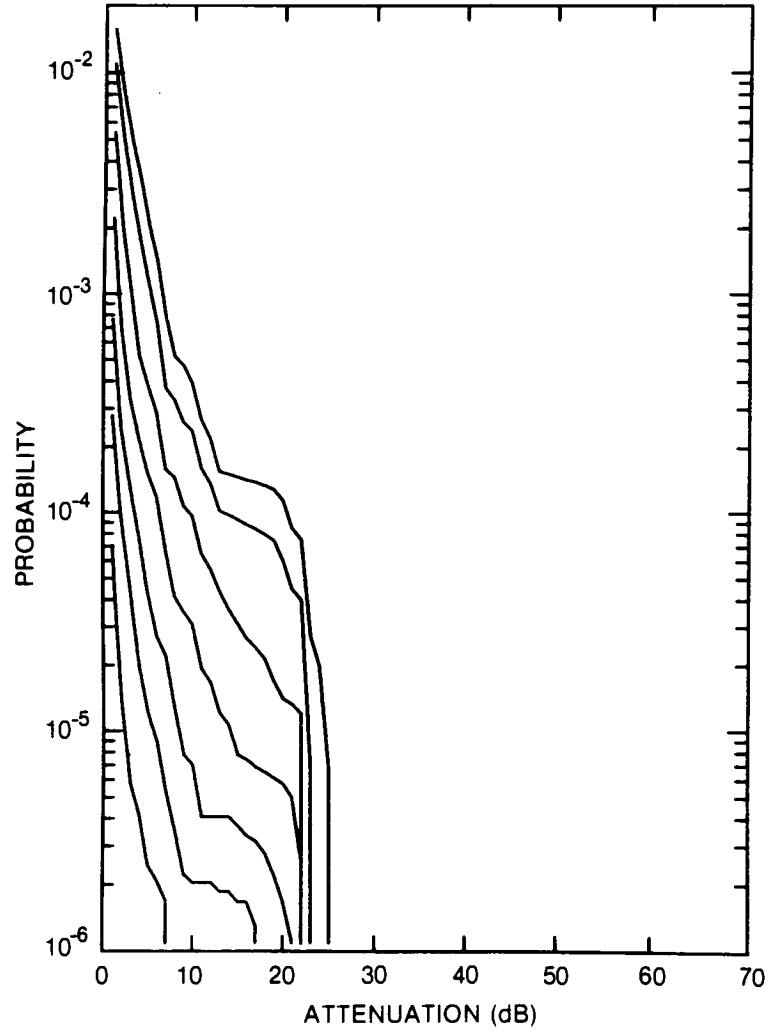

Figure 61. Cumulative distribution of rain attenuation for 15 GHz at Carmacks, YT. Curves, moving from lowest to highest, are for hop lengths of 2, 5, 10, 20, 40, 80 and 120 km, respectively.

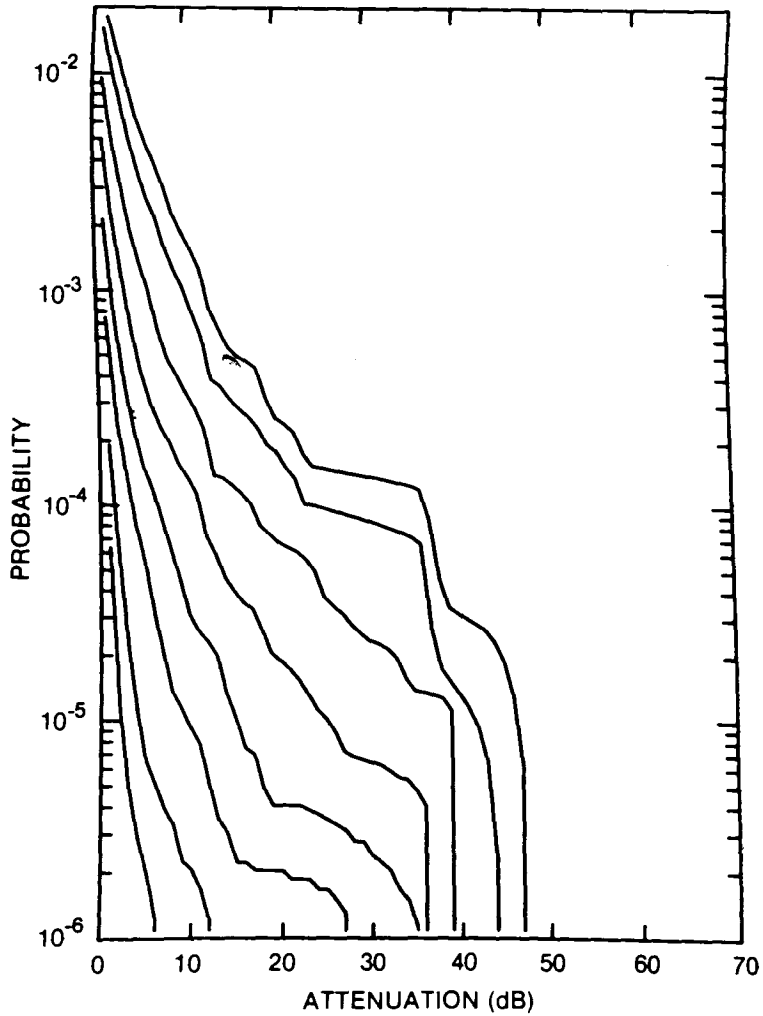

Figure 62. Cumulative distribution of rain attenuation for 20 GHz at Carmacks, YT. Curves, moving from lowest to highest, are for hop lengths of 1, 2, 5, 10, 20, 40, 80 and 120 km, respectively.

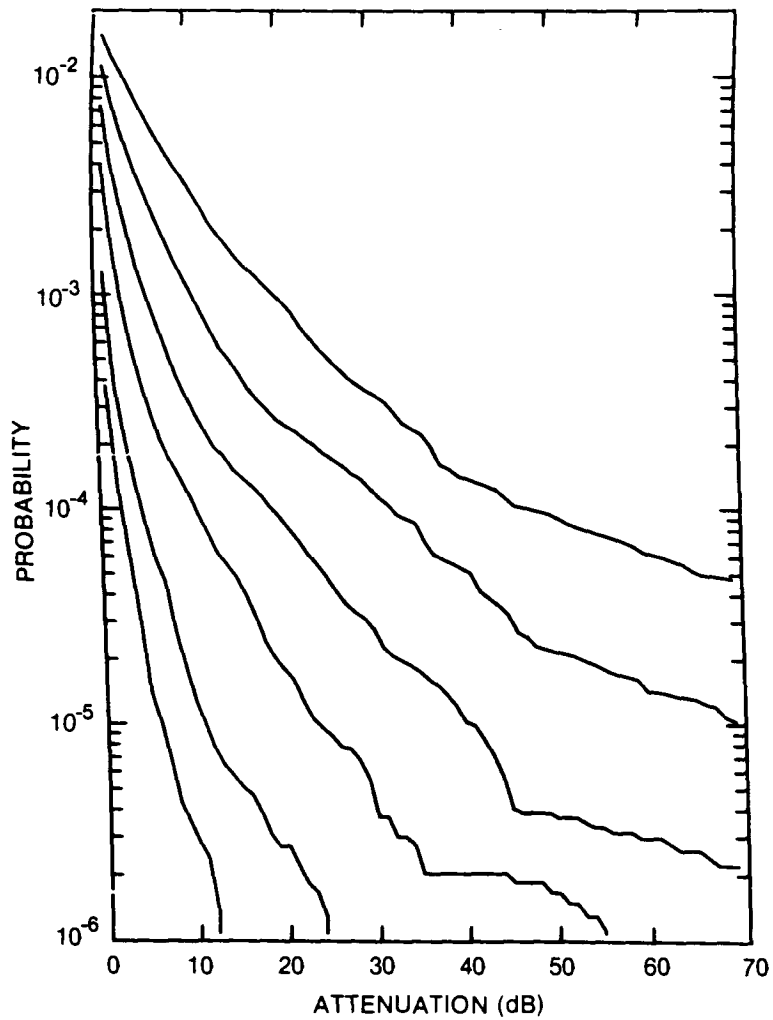

Figure 63. Cumulative distribution of rain attenuation for 35 GHz at Carmacks, YT. Curves, moving from lowest to highest, are for hop lengths of 1, 2, 5, 10, 20 and 40 km, respectively.

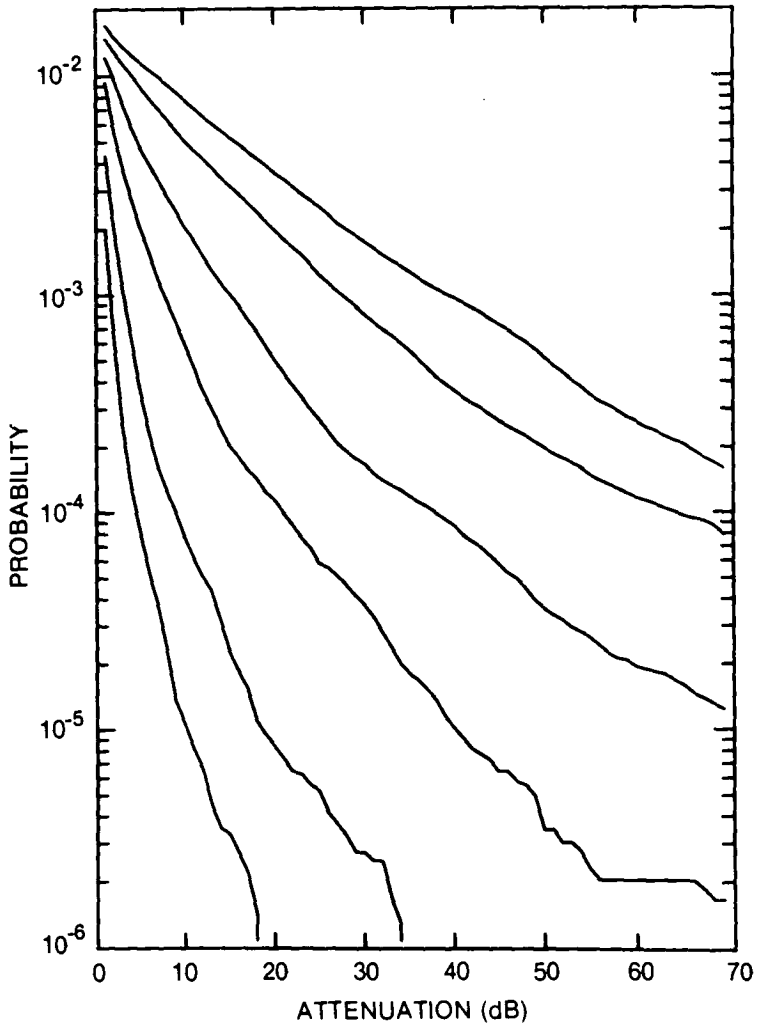

Figure 64. Cumulative distribution of rain attenuation for 56 GHz at Carmacks, YT. Curves, moving from lowest to highest, are for hop lengths of 1, 2, 5, 10, 20 and 30 km, respectively.

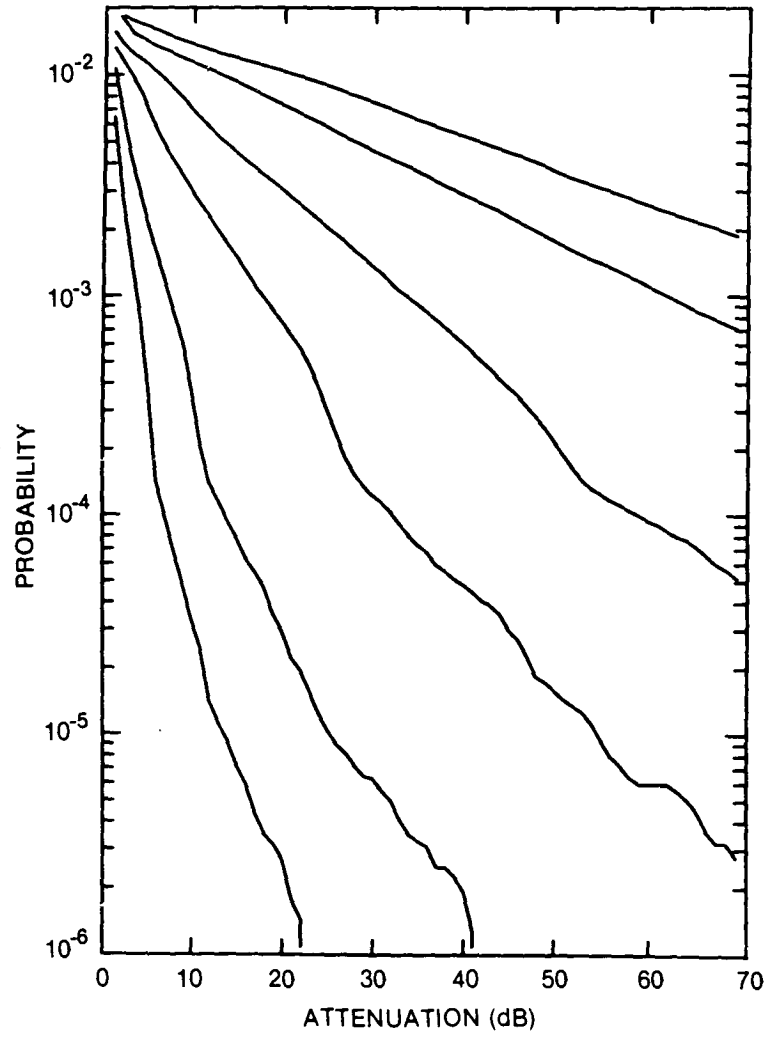

Figure 65. Cumulative distribution of rain attenuation for 100 GHz at Carmacks, YT. Curves, moving from lowest to highest, are for hop lengths of 1, 2, 5, 10, 20 and 30 km, respectively.

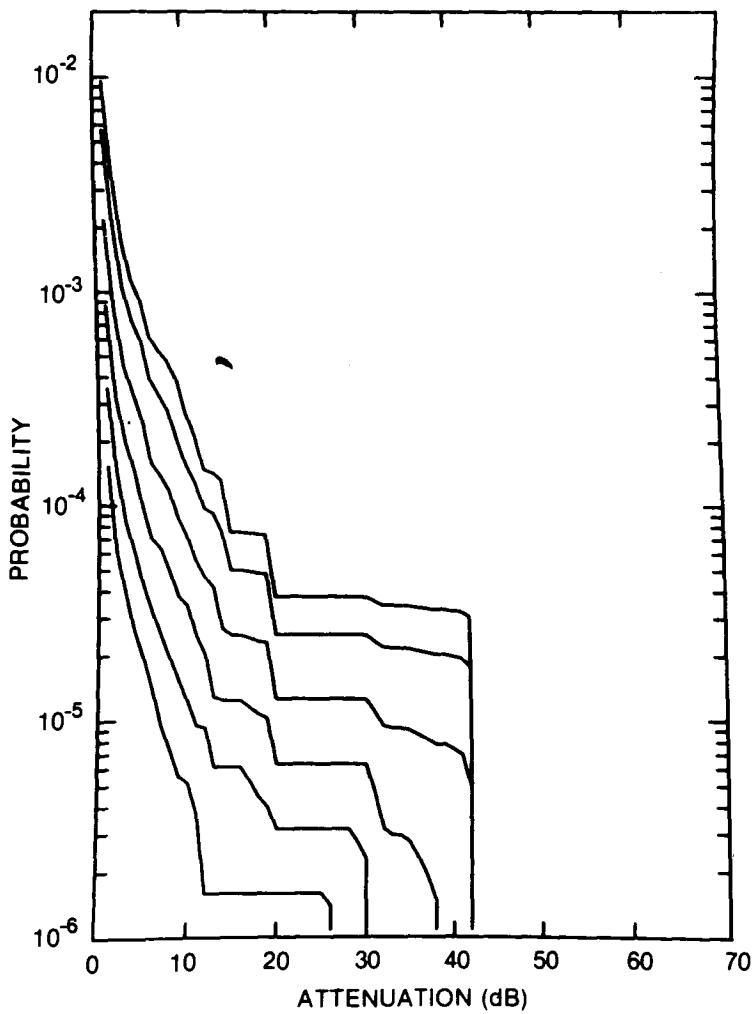

Figure 66. Cumulative distribution of rain attenuation for 8 GHz at Central Patricia, ONT. Curves, moving from lowest to highest, are for hop lengths of 5, 10, 20, 40, 80 and 120 km, respectively.

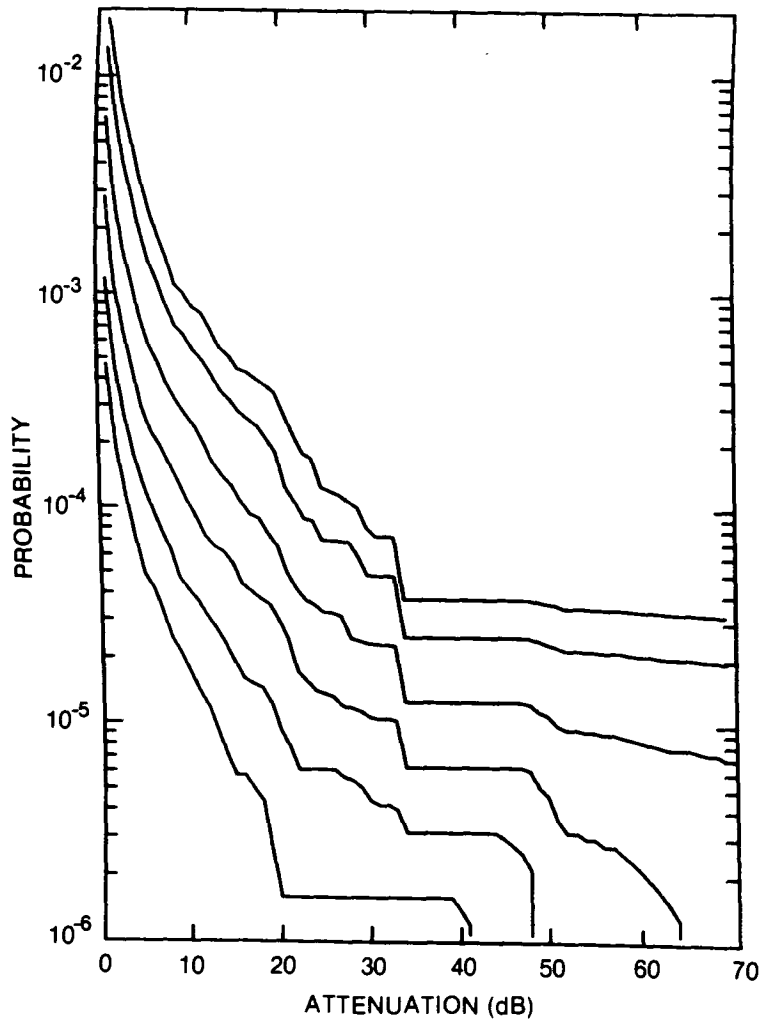

Figure 67. Cumulative distribution of rain attenuation for 11 GHz at Central Patricia, ONT. Curves, moving from lowest to highest, are for hop lengths of 5, 10, 20, 40, 80 and 120 km, respectively.

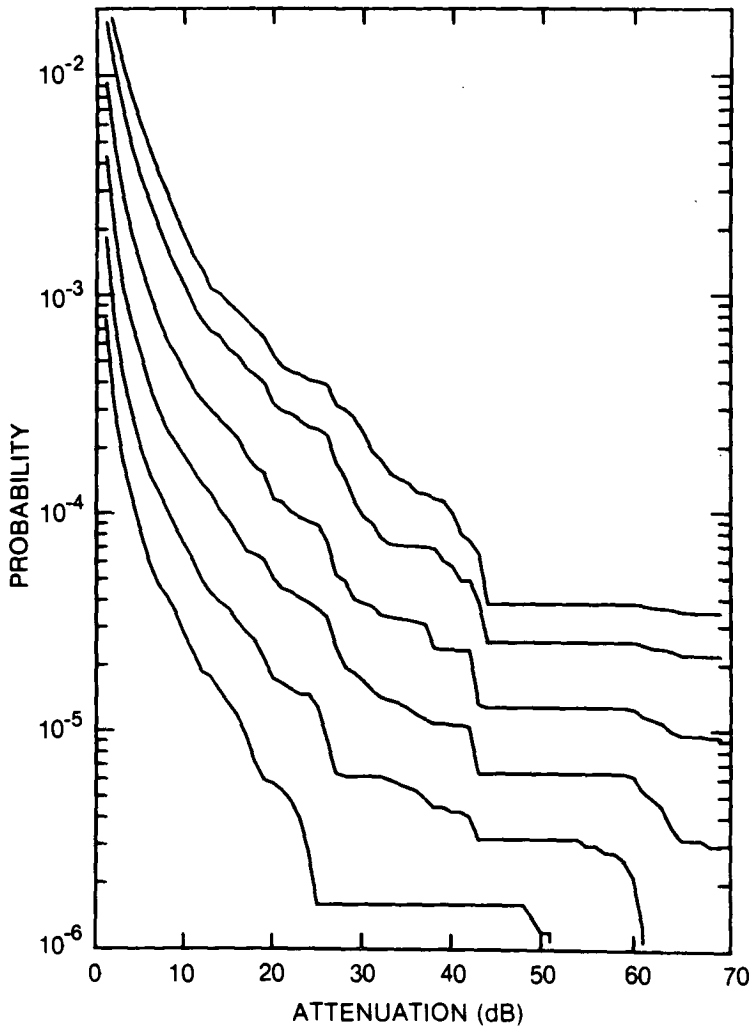

Figure 68. Cumulative distribution of rain attenuation for 12.8 GHZ at Central Patricia, ONT. Curves, moving from lowest to highest, are for hop lengths of 5, 10, 20, 40, 80 and 120 km, respectively.

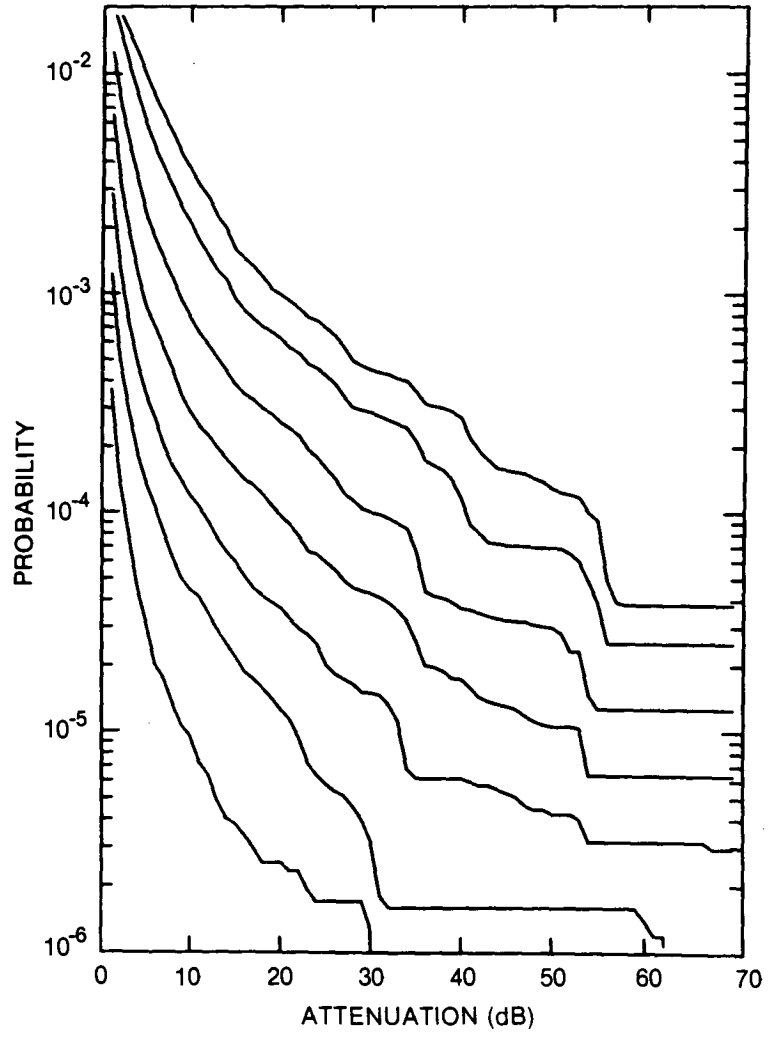

Figure 69. Cumulative distribution of rain attenuation for 15 GHz at Central Patricia, ONT. Curves, moving from lowest to highest, are for hop lengths of 2, 5, 10, 20, 40, 80 and 120 km, respectively.

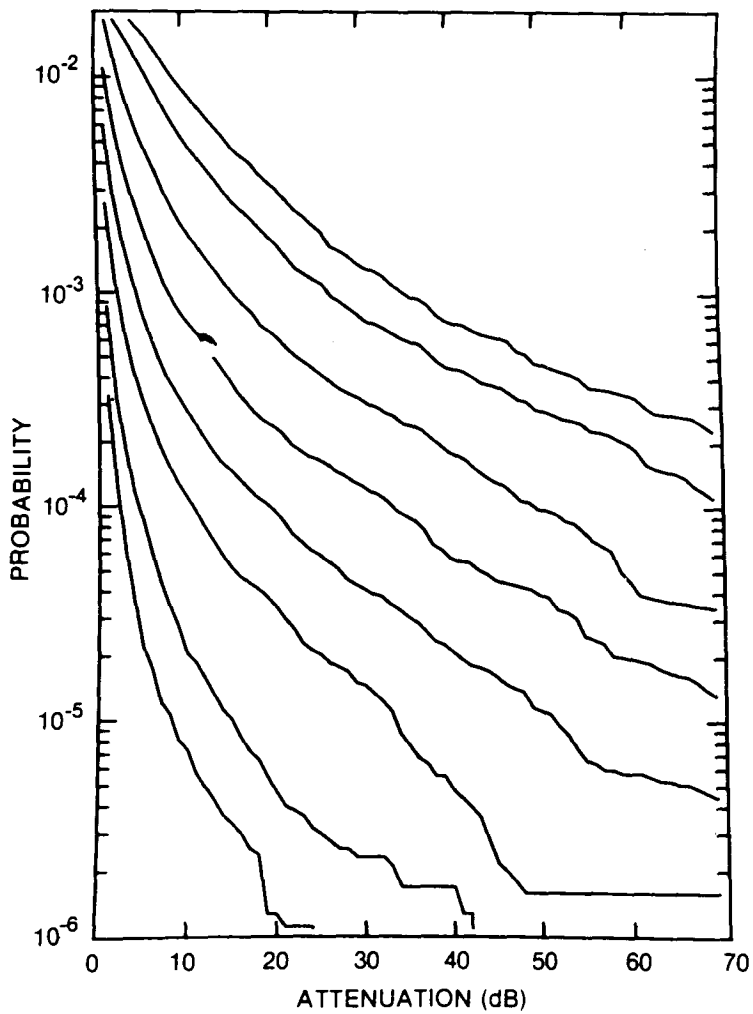

Figure 70. Cumulative distribution of rain attenuation for 20 GHz at Central Patricia, ONT. Curves, moving from lowest to highest, are for hop lengths of 1, 2, 5, 10, 20, 40, 80 and 120 km, respectively.

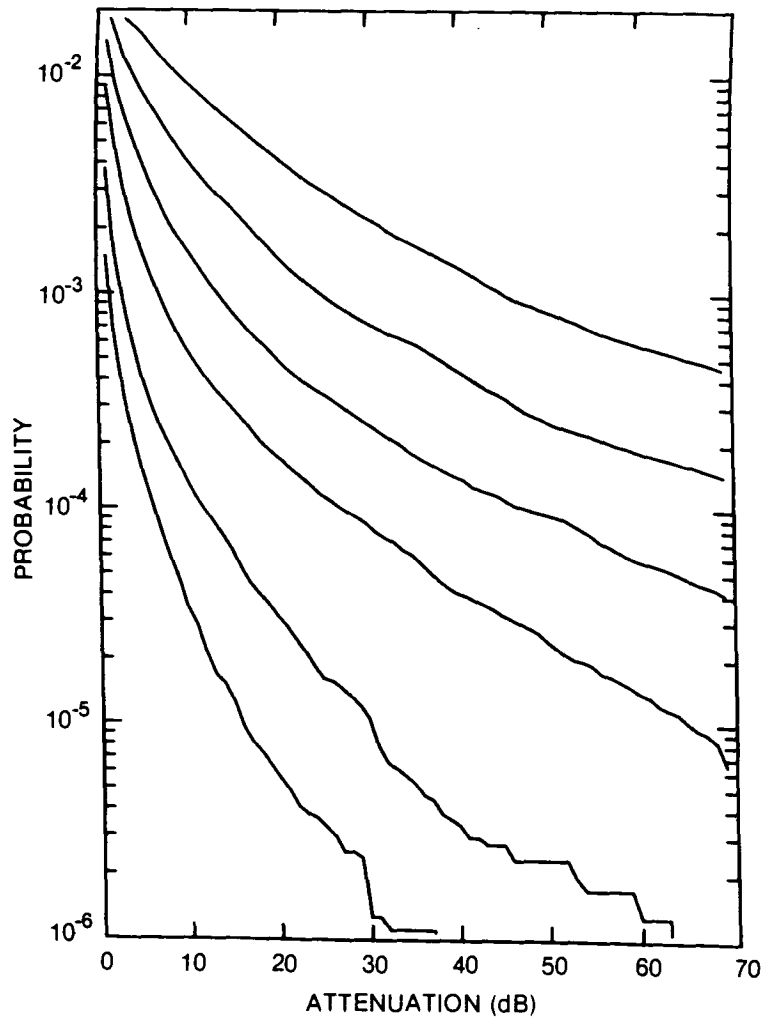

Figure 71. Cumulative distribution of rain attenuation for 35 GHz at Central Patricia, ONT. Curves, moving from lowest to highest, are for hop lengths of 1, 2, 5, 10, 20 and 40 km, respectively.

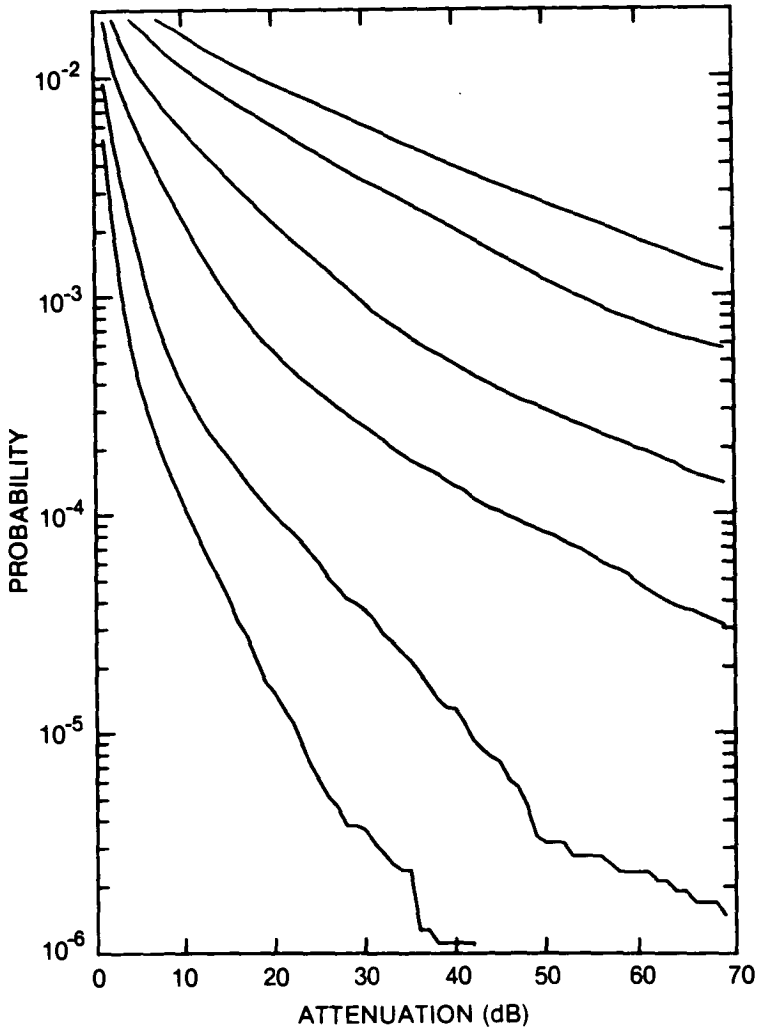

Figure 72. Cumulative distribution of rain attenuation for 56 GHz at Central Patricia, ONT. Curves, moving from lowest to highest, are for hop lengths of 1, 2, 5, 10, 20 and 30 km, respectively.

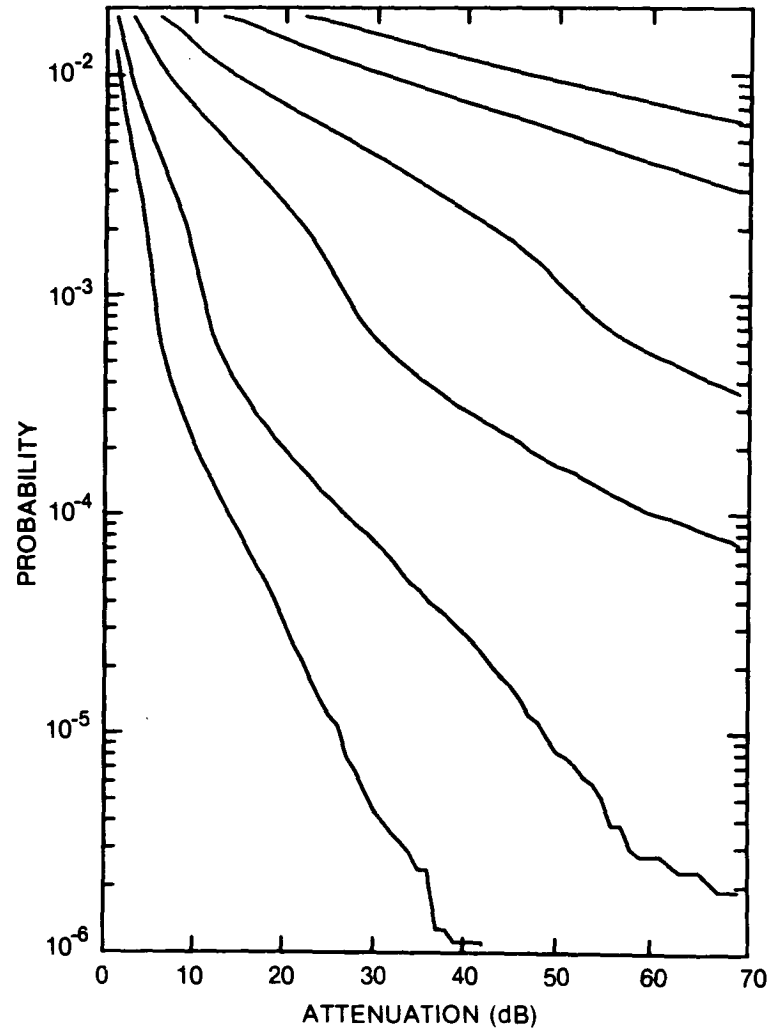

Figure 73. Cumulative distribution of rain attenuation for 100 GHz at Central Patricia, ONT. Curves, moving from lowest to highest, are for hop lengths of 1, 2, 5, 10, 20 and 30 km, respectively.

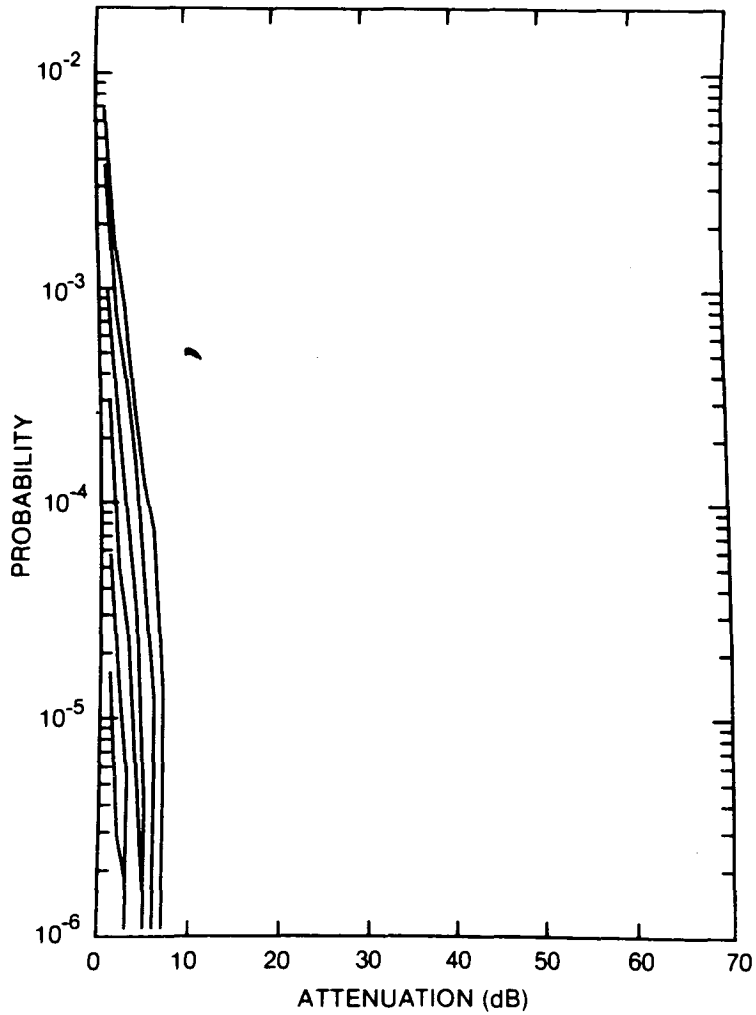

Figure 74. Cumulative distribution of rain attenuation for 8 GHz at Churchill, MAN. Curves, moving from lowest to highest, are for hop lengths of 5, 10, 20, 40, 80 and 120 km, respectively.

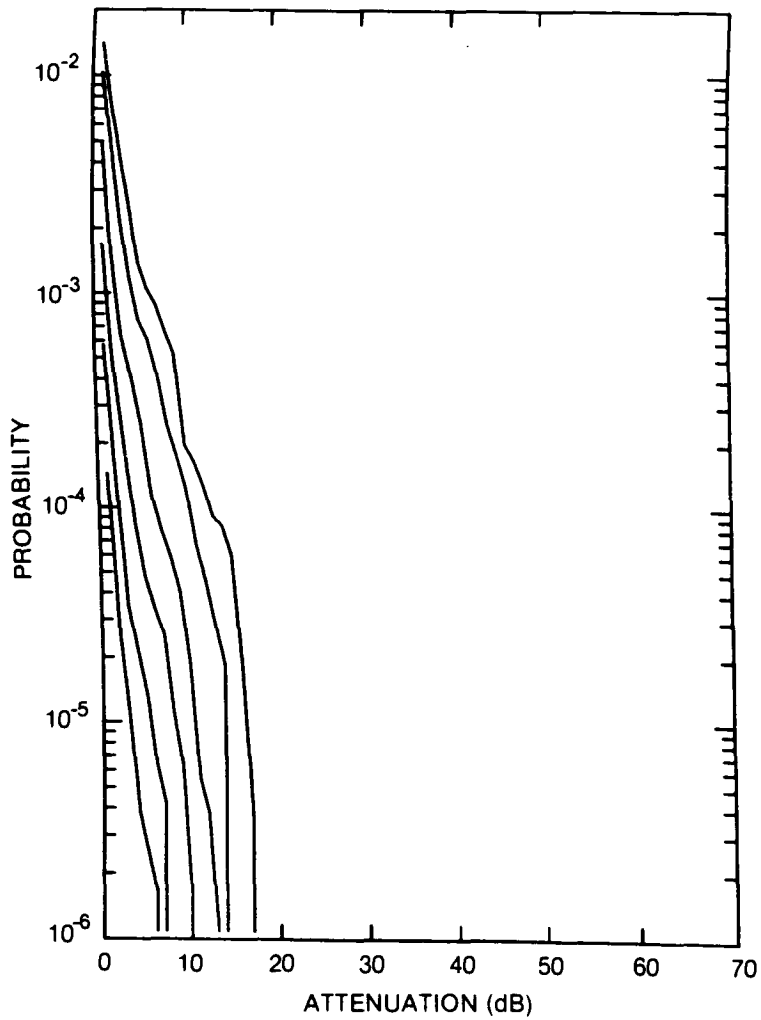

Figure 75. Cumulative distribution of rain attenuation for 11 GHz at Churchill, MAN. Curves, moving from lowest to highest, are for hop lengths of 5, 10, 20, 40, 80 and 120 km, respectively.

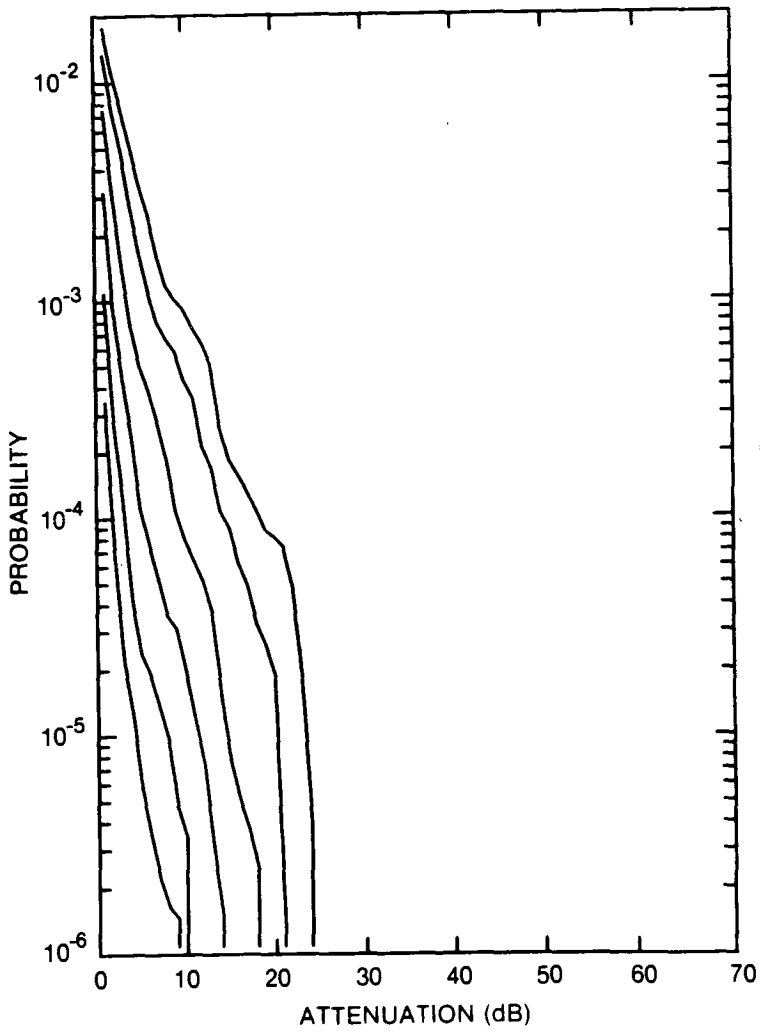

Figure 76. Cumulative distribution of rain attenuation for 12.8 GHz at Churchill, MAN. Curves, moving from lowest to highest, are for hop lengths of 5, 10, 20, 40, 80 and 120 km, respectively.

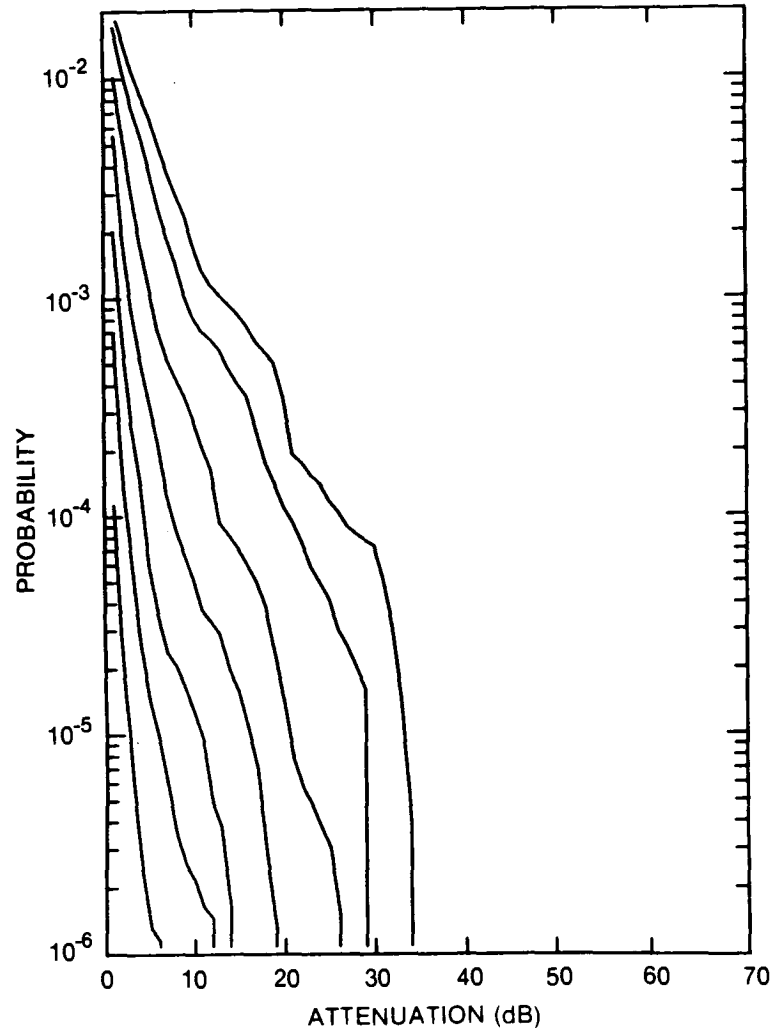

Figure 77. Cumulative distribution of rain attenuation for 15 GHz at Churchill, MAN. Curves, moving from lowest to highest, are for hop lengths of 2, 5, 10, 20, 40, 80 and 120 km, respectively.

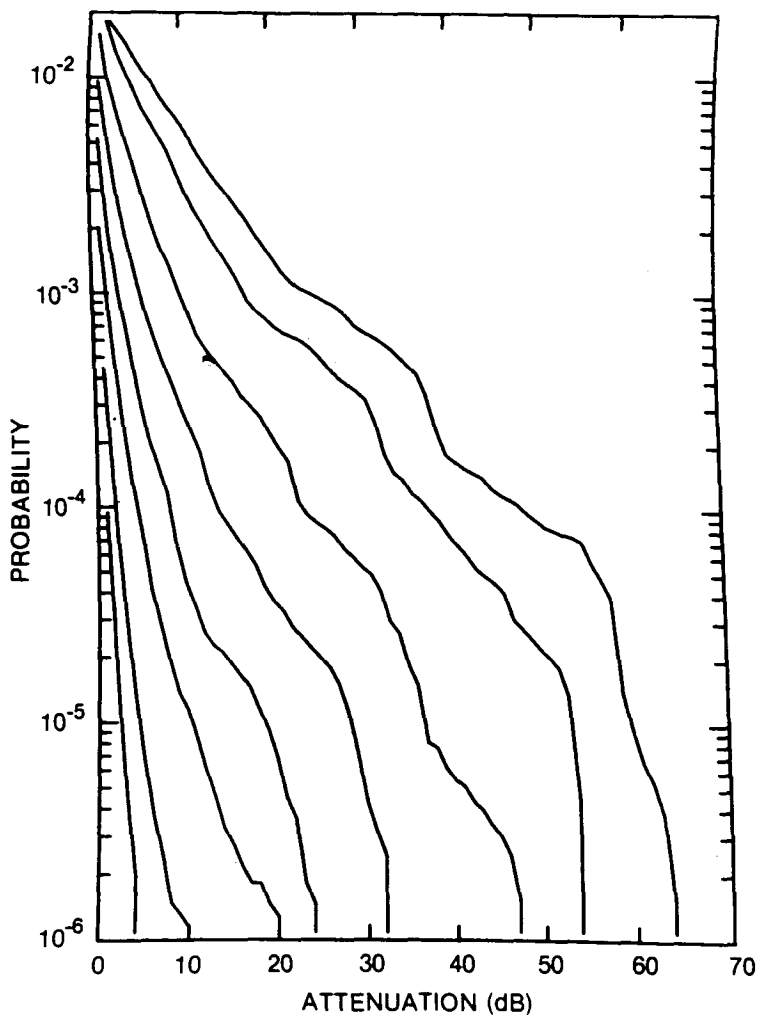

Figure 78. Cumulative distribution of rain attenuation for 20 GHz at Churchill, MAN. Curves, moving from lowest to highest, are for hop lengths of 1, 2, 5, 10, 20, 40, 80 and 120 km, respectively.

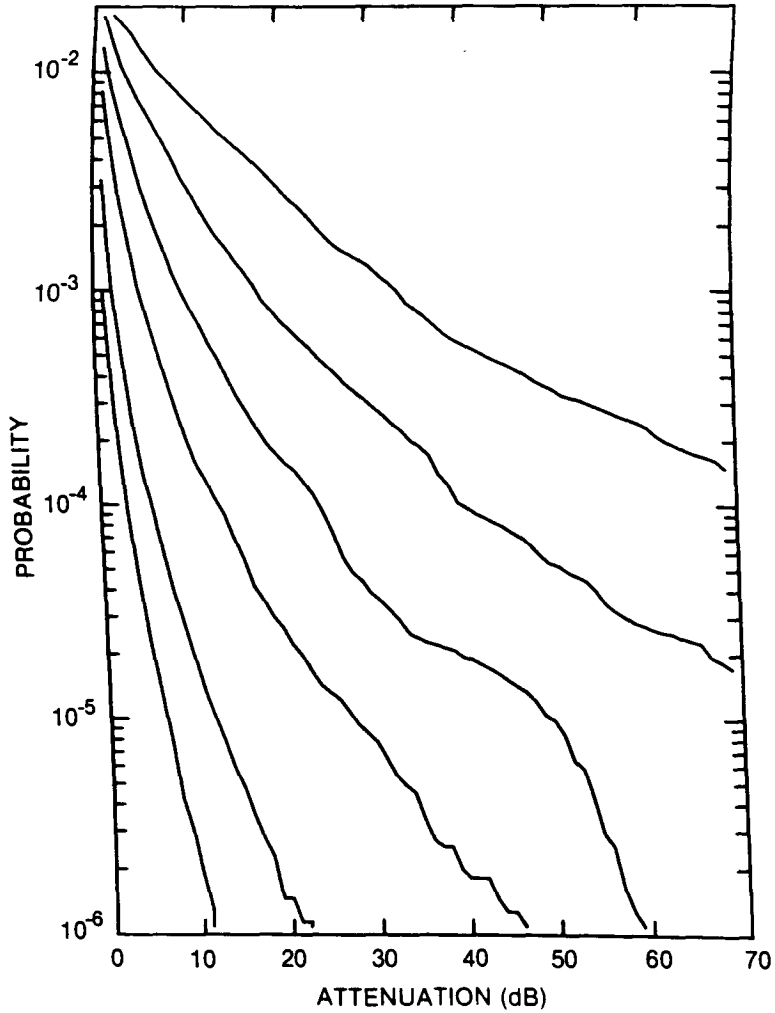

Figure 79. Cumulative distribution of rain attenuation for 35 GHz at Churchill, MAN. Curves, moving from lowest to highest, are for hop lengths of 1, 2, 5, 10, 20 and 40 km, respectively.

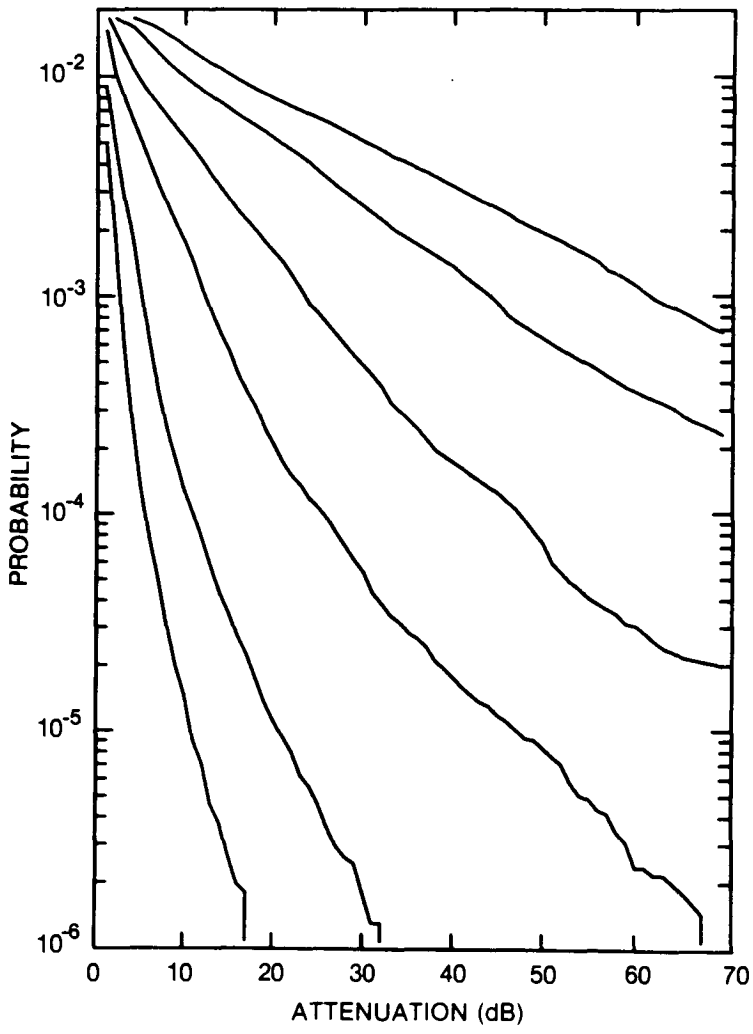

Figure 80. Cumulative distribution of rain attenuation for 56 GHz at Churchill, MAN. Curves, moving from lowest to highest, are for hop lengths of 1, 2, 5, 10, 20 and 30 km, respectively.

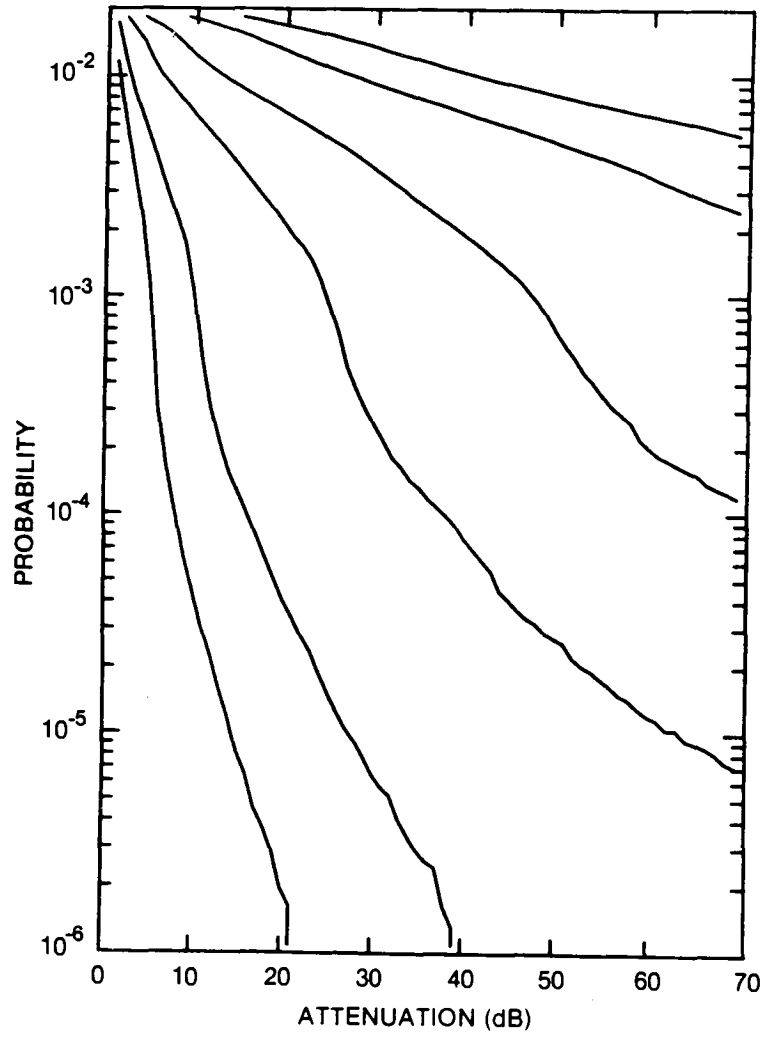

Figure 81. Cumulative distribution of rain attenuation for 100 GHz at Churchill, MAN. Curves, moving from lowest to highest, are for hop lengths of 1, 2, 5, 10, 20 and 30 km, respectively.

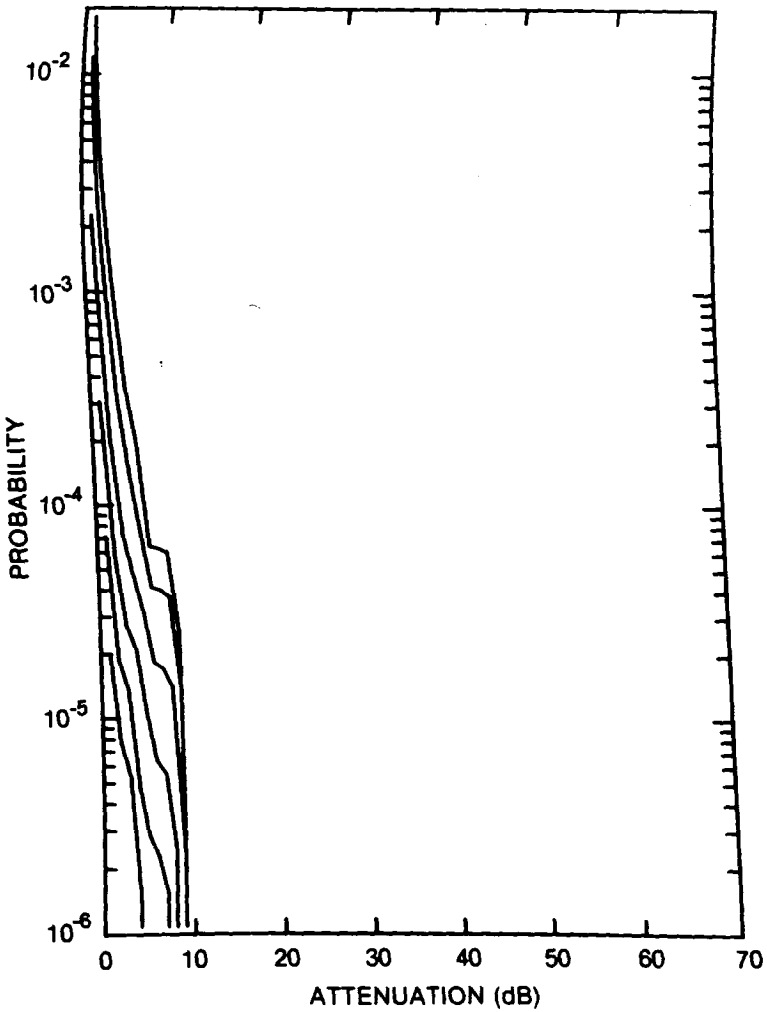

Figure 82. Cumulative distribution of rain attenuation for 8 GHz at Comox, BC. Curves, moving from lowest to highest, are for hop lengths of 5, 10, 20, 40, 80 and 120 km, respectively.

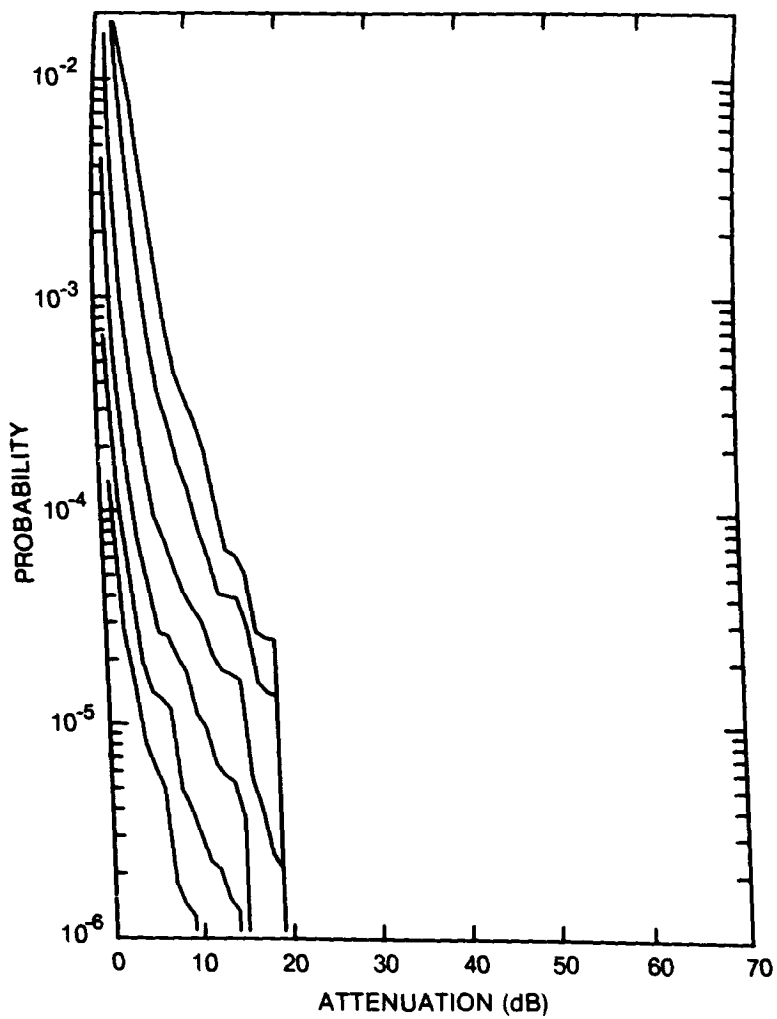

Figure 83. Cumulative distribution of rain attenuation for 11 GHz at Comox, BC. Curves, moving from lowest to highest, are for hop lengths of 5, 10, 20, 40, 80 and 120 km, respectively.

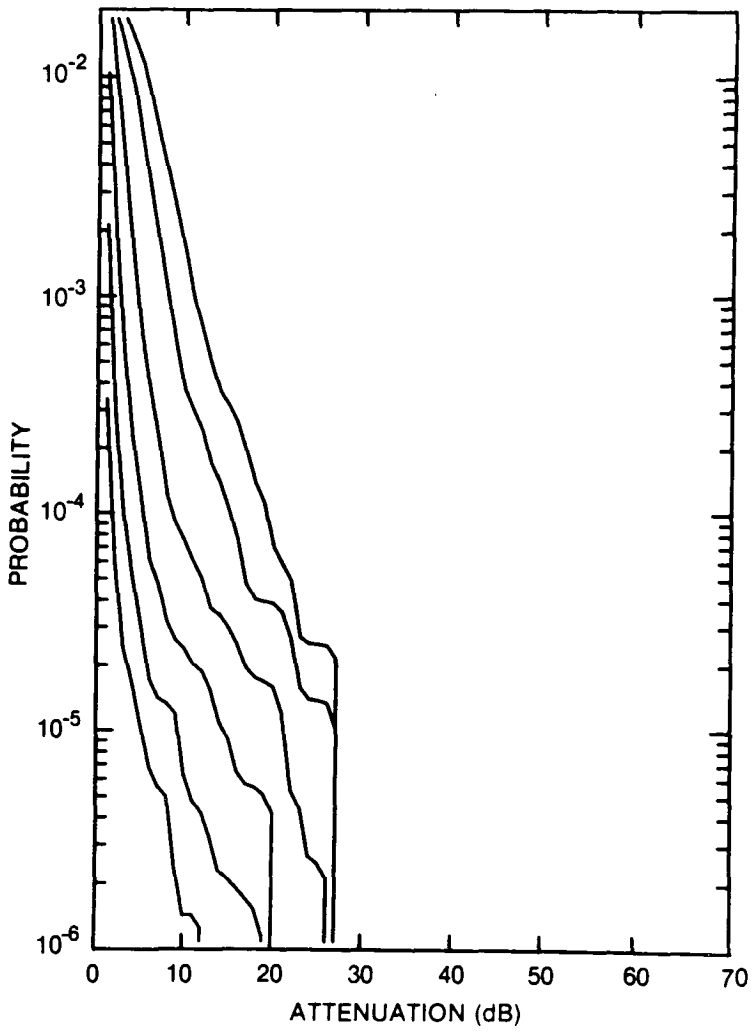

Figure 84. Cumulative distribution of rain attenuation for 12.8 GHz at Comox, BC. Curves, moving from lowest to highest, are for hop lengths of 5, 10, 20, 40, 80 and 120 km, respectively.

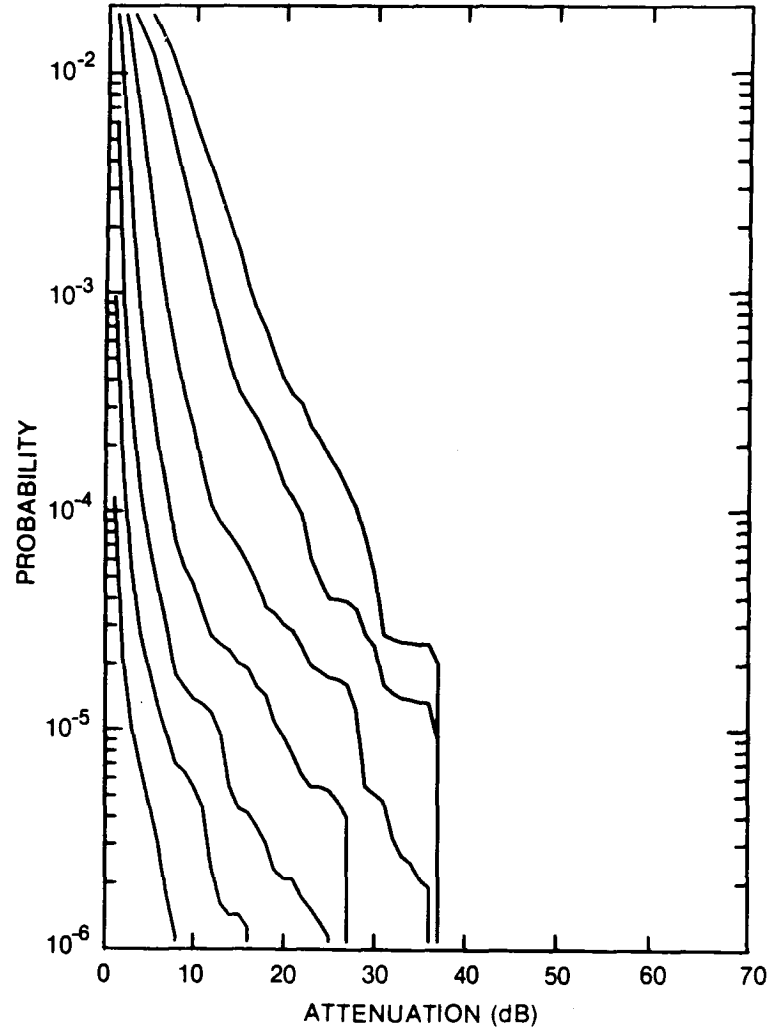

Figure 85. Cumulative distribution of rain attenuation for 15 GHz at Comox, BC. Curves, moving from lowest to highest, are for hop lengths of 2, 5, 10, 20, 40, 80 and 120 km, respectively.

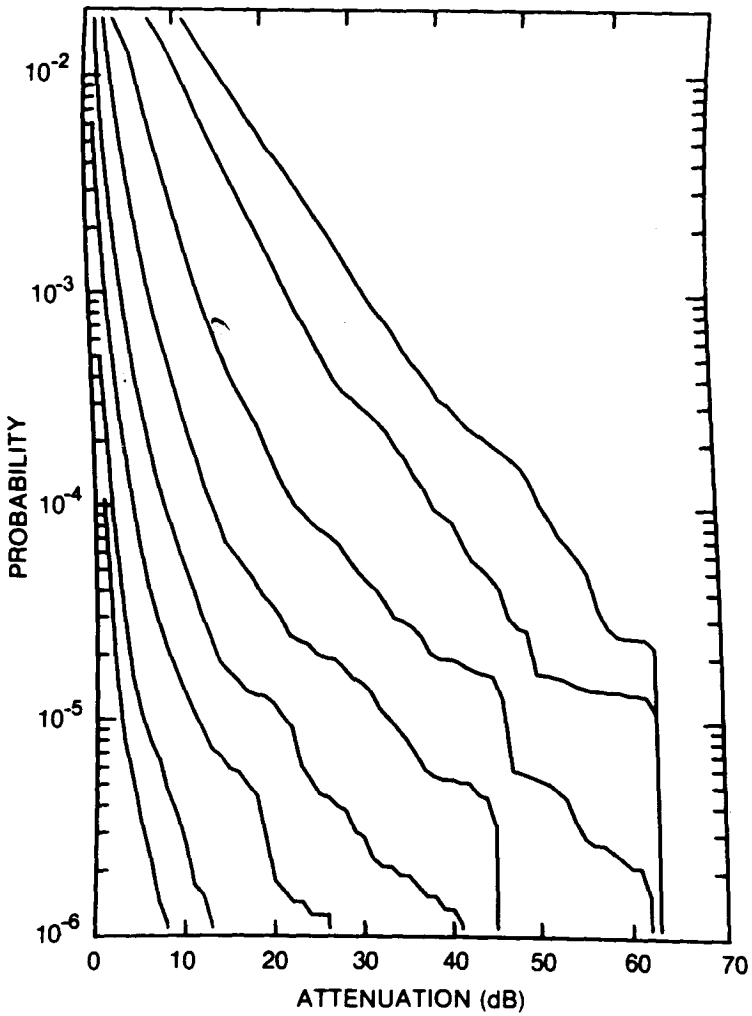

Figure 86. Cumulative distribution of rain attenuation for 20 GHz at Comox, BC. Curves, moving from lowest to highest, are for hop lengths of 1, 2, 5, 10, 10, 40 80 and 120 km, respectively.

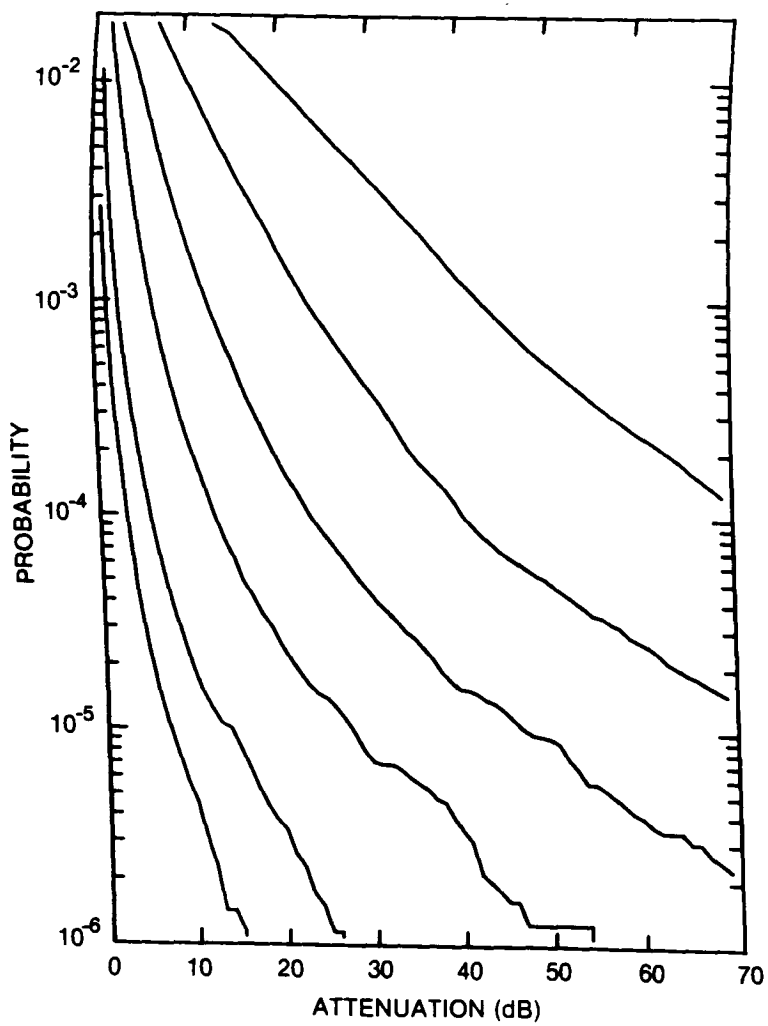

Figure 87. Cumulative distribution of rain attenuation for 35 GHz at Comox, BC. Curves, moving from lowest to highest, are for hop lengths of 1, 2, 4, 10, 20 and 40 km, respectively.

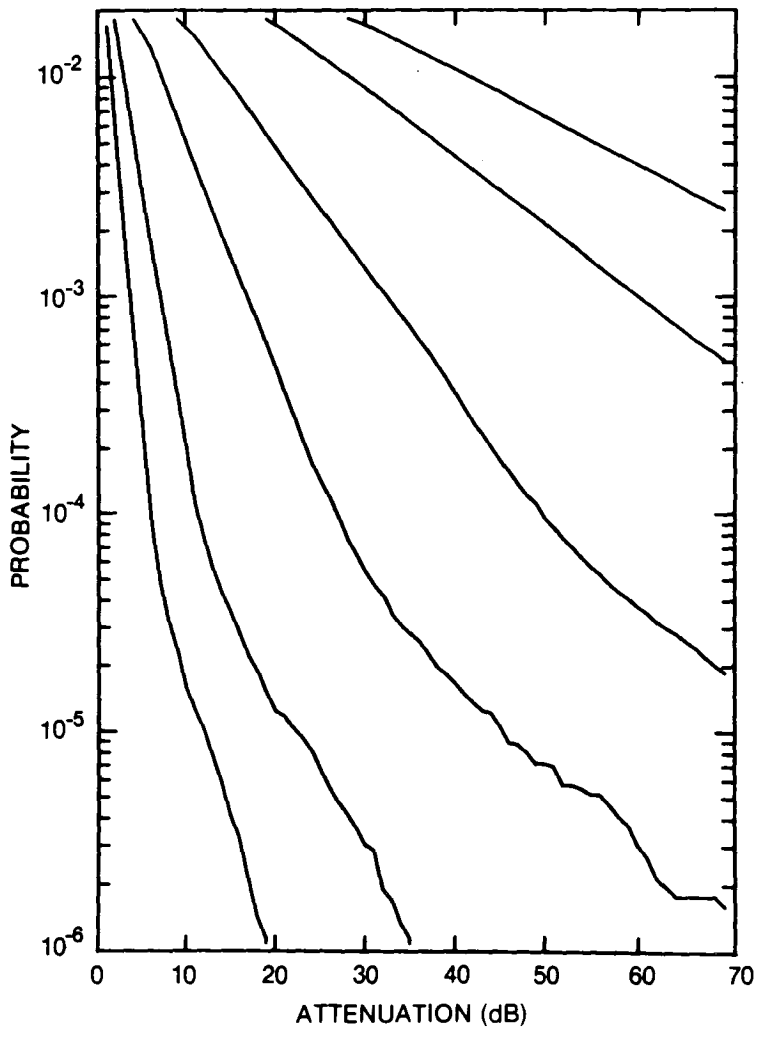

Figure 88. Cumulative distribution of rain attenuation for 56 GHz at Comox, BC. Curves, moving from lowest to highest, are for hop lengths of 1, 2, 5, 10, 20 and 30 km, respectively.

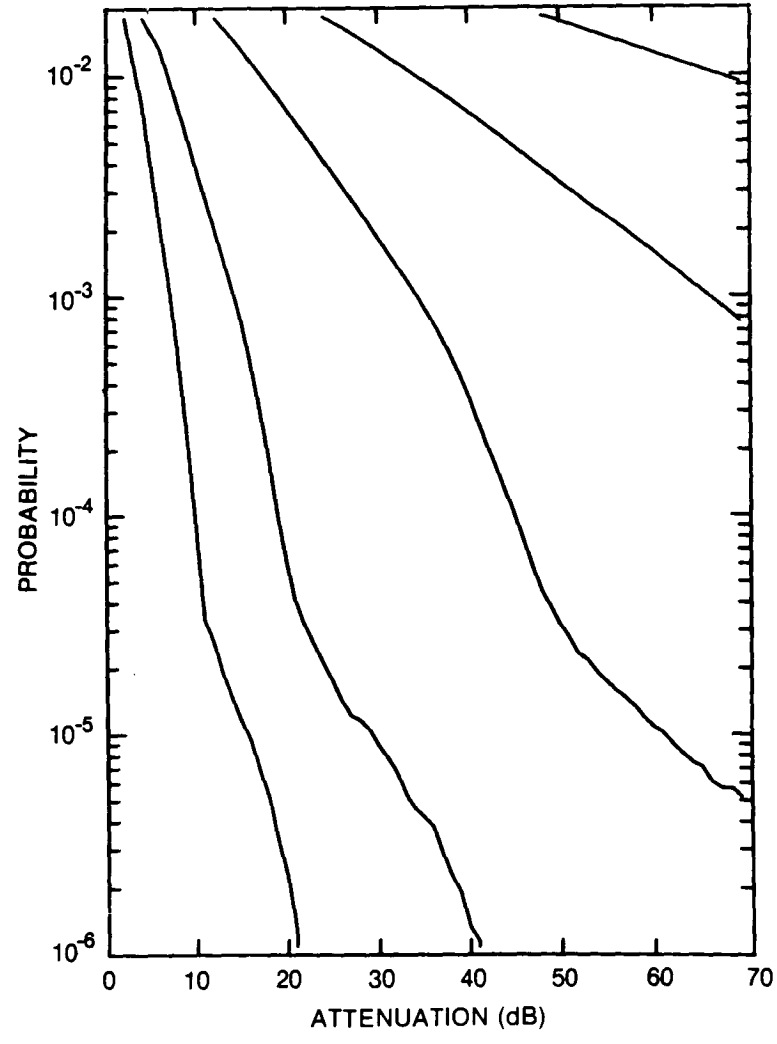

Figure 89. Cumulative distribution of rain attenuation for 100 GHz at Comox, BC. Curves, moving from lowest to highest, are for hop lengths of 1, 2, 5, 10 and 20 km, respectively.

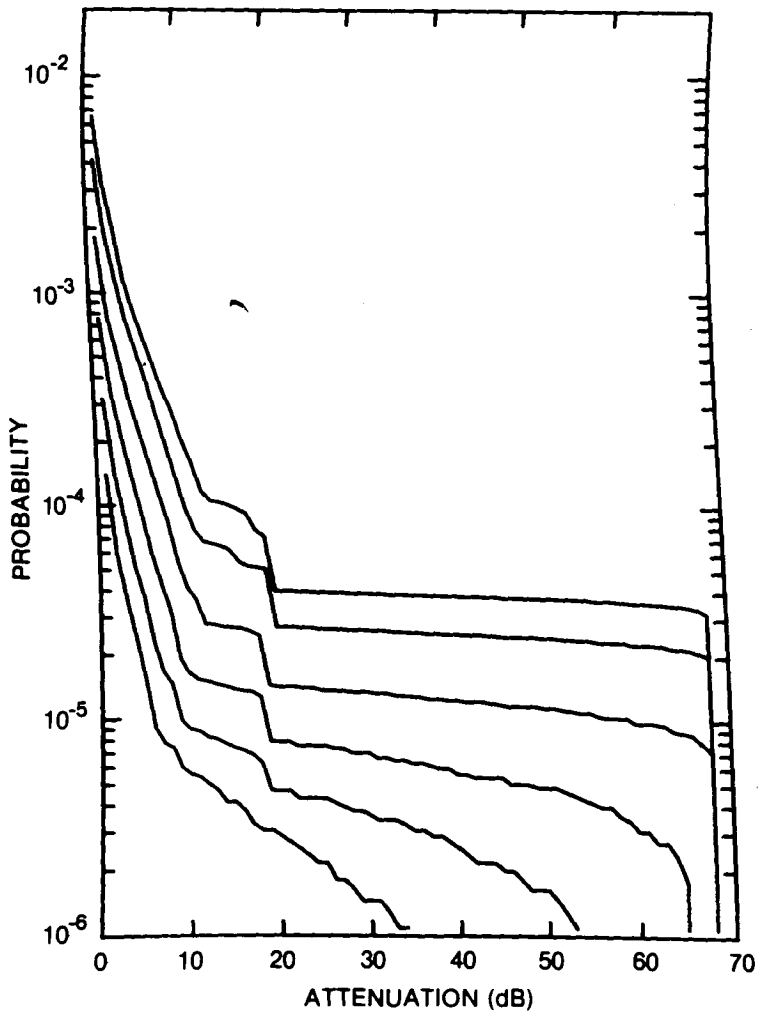

Figure 90. Cumulative distribution of rain attenuation for 8 GHz at Dauphin, MAN. Curves, moving from lowest to highest, are for hop lengths of 5, 10, 20, 40, 80 and 120 km, respectively.

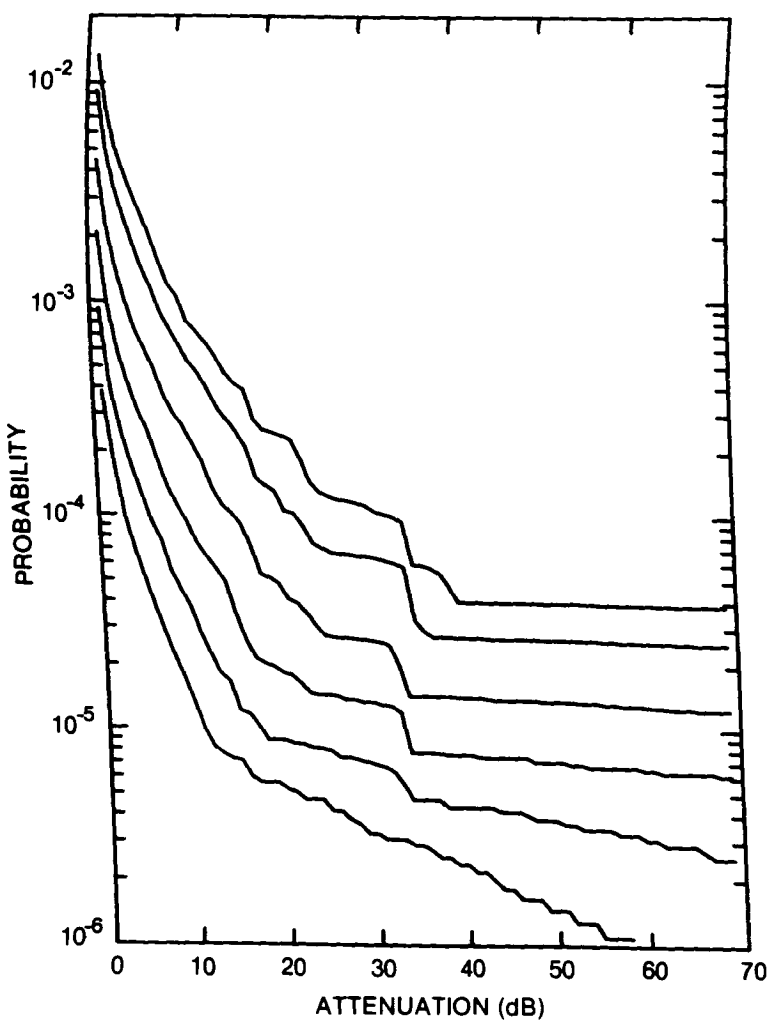

Figure 91. Cumulative distribution of rain attenuation for 11 GHz at Dauphin, MAN. Curves, moving from lowest to highest, are for hop lengths of 5, 10, 20, 40, 80 and 120 km, respectively.

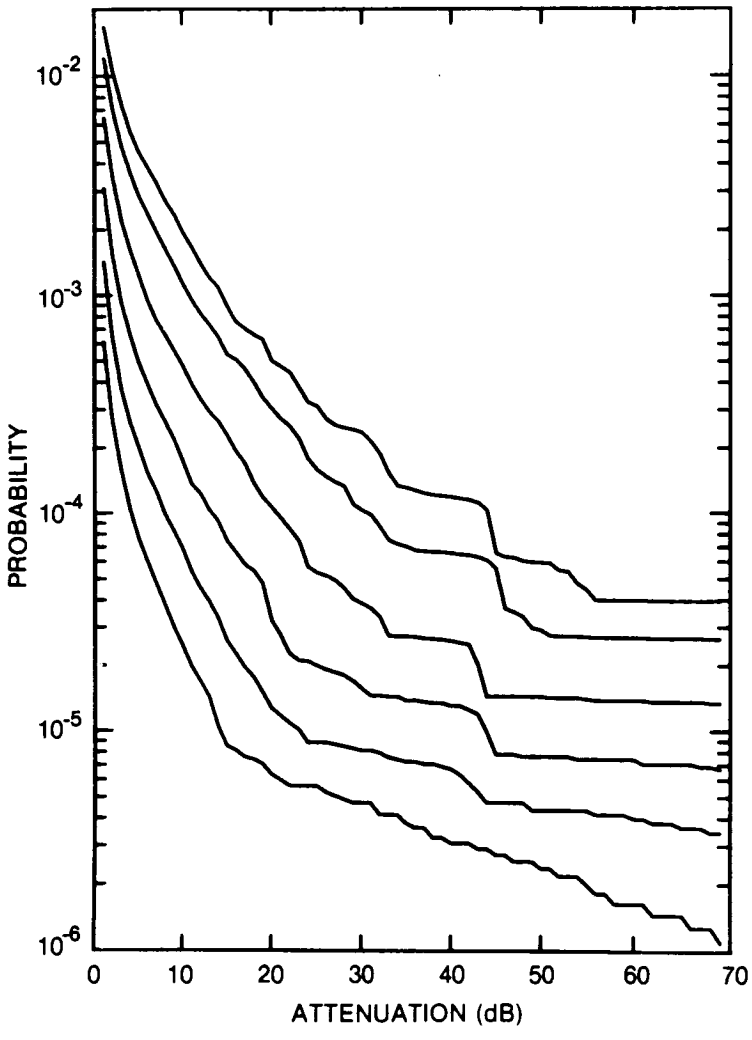

Figure 92. Cumulative distribution of rain attenuation for 12.8 GHz at Dauphin, MAN. Curves, moving from lowest to highest, are for hop lengths of 5, 10, 20, 40, 80 and 120 km, respectively.

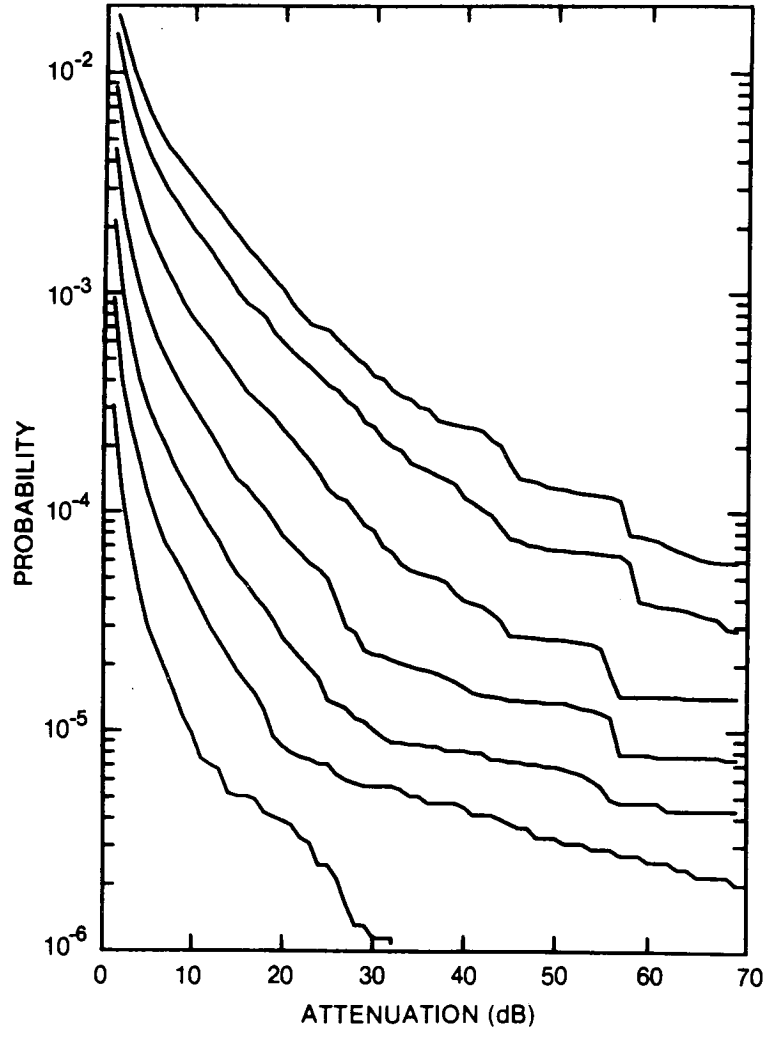

Figure 93. Cumulative distribution of rain attenuation for 15 GHz at Dauphin, MAN. Curves, moving from lowest to highest, are for hop lengths of 2, 5, 10, 20, 40, 80 and 120 km, respectively.

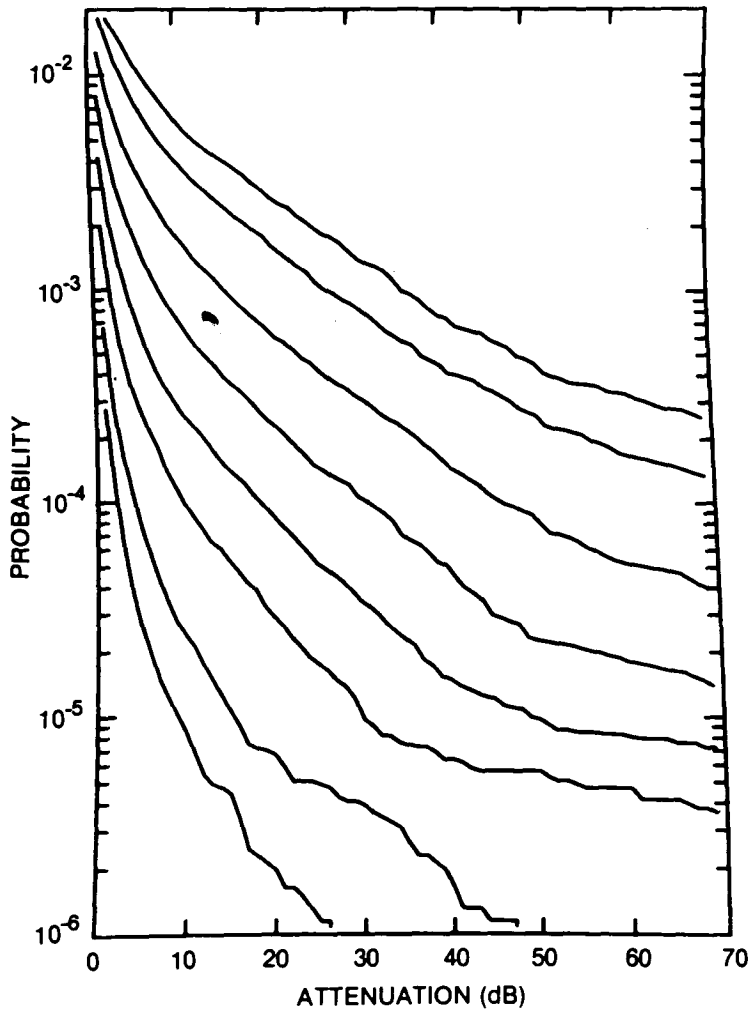

Figure 94. Cumulative distribution of rain attenuation for 20 GHz at Dauphin, MAN. Curves, moving from lowest to highest, are for hop lengths of 1, 2, 5, 10, 20, 40, 80 and 120 km, respectively.

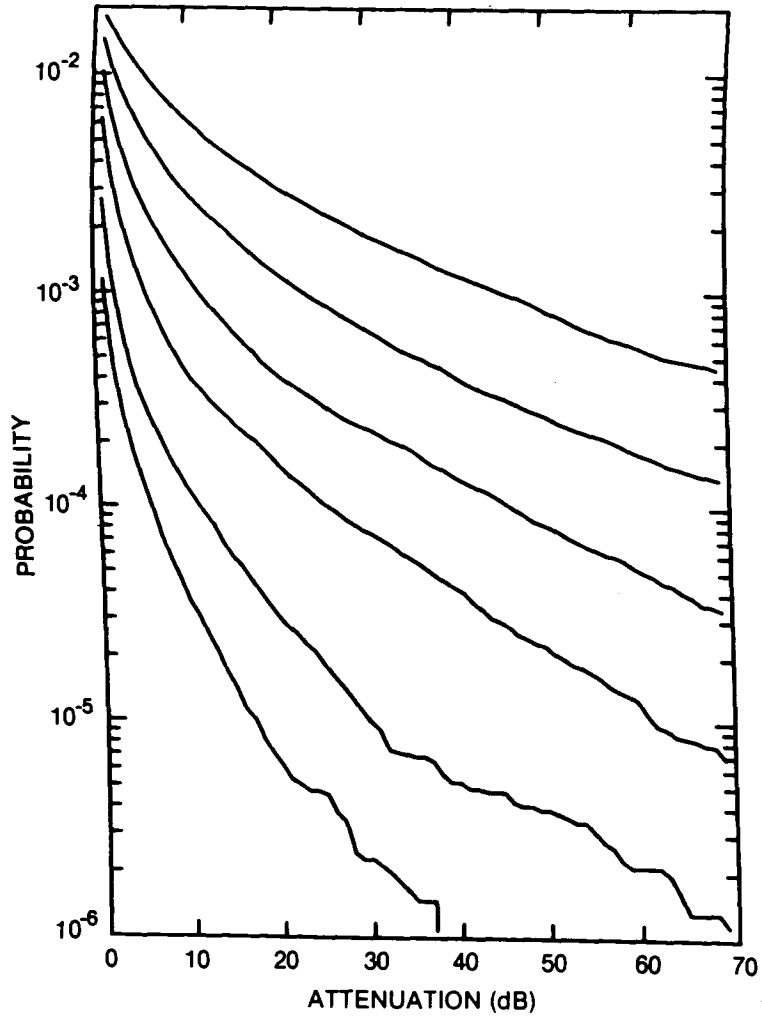

Figure 95. Cumulative distribution of rain attenuation for 35 GHz at Dauphin, MAN. Curves, moving from lowest to highest, are for hop lengths of 1, 2, 5, 10, 20 and 40 km, respectively.

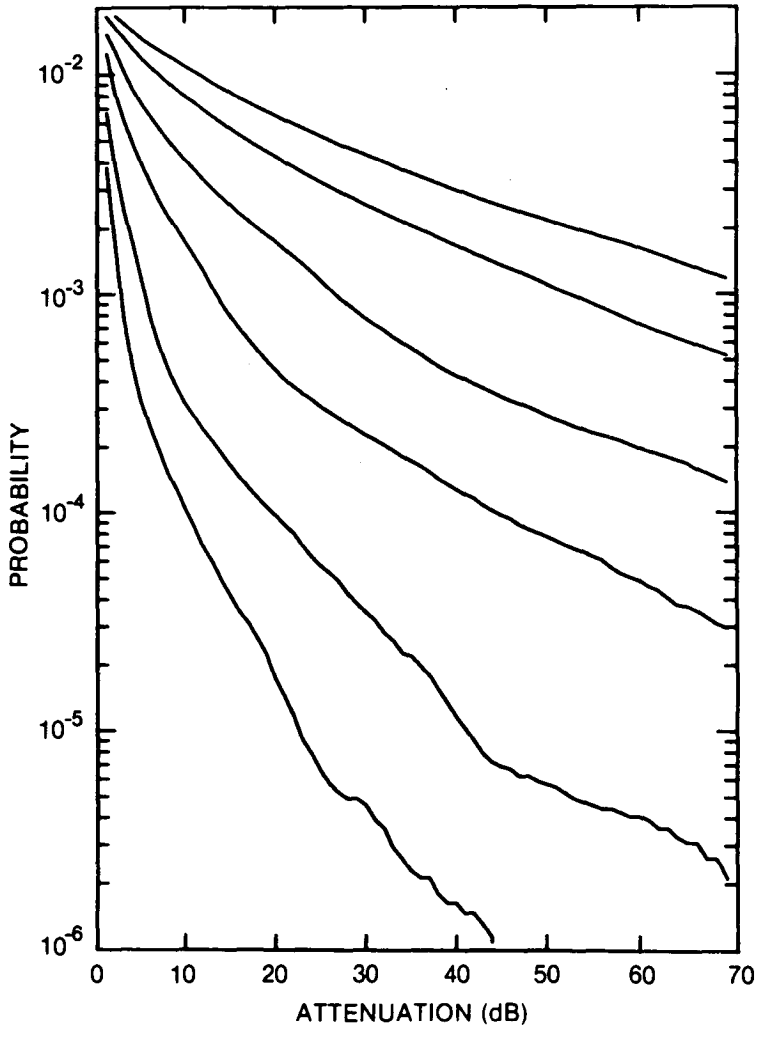

Figure 96. Cumulative distribution of rain attenuation for 56 GHz at Dauphin, MAN. Curves, moving from lowest to highest, are for hop lengths of 1, 2, 5, 10, 20 and 30 km, respectively.

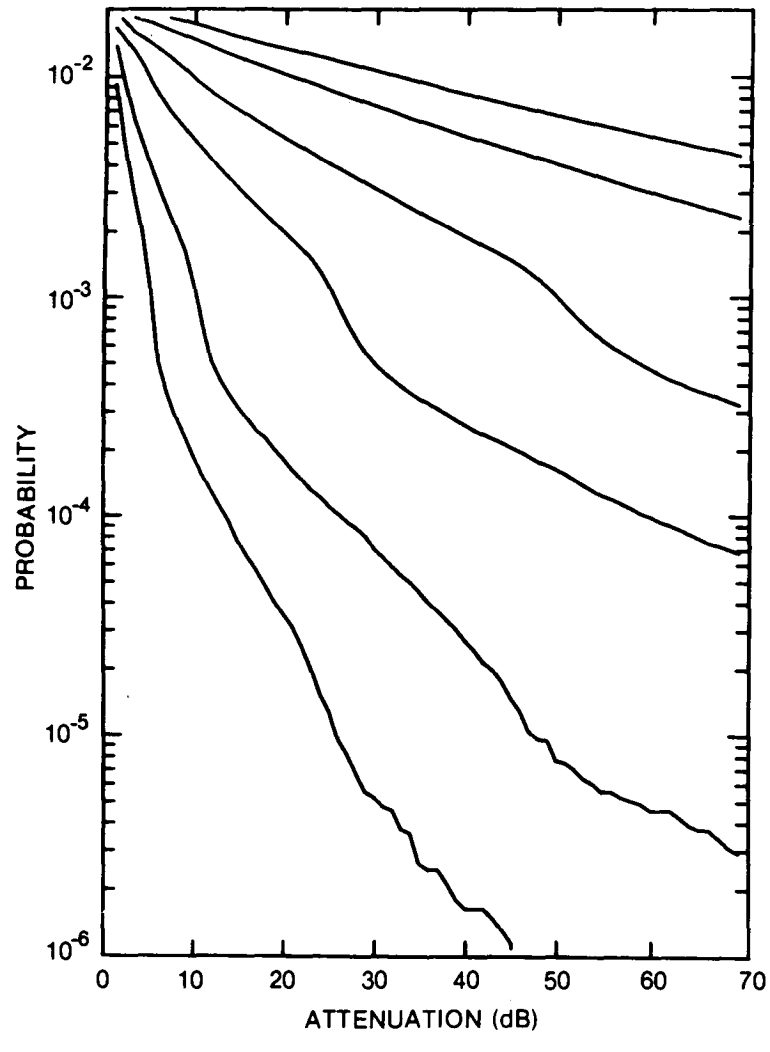

Figure 97. Cumulative distribution of rain attenuation for 100 GHz at Dauphin, MAN. Curves, moving from lowest to highest, are hop lengths of 1, 2, 5, 10, 20 and 30 km, respectively.

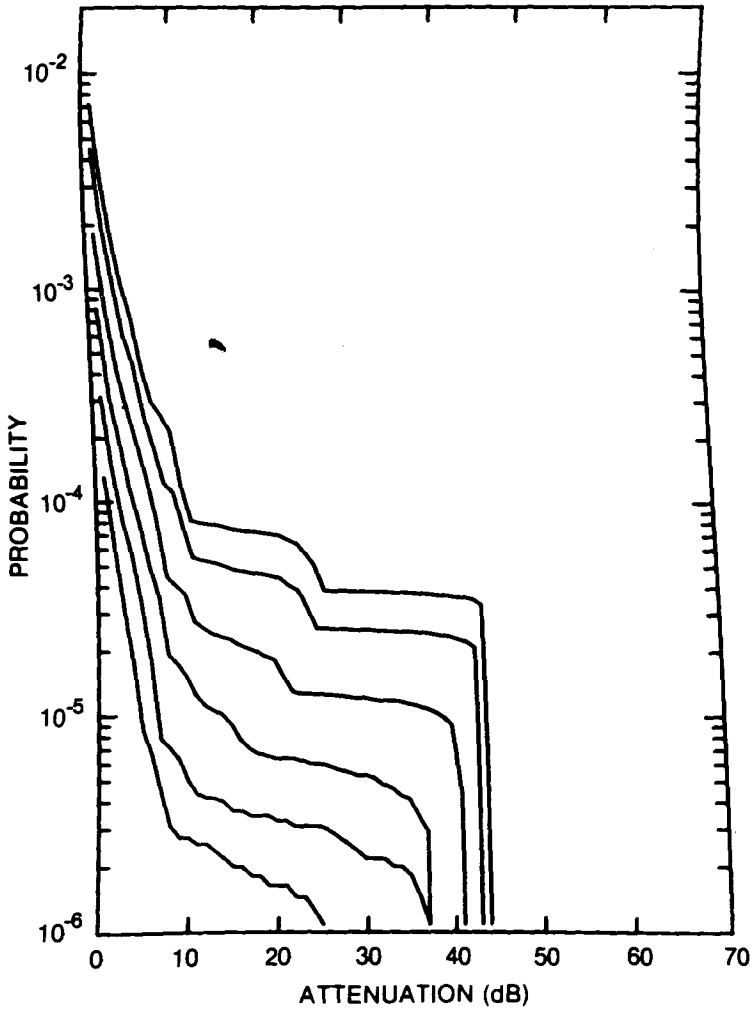

Figure 98. Cumulative distribution of rain attenuation for 8 GHz at Edmonton, ALTA. Curves, moving from lowest to highest, are for hop lengths of 5, 10, 20, 40, 80 and 120 km, respectively.

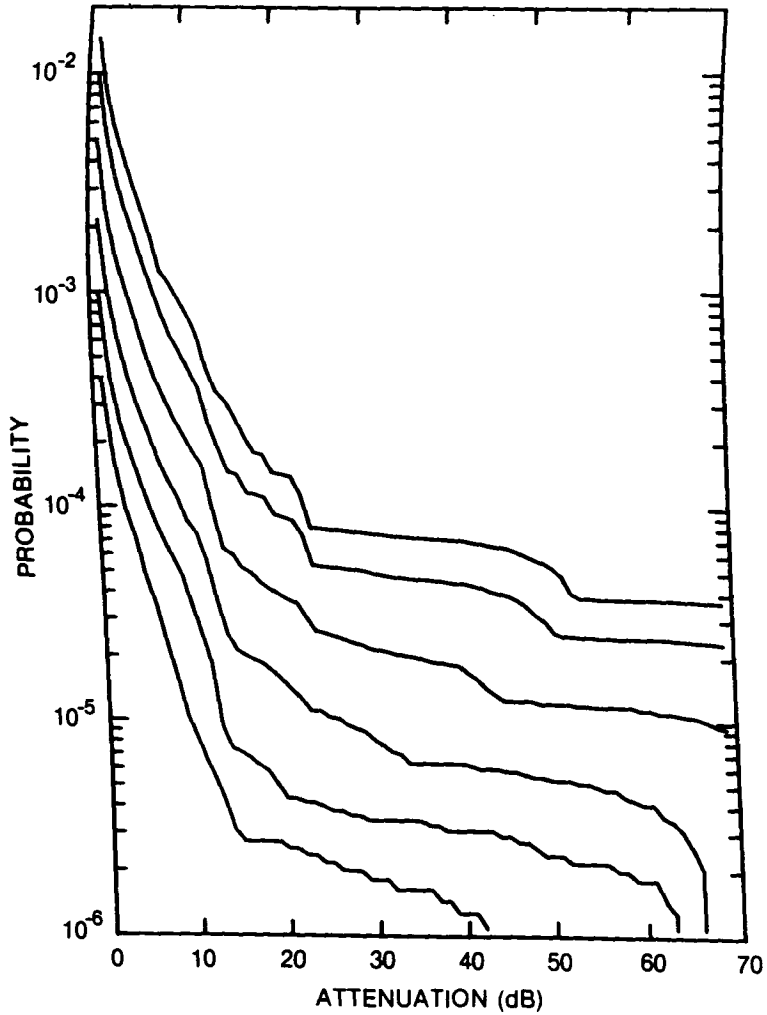

Figure 99. Cumulative distribution of rain attenuation for 11 GHz at Edmonton, ALTA. Curves, moving from lowest to highest, are for hop lengths of 5, 10, 20, 40, 80 and 120 km, respectively.

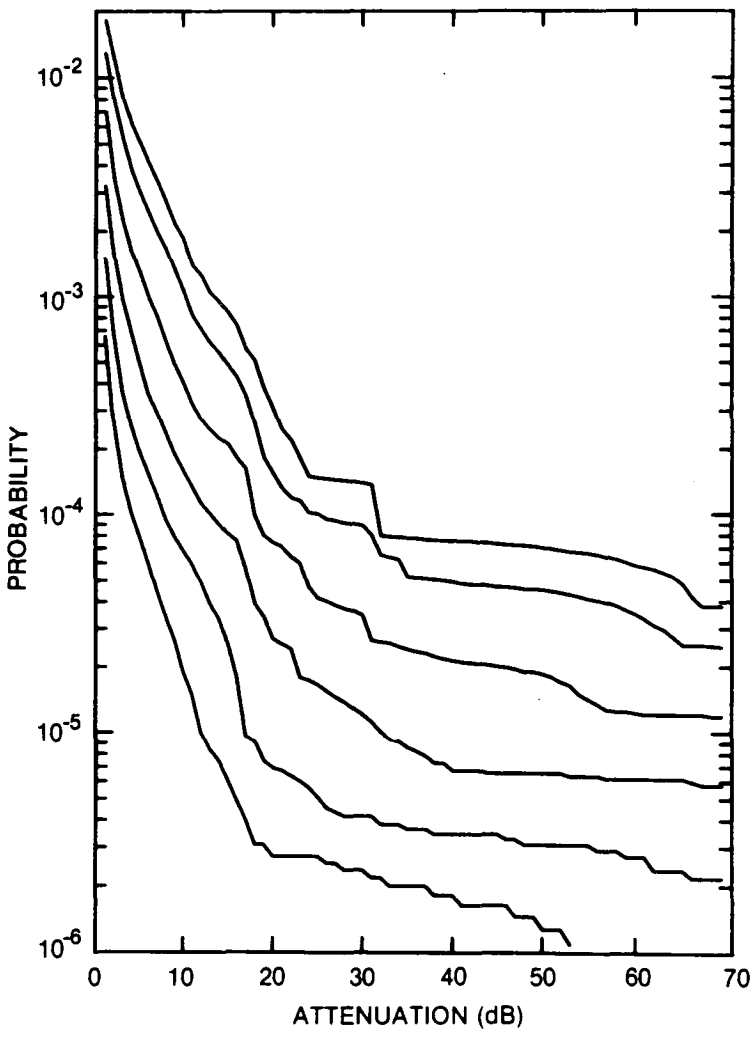

Figure 100. Cumulative distribution of rain attenuation for 12.8 GHz at Edmonton, ALTA. Curves, moving from lowest to highest, are for hop lengths of 5, 10, 20, 40, 80 and 120 km, respectively.

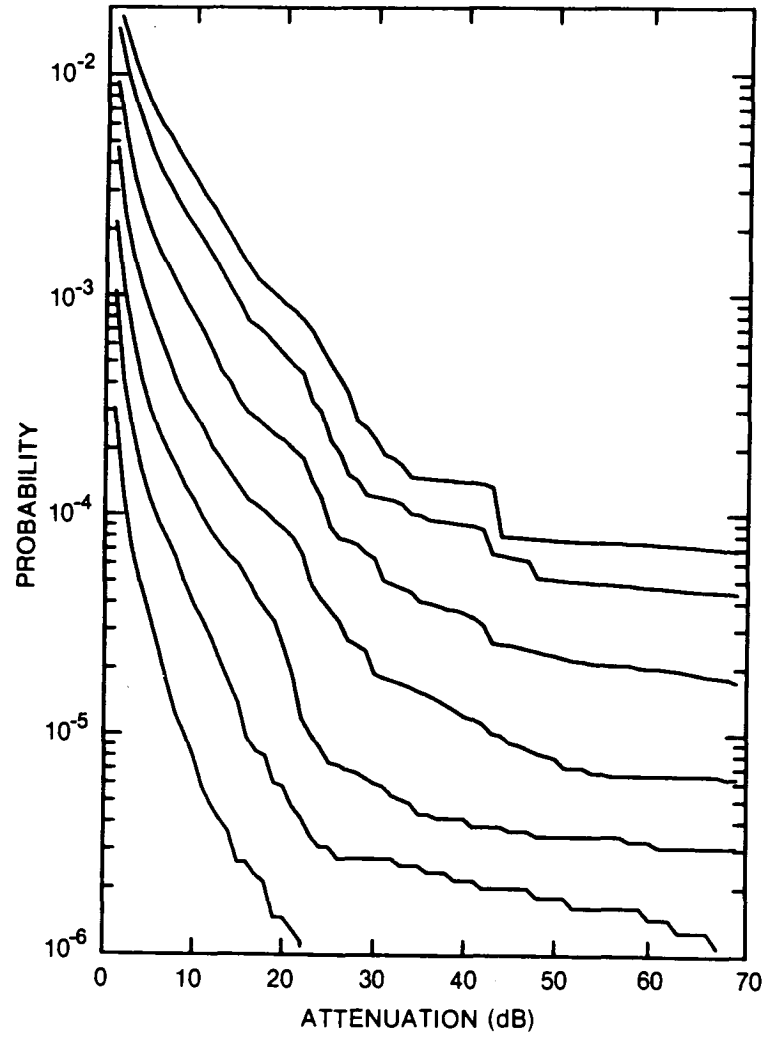

Figure 101. Cumulative distribution of rain attenuation for 15 GHz at Edmonton, ALTA. Curves, moving from lowest to highest, are for hop lengths of 2, 5, 10, 20, 40, 80 and 120 km, respectively.

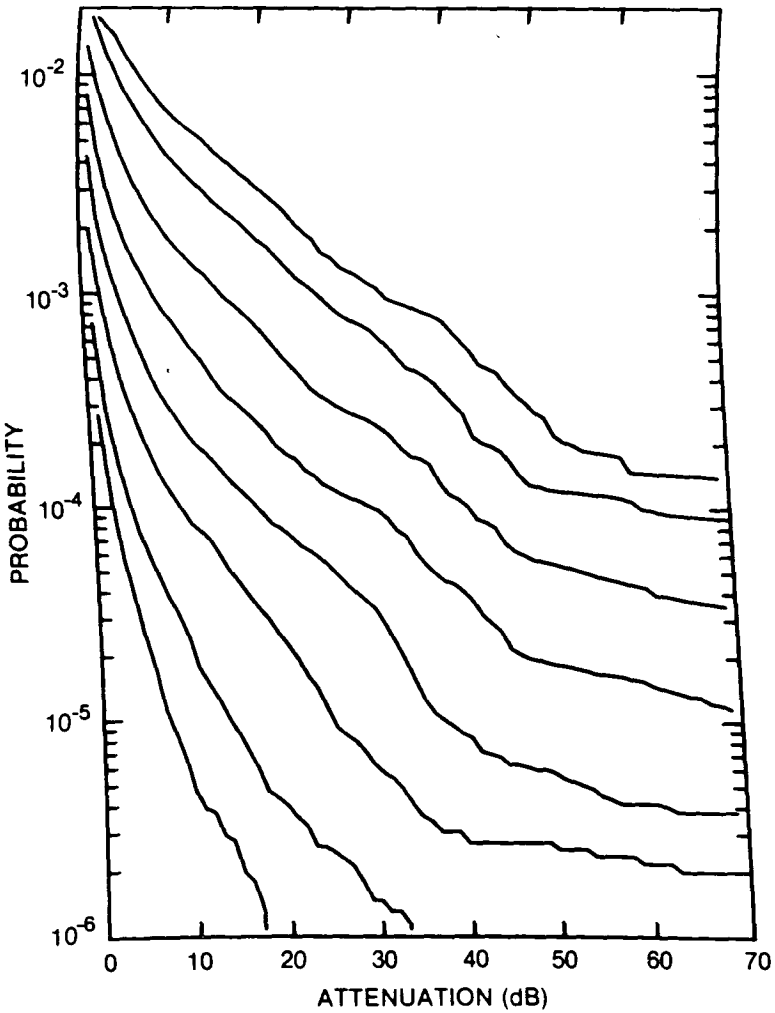

Figure 102. Cumulative distribution of rain attenuation for 20 GHz at Edmonton, ALTA. Curves, moving from lowest to highest, are for hop lengths of 1, 2, 5, 10, 20, 40, 80 and 120 km, respectively.

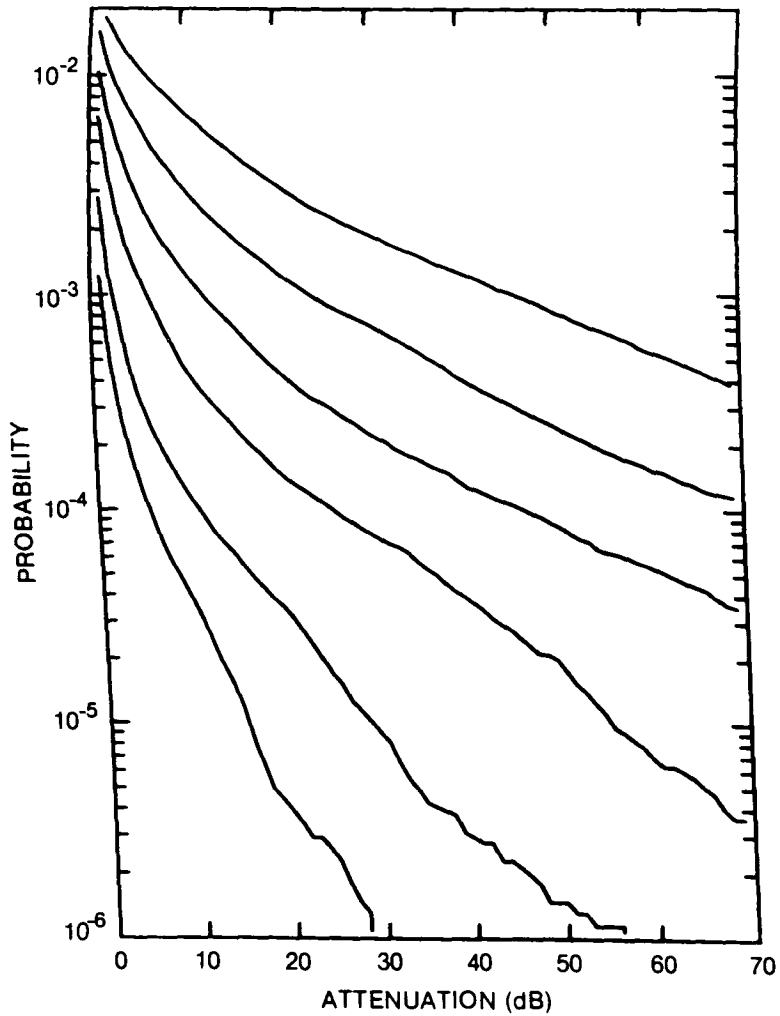

Figure 103. Cumulative distribution of rain attenuation for 35 GHz at Edmonton, ALTA. Curves, moving from lowest to highest, are for hop lengths of 1, 2, 5, 10, 20 and 40 km, respectively.

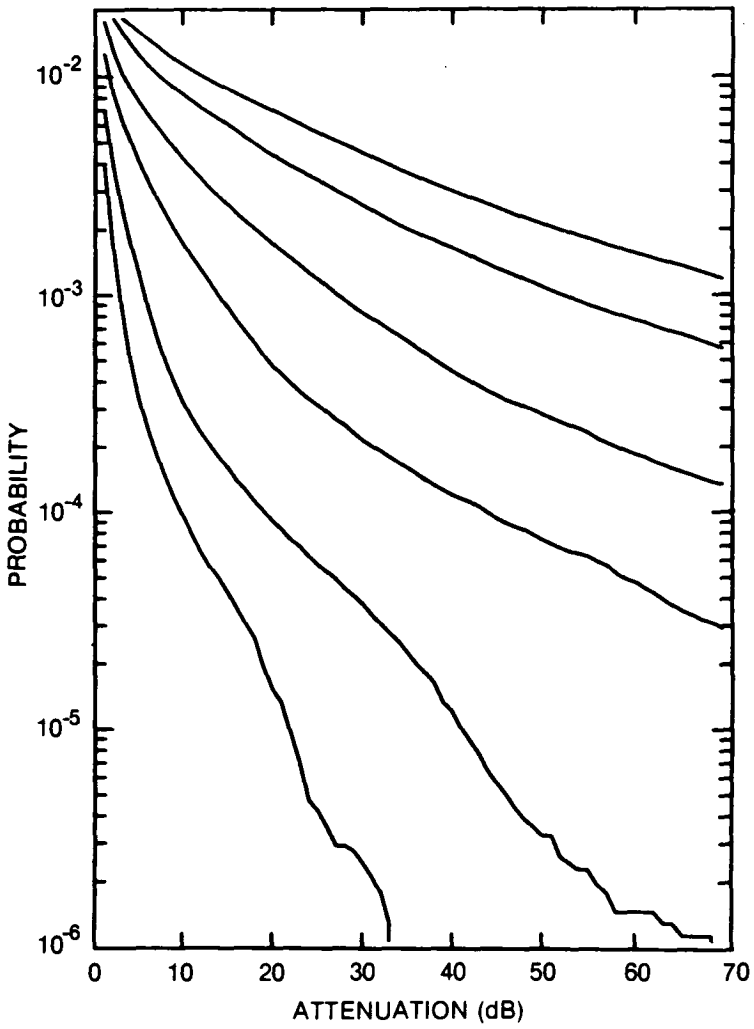

Figure 104. Cumulative distribution of rain attenuation for 56 GHz at Edmonton, ALTA. Curves, moving from lowest to highest, are for hop lengths of 1, 2, 5, 10, 20 and 30 km, respectively.

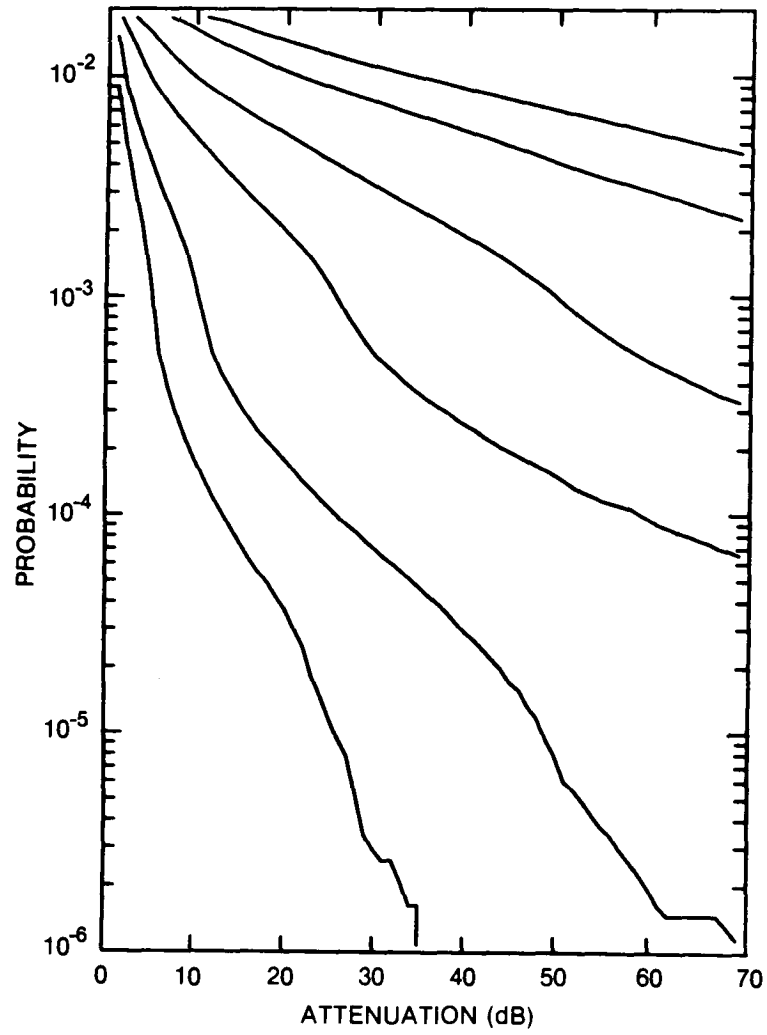

Figure 105. Cumulative distribution of rain attenuation for 100 GHz at Edmonton, ALTA. Curves, moving from lowest to highest, are for hop lengths of 1, 2, 5, 10, 20 and 30 km, respectively.

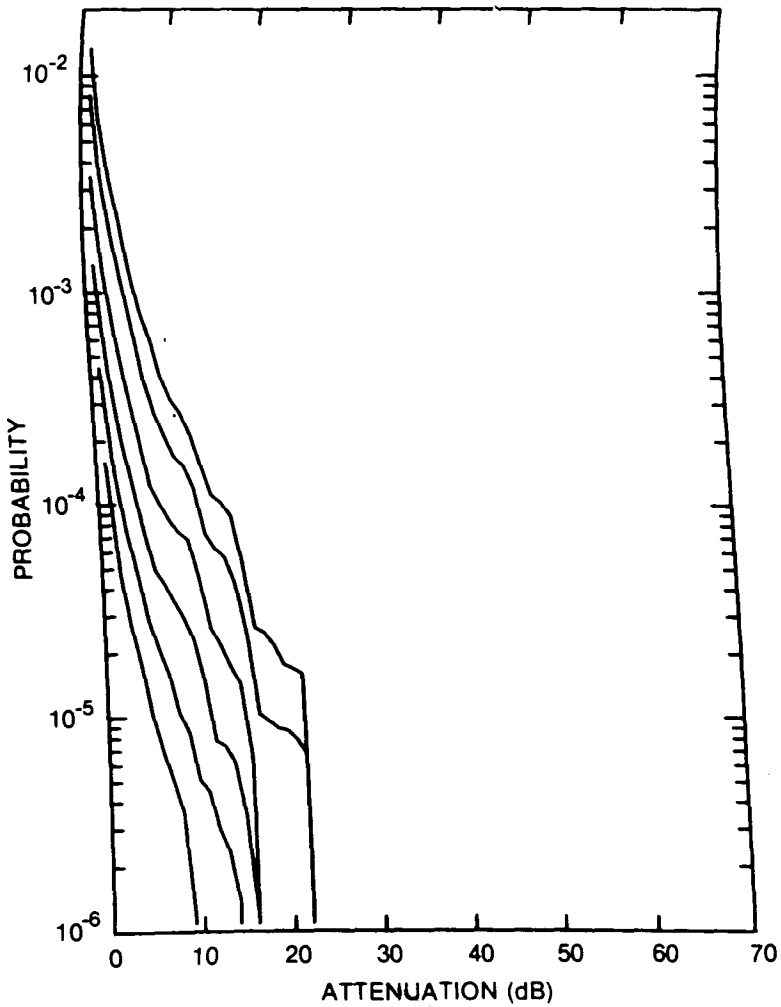

Figure 106. Cumulative distribution of rain attenuation for 8 GHz at Fredericton, NB. Curves, moving from lowest to highest, are for hop lengths of 5, 10, 20, 40, 80 and 120 km, respectively.

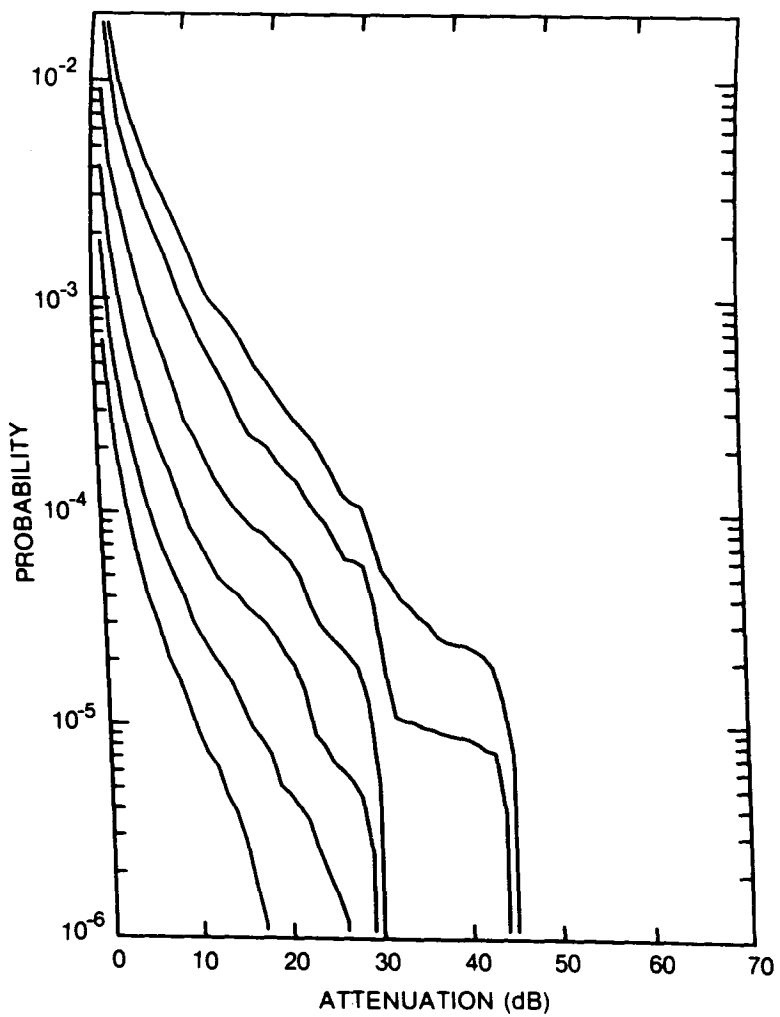

Figure 107. Cumulative distribution of rain attenuation for 11 GHz at Fredericton, NB. Curves, moving from lowest to highest, are for hop lengths of 5, 10, 20, 40, 80 and 120 km, respectively.

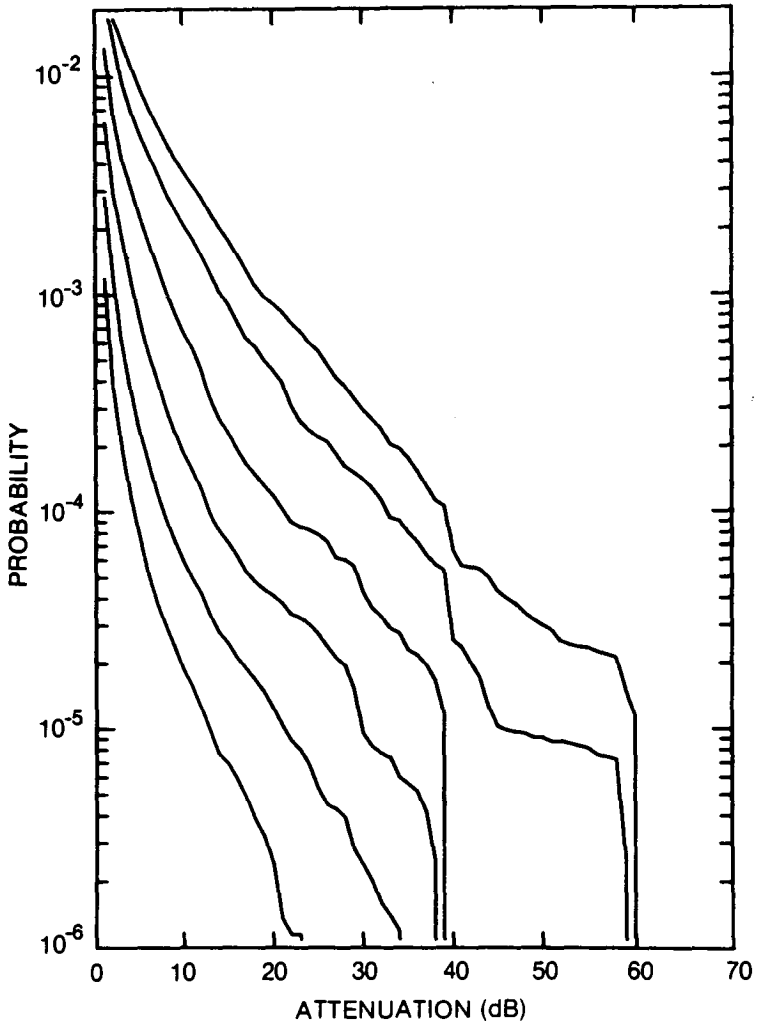

Figure 108. Cumulative distribution of rain attenuation for 12.8 GHz at Fredericton, NB. Curves, moving from lowest to highest, are for hop lengths of 5, 10, 20, 40, 80 and 120 km, respectively.

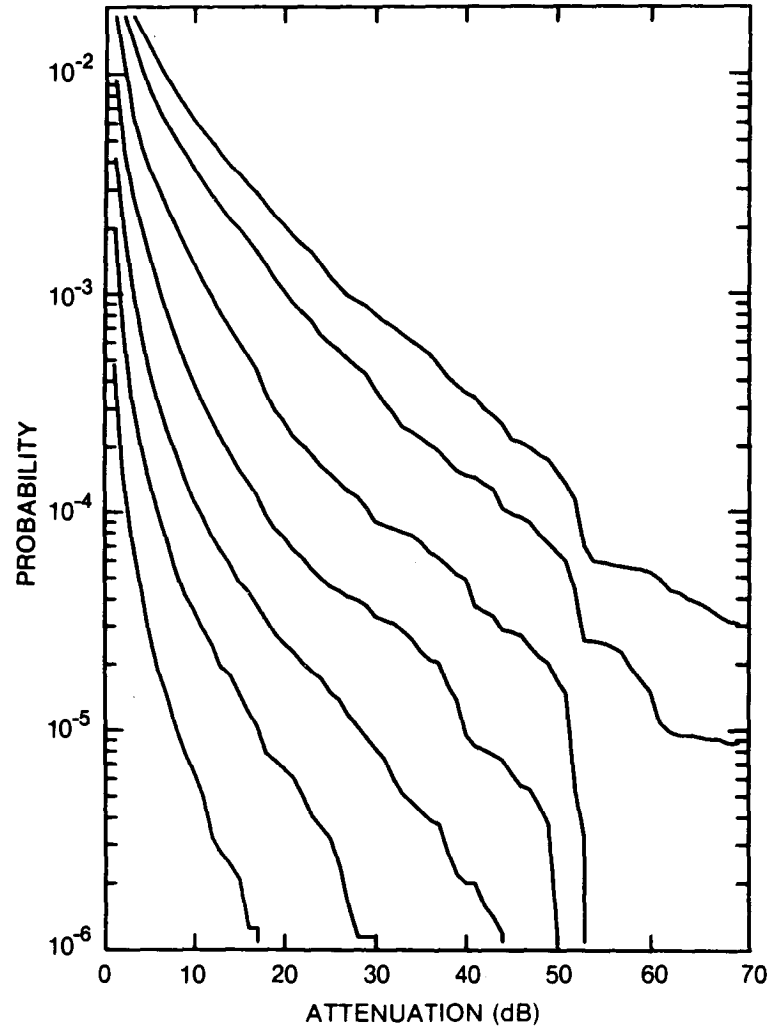

Figure 109. Cumulative distribution of rain attenuation for 15 GHz at Fredericton, NB. Curves, moving from lowest to highest, are for hop lengths of 2, 5, 10, 20, 40, 80 and 120 km, respectively.

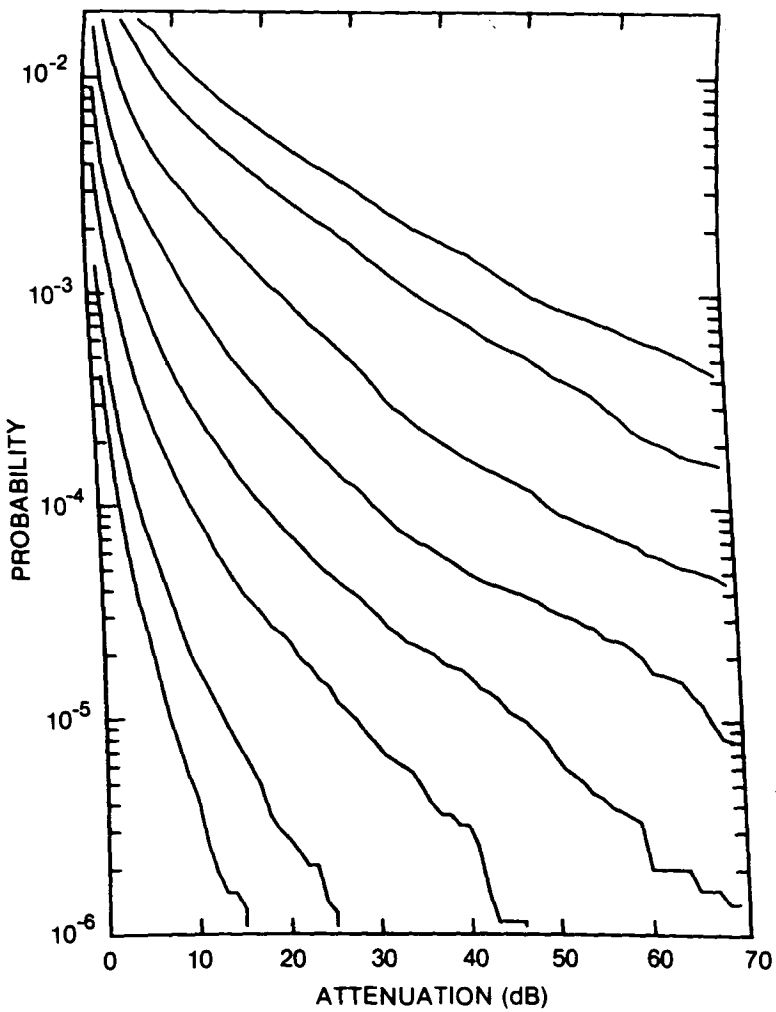

Figure 110. Cumulative distribution of rain attenuation for 20 GHz at Fredericton, NB. Curves, moving from lowest to highest, are for hop lengths of 1, 2, 5, 10, 20, 40, 80 and 120 km, respectively.

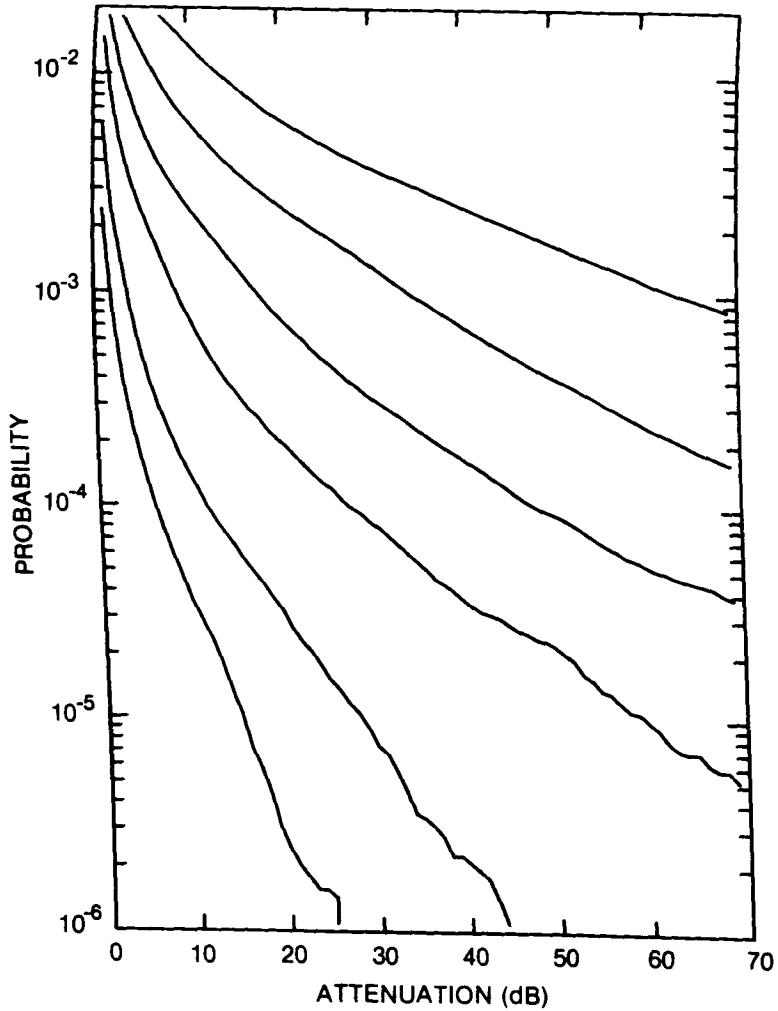

Figure 111. Cumulative distribution of rain attenuation for 35 GHz at Fredericton, ALTA. Curves, moving from lowest to highest, are for hop lengths of 1, 2, 5, 10, 20 and 40 km, respectively.

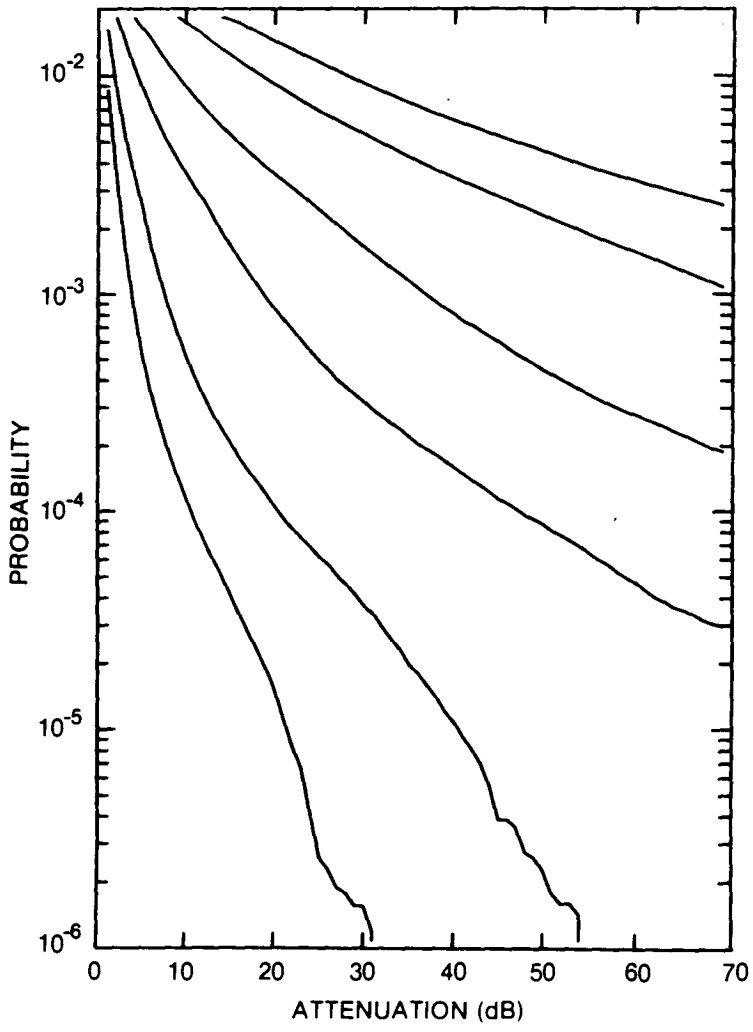

Figure 112. Cumulative distribution of rain attenuation for 56 GHz at Fredericton, NB. Curves, moving from lowest to highest, are for hop lengths of 1, 2, 5, 10, 20 and 30 km, respectively.

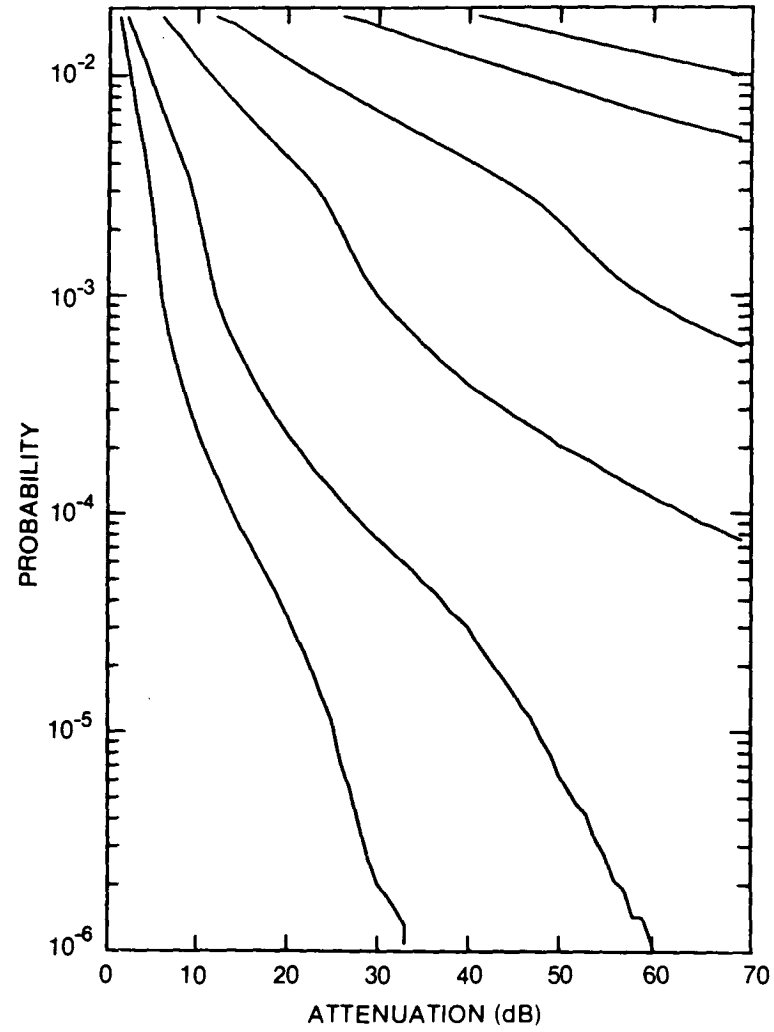

Figure 113. Cumulative distribution of rain attenuation for 100 GHz at Fredericton, NB. Curves, moving from lowest to highest, are for hop lengths of 1, 2, 5, 10, 20 and 30 km, respectively.

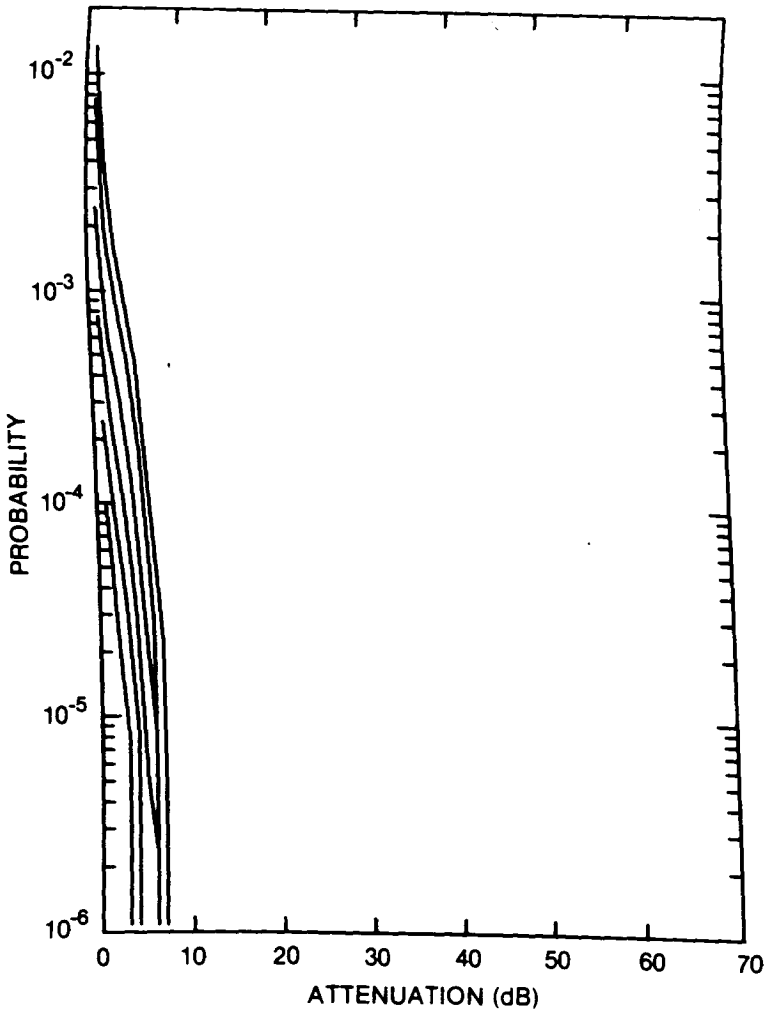

Figure 114. Cumulative distribution of rain attenuation for 8 GHz at Gagnon, QUE. Curves, moving from lowest to highest, are for hop lengths of 5, 10, 20, 40, 80 and 120 km, respectively.

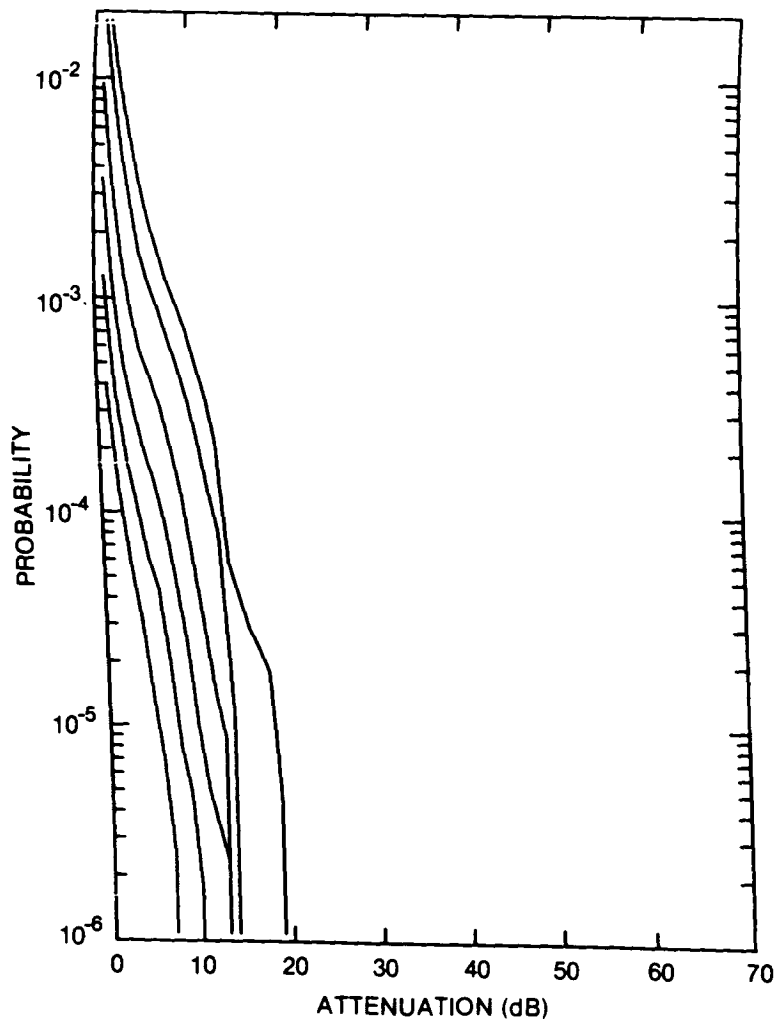

Figure 115. Cumulative distribution of rain attenuation for 11 GHz at Gagnon, QUE. Curves, moving from lowest to highest, are for hop lengths of 5, 10, 20, 40, 80,and 120 km respectively.

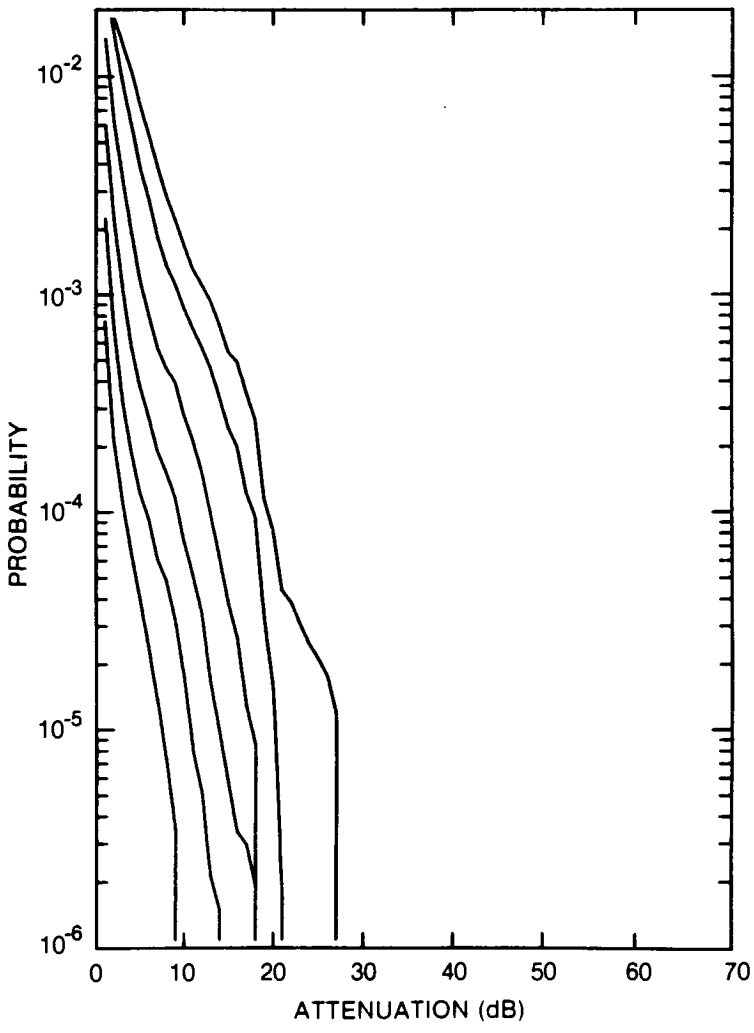

Figure 116. Cumulative distribution of rain attenuation for 12.8 GHz at Gagnon, QUE. Curves, moving from lowest to highest, are for hop lengths of 5, 10, 20, 40, 80 and 120 km, respectively.

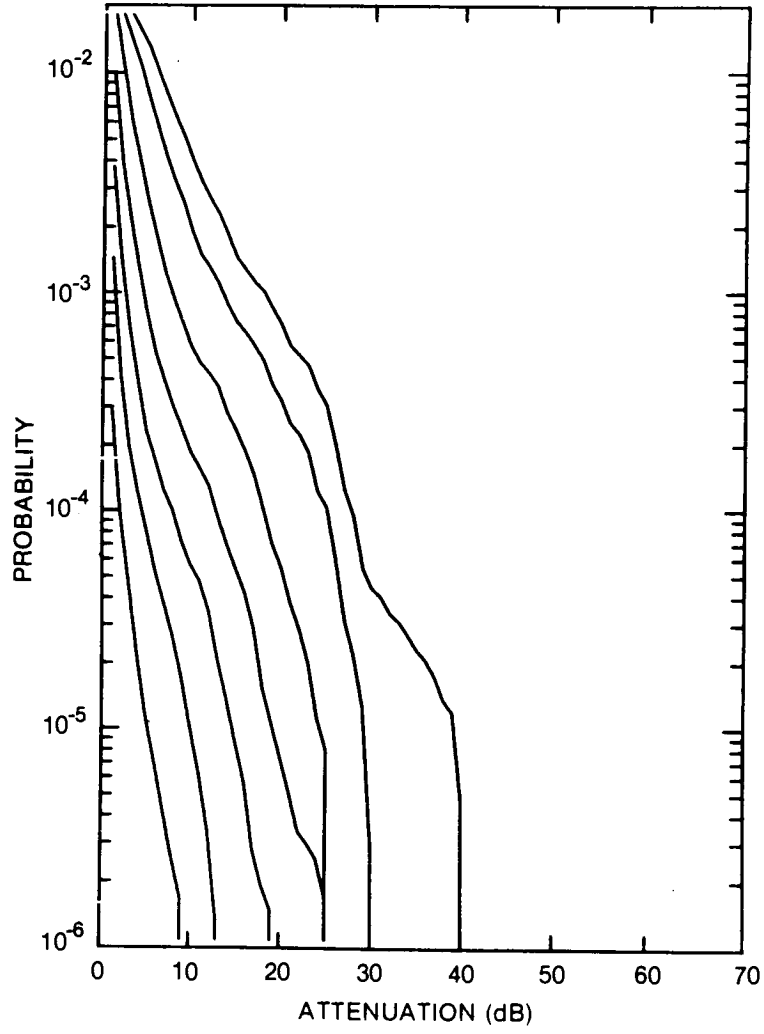

Figure 117. Cumulative distribution of rain attenuation for 15 GHz at Gagnon, QUE. Curves, moving from lowest to highest, are for hop lengths of 2, 5, 10, 20 40, 80 and 120 km, respectively.

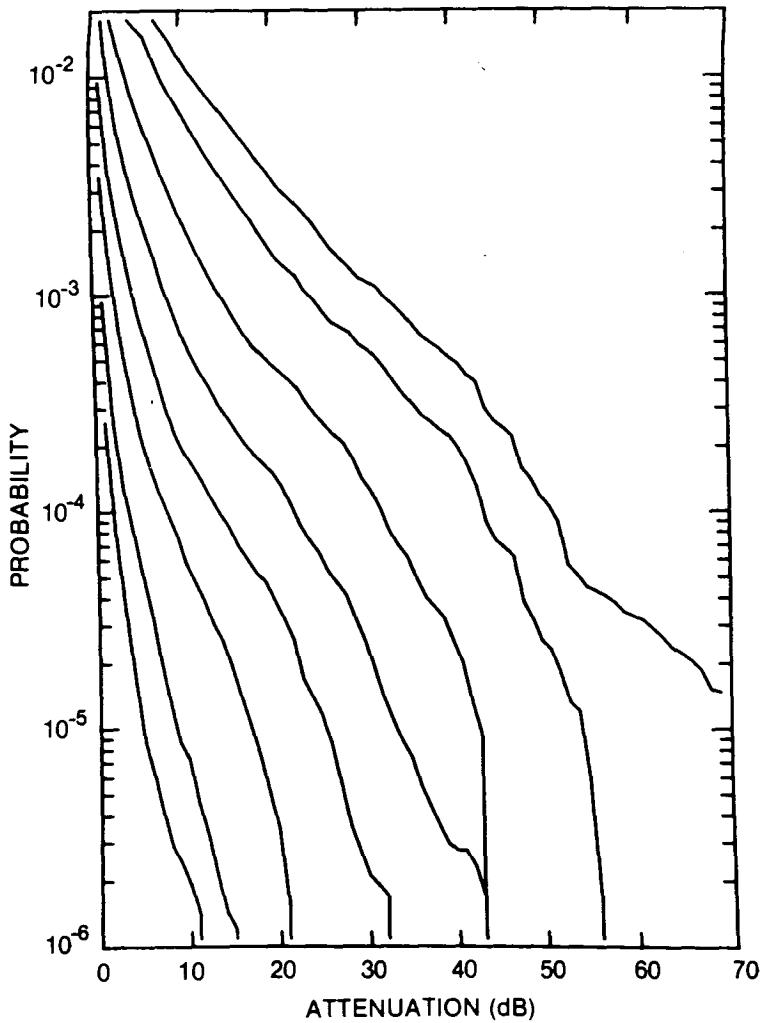

Figure 118. Cumulative distribution of rain attenuation for 20 GHz at Gagnon, QUE. Curves, moving from lowest to highest, are for hop lengths of 1, 2, 5, 10, 10, 40, 80 and 120 km, respectively.

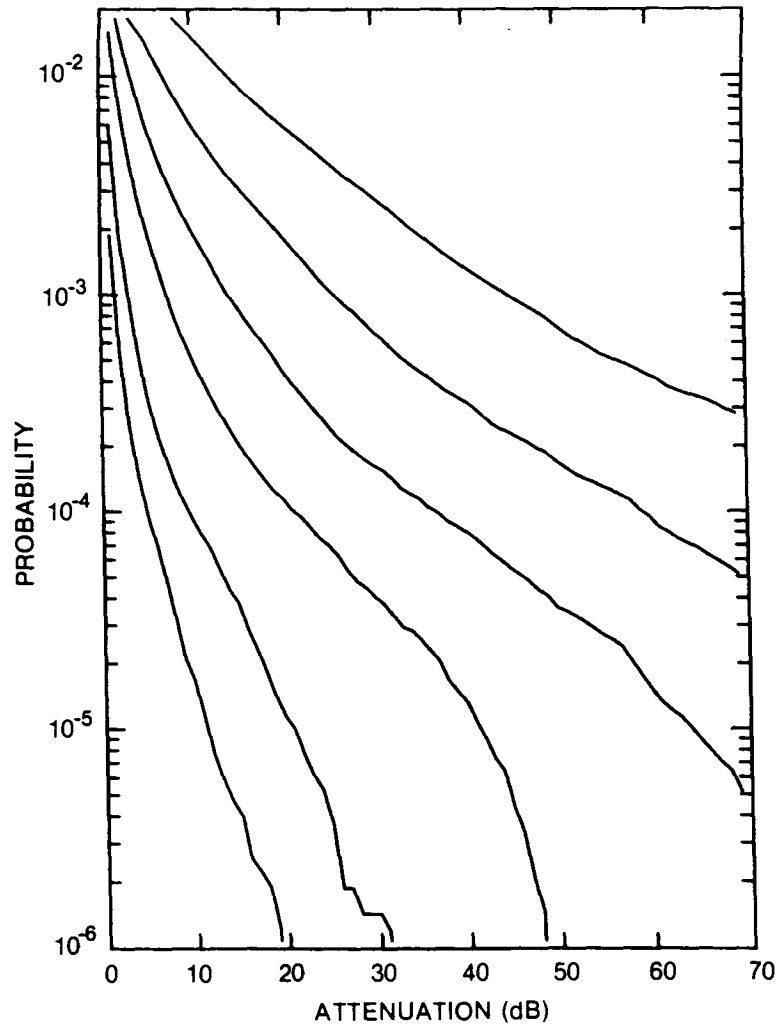

Figure 119. Cumulative distribution of rain attenuation for 35 GHz at Gagnon, QUE. Curves, moving from lowest to highest, are for hop lengths of 1, 2, 5, 10, 20 and 40 km, respectively.

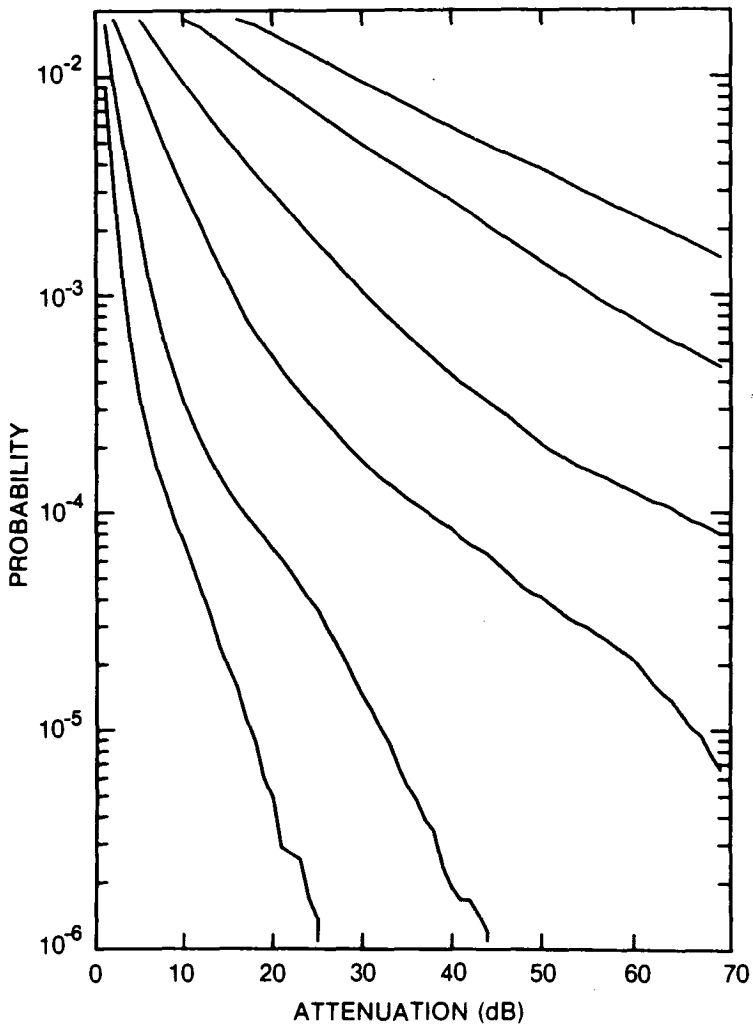

Figure 120. Cumulative distribution of rain attenuation for 56 GHz at Gagnon, QUE. Curves, moving from lowest to highest, are for hop lengths of 1, 2, 5, 10, 20 and 30 km, respectively.

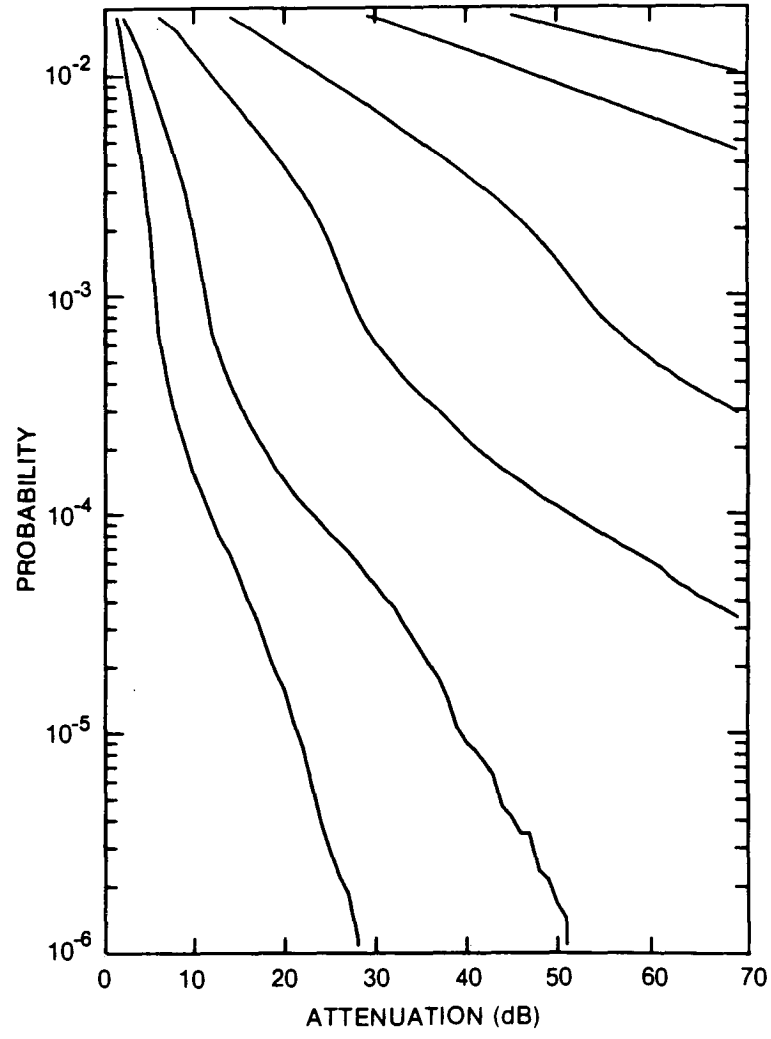

Figure 121. Cumulative distribution of rain attenuation for 100 GHz at Gagnon, QUE. Curves, moving from lowest to highest, are for hop lengths of 1, 2, 5, 10, 20 and 30 km, respectively.

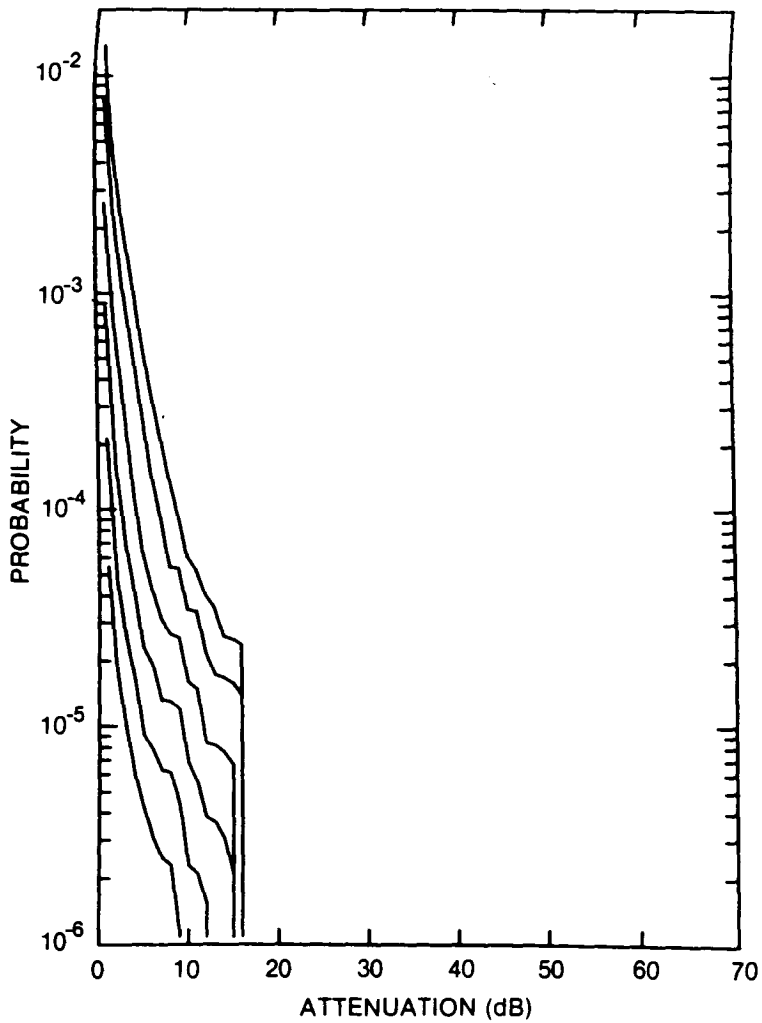

Figure 122. Cumulative distribution of rain attenuation for 8 GHz at Gander, NFLD. Curves, moving from lowest to highest, are for hop lengths of 5, 10, 20, 40, 80 and 120 km, respectively.

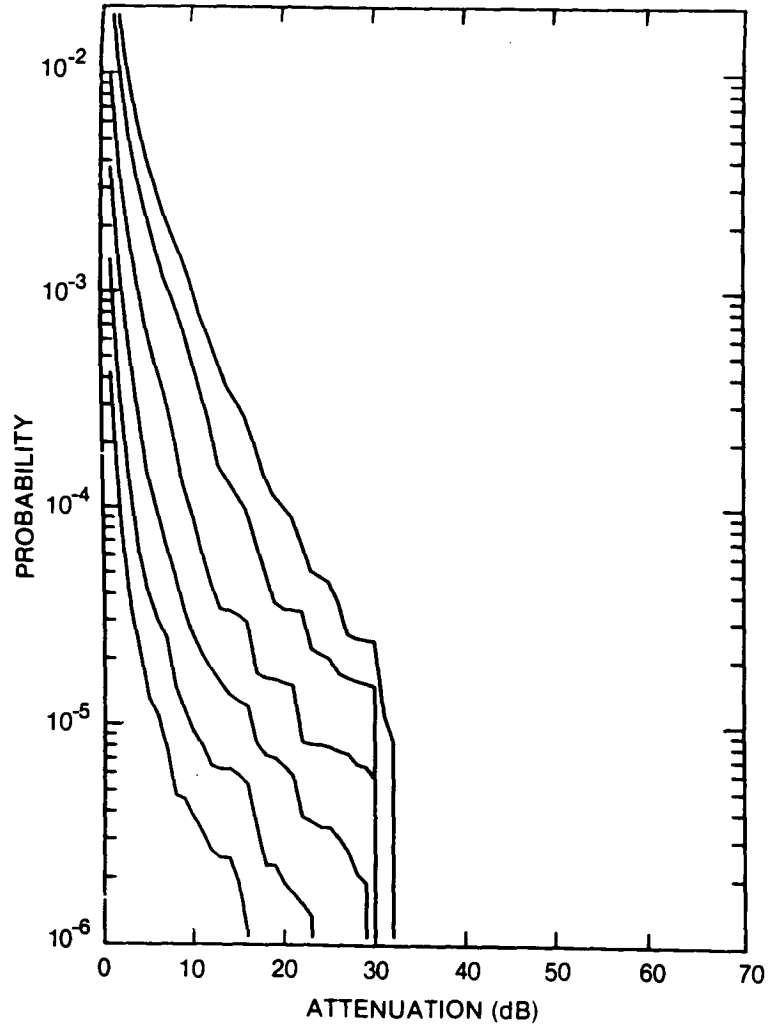

Figure 123. Cumulative distribution of rain attenuation for 11 GHz at Gander, NFLD. Curves, moving from lowest to highest, are for hop lengths of 5, 10, 20, 40, 80 and 120 km, respectively.

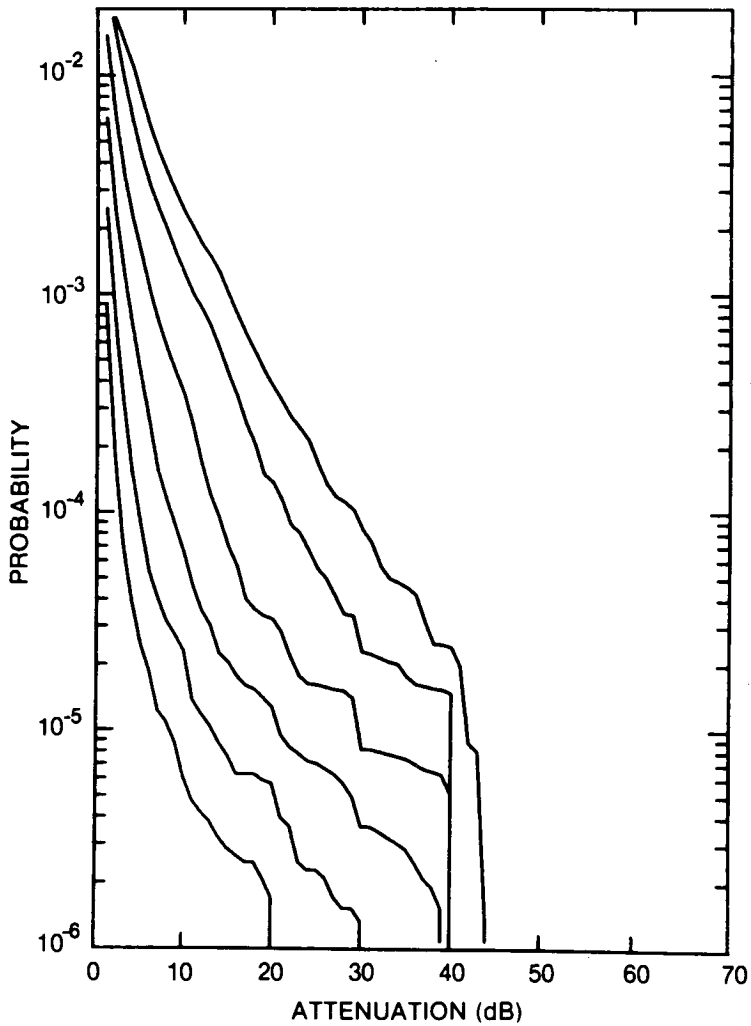

Figure 124. Cumulative distribution of rain attenuation for 12.8 GHz at Gander, NFLD. Curves, moving from lowest to highest, are for hop lengths of 5, 10, 20, 40, 80 and 120 km, respectively.

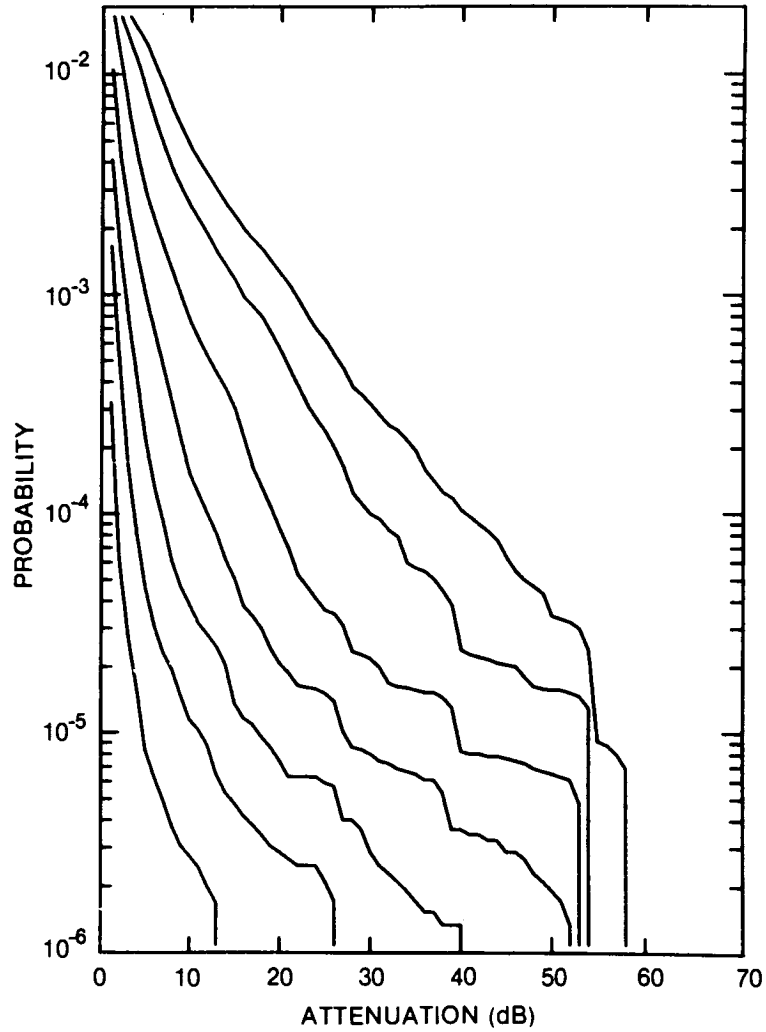

Figure 125. Cumulative distribution of rain attenuation for 15 GHz at Gander, NFLD. Curves, moving from lowest to highest, are for hop lengths of 2, 5, 10, 20, 40, 80 and 120 km, respectively.

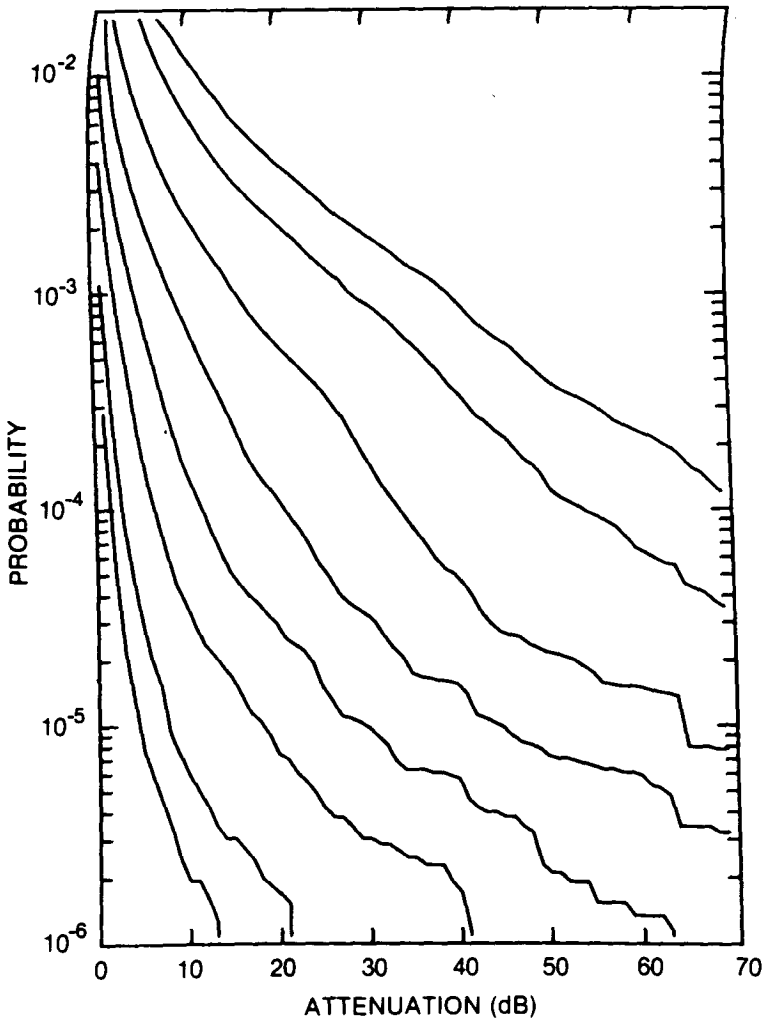

Figure 126. Cumulative distribution of rain attenuation for 20 GHz at Gander, NFLD. Curves, moving from lowest to highest, are for hop lengths of 1, 2, 5, 10, 20, 40, 80 and 120 km, respectively.

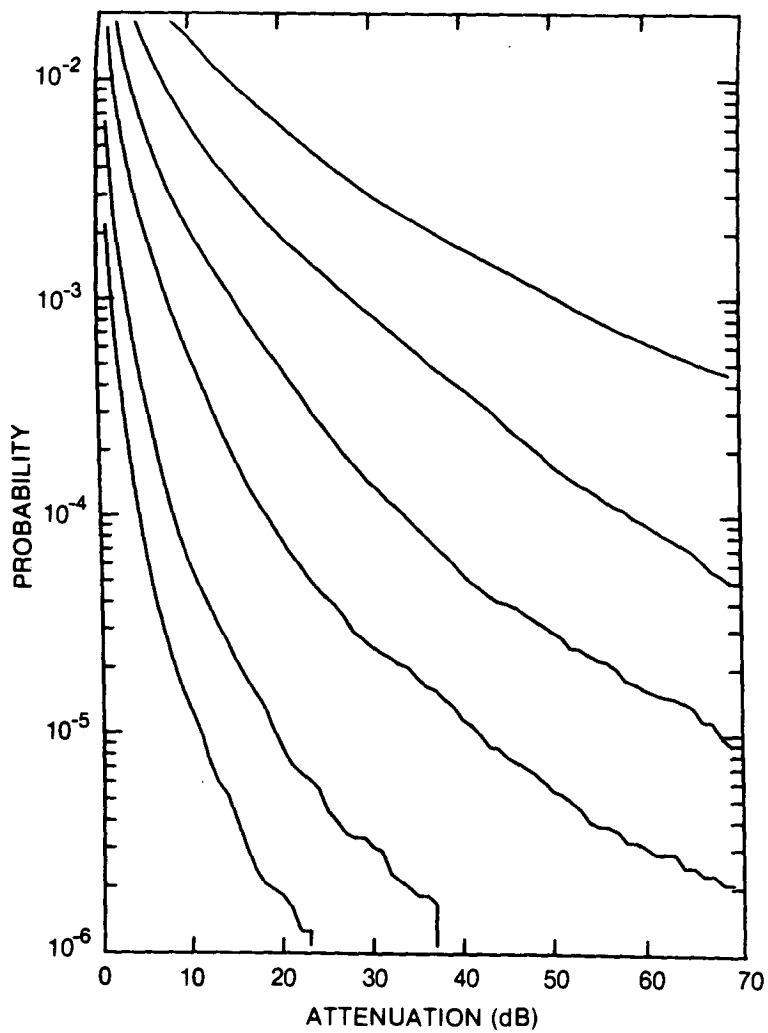

Figure 127. Cumulative distribution of rain attenuation for 35 GHz at Gander, NFLD. Curves, moving from lowest to highest, are for hop lengths of 1, 2, 5, 10, 20 and 40 km, respectively.

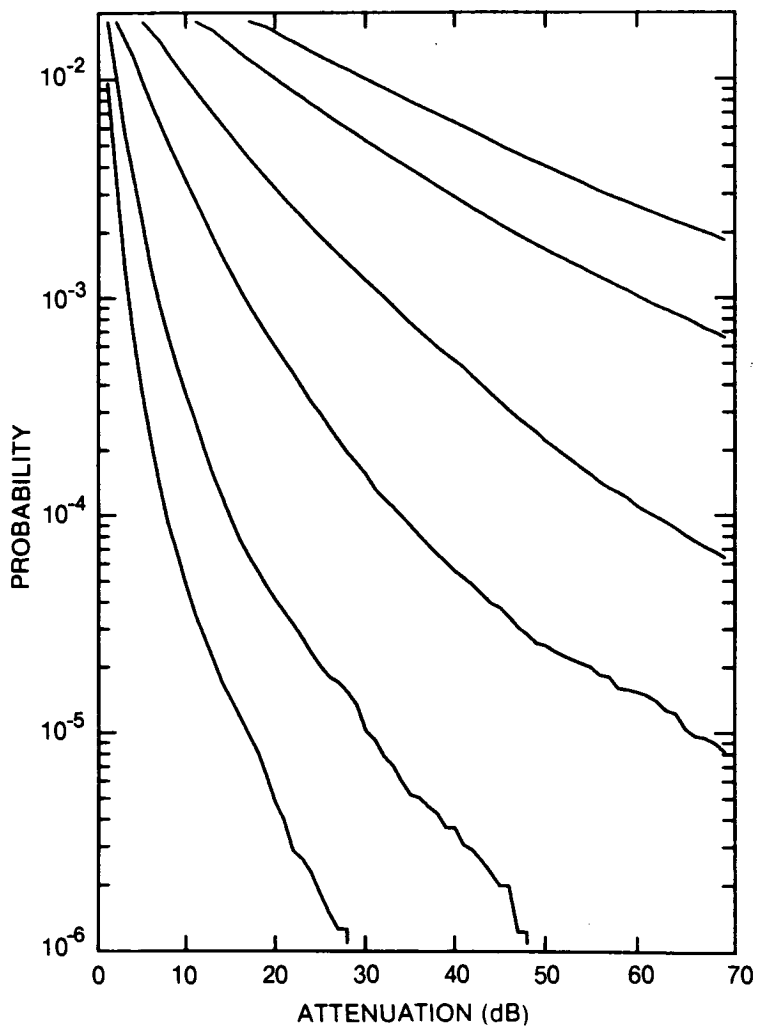

Figure 128. Cumulative distribution of rain attenuation for 56 GHz at Gander, NFLD. Curves, moving from lowest to highest, are for hop lengths of 1, 2, 5, 10, 20 and 30 km, respectively.

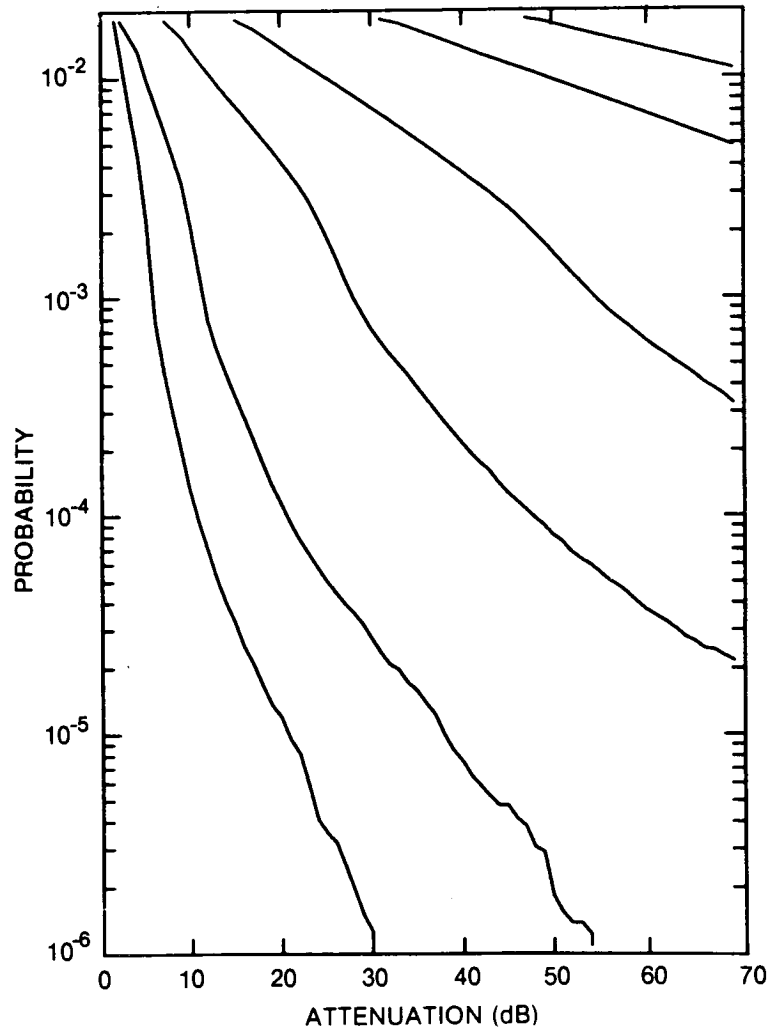

Figure 129. Cumulative distribution of rain attenuation for 100 GHz at Gander, NFLD. Curves, moving from lowest to highest, are for hop lengths of 1, 2, 5, 10, 20 and 30 km, respectively.

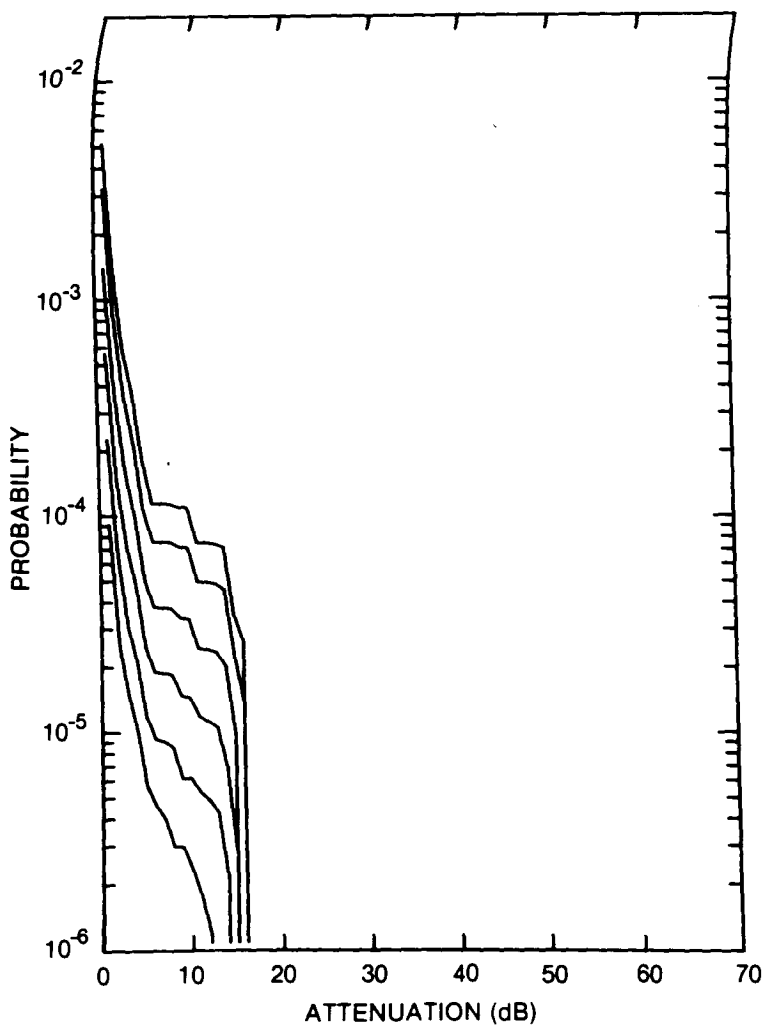

Figure 130. Cumulative distribution of rain attenuation for 8 GHz at Geraldton, ONT. Curves, moving from lowest to highest, are for hop lengths of 5, 10, 20, 40, 80 and 120 km, respectively.

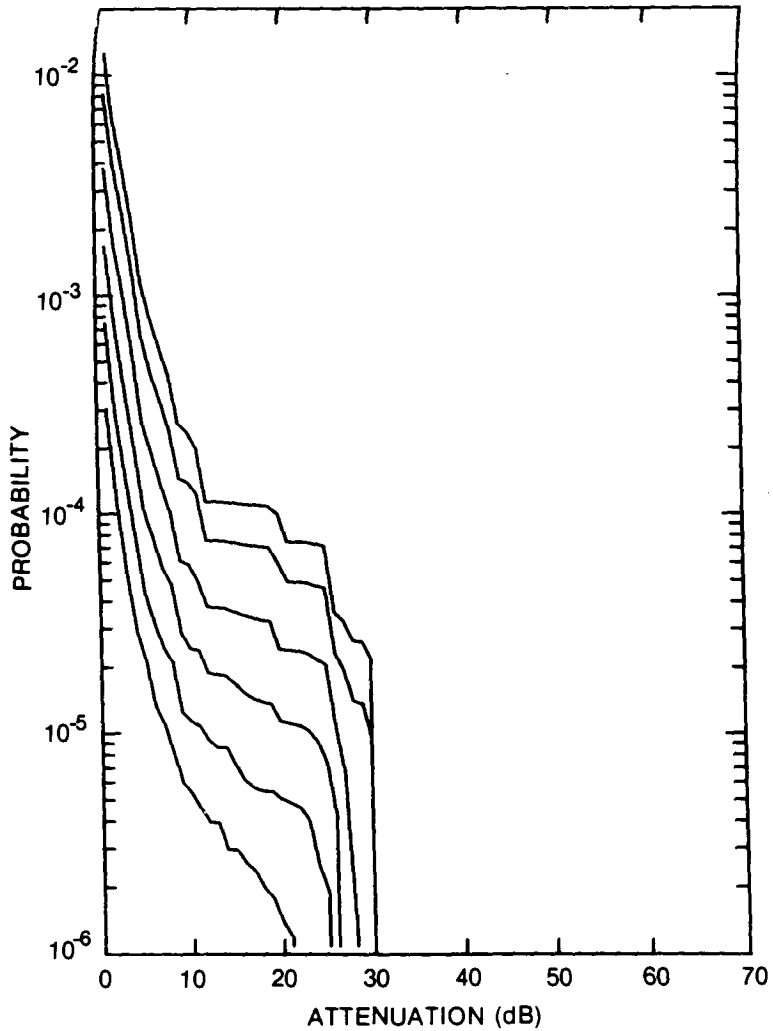

Figure 131. Cumulative distribution of rain attenuation for 11 GHz at Geraldton, ONT. Curves, moving from lowest to highest, are for hop lengths of 5, 10, 20, 40, 80 and 120 km, respectively.

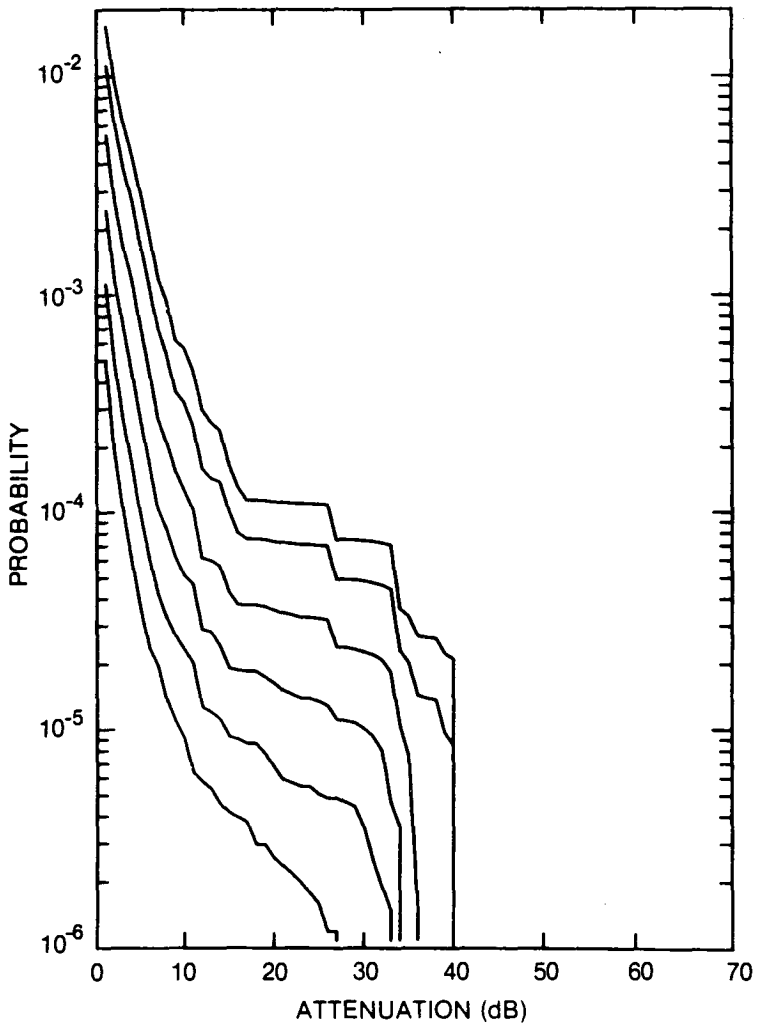

Figure 132. Cumulative distribution of rain attenuation for 12.8 GHz at Geraldton, ONT. Curves, moving from lowest to highest, are for hop lengths of 5, 10, 20, 40, 80 and 120 km, respectively.

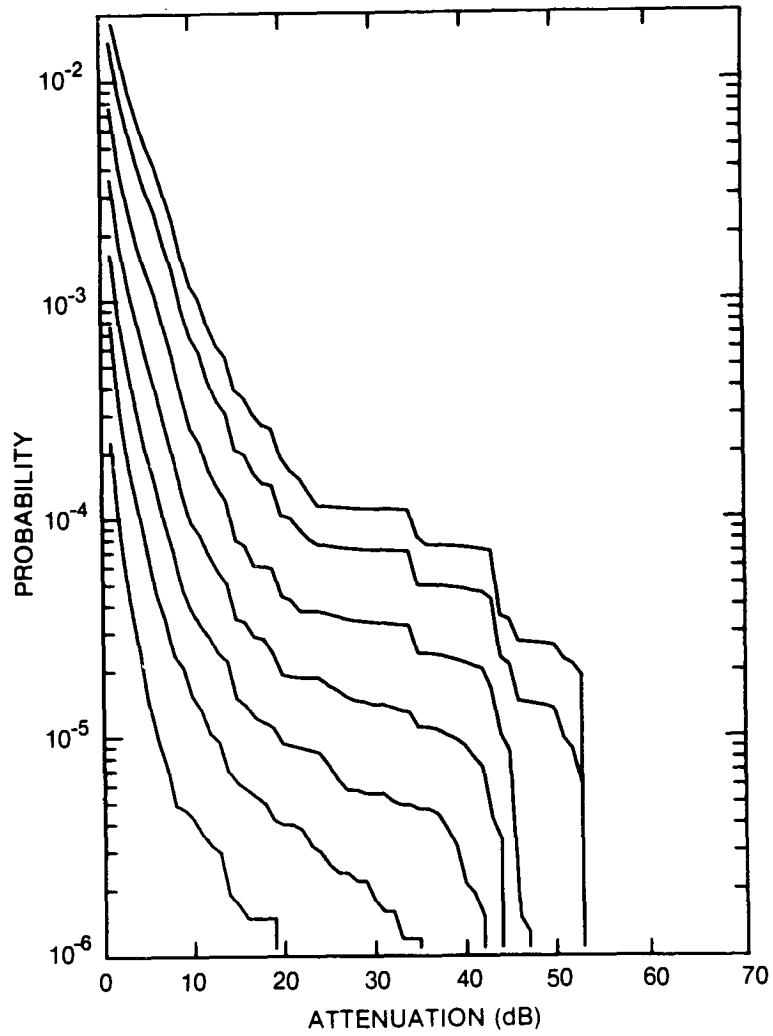

Figure 133. Cumulative distribution of rain attenuation for 15 GHz at Geraldton, ONT. Curves, moving from lowest to highest, are for hop lengths of 2, 5, 10, 20, 40, 80 and 120 km, respectively.

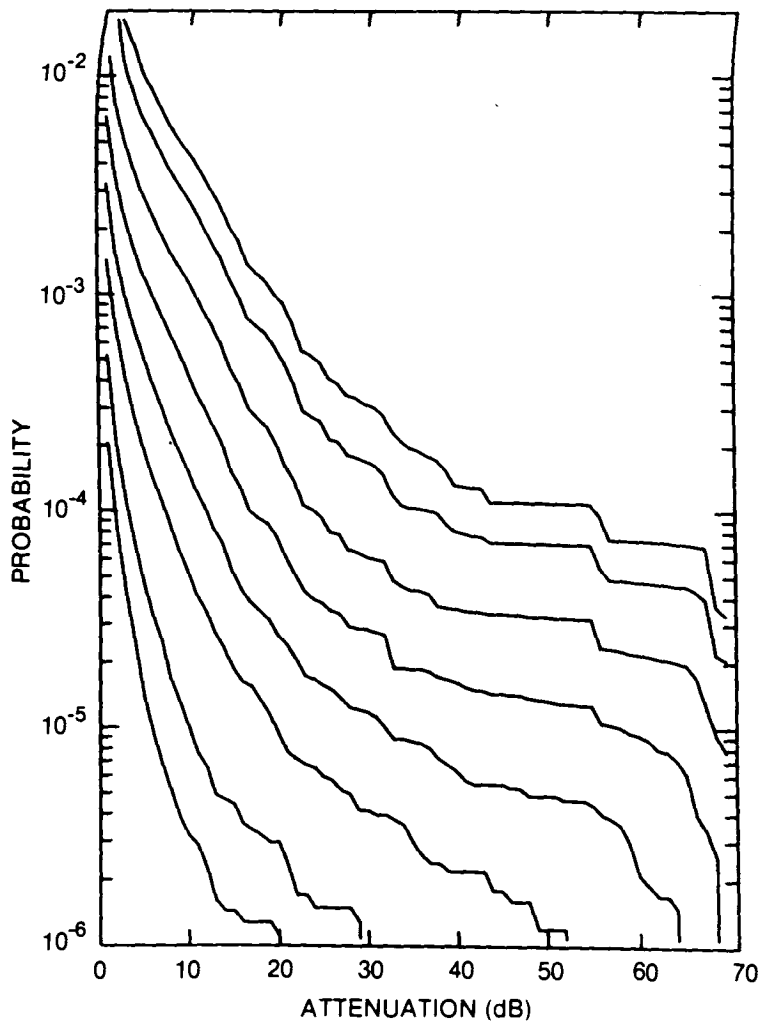

Figure 134. Cumulative distribution of rain attenuation for 20 GHz at Geraldton, ONT. Curves, moving from lowest to highest, are for hop lengths of 1, 2, 5, 10, 20, 40, 80 and 120 km, respectively.

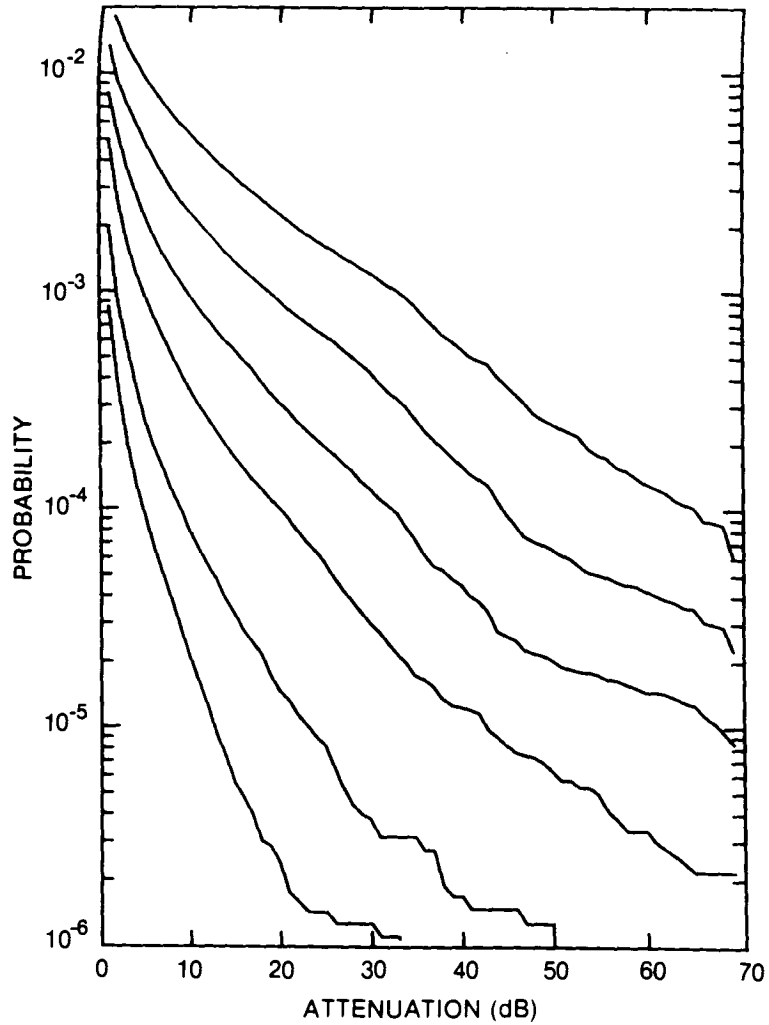

Figure 135. Cumulative distribution of rain attenuation for 35 GHz at Geraldton, ONT. Curves, moving from lowest to highest, are for hop lengths of 1, 2, 5, 10, 20 and 40 km, respectively.

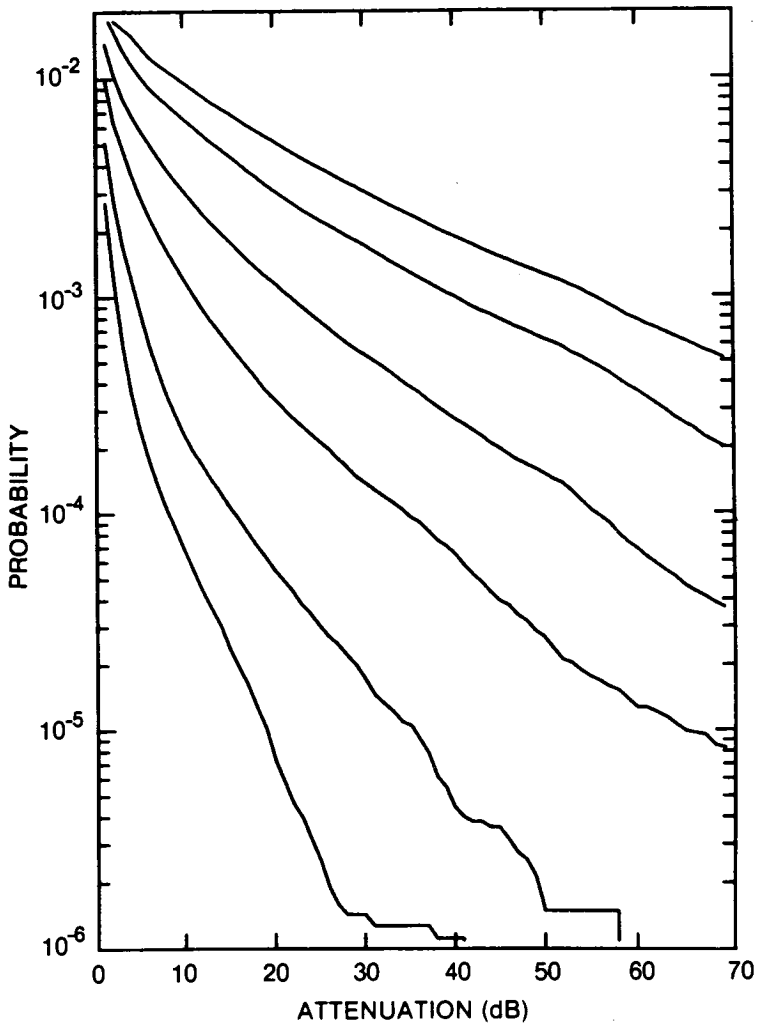

Figure 136. Cumulative distribution of rain attenuation for 56 GHz at Geraldton, ONT. Curves, moving from lowest to highest, are for hop lengths of 1, 2, 5, 10, 20 and 30 km, respectively.

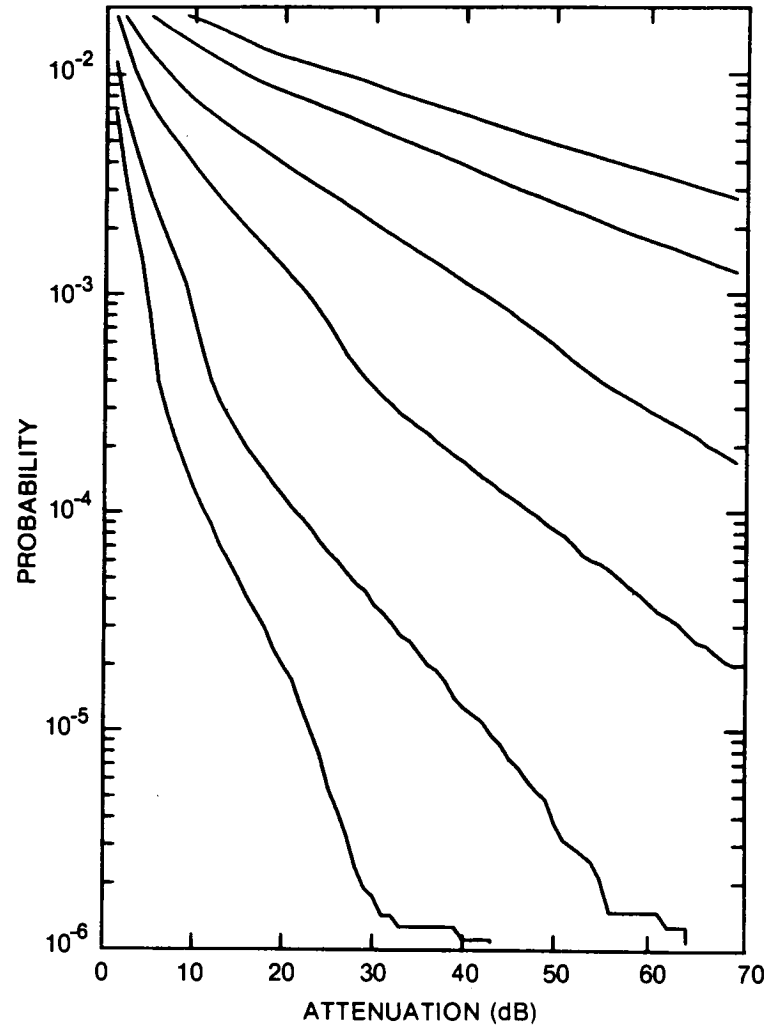

Figure 137. Cumulative distribution of rain attenuation for 100 GHz at Geraldton, ONT. Curves, moving from lowest to highest, are for hop lengths of 1, 2, 5, 10, 20 and 30 km, respectively.

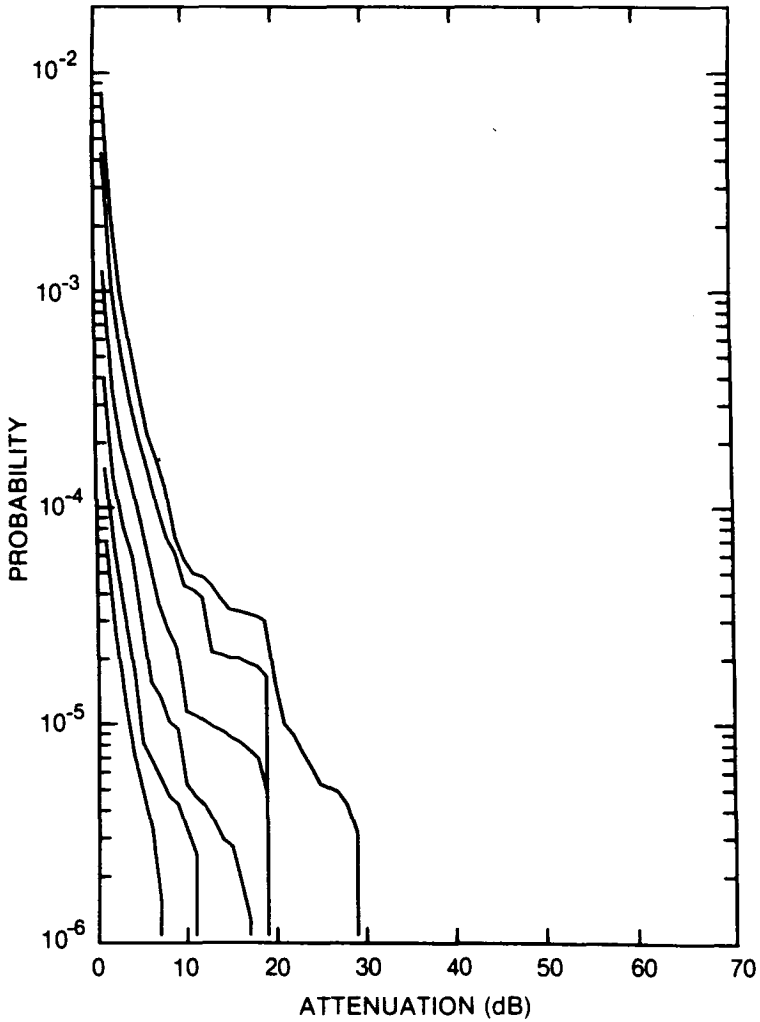

Figure 138. Cumulative distribution of rain attenuation for 8 GHz at Goose Bay, NFLD. Curves, moving from lowest to highest, are for hop lengths of 5, 10, 20, 40, 80 and 120 km, respectively.

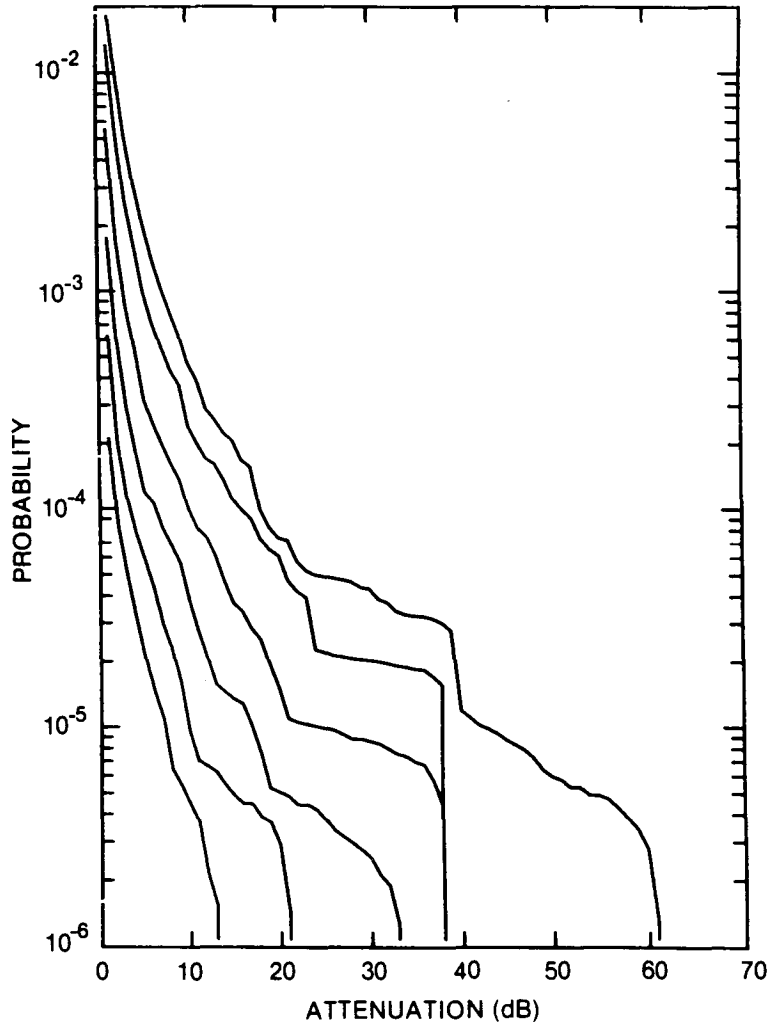

Figure 139. Cumulative distribution of rain attenuation for 11 GHz at Goose Bay, NFLD. Curves, moving from lowest to highest, are for hop lengths of 5, 10, 20, 40, 80 and 120 km, respectively.

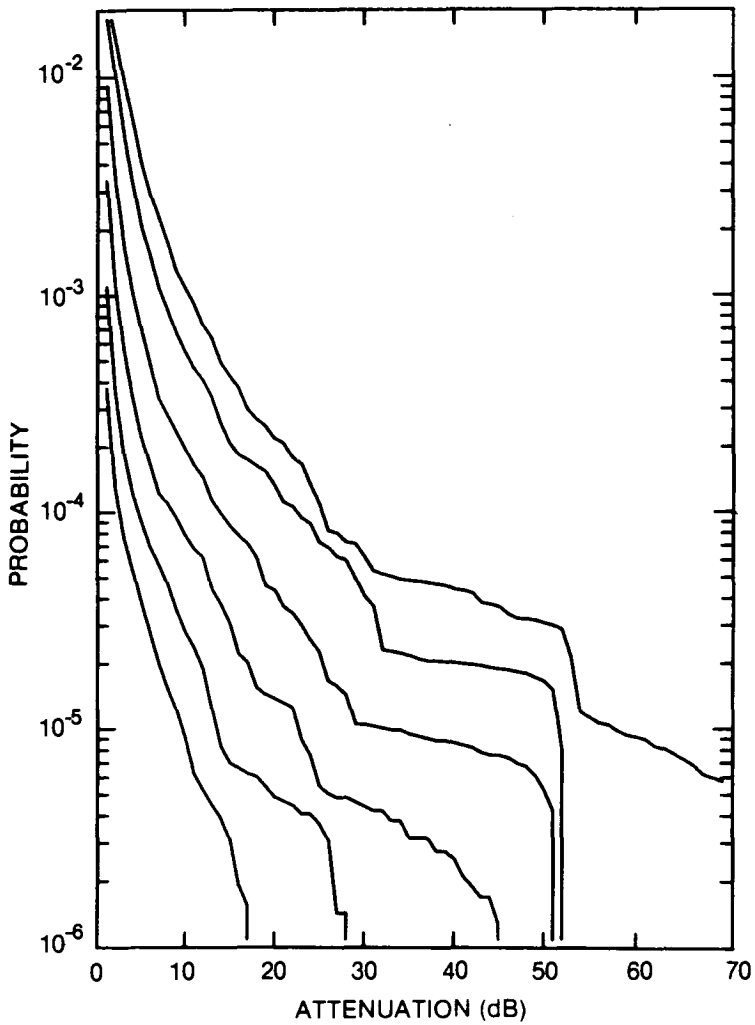

Figure 140. Cumulative distribution of rain attenuation for 12.8 GHZ at Goose Bay, NFLD. Curves, moving from lowest to highest, are for hop lengths of 5, 10, 20, 40, 80 and 120 km, respectively.

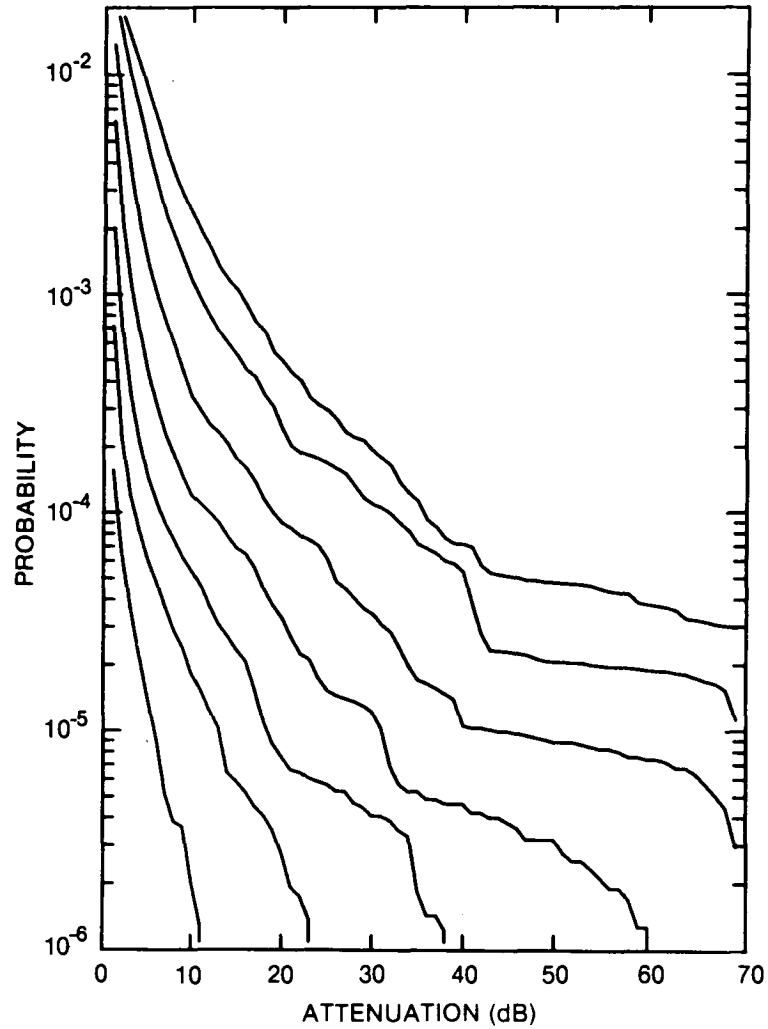

Figure 141. Cumulative distribution of rain attenuation for 15 GHz at Goose Bay, NFLD. Curves, moving from lowest to highest, are for hop lengths of 2, 5, 10, 20, 40, 80 and 120 km, respectively.

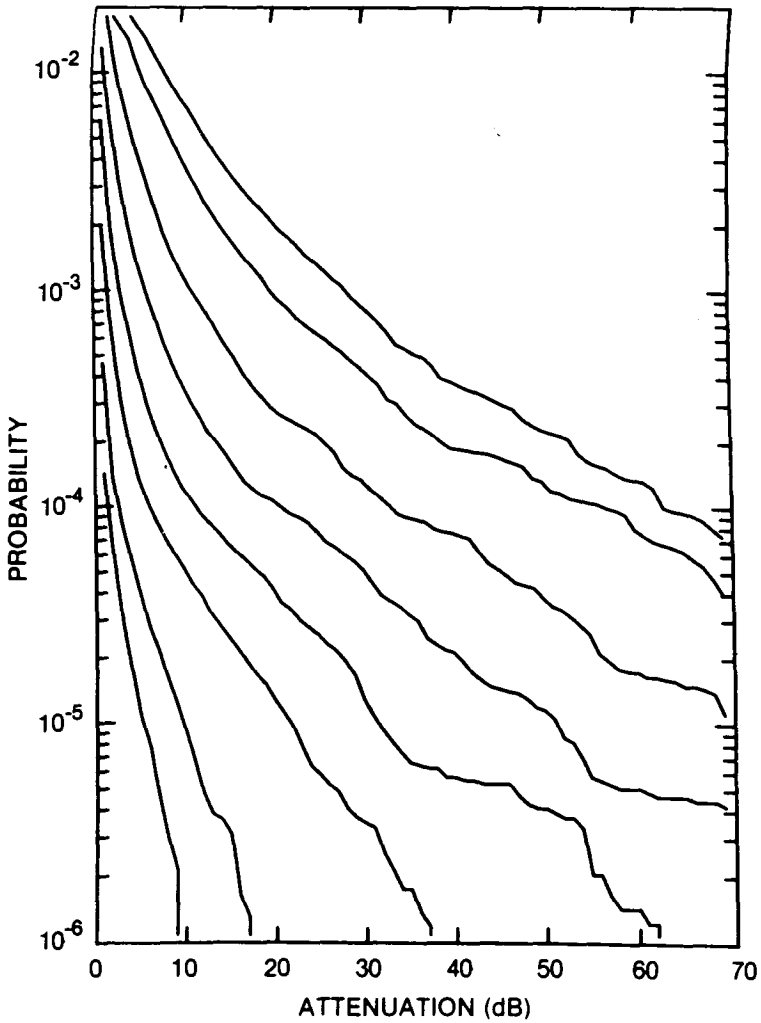

Figure 142. Cumulative distribution of rain attenuation for 20 GHz at Goose Bay, NFLD. Curves, moving from lowest to highest, are for hop lengths of 1, 2, 5, 10, 20, 40, 80 and 120 km, respectively.

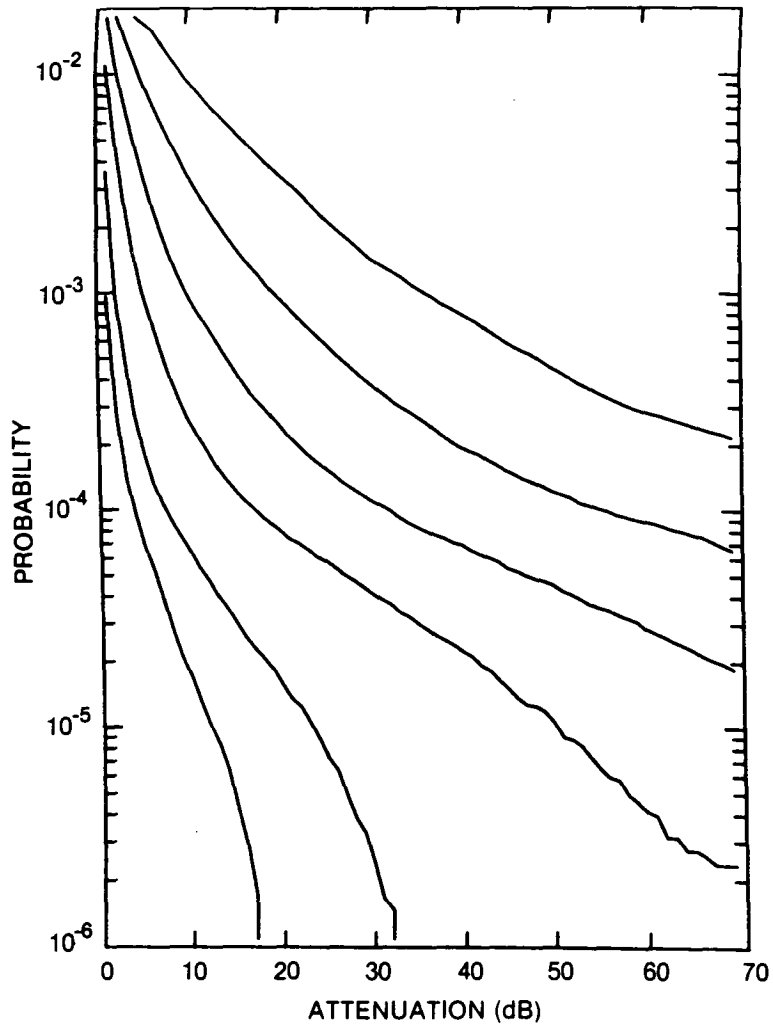

Figure 143. Cumulative distribution of rain attenuation for 35 GHz at Goose Bay, NFLD. Curves, moving from lowest to highest, are for hop lengths of 1, 2, 5, 10, 20 and 40 km, respectively.

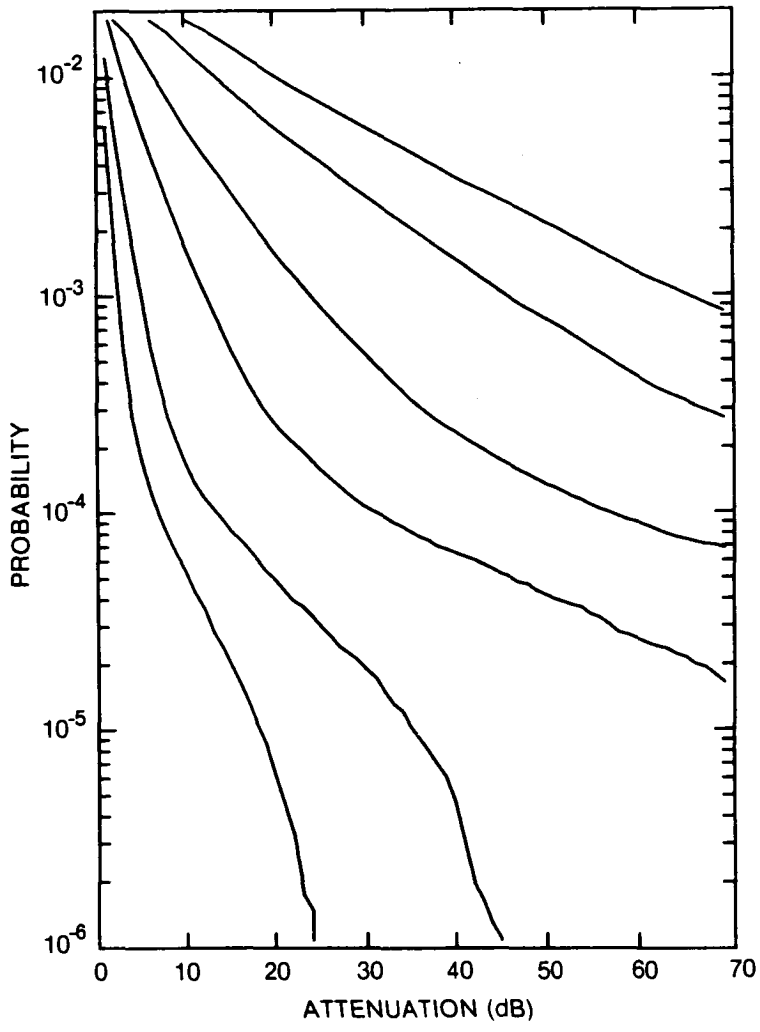

Figure 144. Cumulative distribution of rain attenuation for 56 GHz at Goose Bay, NFLD. Curves, moving from lowest to highest, are for hop lengths of 1, 2, 5, 10, 20 and 30 km, respectively.

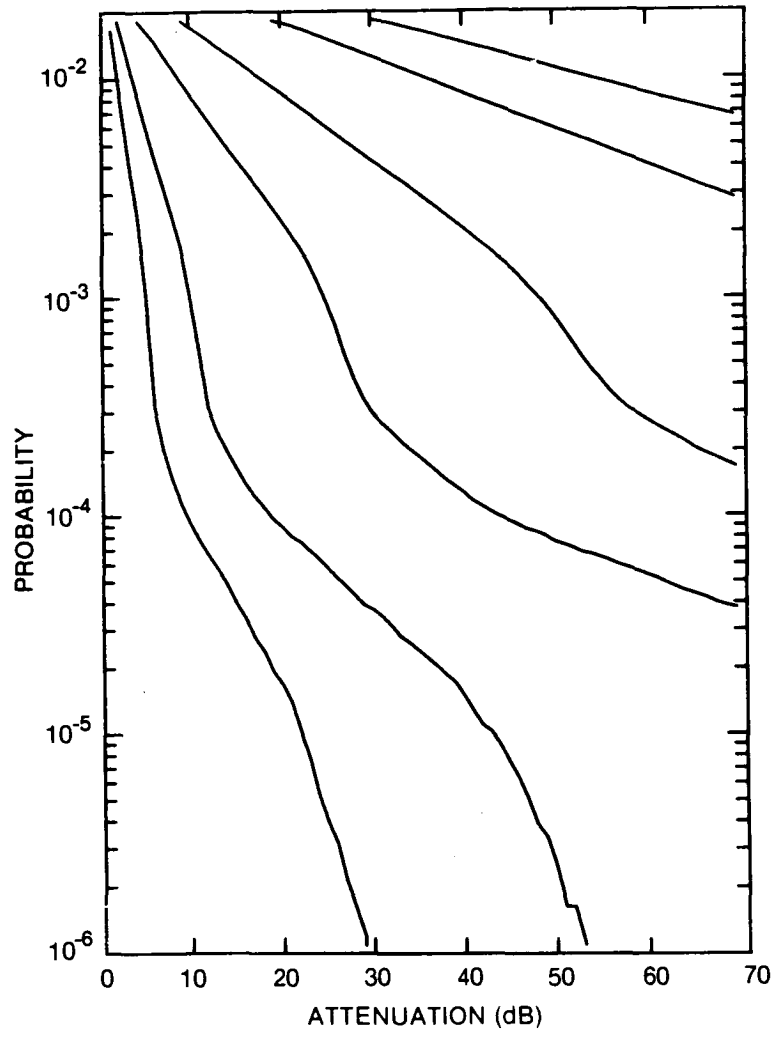

Figure 145. Cumulative distribution of rain attenuation for 100 GHz at Goose Bay, NFLD. Curves, moving from lowest to highest, are for hop lengths of 1, 2, 5, 10, 20 and 30 km, respectively.

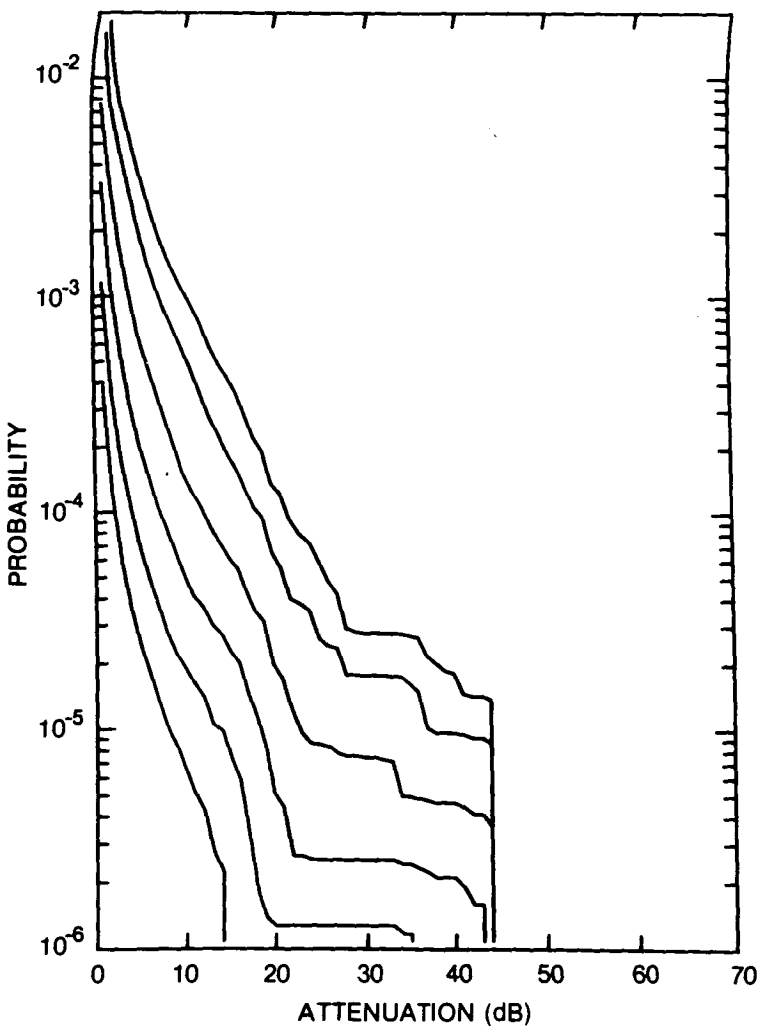

Figure 146. Cumulative distribution of rain attenuation for 8 GHz at Halifax, NS. Curves, moving from lowest to highest, are for hop lengths of 5, 10, 20, 40, 80 and 120 km, respectively.

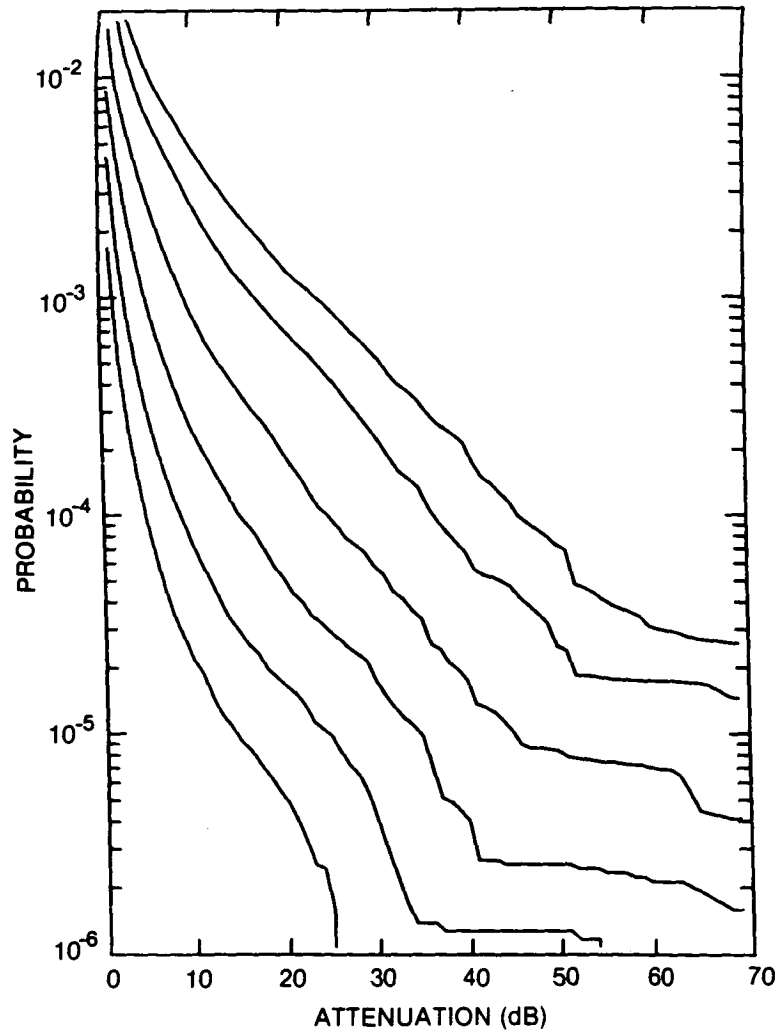

Figure 147. Cumulative distribution of rain attenuation for 11 GHz at Halifax, NS. Curves, moving from lowest to highest, are for hop lengths of 5, 10, 20, 40, 80 and 120 km, respectively.

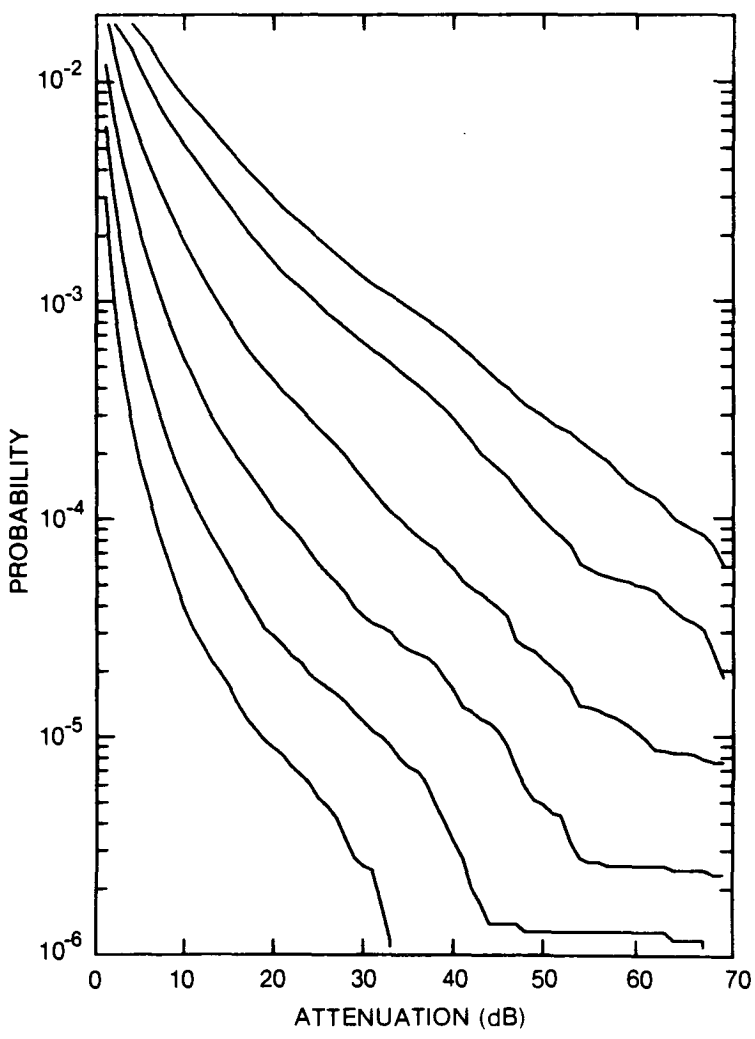

Figure 148. Cumulative distribution of rain attenuation for 12.8 GHz at Halifax, NS. Curves, moving from lowest to highest, are for hop lengths of 5, 10, 20, 40, 80 and 120 km, respectively.

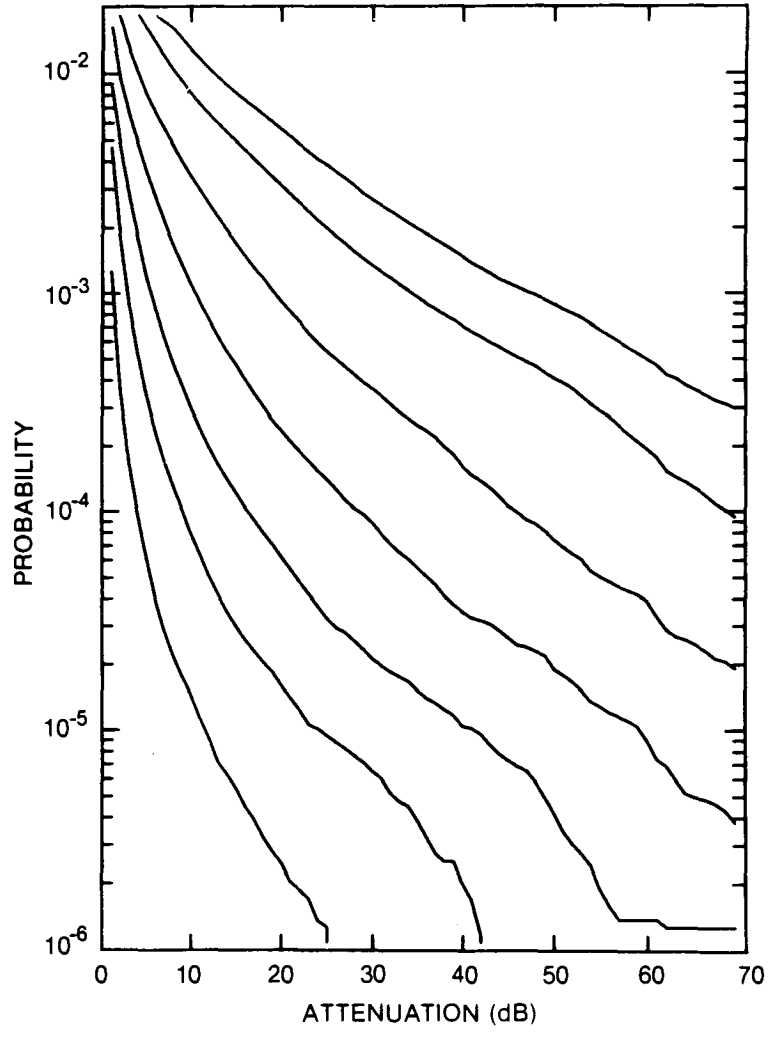

Figure 149. Cumulative distribution of rain attenuation for 15 GHz at Halifax, NS. Curves, moving from lowest to highest, are for hop lengths of 2, 5, 10, 20, 40, 80 and 120 km, respectively.

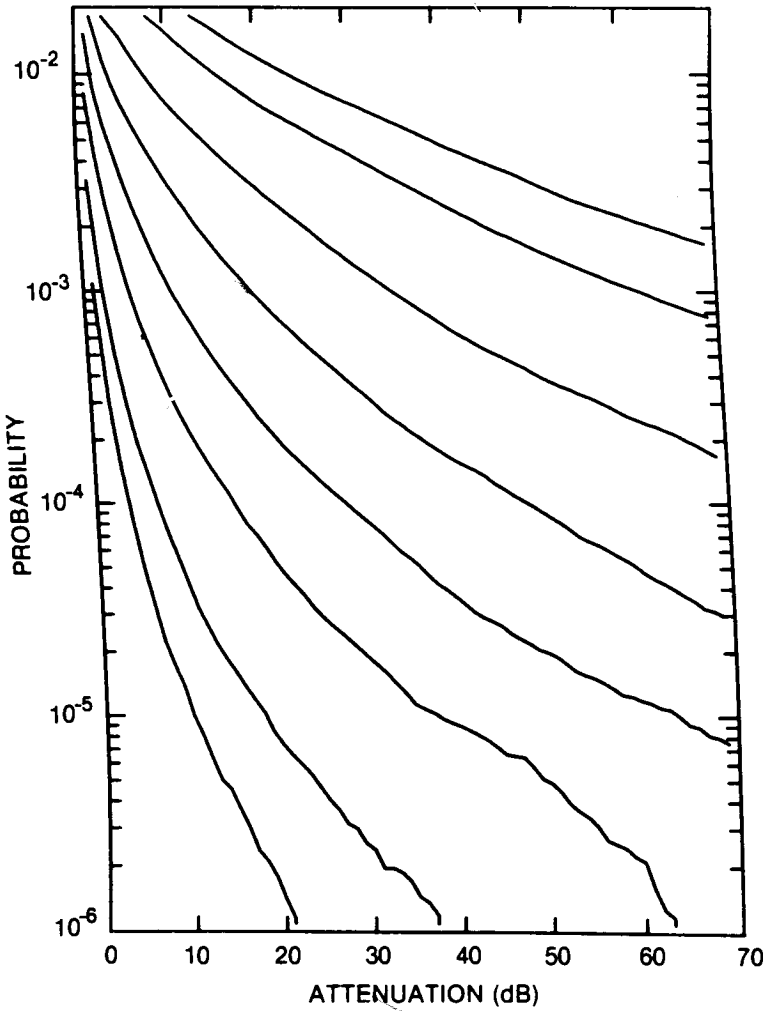

Figure 150. Cumulative distribution of rain attenuation for 20 GHz at Halifax, NS. Curves, moving from lowest to highest, are for hop lengths of 1, 2, 5, 10, 20, 40, 80 and 120 km, respectively.

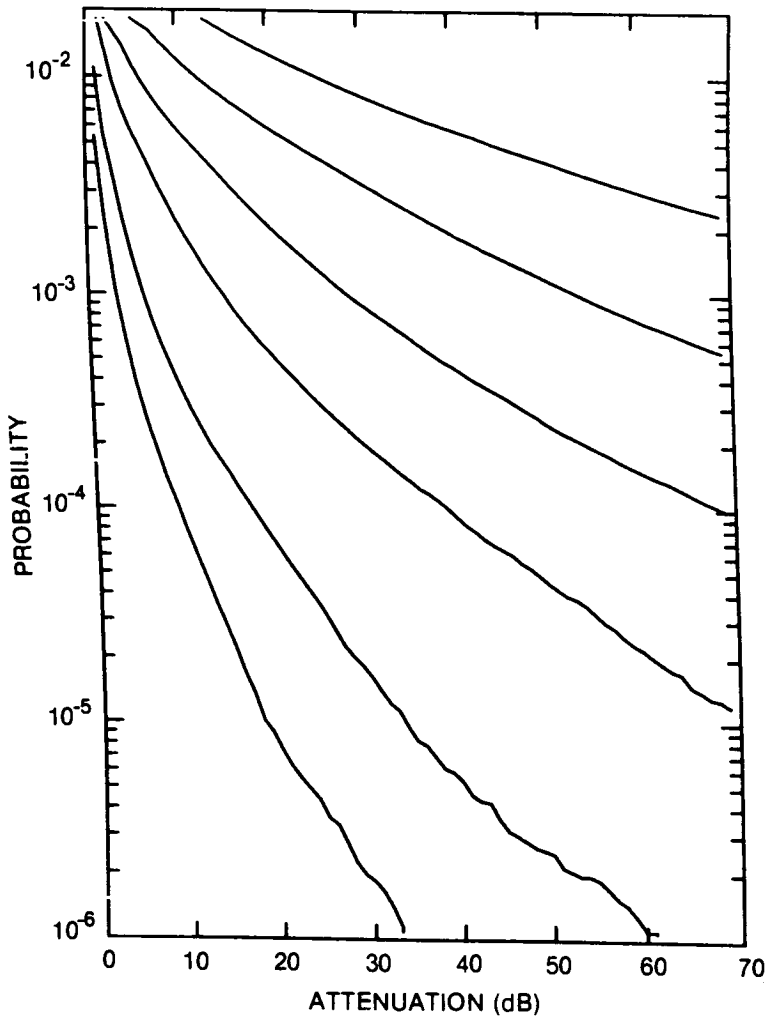

Figure 151. Cumulative distribution of rain attenuation for 35 GHz at Halifax, NS. Curves, moving from lowest to highest, are for hop lengths of 1, 2, 5, 10, 20 and 40 km, respectively.

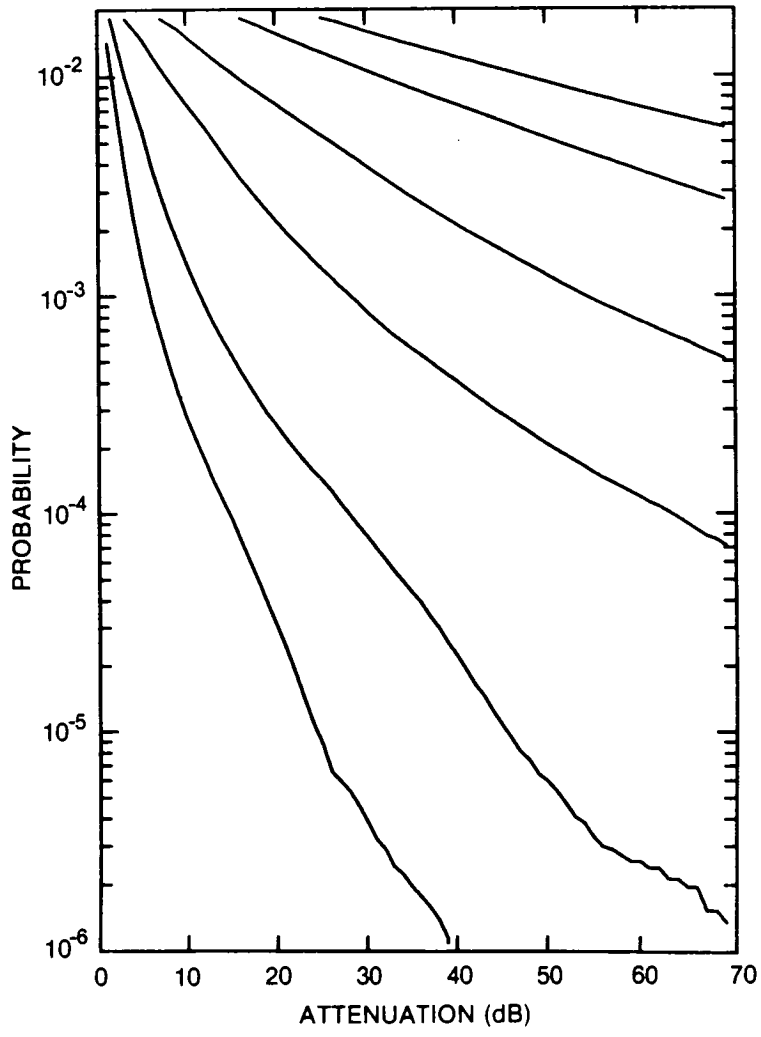

Figure 152. Cumulative distribution of rain attenuation for 56 GHz at Halifax, NS. Curves, moving from lowest to highest, are for hop lengths of 1, 2, 5, 10, 20 and 30 km, respectively.

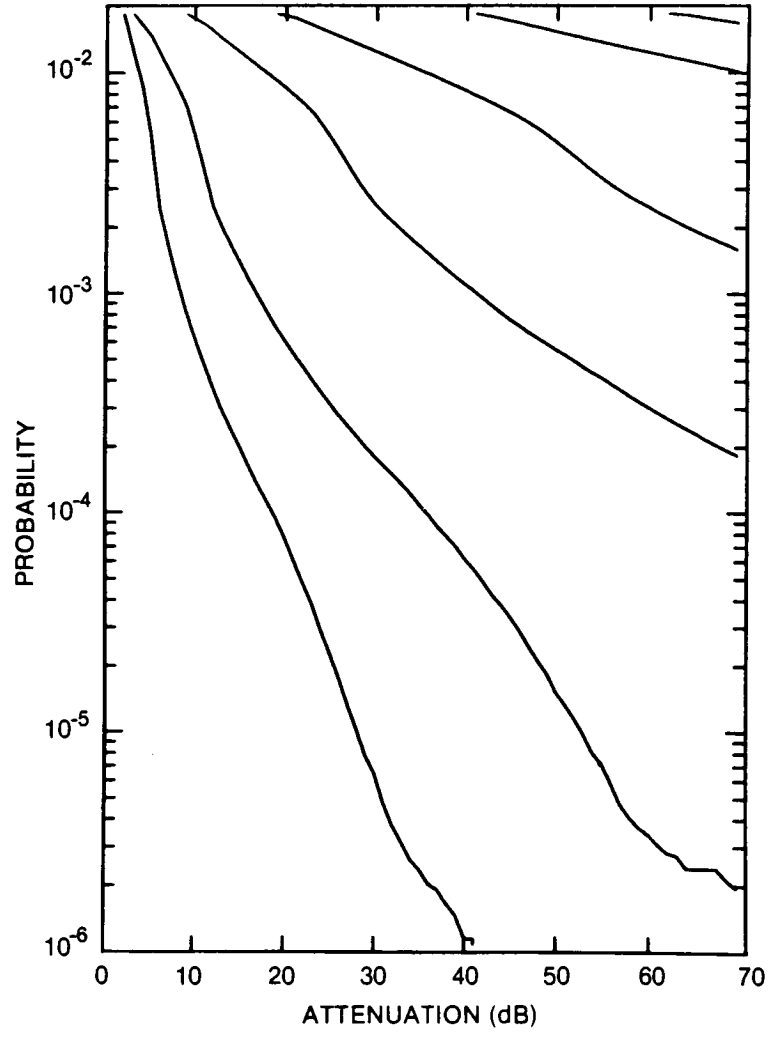

Figure 153. Cumulative distribution of rain attenuation for 100 GHz at Halifax, NS. Curves, moving from lowest to highest, are for hop lengths of 1, 2, 5, 10, 20 and 30 km, respectively.

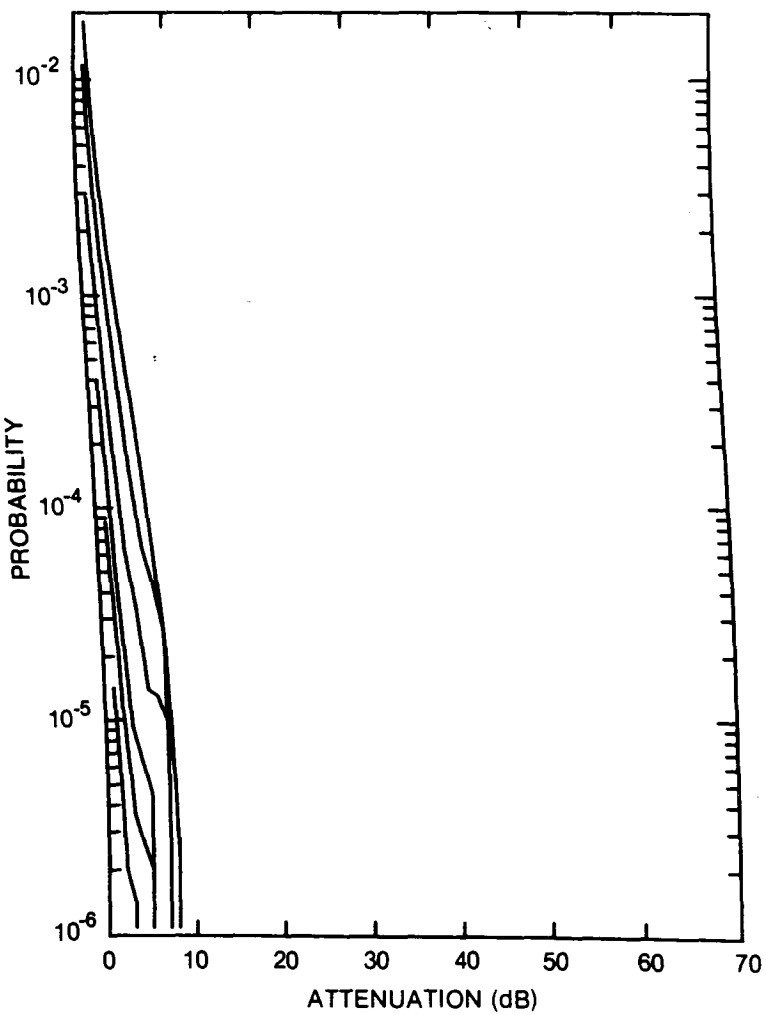

Figure 154. Cumulative distribution of rain attenuation for 8 GHz at Hope, BC. Curves, moving from lowest to highest, are for hop lengths of 5, 10, 20, 40, 80 and 120 km, respectively.

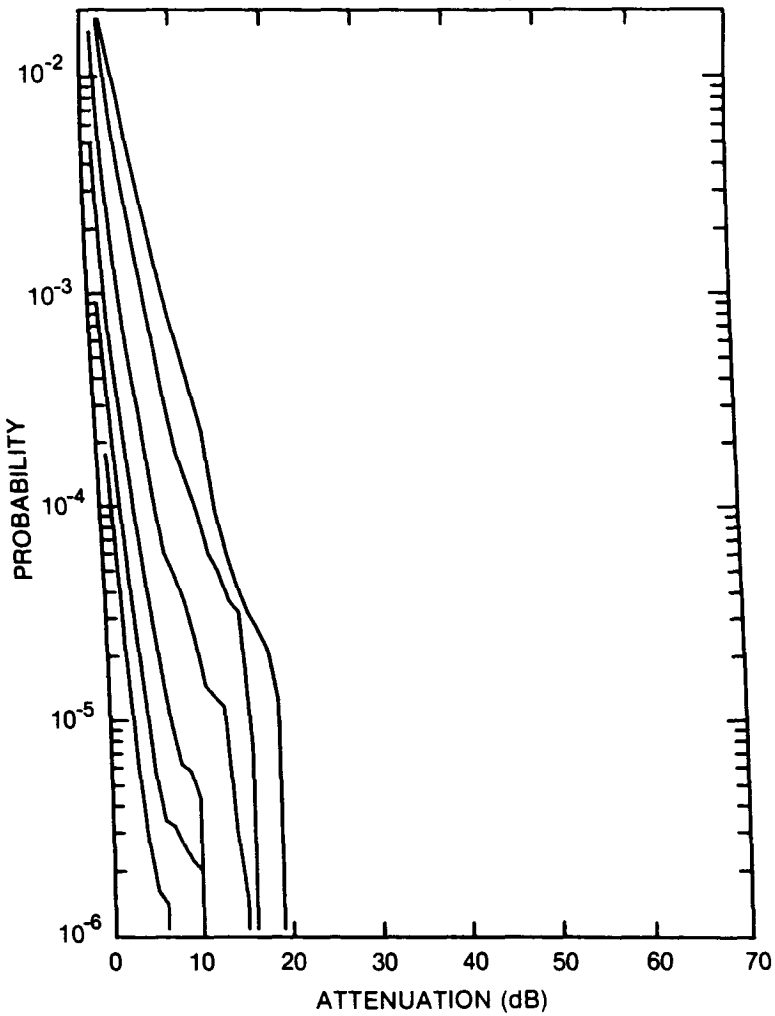

Figure 155. Cumulative distribution of rain attenuation for 11 GHz at Hope, BC. Curves, moving from lowest to highest, are for hop lengths of 5, 10, 20, 40, 80 and 120 km, respectively.

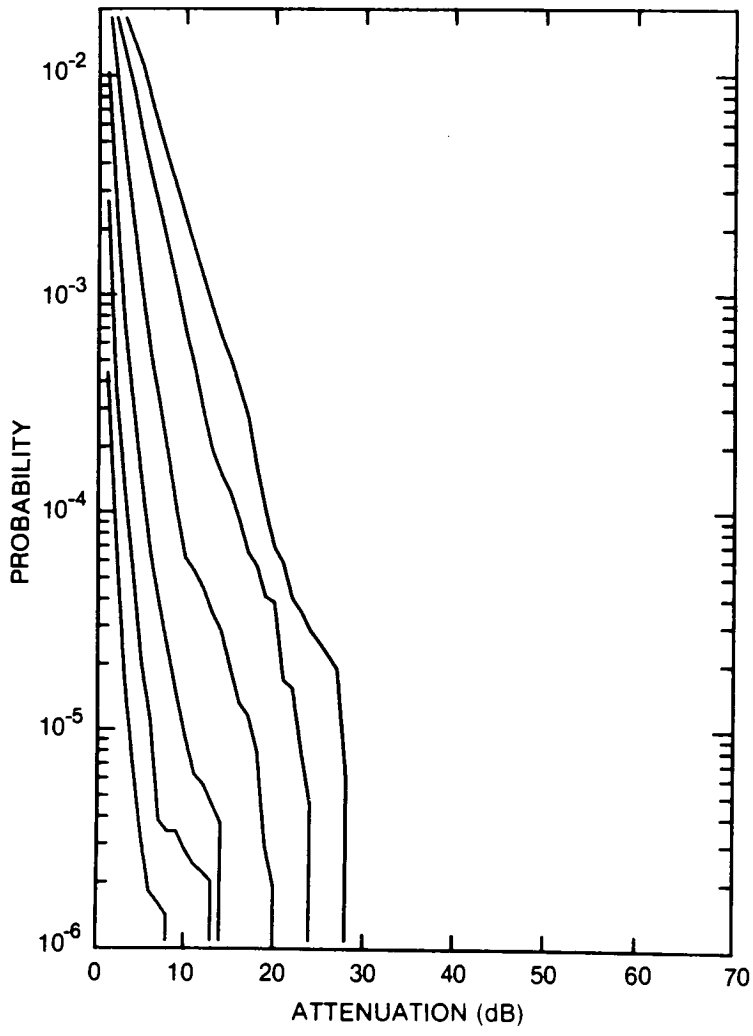

Figure 156. Cumulative distribution of rain attenuation for 12.8 GHz at Hope, BC. Curves, moving from lowest to highest, are for hop lengths of 5, 10, 20, 40, 80 and 120 km, respectively.

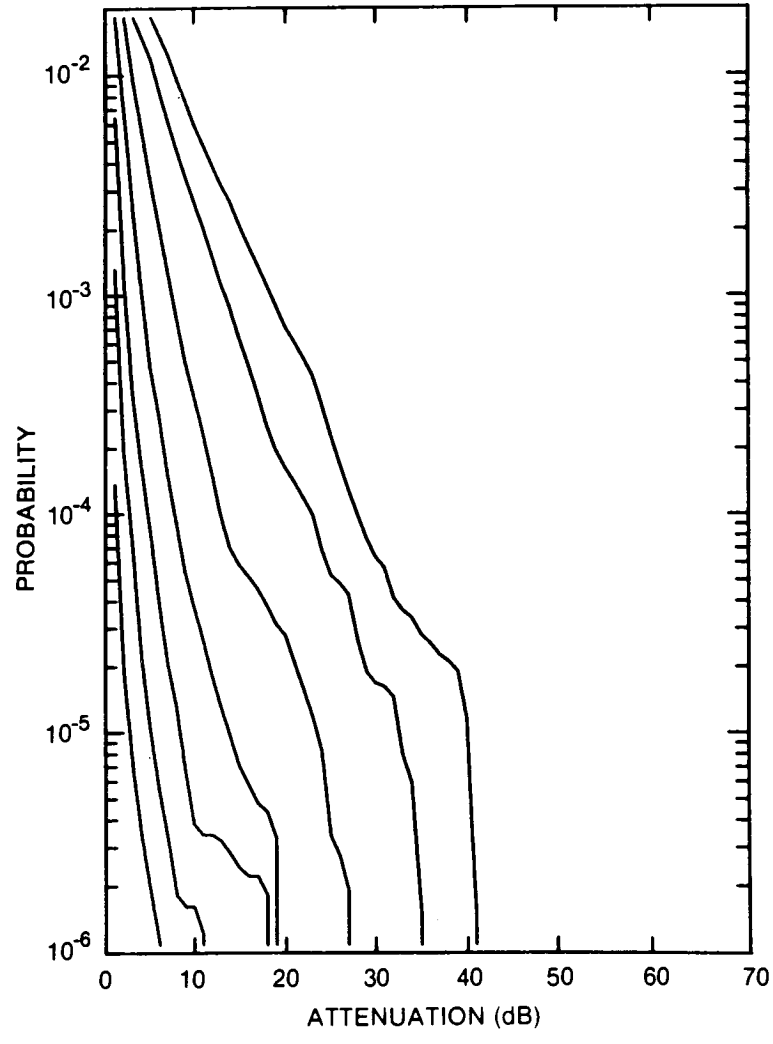

Figure 157. Cumulative distribution of rain attenuation for 15 GHz at Hope, BC. Curves, moving from lowest to highest, are for hop lengths of 2, 5, 10, 20, 40, 80, and 120 km, respectively.

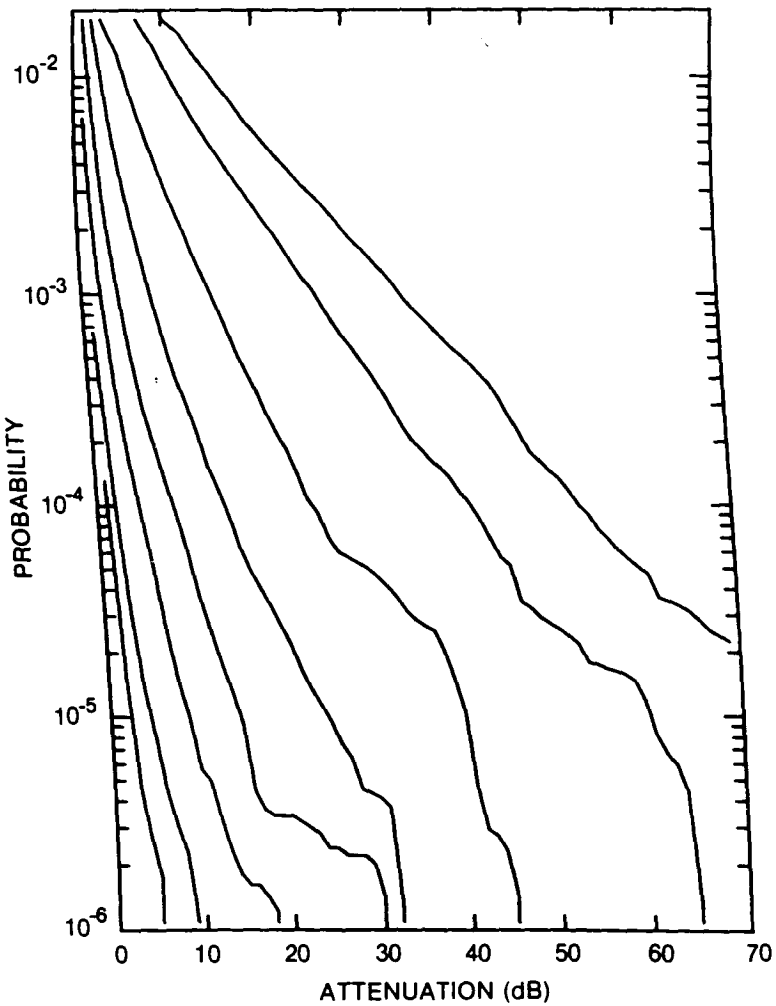

Figure 158. Cumulative distribution of rain attenuation for 20 GHz at Hope, BC. Curves, moving from lowest to highest, are for hop lengths of 1, 2, 5, 10, 20, 40, 80 and 120 km, respectively.

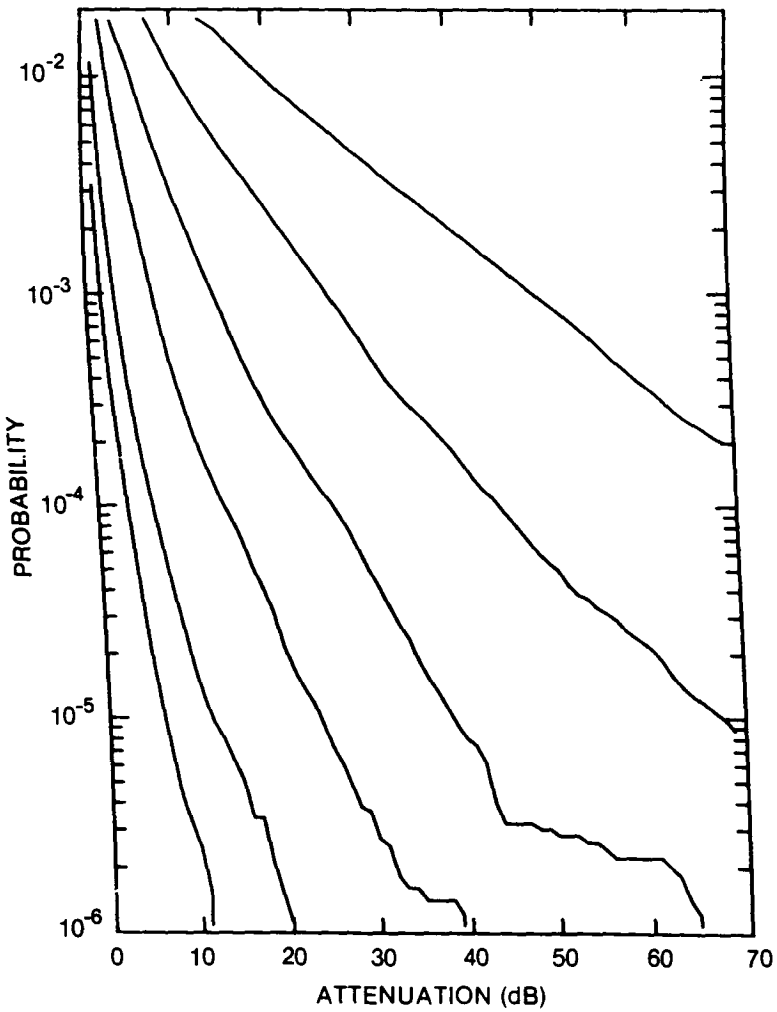

Figure 159. Cumulative distribution of rain attenuation for 35 GHz at Hope, BC. Curves, moving from lowest to highest, are for hop lengths of 1, 2, 5, 10, 20 and 40 km, respectively.

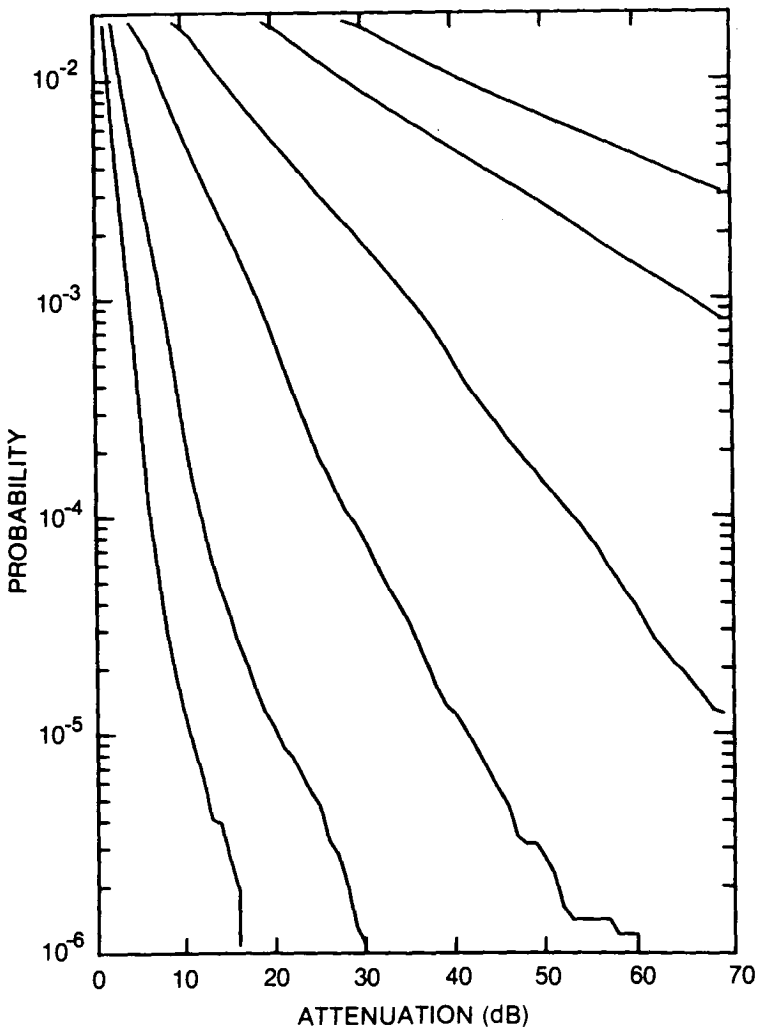

Figure 160. Cumulative distribution of rain attenuation for 56 GHz at Hope, BC. Curves, moving from lowest to highest, are for hop lengths of 1, 2, 5, 10, 20 and 30 km, respectively.

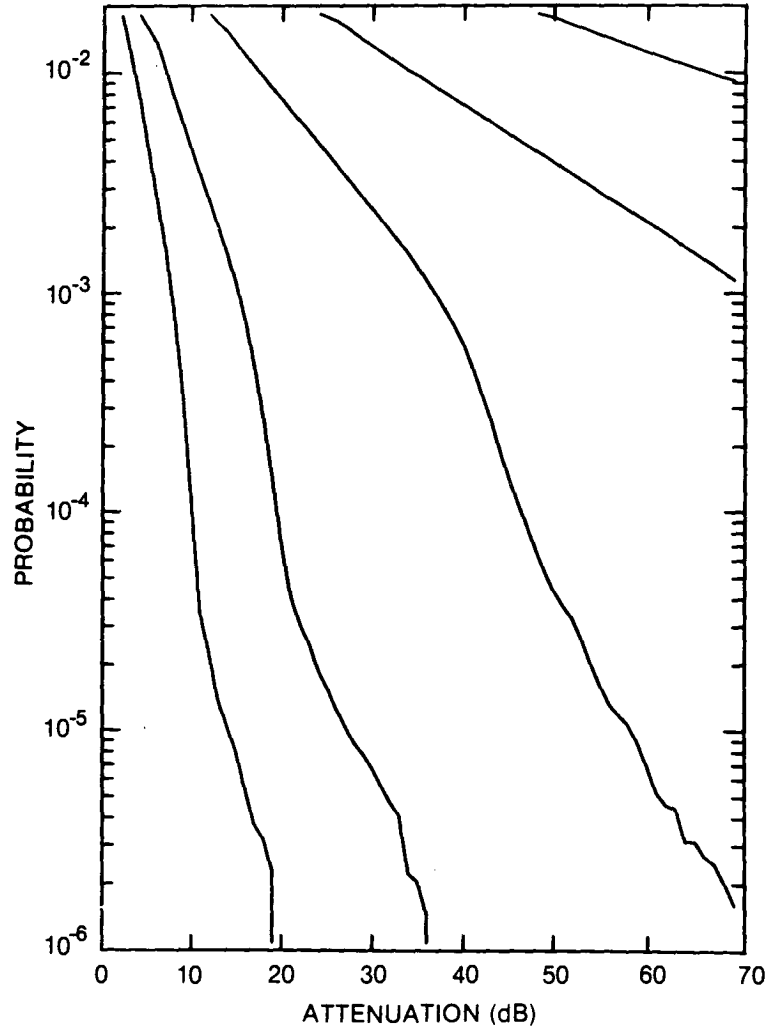

Figure 161. Cumulative Distribution of rain attenuation for 100 GHz at Hope, BC. Curves, moving from lowest to highest, are for hop lengths of 1, 2, 5, 10, and 20 km, respectively.

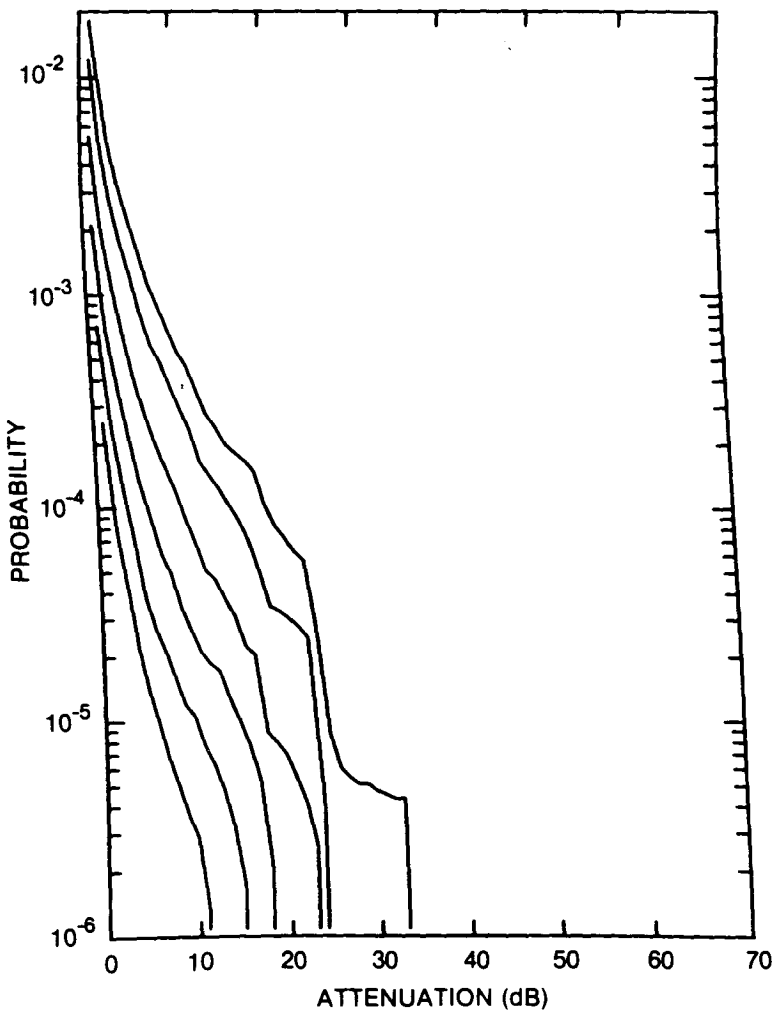

Figure 162. Cumulative distribution of rain attenuation for 8 GHz at Kentville, NS. Curves, moving from lowest to highest, are for hop lengths of 5, 10, 20, 40, 80 and 120 km, respectively.

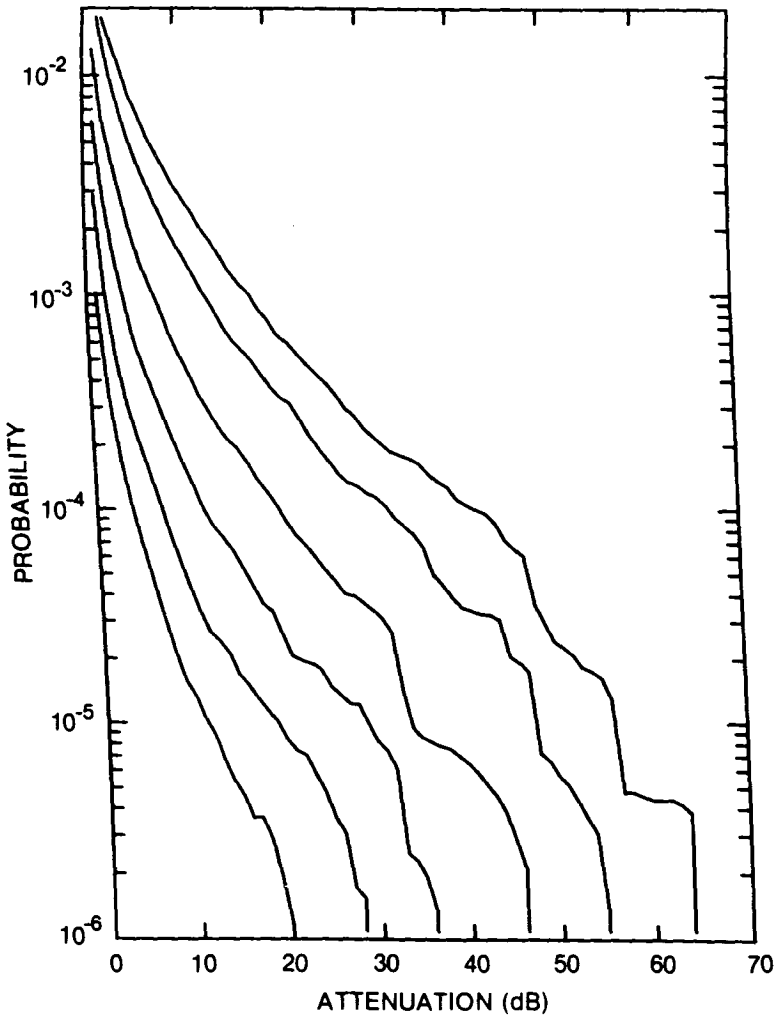

Figure 163. Cumulative distribution of rain attenuation for 11 GHz at Kentville, NS. Curves, moving from lowest to highest, are for hop lengths of 5, 10, 20, 40, 80 and 120 km, respectively.

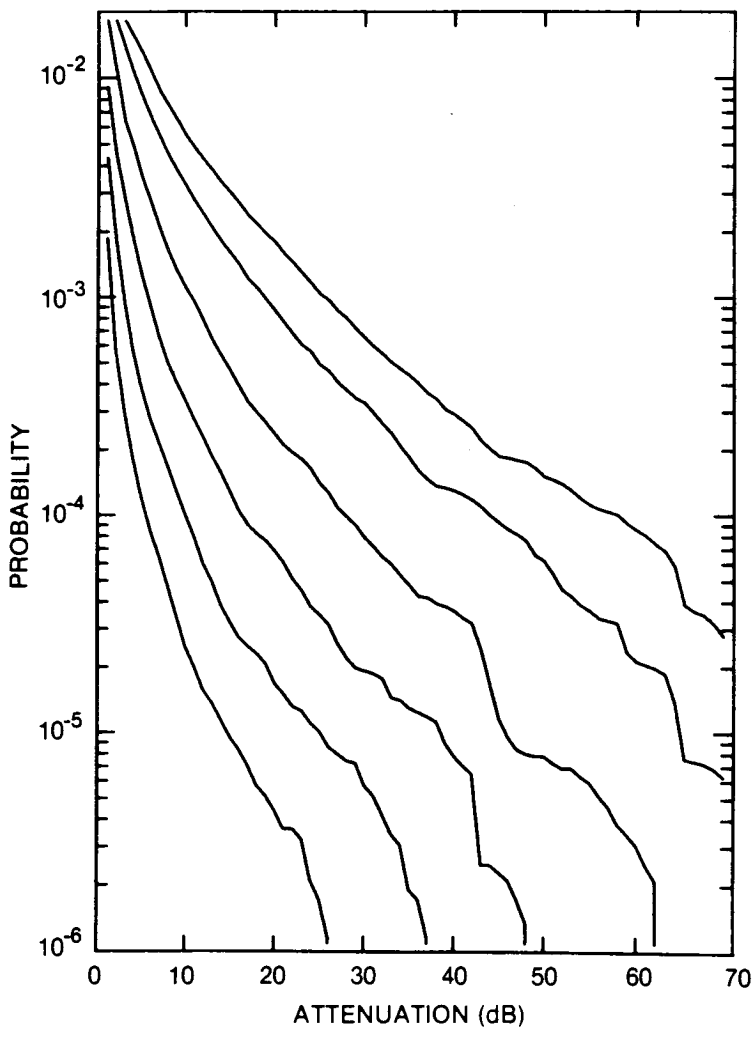

Figure 164. Cumulative distribution of rain attenuation for 12.8 GHz at Kentville, NS. Curves, moving from lowest to highest, are for hop lengths of 5, 10, 20, 40, 80 and 120 km, respectively.

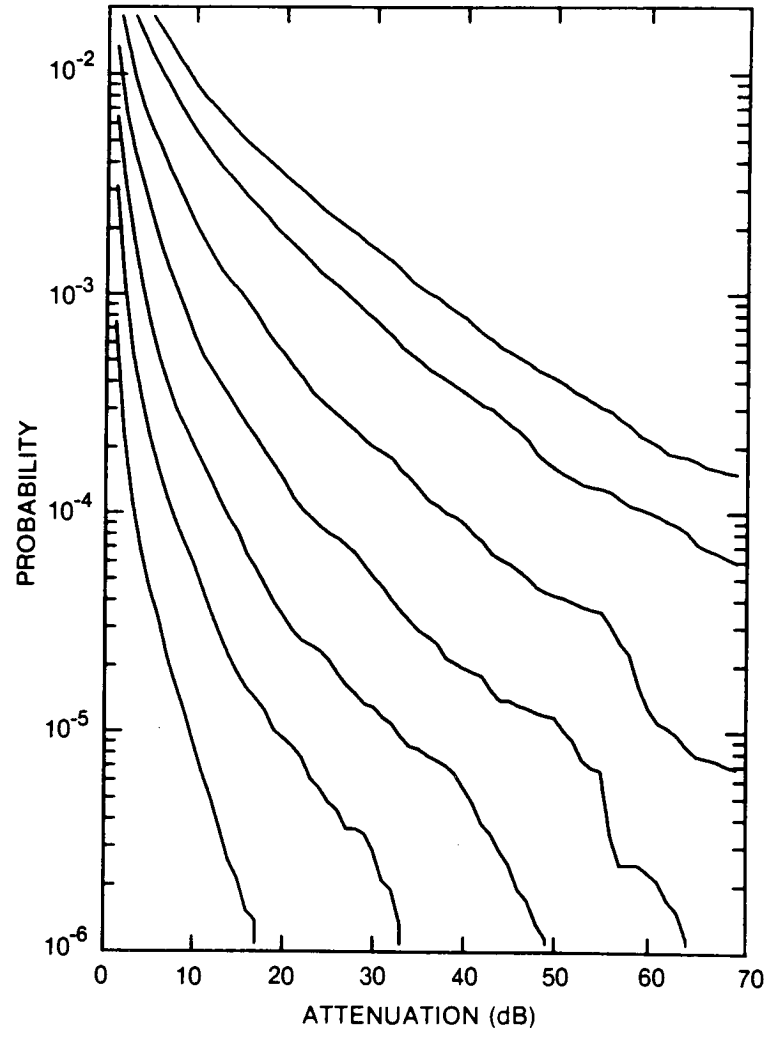

Figure 165. Cumulative distribution of rain attenuation for 15 GHz at Kentville, NS. Curves, moving from lowest to highest, are for hop lengths of 2, 5, 10, 20, 40, 80 and 120 km, respectively.

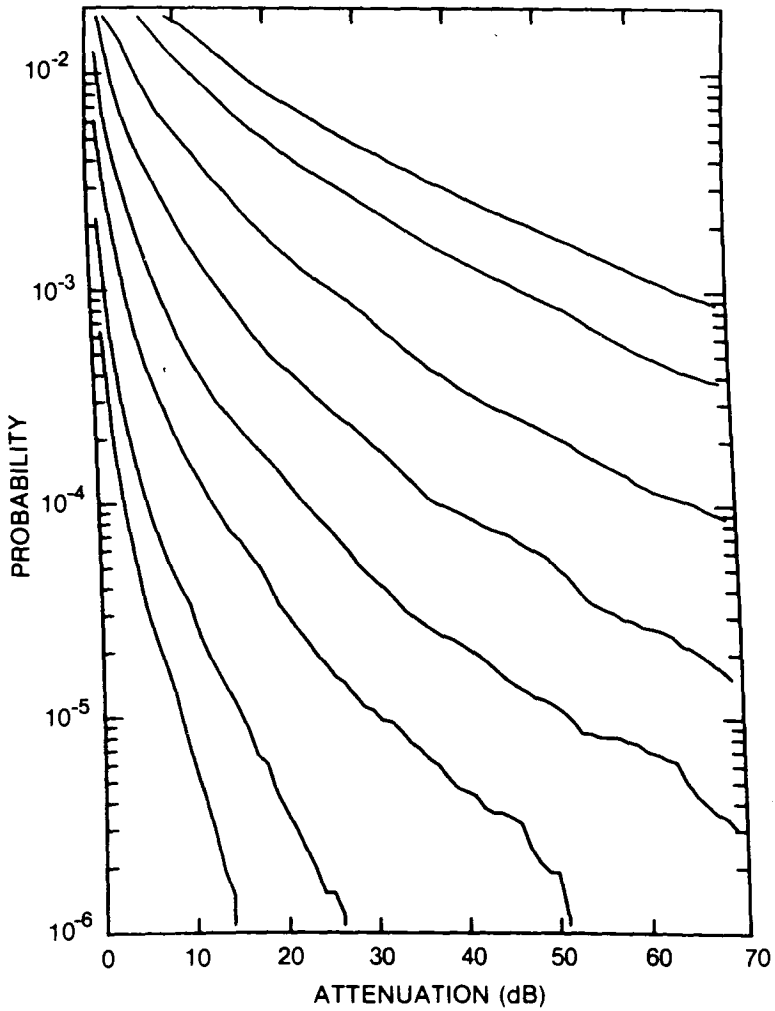

Figure 166. Cumulative distribution of rain attenuation for 20 GHz at Kentville, NS. Curves, moving from lowest to highest, are for hop lengths of 1, 2, 5, 10, 20, 40, 80 and 120 km, respectively.

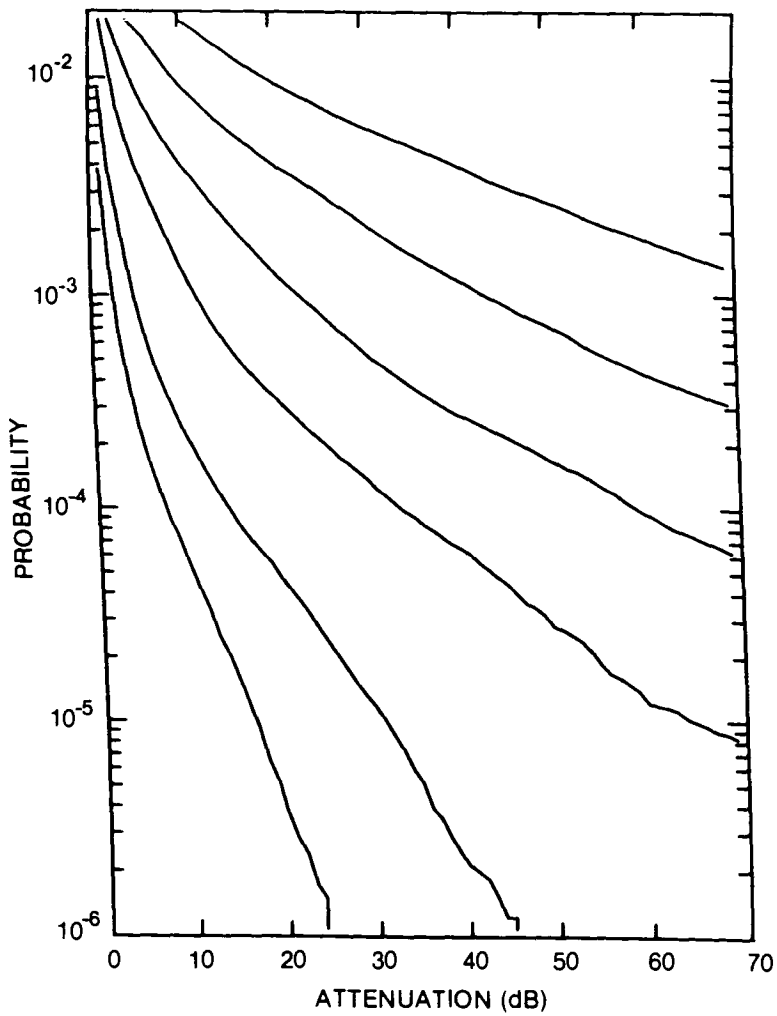

Figure 167. Cumulative distribution of rain attenuation for 35 GHz at Kentville, NS. Curves, moving from lowest to highest, are for hop lengths of 1, 2, 5, 10, 20 and 40 km, respectively.

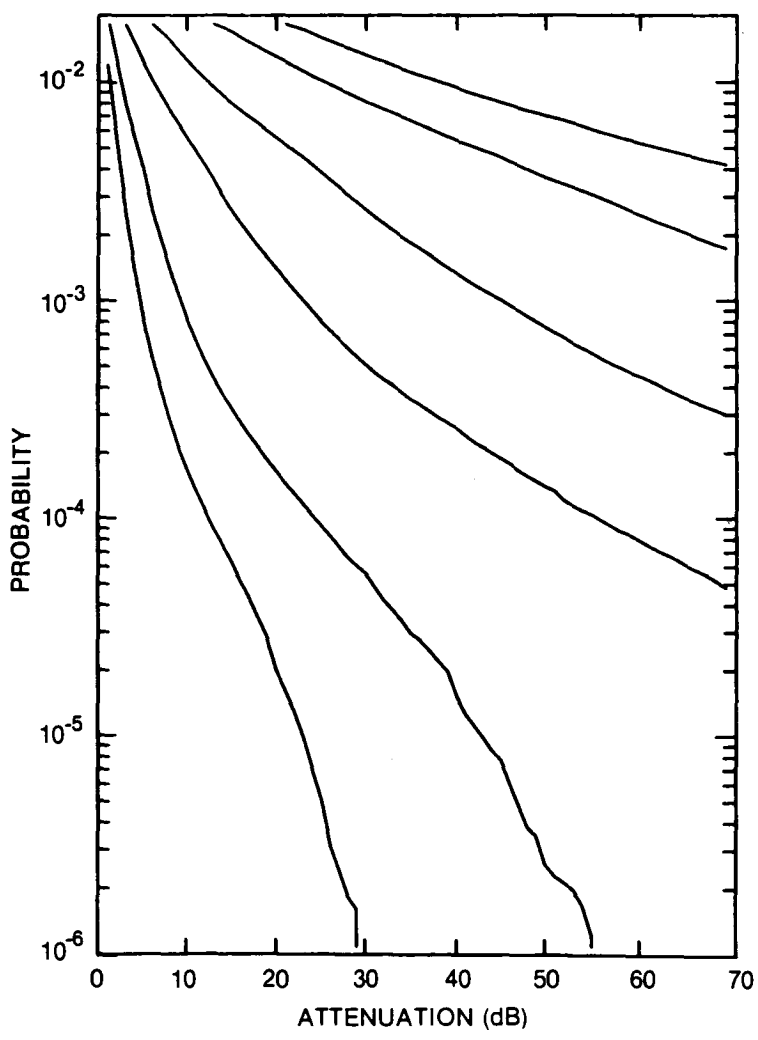

Figure 168. Cumulative distribution of rain attenuation for 56 GHz at Kentville, NS. Curves, moving from lowest to highest, are for hop lengths of 1, 2, 5, 10, 20 and 30 km, respectively.

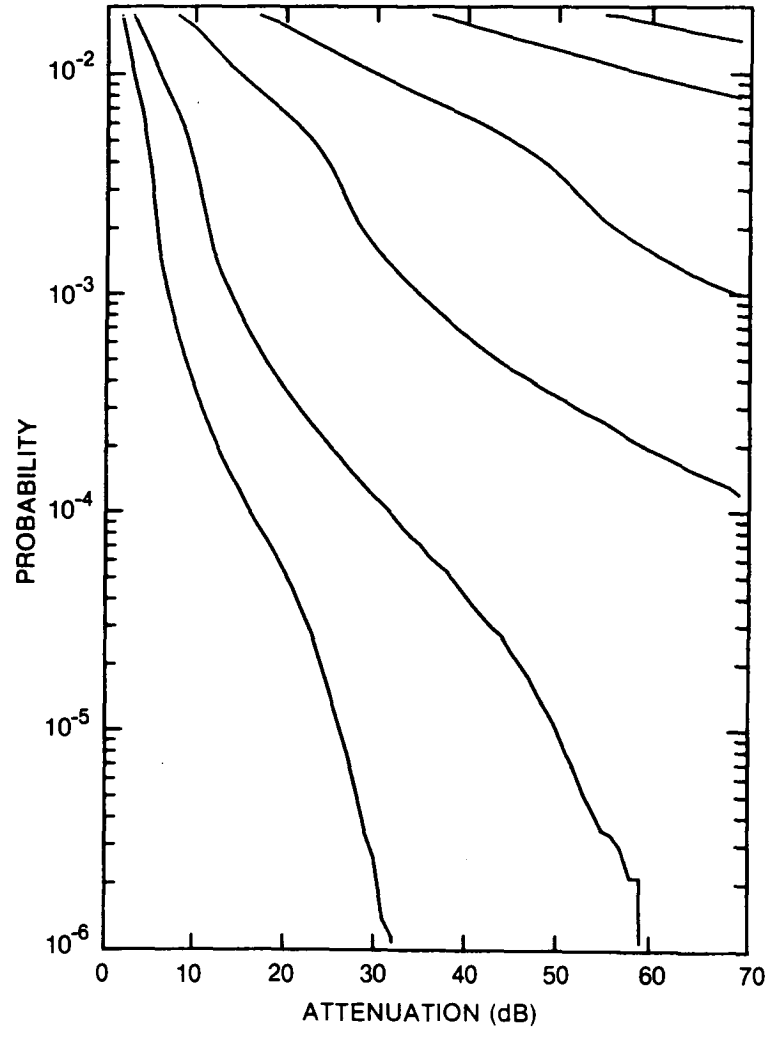

Figure 169. Cumulative distribution of rain attenuation for 100 GHz at Kentville, NS. Curves, moving from lowest to highest, are for hop lengths of 1, 2, 5, 10, 20 and 30 km, respectively.

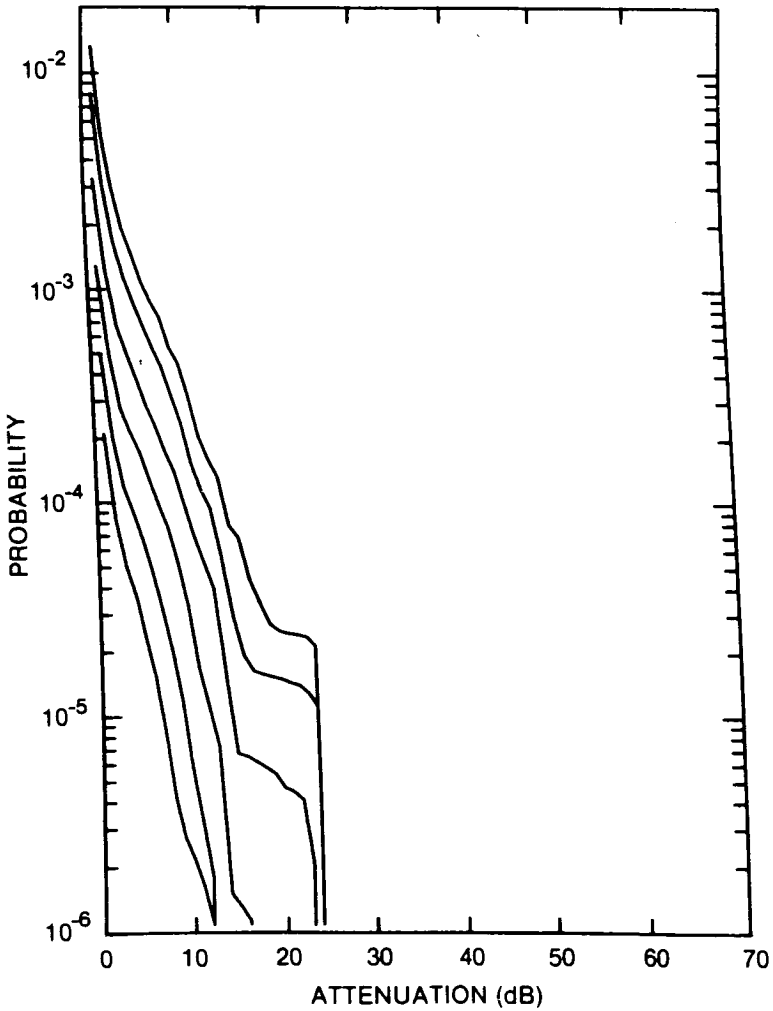

Figure 170. Cumulative distribution of rain attenuation for 8 GHz at Kingston, ONT. Curves, moving from lowest to highest, are for hop lengths of 5, 10, 20, 40, 80 and 120 km, respectively.

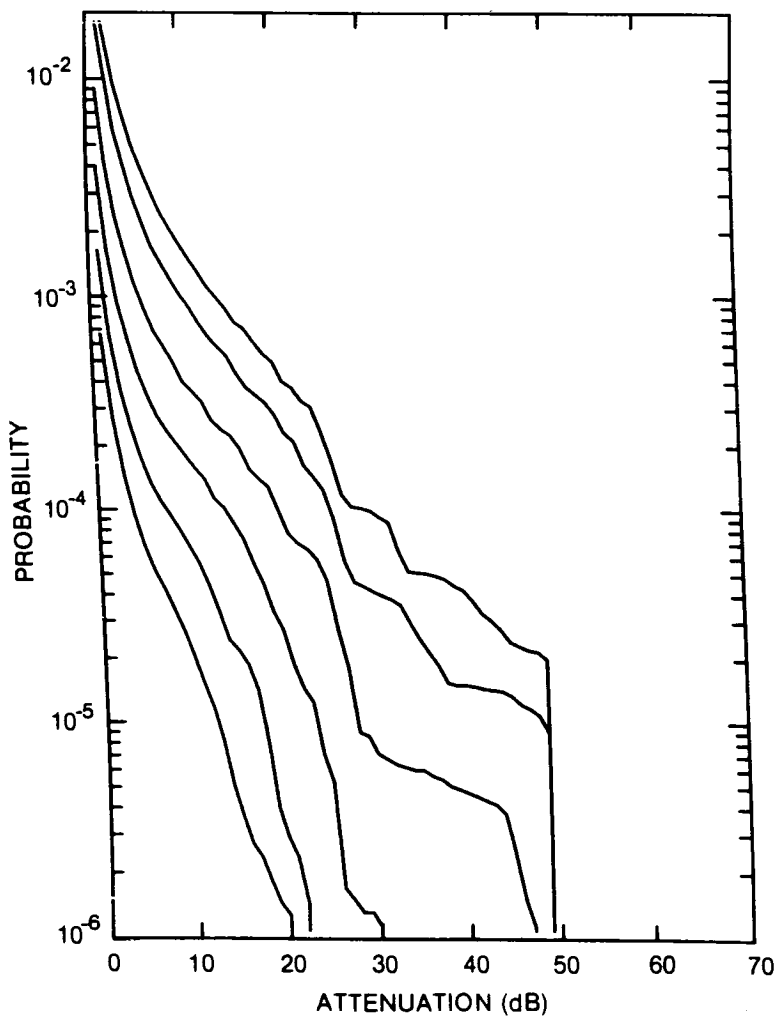

Figure 171. Cumulative distribution of rain attenuation for 11 GHz at Kingston, ONT. Curves, moving from lowest to highest, are for hop lengths of 5, 10, 20, 40, 80 and 120 km, respectively.

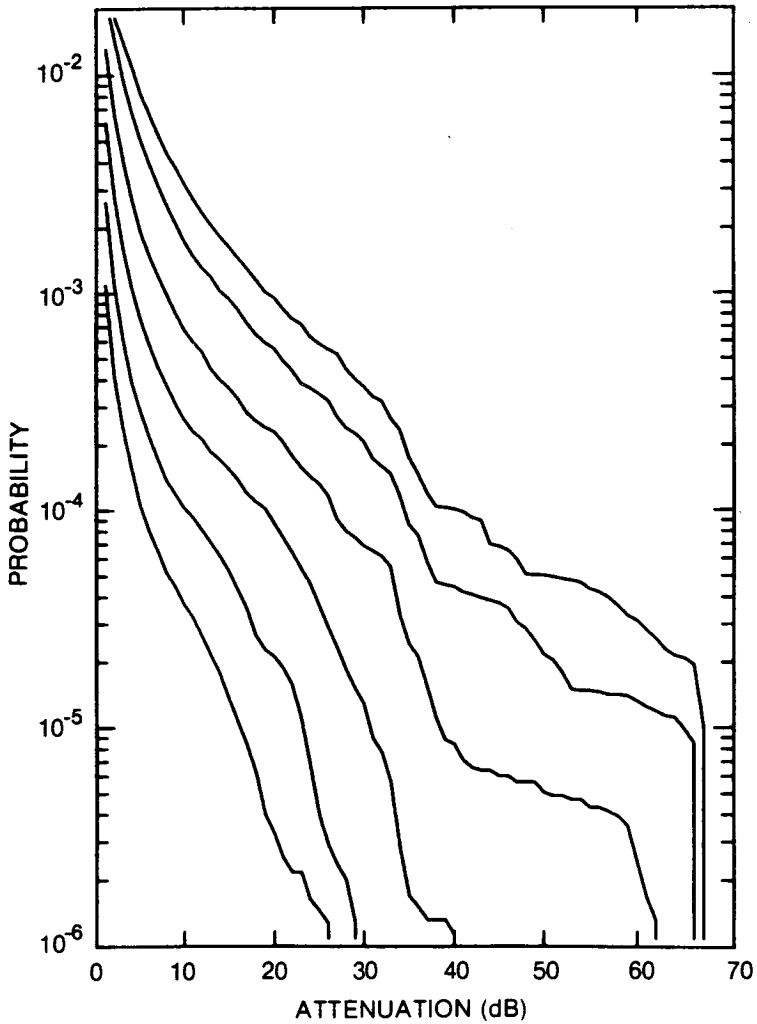

Figure 172. Cumulative distribution of rain attenuation for 12.8 GHz at Kingston, ONT. Curves, moving from lowest to highest, are for hop lengths of 5, 10, 20, 40, 80 and 120 km, respectively.

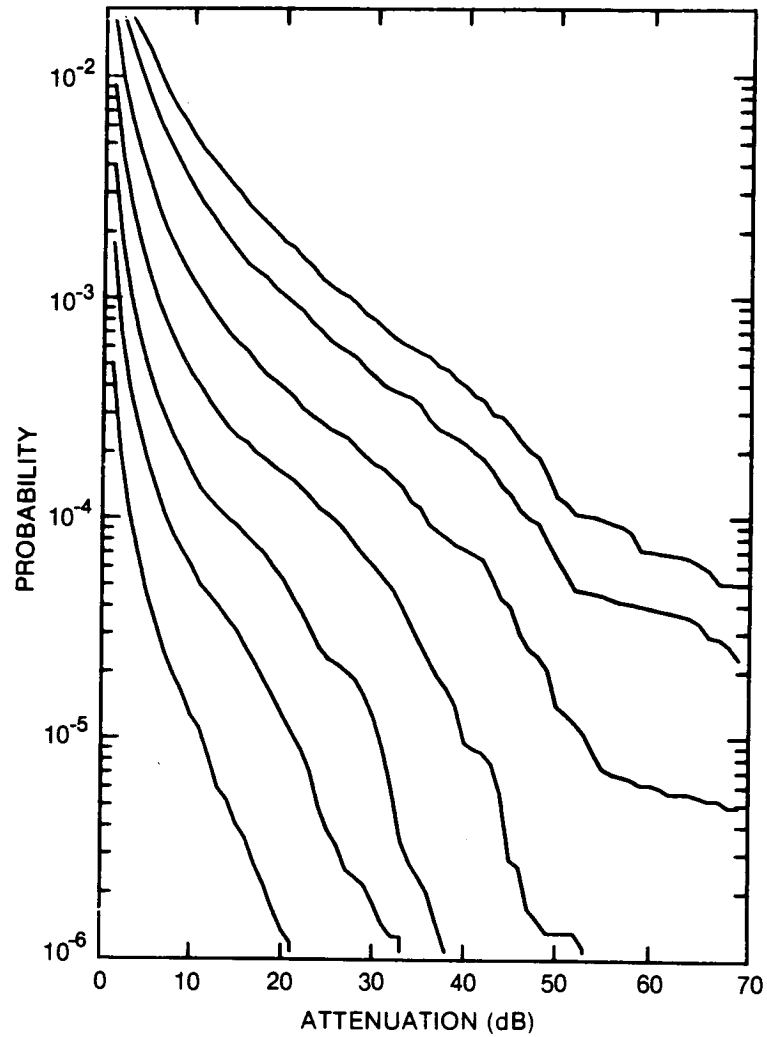

Figure 173. Cumulative distribution of rain attenuation for 15 GHz at Kingston, ONT. Curves, moving from lowest to highest, are for hop lengths of 2, 5, 10, 20, 40, 80 and 120 km, respectively.

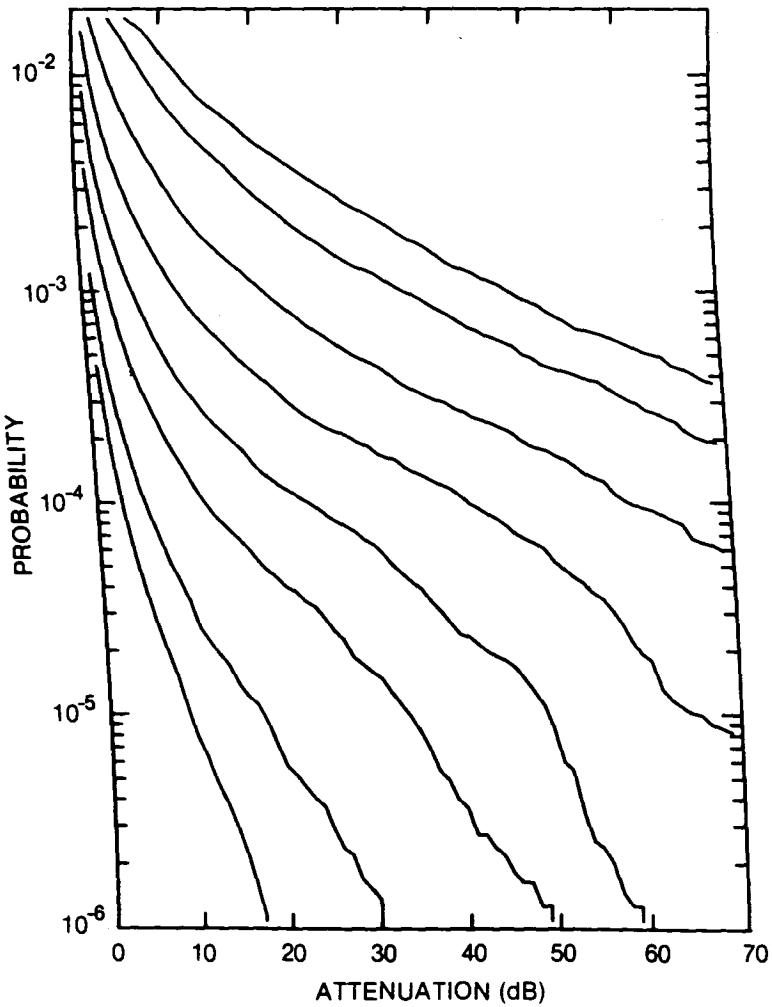

Figure 174. Cumulative distribution of rain attenuation for 20 GHz at Kingston, ONT. Curves, moving from lowest to highest, are for hop lengths of 1, 2, 5, 10, 20, 40, 80 and 120 km, respectively.

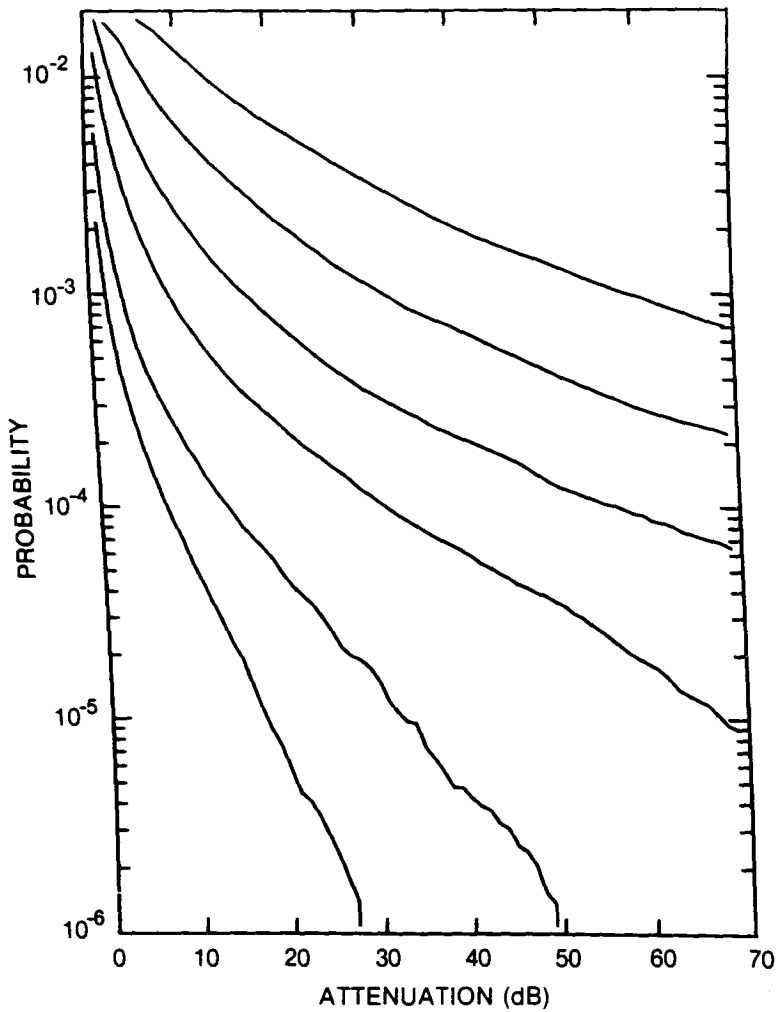

Figure 175. Cumulative distribution of rain attenuation for 35 GHz at Kingston, ONT. Curves, moving from lowest to highest, are for hop lengths of 1, 2, 5, 10, 20 and 40 km, respectively.

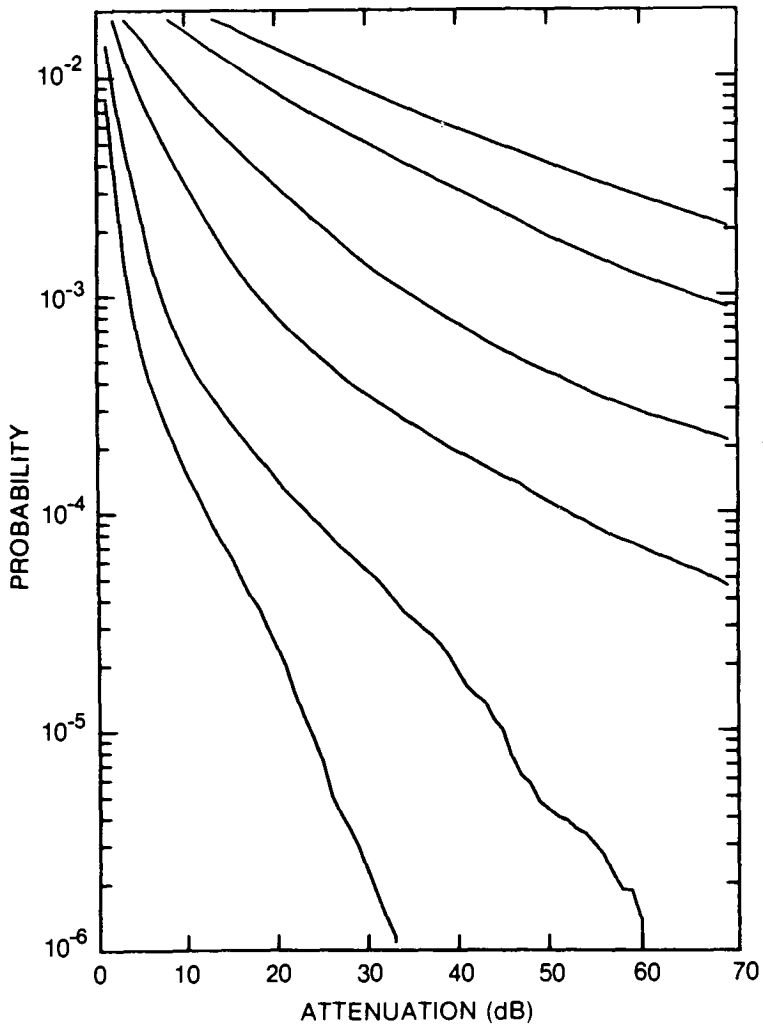

Figure 176. Cumulative distribution of rain attenuation for 56 GHz at Kingston, ONT. Curves, moving from lowest to highest, are for hop lengths of 1, 2, 5, 10, 20 and 30 km, respectively.

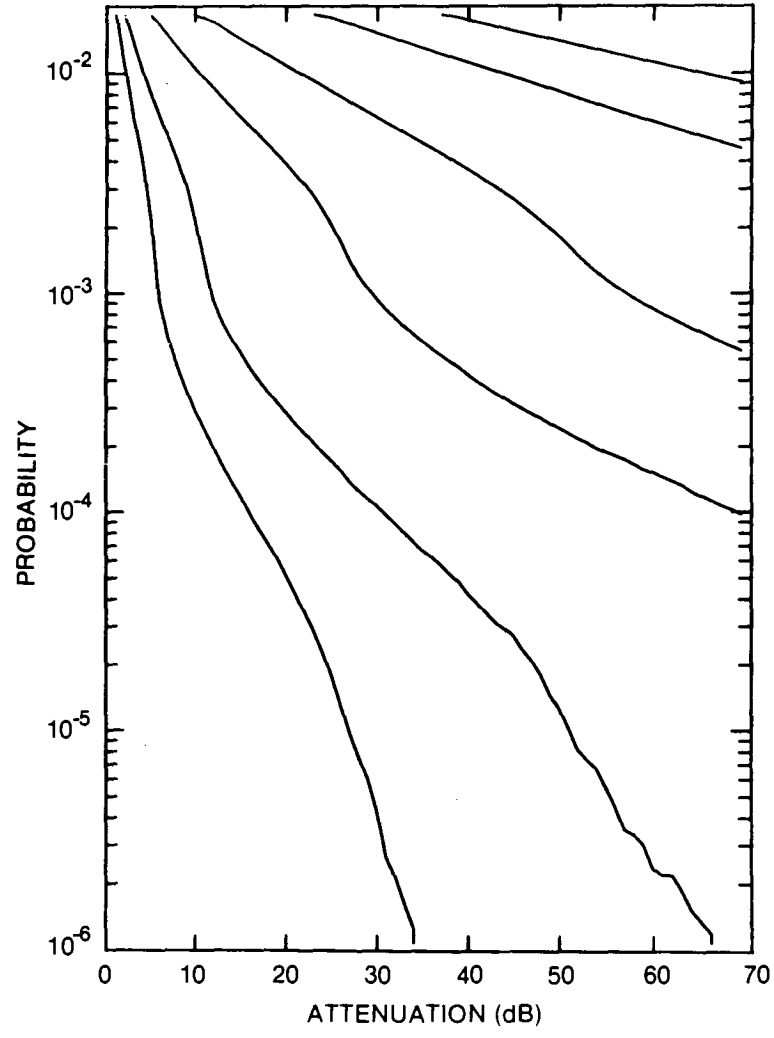

Figure 177. Cumulative distribution of rain attenuation for 100 GHz at Kingston, ONT. Curves, moving from lowest to highest, are for hop lengths of 1, 2, 5, 10, 20 and 30 km, respectively.

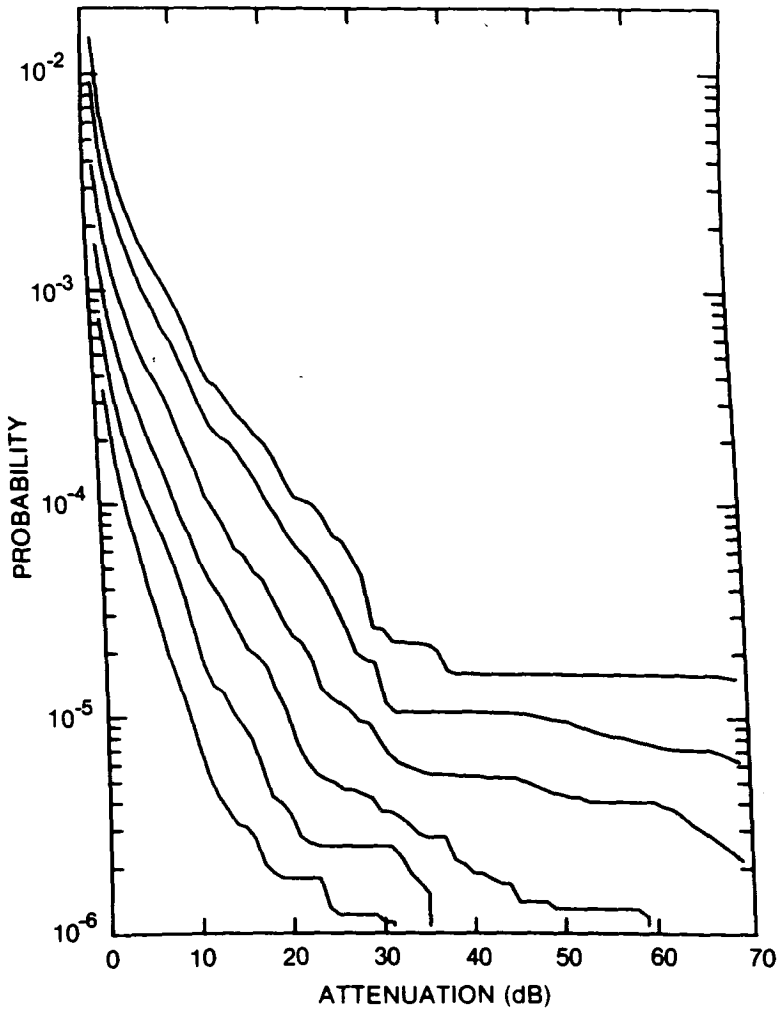

Figure 178. Cumulative distribution of rain attenuation for 8 GHz at London, ONT. Curves, moving from lowest to highest, are for hop lengths of 5, 10, 20, 40, 80 and 120 km, respectively.

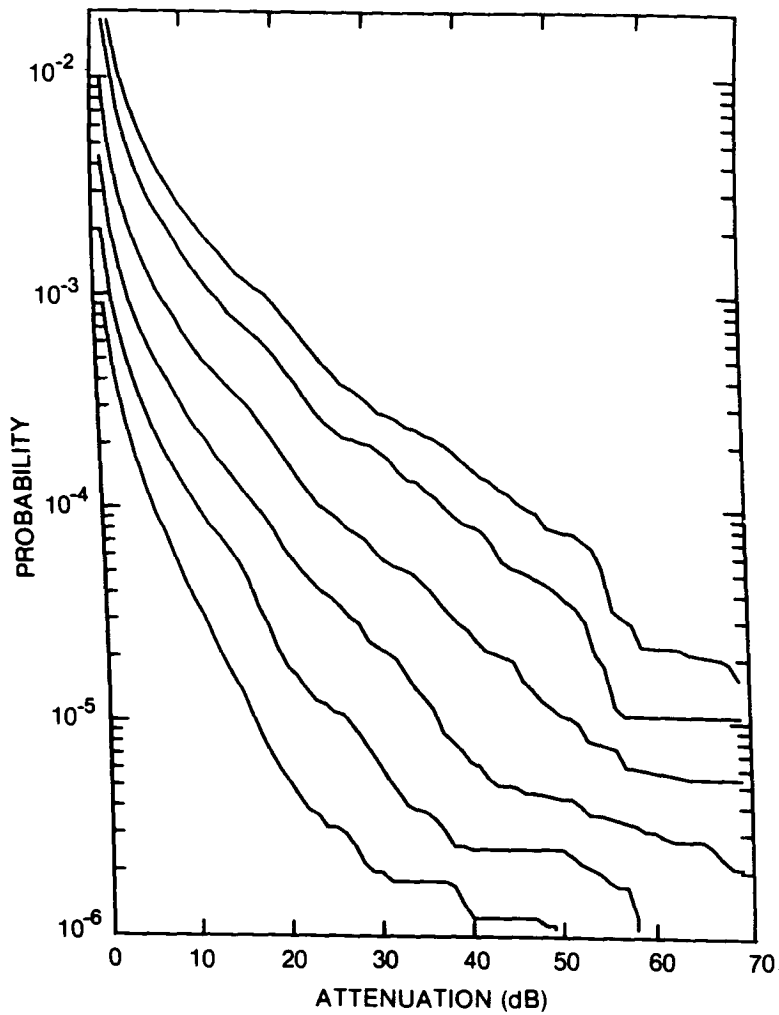

Figure 179. Cumulative distribution of rain attenuation for 11 GHz at London, ONT. Curves, moving from lowest to highest, are for hop lengths of 5, 10, 20, 40, 80 and 120 km, respectively.

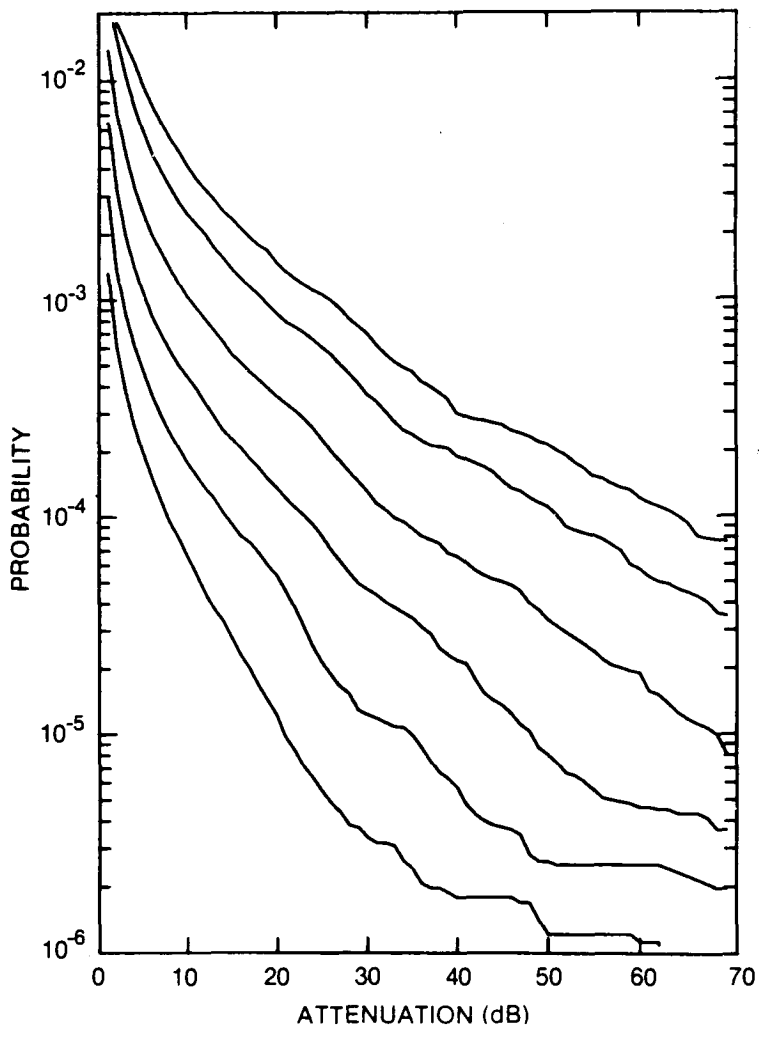

Figure 180. Cumulative distribution of rain attenuation for 12.8 GHz at London, ONT. Curves, moving from lowest to highest, are for hop lengths of 5, 10, 20, 40, 80 and 120 km, respectively.

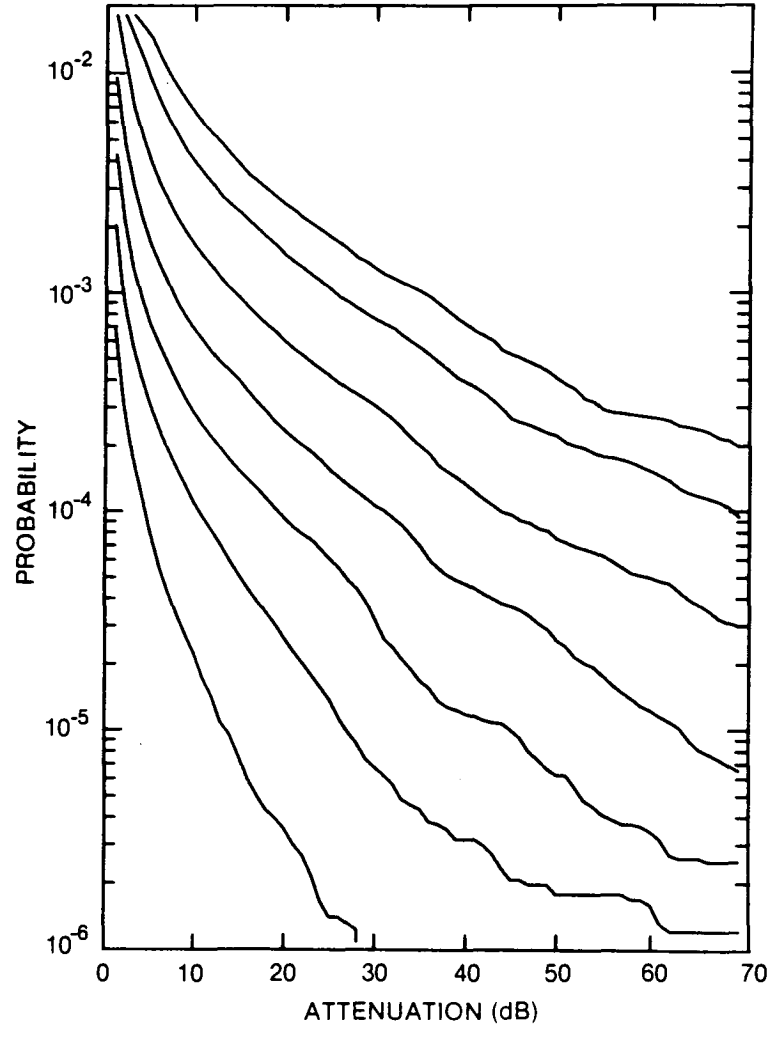

Figure 181. Cumulative distribution of rain attenuation for 15 GHz at London, ONT. Curves, moving from lowest to highest, are for hop lengths of 2, 5, 10, 20, 40, 80 and 120 km, respectively.

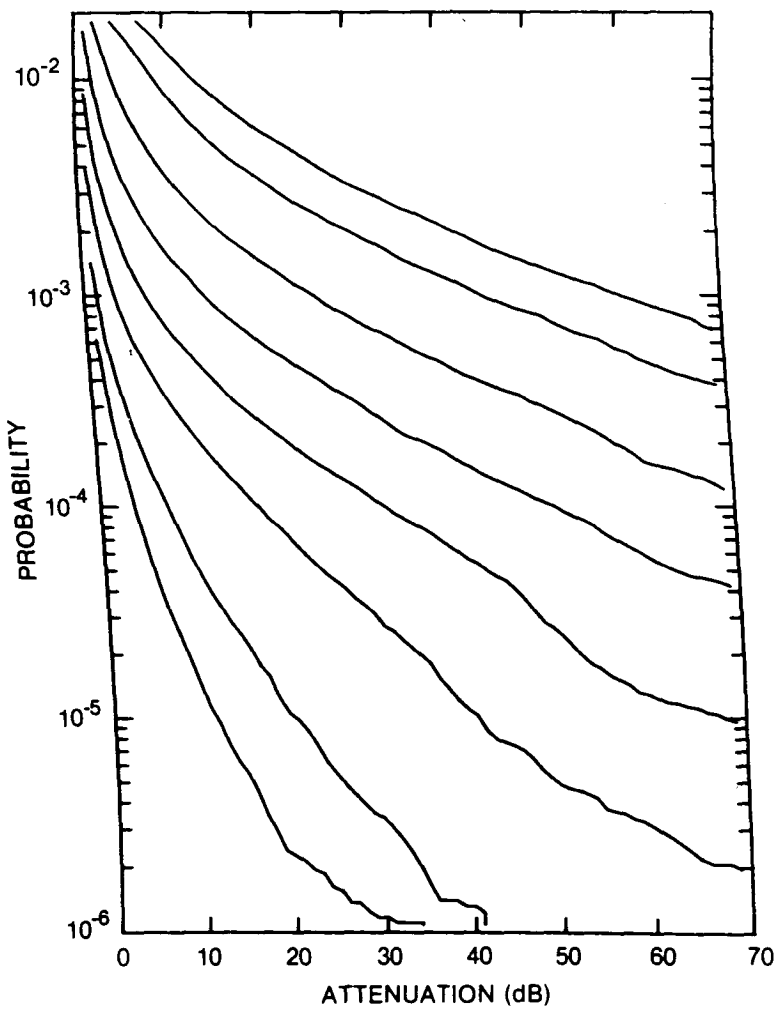

Figure 182. Cumulative distribution of rain attenuation for 20 GHz at London, ONT. Curves, moving from lowest to highest, are for hop lengths of 1, 2, 5, 10, 20, 40, 80 and 120 km, respectively.

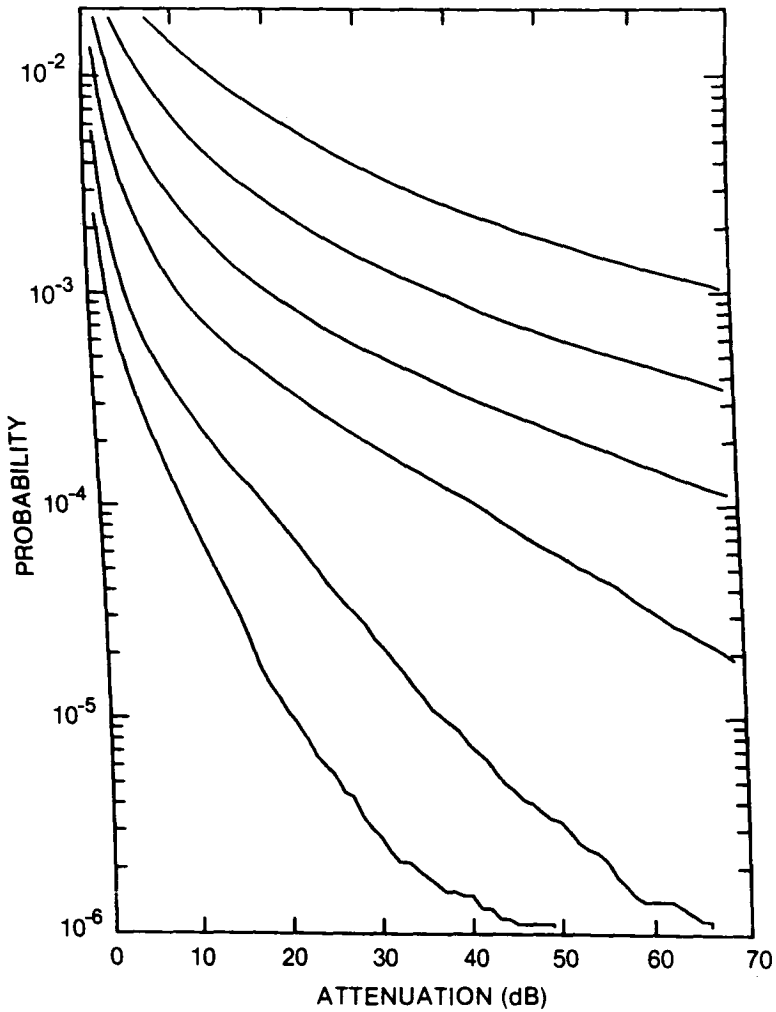

Figure 183. Cumulative distribution of rain attenuation for 35 GHz at London, ONT. Curves, moving from lowest to highest, are for hop lengths of 1, 2, 5, 10, 20 and 40 km, respectively.

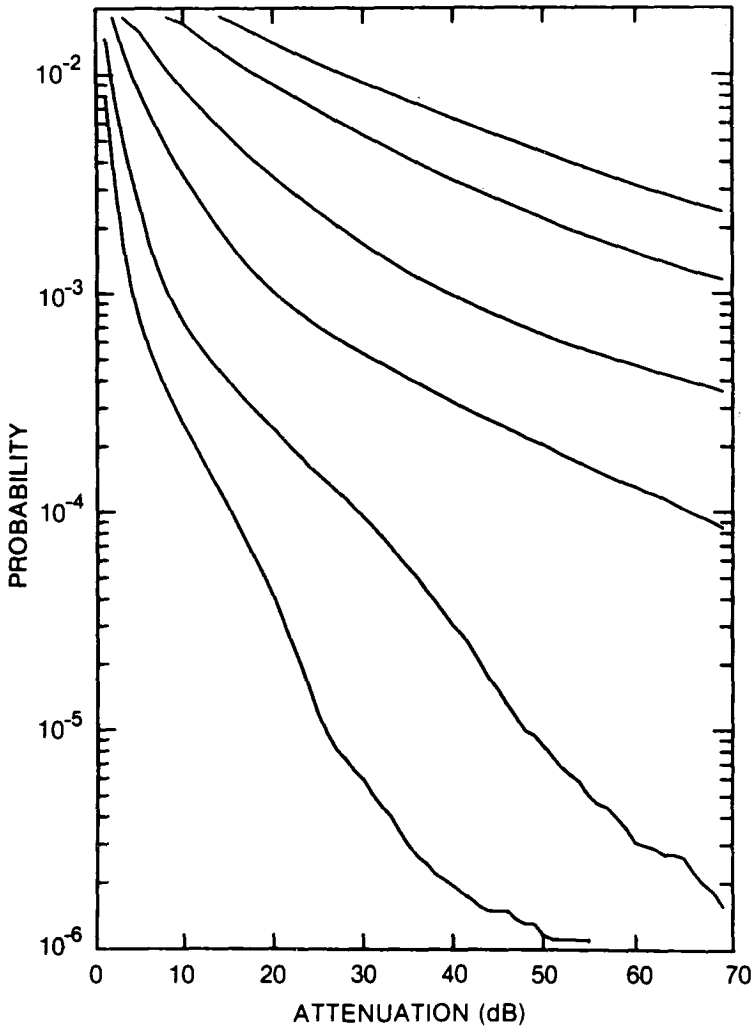

Figure 184. Cumulative distribution of rain attenuation for 56 GHz at London, ONT. Curves, moving from lowest to highest, are for hop lengths of 1, 2, 5, 10, 20 and 30 km, respectively.

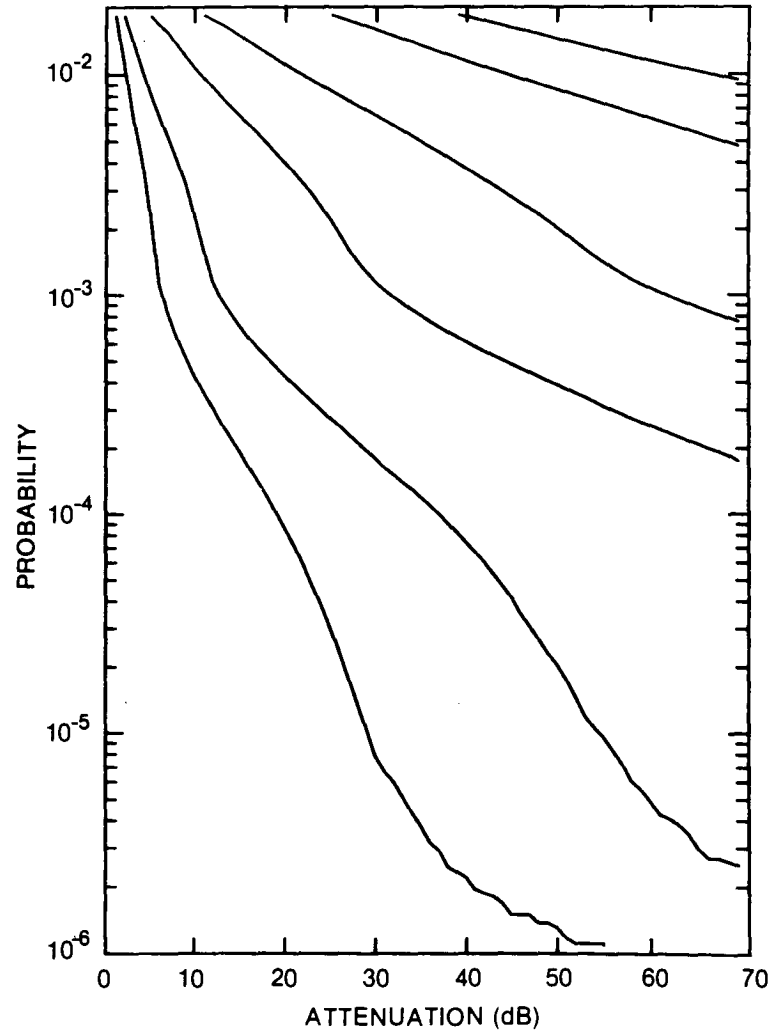

Figure 185. Cumulative distribution of rain attenuation for 100 GHz at London, ONT. Curves, moving from lowest to highest, are for hop lengths of 1, 2, 5, 10, 20 and 30 km, respectively.

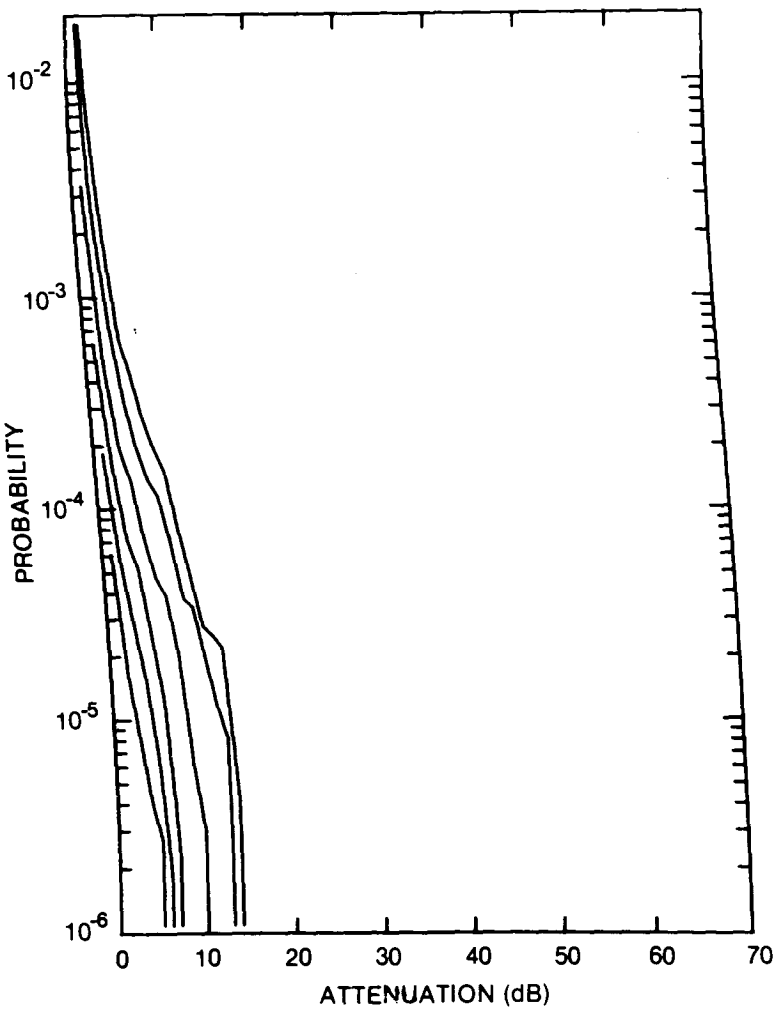

Figure 186. Cumulative distribution of rain attenuation for 8 GHz at Mission, BC. Curves, moving from lowest to highest, are for hop lengths of 5, 10, 20, 40, 80 and 120 km, respectively.

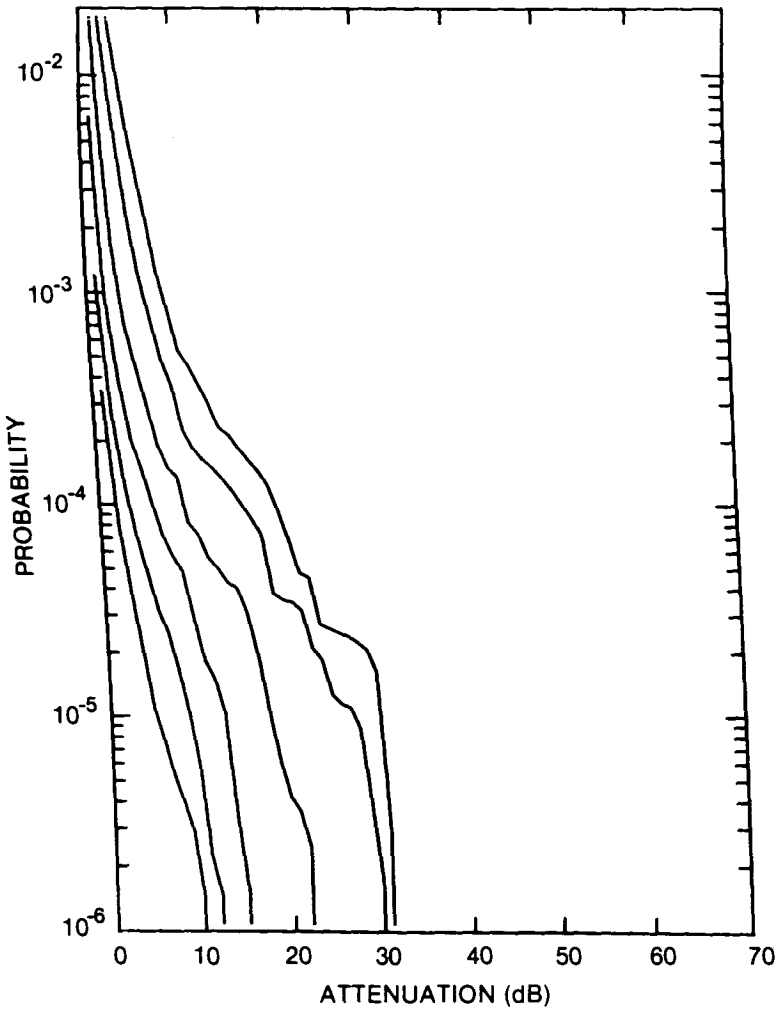

Figure 187. Cumulative distribution of rain attenuation for 11 GHz at Mission, BC. Curves, moving from lowest to highest, are for hop lengths of 5, 10, 20, 40, 80 and 120 km, respectively.

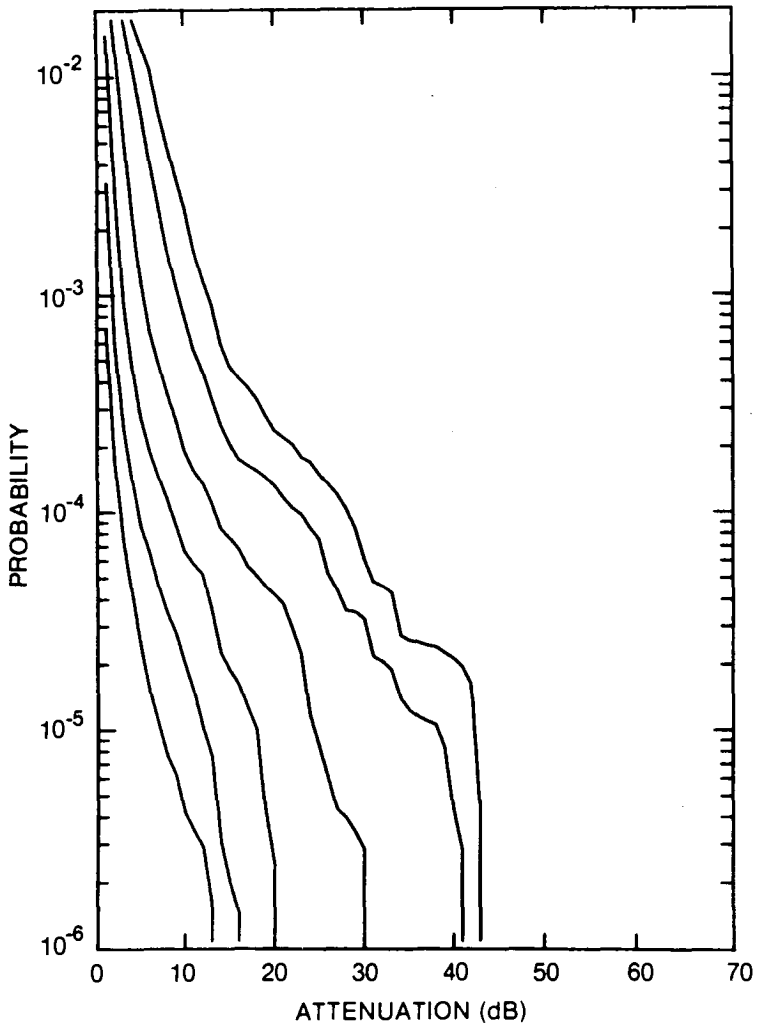

Figure 188. Cumulative distribution of rain attenuation for 12.8 GHz at Mission, BC. Curves, moving from lowest to highest, are for hop lengths of 5, 10, 20, 40, 80 and 120 km, respectively.

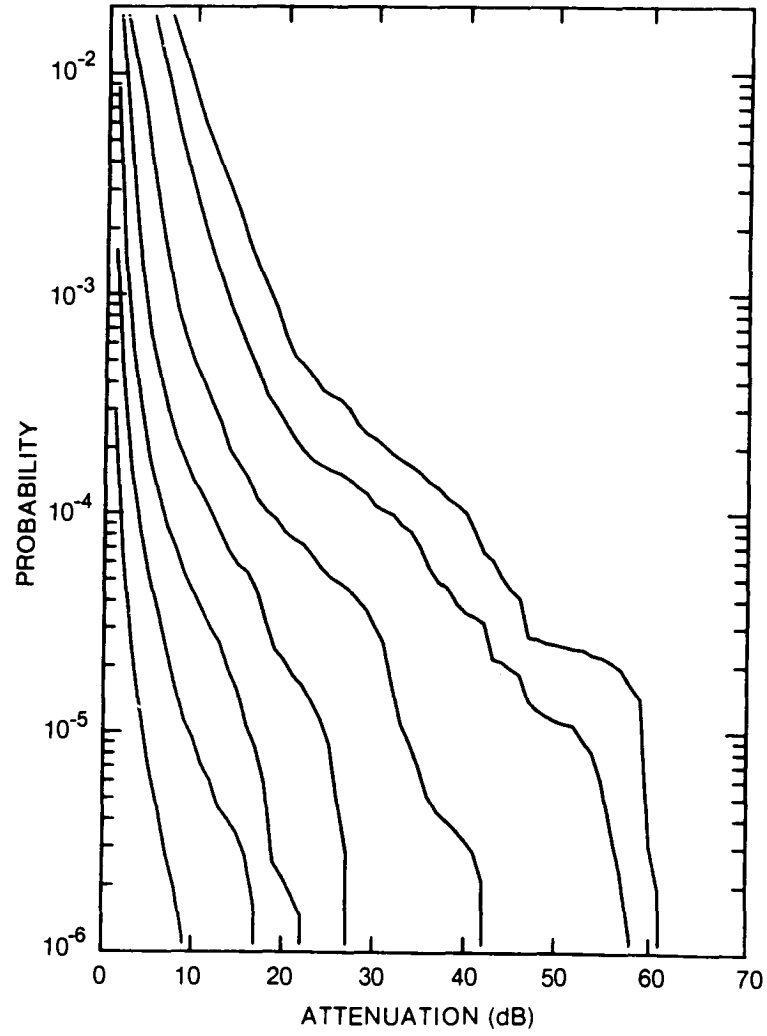

Figure 189. Cumulative distribution of rain attenuation for 15 GHz at Mission, BC. Curves, moving from lowest to highest, are for hop lengths of 2, 5, 10, 20, 40, 80 and 120 km, respectively.

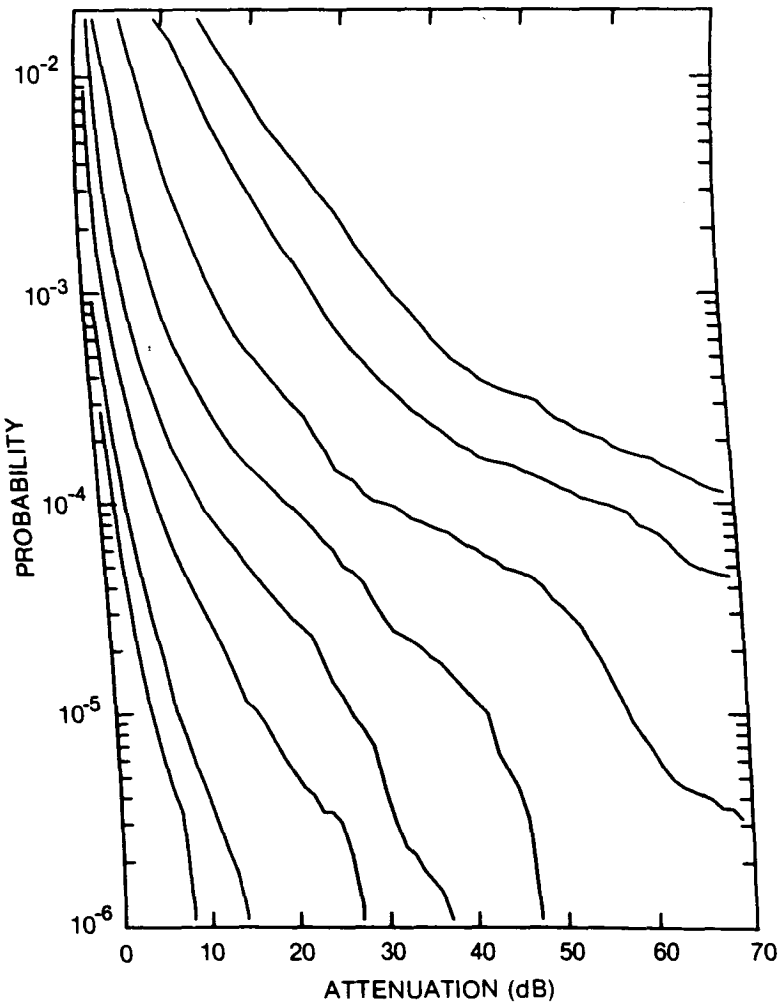

Figure 190. Cumulative distribution of rain attenuation for 20 GHz at Mission, BC. Curves, moving from lowest to highest, are for hop lengths of 1, 2, 5, 10, 20 40, 80 and 120 km, respectively.

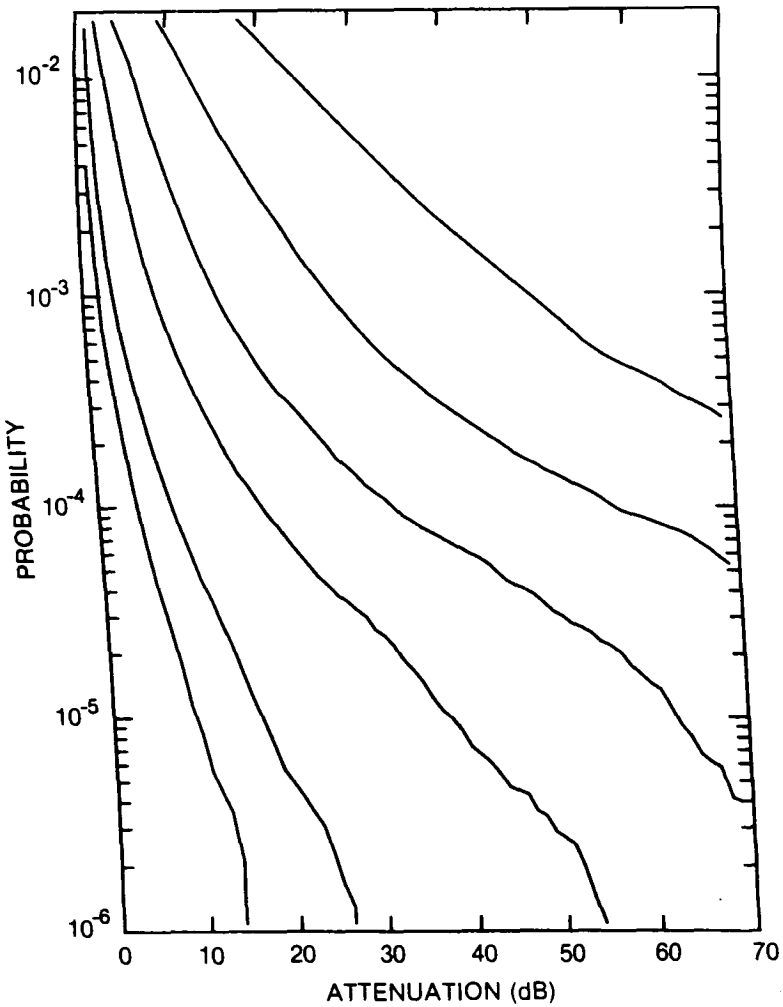

Figure 191. Cumulative distribution of rain attenuation for 35 GHz at Mission, BC. Curves, moving from lowest to highest, are for hop lengths of 1, 2, 5, 10, 20 and 40 km, respectively.

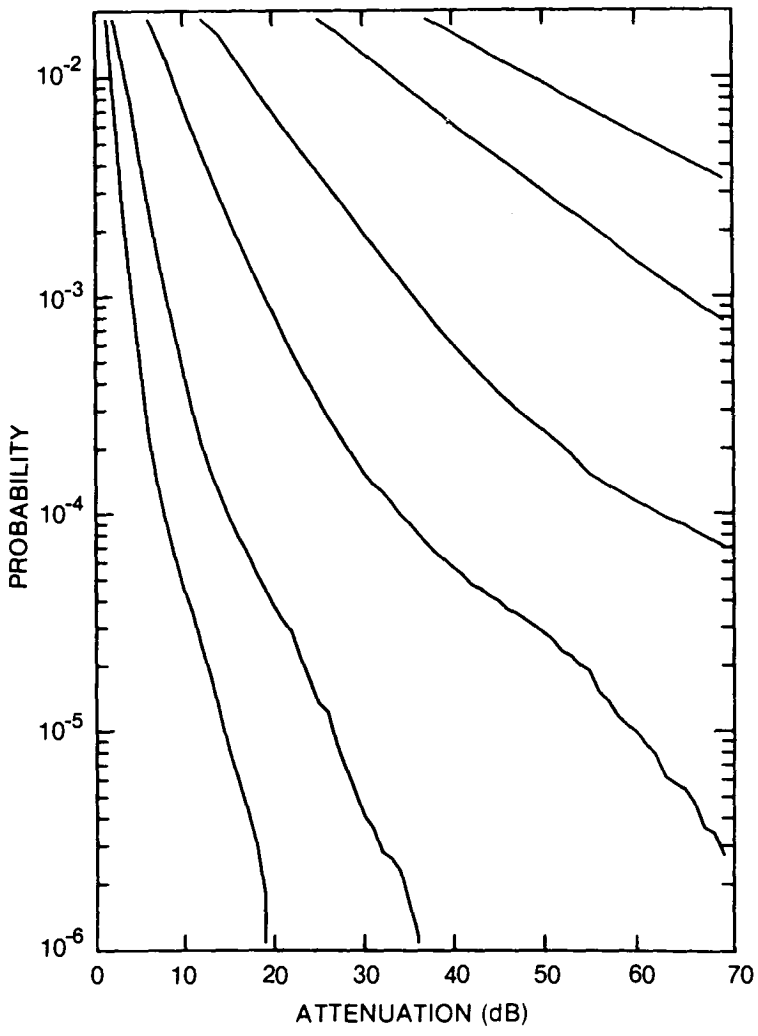

Figure 192. Cumulative distribution of rain attenuation for 56 GHz at Mission, BC. Curves, moving from lowest to highest, are for hop lengths of 1, 2, 5, 10, 20 and 30 km, respectively.

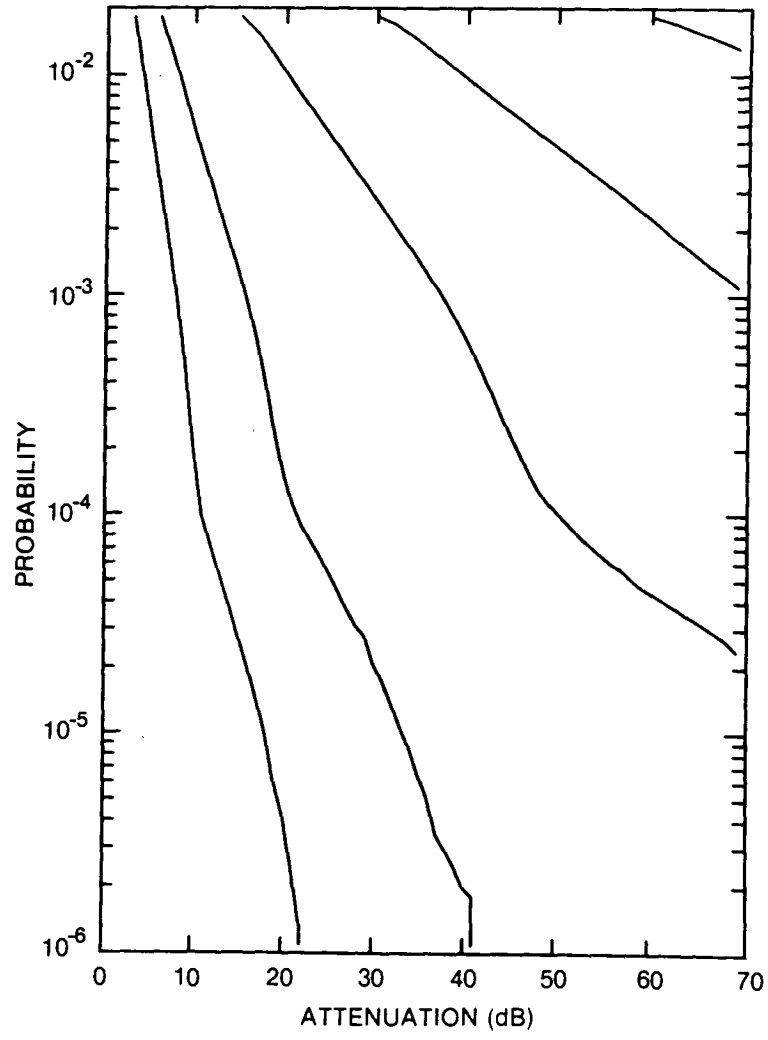

Figure 193. Cumulative distribution of rain attenuation for 100 GHz at Mission, BC. Curves, moving from lowest to highest, are for hop lengths of 1, 2, 5, 10 and 20 km, respectively.

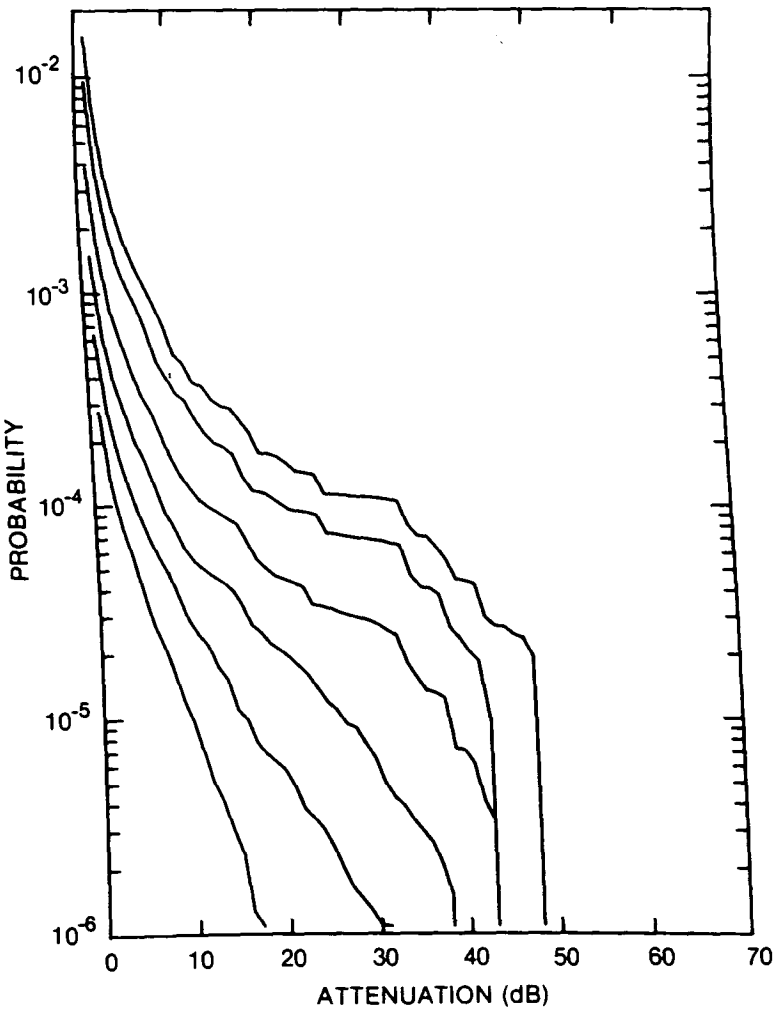

Figure 194. Cumulative distribution of rain attenuation for 8 GHz at Montreal, QUE. Curves, moving from lowest to highest, are for hop lengths of 5, 10, 20, 40, 80 and 120 km, respectively.

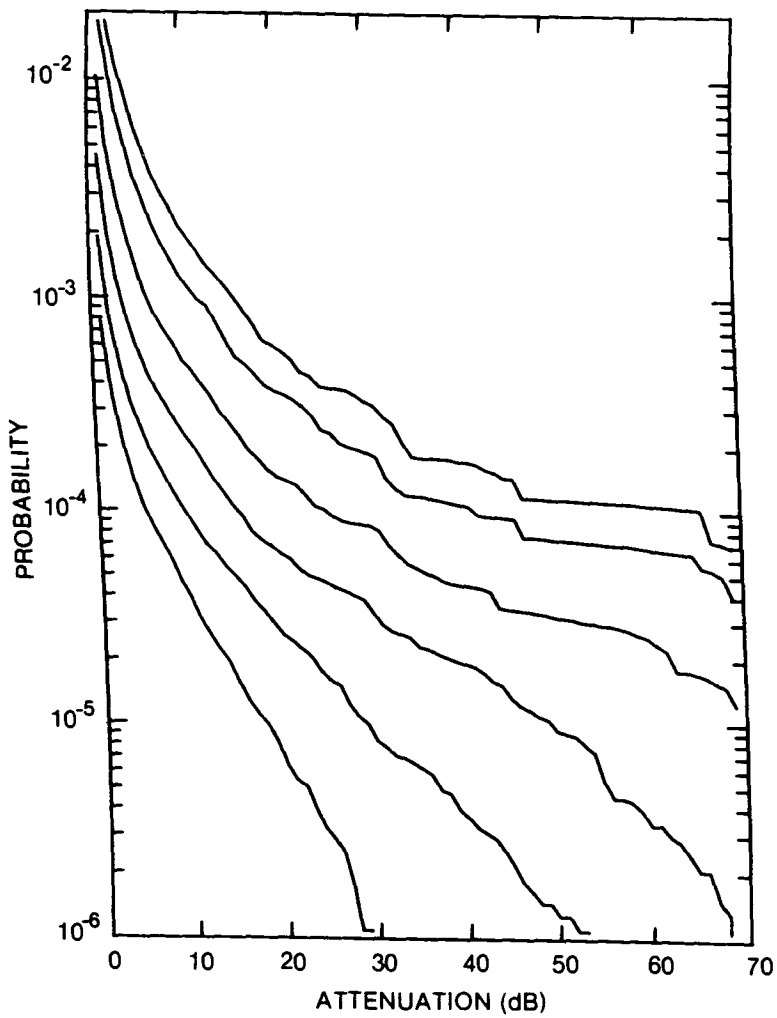

Figure 195. Cumulative distribution of rain attenuation for 11 GHz at Montreal, QUE. Curves, moving from lowest to highest, are for hop lengths of 5, 10, 20, 40, 80 and 120 km, respectively.

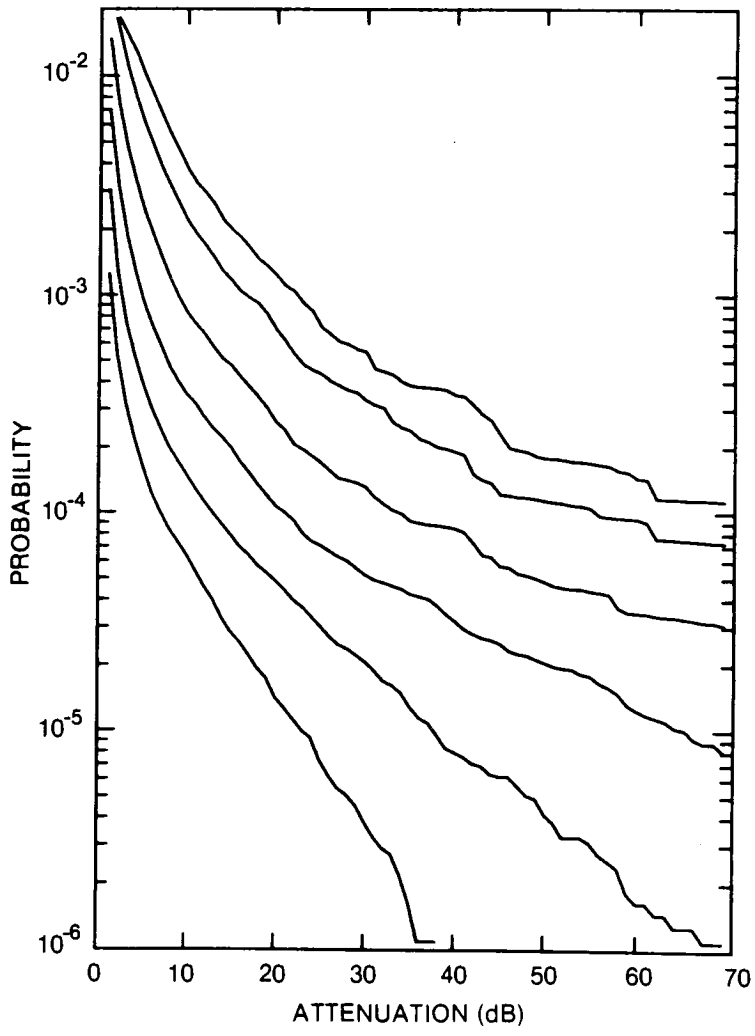

Figure 196. Cumulative distribution of rain attenuation for 12.8 GHz at Montreal, QUE. Curves, moving from lowest to highest, are for hop lengths of 5, 10, 20, 40, 80 and 120 km, respectively.

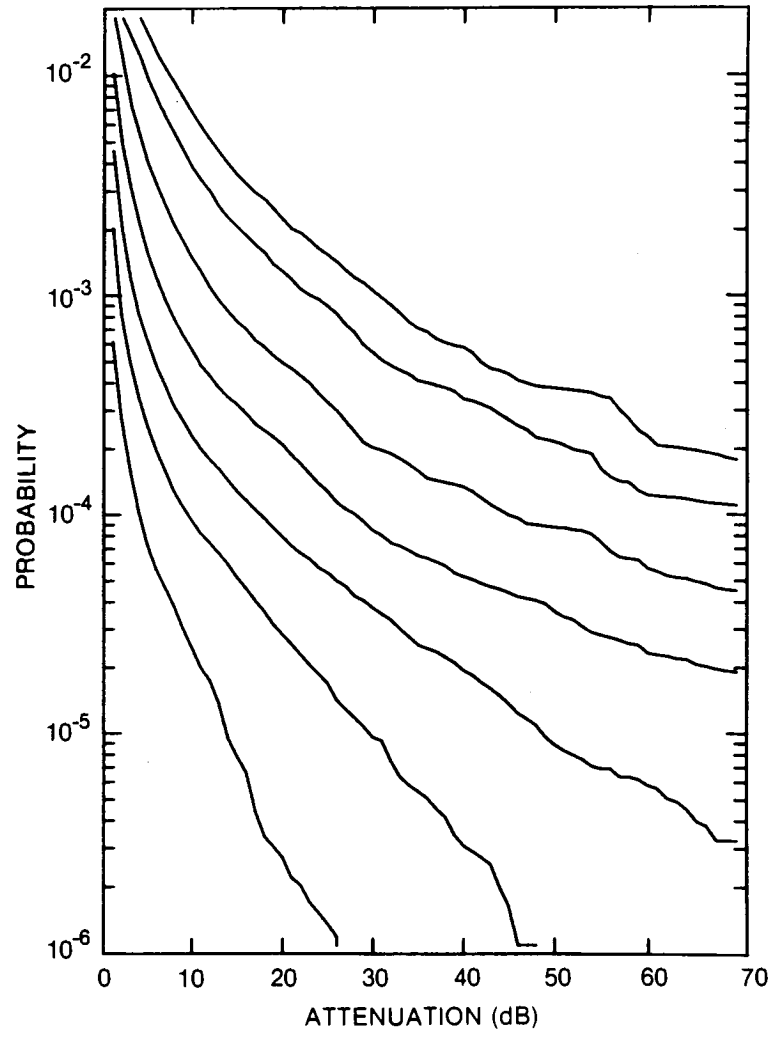

Figure 197. Cumulative distribution of rain attenuation for 15 GHz at Montreal, QUE. Curves, moving from lowest to highest, are for hop lengths of 2, 5, 10, 20, 40, 80 and 120 km, respectively.

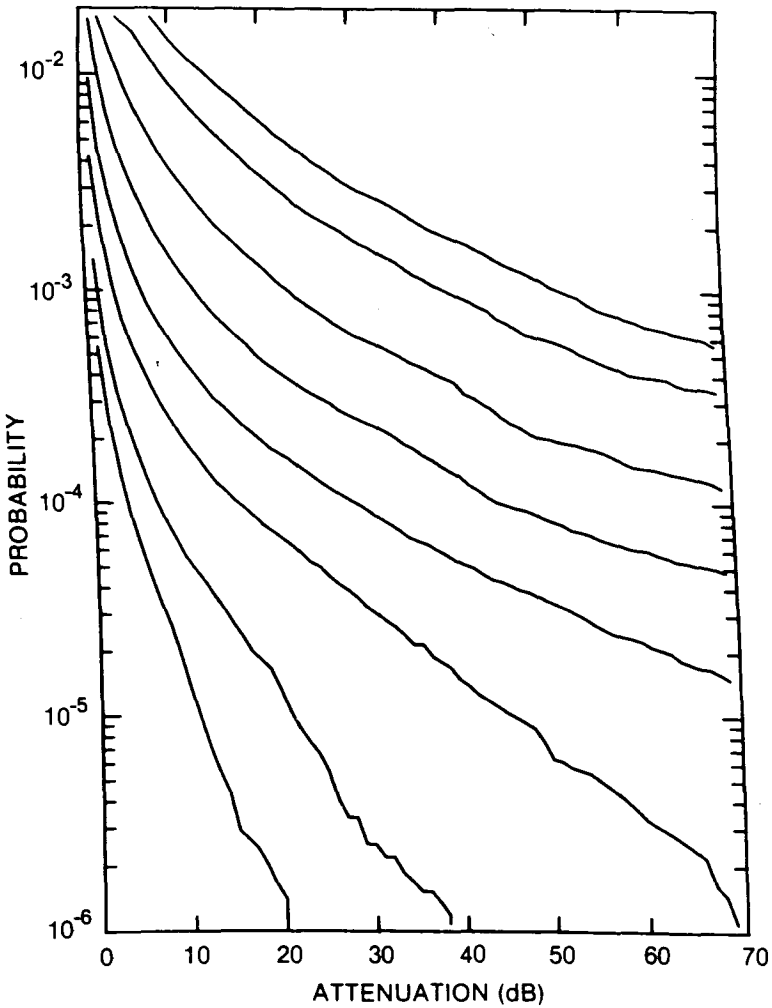

Figure 198. Cumulative distribution of rain attenuation for 20 GHz at Montreal, QUE. Curves, moving from lowest to highest, are for hop lengths of 1, 2, 5, 10, 20, 40, 80 and 120 km, respectively.

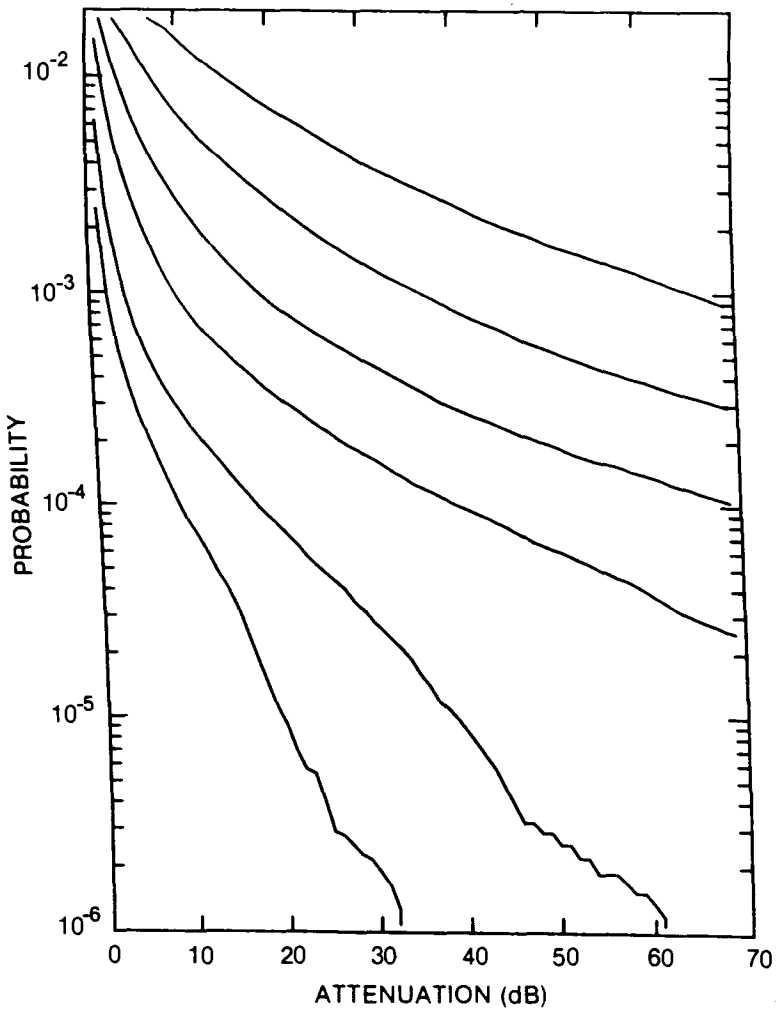

Figure 199. Cumulative distribution of rain attenuation for 35 GHz at Montreal, QUE. Curves, moving from lowest to highest, are for hop lengths of 1, 2, 5, 10, 20 and 40 km, respectively.

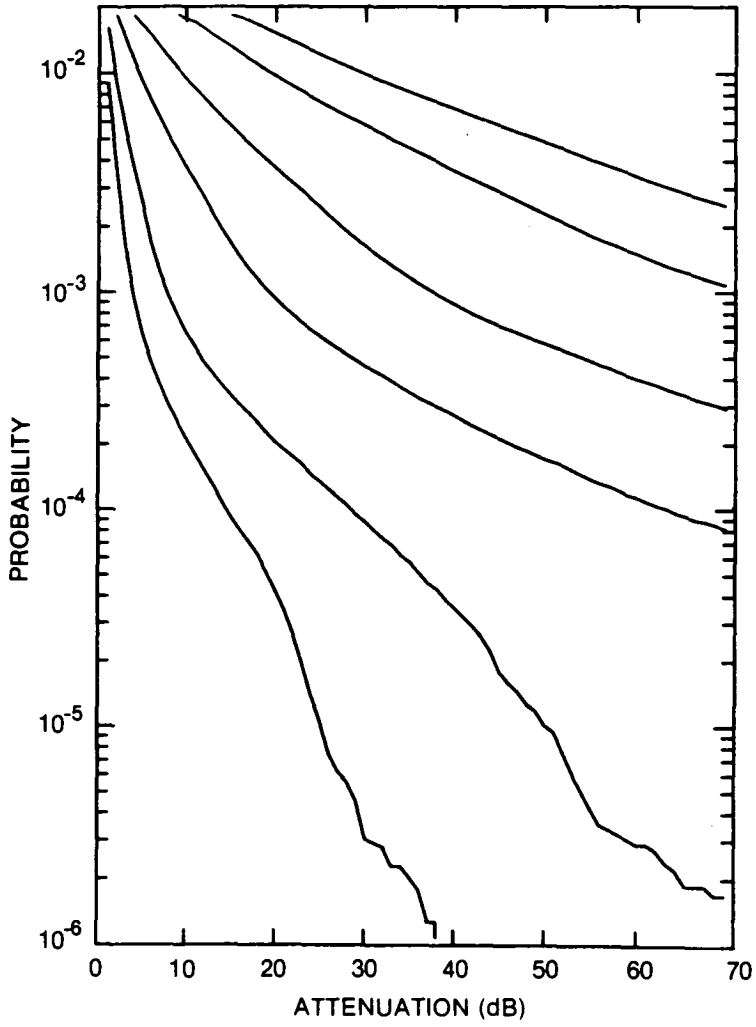

Figure 200. Cumulative distribution of rain attenuation for 56 GHz at Montreal, QUE. Curves, moving from lowest to highest, are for hop lengths of 1, 2, 5, 10, 20 and 30 km, respectively.

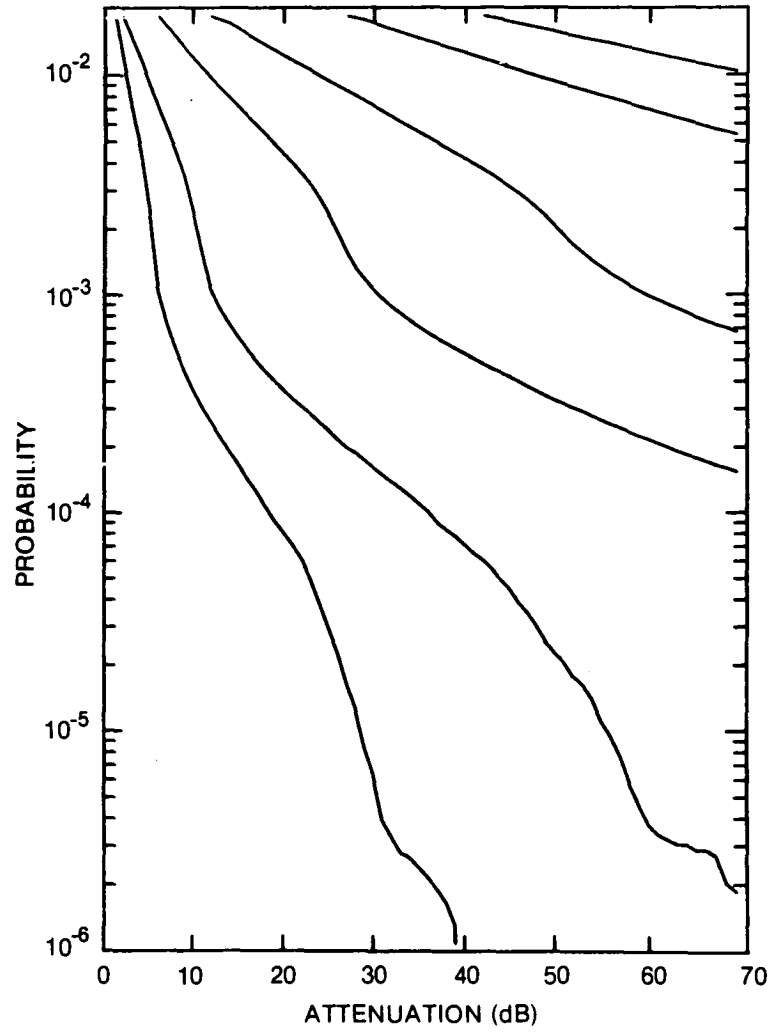

Figure 201. Cumulative distribution of rain attenuation for 100 GHz at Montreal, QUE. Curves, moving from lowest to highest, are for hop lengths of 1, 2, 5, 10, 20 and 30 km, respectively.

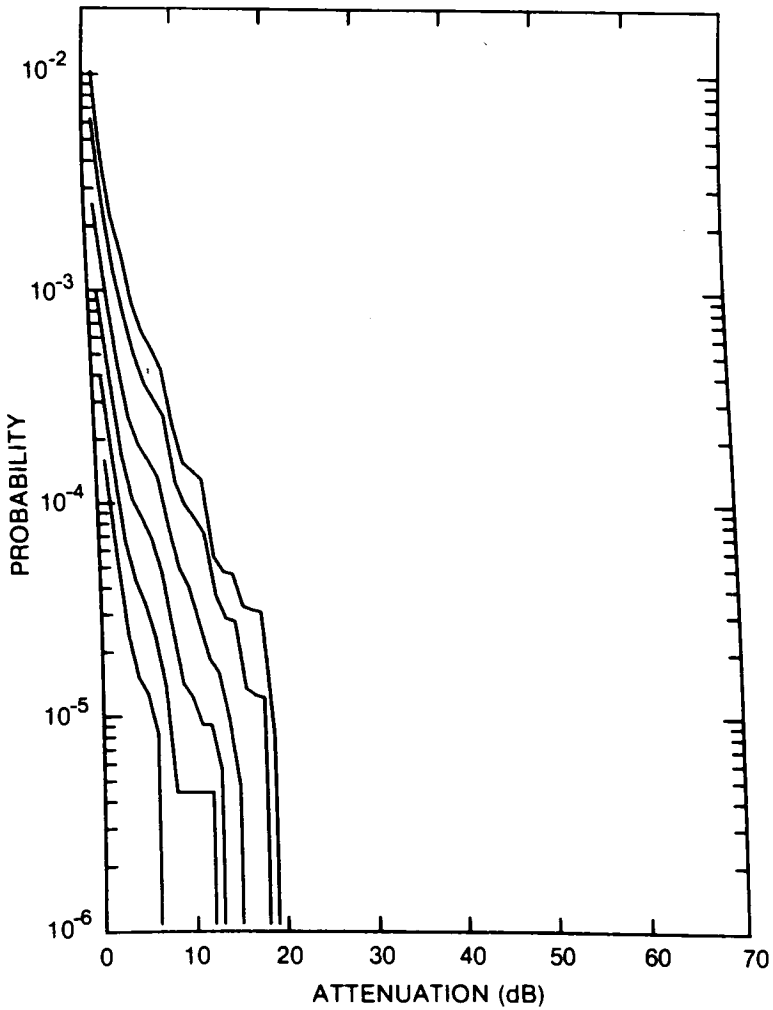

Figure 202. Cumulative distribution of rain attenuation for 8 GHz at Moosonee, ONT. Curves, moving from lowest to highest, are for hop lengths of 5, 10, 20, 40, 80 and 120 km, respectively.

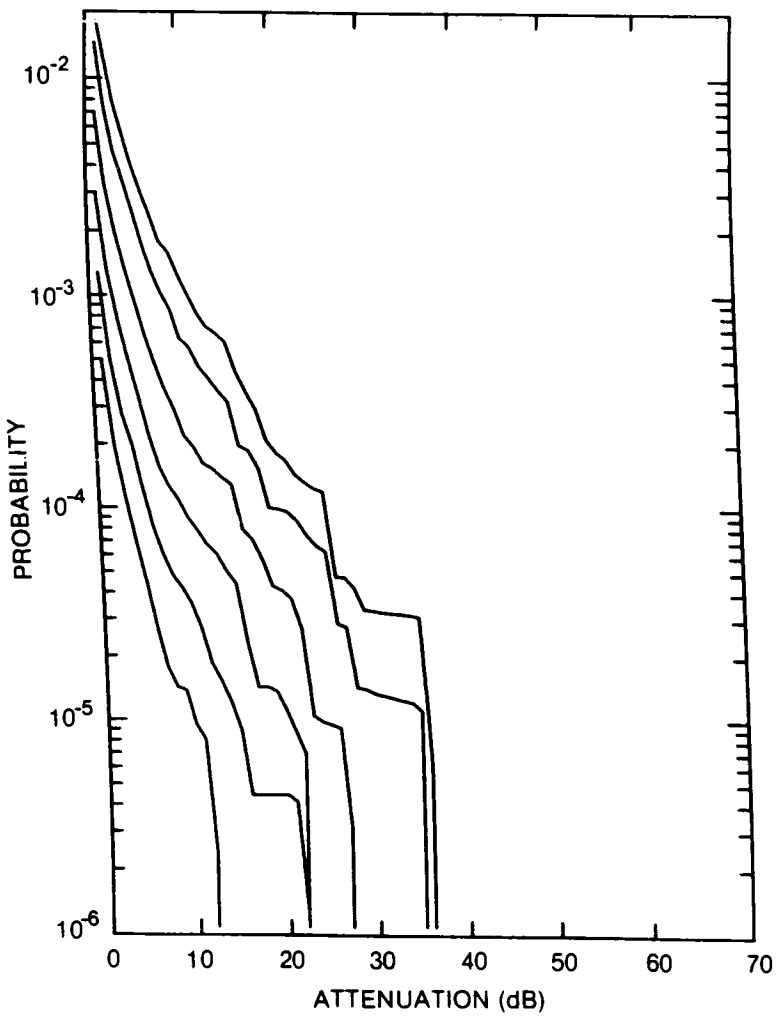

Figure 203. Cumulative distribution of rain attenuation for 11 GHz at Moosonee, ONT. Curves, moving from lowest to highest, are for hop lengths of 5, 10, 20, 40, 80 and 120 km, respectively.

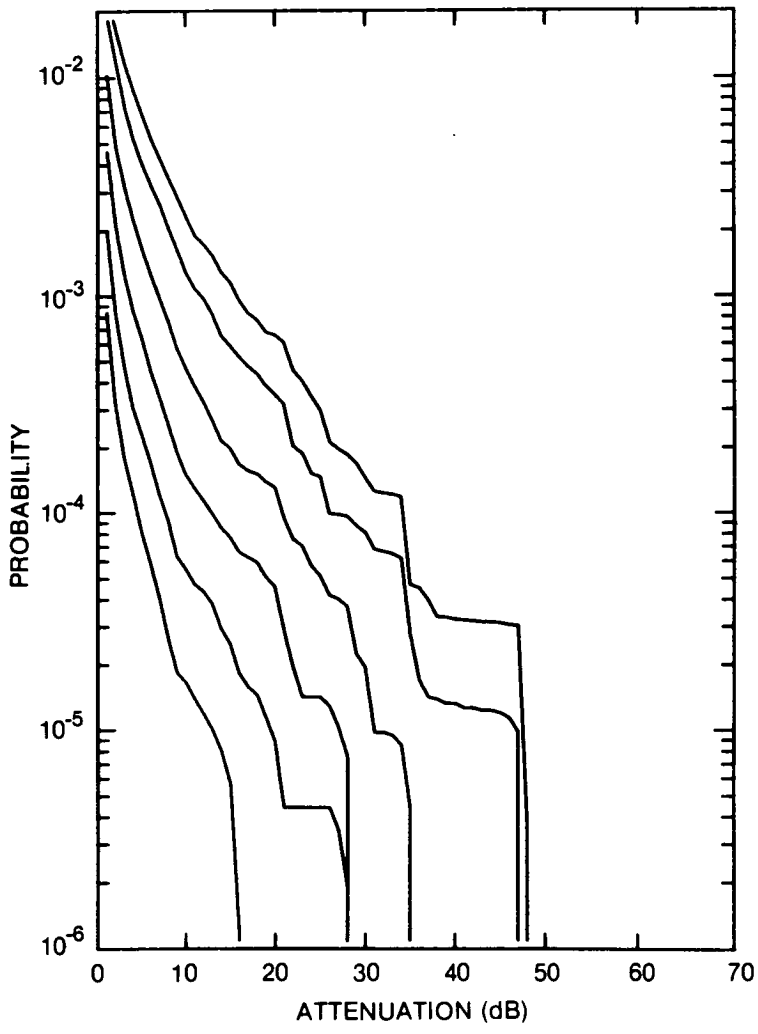

Figure 204. Cumulative distribution of rain attenuation for 12.8 GHz at Moosonee, ONT. Curves, moving from lowest to highest, are for hop lengths of 5, 10, 20, 40, 80 and 120 km, respectively.

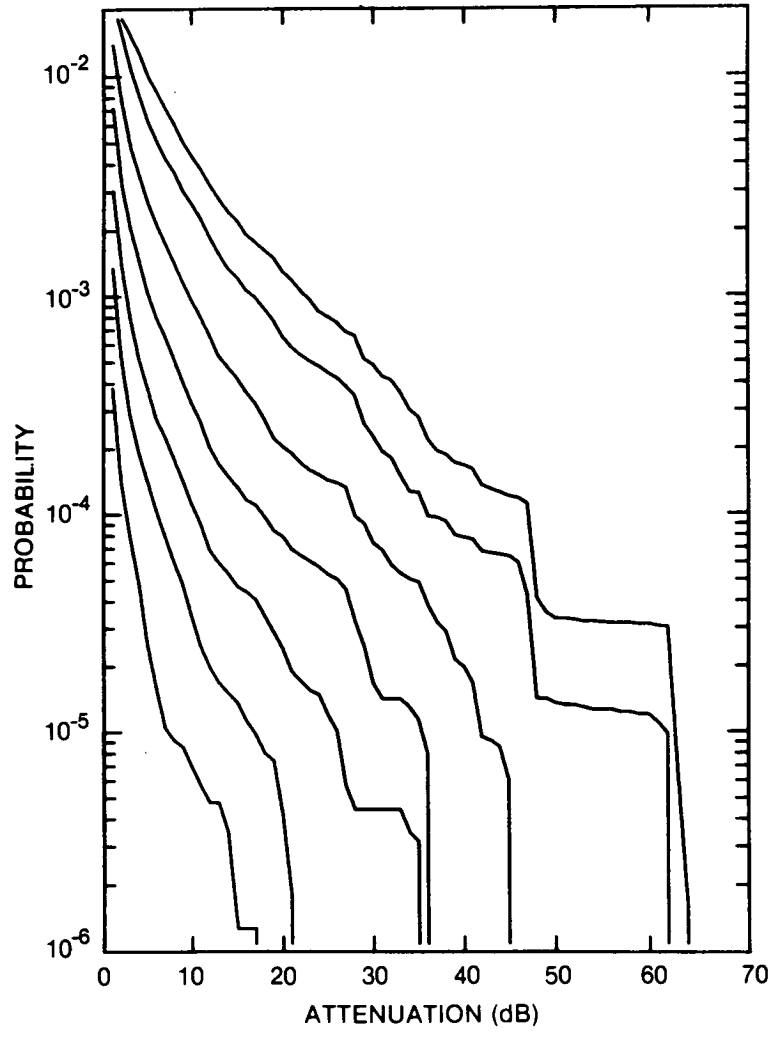

Figure 205. Cumulative distribution of rain attenuation for 15 GHz at Moosonee, ONT. Curves, moving from lowest to highest, are for hop lengths of 2, 5, 10, 20, 40, 80 and 120 km, respectively.

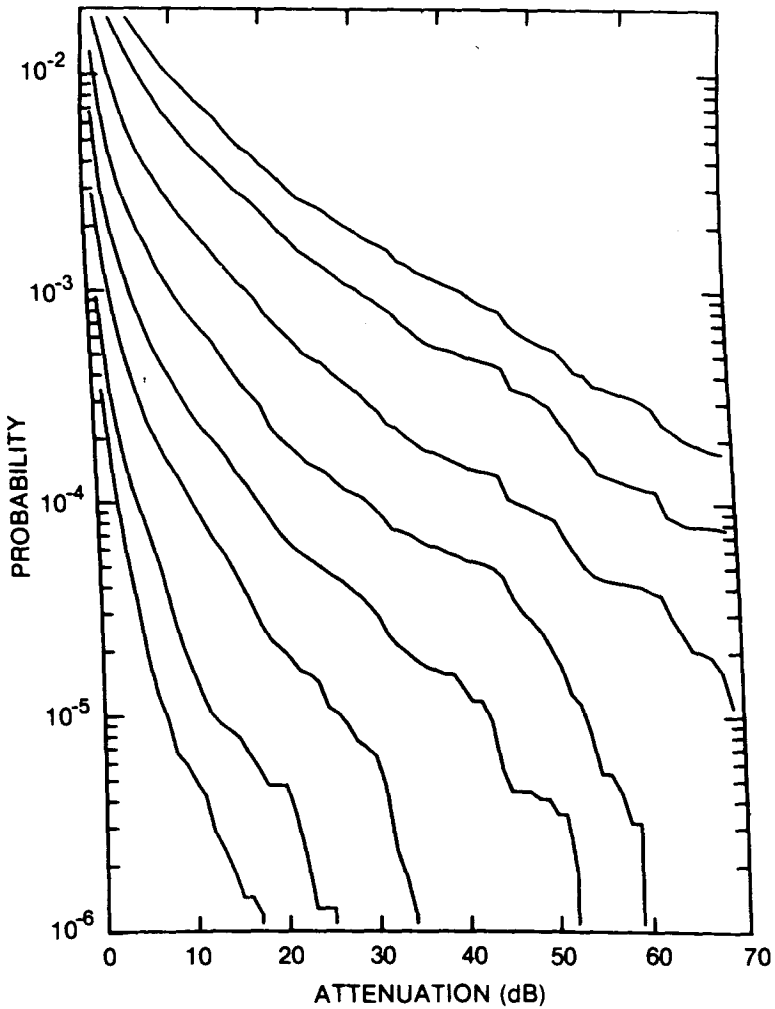

Figure 206. Cumulative distribution of rain attenuation for 20 GHz at Moosonee, ONT. Curves, moving from lowest to highest, are for hop lengths of 1, 2, 5, 10, 20, 40, 80 and 120 km, respectively.

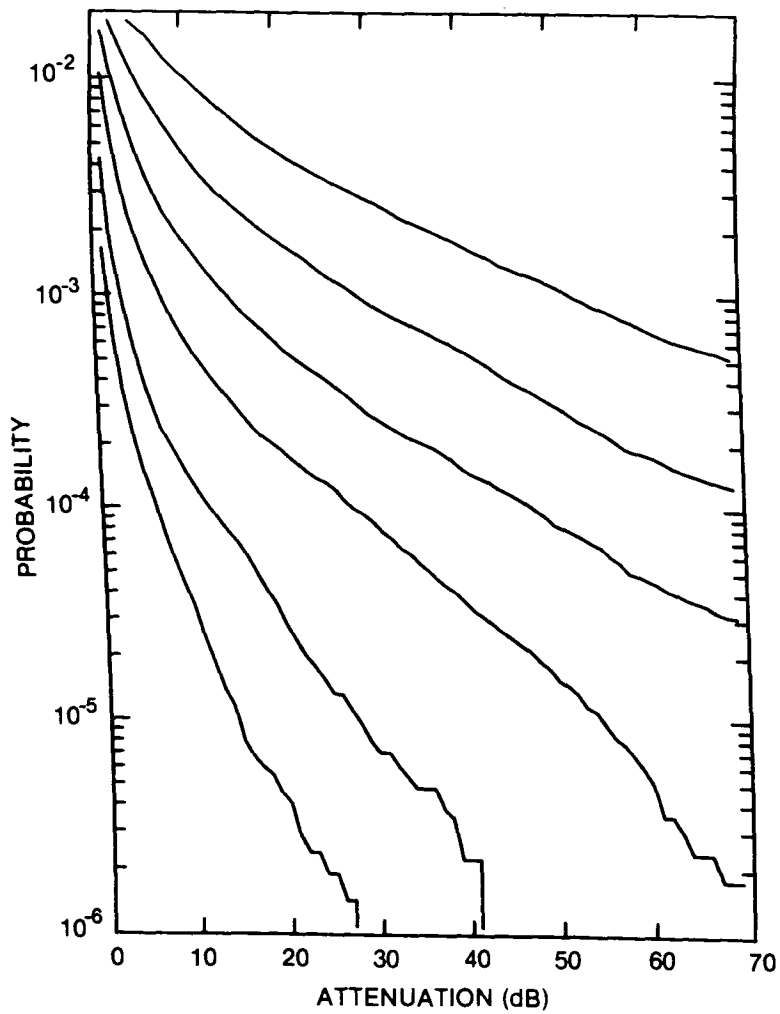

Figure 207. Cumulative distribution of rain attenuation for 35 GHz at Moosonee, ONT. Curves, moving from lowest to highest, are for hop lengths of 1, 2, 5, 10, 20, and 40 km, respectively.

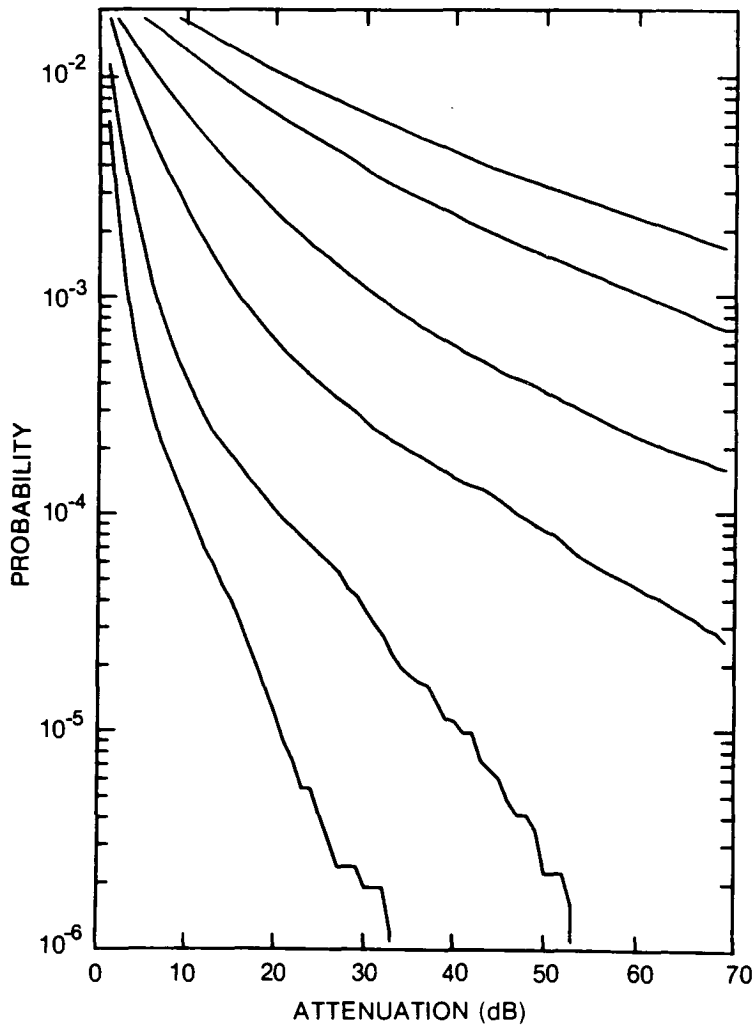

Figure 208. Cumulative distribution of rain attenuation for 56 GHz at Moosonee, ONT. Curves, moving from lowest to highest, are for hop lengths of 1, 2, 5, 10, 20 and 30 km, respectively.

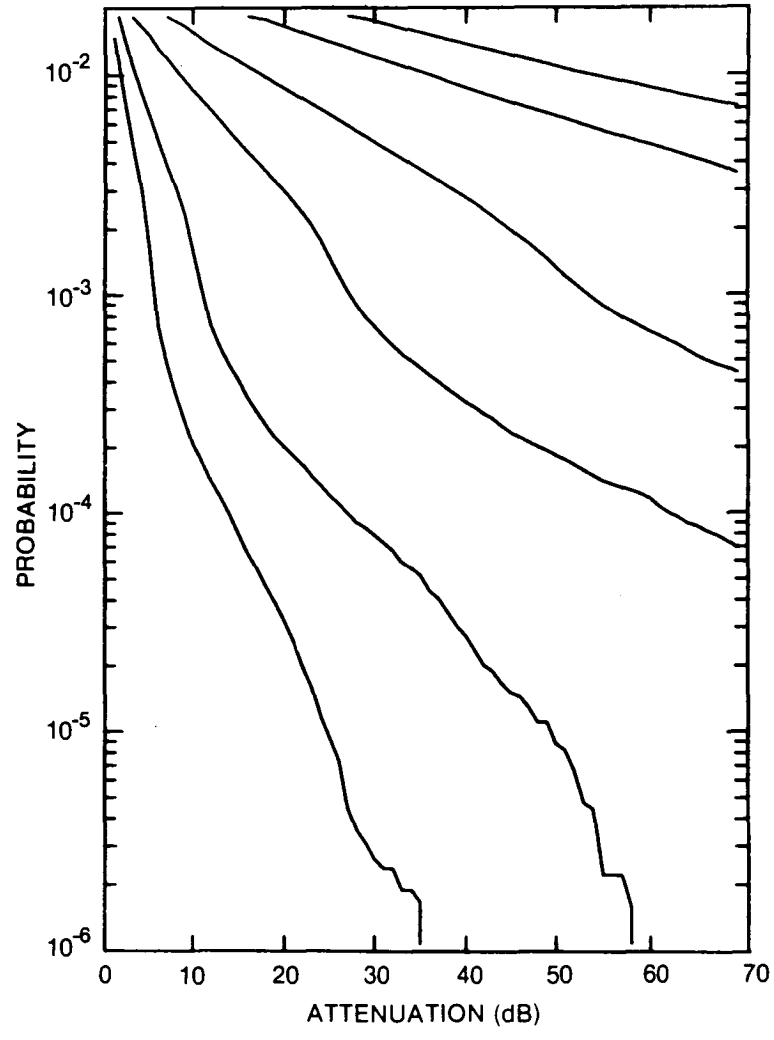

Figure 209. Cumulative distribution of rain attenuation for 100 GHz at Moosonee, ONT. Curves, moving from lowest to highest, are for hop lengths of 1, 2, 5, 10, 20 and 30 km, respectively.

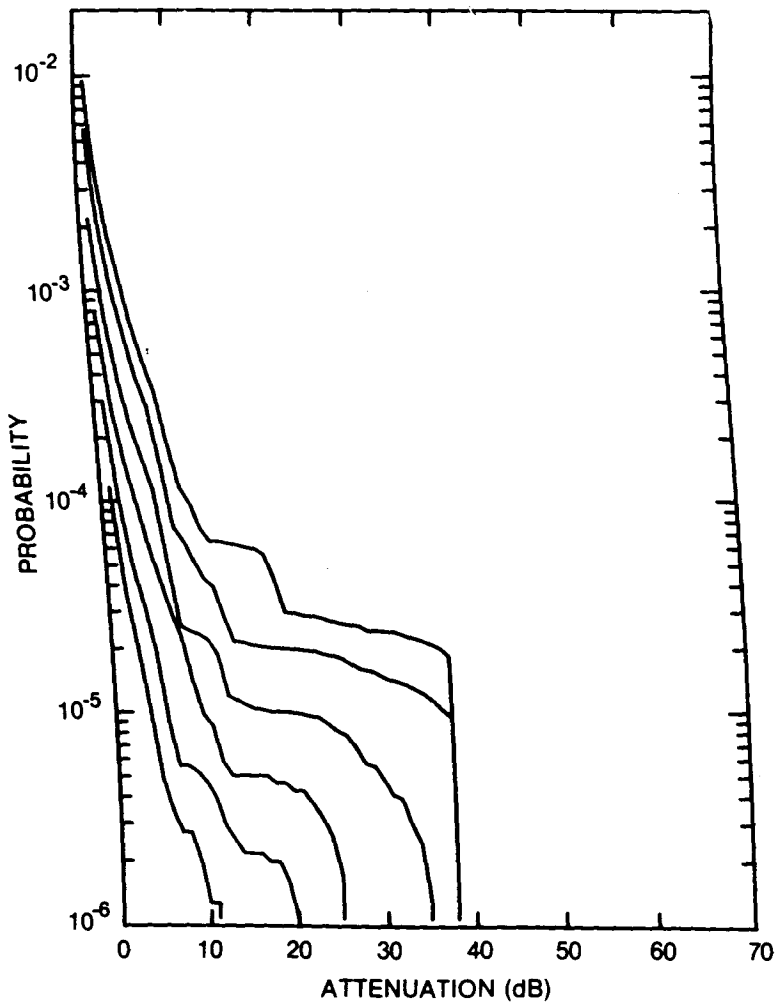

Figure 210. Cumulative distribution of rain attenuation for 8 GHz at Normandin, QUE. Curves, moving from lowest to highest, are for hop lengths of 5, 10, 20, 40, 80 and 120 km, respectively.

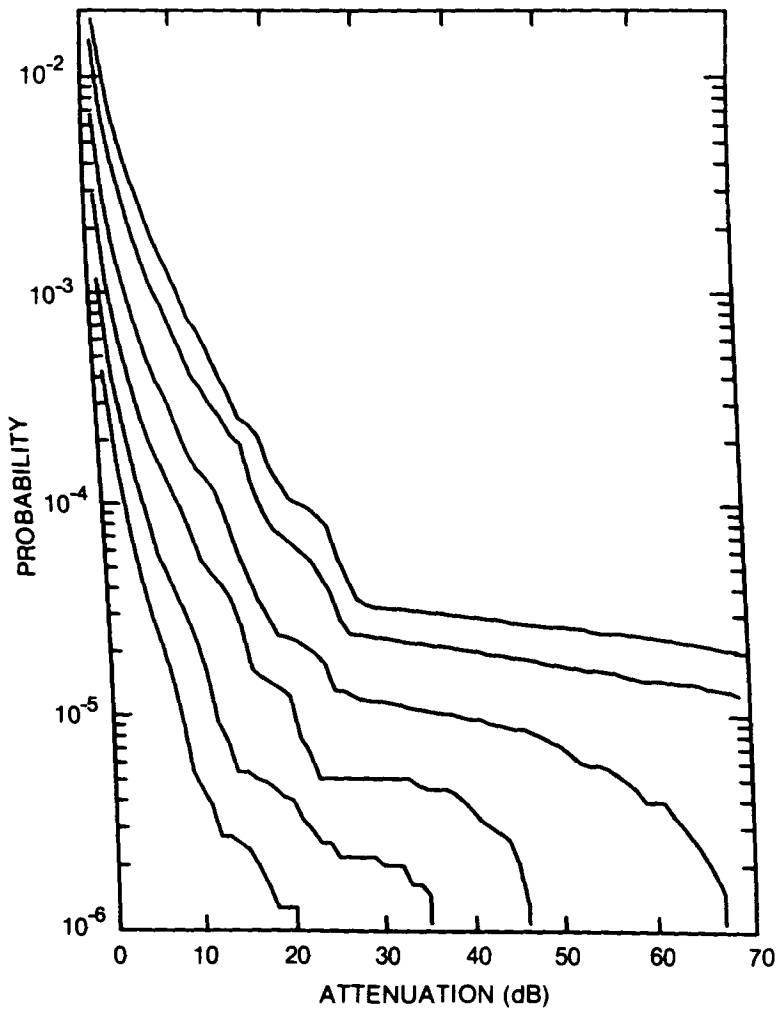

Figure 211. Cumulative distribution of rain attenuation for 11 GHz at Normandin, QUE. Curves, moving from lowest to highest, are for hop lengths of 5, 10, 20, 40, 80 and 120 km, respectively.

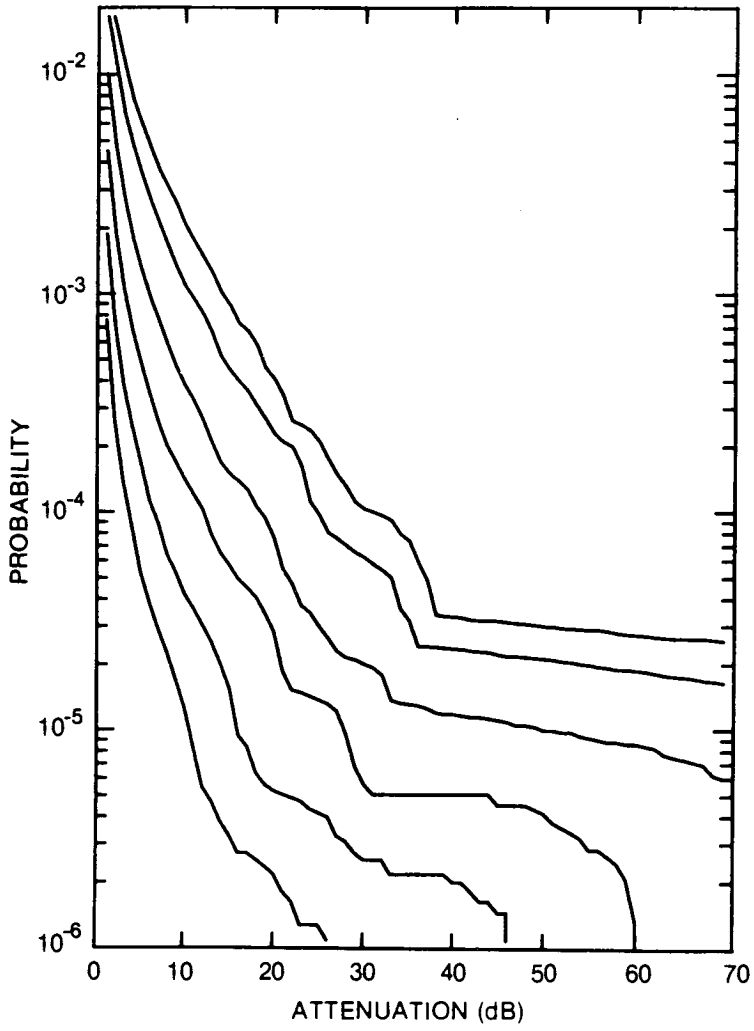

Figure 212. Cumulative distribution of rain attenuation for 12.8 GHz at Normandin, QUE. Curves, moving from lowest to highest, are for hop lengths of 5, 10, 20, 40, 80 and 120 km, respectively.

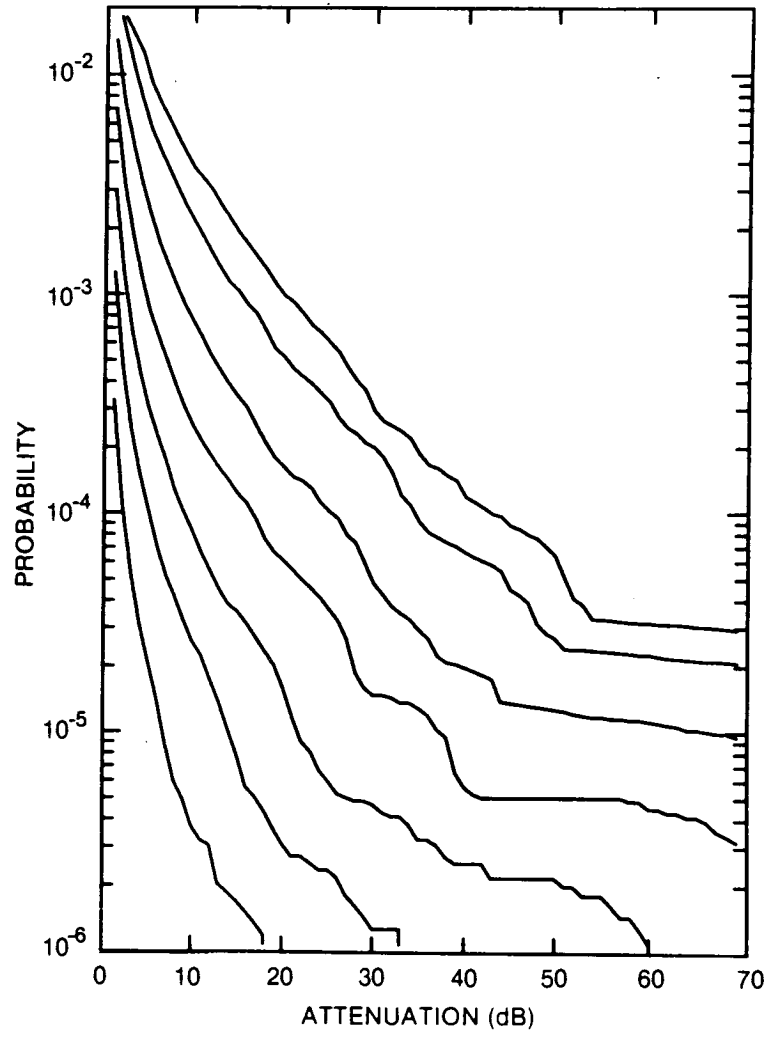

Figure 213. Cumulative distribution of rain attenuation for 15 GHz at Normandin, QUE. Curves, moving from lowest to highest, are for hop lengths of 2, 5, 10, 20, 40, 80 and 120 km, respectively.

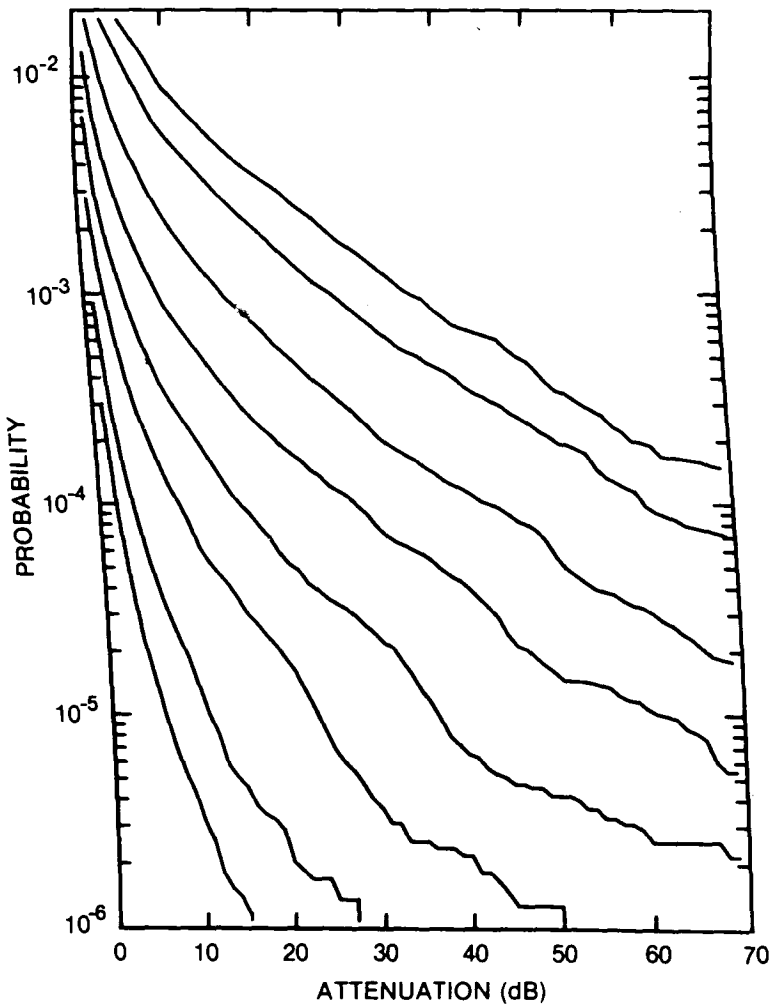

Figure 214. Cumulative distribution of rain attenuation for 20 GHz at Normandin, QUE. Curves, moving from lowest to highest, are for hop lengths of 1, 2, 5, 10, 20, 40, 80 and 120 km, respectively.

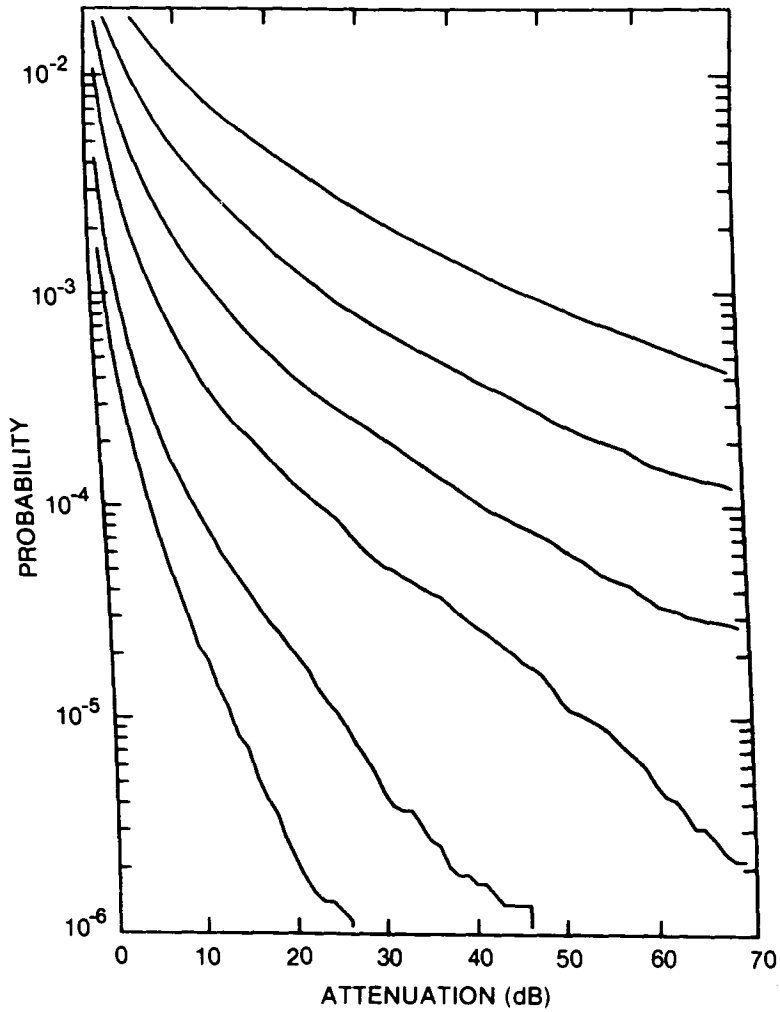

Figure 215. Cumulative distribution of rain attenuation for 35 GHz at Normandin, QUE. Curves, moving from lowest to highest, are for hop lengths of 1, 2, 5, 10, 20 and 40 km, respectively.

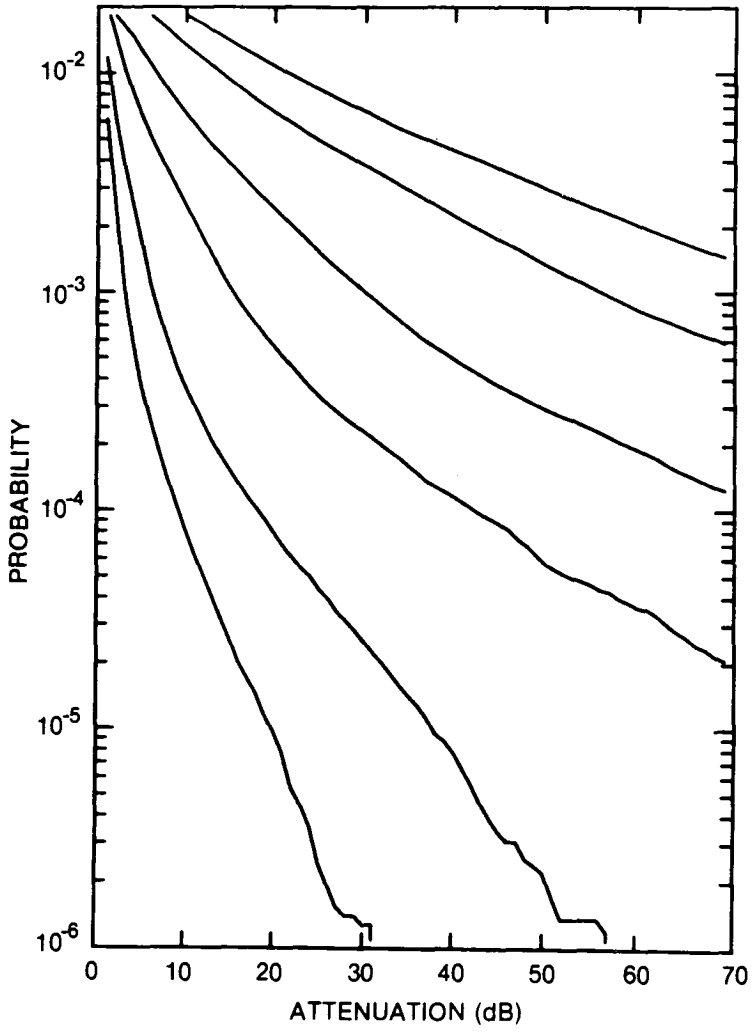

Figure 216. Cumulative distribution of rain attenuation for 56 GHz at Normandin, QUE. Curves, moving from lowest to highest, are for hop lengths of 1, 2, 5, 10, 20 and 30 km, respectively.

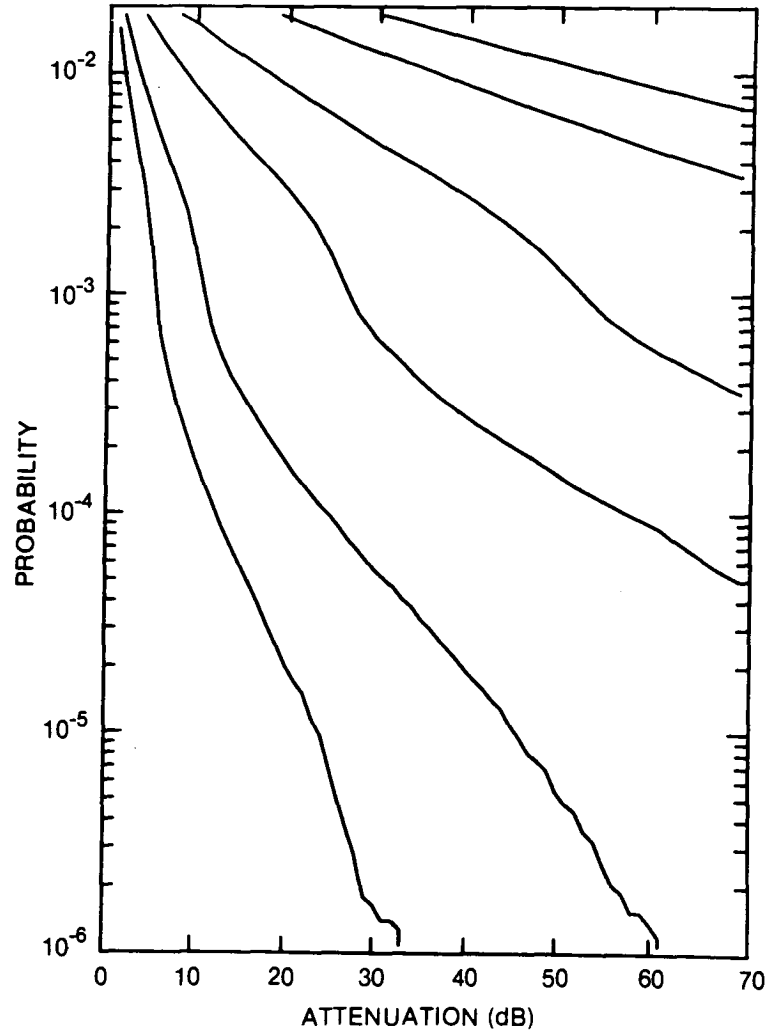

Figure 217. Cumulative distribution of rain attenuation for 100 GHz at Normandin, QUE. Curves, moving from lowest to highest, are for hop lengths of 1, 2, 5, 10, 20 and 30 km, respectively.

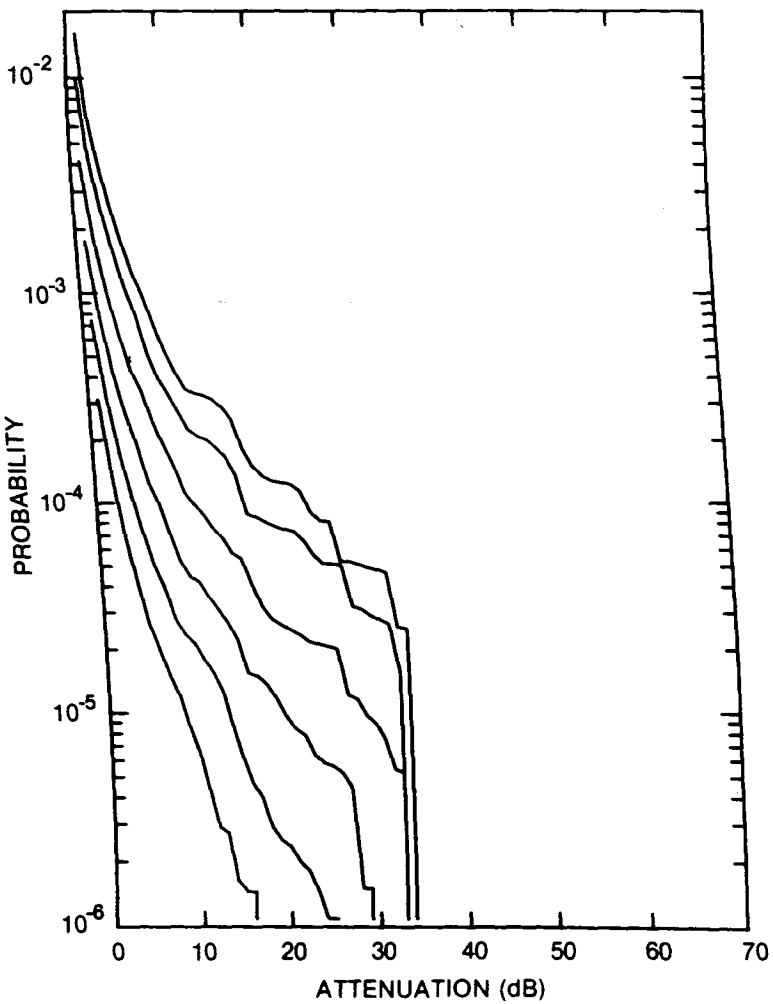

Figure 218. Cumulative distribution of rain attenuation for 8 GHz at North Bay, ONT. Curves, moving from lowest to highest, are for hop lengths of 5, 10, 20, 40, 80 and 120 km, respectively.

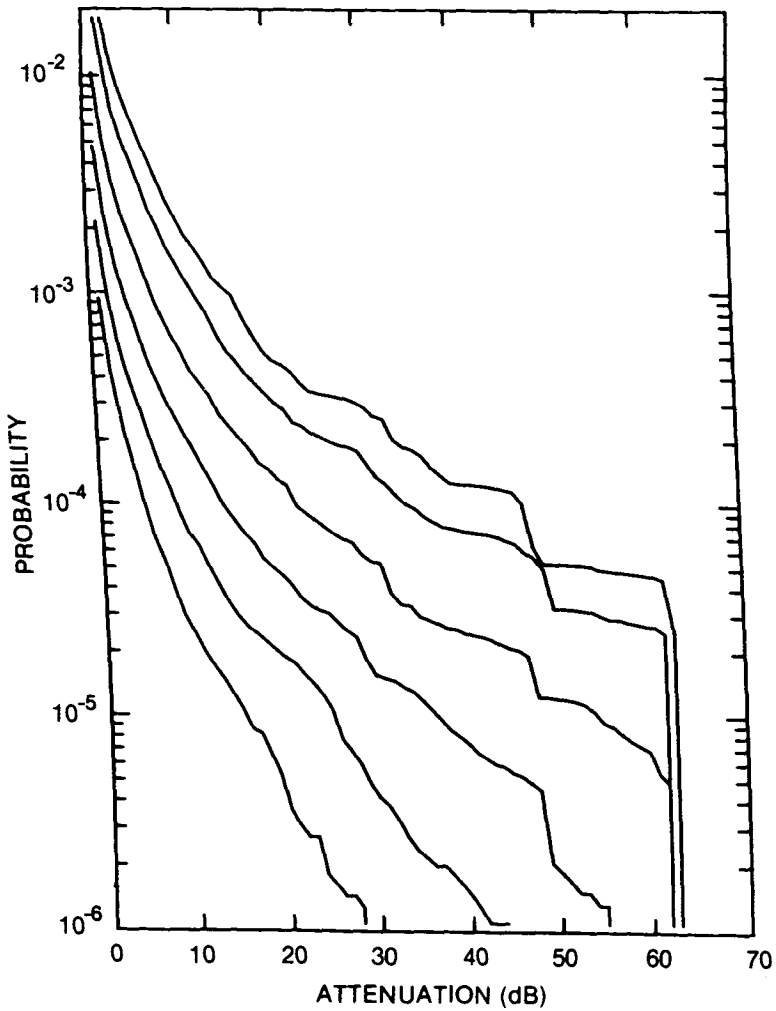

Figure 219. Cumulative distribution of rain attenuation for 11 GHz at North Bay, ONT. Curves, moving from lowest to highest, are for hop lengths of 5, 10, 20, 40, 80 and 120 km, respectively.

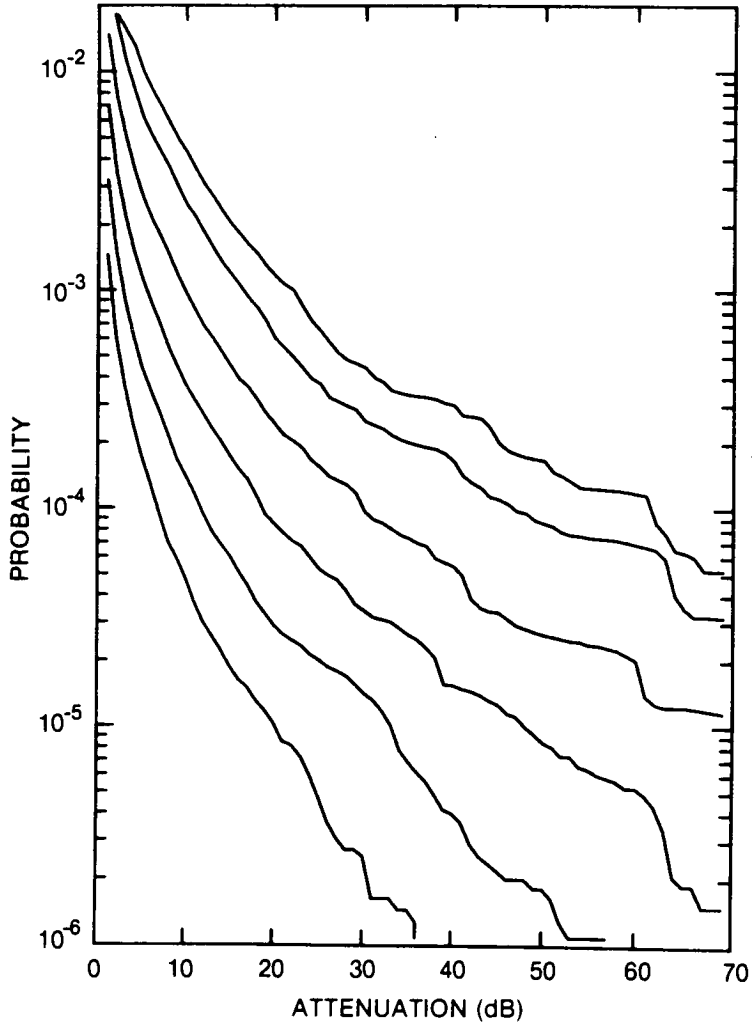

Figure 220. Cumulative distribution of rain attenuation for 12.8 GHz at North Bay, ONT. Curves, moving from lowest to highest, are for hop lengths of 5, 10, 20, 40, 80 and 120 km, respectively.

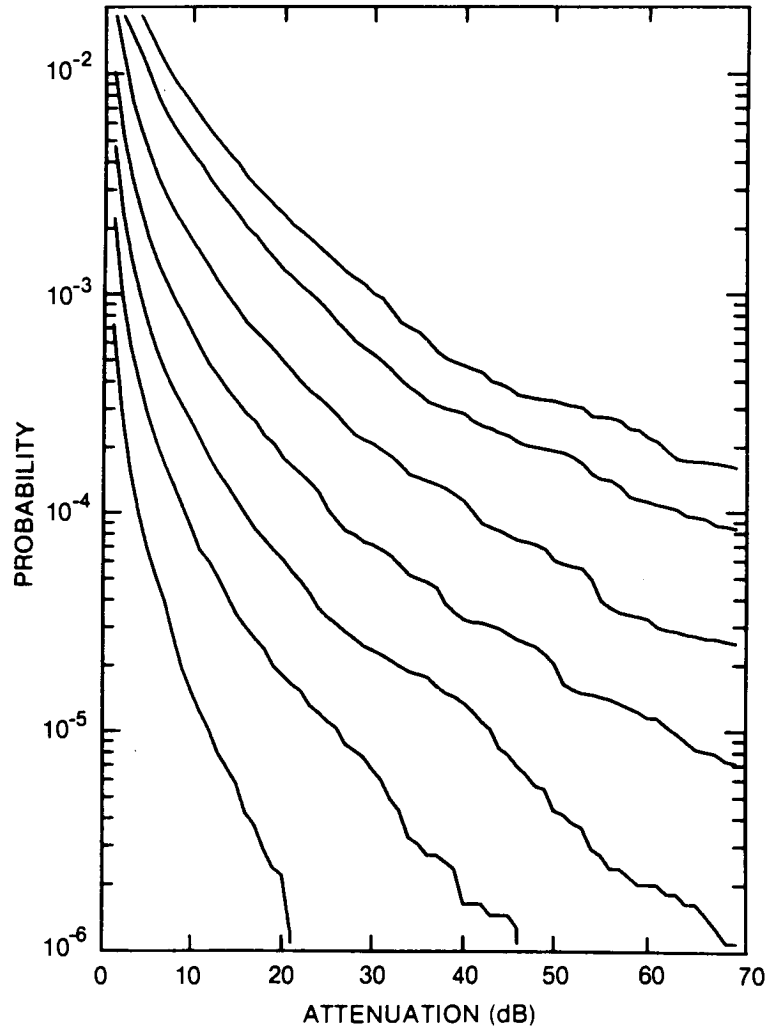

Figure 221. Cumulative distribution of rain attenuation for 15 GHz at North Bay, ONT. Curves, moving from lowest to highest, are for hop lengths of 2, 5, 10, 20, 40, 80 and 120 km, respectively.

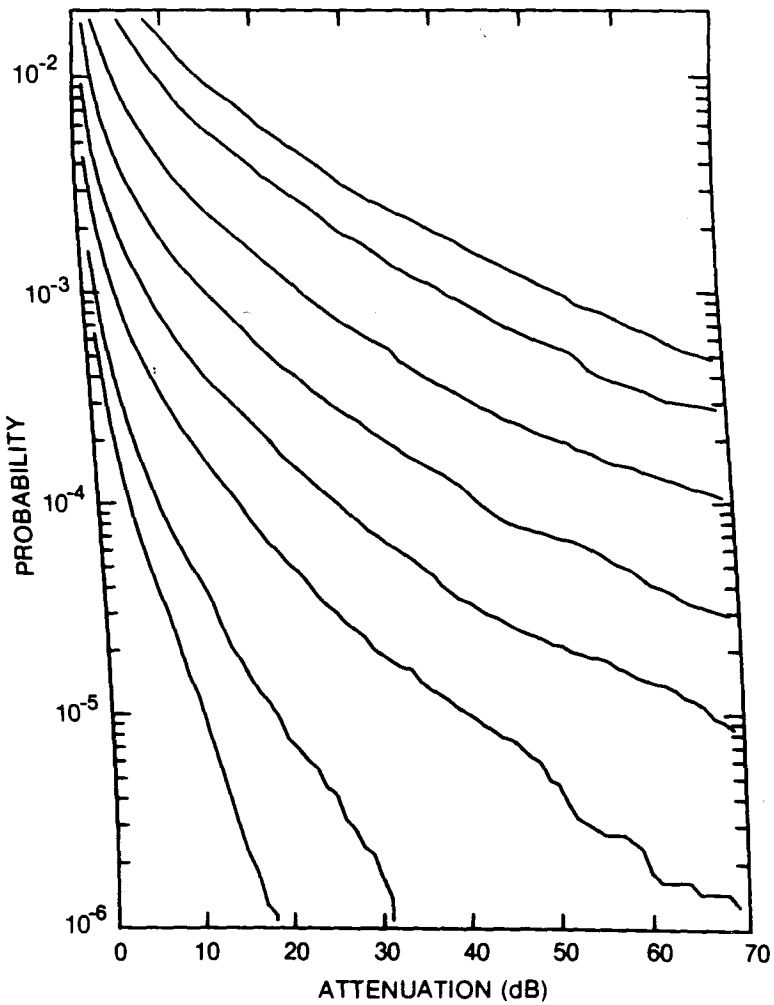

Figure 222. Cumulative distribution of rain attenuation for 20 GHz at North Bay, ONT. Curves, moving from lowest to highest, are for hop lengths of 1, 2, 5, 10, 20, 40, 80 and 120 km, respectively.

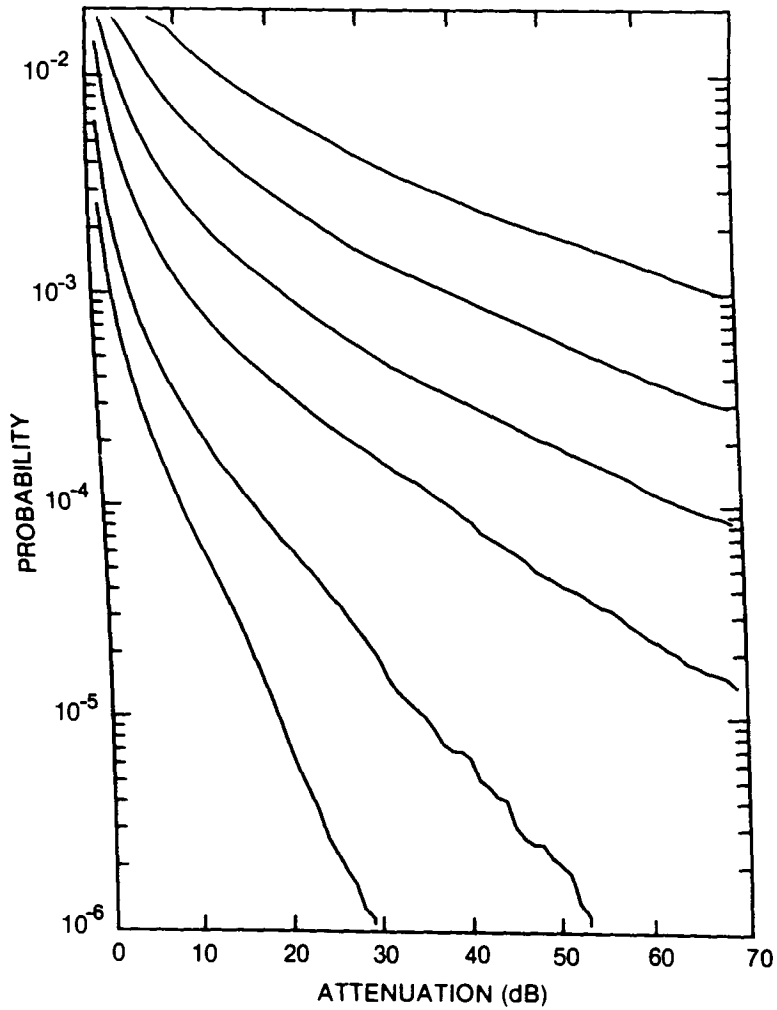

Figure 223. Cumulative distribution of rain attenuation for 35 GHz at North Bay, ONT. Curves, moving from lowest to highest, are for hop lengths of 1, 2, 5, 10, 20 and 40 km, respectively.

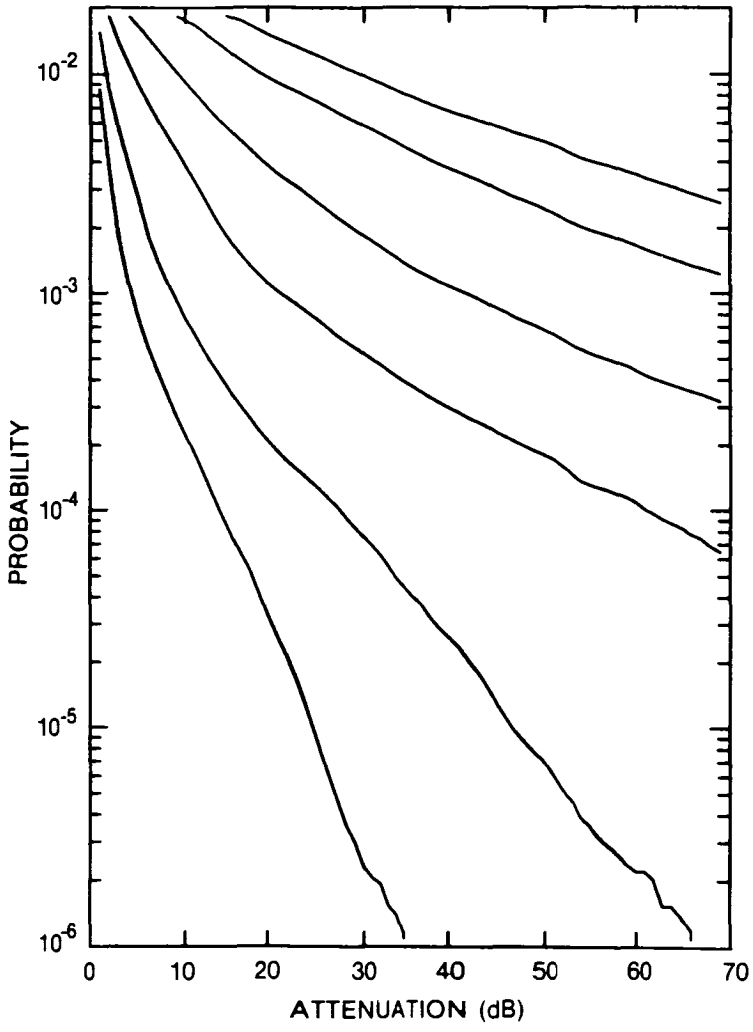

Figure 224. Cumulative distribution of rain attenuation for 56 GHz at North Bay, ONT. Curves, moving from lowest to highest, are for hop lengths of 1, 2, 5, 10, 20 and 30 km, respectively.

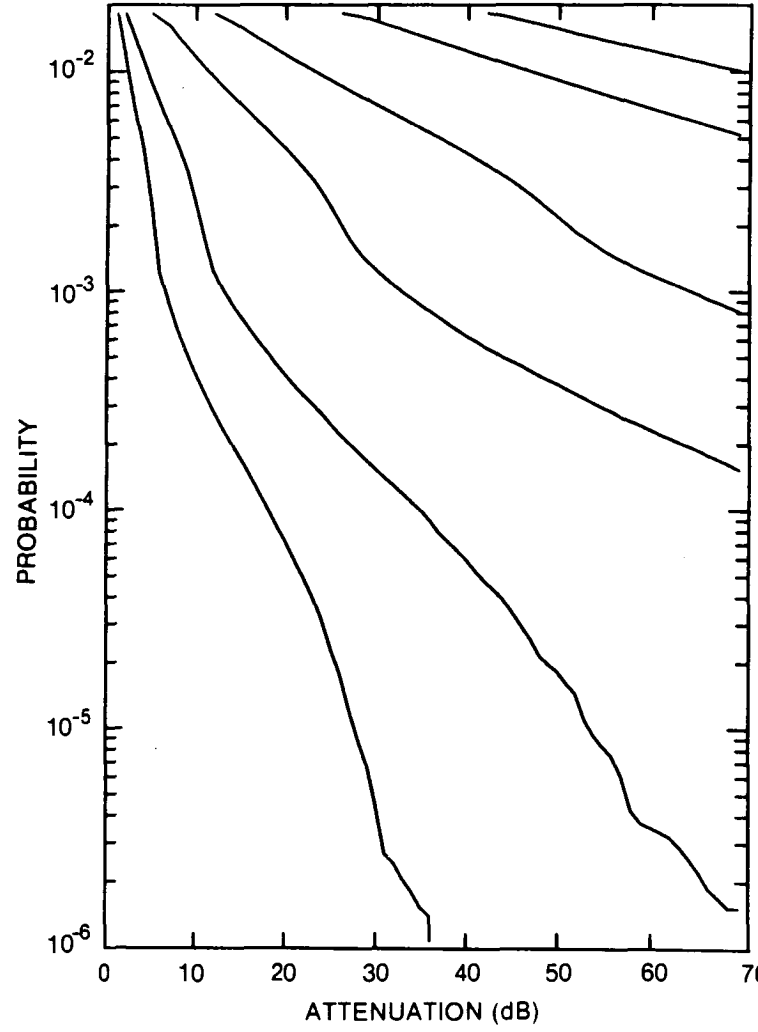

Figure 225. Cumulative distribution of rain attenuation for 100 GHz at North Bay, ONT. Curves, moving from lowest to highest, are for hop lengths of 1, 2, 5, 10, 20 and 30 km, respectively.

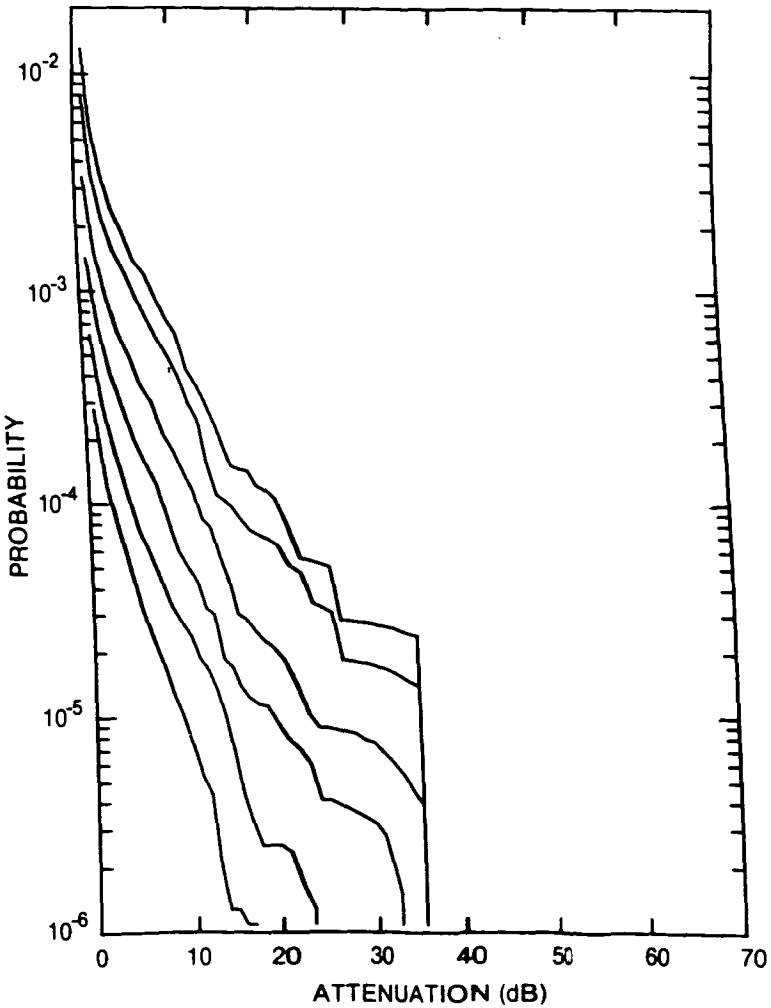

Figure 226. Cumulative distribution of rain attenuation for 8 GHz at Ottawa, ONT. Curves, moving from lowest to highest, are for hop lengths of 5, 10, 20, 40, 80 and 120 km, respectively.

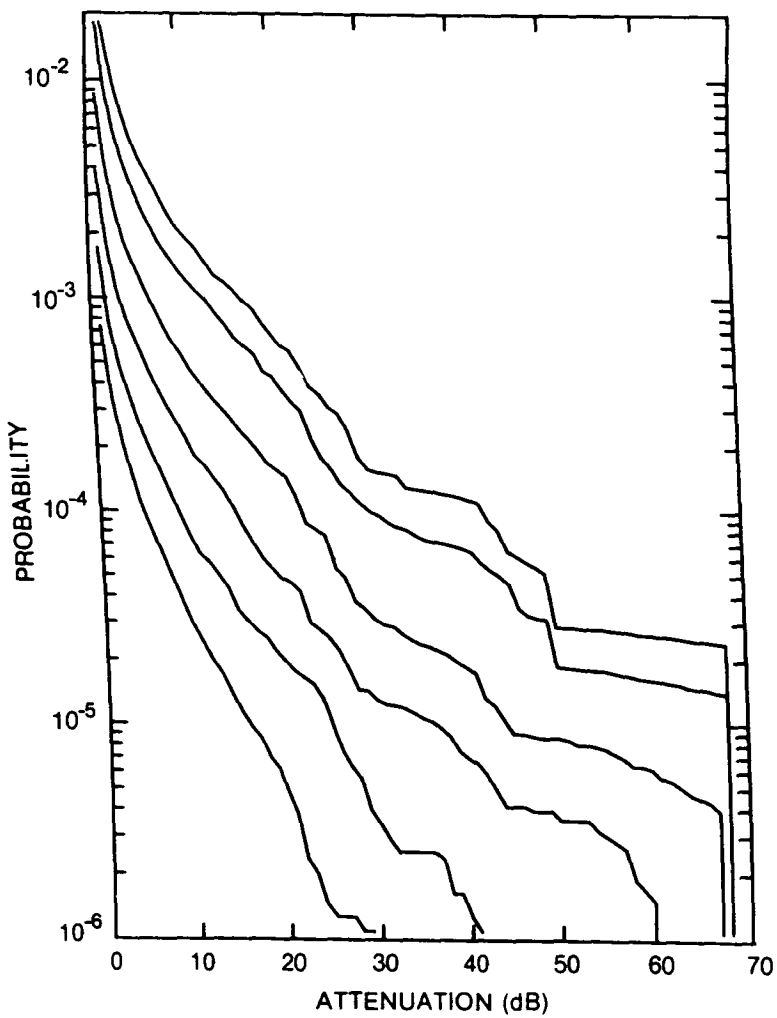

Figure 227. Cumulative distribution of rain attenuation for 11 GHz at Ottawa, ONT. Curves, moving from lowest to highest, are for hop lengths of 5, 10, 20, 40, 80 and 120 km, respectively.

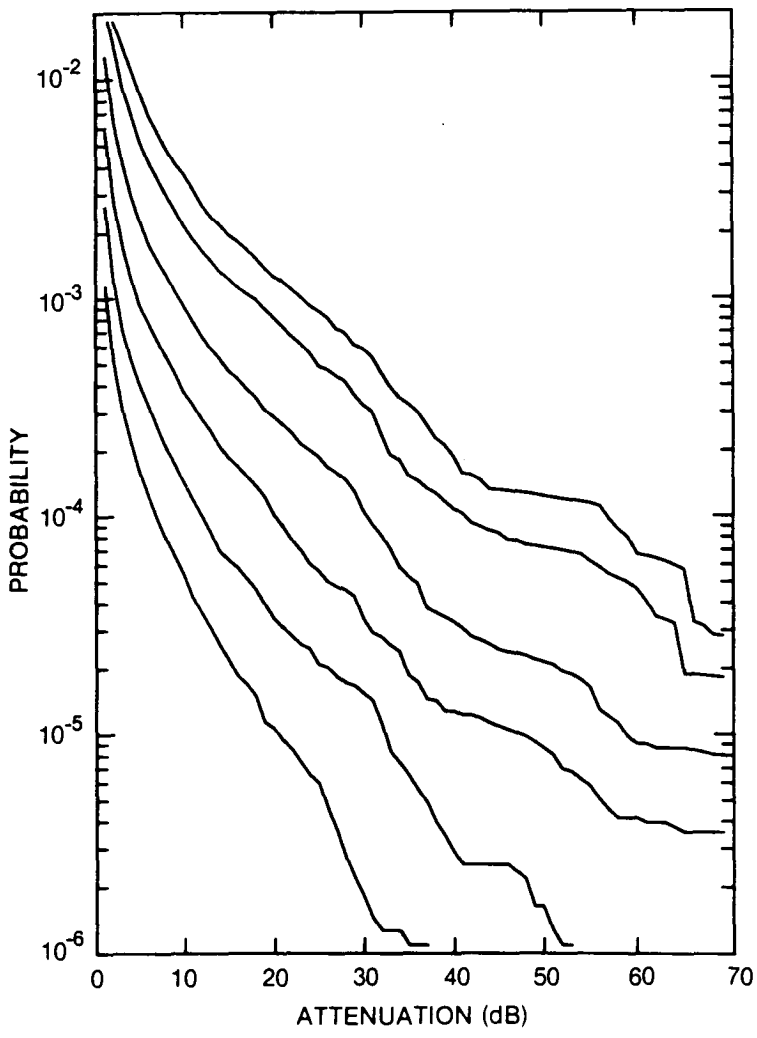

Figure 228. Cumulative distribution of rain attenuation for 12.8 GHz at Ottawa, ONT. Curves, moving from lowest to highest, are for hop lengths of 5, 10, 20, 40, 80 and 120 km, respectively.

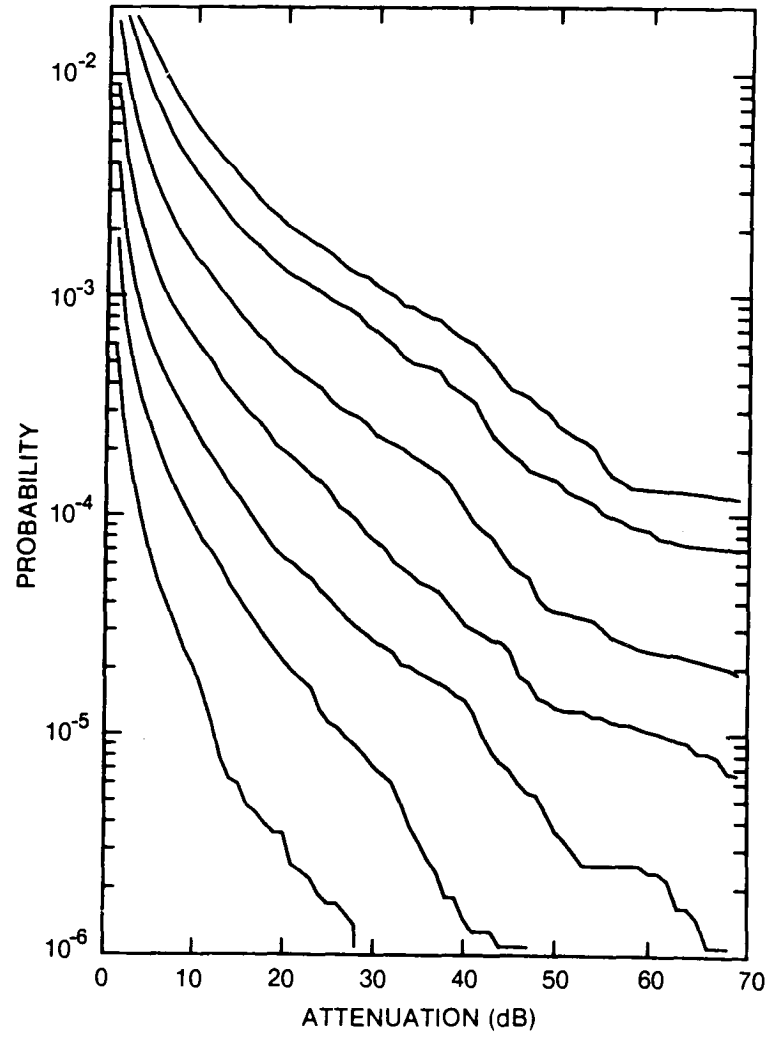

Figure 229. Cumulative distribution of rain attenuation for 15 GHz at Ottawa, ONT. Curves, moving from lowest to highest, are for hop lengths of 2, 5, 10, 20, 40, 80 and 120 km, respectively.

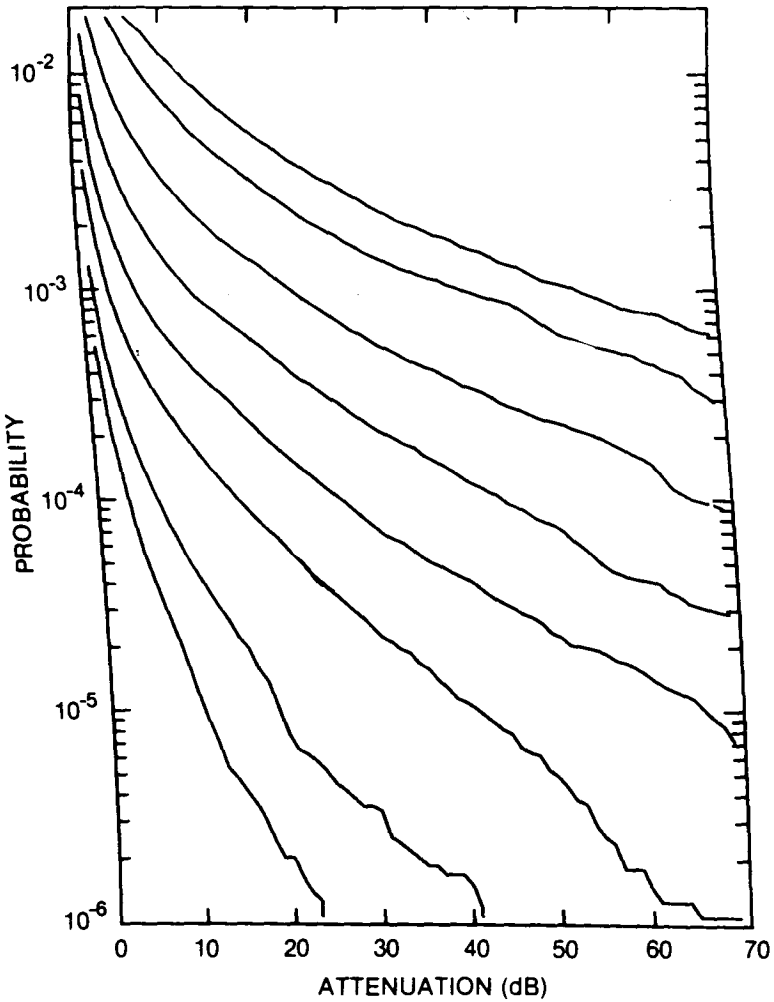

Figure 230. Cumulative distribution of rain attenuation for 20 GHz at Ottawa, ONT. Curves, moving from lowest to highest, are for hop lengths of 1, 2, 5, 10, 20, 40 80 and 120 km, respectively.

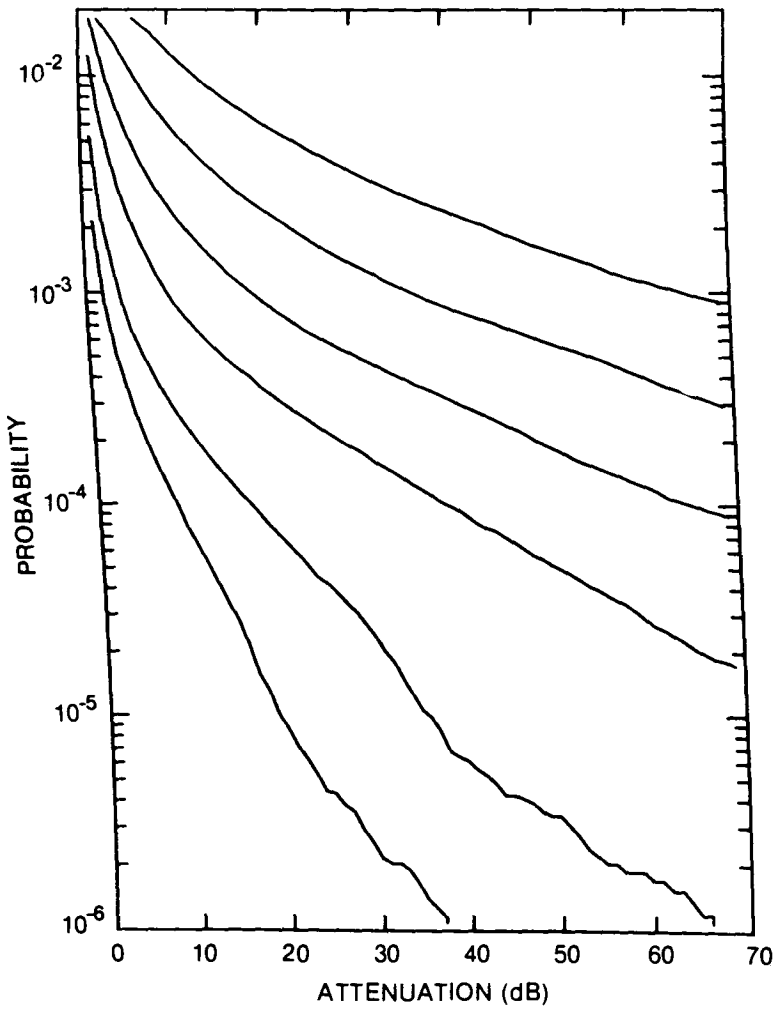

Figure 231. Cumulative distribution of rain attenuation for 35 GHz at Ottawa, ONT. Curves, moving from lowest to highest, are for hop lengths of 1, 2, 5, 10, 20 and 40 km, respectively.

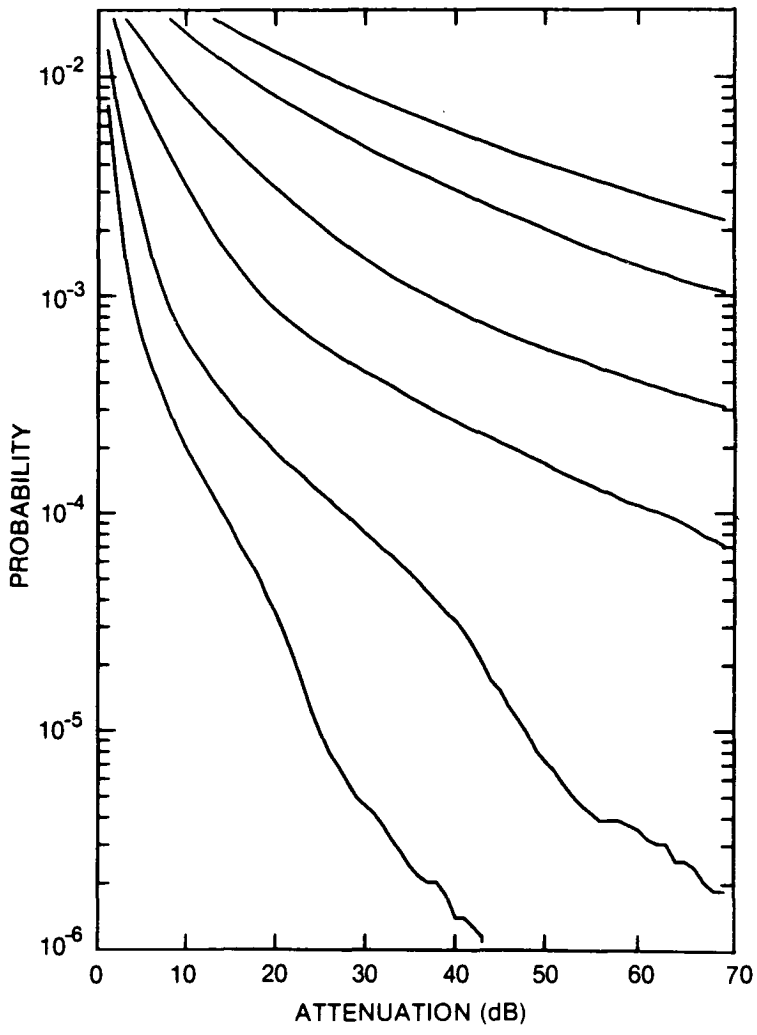

Figure 232. Cumulative distribution of rain attenuation for 56 GHz at Ottawa, ONT. Curves, moving from lowest to highest, are for hop lengths of 1, 2, 5, 10, 20 and 30 km, respectively.

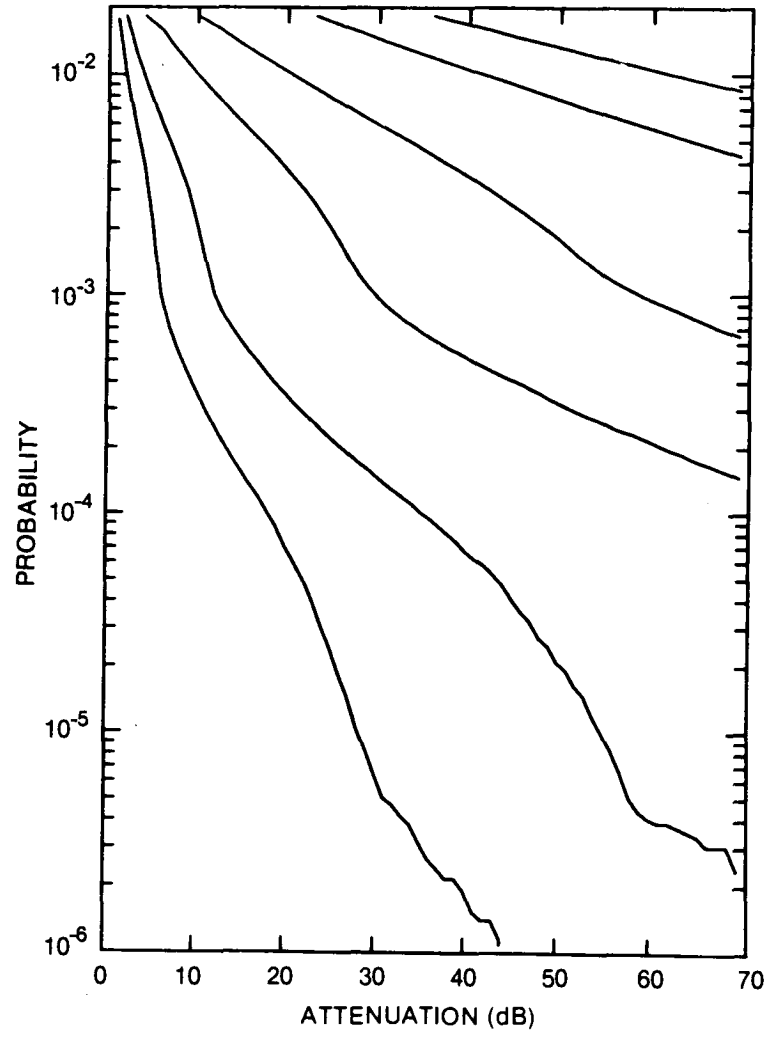

Figure 233. Cumulative distribution of rain attenuation for 100 GHz at Ottawa, ONT. Curves, moving from lowest to highest, are for hop lengths of 1, 2, 5, 10, 20 and 30 km, respectively.

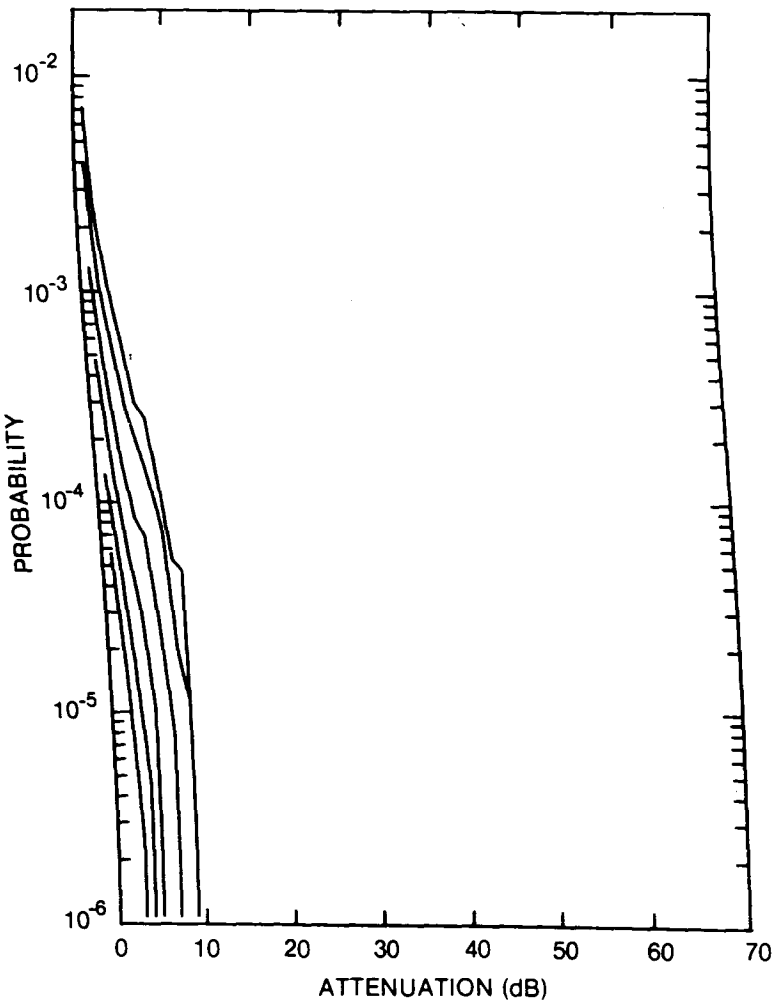

Figure 234. Cumulative distribution of rain attenuation for 8 GHz at Poste de la Baleine, QUE. Curves, moving from lowest to highest, are for hop lengths of 5, 10, 20, 40, 80 and 120 km, respectively.

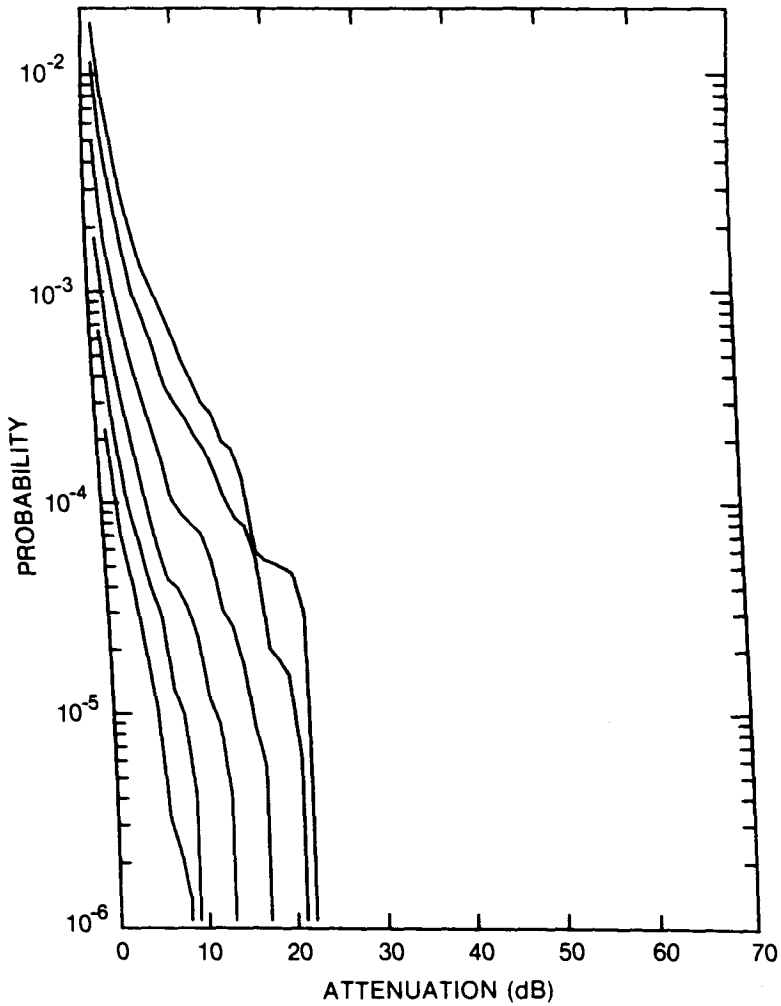

Figure 235. Cumulative distribution of rain attenuation for 11 GHz at Poste de la Baleine, QUE. Curves, moving from lowest to highest, are for hop lengths of 5, 10, 20, 40, 80 and 120 km, respectively.

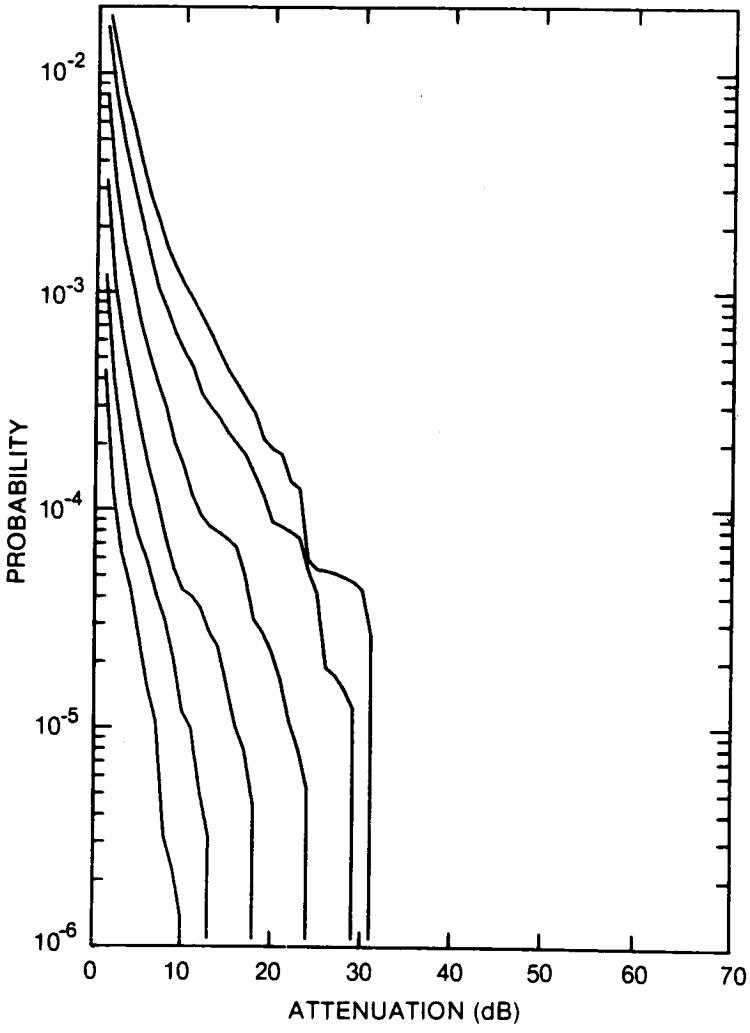

Figure 236. Cumulative distribution of rain attenuation for 12.8 GHz at Poste de la Baleine, QUE. Curves, moving from lowest to highest, are for hop lengths of 5, 10, 20, 40, 80 and 120 km, respectively.

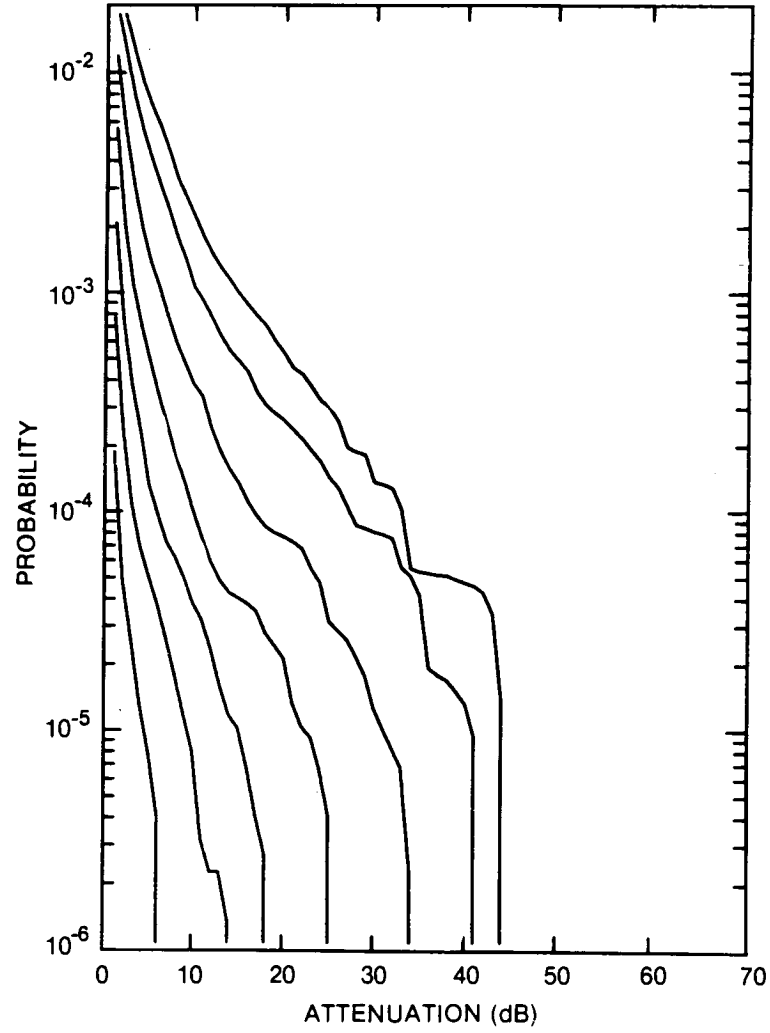

Figure 237. Cumulative distribution of rain attenuation for 15 GHz at Poste de la Baleine, QUE. Curves, moving from lowest to highest, are for hop lengths of 2, 5, 10, 20, 40, 80 and 120 km, respectively.

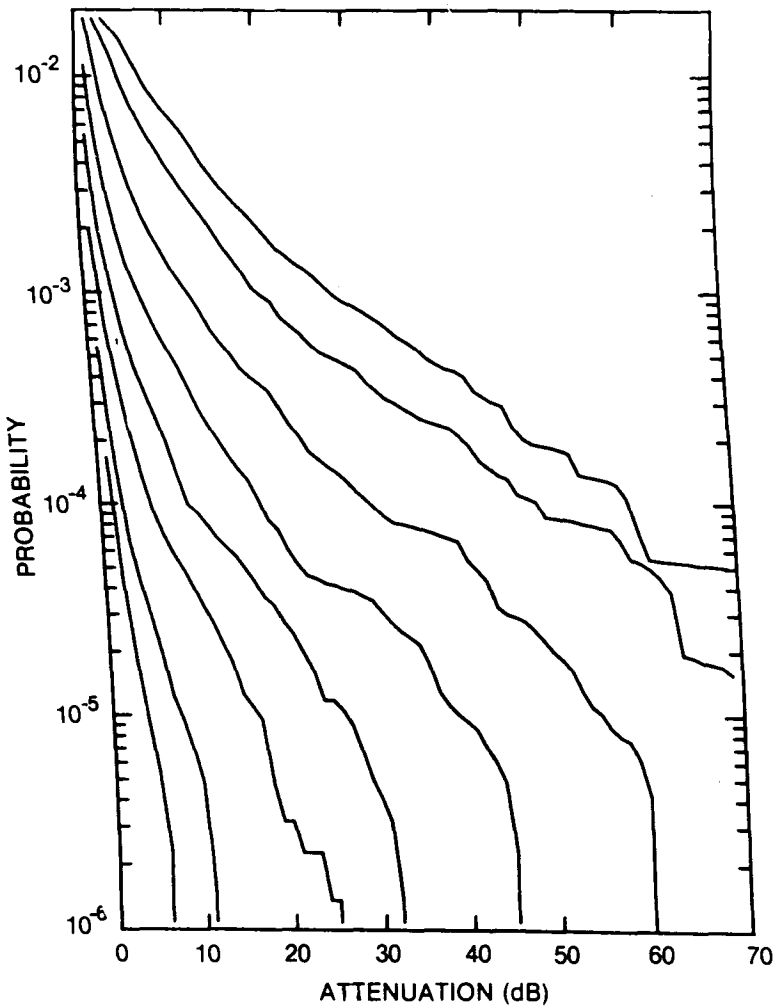

Figure 238. Cumulative distribution of rain attenuation for 20 GHz at Poste de la Baleine, QUE. Curves, moving from lowest to highest, are for hop lengths of 1, 2, 5, 10, 20, 40, 80 and 120 km, respectively.

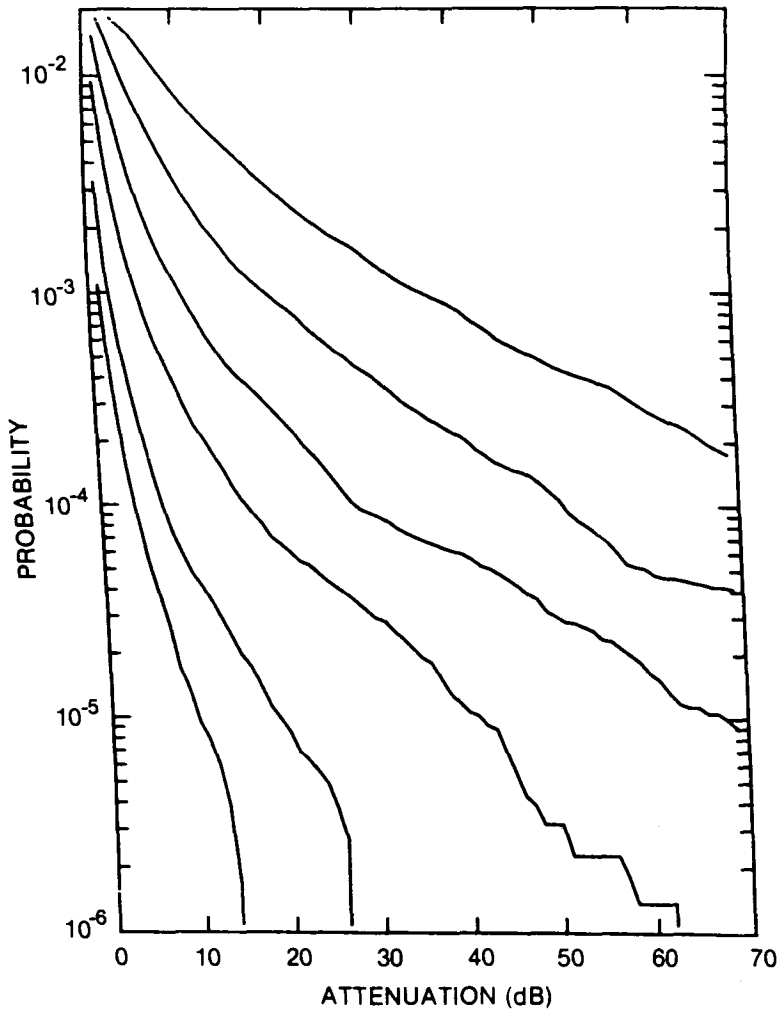

Figure 239. Cumulative distribution of rain attenuation for 35 GHz at Poste de la Baleine, QUE. Curves, moving from lowest to highest, are for hop lengths of 1, 2, 5, 10, 20 and 40 km, respectively.

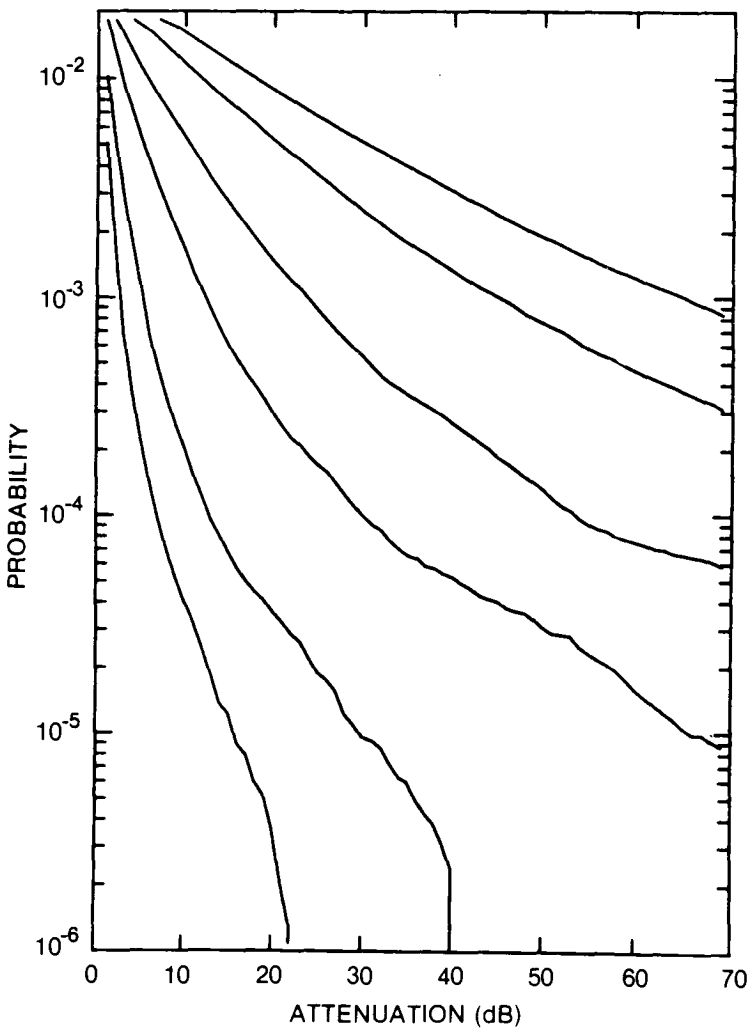

Figure 240. Cumulative distribution of rain attenuation for 56 GHz at Poste de la Baleine, QUE. Curves, moving from lowest to highest, are for hop lengths of 1, 2, 5, 10, 20 and 30 km, respectively.

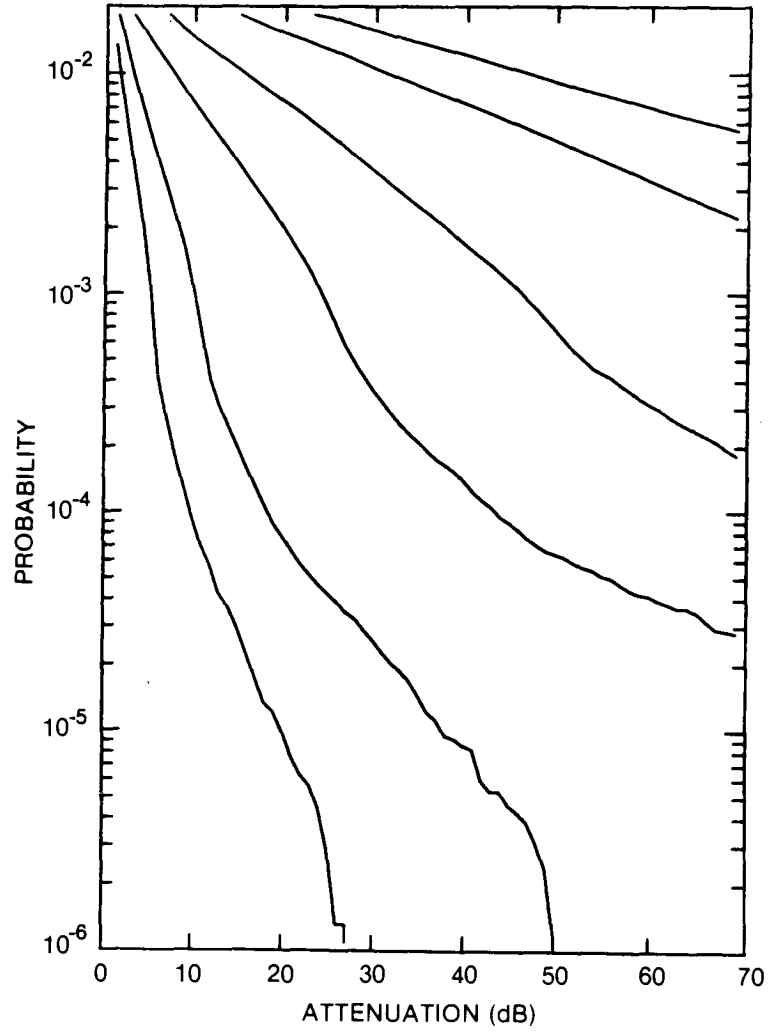

Figure 241. Cumulative distribution of rain attenuation for 100 GHz at Poste de la Baleine, QUE. Curves, moving from lowest to highest, are for hop lengths of 1, 2, 5, 10, 20 and 30 km, respectively.

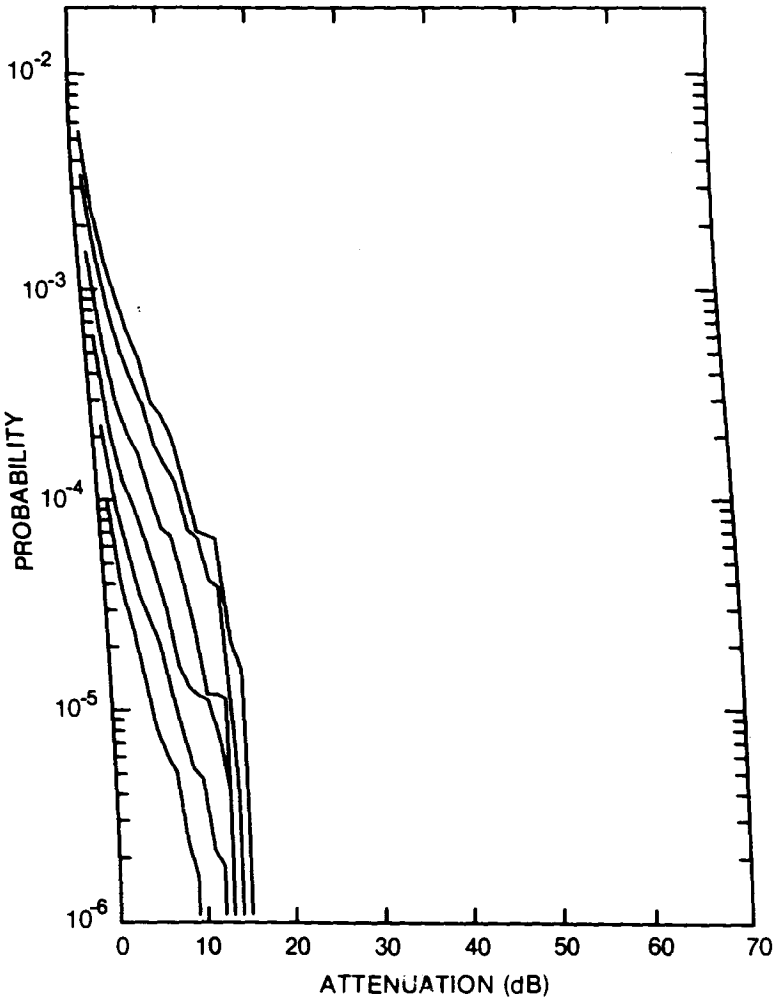

Figure 242. Cumulative distribution of rain attenuation for 8 GHz at Prince Albert, SASK. Curves, moving from lowest to highest, are for hop lengths of 5, 10, 20, 40, 80 and 120 km, respectively.

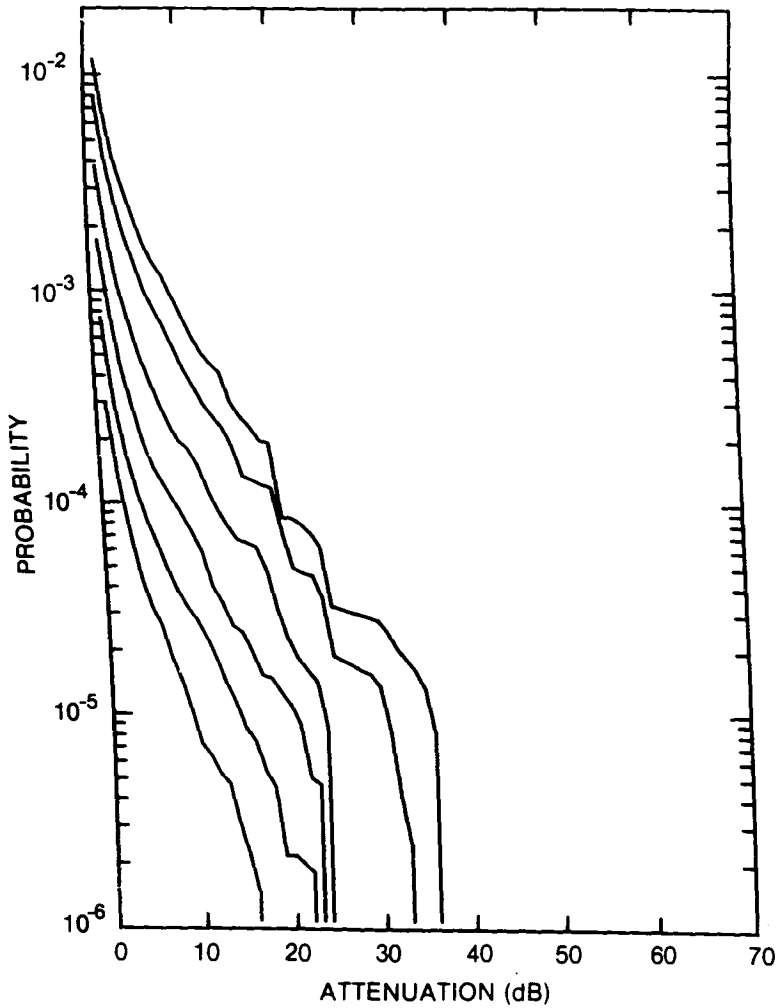

Figure 243. Cumulative distribution of rain attenuation for 11 GHz at Prince Albert, SASK. Curves, moving from lowest to highest, are for hop lengths of 5, 10, 20, 40, 80 and 120 km, respectively.

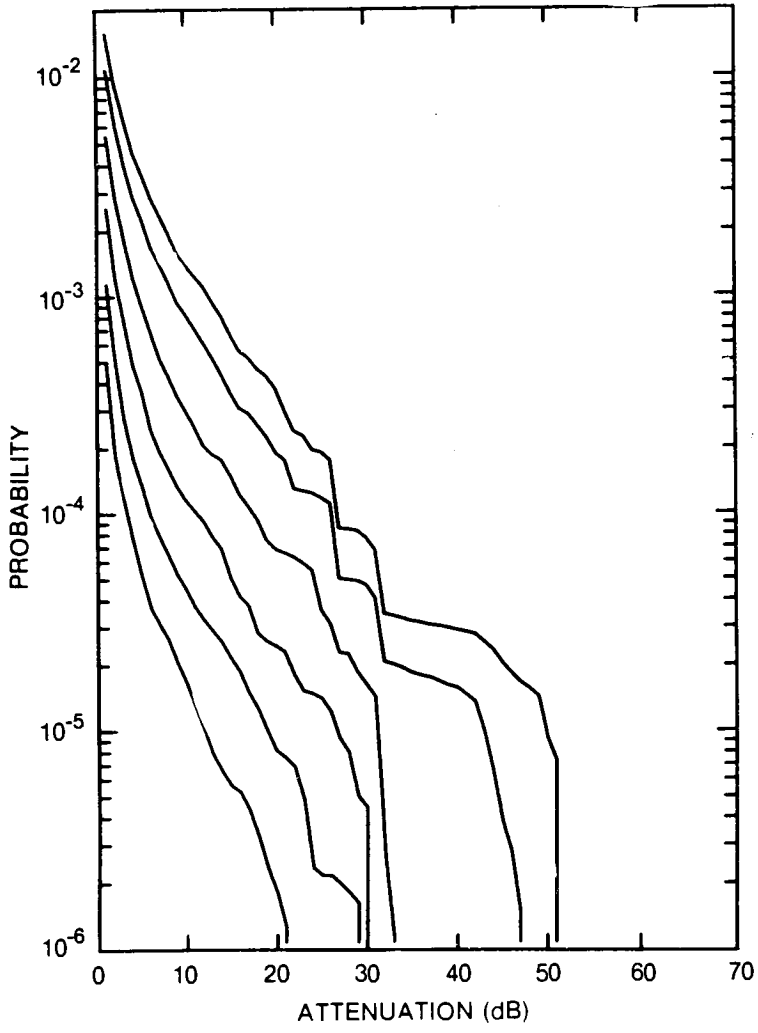

Figure 244. Cumulative distribution of rain attenuation for 12.8 GHz at Prince Albert, SASK. Curves, moving from lowest to highest, are for hop lengths of 5, 10, 20, 40, 80 and 120 km, respectively.

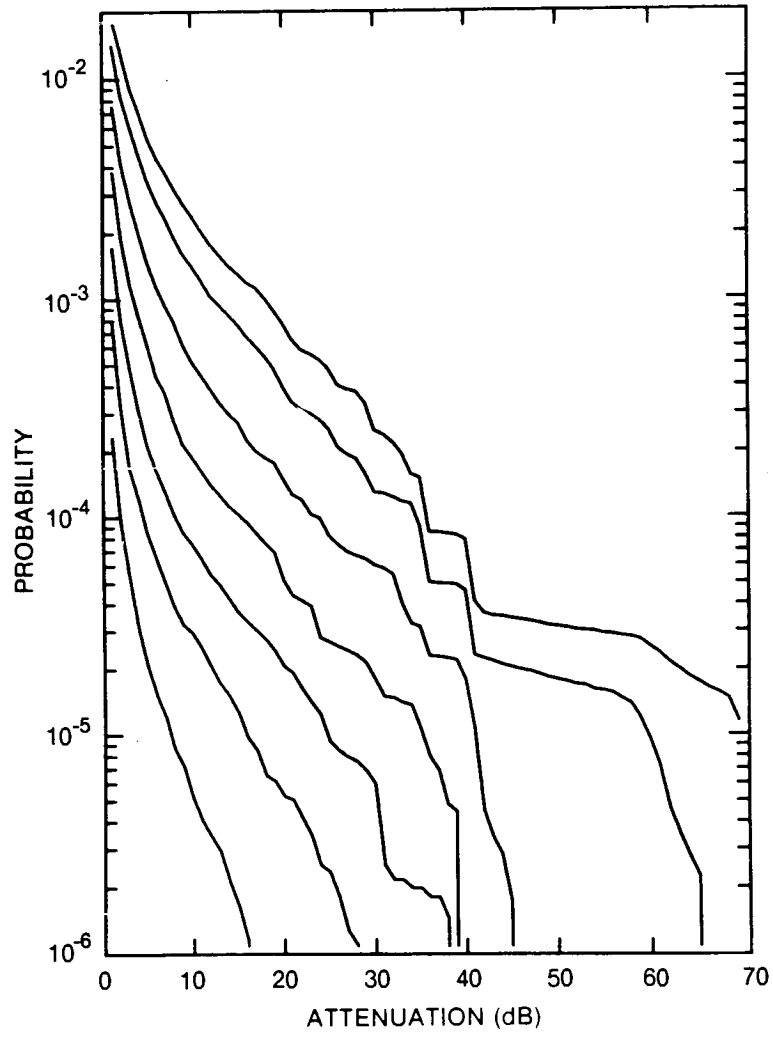

Figure 245. Cumulative distribution of rain attenuation for 15 GHz at Prince Albert, SASK. Curves, moving from lowest to highest, are for hop lengths of 2, 5, 10, 20, 40, 80 and 120 km, respectively.

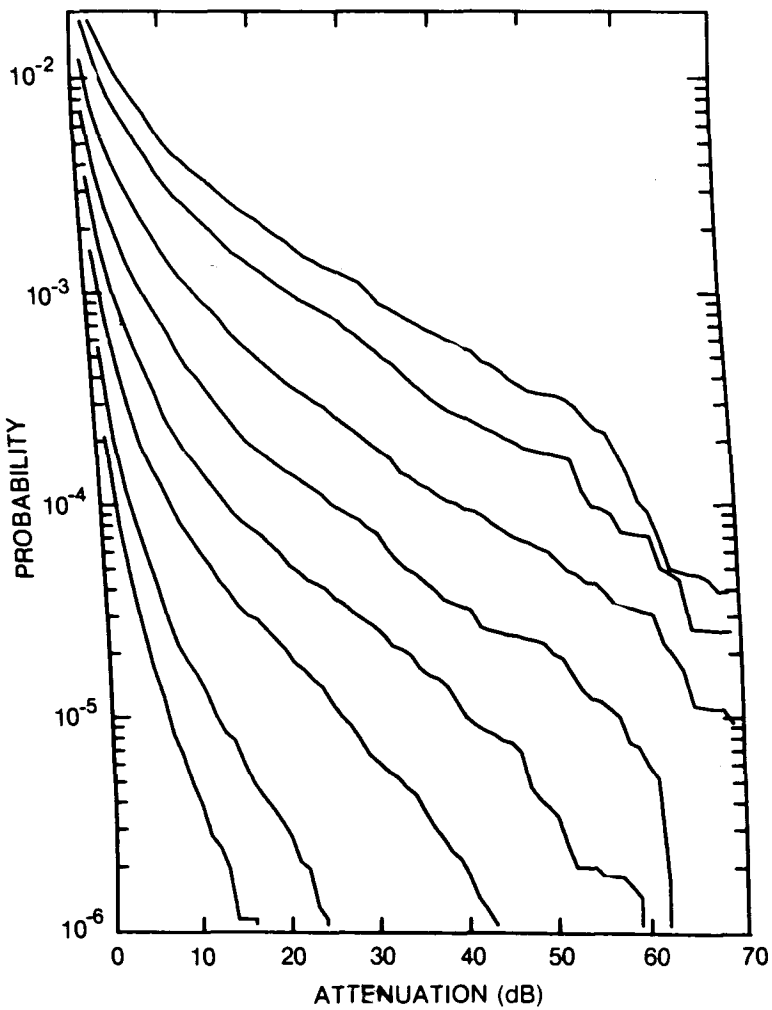

Figure 246. Cumulative distribution of rain attenuation for 20 GHz at Prince Albert, SASK. Curves, moving from lowest to highest, are for hop lengths of 1, 2, 5, 10, 20, 40, 80 and 120 km, respectively.

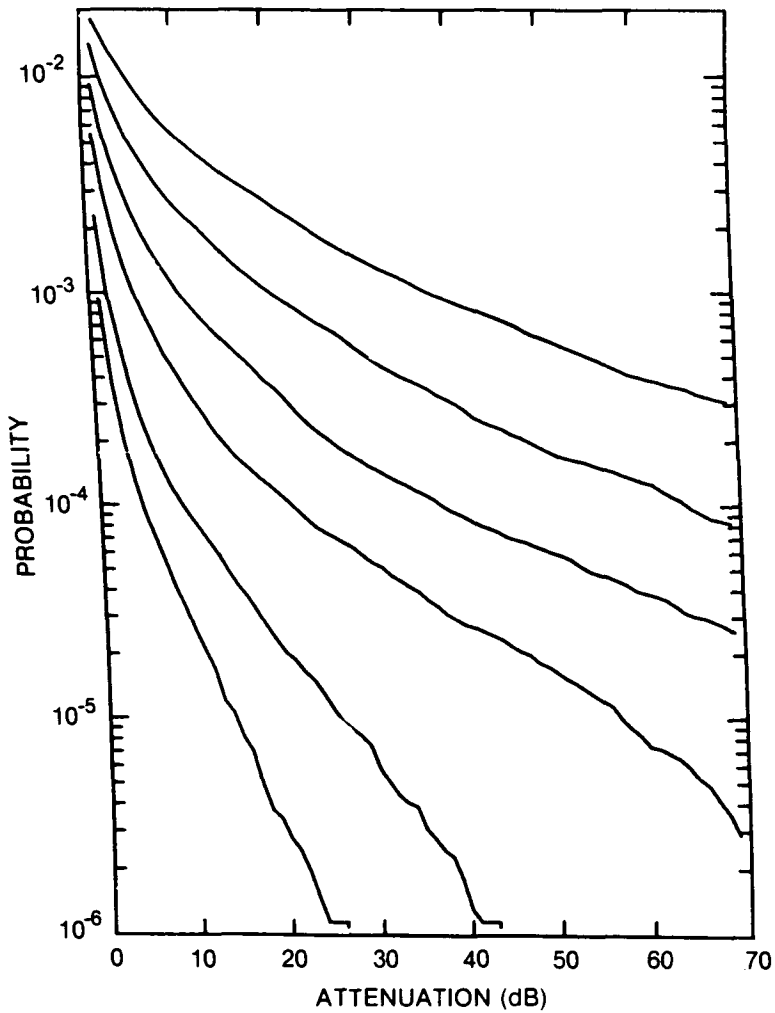

Figure 247. Cumulative distribution of rain attenuation for 35 GHz at Prince Albert, SASK. Curves, moving from lowest to highest, are for hop lengths of 1, 2, 5, 10, 20 and 40 km, respectively.

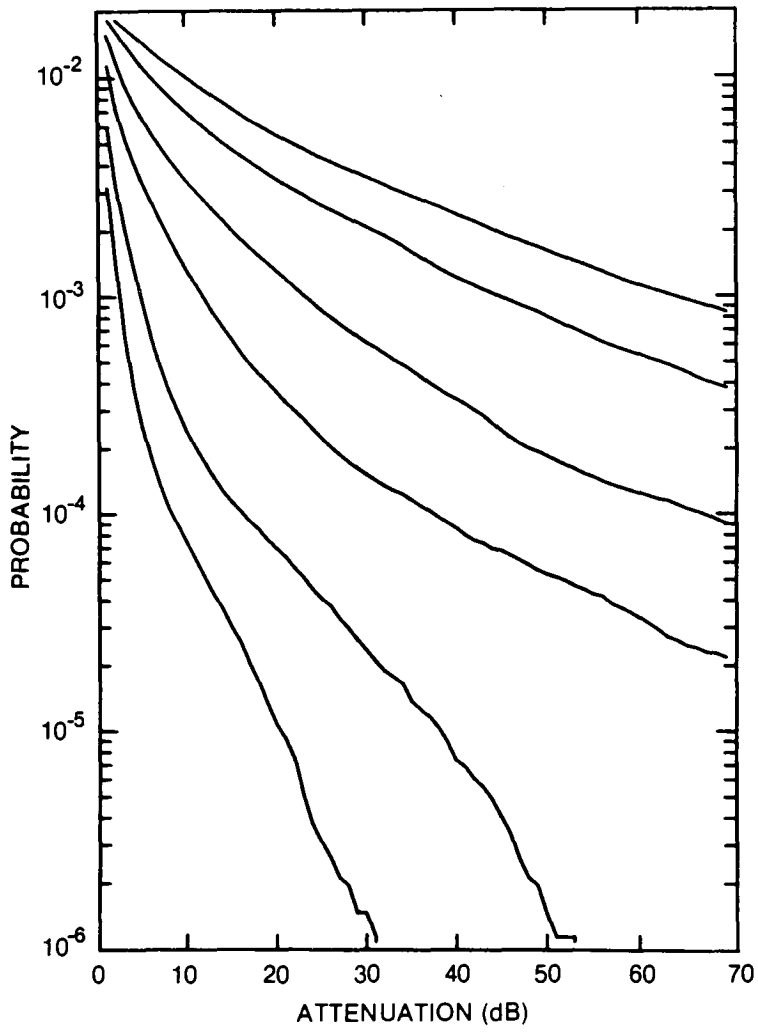

Figure 248. Cumulative distribution of rain attenuation for 56 GHz at Prince Albert, SASK. Curves, moving from lowest to highest, are for hop lengths of 1, 2, 5, 10, 20 and 30 km, respectively.

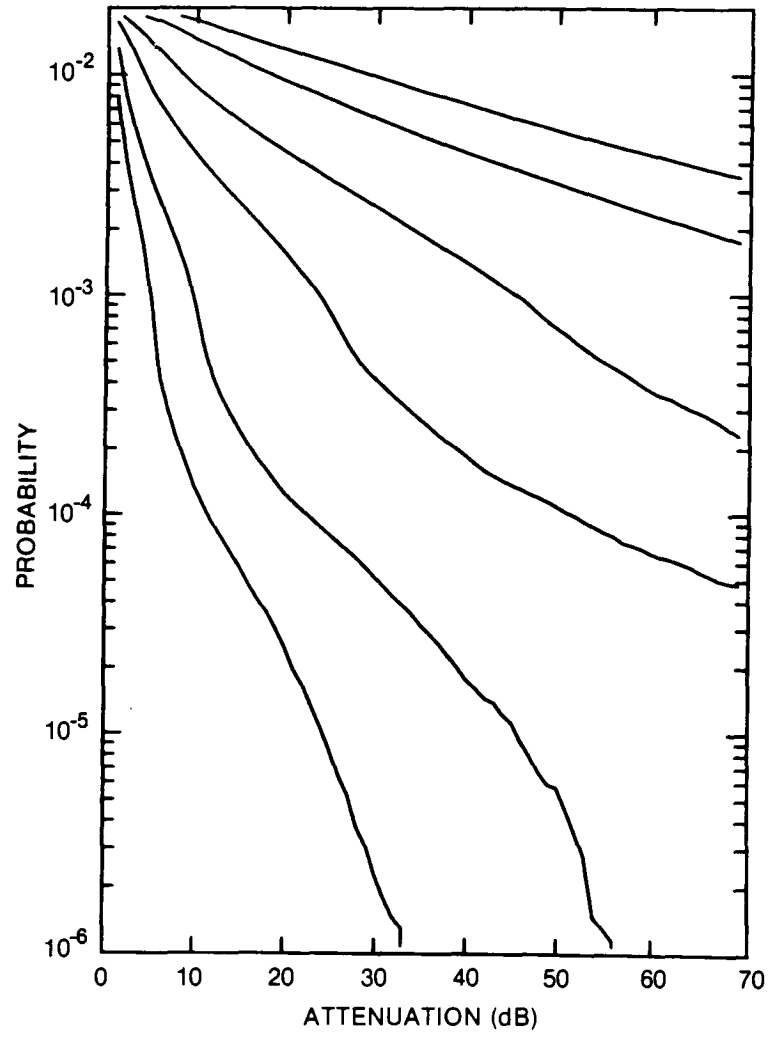

Figure 249. Cumulative distribution of rain attenuation for 100 GHz at Prince Albert, SASK. Curves, moving from lowest to highest, are for hop lengths of 1, 2, 5, 10, 20 and 30 km, respectively.

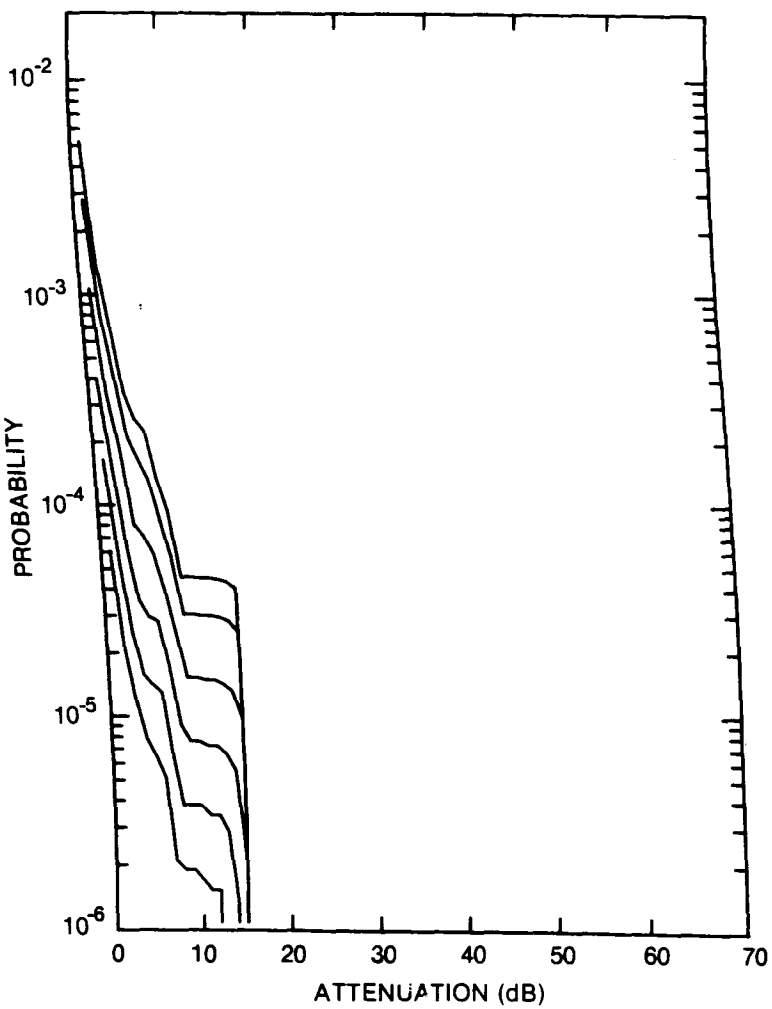

Figure 250. Cumulative distribution of rain attenuation for 8 GHz at Prince George, BC. Curves, moving from lowest to highest, are for hop lengths of 5, 10, 20, 40, 80 and 120 km, respectively.

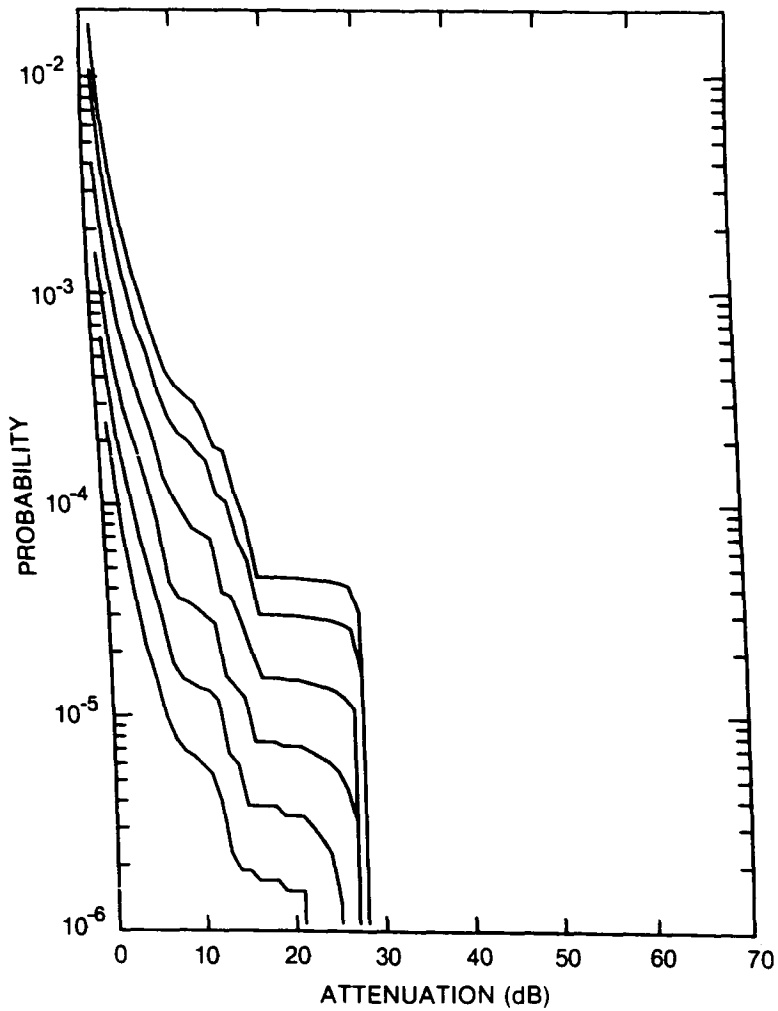

Figure 251. Cumulative distribution of rain attenuation for 11 GHz at Prince George, BC. Curves, moving from lowest to highest, are for hop lengths of 5, 10, 20, 40, 80 and 120 km, respectively.

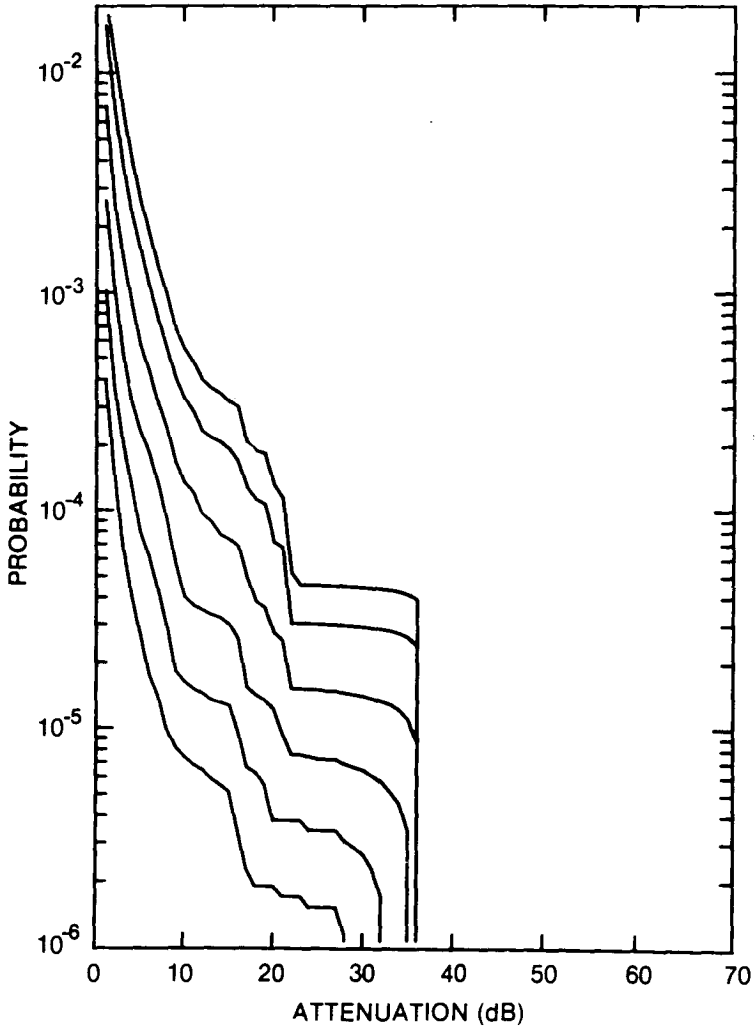

Figure 252. Cumulative distribution of rain attenuation for 12.8 GHz at Prince George, BC. Curves, moving from lowest to highest, are for hop lengths of 5, 10, 20, 40, 80 and 120 km, respectively.

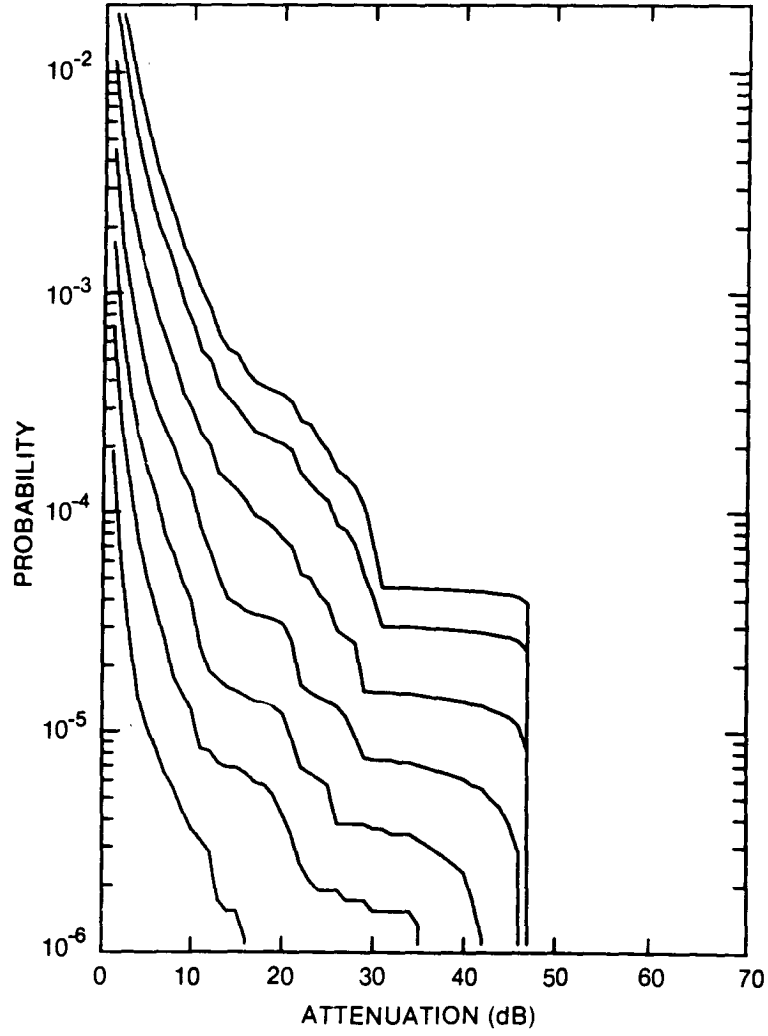

Figure 253. Cumulative distribution of rain attenuation for 15 GHz at Prince George, BC. Curves, moving from lowest to highest, are for hop lengths of 2, 5, 10, 20, 40, 80 and 120 km, respectively.

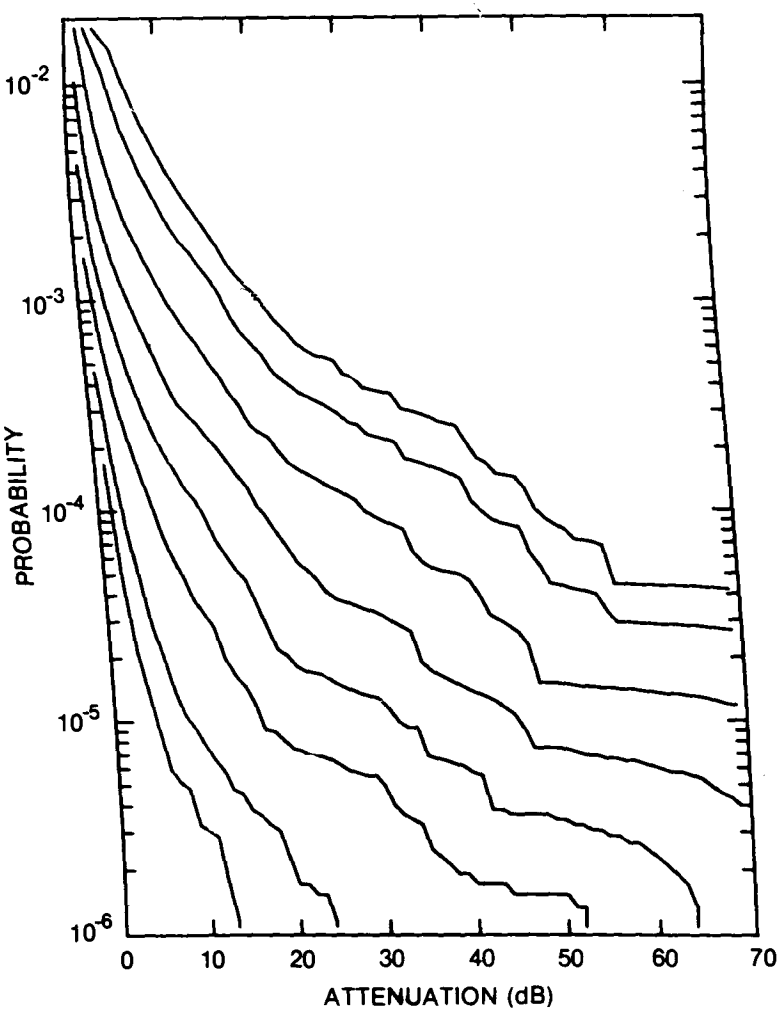

Figure 254. Cumulative distribution of rain attenuation for 20 GHz at Prince George, BC. Curves, moving from lowest to highest, are for hop lengths of 1, 2, 5, 10, 20, 40, 80 and 120 km, respectively.

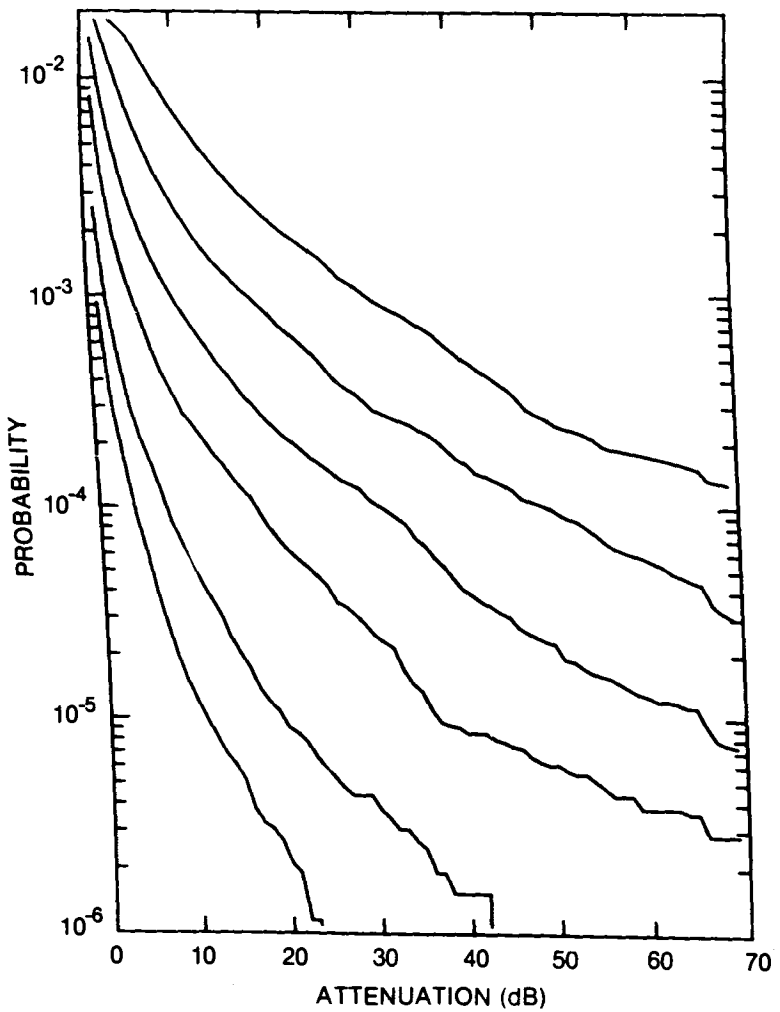

Figure 255. Cumulative distribution of rain attenuation for 35 GHz at Prince George, BC. Curves, moving from lowest to highest, are for hop lengths of 1, 2, 5, 10, 20 and 40 km, respectively.

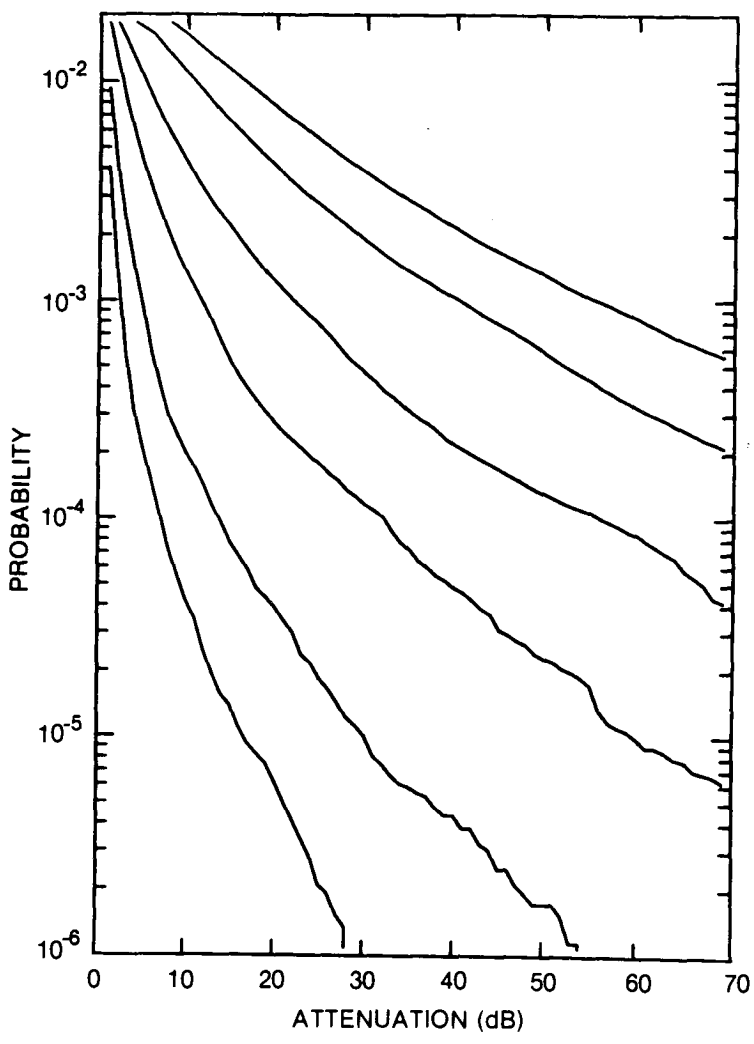

Figure 256. Cumulative distribution of rain attenuation for 56 GHz at Prince George, BC. Curves, moving from lowest to highest, are for hop lengths of 1, 2, 5, 10, 20 and 30 km, respectively.

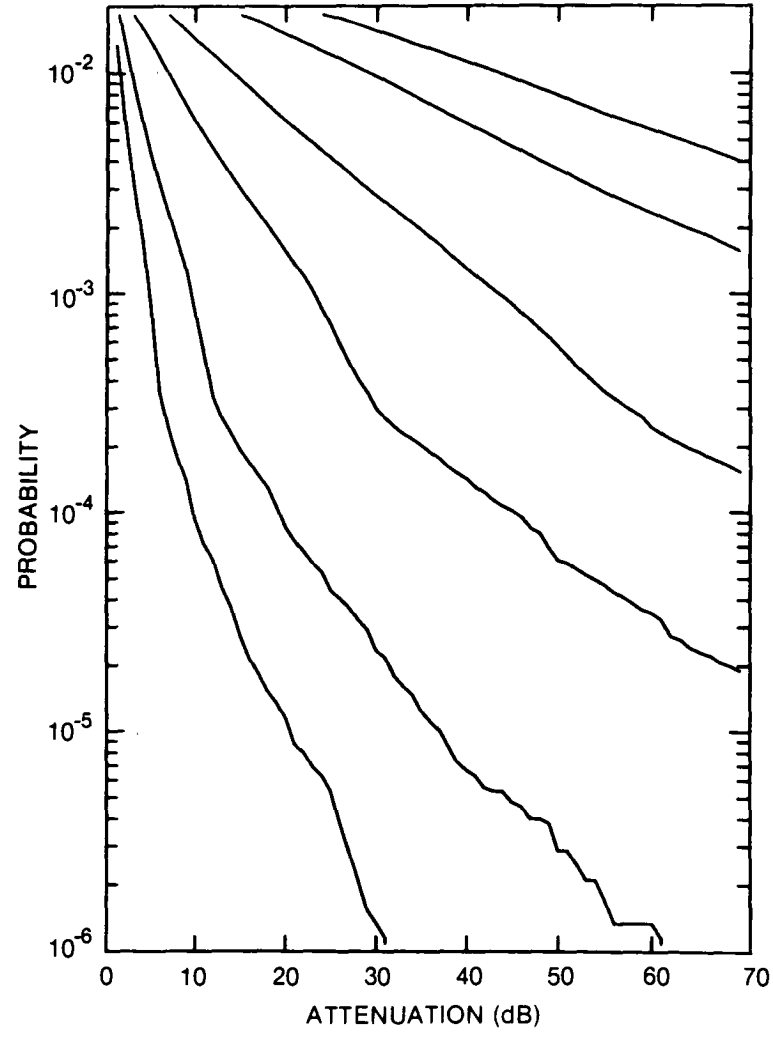

Figure 257. Cumulative distribution of rain attenuation for 100 GHz at Prince George, BC. Curves, moving from lowest to highest, are for hop lengths of 1, 2, 5, 10, 20 and 30 km, respectively.

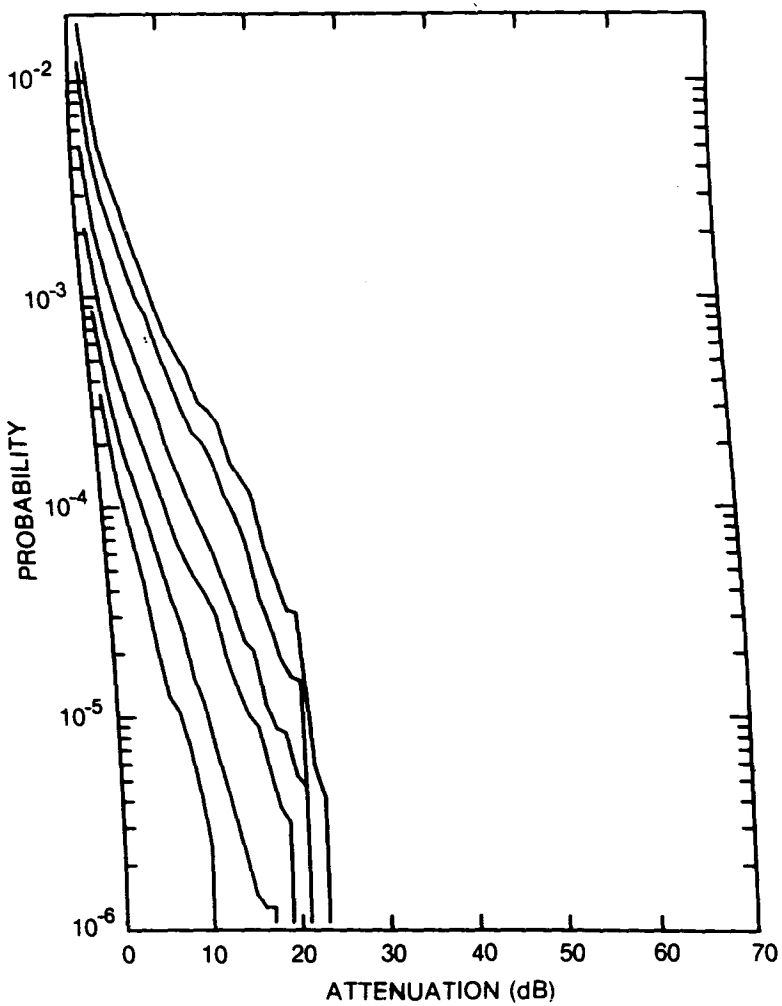

Figure 258. Cumulative distribution of rain attenuation for 8 GHz at Quebec, QUE. Curves, moving from lowest to highest, are for hop lengths of 5, 10, 20, 40, 80 and 120 km, respectively.

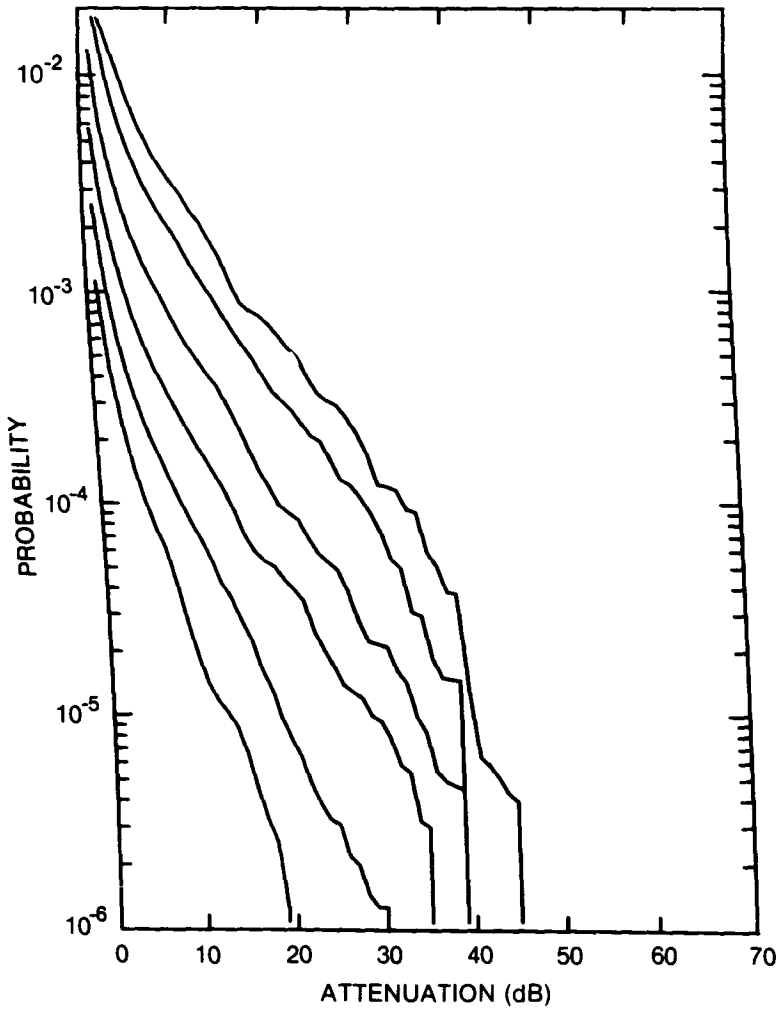

Figure 259. Cumulative distribution of rain attenuation for 11 GHz at Quebec, QUE. Curves, moving from lowest to highest, are for hop lengths of 5, 10, 20, 40, 80 and 120 km, respectively.

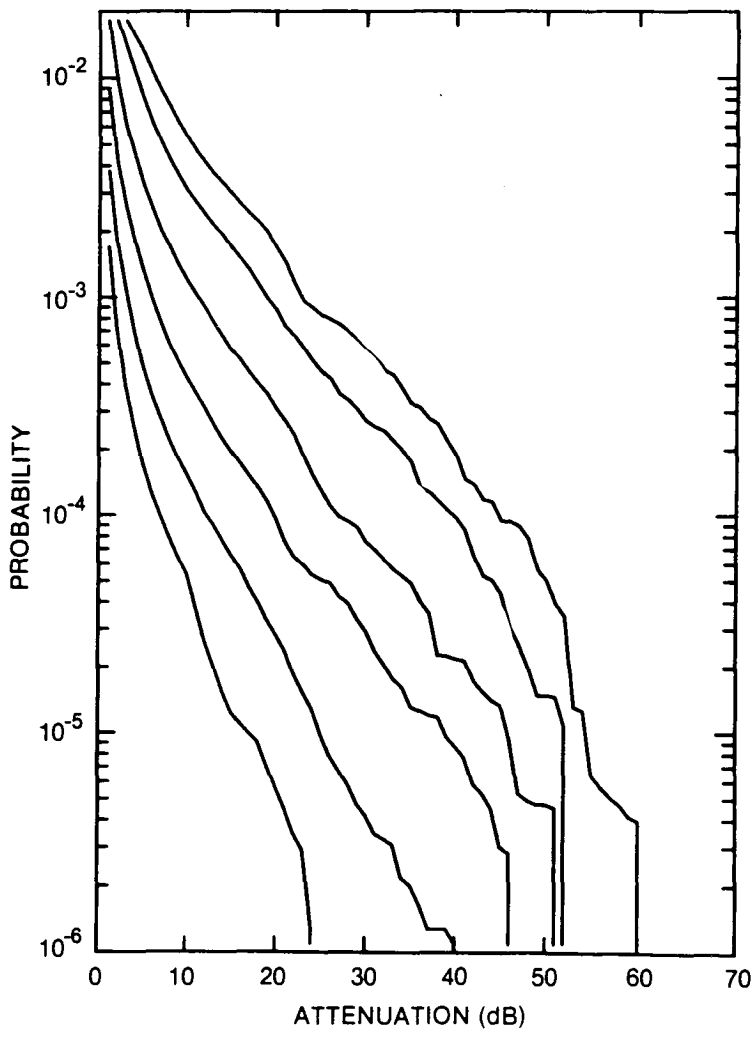

Figure 260. Cumulative distribution of rain attenuation for 12.8 GHz at Quebec, QUE. Curves, moving from lowest to highest, are for hop lengths of 5, 10, 20, 40, 80 and 120 km, respectively.

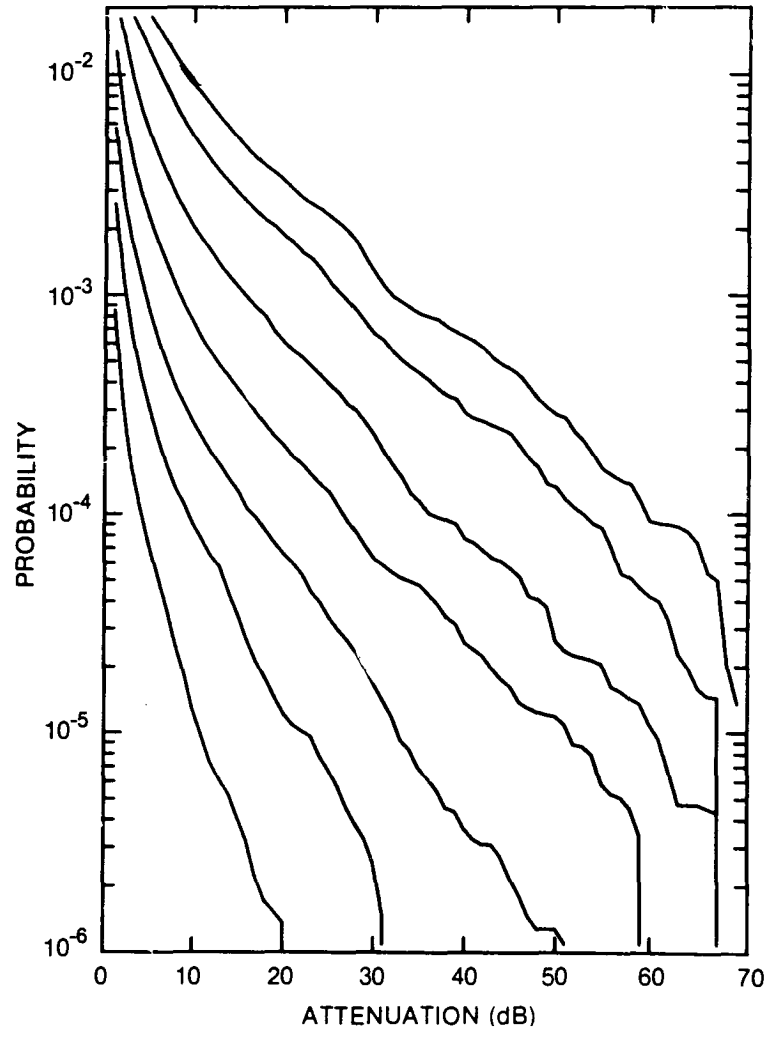

Figure 261. Cumulative distribution of rain attenuation for 15 GHz at Quebec, QUE. Curves, moving from lowest to highest, are for hop lengths of 2, 5, 10, 20, 40, 80 and 120 km, respectively.

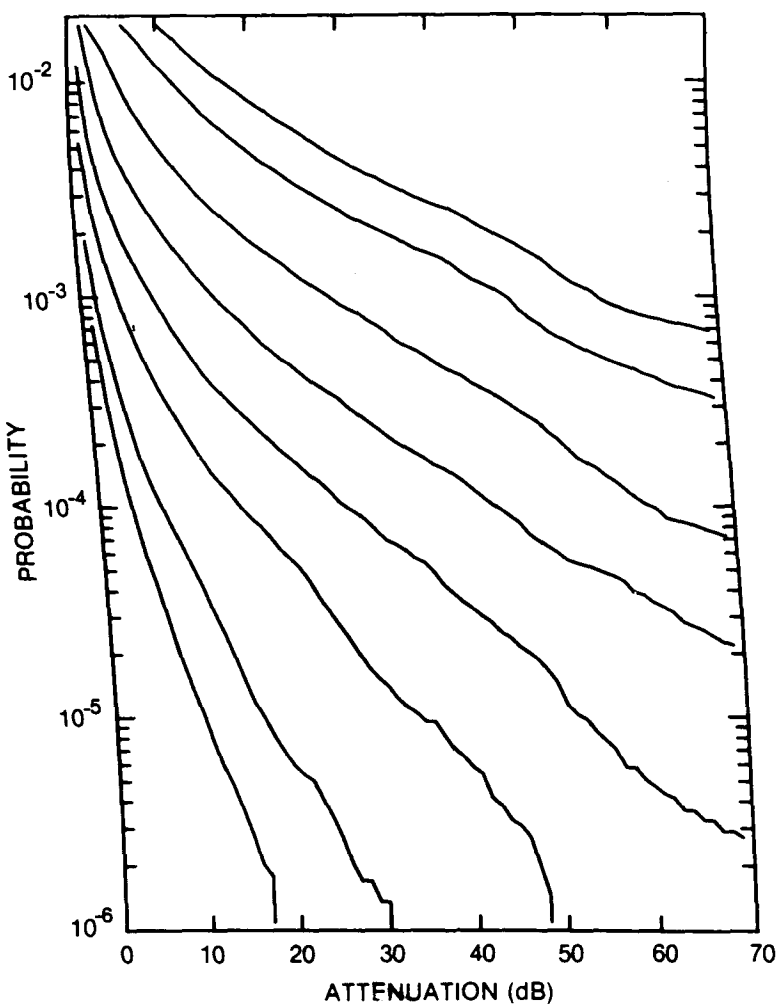

Figure 262. Cumulative distribution of rain attenuation for 20 GHz at Quebec, QUE. Curves, moving from lowest to highest, are for hop lengths of 1, 2, 5, 10, 20, 40, 80 and 120 km, respectively.

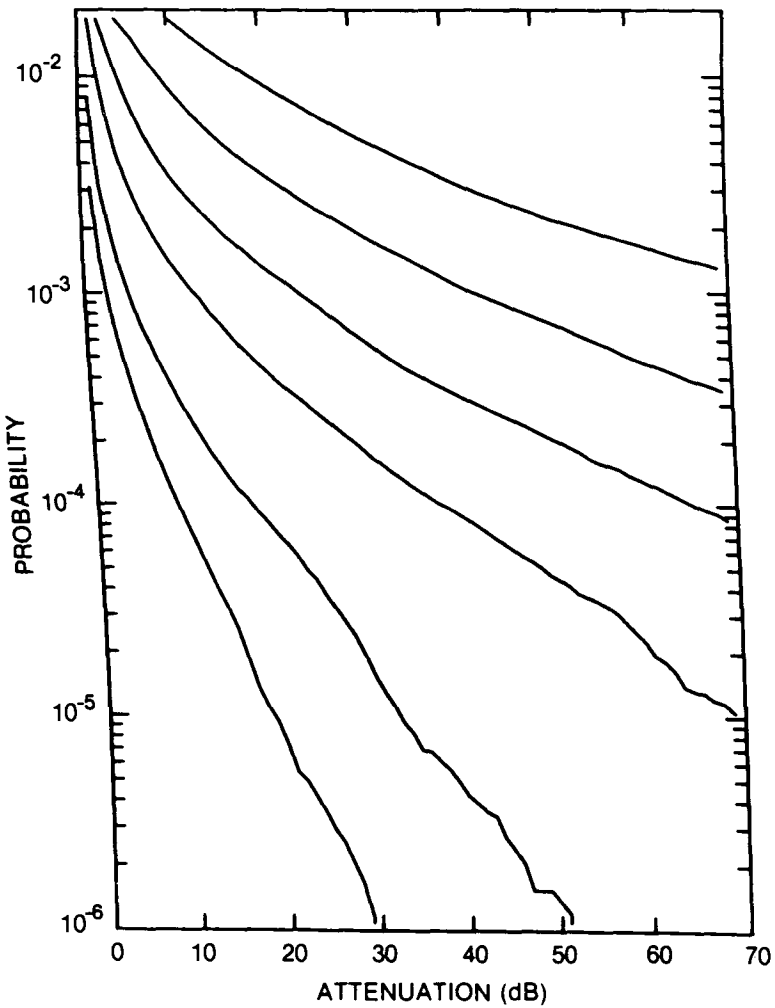

Figure 263. Cumulative distribution of rain attenuation for 35 GHz at Quebec, QUE. Curves, moving from lowest to highest, are for hop lengths of 1, 2, 5, 10, 20 and 40 km, respectively.

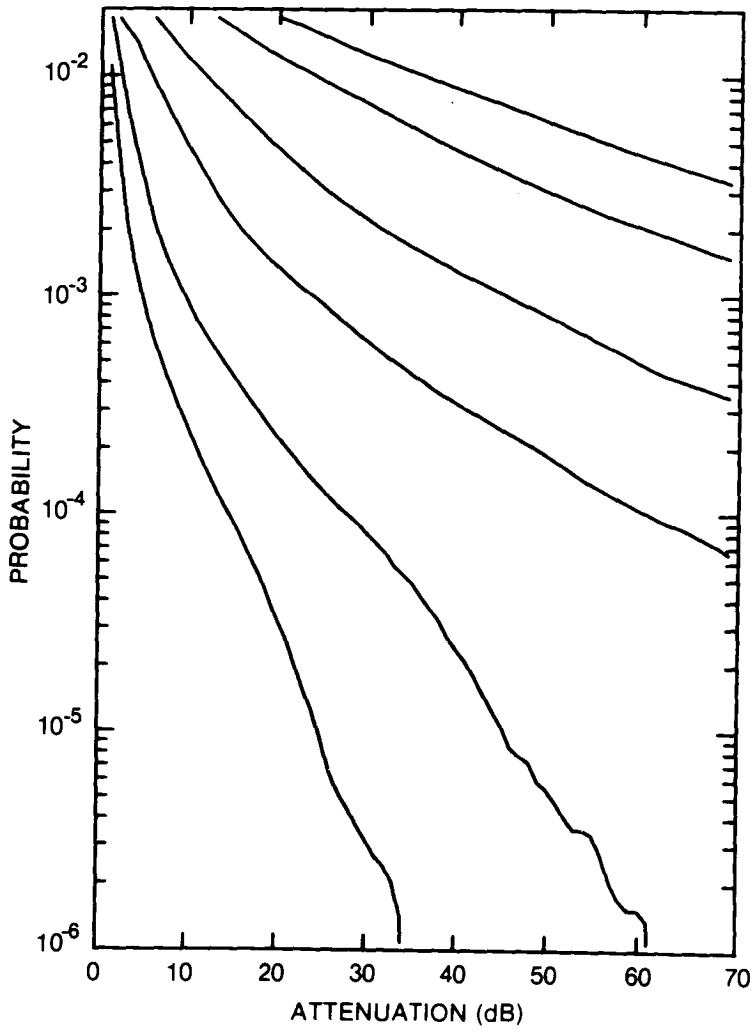

Figure 264. Cumulative distribution of rain attenuation for 56 GHz at Quebec, QUE. Curves, moving from lowest to highest, are for hop lengths of 1, 2, 5, 10, 20 and 30 km, respectively.

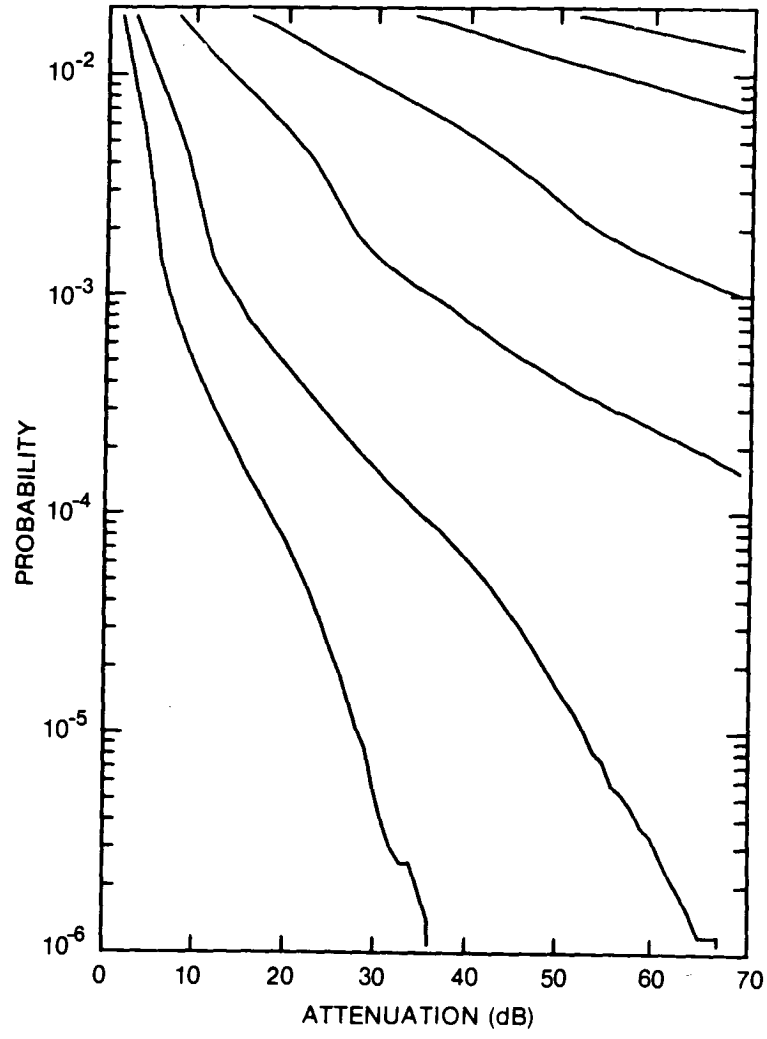

Figure 265. Cumulative distribution of rain attenuation for 100 GHz at Quebec, QUE. Curves, moving from lowest to highest, are for hop lengths of 1, 2, 5, 10, 20 and 30 km, respectively.

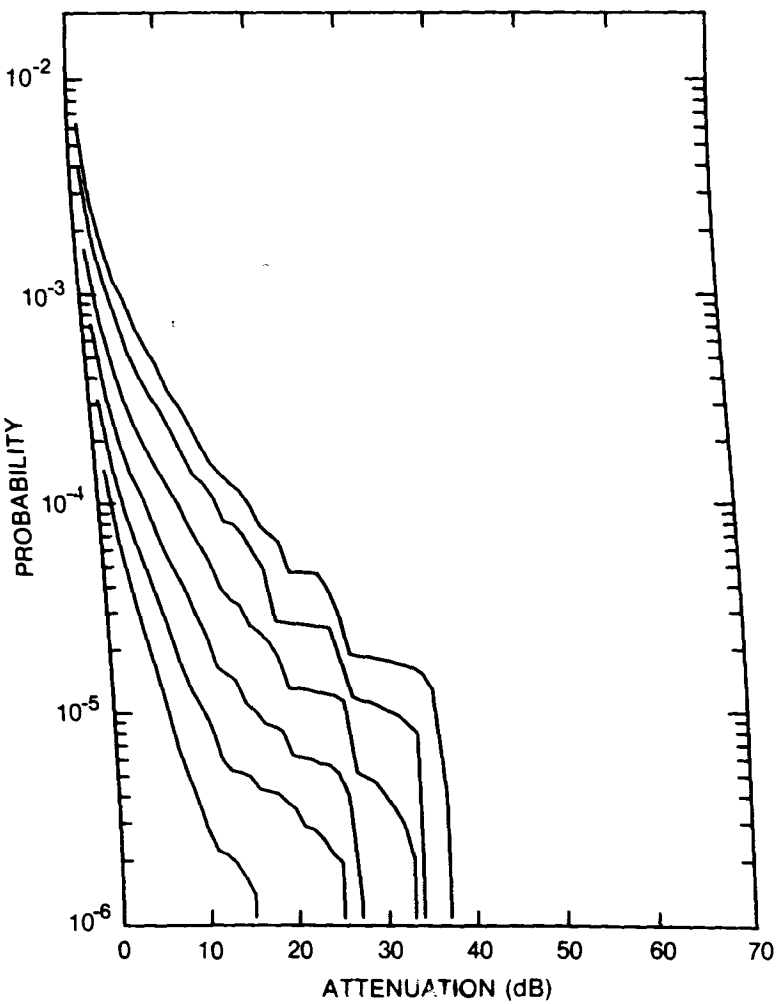

Figure 266. Cumulative distribution of rain attenuation for 8 GHz at Regina, SASK. Curves, moving from lowest to highest, are for hop lengths of 5, 10, 20, 40, 80 and 120 km, respectively.

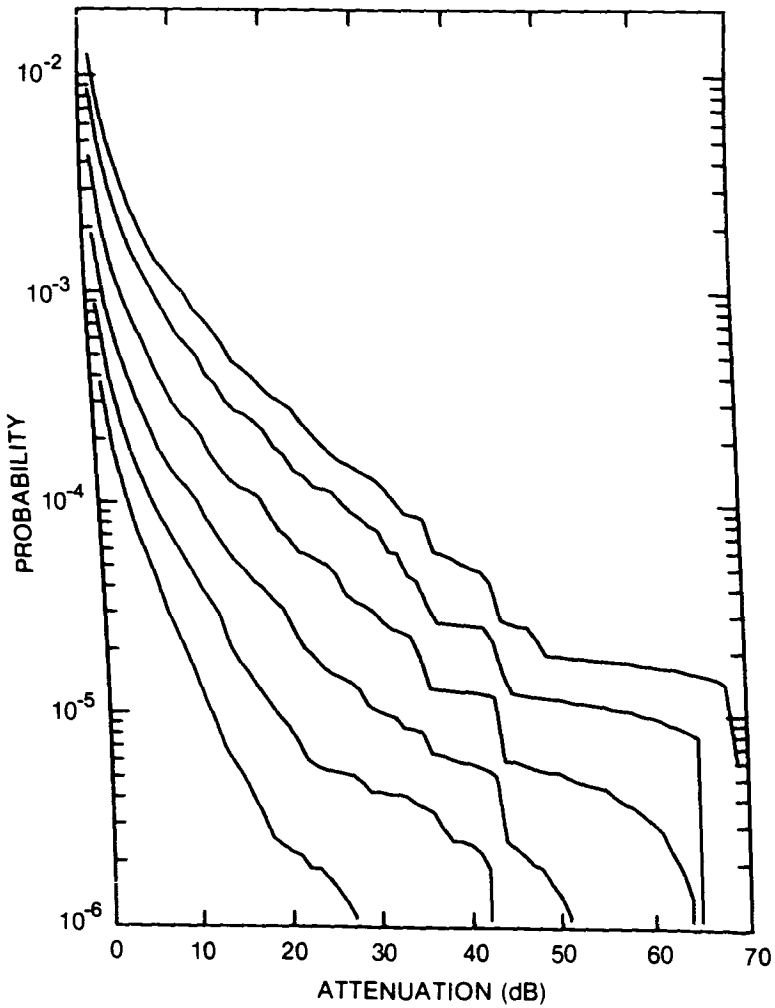

Figure 267. Cumulative distribution of rain attenuation for 11 GHz at Regina, SASK. Curves, moving from lowest to highest, are for hop lengths of 5, 10, 20, 40, 80 and 120 km, respectively.

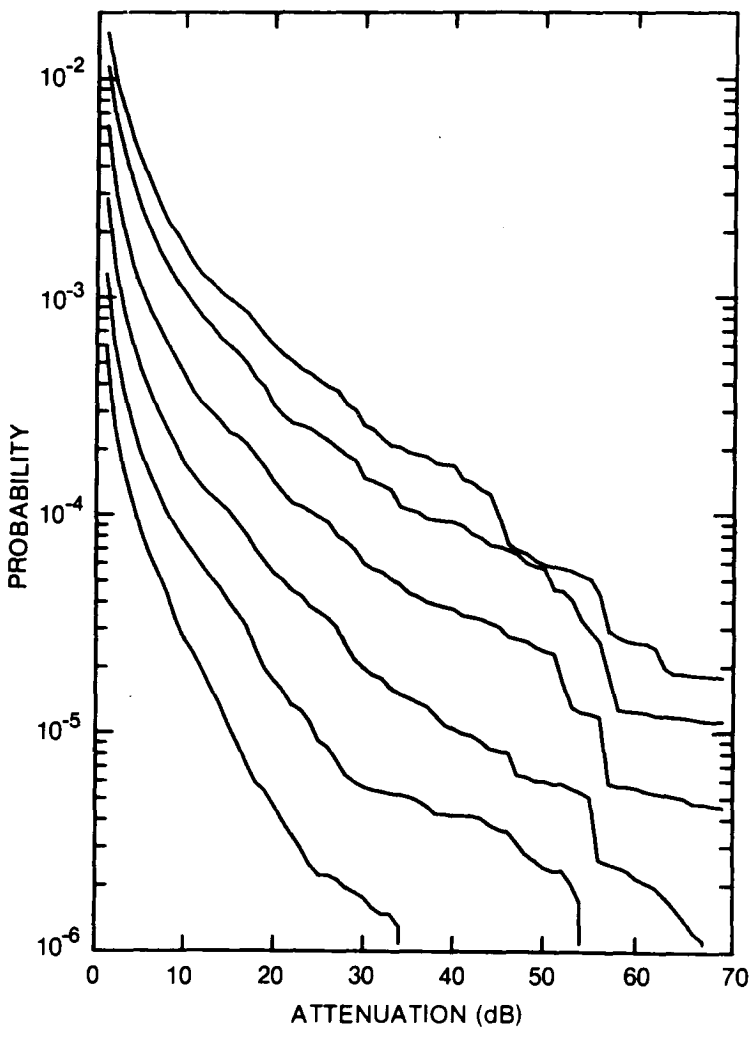

Figure 268. Cumulative distribution of rain attenuation for 12.8 GHz at Regina, SASK. Curves, moving from lowest to highest, are for hop lengths of 5, 10, 20, 40, 80 and 120 km, respectively.

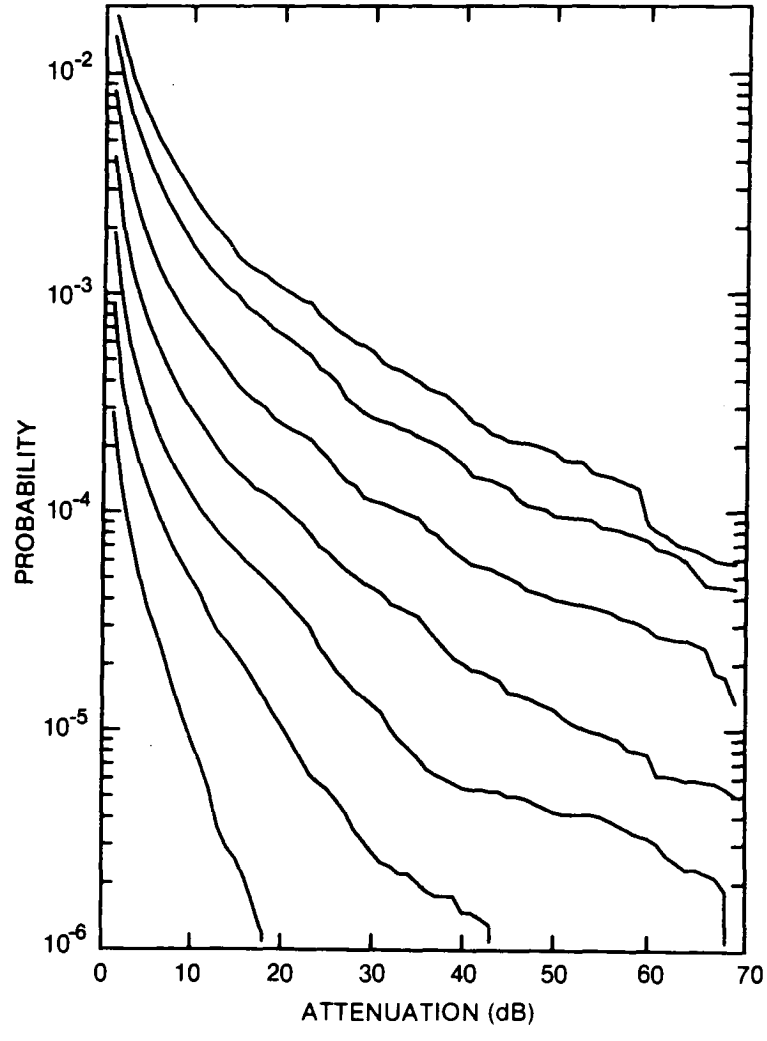

Figure 269. Cumulative distribution of rain attenuation for 15 GHz at Regina, SASK. Curves, moving from lowest to highest, are for hop lengths of 2, 5, 10, 20, 40, 80 and 120 km, respectively.

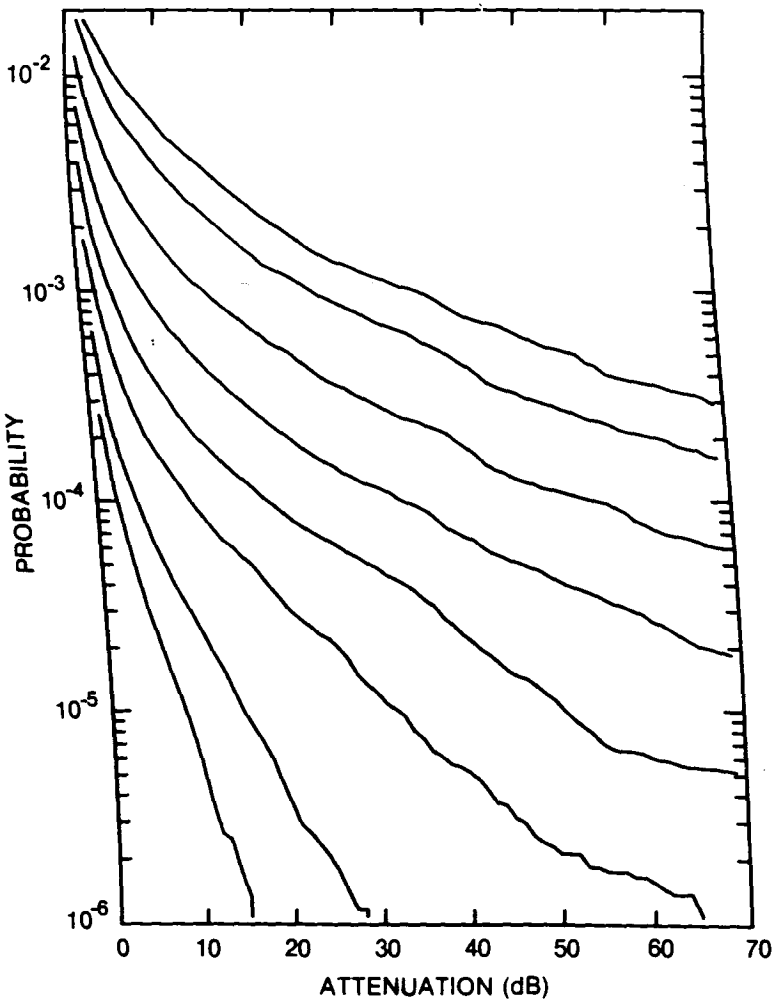

Figure 270. Cumulative distribution of rain attenuation for 20 GHz at Regina, SASK. Curves, moving from lowest to highest, are for hop lengths of 1, 2, 5, 10, 20, 40, 80 and 120 km, respectively.

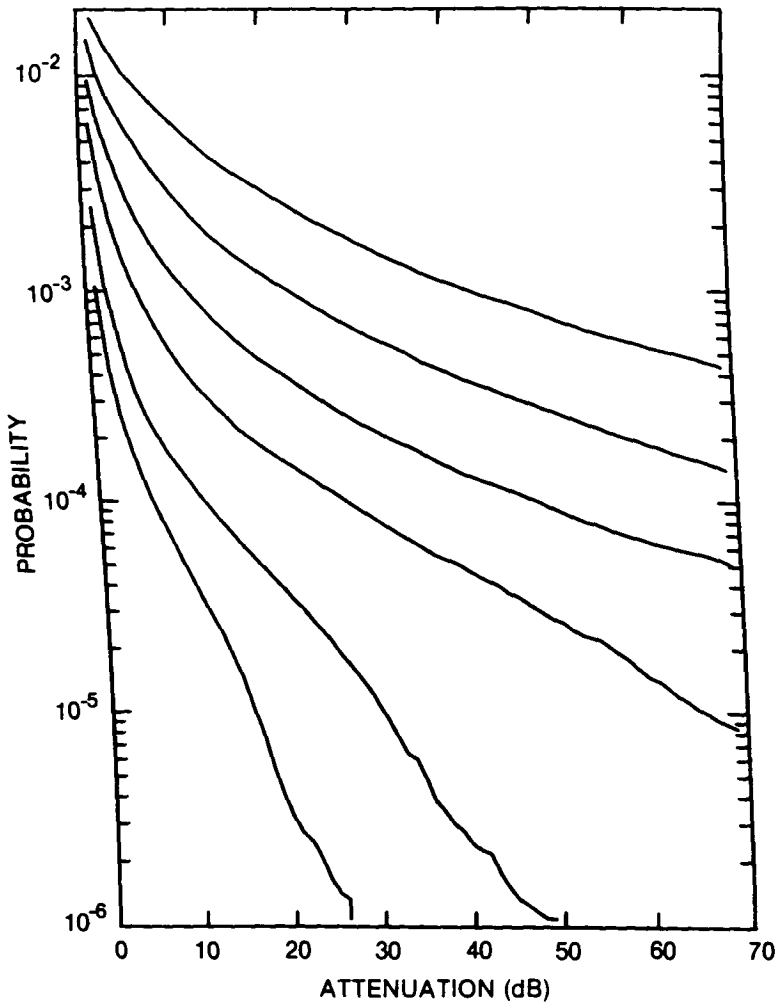

Figure 271. Cumulative distribution of rain attenuation for 35 GHz at Regina, SASK. Curves, moving from lowest to highest, are for hop lengths of 1, 2, 5, 10, 20 and 40 km, respectively.

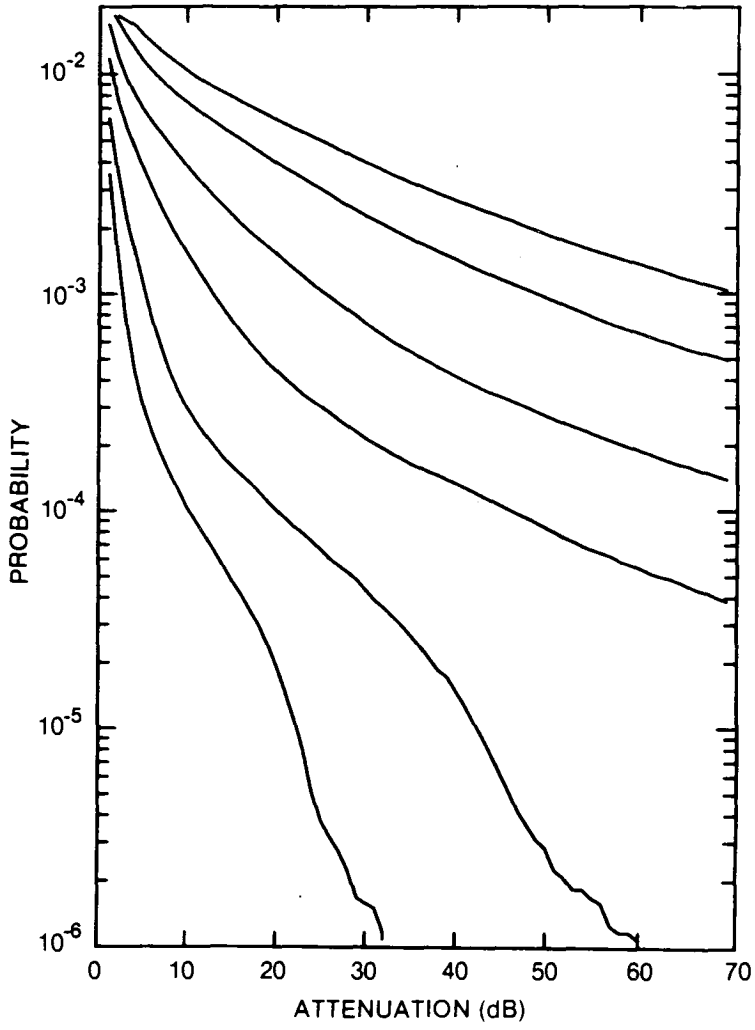

Figure 272. Cumulative distribution of rain attenuation for 56 GHz at Regina, SASK. Curves, moving from lowest to highest, are for hop lengths of 1, 2, 5, 10, 20 and 30 km, respectively.

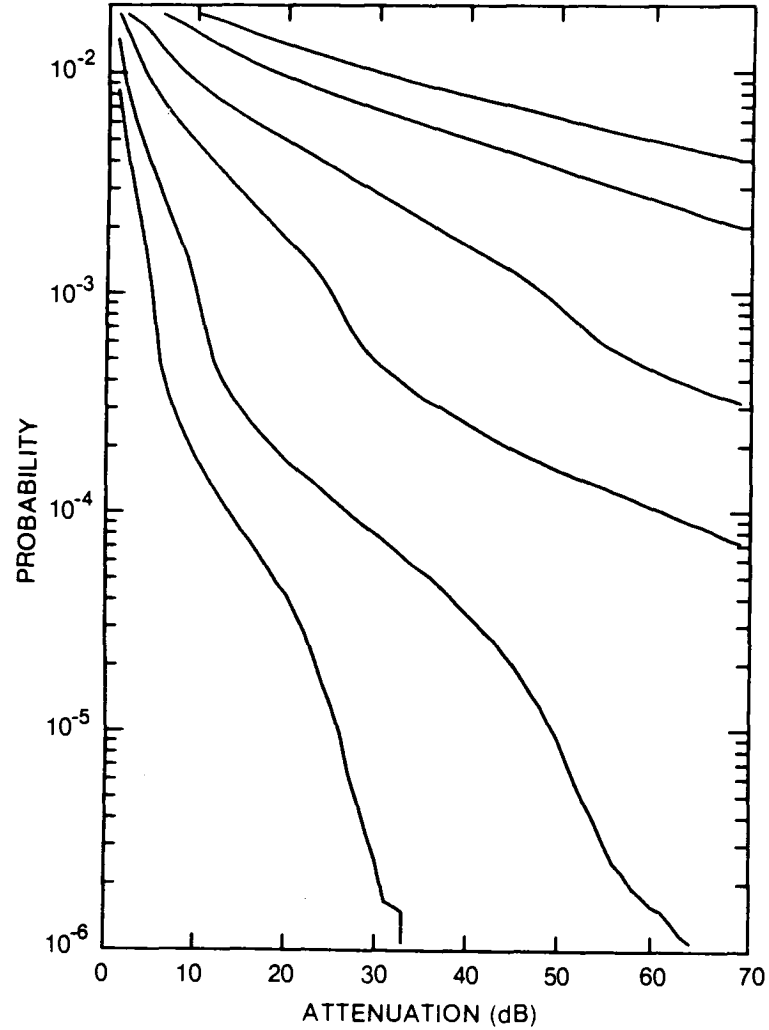

Figure 273. Cumulative distribution of rain attenuation for 100 GHz at Regina, SASK. Curves, moving from lowest to highest, are for hop lengths of 1, 2, 5, 10, 20 and 30 km, respectively.

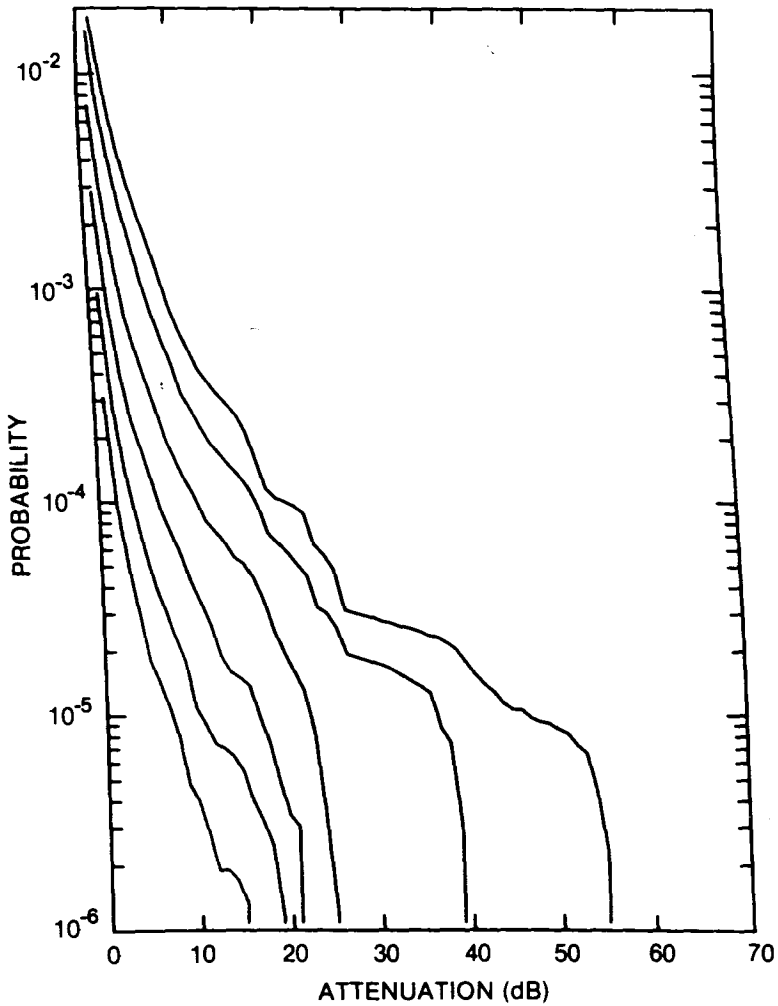

Figure 274. Cumulative distribution of rain attenuation for 8 GHz at Saint John, NB. Curves, moving from lowest to highest, are for hop lengths of 5, 10, 20, 40, 80 and 120 km, respectively.

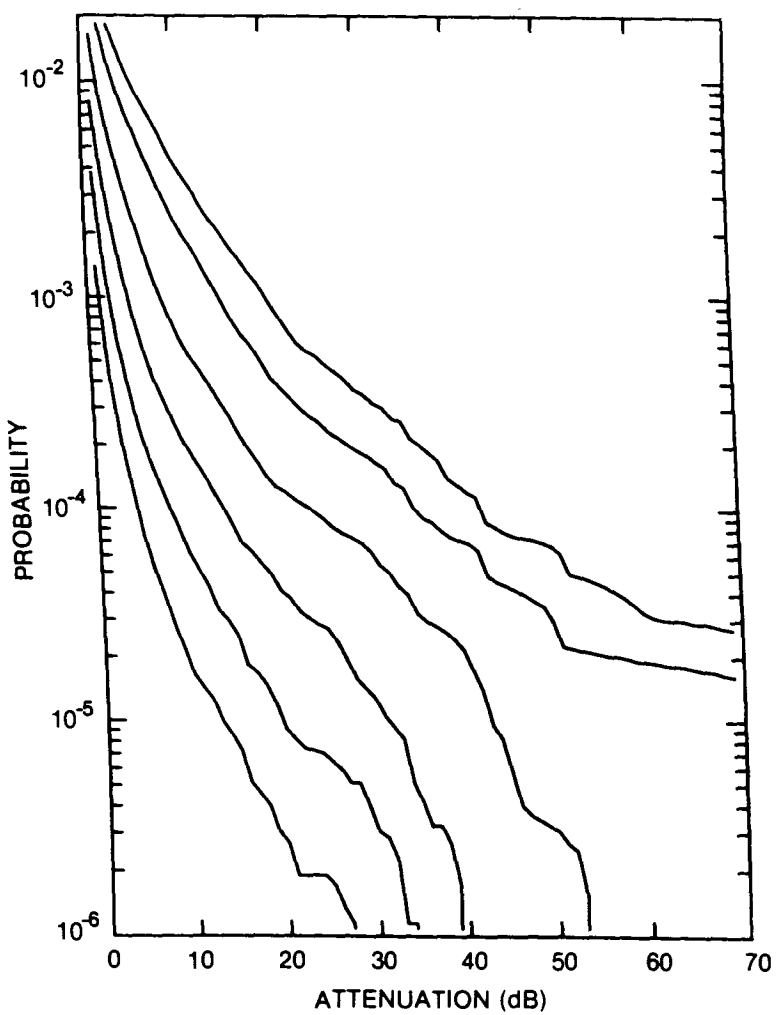

Figure 275. Cumulative distribution of rain attenuation for 11 GHz at Saint John, NB. Curves, moving from lowest to highest, are for hop lenghts of 5, 10, 20, 40, 80 and 120 km, respectively.

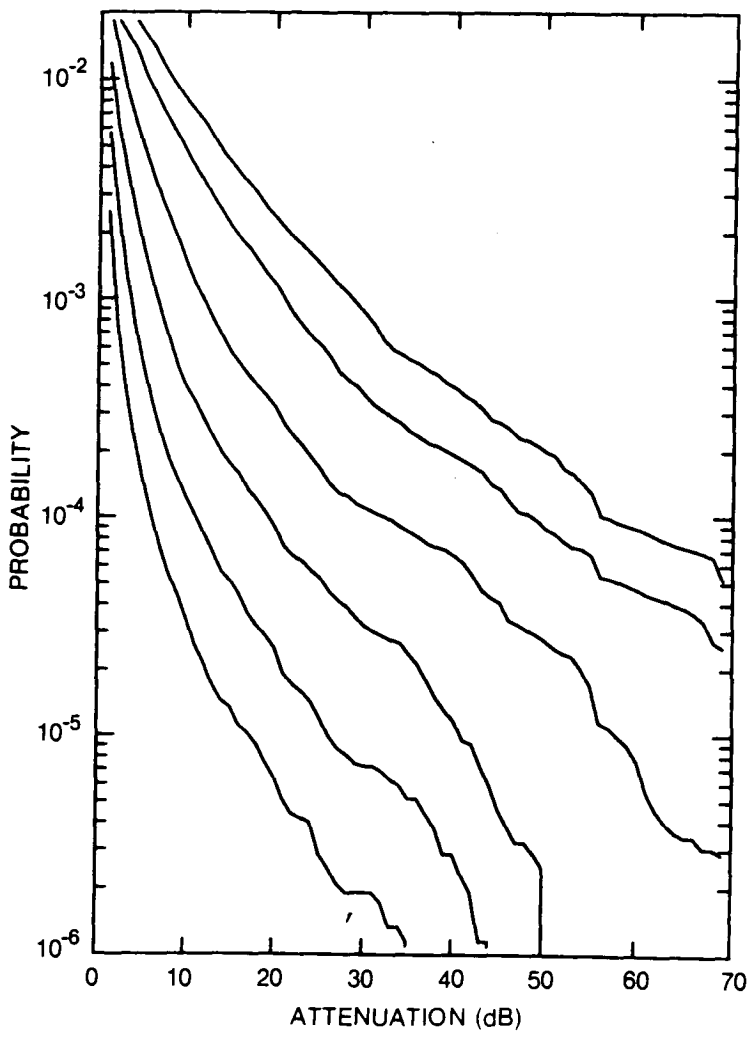

Figure 276. Cumulative distribution of rain attenuation for 12.8 GHz at Saint John, N8. Curves, moving from lowest to highest, are for hop lengths of 5, 10, 20, 40, 80 and 120 km, respectively.

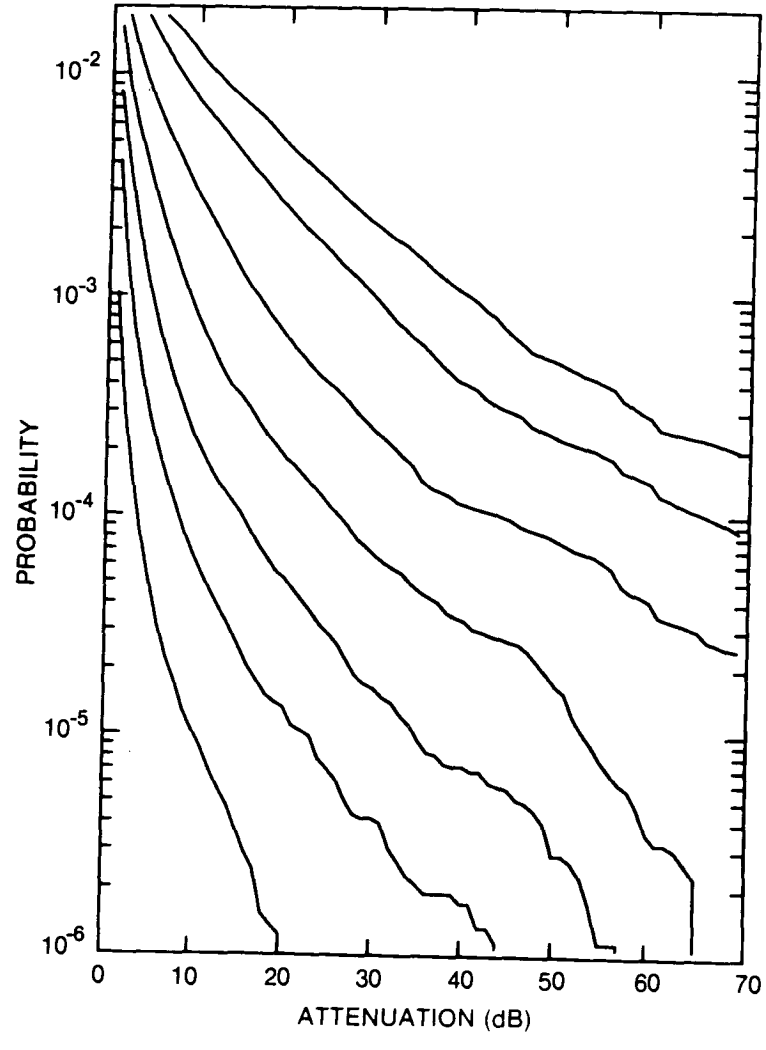

Figure 277. Cumulative distribution of rain attenuation for 15 GHz at Saint John, NB. Curves, moving from lowest to highest, are for hop lengths of 2, 5, 10, 20, 40, 80 and 120 km, respectively.

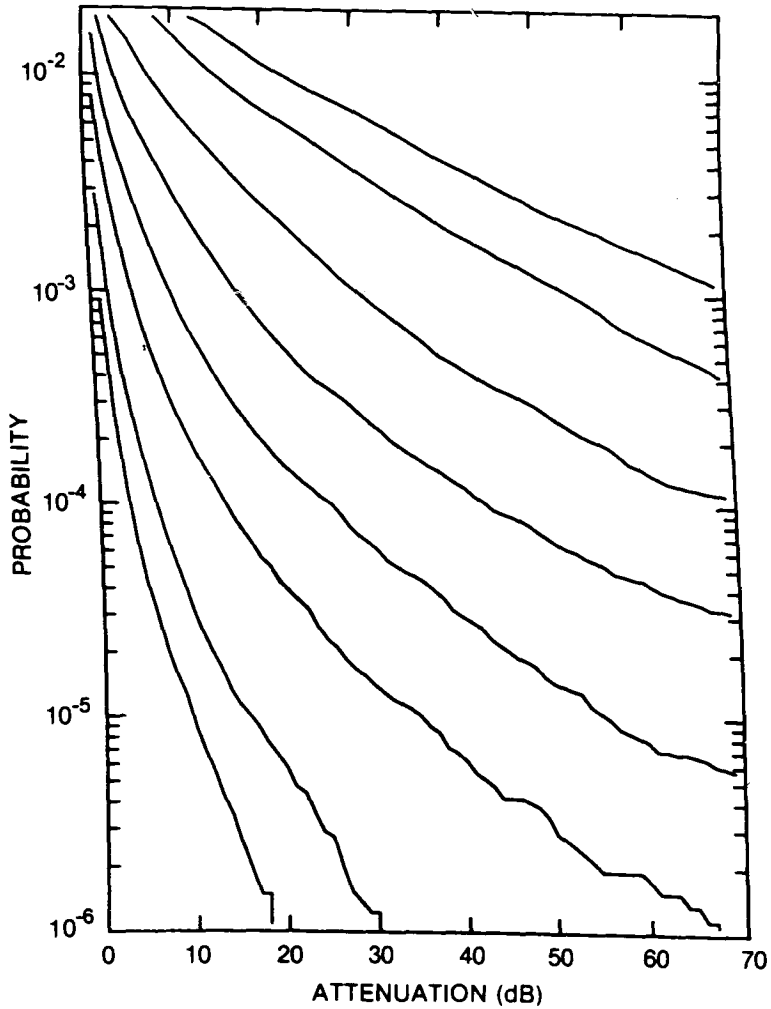

Figure 278. Cumulative distribution of rain attenuation for 20 GHz at Saint John, NB. Curves, moving from lowest to highest, are for hop lengths of 1, 2, 5, 10, 20, 40, 80 and 120 km, respectively.

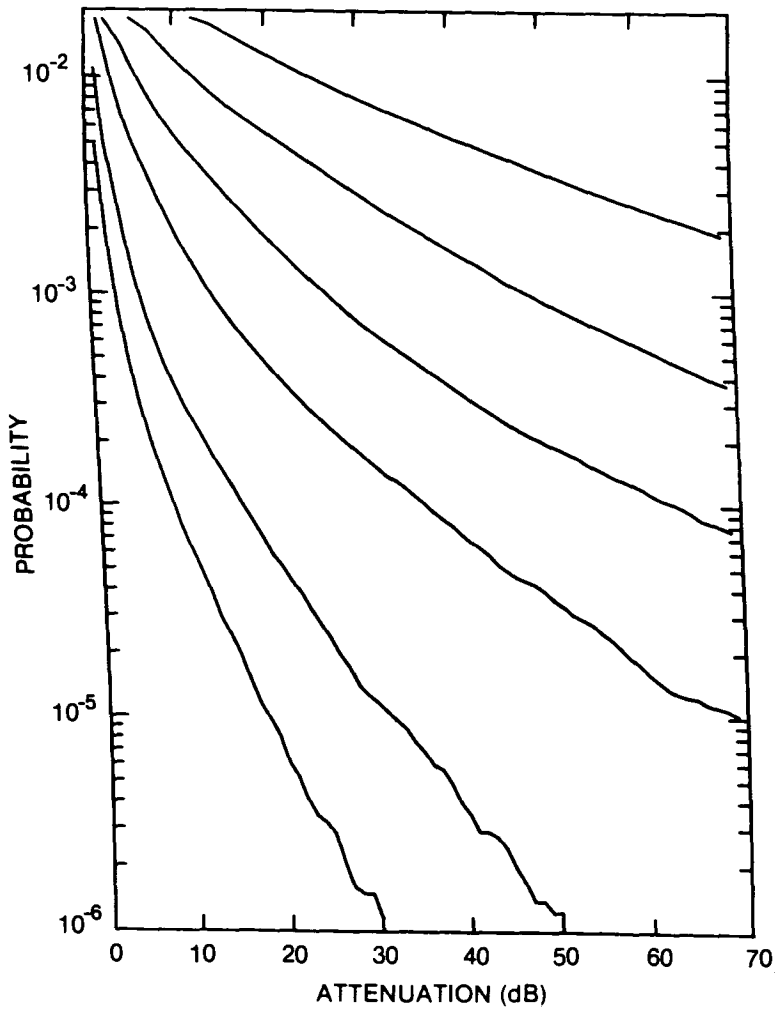

Figure 279. Cumulative distribution of rain attenuation for 35 GHz at Saint John, NB. Curves, moving from lowest to highest, are for hop lengths of 1, 2, 5, 10, 20 and 40 km, respectively.

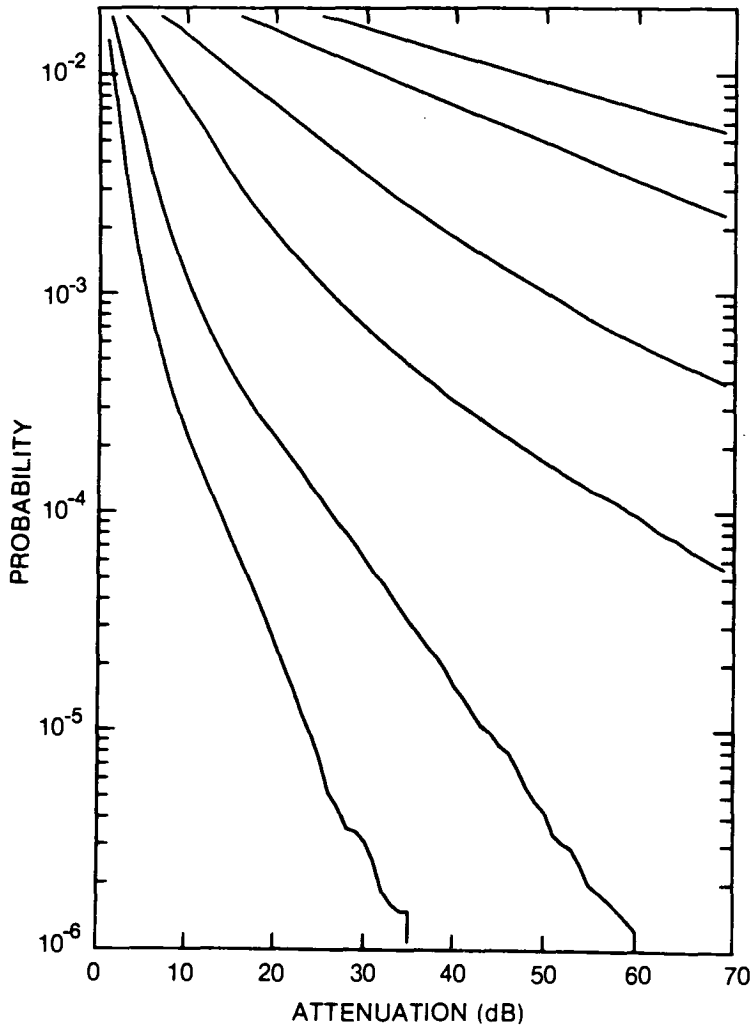

Figure 280. Cumulative distribution of rain attenuation for 56 GHz at Saint John, NB. Curves, moving from lowest to highest, are for hop lengths of 1, 2, 5, 10, 20 and 30 km, respectively.

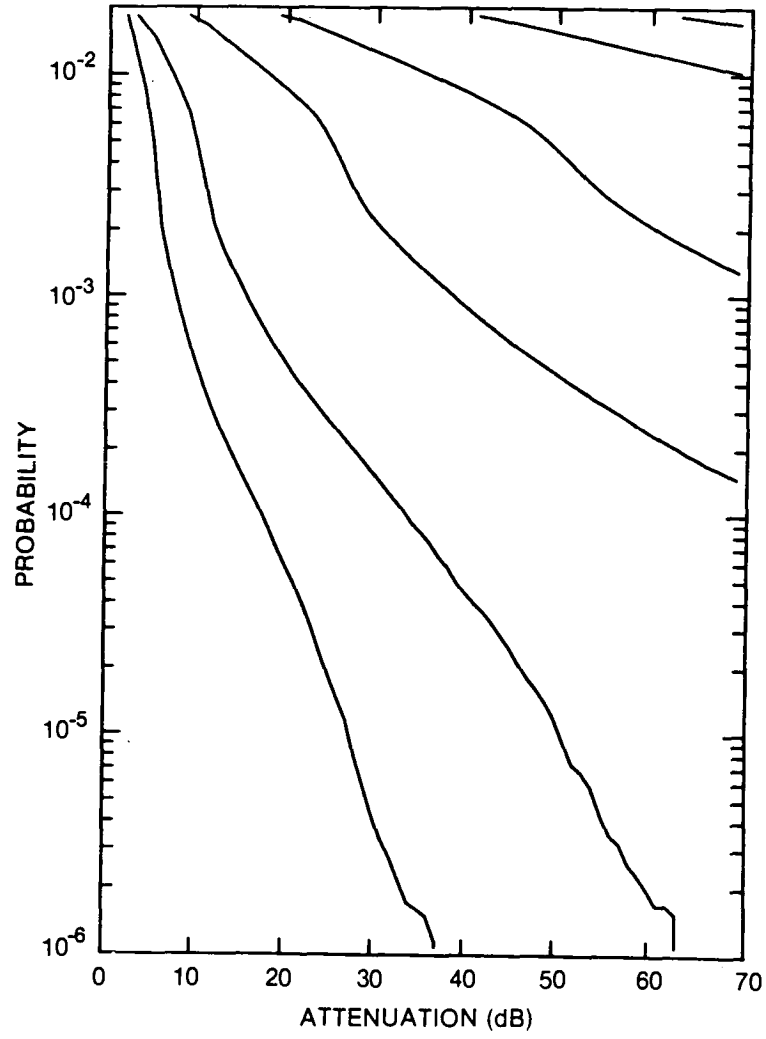

Figure 281. Cumulative distribution of rain attenuation for 100 GHz at Saint John, NB. Curves, moving from lowest to highest, are for hop lengths of 1, 2, 5, 10, 20 and 30 km, respectively.

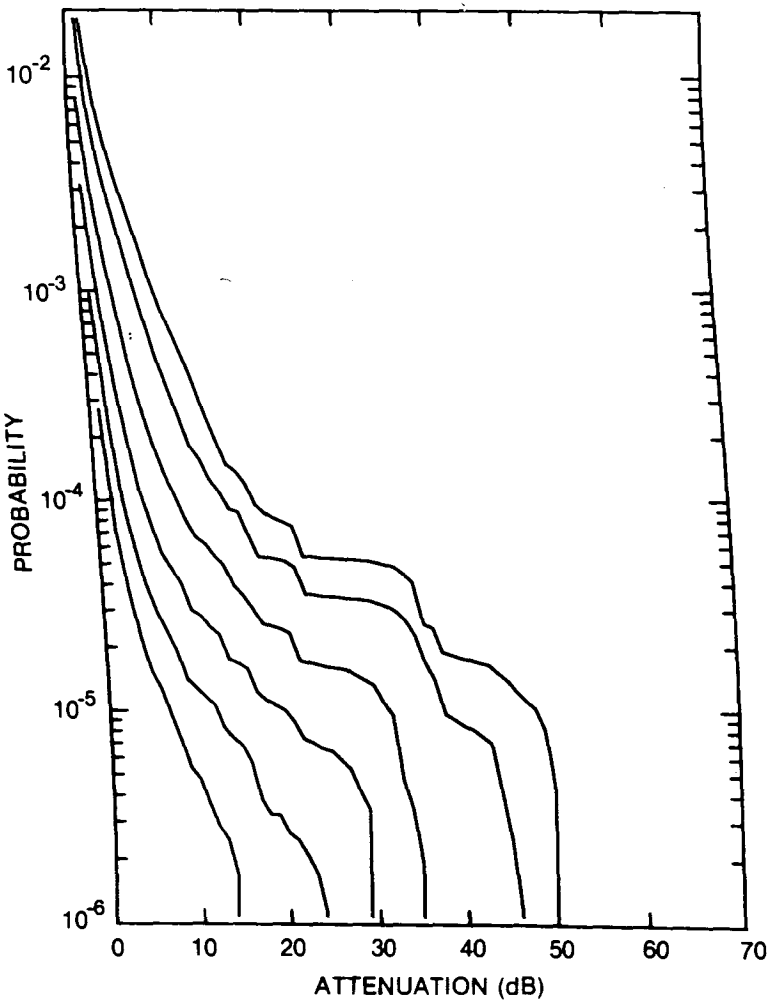

Figure 282. Cumulative distribution of rain attenuation for 8 GHz at St. John's, NFLD. Curves, moving from lowest to highest, are for hop lengths of 5, 10, 20, 40, 80 and 120 km, respectively.

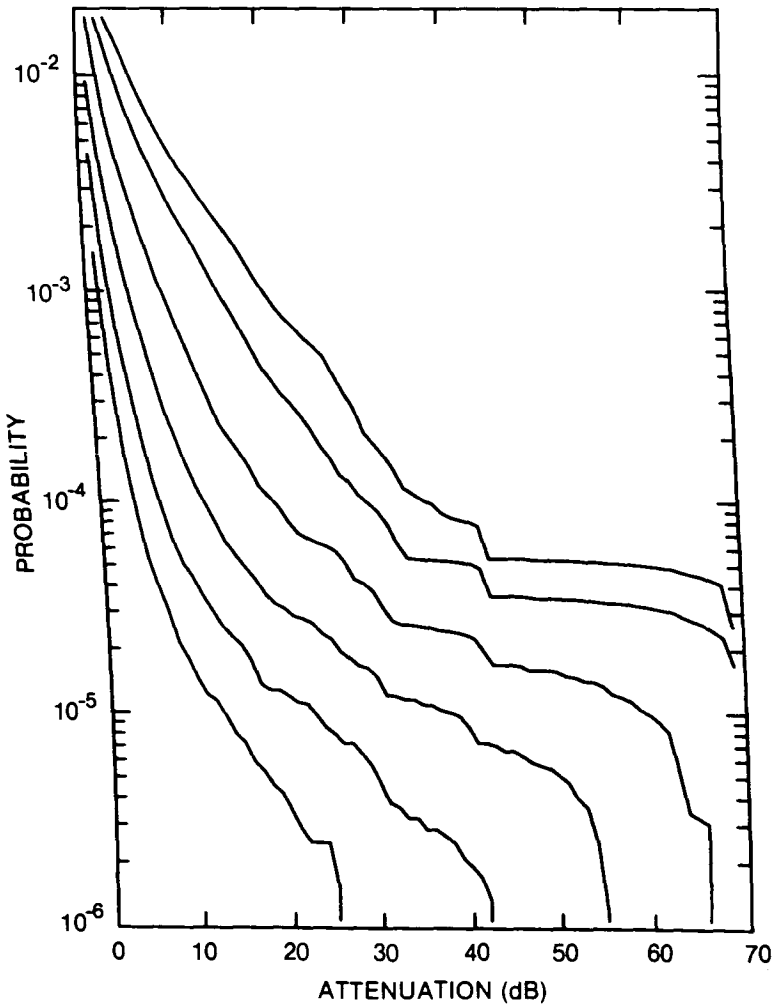

Figure 283. Cumulative distribution of rain attenuation for 11 GHz at St. John's, NFLD. Curves, moving from lowest to highest, are for hop lengths of 5, 10, 20, 40, 80 and 120 km, respectively.

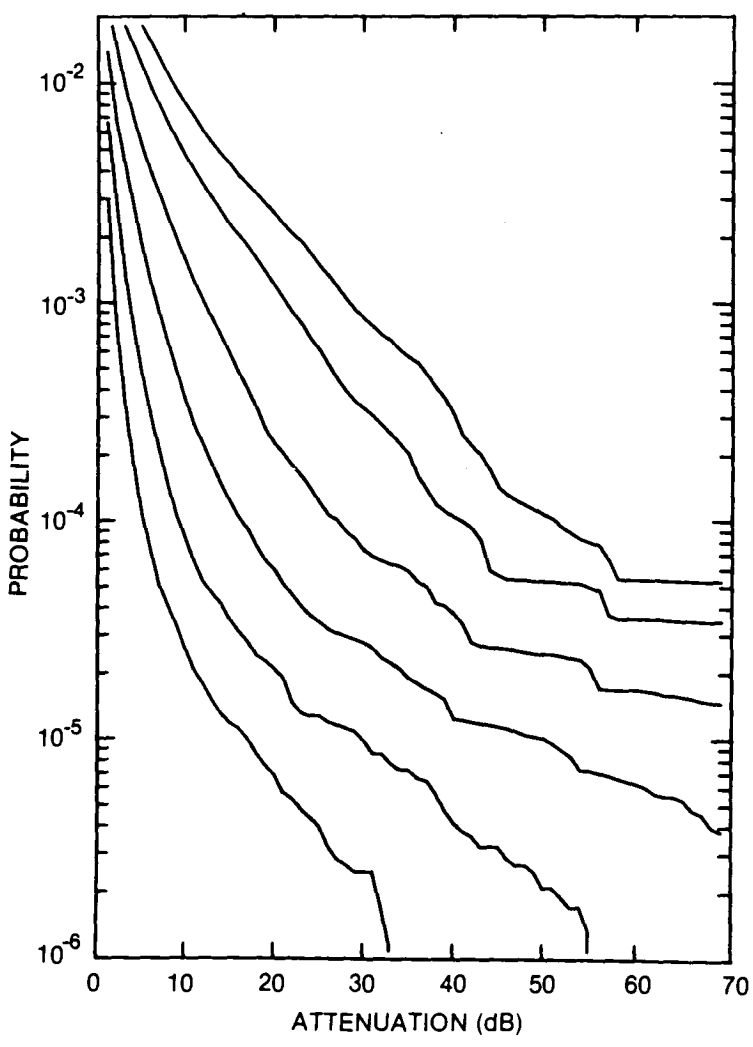

Figure 284. Cumulative distribution of rain attenuation for 12.8 GHz at St. John's, NFLD. Curves, moving from lowest to highest, are for hop lengths of 5, 10, 20, 40, 80 and 120 km, respectively.

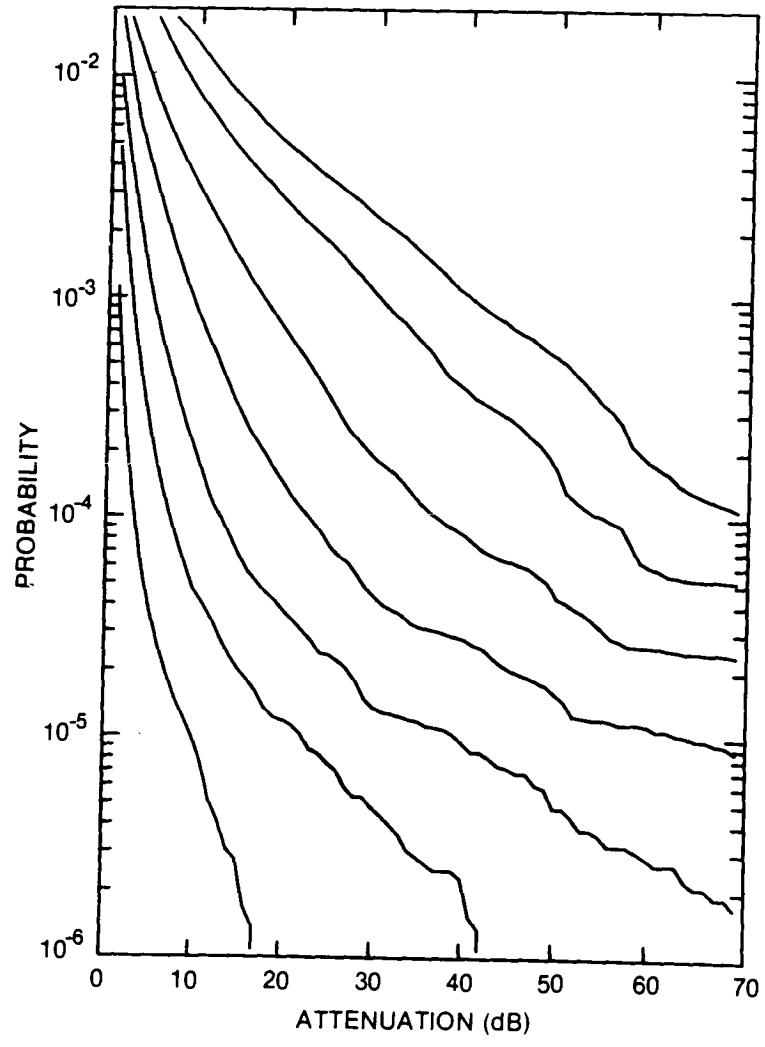

Figure 285. Cumulative distribution of rain attenuation for 15 GHz at St. John's, NFLD. Curves, moving from lowest to highest, are for hop lenghts of 2, 5, 10, 20, 40, 80 and 120 km, respectively.

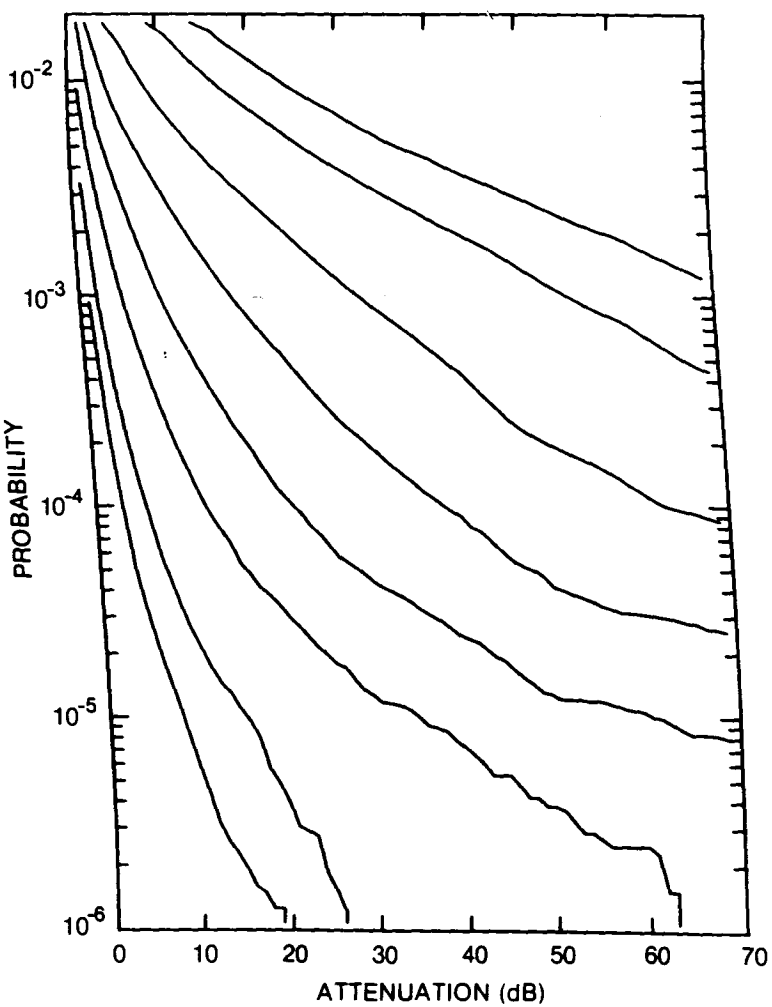

Figure 286. Cumulative distribution of rain attenuation for 20 GHz at St. John's, NFLD. Curves, moving from lowest to highest, are for hop lengths of 1, 2, 5, 10, 20, 40, 80 and 120 km, respectively.

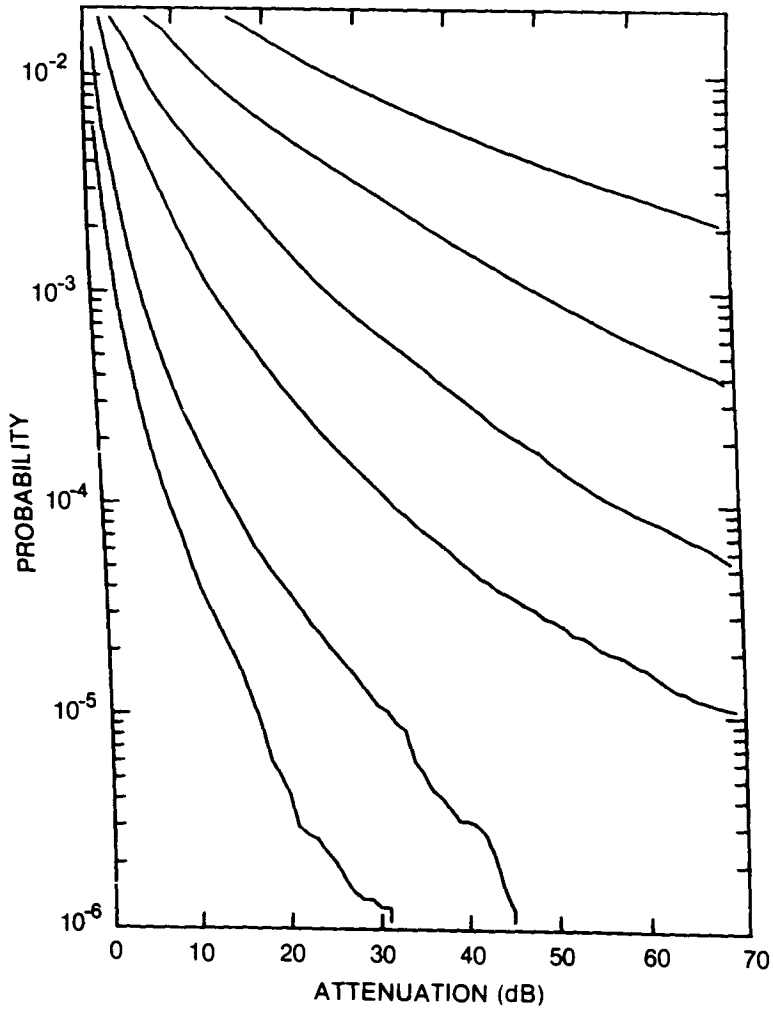

Figure 287. Cumulative distribution of rain attenuation for 35 GHz at St. John's, NFLD. Curves, moving from lowest to highest, are for hop lengths of 1, 2, 5, 10, 20 and 40 km, respectively.

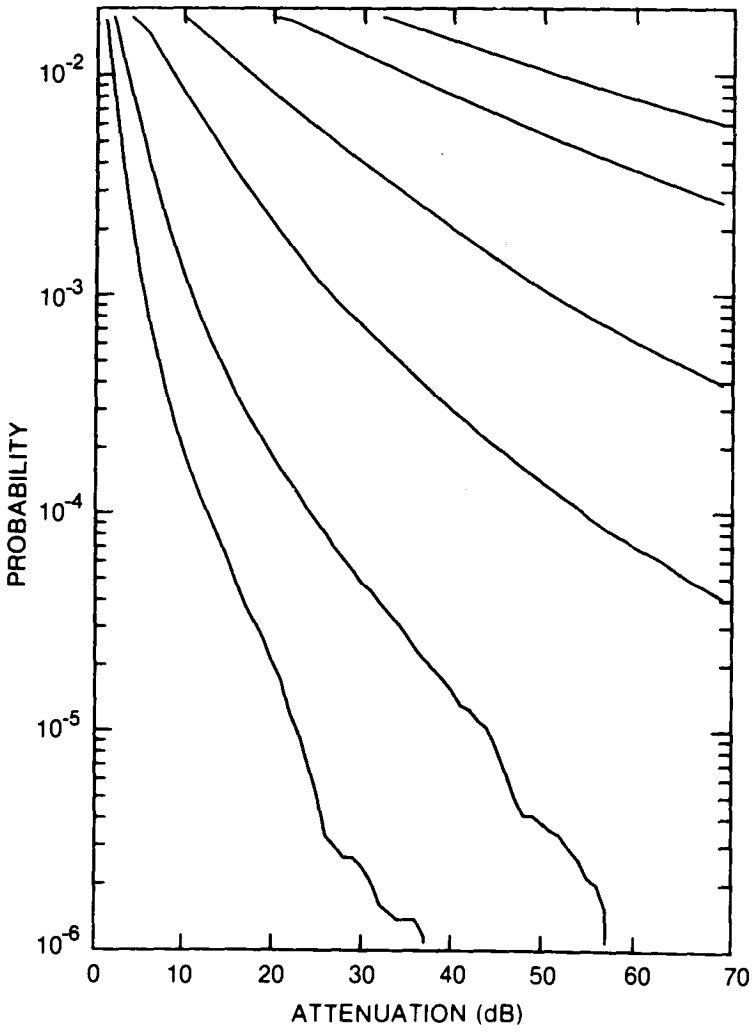

Figure 288. Cumulative distribution of rain attenuation for 56 GHz at St. John's, NFLD. Curves, moving from lowest to highest, are for hop lengths of 1, 2, 5, 10, 20 and 30 km, respectively.

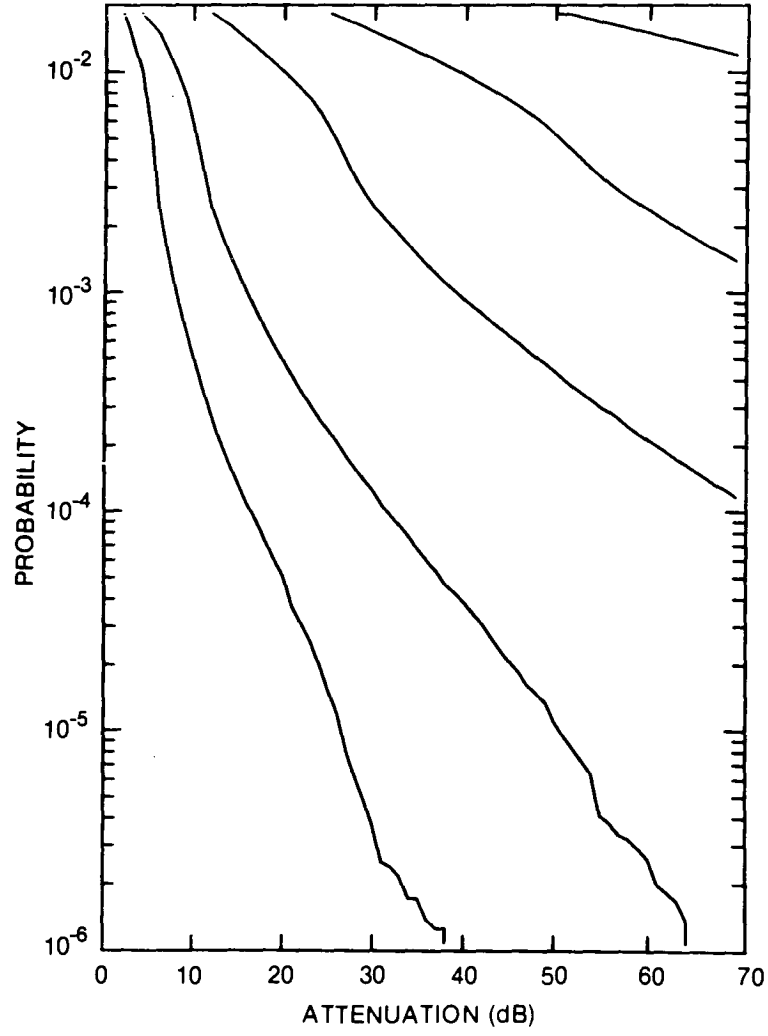

Figure 289. Cumulative distribution of rain attenuation for 100 GHz at St. John's, NFLD. Curves, moving from lowest to highest, are for hop lengths of 1, 2, 5, 10, and 20 km, respectively.

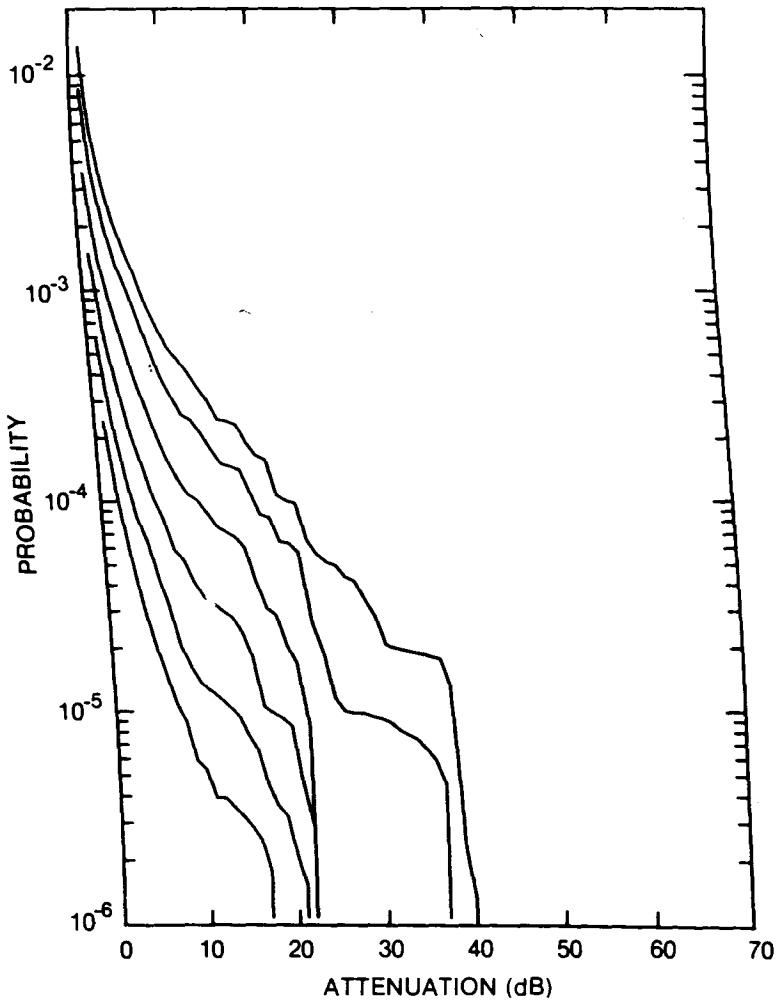

Figure 290. Cumulative distribution of rain attenuation for 8 GHz at Sault Ste. Marie, ONT. Curves, moving from lowest to highest, are for hop lengths of 5, 10, 20, 40, 80 and 120 km, respectively.

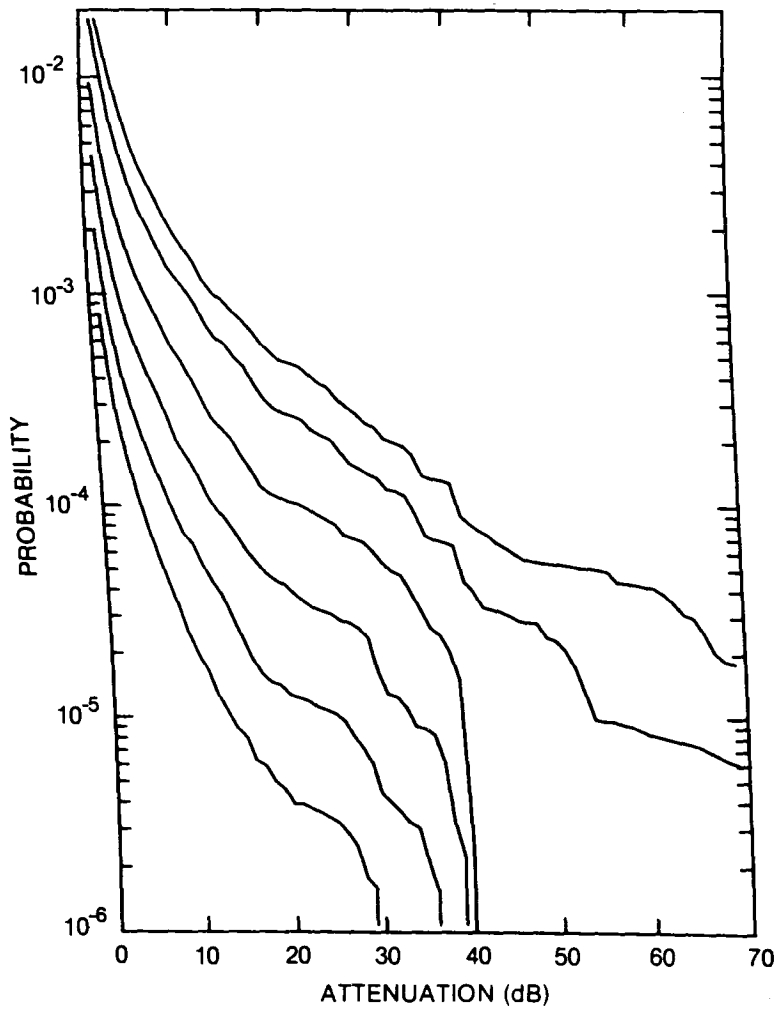

Figure 291. Cumulative distribution of rain attenuation for 11 GHz at Sault Ste. Marie, ONT. Curves, moving from lowest to highest, are for hop lengths of 5, 10, 20, 40, 80 and 120 km, respectively.

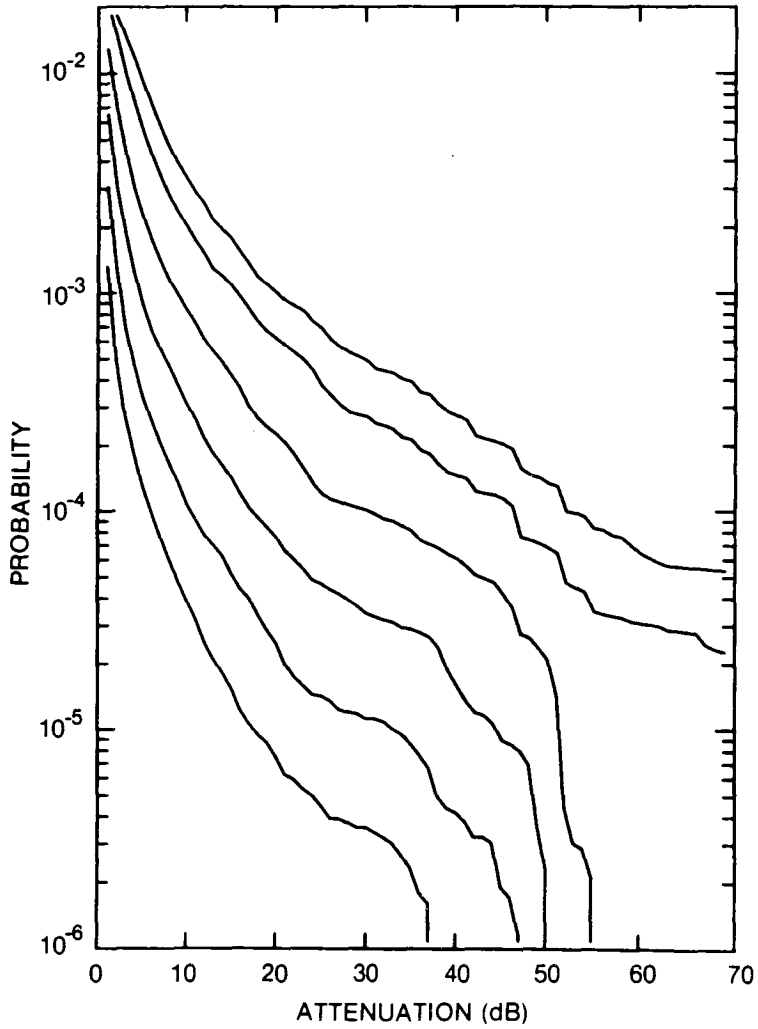

Figure 292. Cumulative distribution of rain attenuation for 12.8 GHz at Sault Ste. Marie, ONT. Curves, moving from lowest to highest, are for hop lengths of 5, 10, 20, 40, 80 and 120 km, respectively.

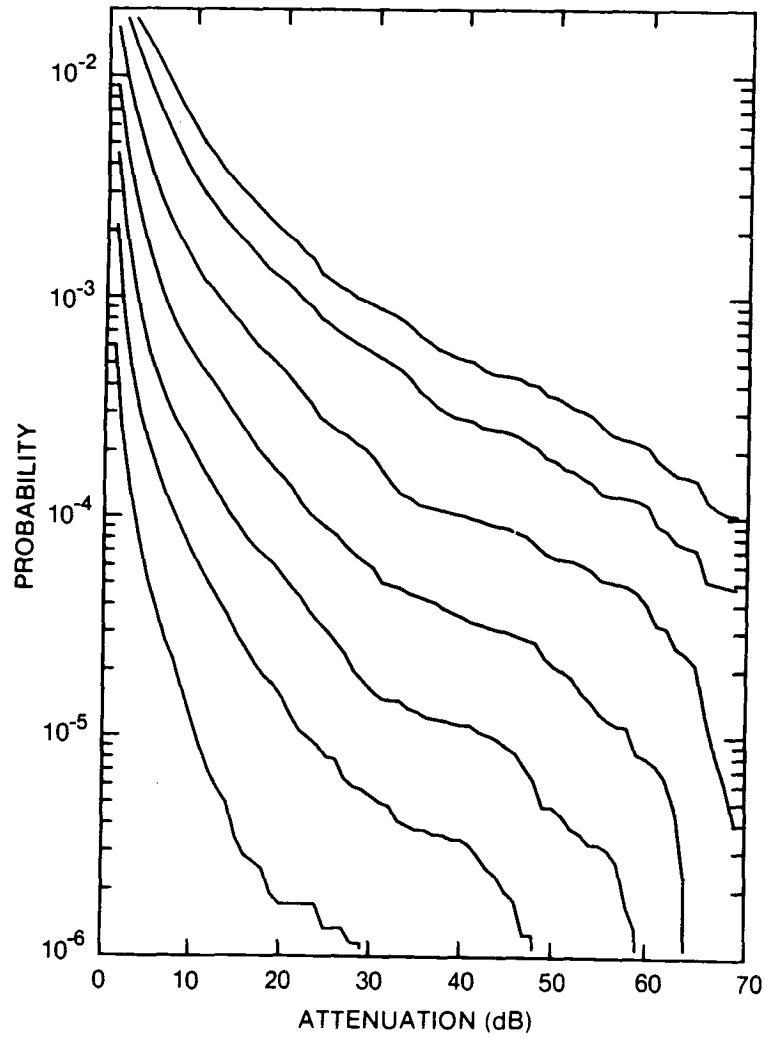

Figure 293. Cumulative distribution of rain attenuation for 15 GHz at Sault Ste. Marie, ONT. Curves, moving from lowest to highest, are for hop lengths of 2, 5, 10, 20, 40, 80 and 120 km, respectively.

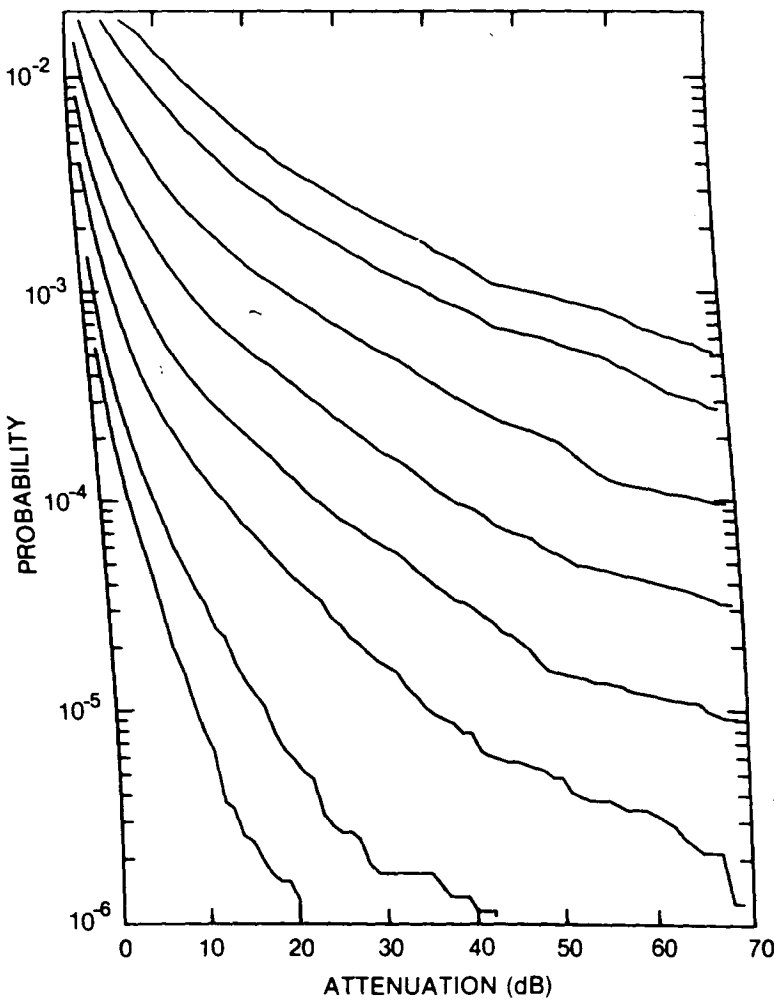

Figure 294. Cumulative distribution of rain attenuation for 20 GHz at Sault Ste. Marie, ONT. Curves, moving from lowest to highest, are for hop lengths of 1, 2, 5, 10, 20, 40, 80 and 120 km, respectively.

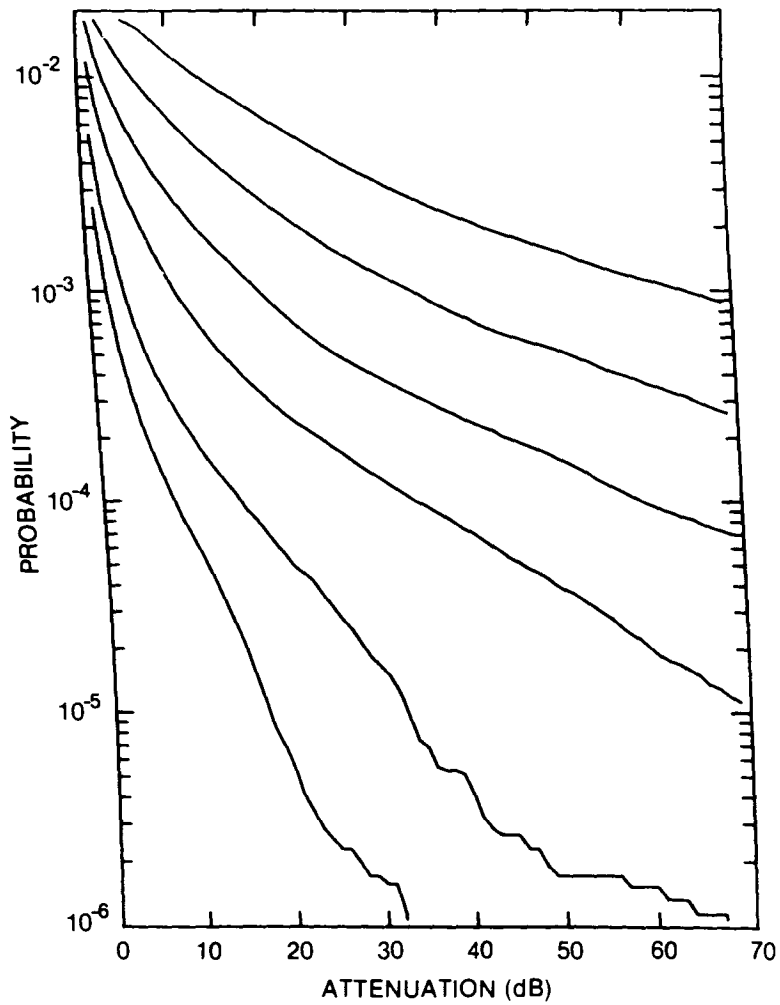

Figure 295. Cumulative distribution of rain attenuation for 35 GHz at Sault Ste. Marie, ONT. Curves, moving from lowest to highest, are for hop lengths of 1, 2, 5, 10, 20 and 40 km, respectively.

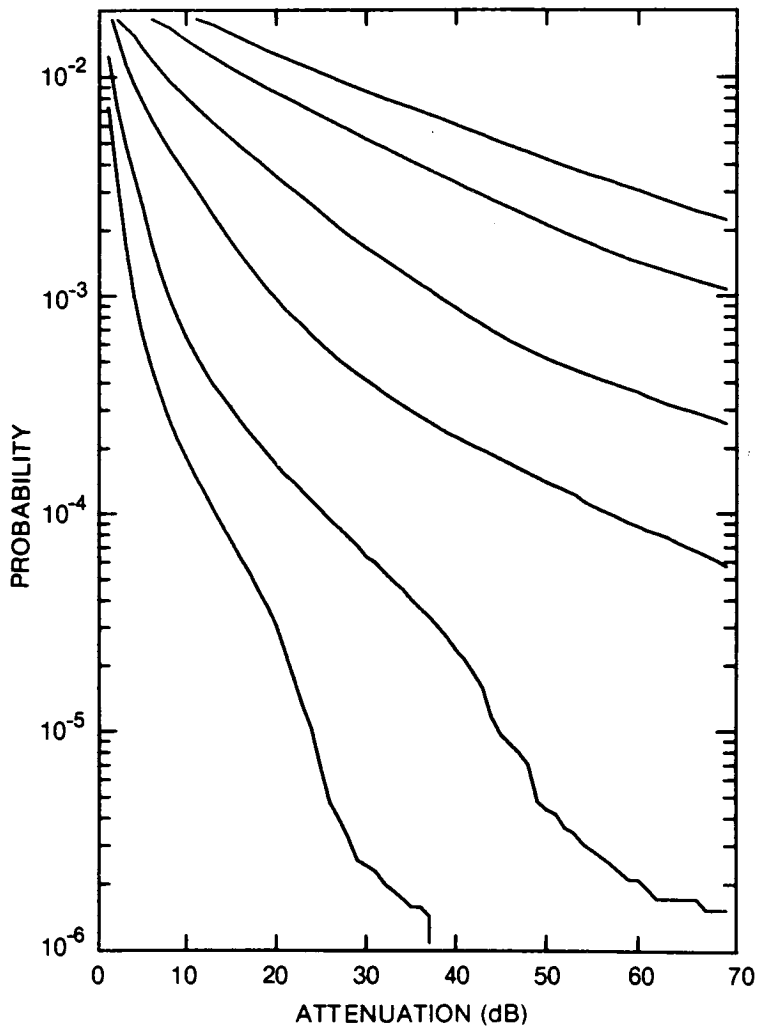

Figure 296. Cumulative distribution of rain attenuation for 56 GHz at Sault Ste. Marie, ONT. Curves, moving from lowest to highest, are for hop lengths of 1, 2, 5, 10, 20 and 30 km, respectively.

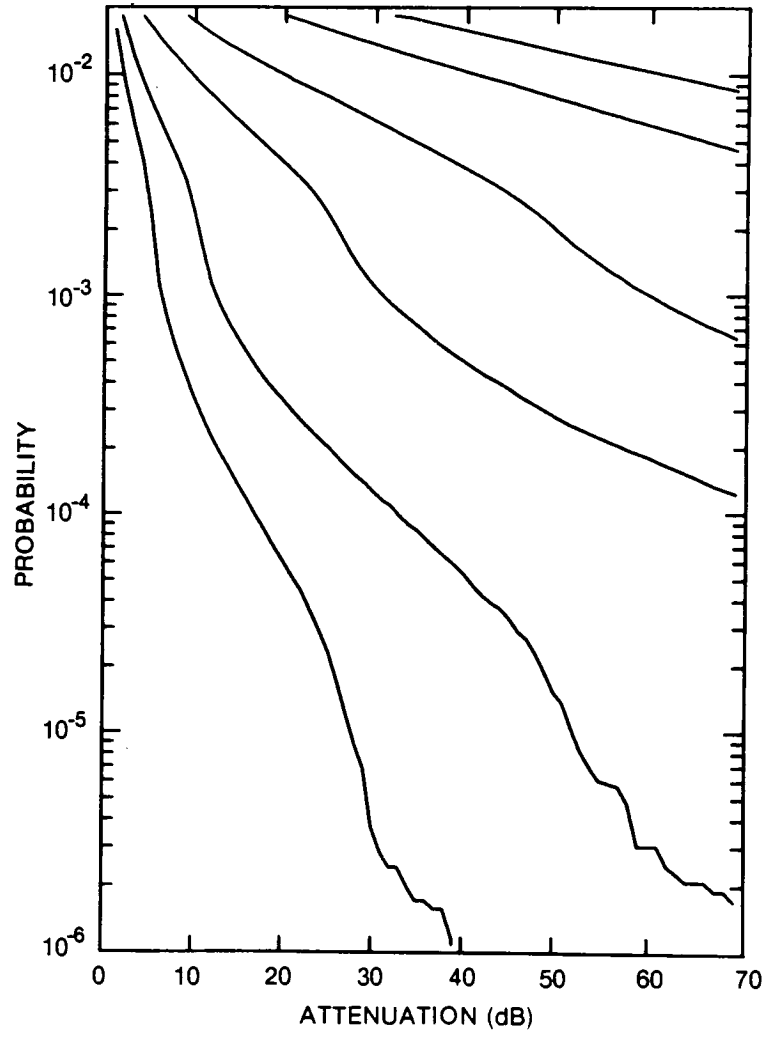

Figure 297. Cumulative distribution of rain attenuation for 100 GHz at Sault Ste. Marie, ONT. Curves, moving from lowest to highest, are for hop lengths of 1, 2, 5, 10, 20 and 30 km, respectively.

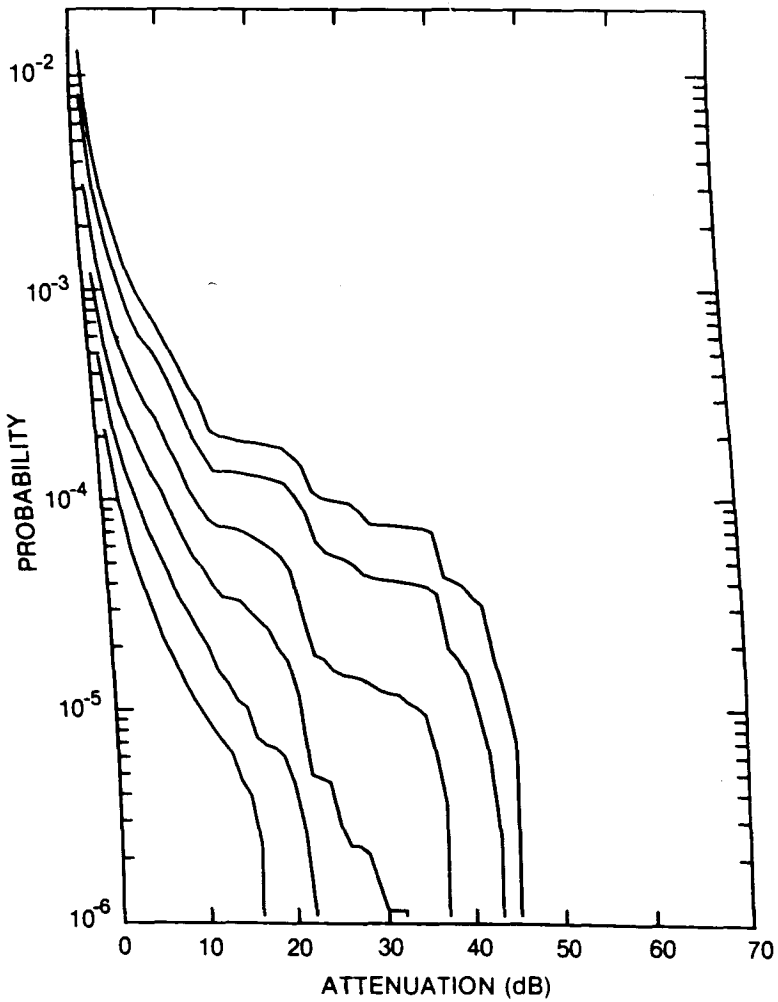

Figure 298. Cumulative distribution of rain attenuation for 8 GHz at Sioux Lookout, ONT. Curves, moving from lowest to highest, are for hop lengths of 5, 10, 20, 40, 80 and 120 km, respectively.

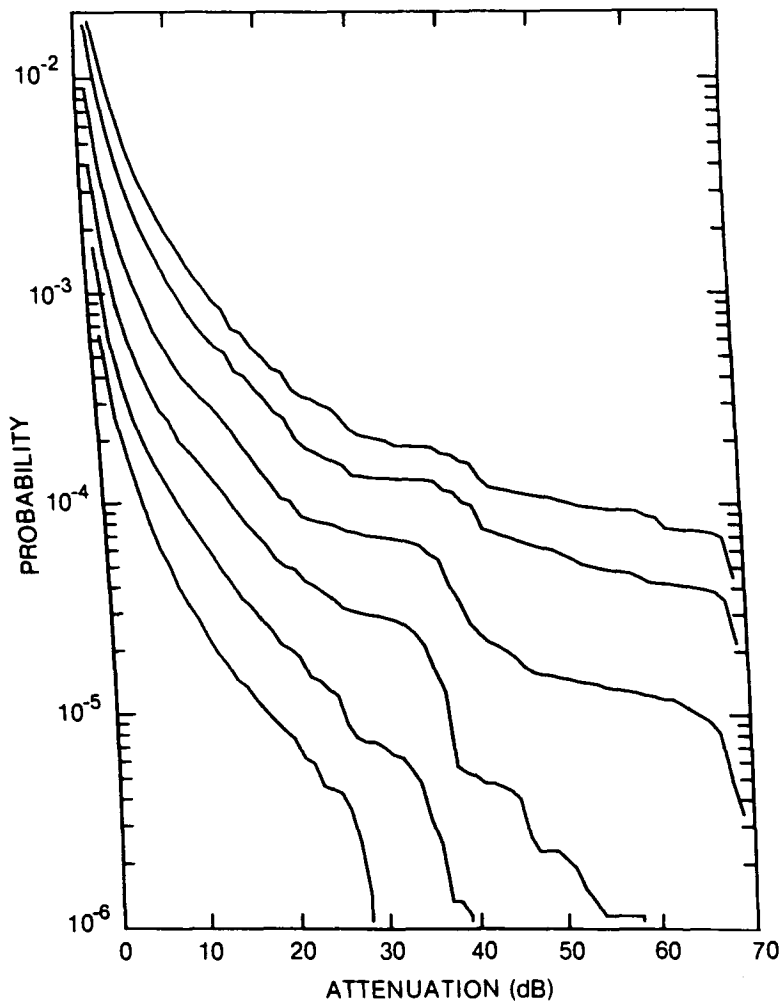

Figure 299. Cumulative distribution of rain attenuation for 11 GHz at Sioux Lookout, ONT. Curves, moving from lowest to highest, are for hop lengths of 5, 10, 20, 40, 80 and 120 km, respectively.

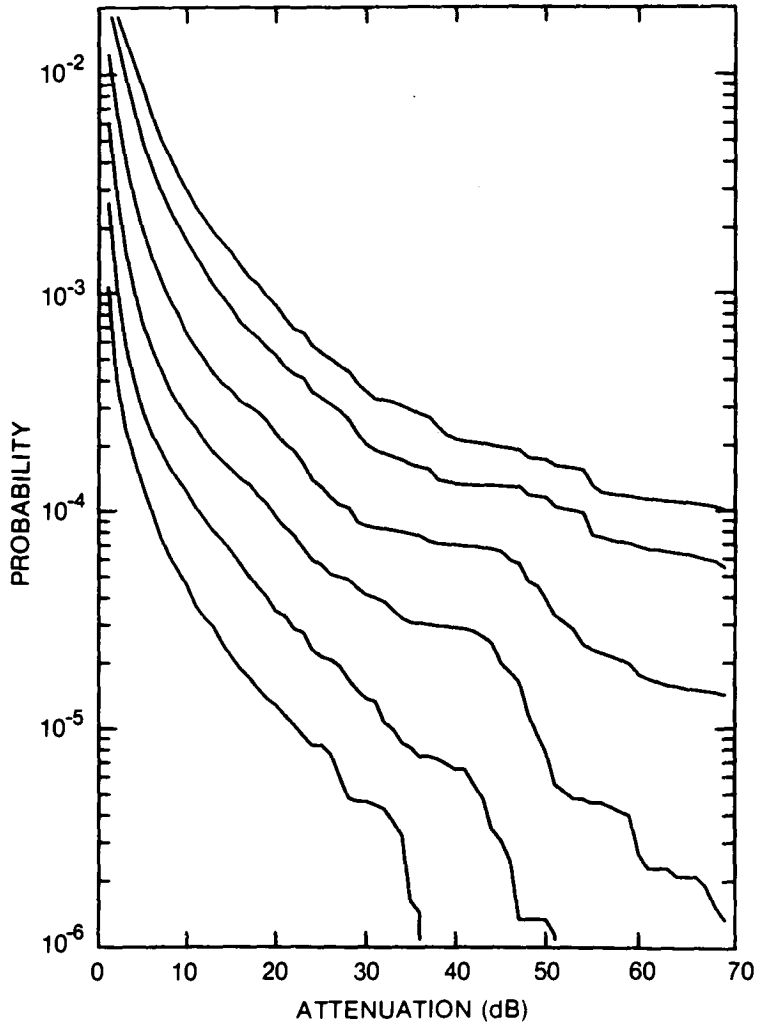

Figure 300. Cumulative distribution of rain attenuation for 12.8 GHz at Sioux Lookout, ONT. Curves, moving from lowest to highest, are for hop lengths of 5, 10, 20, 40, 80 and 120 km, respectively.

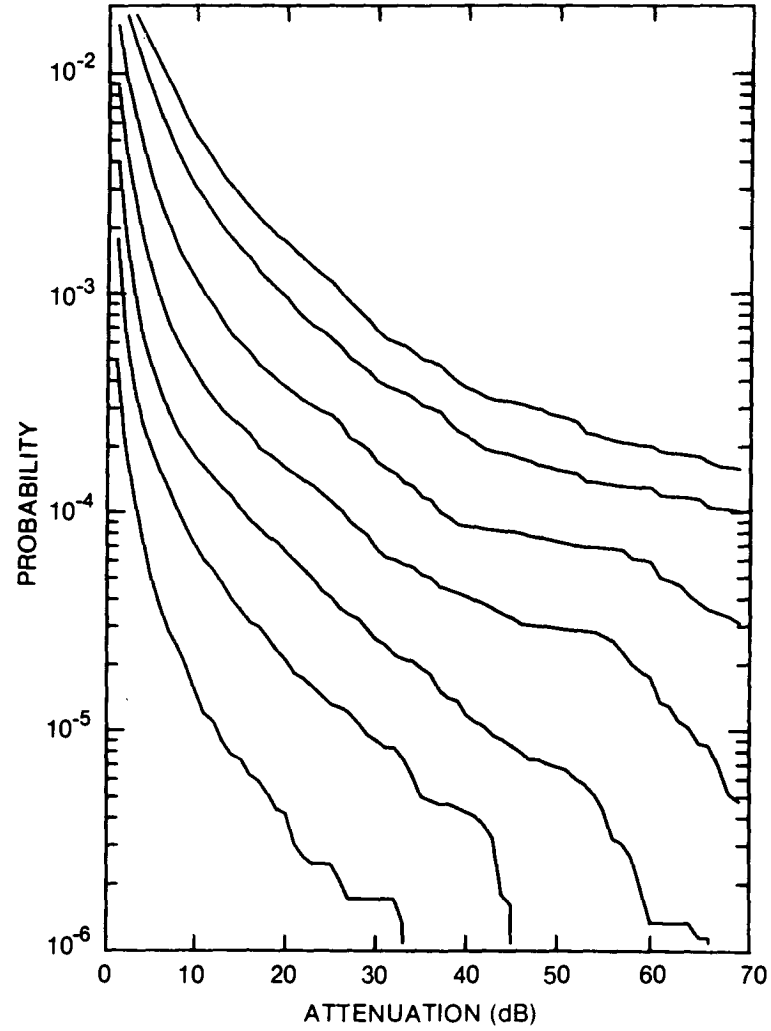

Figure 301. Cumulative distribution of rain attenuation for 15 GHz at Sioux Lookout, ONT. Curves, moving from lowest to highest, are for hop lengths of 2, 5, 10, 20, 40, 80 and 120 km, respectively.

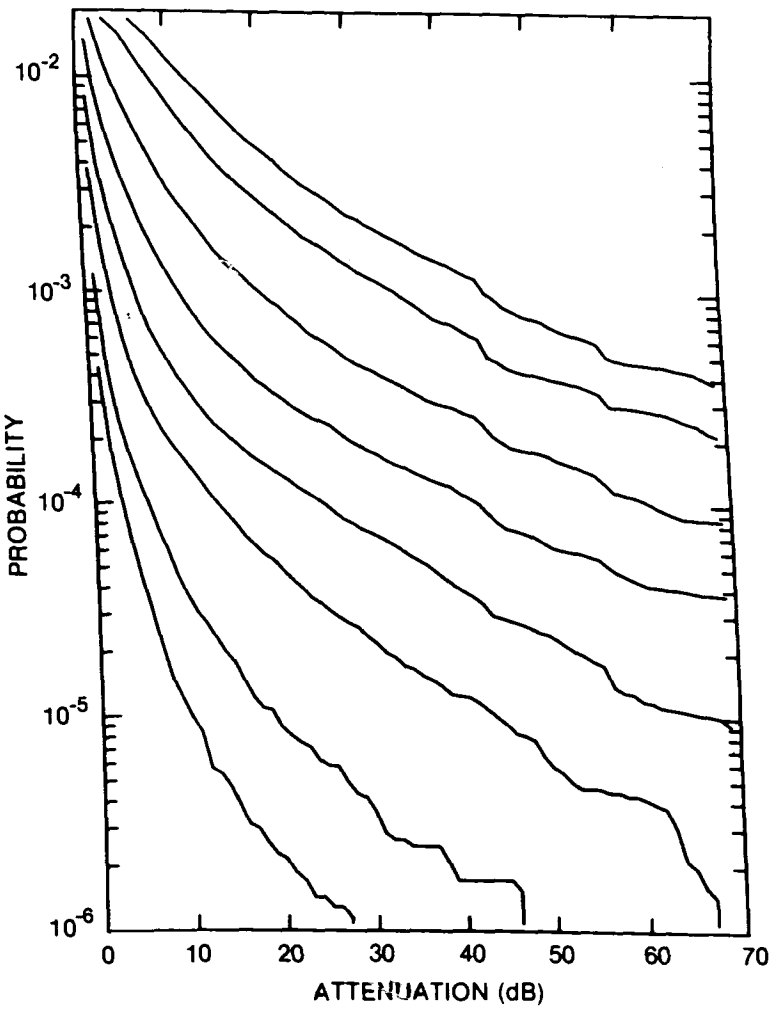

Figure 302. Cumulative distribution of rain attenuation for 20 GHz at Sioux Lookout, ONT. Curves, moving from lowest to highest, are for hop lengths of 1, 2, 5, 10, 20, 40, 80 and 120 km, respectively.

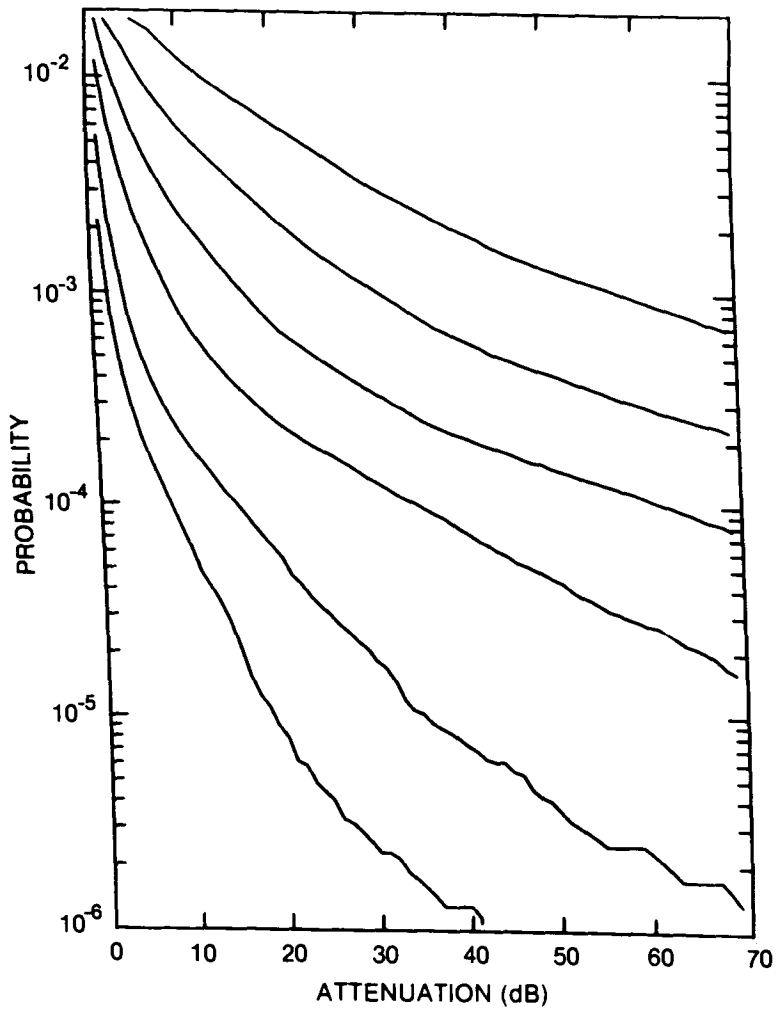

Figure 303. Cumulative distribution of rain attenuation for 35 GHz at Sioux Lookout, ONT. Curves, moving from lowest to highest, are for hop lengths of 1, 2, 5, 10, 20 and 40 km, respectively.

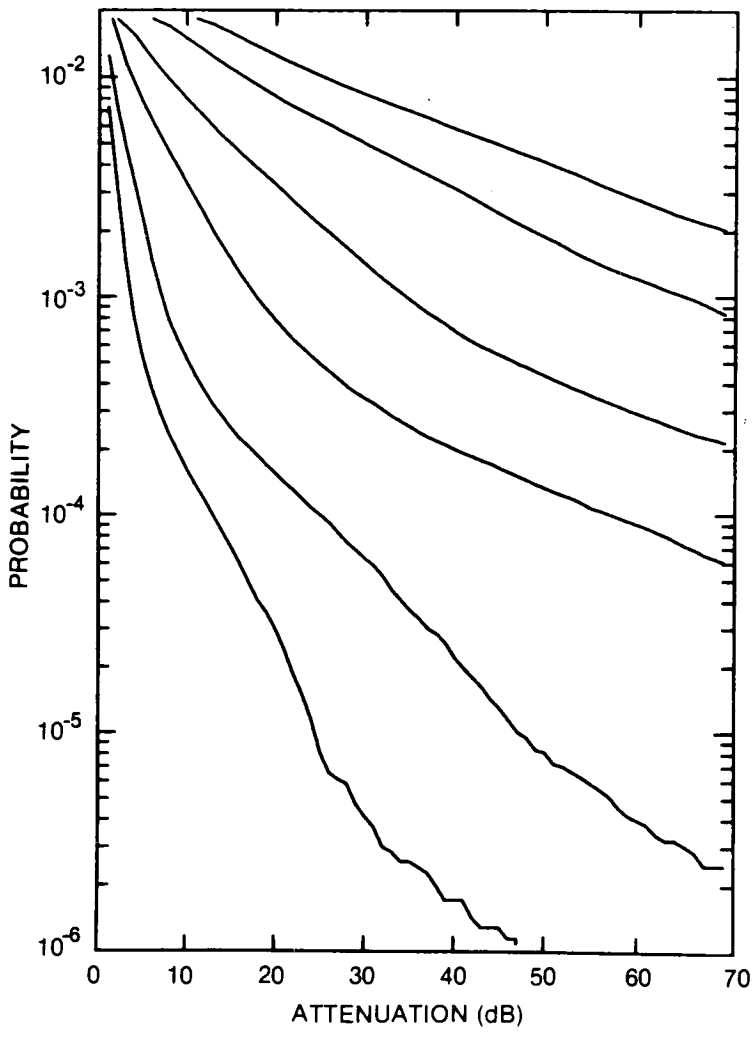

Figure 304. Cumulative distribution of rain attenuation for 56 GHz at Sioux Lookout, ONT. Curves, moving from lowest to highest, are for hop lengths of 1. 2, 5, 10, 20 and 30 km, respectively.

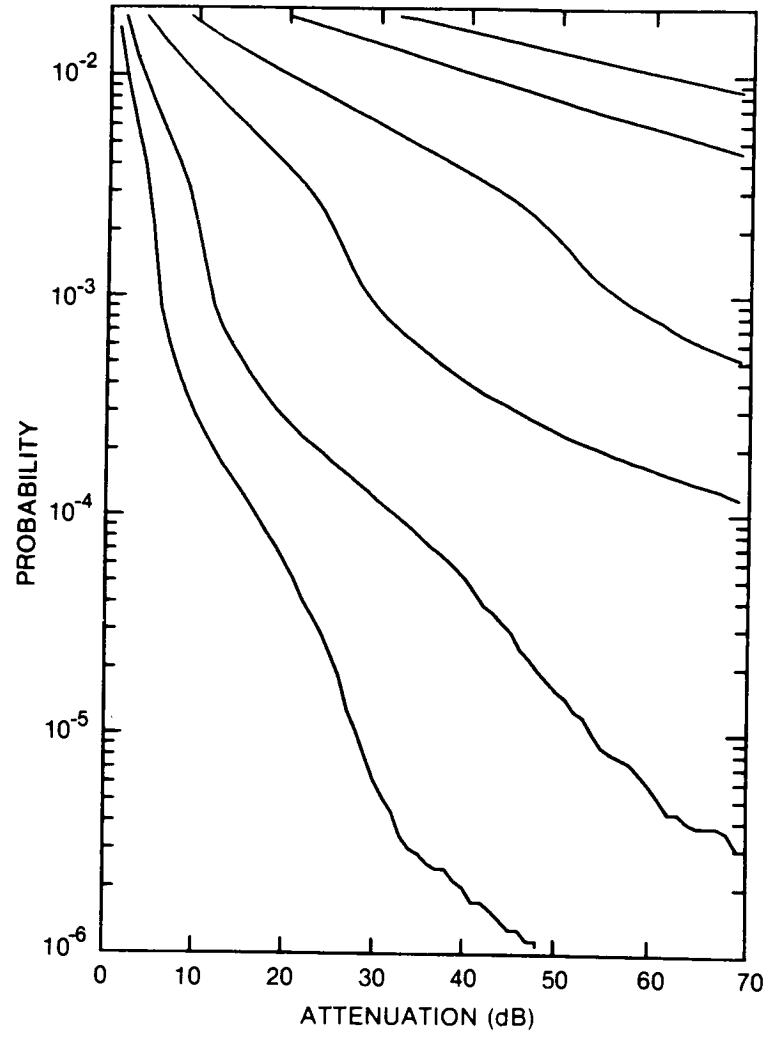

Figure 305. Cumulative distribution of rain attenuation for 100 GHz at Sioux Lookout, ONT. Curves, moving from lowest to highest, are for hop lengths of 1, 2, 5, 10, 20 and 30 km, respectively.

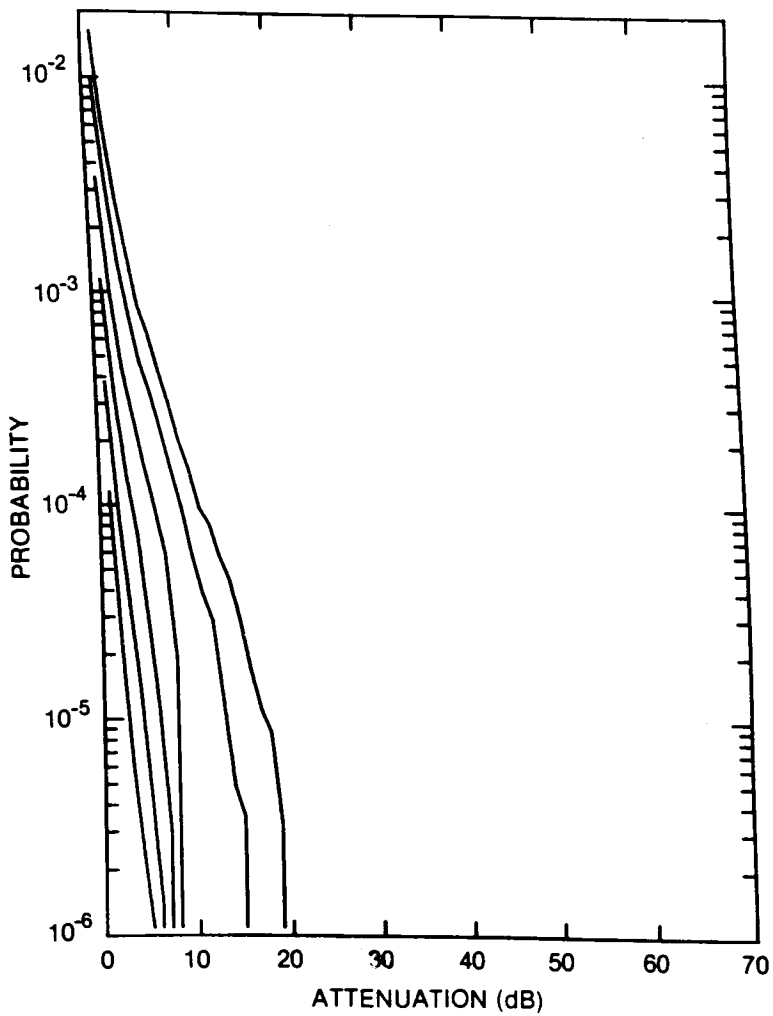

Figure 306. Cumulative distribution of rain attenuation for 8 GHz at Stephenville, NFLD. Curves, moving from lowest to highest, are for hop lengths of 5, 10, 20, 40, 80 and 120 km, respectively.

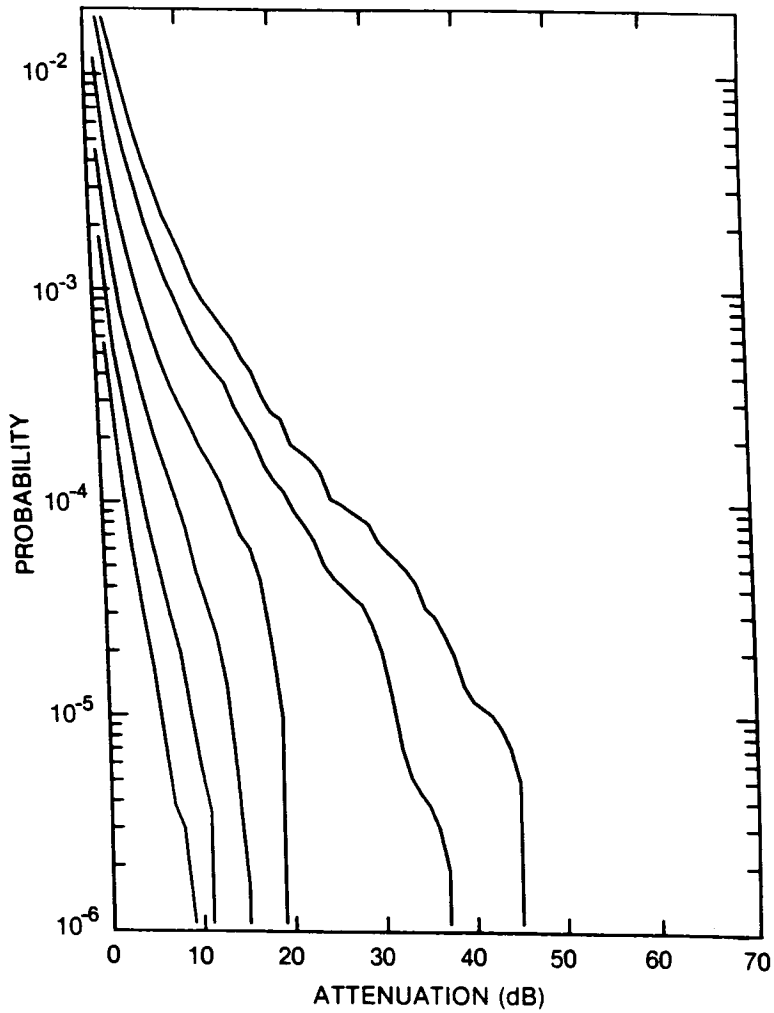

Figure 307. Cumulative distribution of rain attenuation for 11 GHz at Stephenville, NFLD. Curves, moving from lowest to highest, are for hop lengths of 5, 10, 20, 40, 80 and 120 km, respectively.

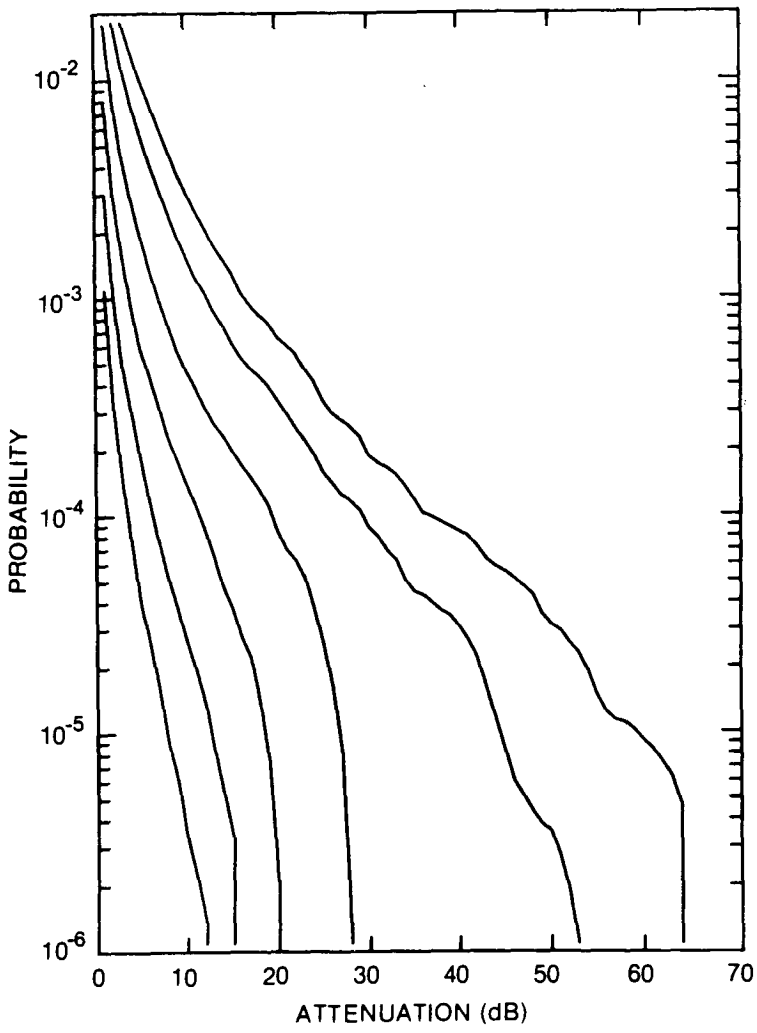

Figure 308. Cumulative distribution of rain attenuation for 12.8 GHz at Stephenville, NFLD. Curves, moving from lowest to highest, are for hop lengths of 5, 10, 20, 40, 80 and 120 km, respectively.

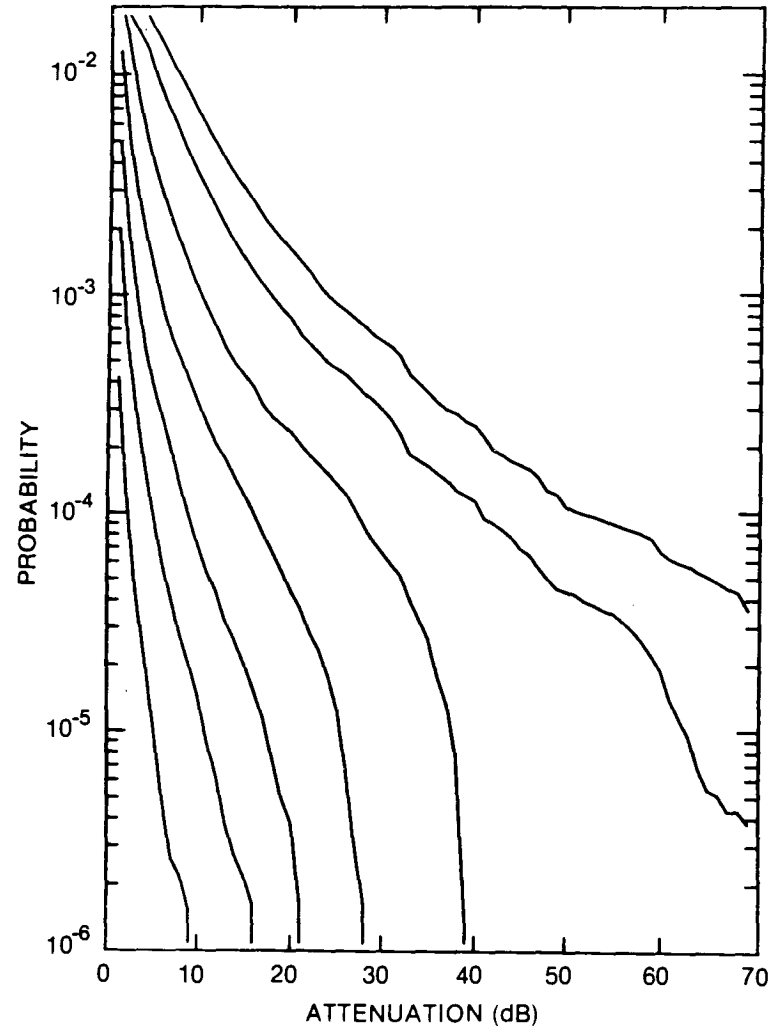

Figure 309. Cumulative distribution of rain attenuation for 15 GHz at Stephenville, NFLD. Curves, moving from lowest to highest, are for hop lengths of 2, 5, 10, 20, 40, 80 and 120 km, respectively.

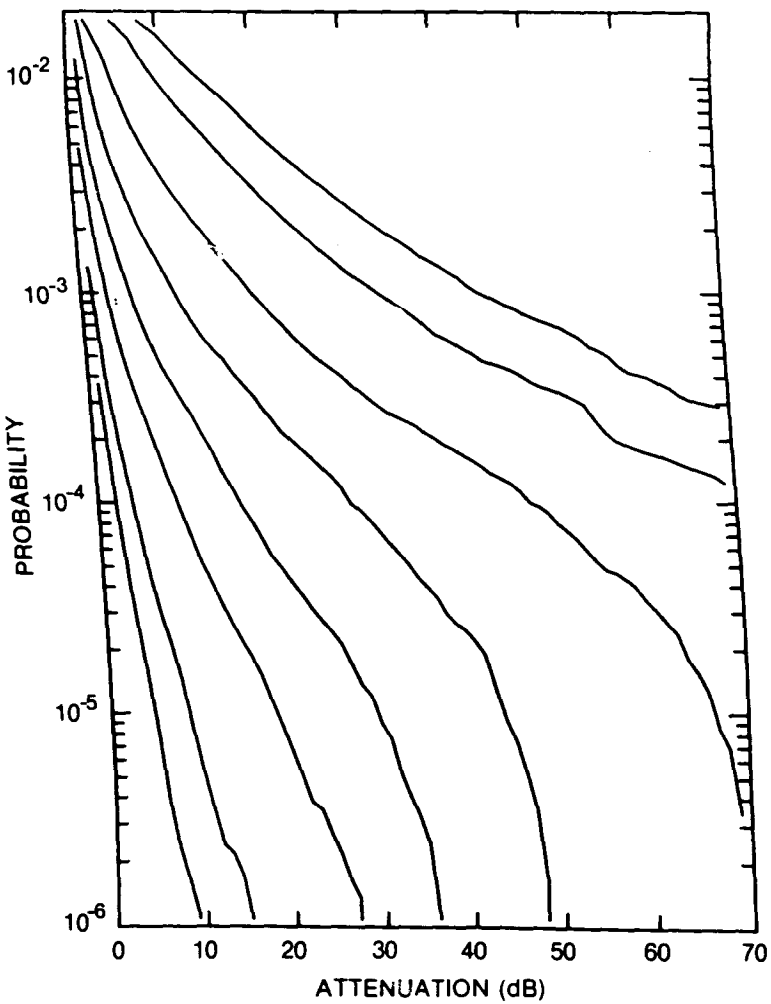

Figure 310. Cumulative distribution of rain attenuation for 20 GHz at Stephenville, NFLD. Curves, moving from lowest to highest, are for hop lengths of 1, 2, 5, 10, 20, 40, 80 and 120 km, respectively.

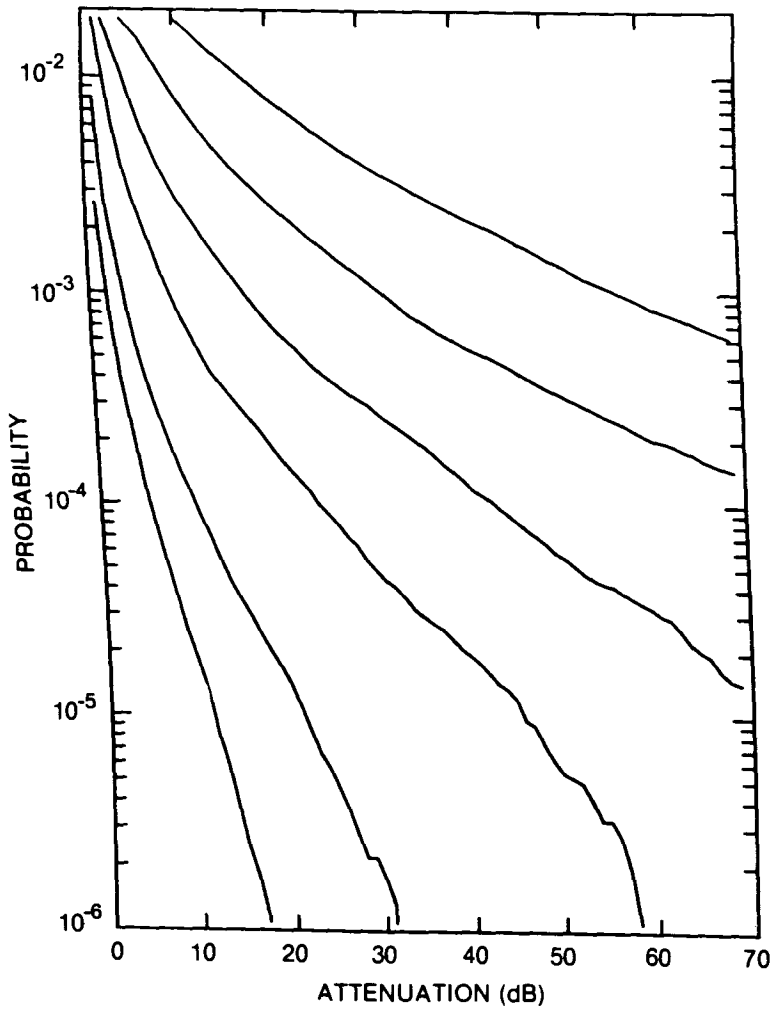

Figure 311. Cumulative distribution of rain attenuation for 35 GHz at Stephenville, NFLD. Curves, moving from lowest to highest, are for hop lengths of 1, 2, 5, 10, 20 and 40 km, respectively.

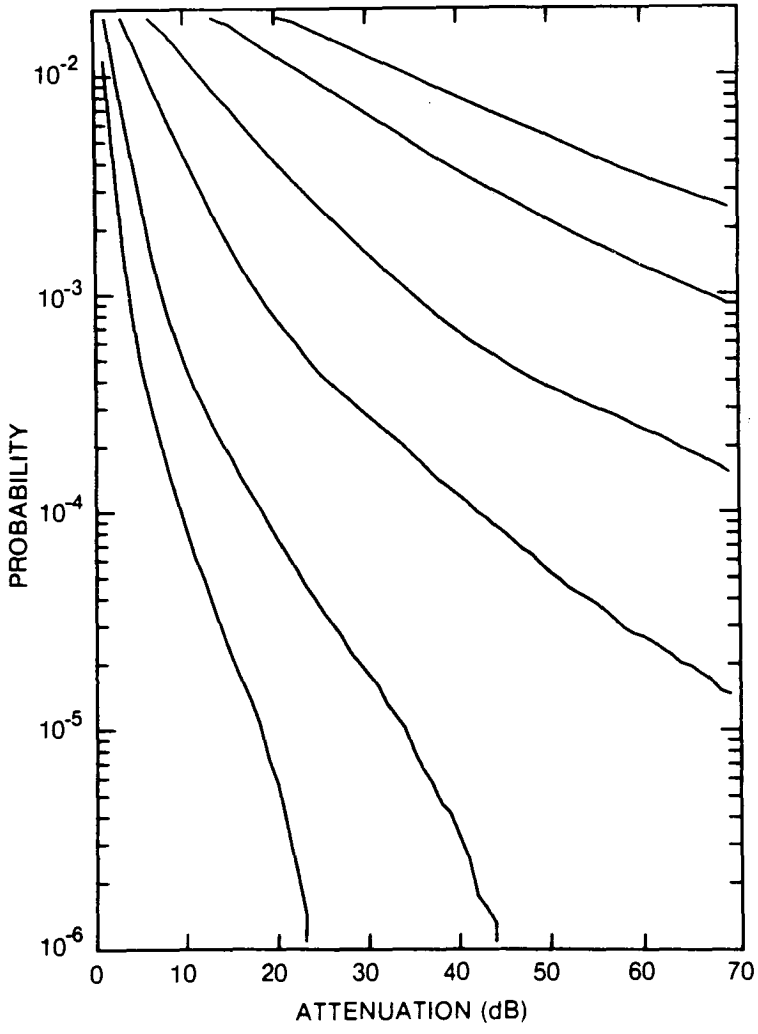

Figure 312. Cumulative distribution of rain attenuation for 56 GHz at Stephenville, NFLD. Curves, moving from lowest to highest, are for hop lengths of 1, 2, 5, 10, 20 and 30 km, respectively.

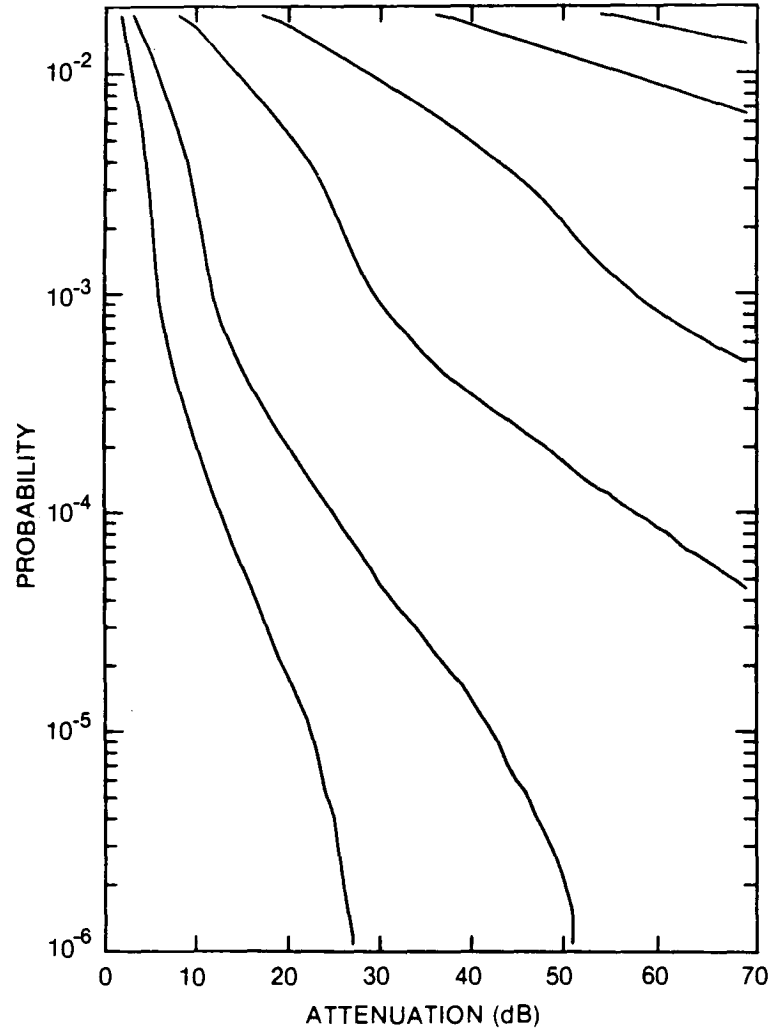

Figure 313. Cumulative distribution of rain attenuation for 100 GHz at Stephenville, NFLD. Curves, moving from lowest to highest, are for hop lengths of 1, 2, 5, 10, 20 and 30 km, respectively.

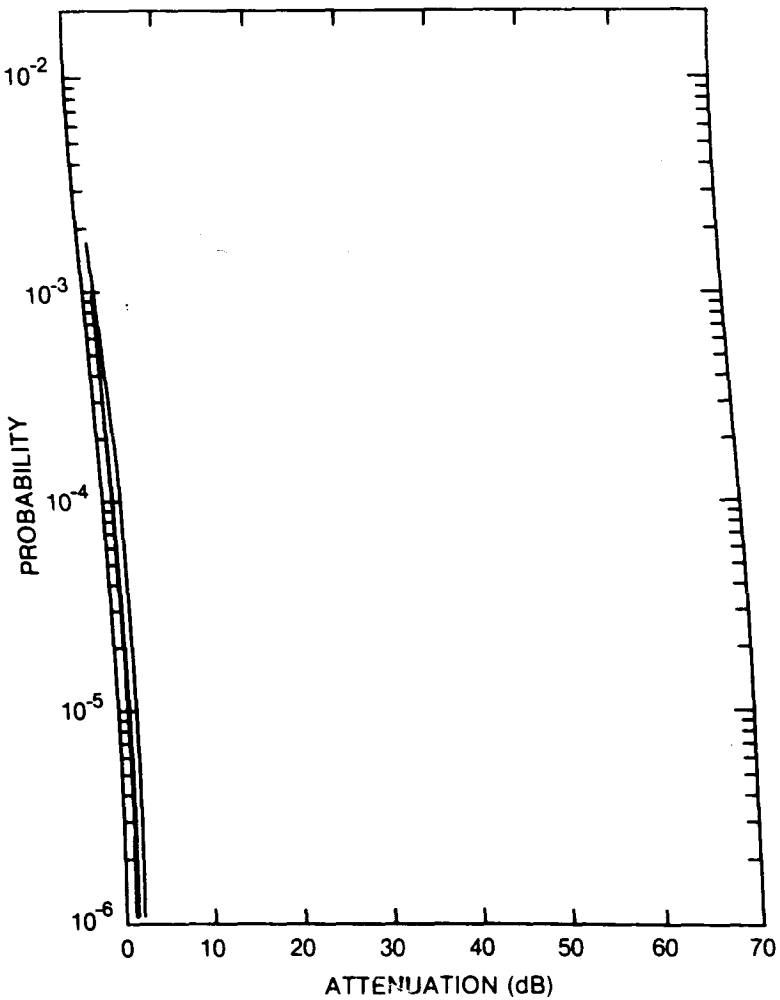

Figure 314. Cumulative distribution of rain attenuation for 8 GHz at Summerland, BC. The distribution for a 120 km hop length is barely distinguishable from the merged curves for lengths of 5 to 80 km.

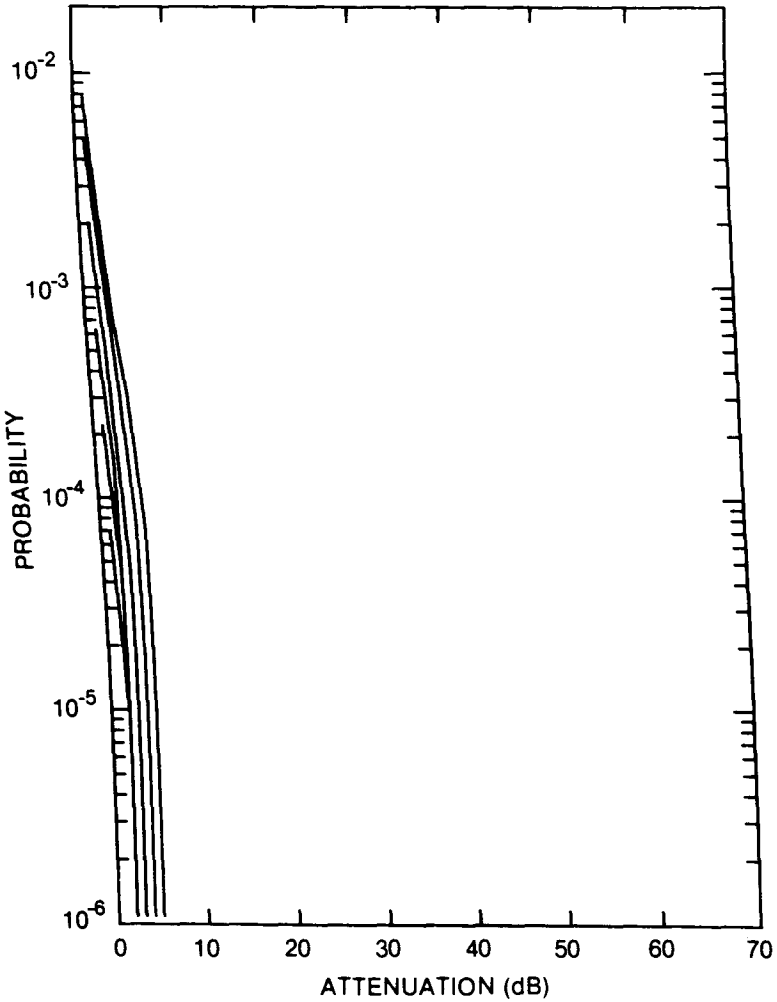

Figure 315. Cumulative distribution of rain attenuation for 11 GHz at Summerland, BC. Curves, moving from lowest to highest, are for hop lengths of 5, 10, 20, 40, 80 and 120 km, respectively.

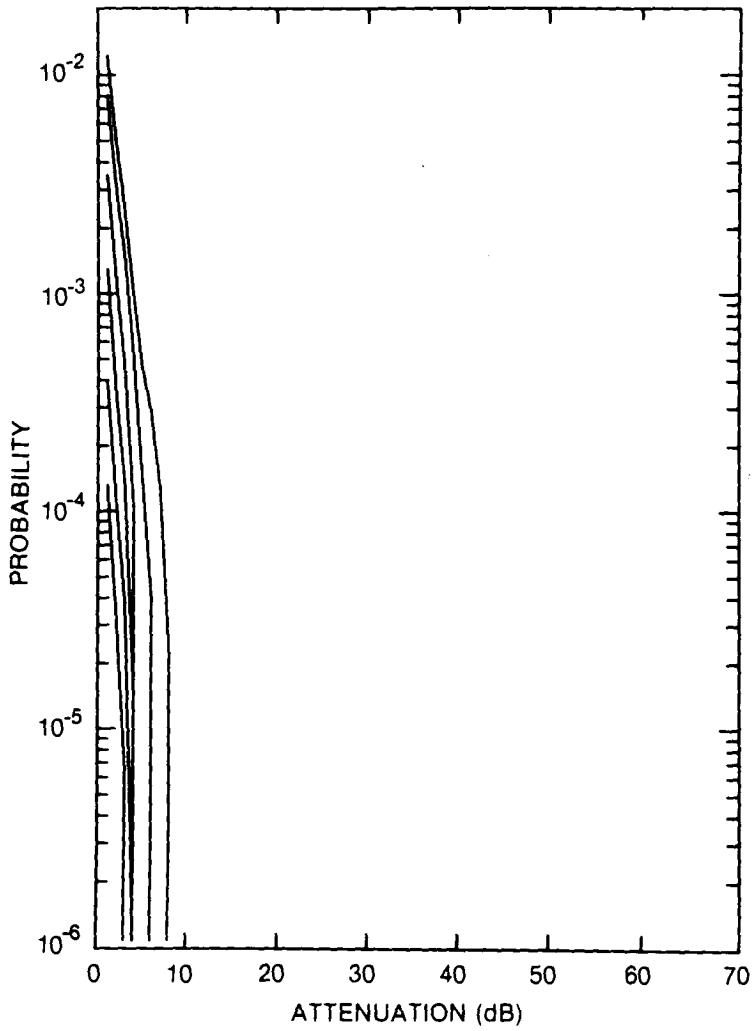

Figure 316. Cumulative distribution of rain attenuation for 12.8 GHz at Summerland, BC. Curves, moving from lowest to highest, are for hop lengths of 5, 10, 20, 40, 80 and 120 km, respectively.

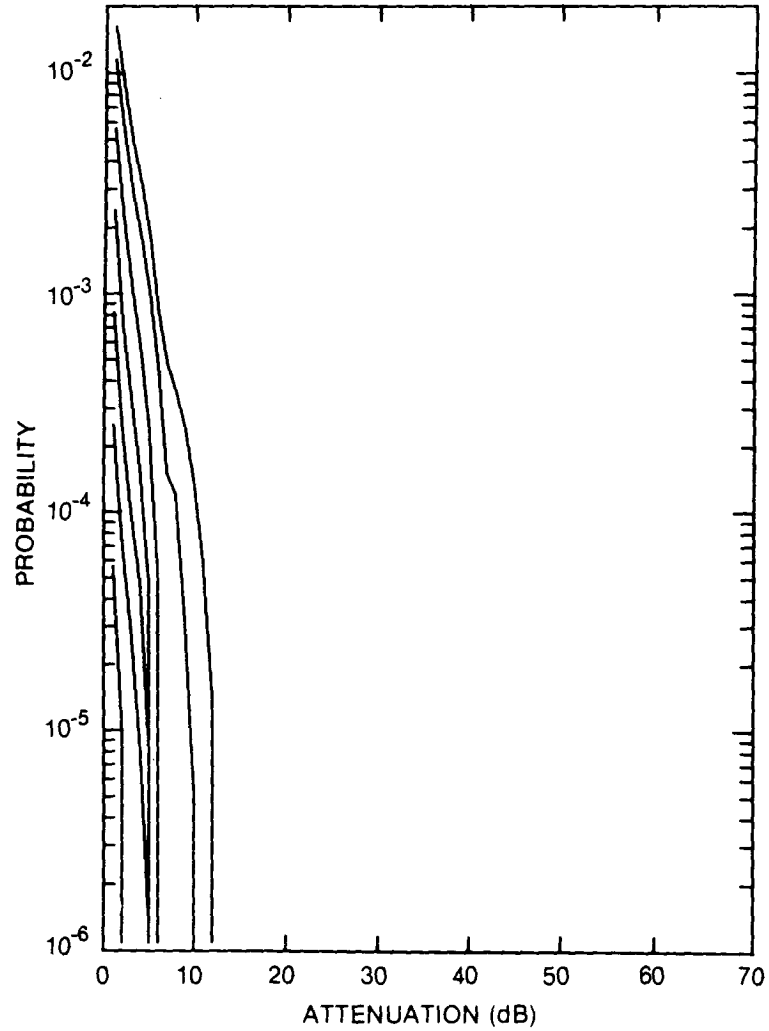

Figure 317. Cumulative distribution of rain attenuation for 15 GHz at Summerland, BC. Curves, moving from lowest to highest, are for hop lengths of 2, 5, 10, 20, 40, 80 and 120 km, respectively.

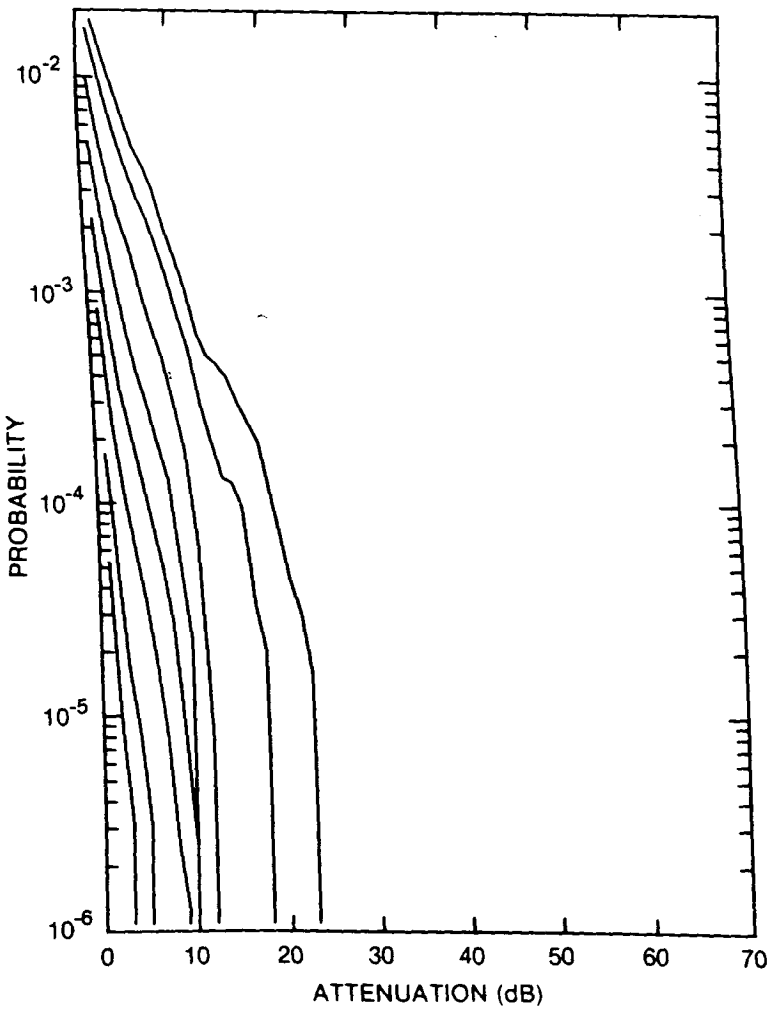

Figure 318. Cumulative distribution of rain attenuation for 20 GHz at Summerland, BC. Curves, moving from lowest to highest, are for hop lengths of 1, 2, 5, 10, 20, 40, 80 and 120 km, respectively.

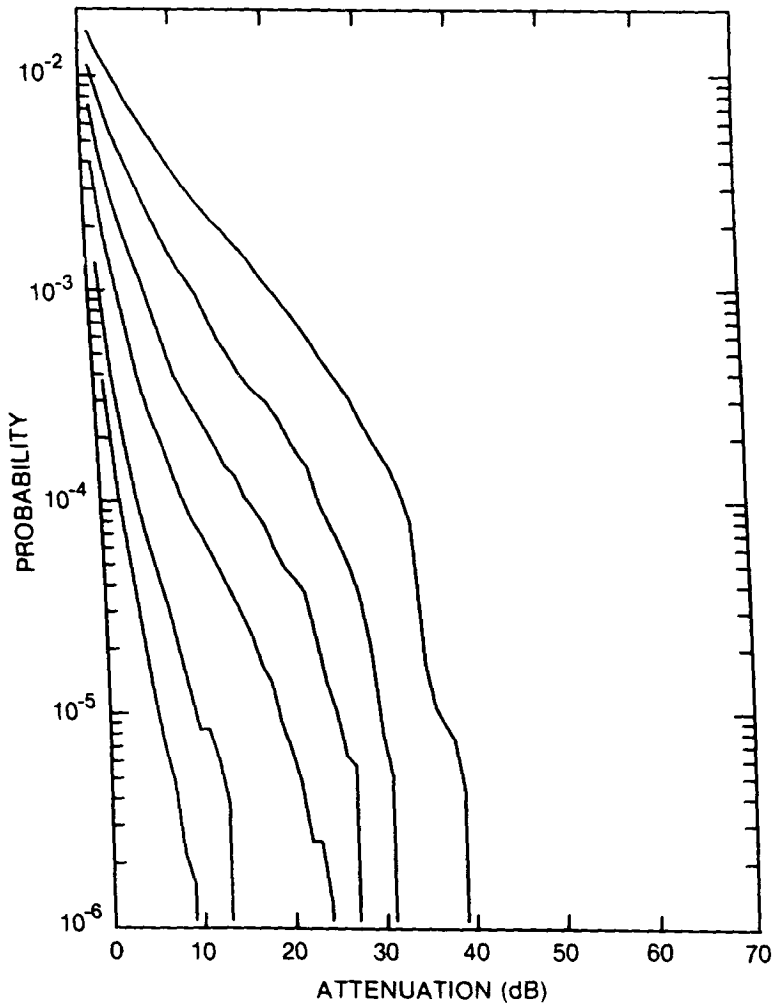

Figure 319. Cumulative distribution of rain attenuation for 35 GHz at Summerland, BC. Curves, moving from lowest to highest, are for hop lengths of 1, 2, 5, 10, 20 and 40 km, respectively.

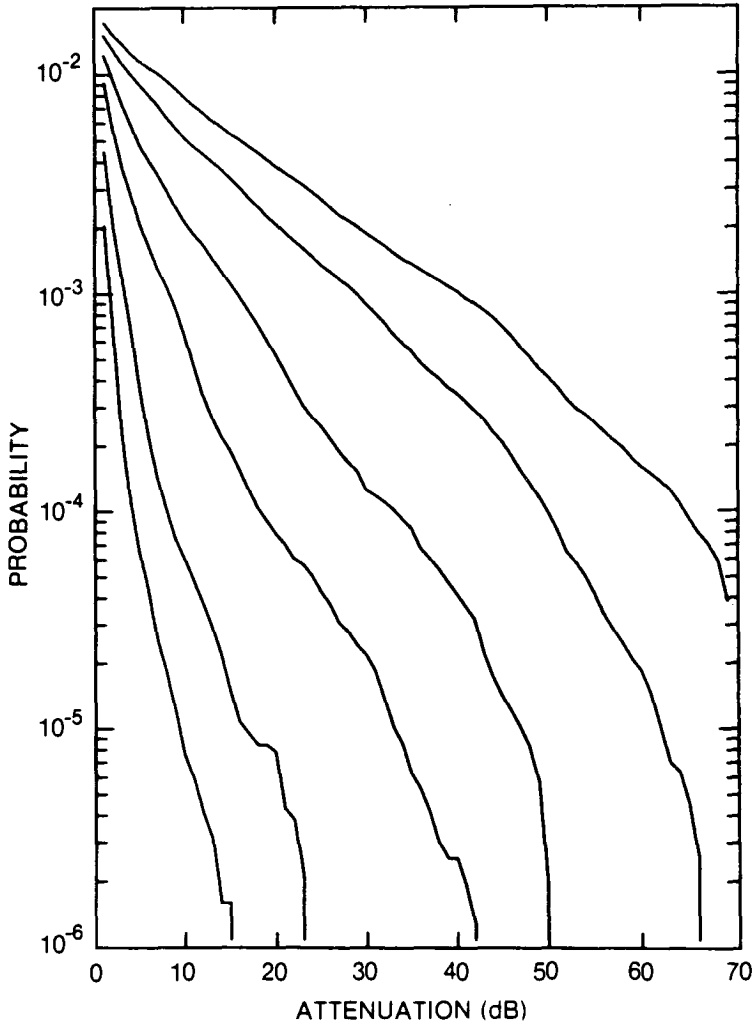

Figure 320. Cumulative distribution of rain attenuation for 56 GHz at Summerland, BC. Curves, moving from lowest to highest, are for hop lengths of 1, 2, 5, 10, 20 and 30 km, respectively.

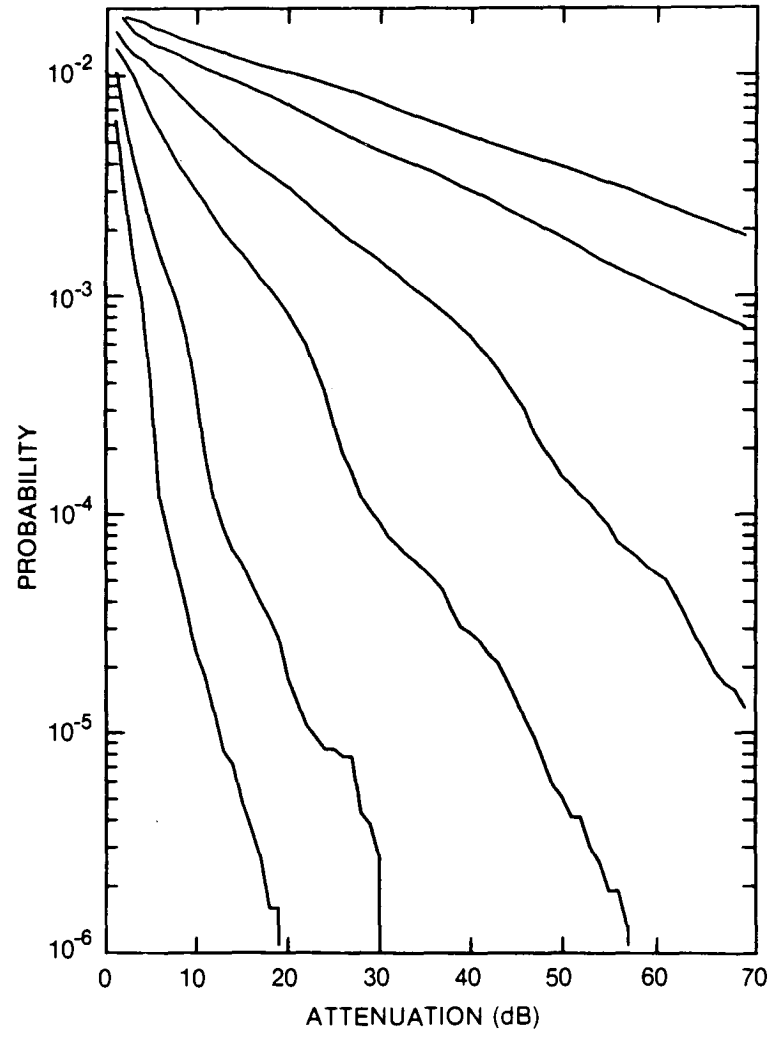

Figure 321. Cumulative distribution of rain attenuation for 100 GHz at Summerland, BC. Curves, moving from lowest to highest, are for hop lengths of 1, 2, 5, 10, 20 and 30 km, respectively.

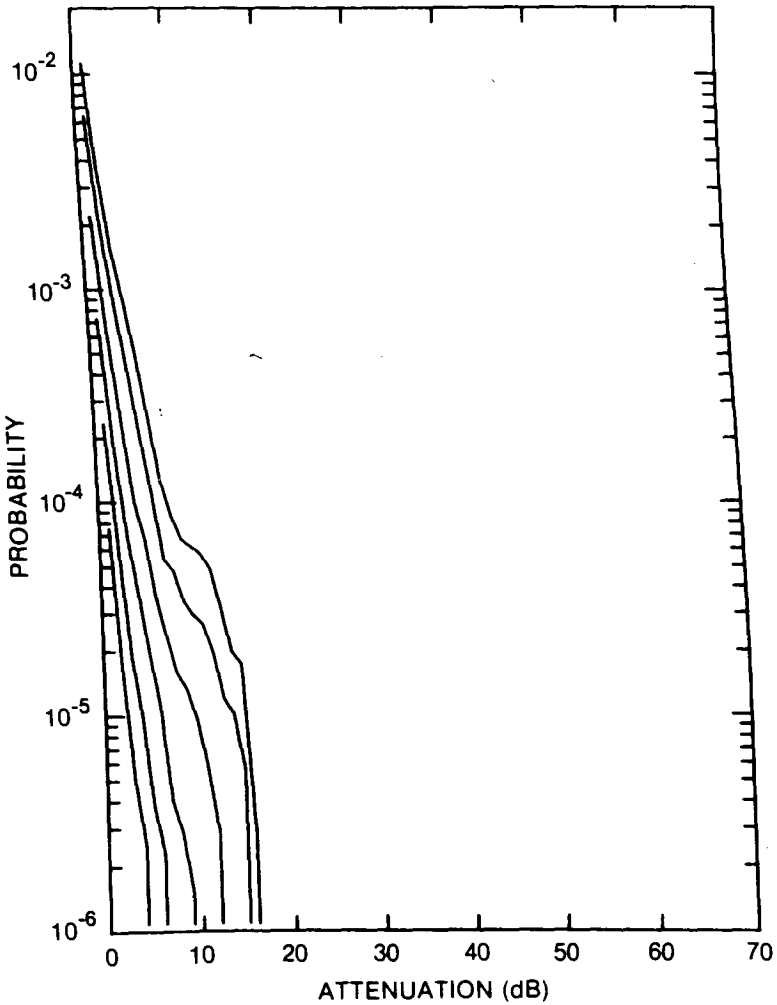

Figure 322. Cumulative distribution of rain attenuation for 8 GHz at Summerside, PEI. Curves, moving from lowest to highest, are for hop lengths of 5, 10, 20, 40, and 80 120 km, respectively.

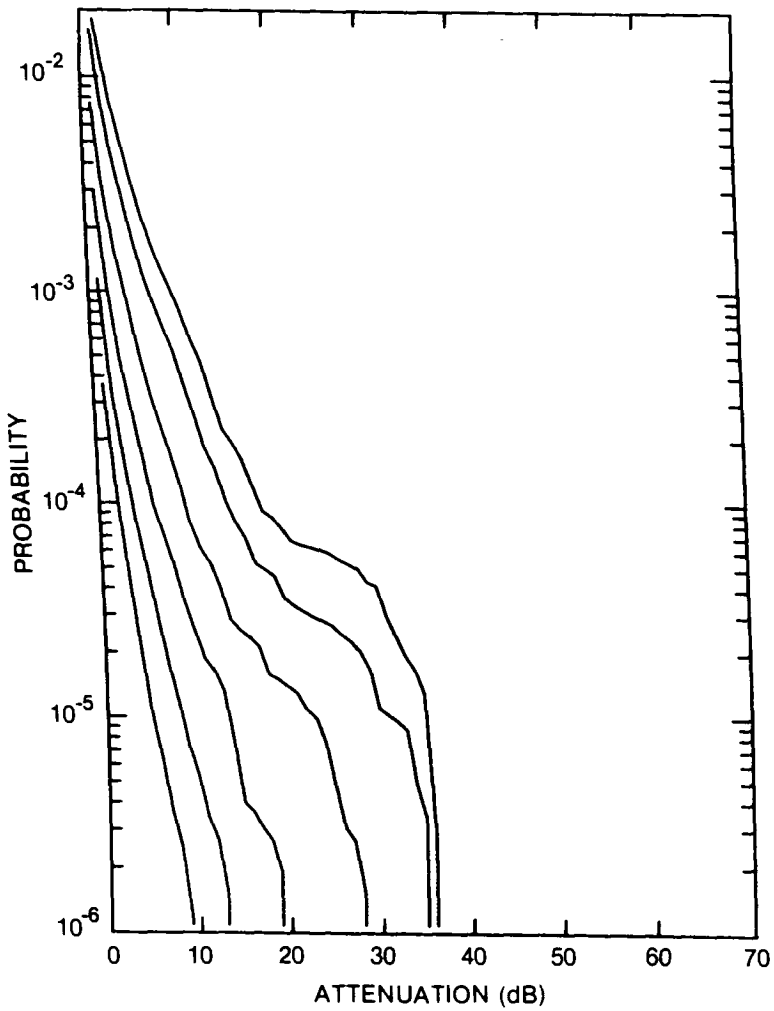

Figure 323. Cumulative distribution of rain attenuation for 11 GHz at Summerside, PEI. Curves, moving from lowest to highest, are for hop lengths of 5, 10, 20, 40, 80 and 120 km, respectively.

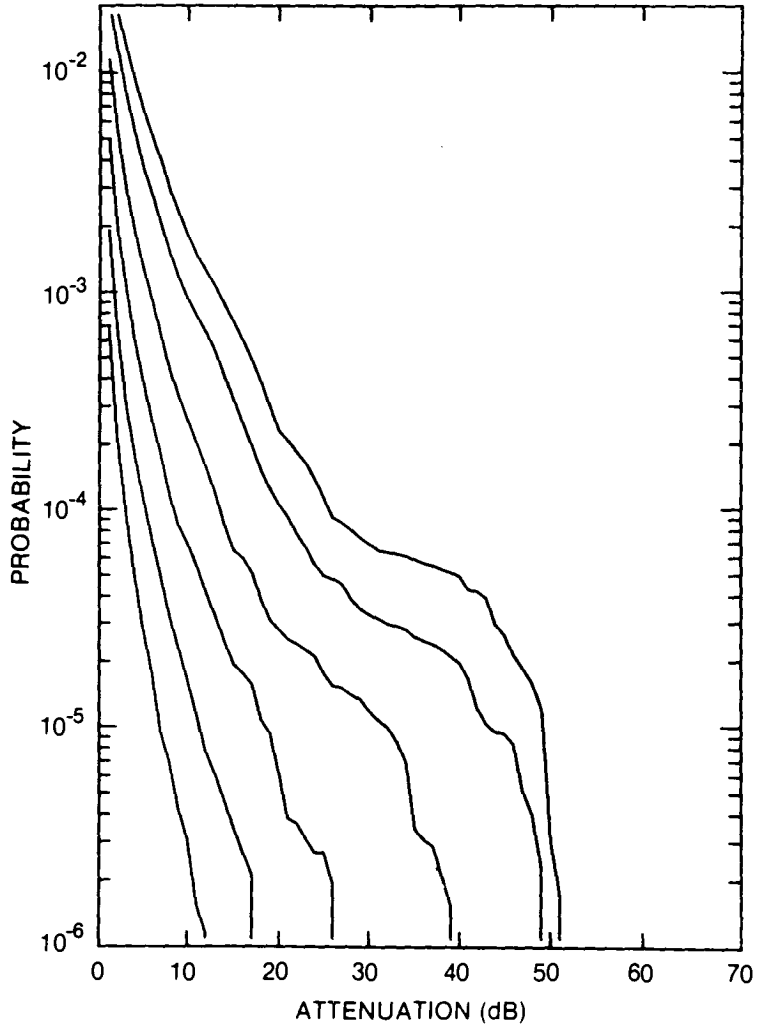

Figure 324. Cumulative distribution of rain attenuation for 12.8 GHz at Summerside, PEI. Curves, moving from lowest to highest, are for hop lengths of 5, 10, 20, 40, 80, and 120 km, respectively.

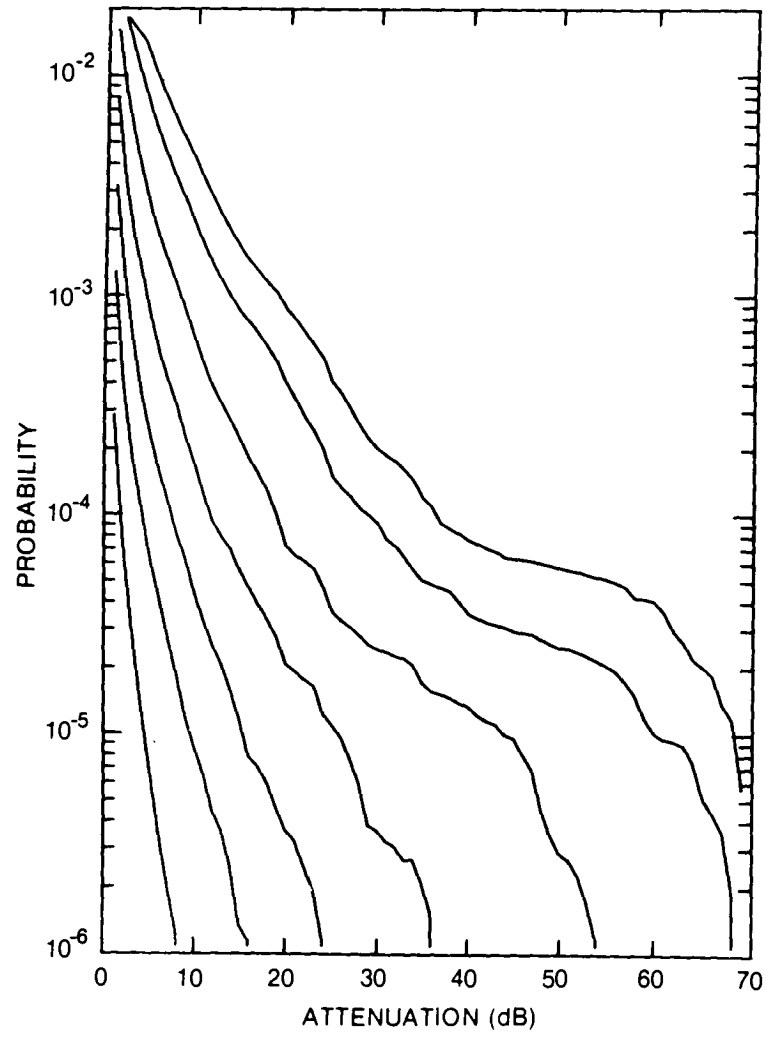

Figure 325. Cumulative distribution of rain attenuation for 15 GHz at Summerside, PEI. Curves, moving from lowest to highest, are for hop lengths of 2, 5, 10, 20, 40, 80 and 120 km, respectively.

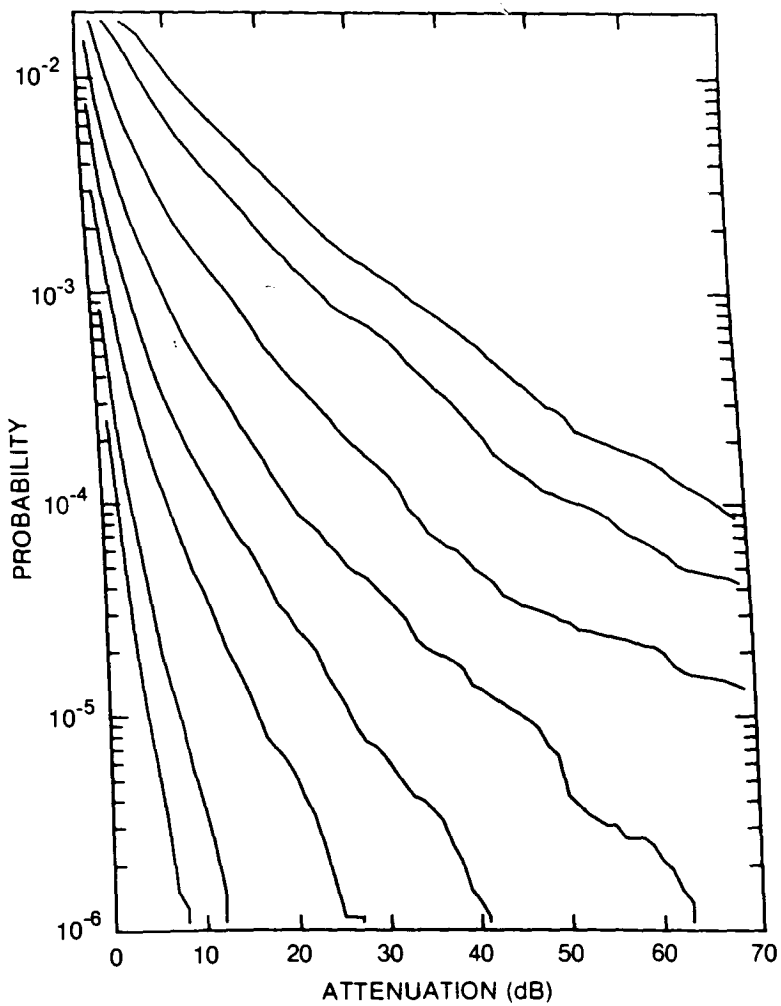

Figure 326. Cumulative distribution of rain attenuation for 20 GHz at Summerside, PEI. Curves, moving from lowest to highest, are for hop lengths of 1, 2, 5, 10, 20, 40, 80 and 120 km, respectively.

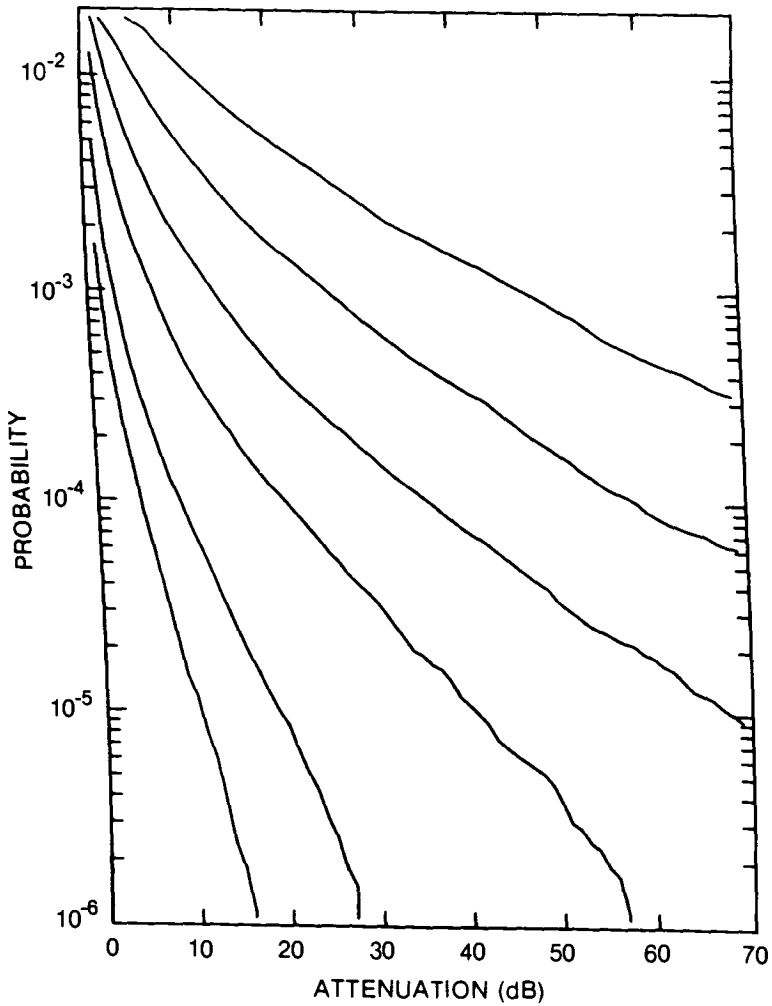

Figure 327. Cumulative distribution of rain attenuation for 35 GHz at Summerside, PEI. Curves, moving from lowest to highest, are for hop lengths of 1, 2, 5, 10, 20 and 40 km, respectively.

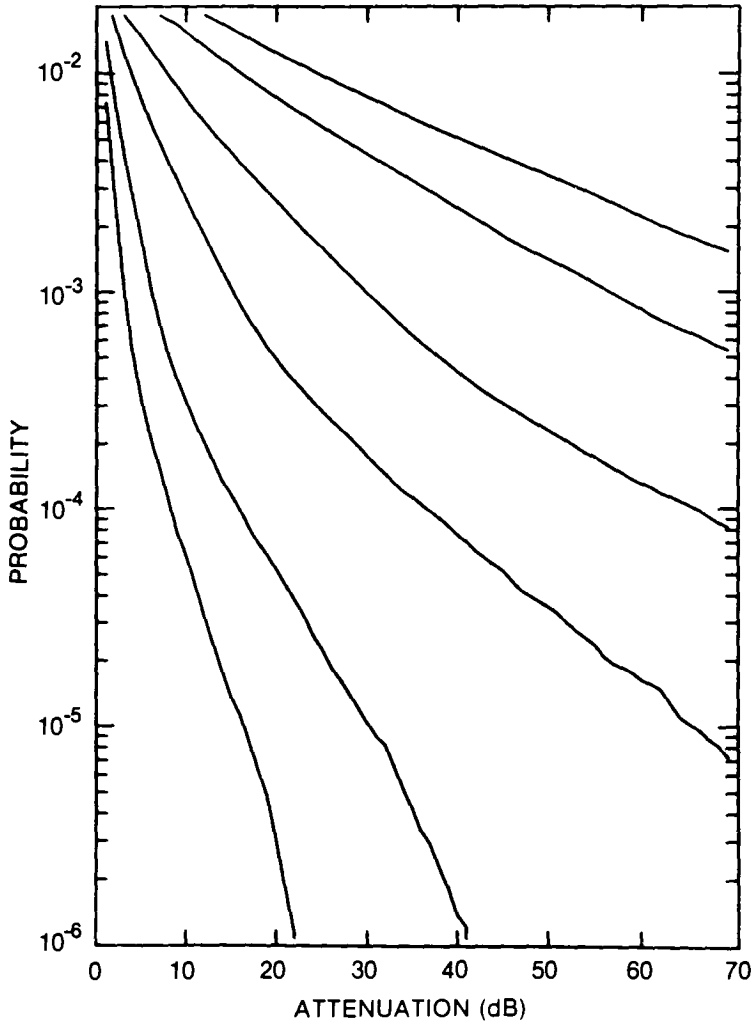

Figure 328. Cumulative distribution of rain attenuation for 56 GHz at Summerside, PEI. Curves, moving from lowest to highest, are for hop lengths of 1, 2, 5, 10, 20 and 30 km, respectively.

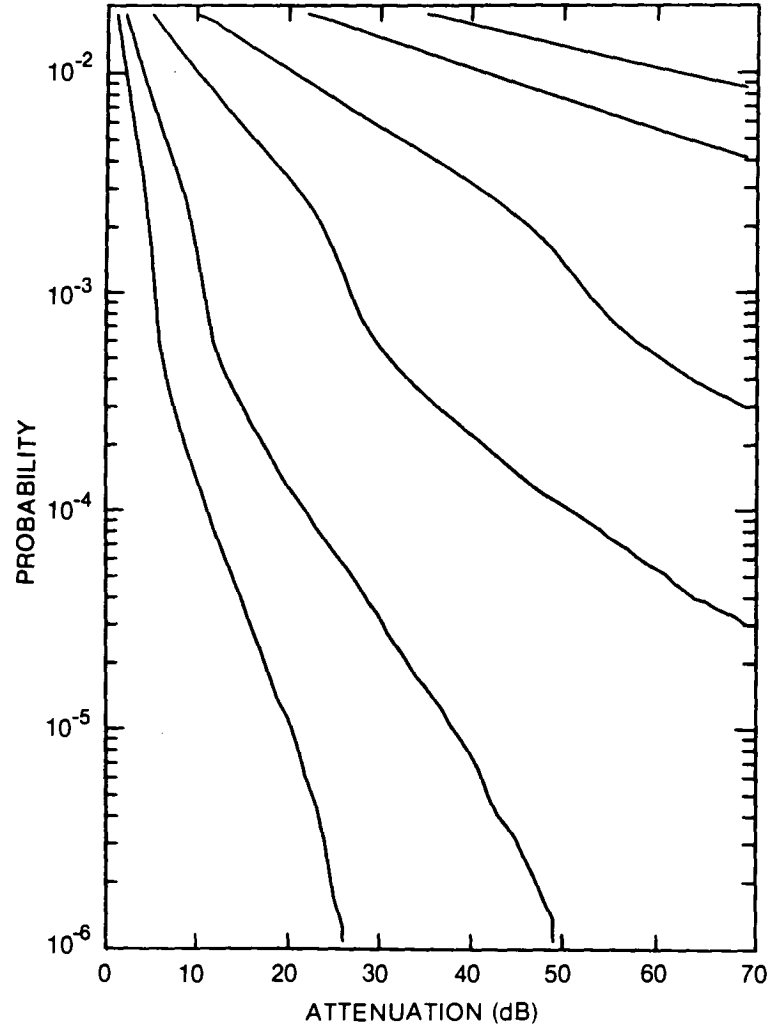

Figure 329. Cumulative distribution of rain attenuation for 100 GHz at Summerside, PEI. Curves, moving from lowest to highest, are for hop lengths of 1, 2, 5, 10, 20 and 30 km, respectively.

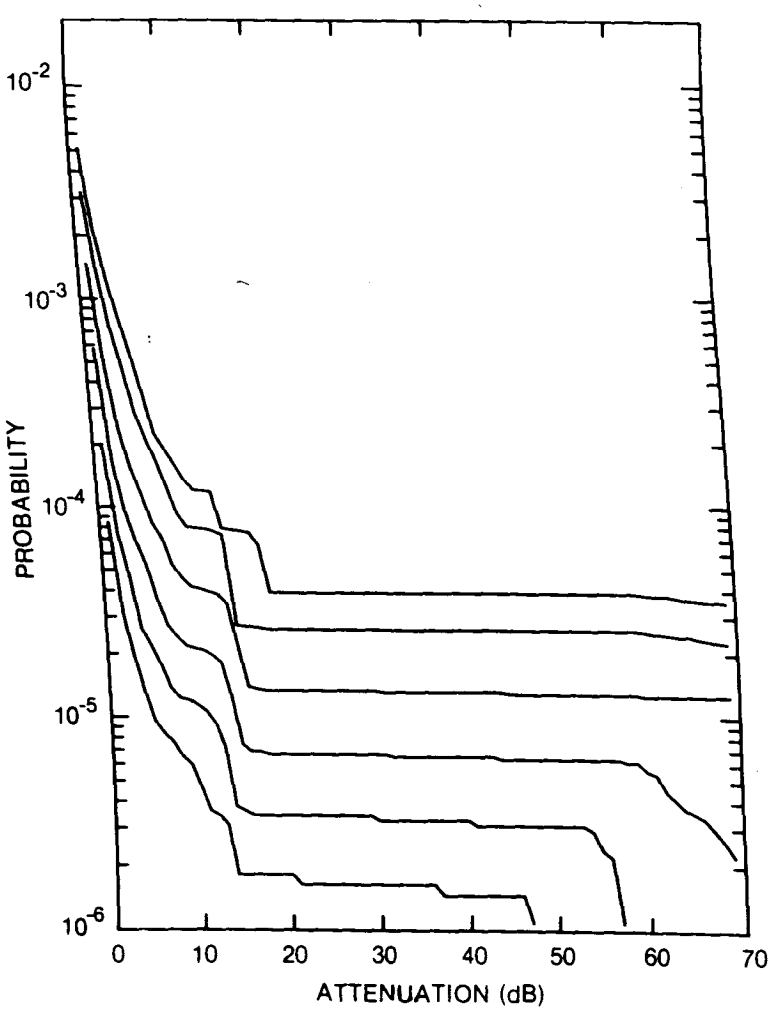

Figure 330. Cumulative distribution of rain attenuation for 8 GHz at Swift Current, SASK. Curves, moving from lowest to highest, are for hop lengths of 5, 10, 20, 40, 80 and 120 km, respectively.

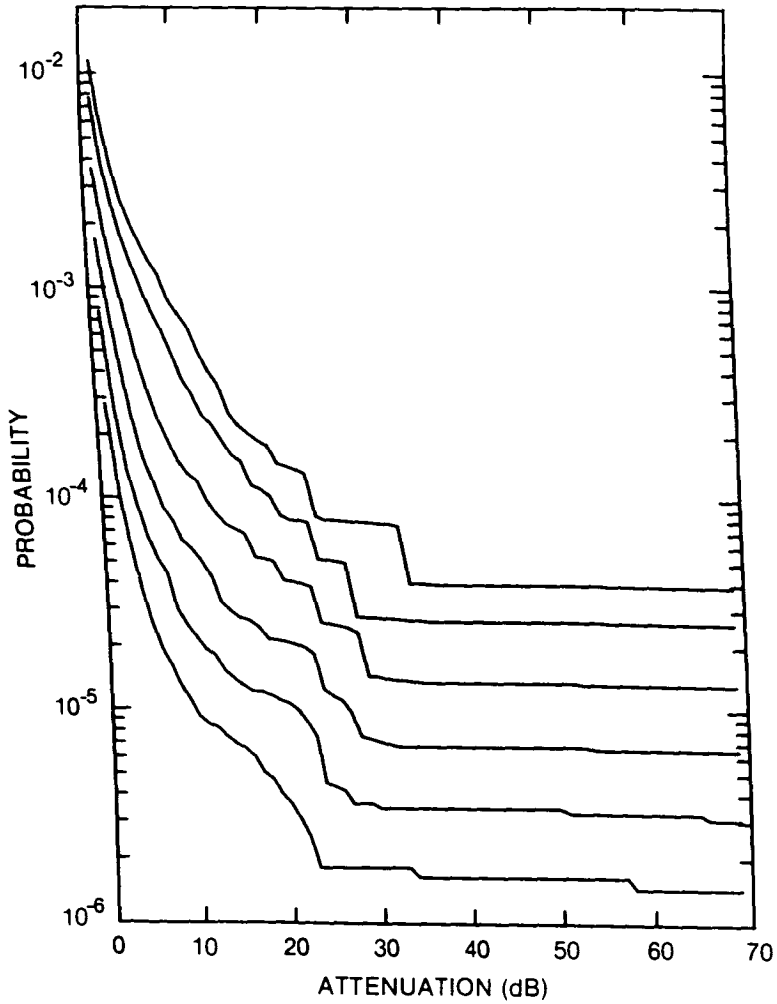

Figure 331. Cumulative distribution of rain attenuation for 11 GHz at Swift Current, SASK. Curves, moving from lowest to highest, are for hop lengths of 5, 10, 20, 40, 80 and 120 km, respectively.

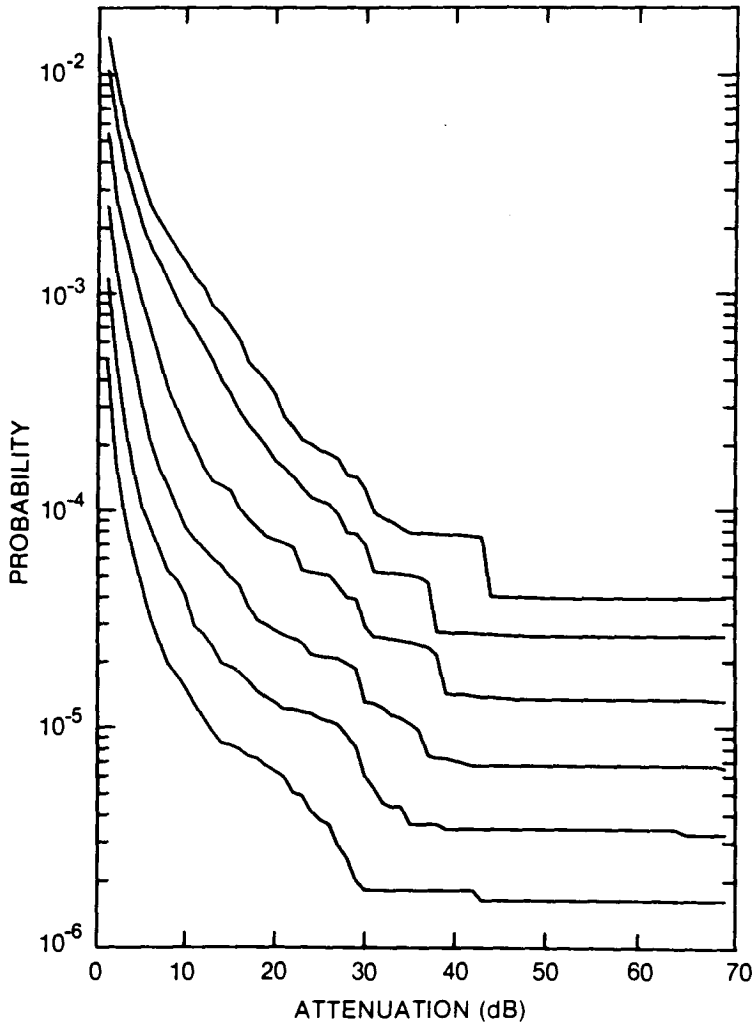

Figure 332. Cumulative distribution of rain attenuation for 12.8 GHz at Swift Current, SASK. Curves, moving from lowest to highest, are for hop lengths of 5, 10, 20, 40, 80 and 120 km, respectively.

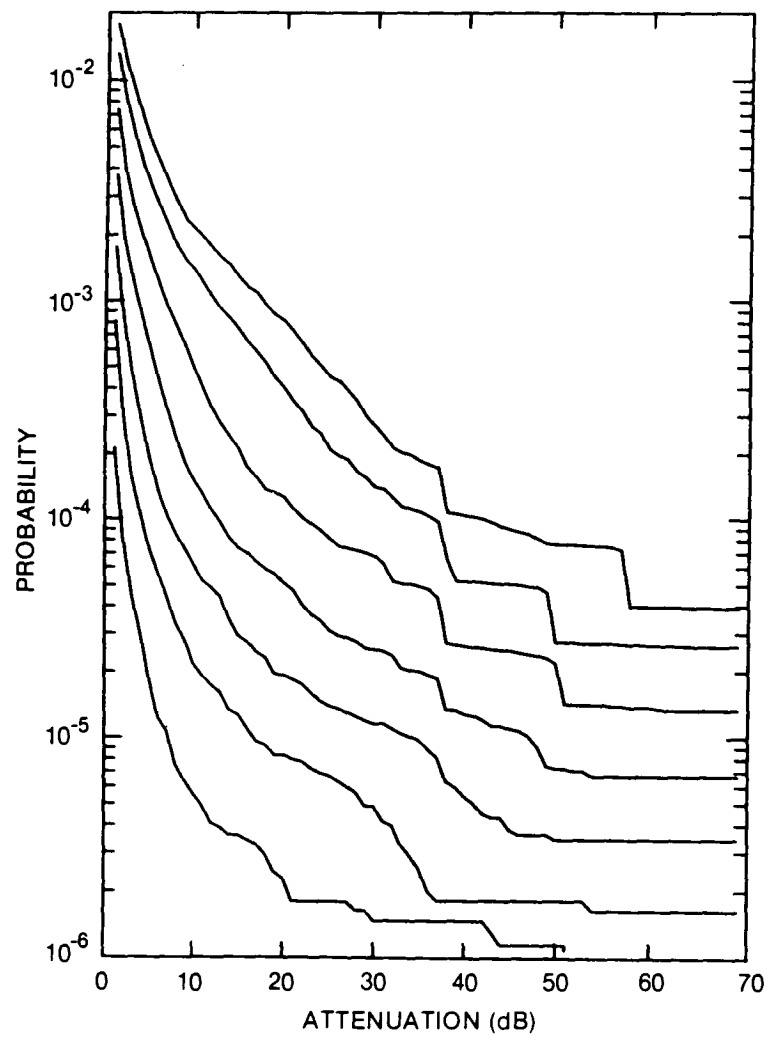

Figure 333. Cumulative distribution of rain attenuation for 15 GHz at Swift Current, SASK. Curves, moving from lowest to highest, are for hop lengths of 2, 5, 10, 20, 40, 80 and 120 km, respectively.

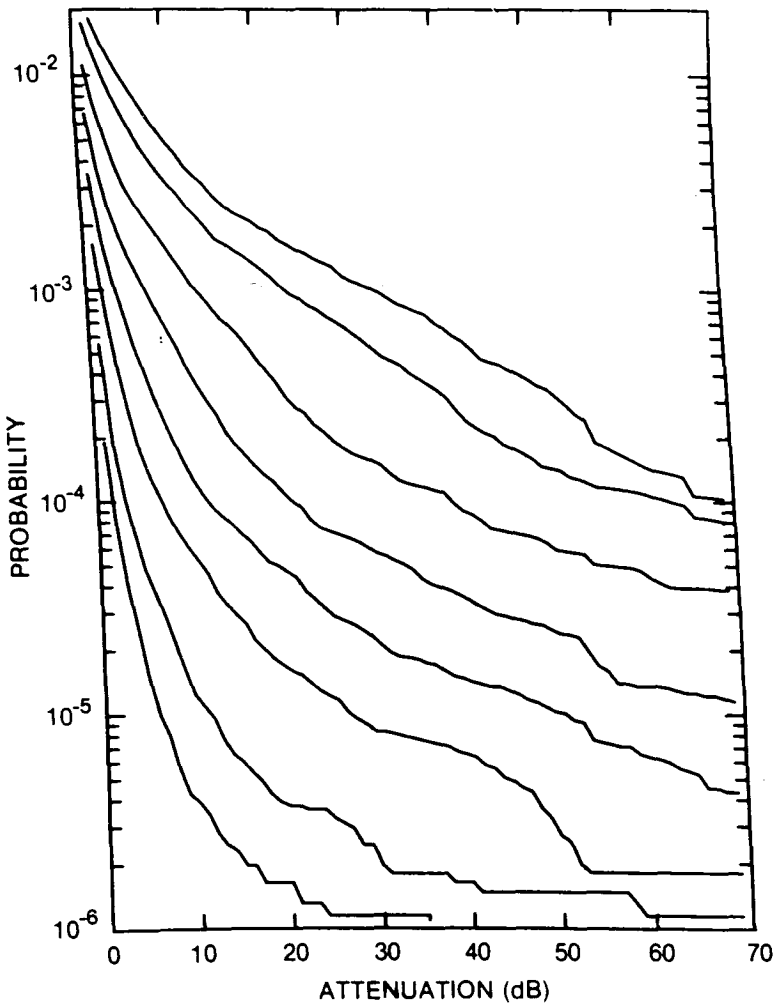

Figure 334. Cumulative distribution of rain attenuation for 20 GHz at Swift Current, SASK. Curves, moving from lowest to highest, are for hop lengths of 1, 2, 5, 10, 20, 40, 80 and 120 km, respectively.

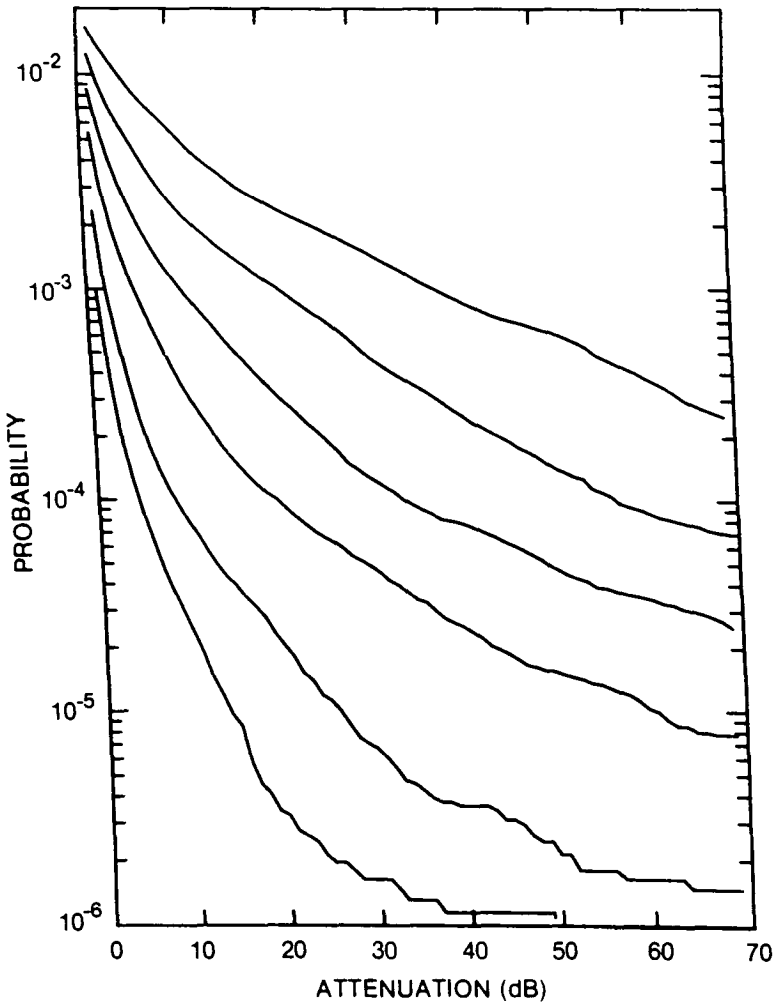

Figure 335. Cumulative distribution of rain attenuation for 35 GHz at Swift Current, SASK. Curves, moving from lowest to highest, are for hop lengths of 1, 2, 5, 10, 20 and 40 km, respectively.

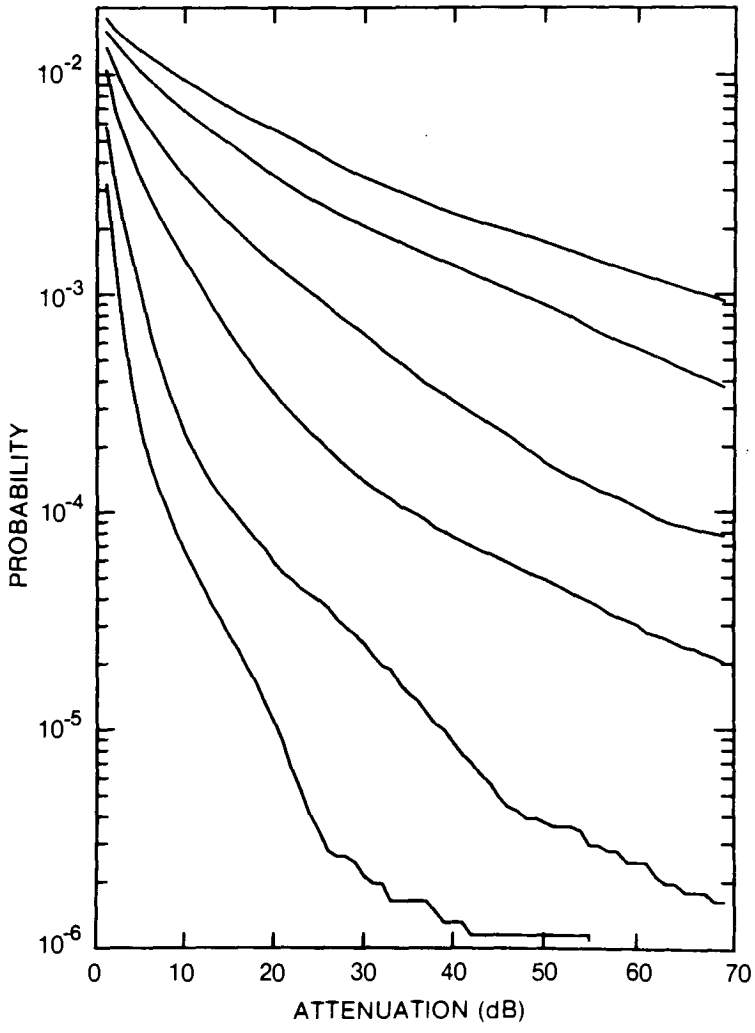

Figure 336. Cumulative distribution of rain attenuation for 56 GHz at Swift Current, SASK. Curves, moving from lowest to highest, are for hop lengths of 1, 2, 5, 10, 20 and 30 km, respectively.

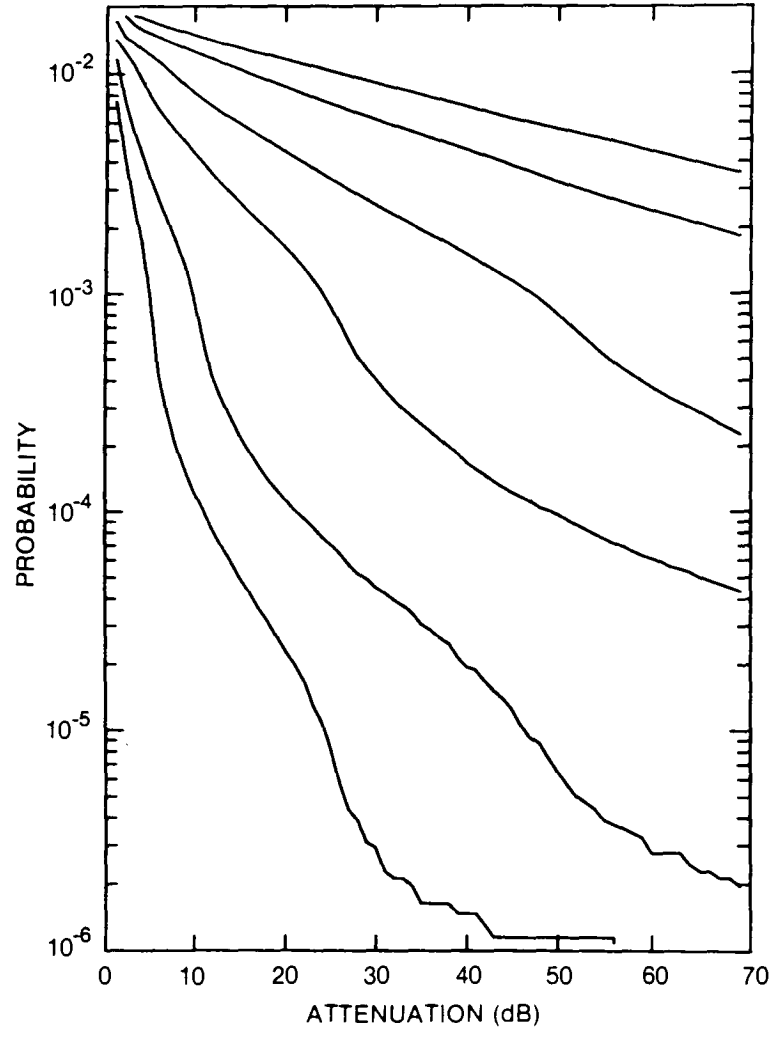

Figure 337. Cumulative distribution of rain attenuation for 100 GHz at Swift Current, SASK. Curves, moving from lowest to highest, are for hop lengths of 1, 2, 5, 10, 20 and 30 km, respectively.

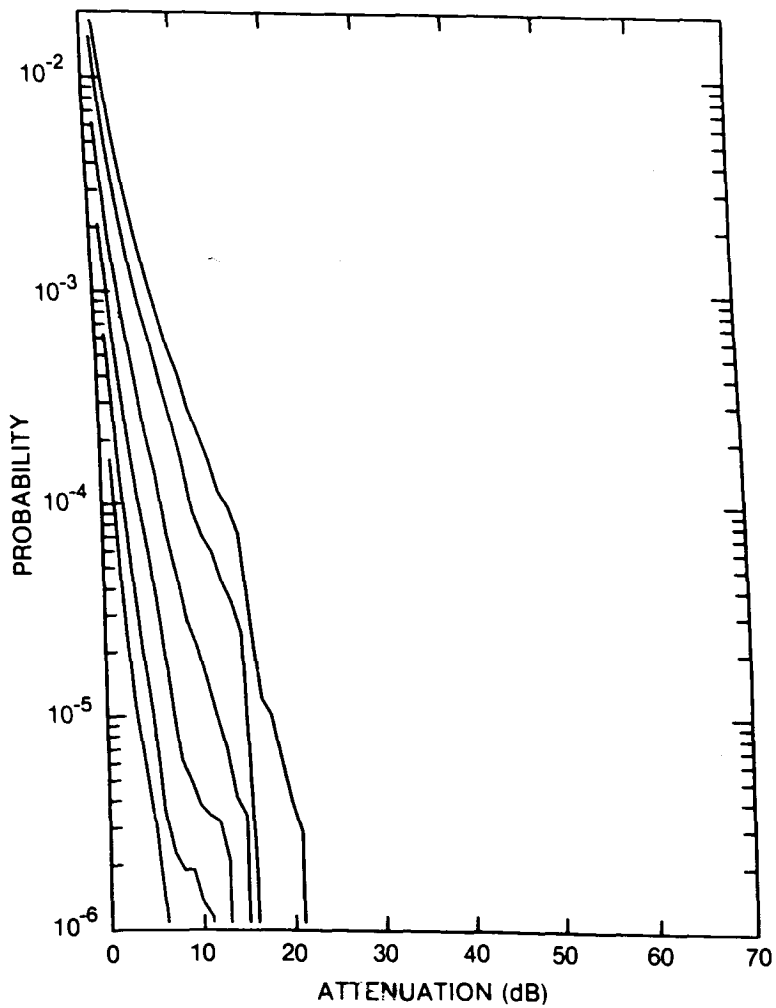

Figure 338. Cumulative distribution of rain attenuation for 8 GHz at Sydney, NS. Curves, moving from lowest to highest, are for hop lengths of 5, 10, 20, 40, 80 and 120 km, respectively.

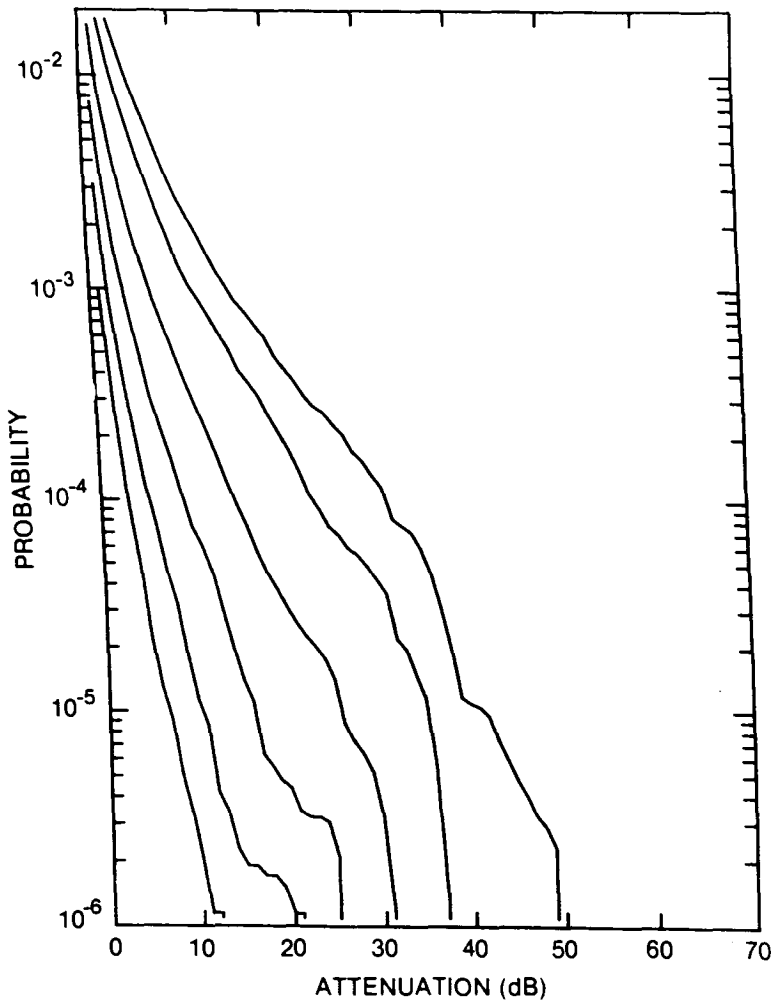

Figure 339. Cumulative distribution of rain attenuation for 11 GHz at Sydney, NS. Curves, moving from lowest to highest, are for hop lenghts of 5, 10, 20, 40, 80 and 120 km, respectively.

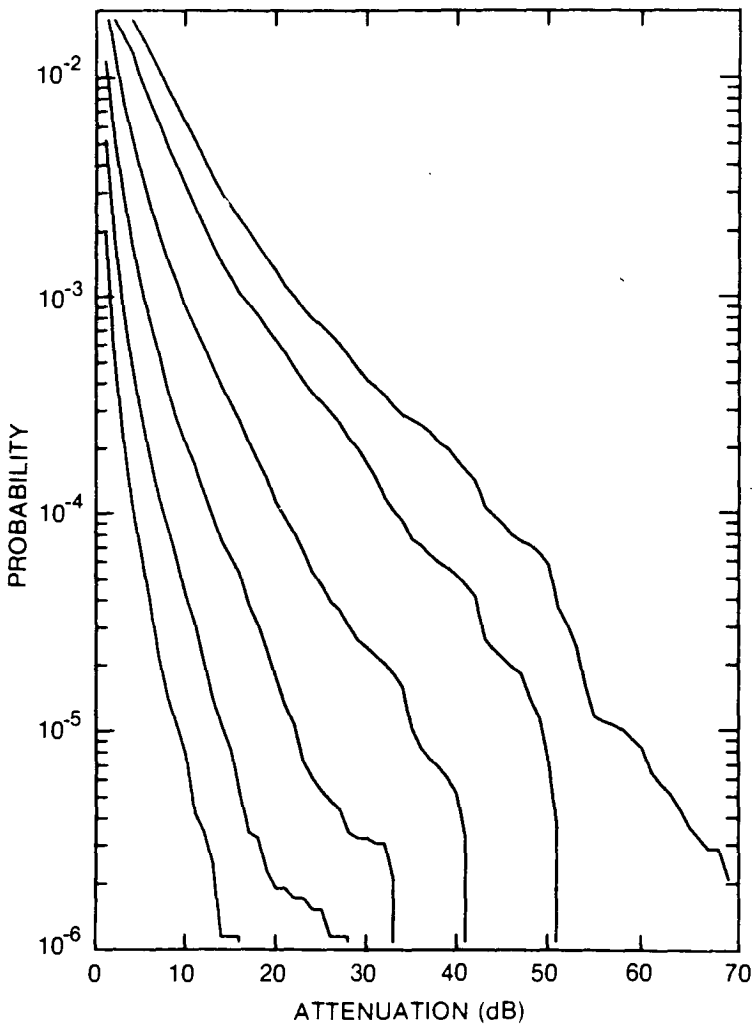

Figure 340. Cumulative distribution of rain attenuation for 12.8 GHz at Sydney, NS. Curves, moving from lowest to highest, are for hop lengths of 5, 10, 20, 40, 80 and 120 km, respectively.

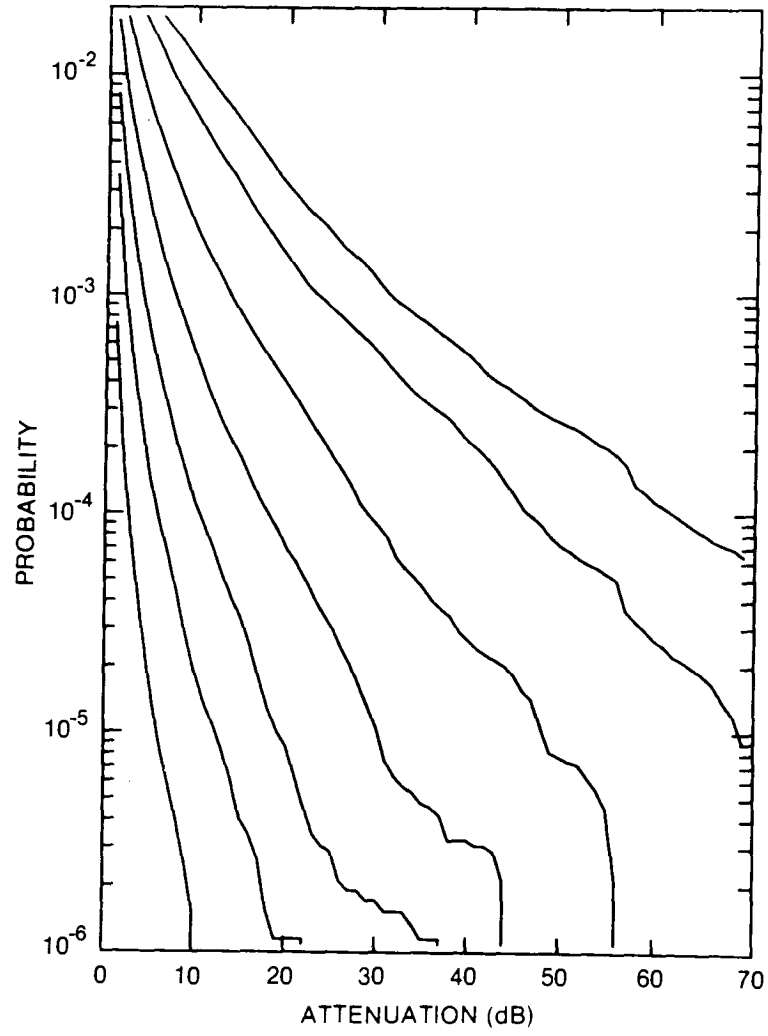

Figure 341. Cumulative distribution of rain attenuation for 15 GHz at Sydney, NS. Curves, moving from lowest to highest, are for hop lengths of 2, 5, 10, 20, 40, 80 and 120 km, respectively.

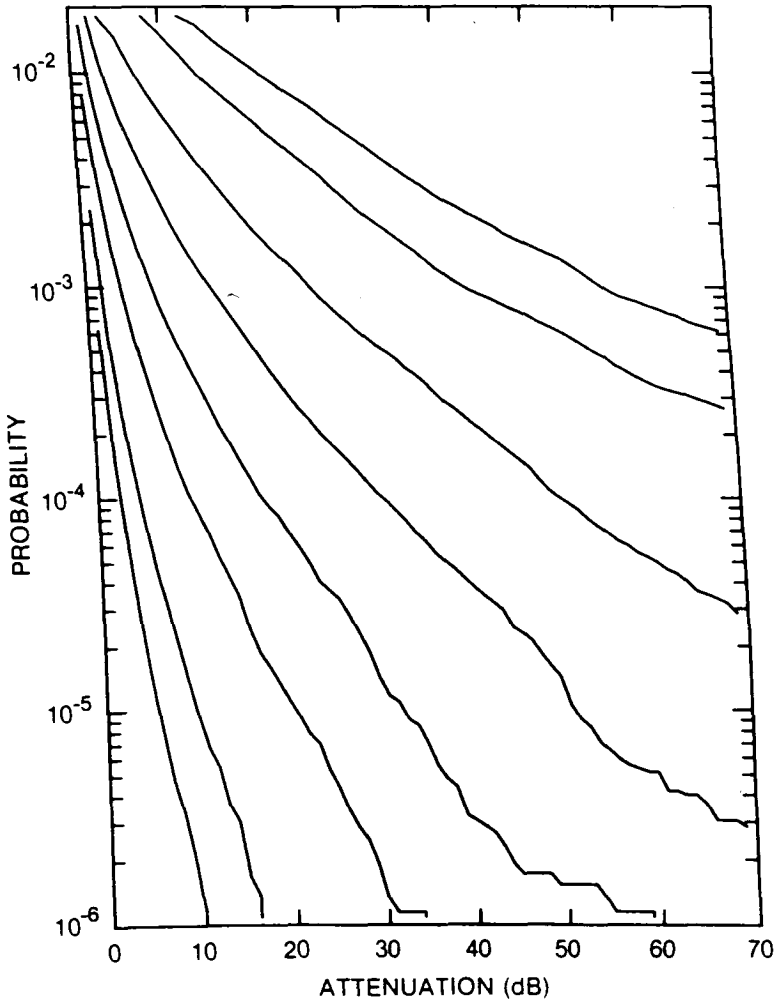

Figure 342. Cumulative distribution of rain attenuation for 20 GHz at Sydney, NS. Curves, moving from lowest to highest, are for hop lengths of 1, 2, 5, 10, 20, 40, 80 and 120 km, respectively.

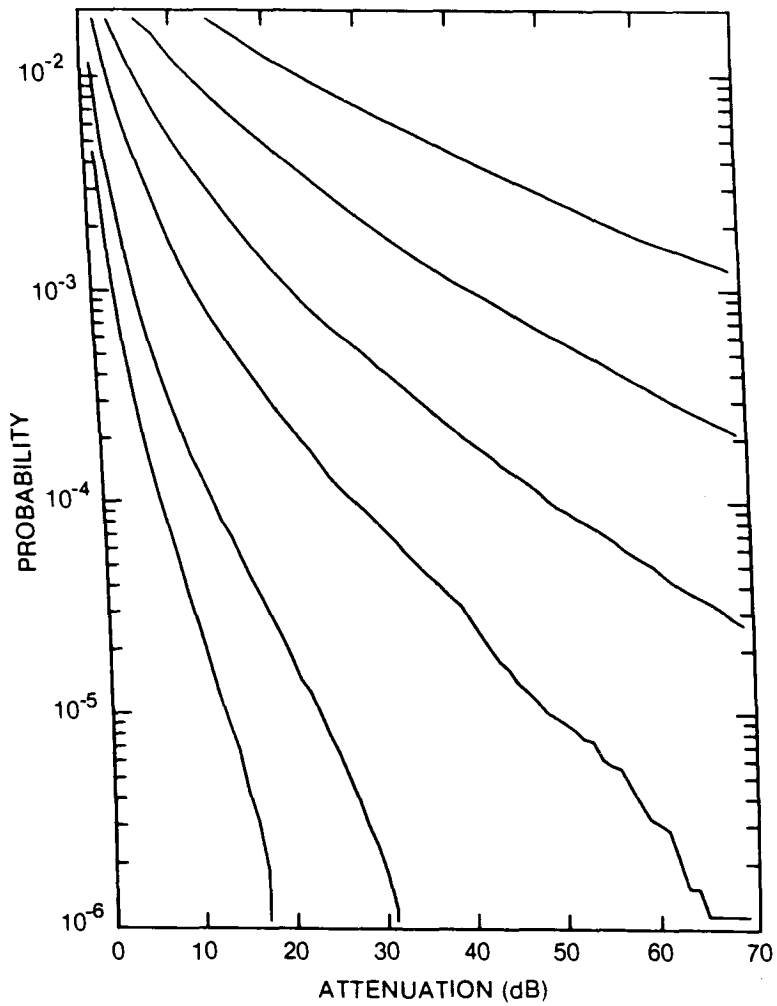

Figure 343. Cumulative distribution of rain attenuation for 35 GHz at Sydney, NS. Curves, moving from lowest to highest, are for hop lengths of 1, 2, 5, 10, 20 and 40 km, respectively.

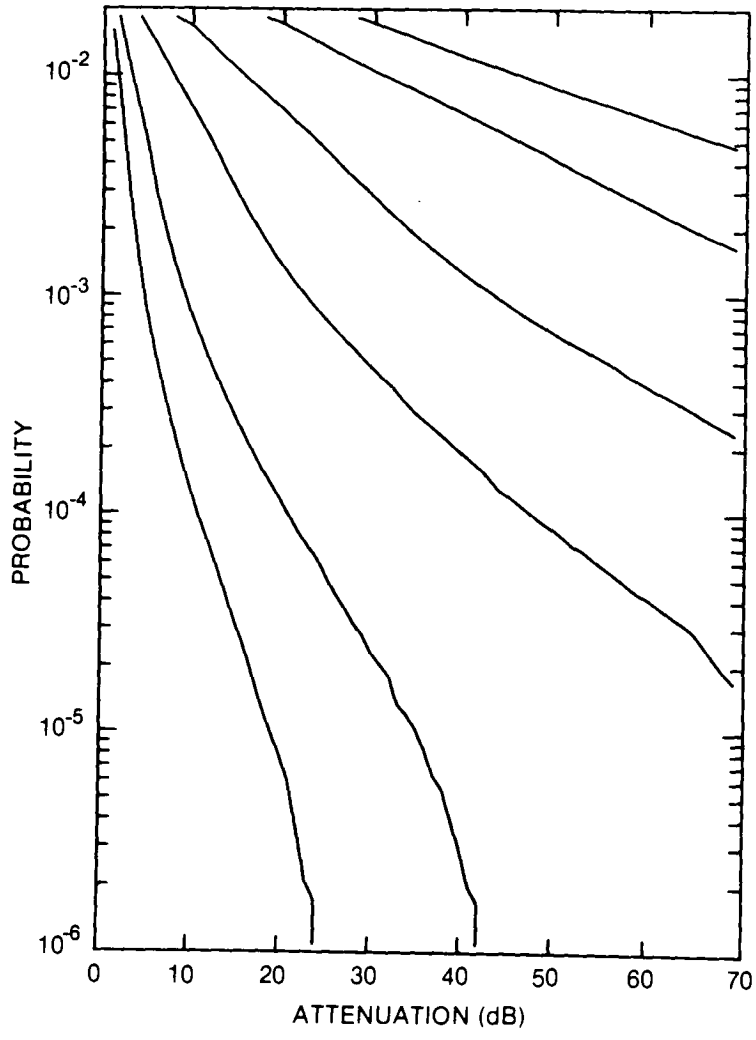

Figure 344. Cumulative distribution of rain attenuation for 56 GHz at Sydney, NS. Curves, moving from lowest to highest, are for hop lengths of 1, 2, 5, 10, 20 and 30 km, respectively.

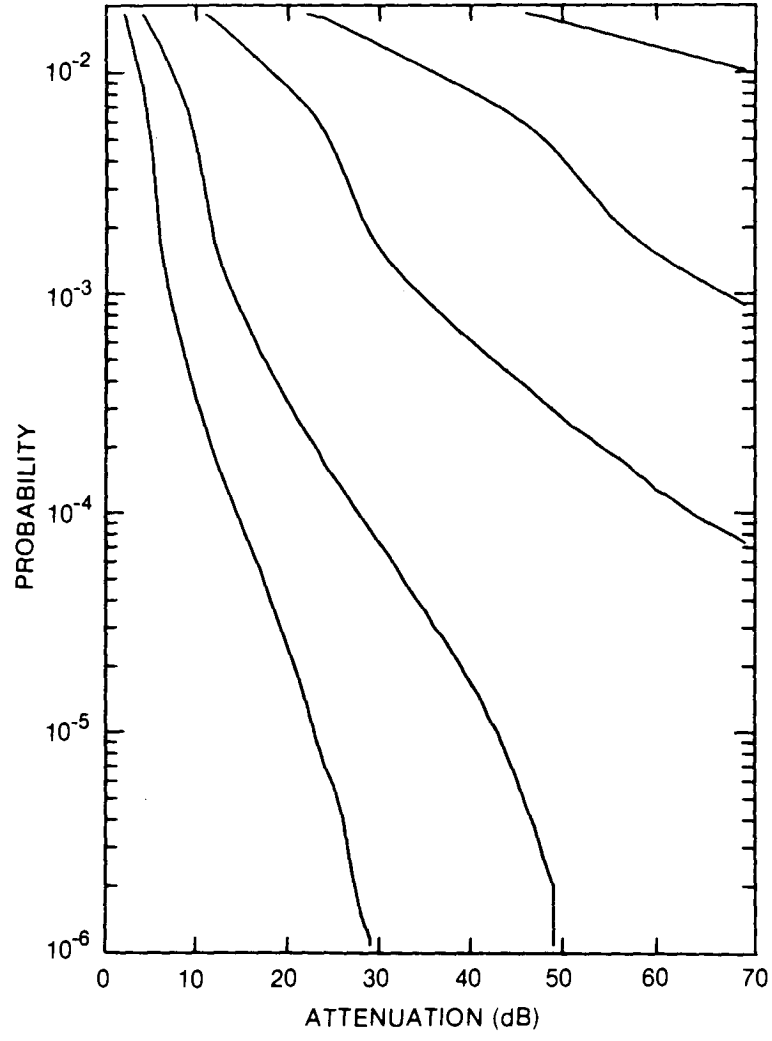

Figure 345. Cumulative distribution of rain attenuation for 100 GHz at Sydney, NS. Curves, moving from lowest to highest, are for hop lengths of 1, 2, 5, 10 and 20 km, respectively.

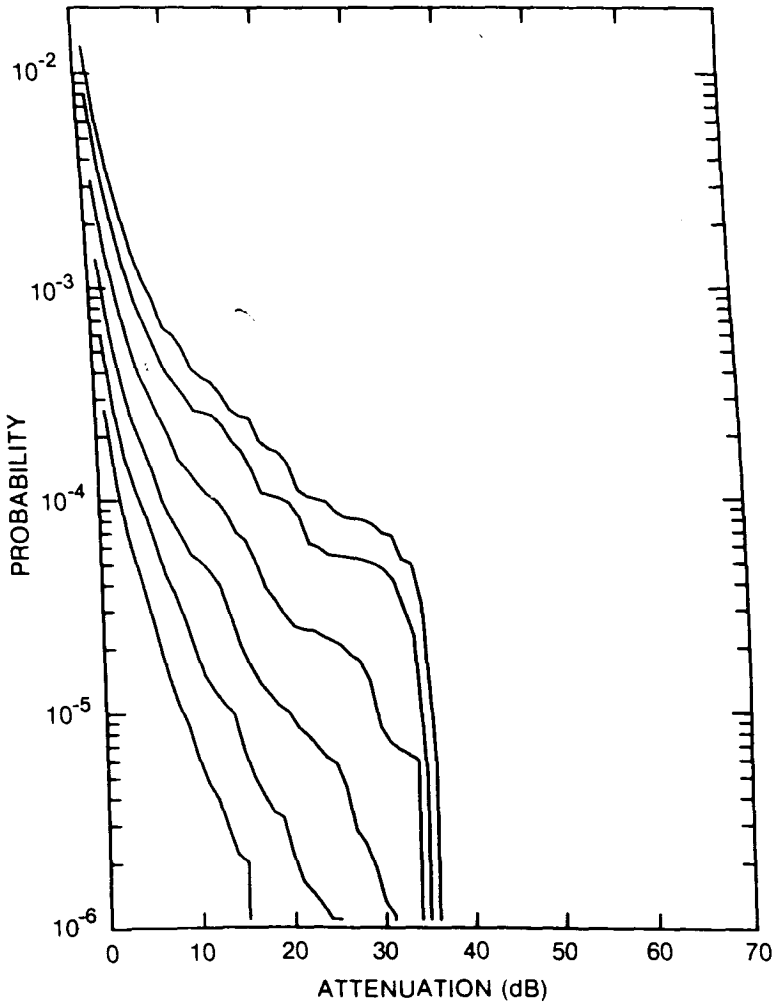

Figure 346. Cumulative distribution of rain attenuation for 8 GHz at Toronto, ONT. Curves, moving from lowest to highest, are for hop lengths of 5, 10, 20, 40, 80 and 120 km, respectively.

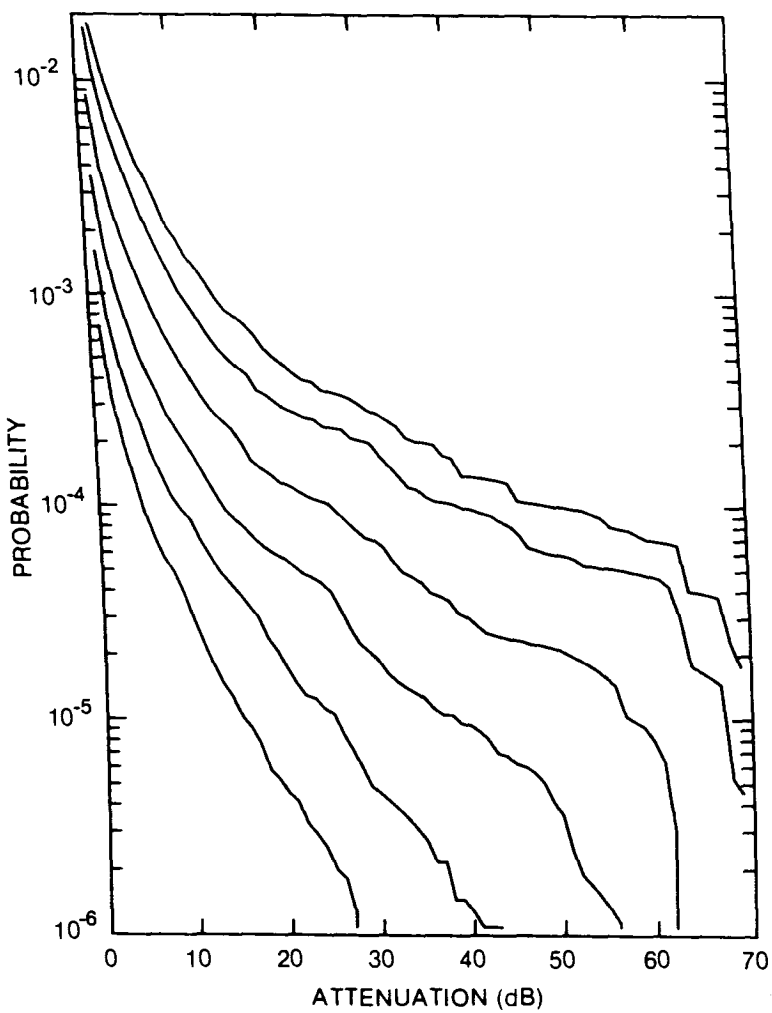

Figure 347. Cumulative distribution of rain attenuation for 11 GHz at Toronto, ONT. Curves, moving from lowest to highest, are for hop lengths of 5, 10, 20, 40, 80 and 120 km, respectively.

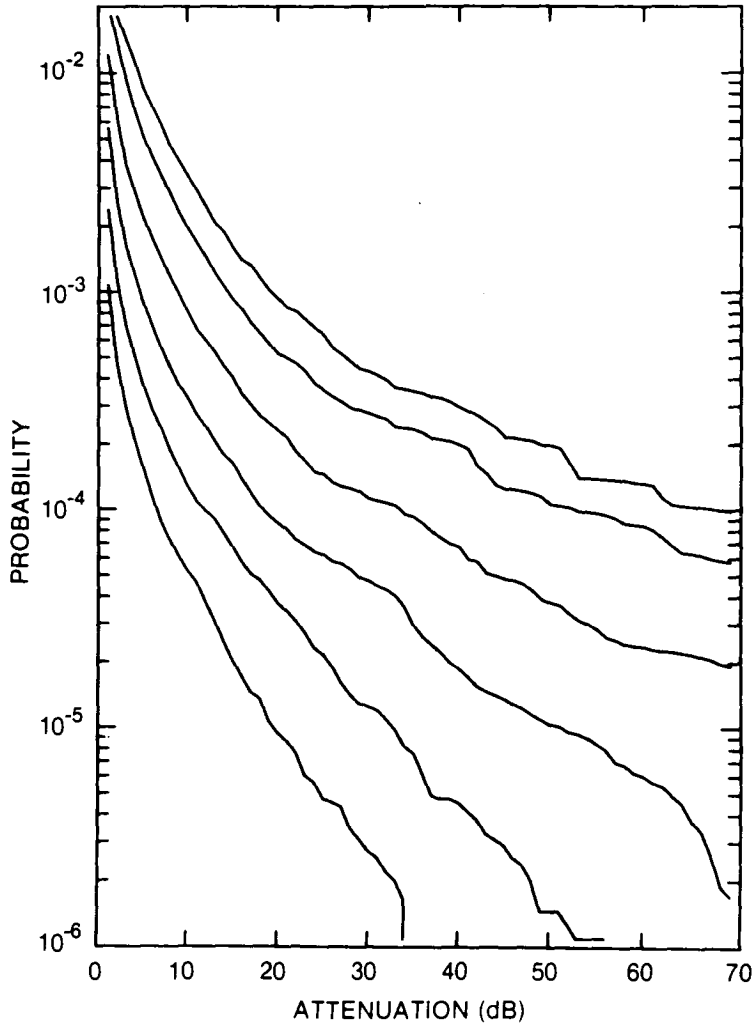

Figure 348. Cumulative distribution of rain attenuation for 12.8 GHz at Toronto, ONT. Curves, moving from lowest to highest, are for hop lengths of 5, 10, 20, 40, 80 and 120 km, respectively.

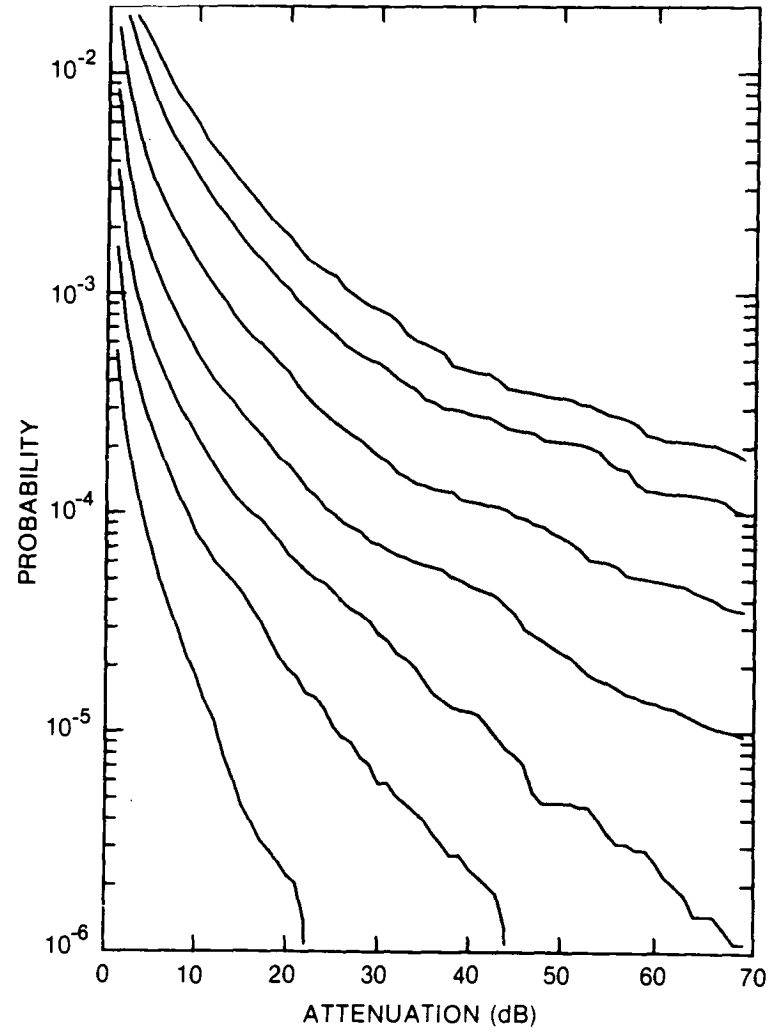

Figure 349. Cumulative distribution of rain attenuation for 15 GHz at Toronto, ONT. Curves, moving from lowest to highest, are for hop lengths of 2, 5, 10, 20, 40, 80 and 120 km, respectively.

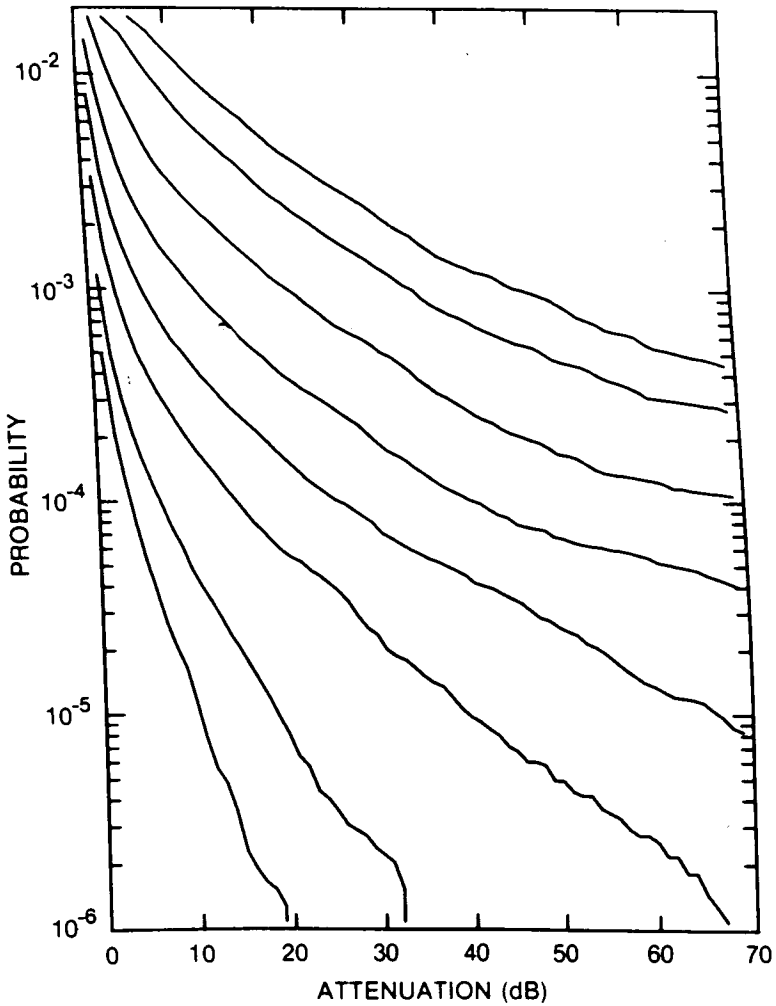

Figure 350. Cumulative distribution of rain attenuation for 20 GHz at Toronto, ONT. Curves, moving from lowest to highest are for hop lengths of 1, 2, 5, 10, 20, 40, 80 and 120 km, respectively.

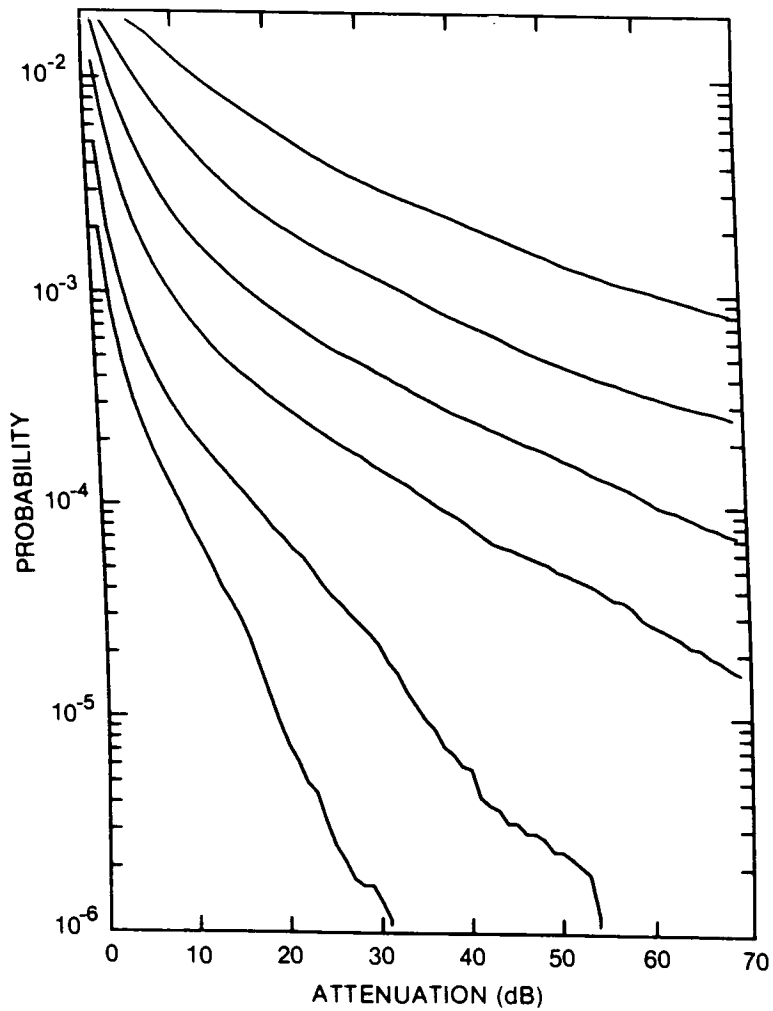

Figure 351. Cumulative distribution of rain attenuation for 35 GHz at Toronto, ONT. Curves, moving from lowest to highest, are for hop lengths of 1, 2, 5, 10, 20 and 40 km, respectively.

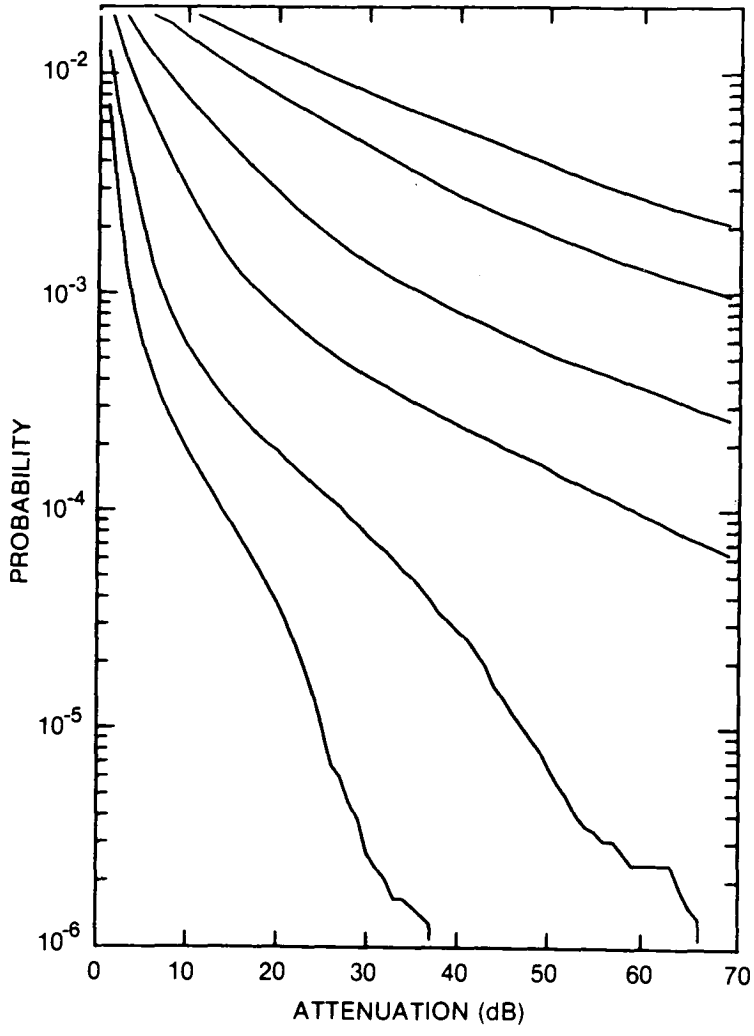

Figure 352. Cumulative distribution of rain attenuation for 56 GHz at Toronto, ONT. Curves, moving from lowest to highest, are for hop lengths of 1, 2, 5, 10, 20 and 30 km, respectively.

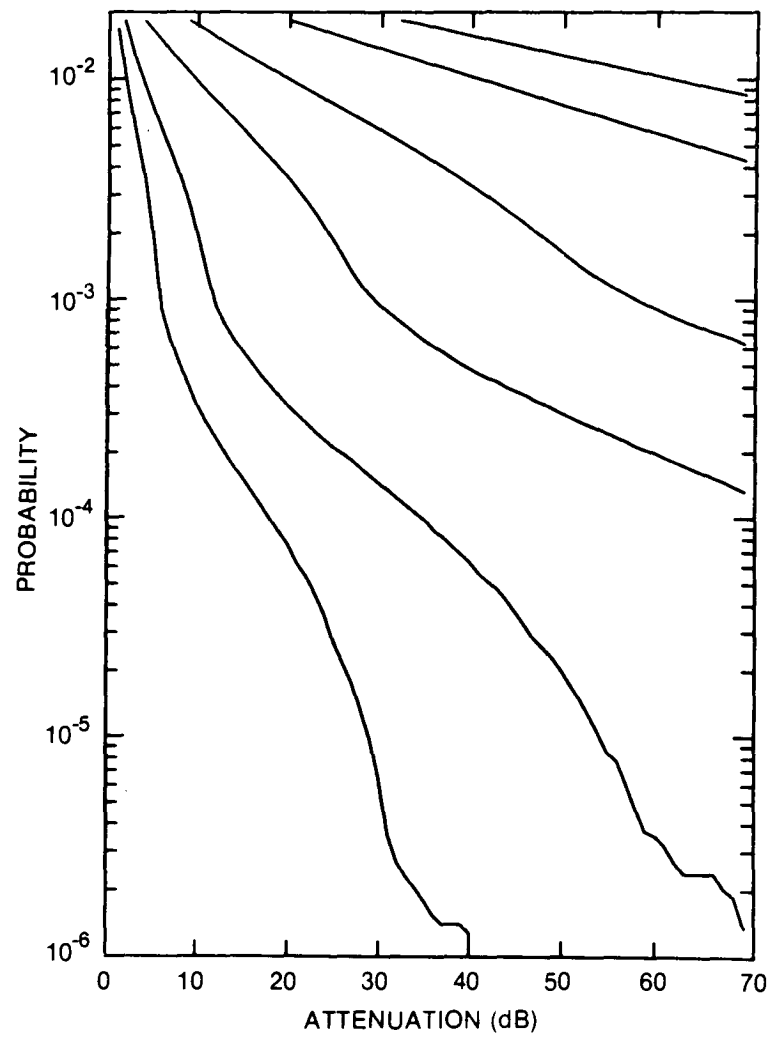

Figure 353. Cumulative distribution of rain attenuation for 100 GHz at Toronto, ONT. Curves, moving from lowest to highest, are for hop lengths of 1, 2, 5, 10, 20 and 30 km, respectively.

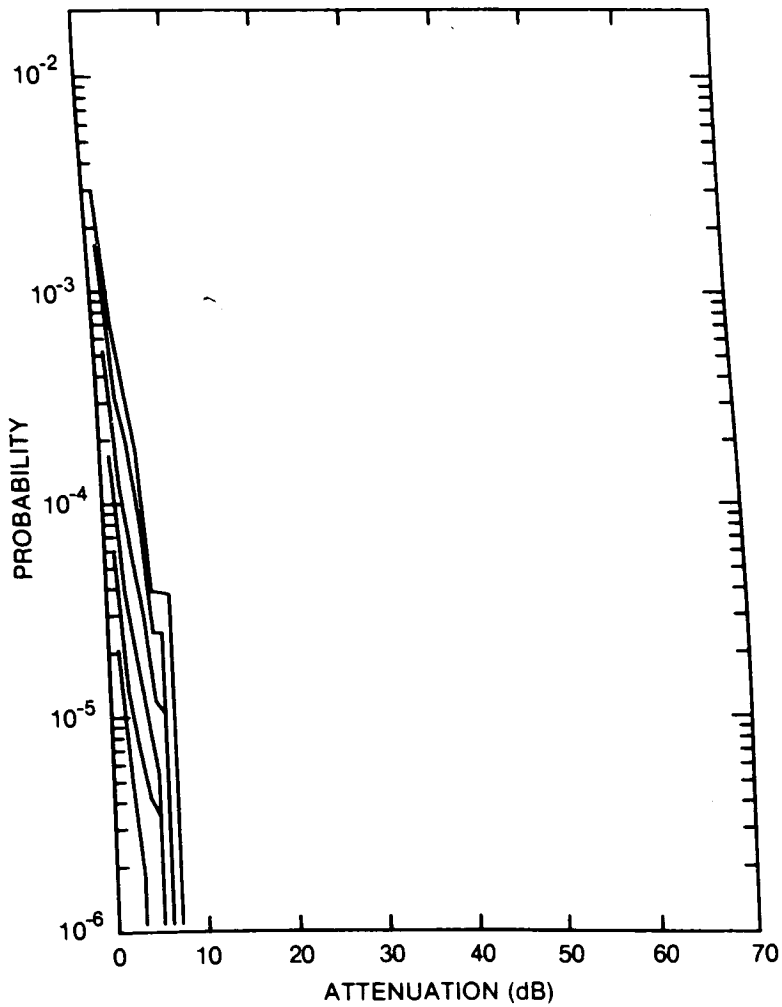

Figure 354. Cumulative distribution of rain attenuation for 8 GHz at Uranium City, SASK. Curves, moving from lowest to highest, are for hop lengths of 5, 10, 20, 40, 80 and 120 km, respectively.

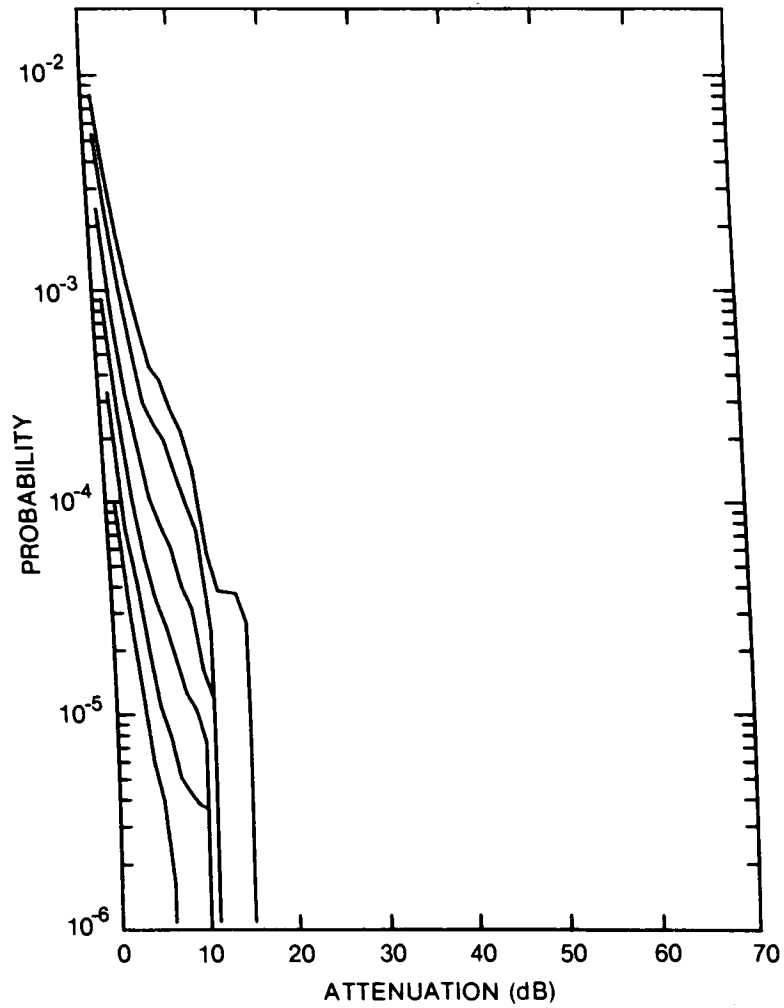

Figure 355. Cumulative distribution of rain attenuation for 11 GHz at Uranium City, SASK. Curves, moving from lowest to highest, are for hop lengths of 5, 10, 20, 40, 80 and 120 km, respectively.

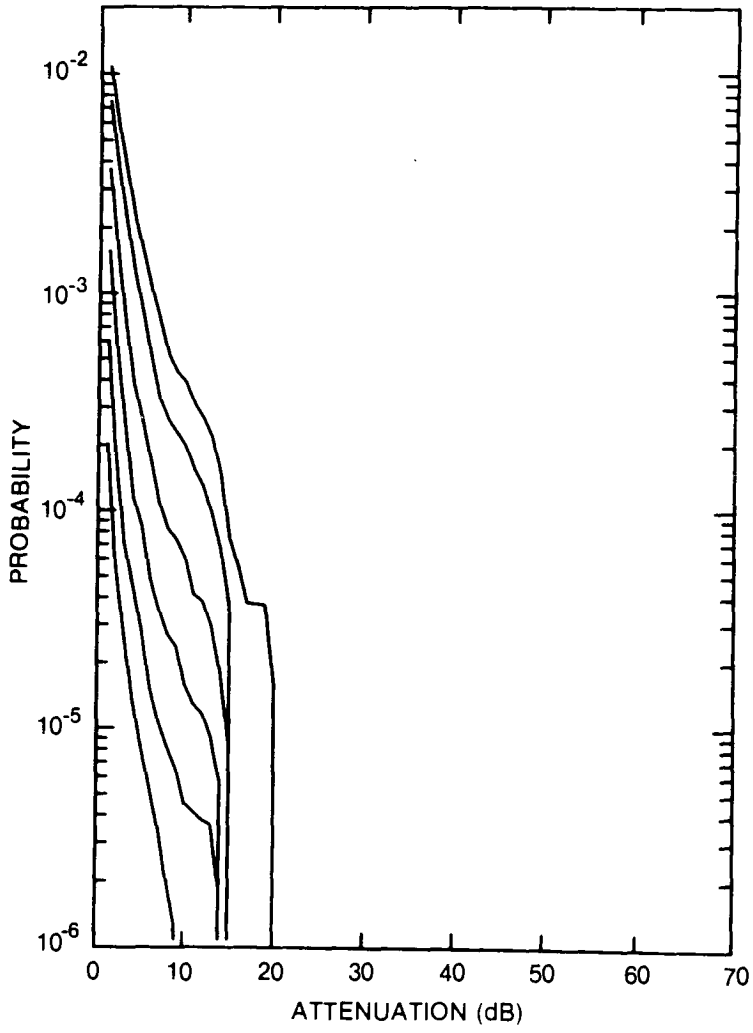

Figure 356. Cumulative distribution of rain attenuation for 12.8 GHz at Uranium City, SASK. Curves, moving from lowest to highest, are for hop lengths of 5, 10, 20, 40, 80 and 120 km, respectively.

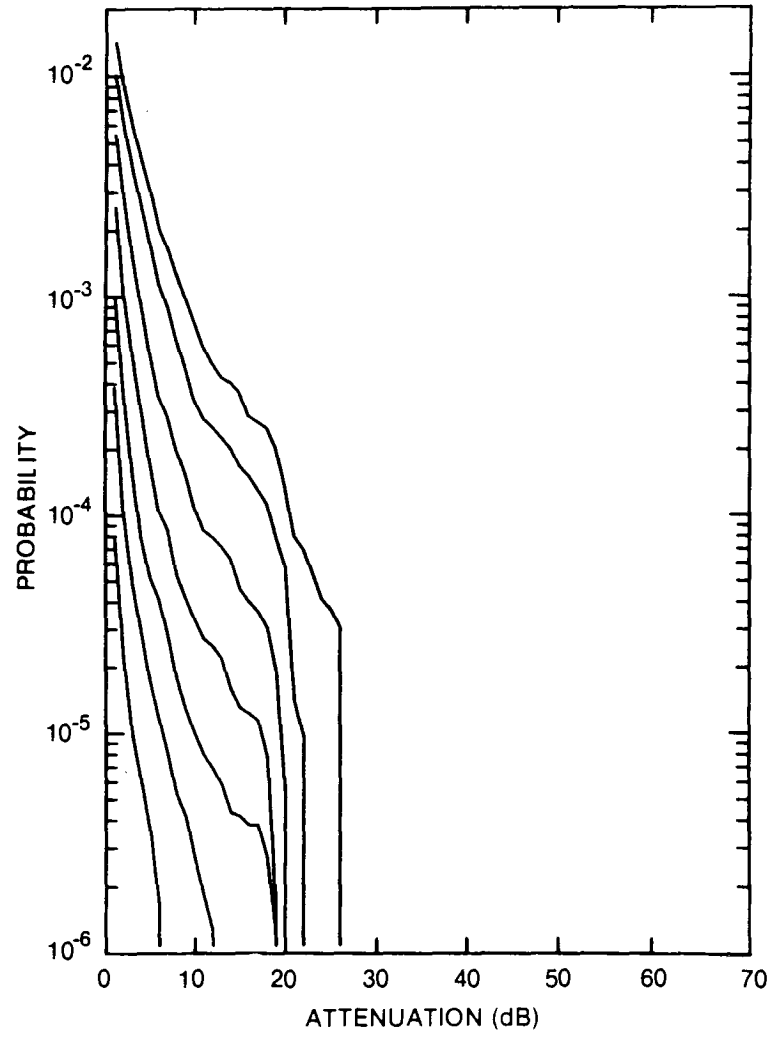

Figure 357. Cumulative distribution of rain attenuation for 15 GHz at Uranium City, SASK. Curves, moving from lowest to highest, are for hop lengths of 2, 5, 10, 20, 40, 80 and 120 km, respectively.

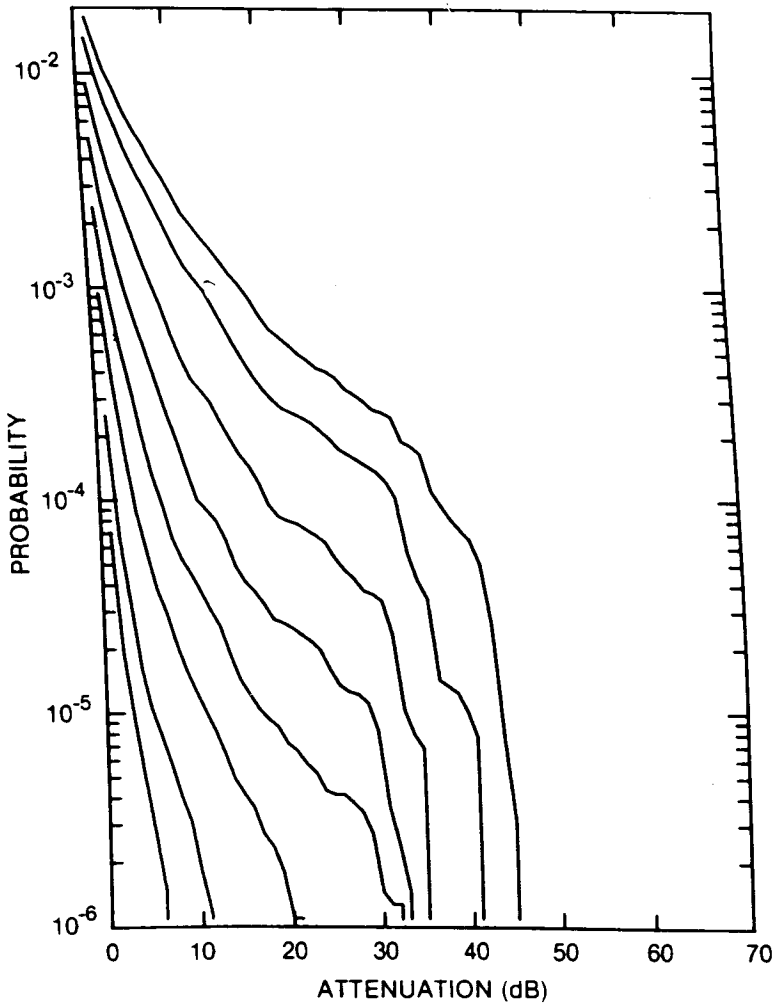

Figure 358. Cumulative distribution of rain attenuation for 20 GHz at Uranium City, SASK. Curves, moving from lowest to highest, are for hop lengths of 1, 2, 5, 10, 20, 40, 80 and 120 km, respectively.

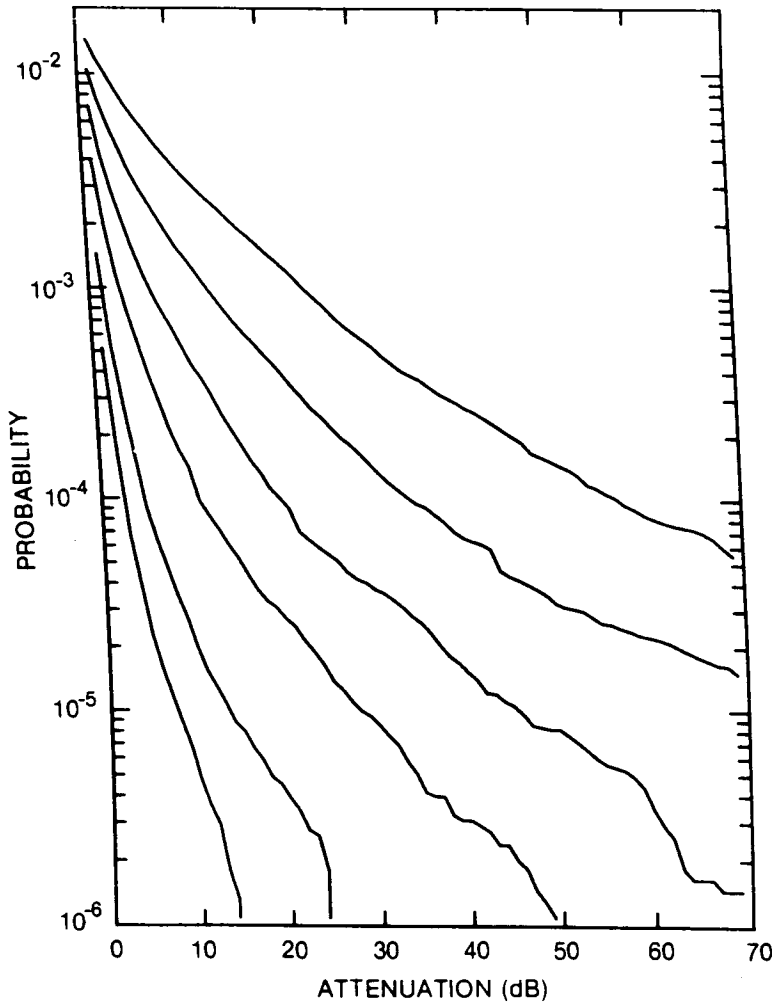

Figure 359. Cumulative distribution of rain attenuation for 35 GHz at Uranium City, SASK. Curves, moving from lowest to highest, are for hop lengths of 1, 2, 5, 10, 20 and 40 km, respectively.

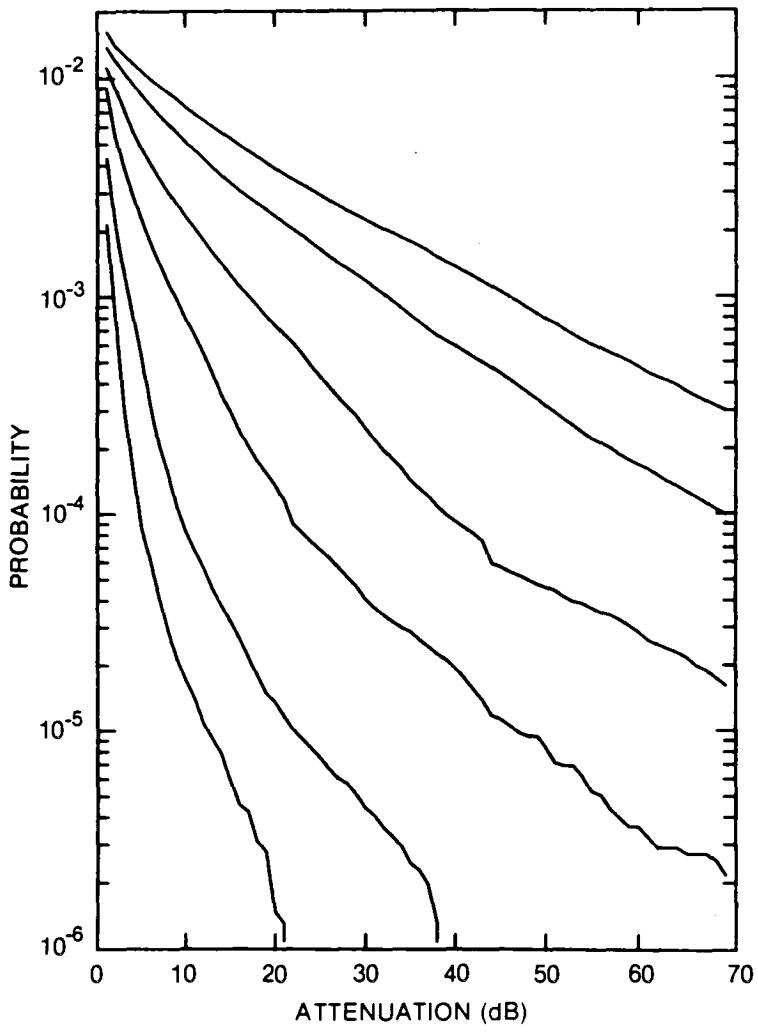

Figure 360. Cumulative distribution of rain attenuation for 56 GHz at Uranium City, SASK. Curves, moving from lowest to highest, are for hop lengths of 1, 2, 5, 10, 20 and 30 km, respectively.

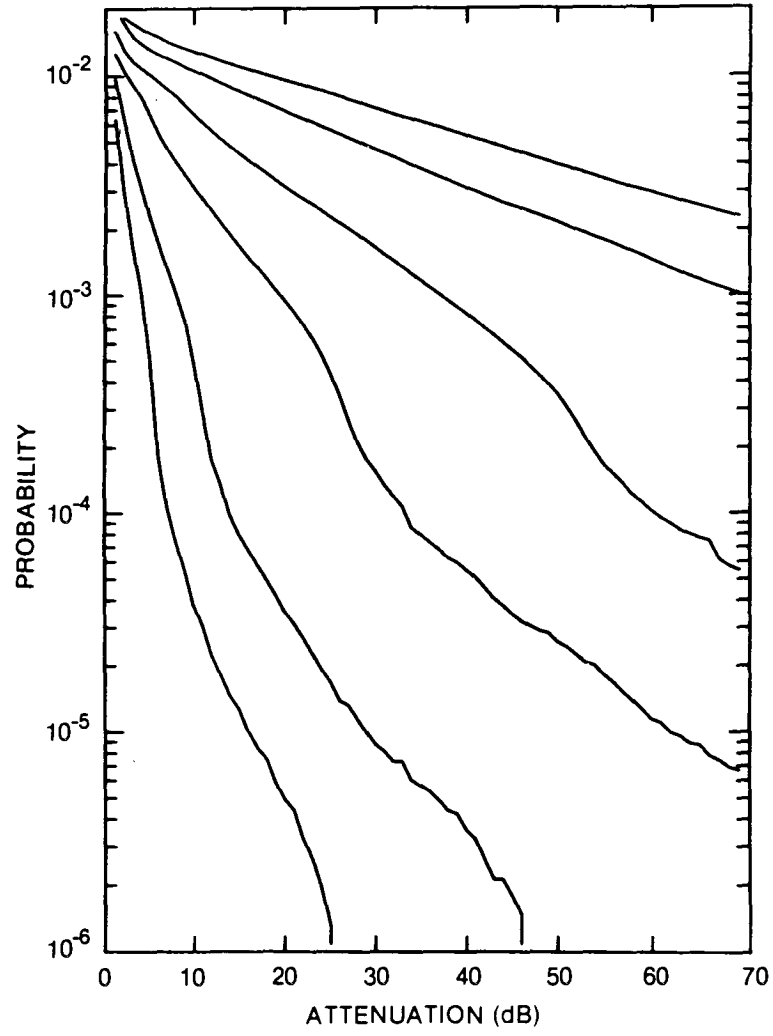

Figure 361. Cumulative distribution of rain attenuation for 100 GHz at Uranium City, SASK. Curves, moving from lowest to highest, are for hop lengths of 1, 2, 5, 10, 20 and 30 km, respectively.

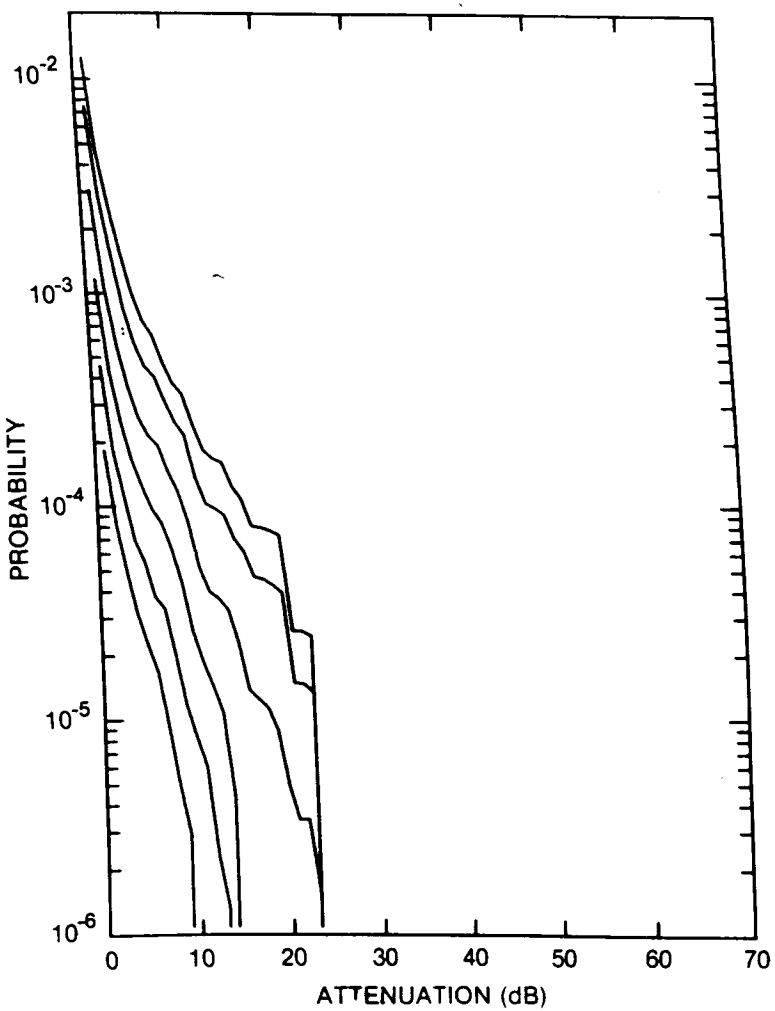

Figure 362. Cumulative distribution of rain attenuation for 8 GHz at Val d'Or, QUE. Curves, moving from lowest to highest, are for hop lengths of 5, 10, 20, 40, 80 and 120 km, respectively.

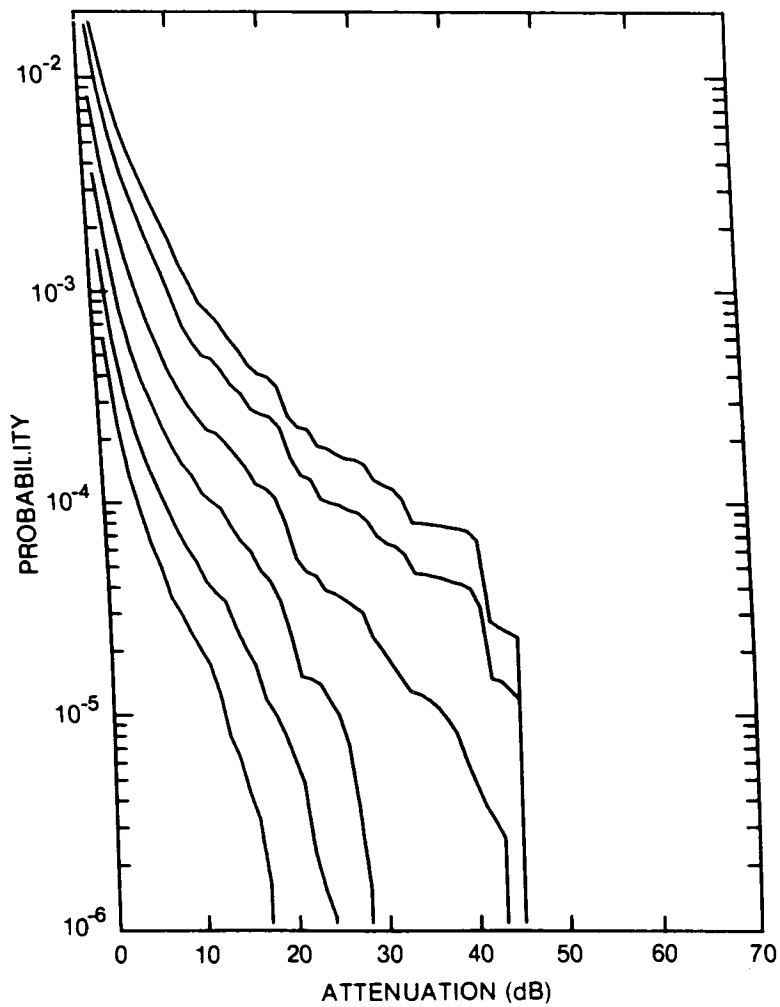

Figure 363. Cumulative distribution of rain attenuation for 11 GHz at Val d'Or, QUE. Curves, moving from lowest to highest, are for hop lengths of 5, 10, 20, 40, 80 and 120 km, respectively.

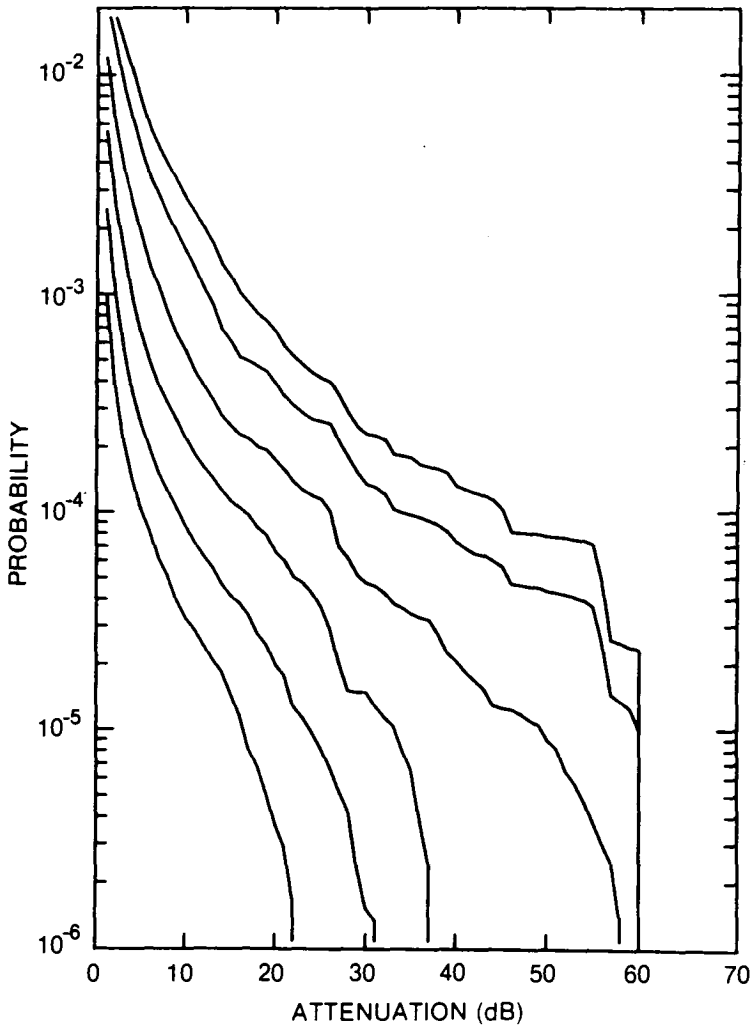

Figure 364. Cumulative distribution of rain attenuation for 12.8 GHz at Val d'Or, QUE. Curves moving from lowest to highest, are for hop lengths of 5, 10, 20, 40, 80 and 120 km, respectively.

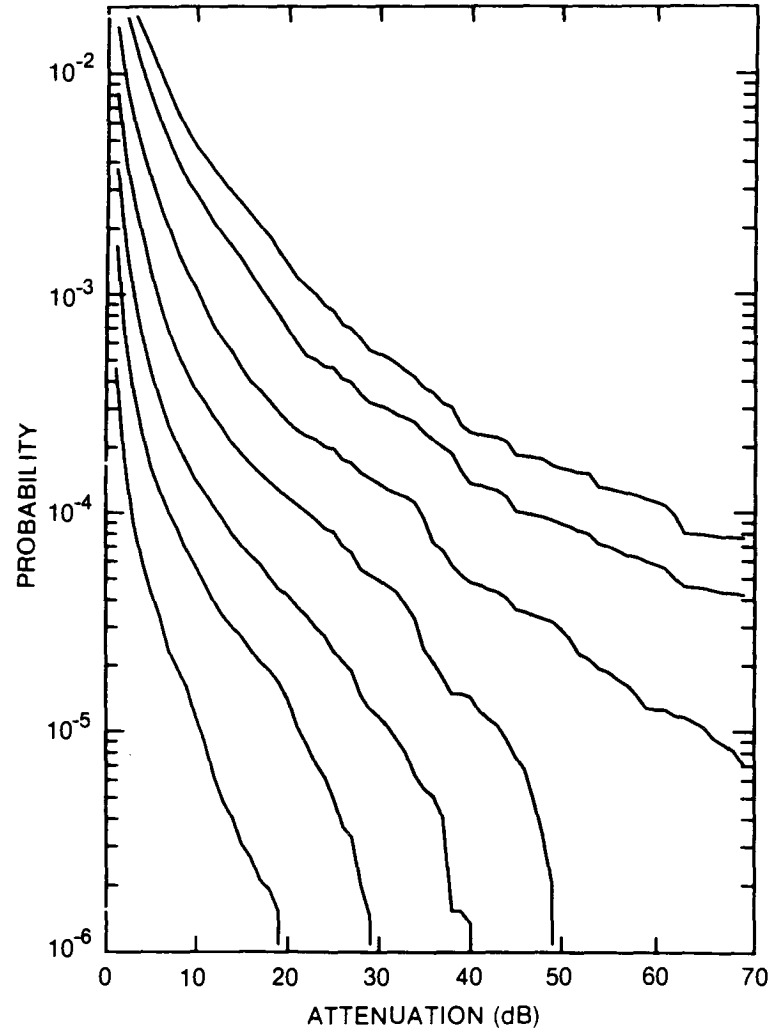

Figure 365. Cumulative distribution of rain attenuation for 15 GHz at Val d'Or, QUE. Curves, moving from lowest to highest, are for hop lengths of 2, 5, 10, 20, 40, 80 and 120 km, respectively.

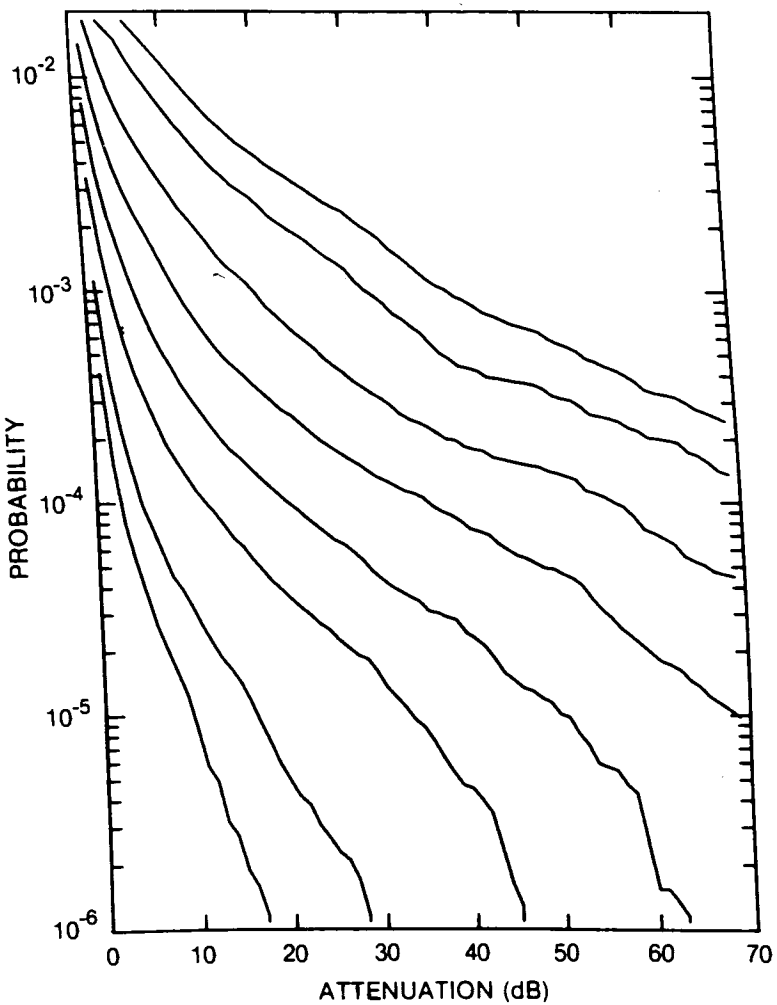

Figure 366. Cumulative distribution of rain attenuation for 20 GHz at Val d'Or, QUE. Curves, moving from lowest to highest, are for hop lengths of 1, 2, 5, 10, 20, 40, 80 and 120 km, respectively.

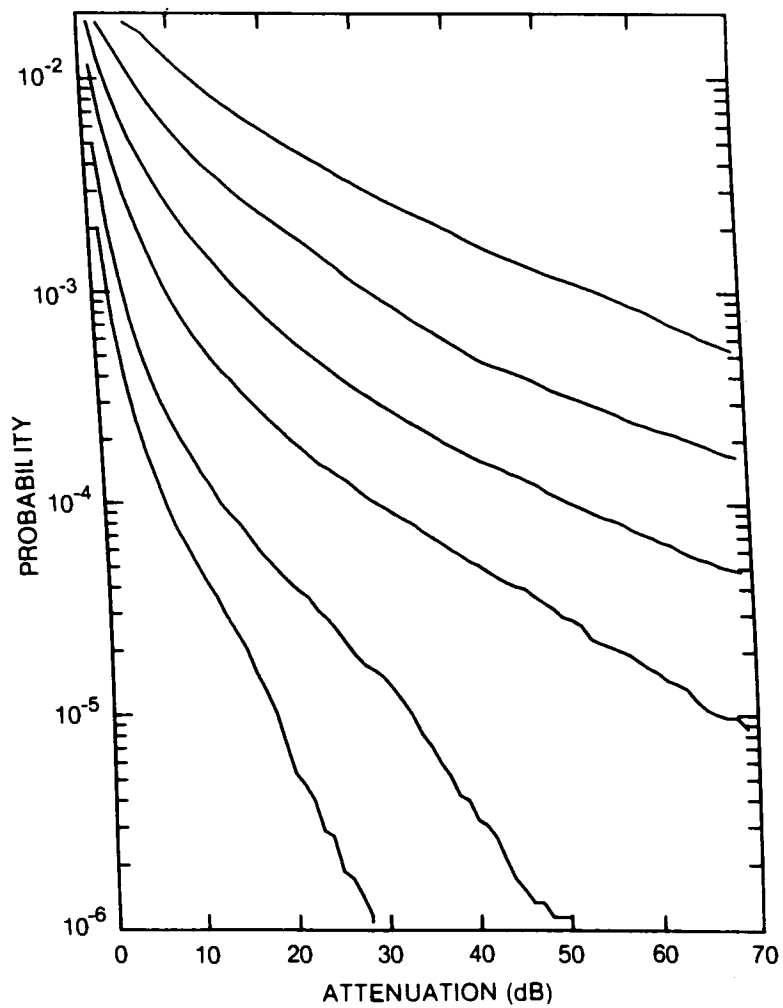

Figure 367. Cumulative distribution of rain attenuation for 35 GHz at Val d'Or, QUE. Curves, moving from lowest to highest, are for hop lengths of 1, 2, 5, 10, 20 and 40 km, respectively.

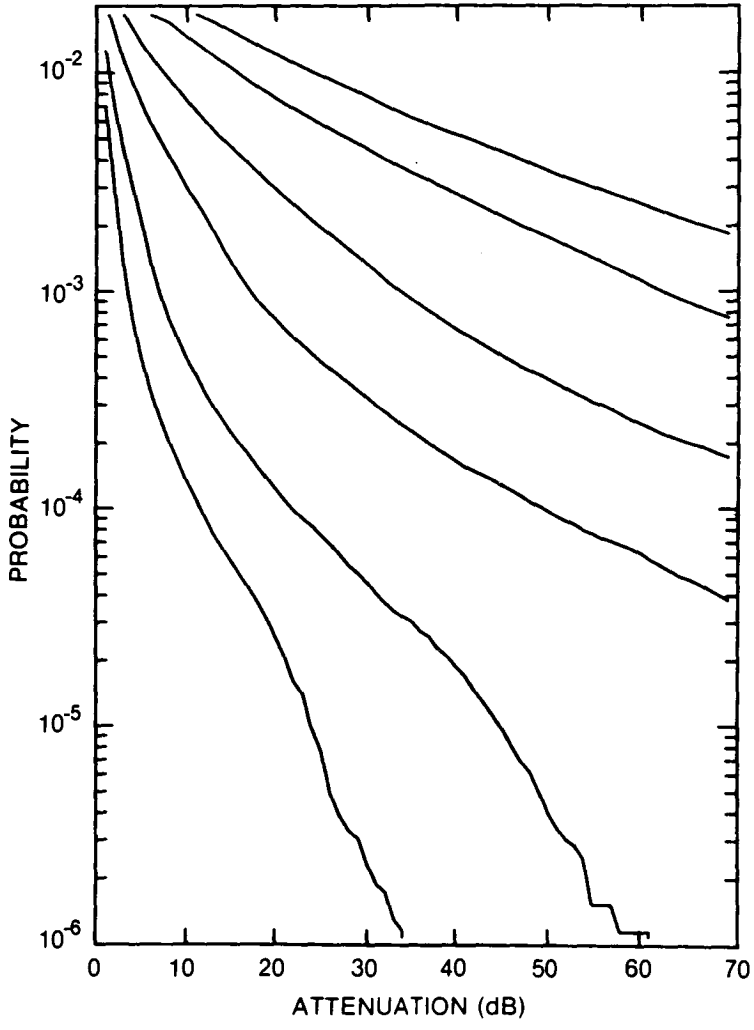

Figure 368. Cumulative distribution of rain attenuation for 56 GHz at Val d'Or, QUE. Curves, moving from lowest to highest, are for hop lengths of 1, 2, 5, 10, 20 and 30 km, respectively.

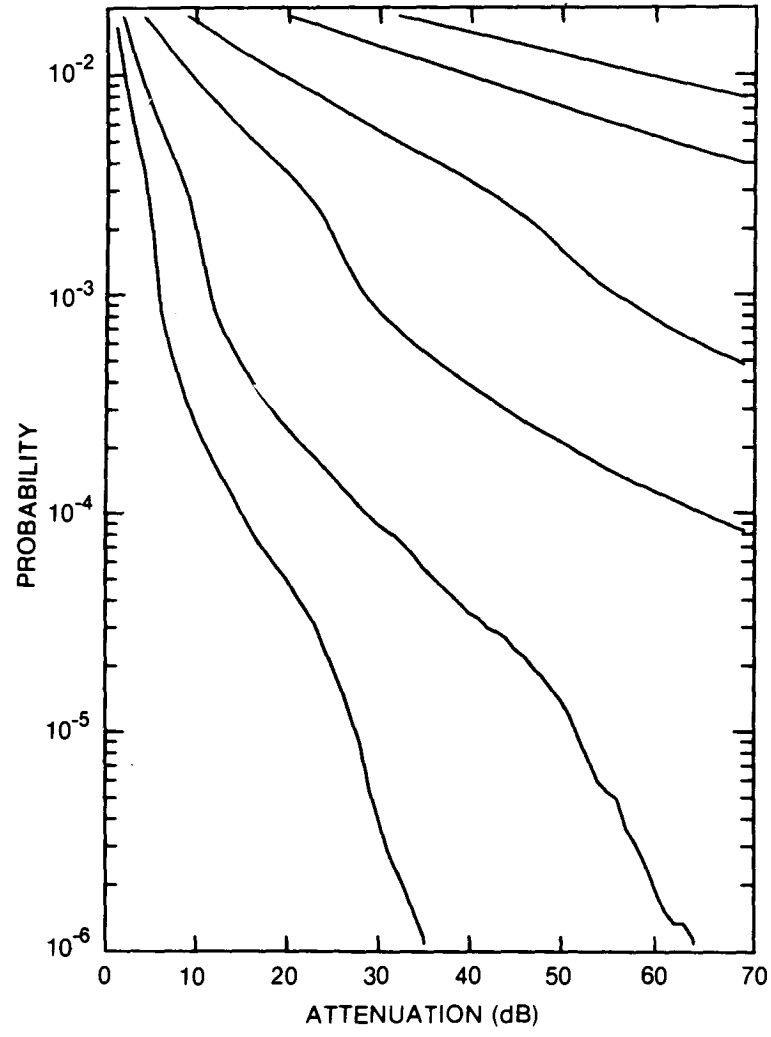

Figure 369. Cumulative distribution of rain attenuation for 100 GHz at Val d'Or, QUE. Curves, moving from lowest to highest, are for hop lengths of 1, 2, 5, 10, 20 and 30 km, respectively.

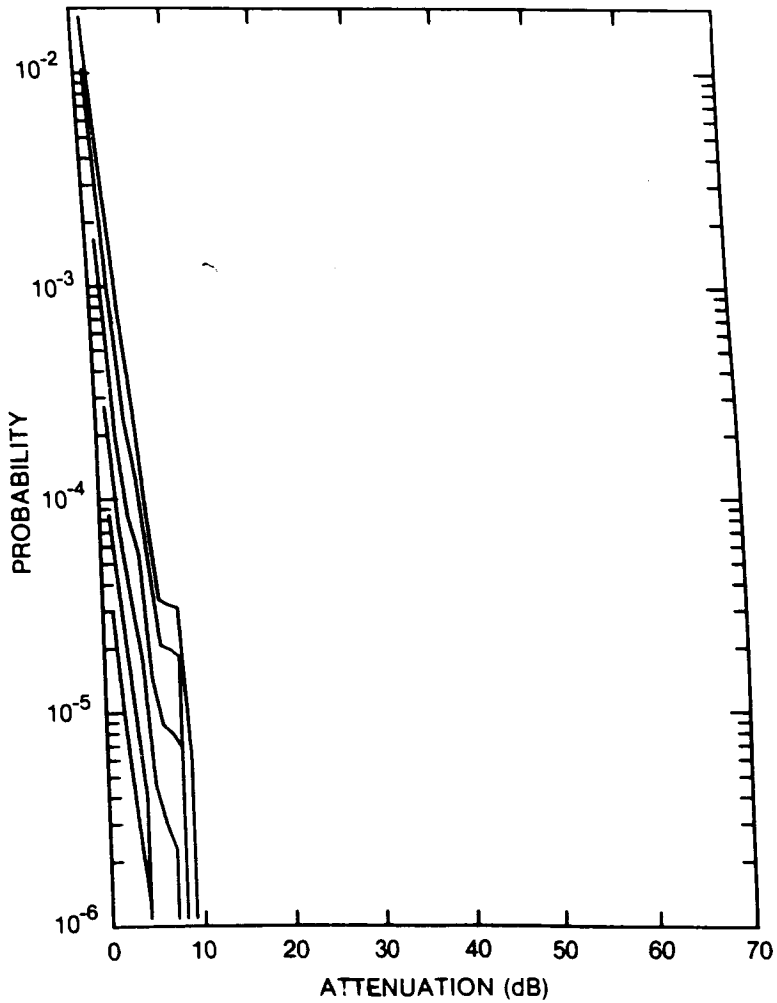

Figure 370. Cumulative distribution of rain attenuation for 8 GHz at Vancouver, BC. Curves, moving from lowest to highest, are for hop lengths of 5, 10, 20, 40, 80 and 120 km, respectively.

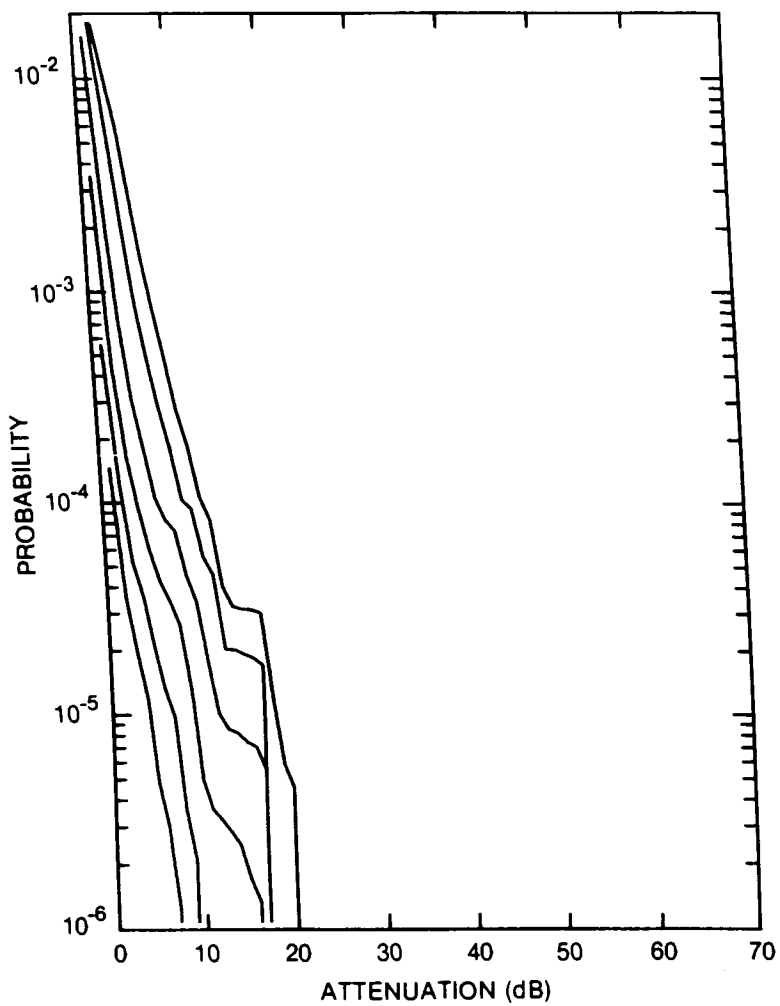

Figure 371. Cumulative distribution of rain attenuation for 11 GHz at Vancouver, BC. Curves, moving from lowest to highest, are for hop lengths of 5, 10, 20, 40, 80 and 120 km, respectively.

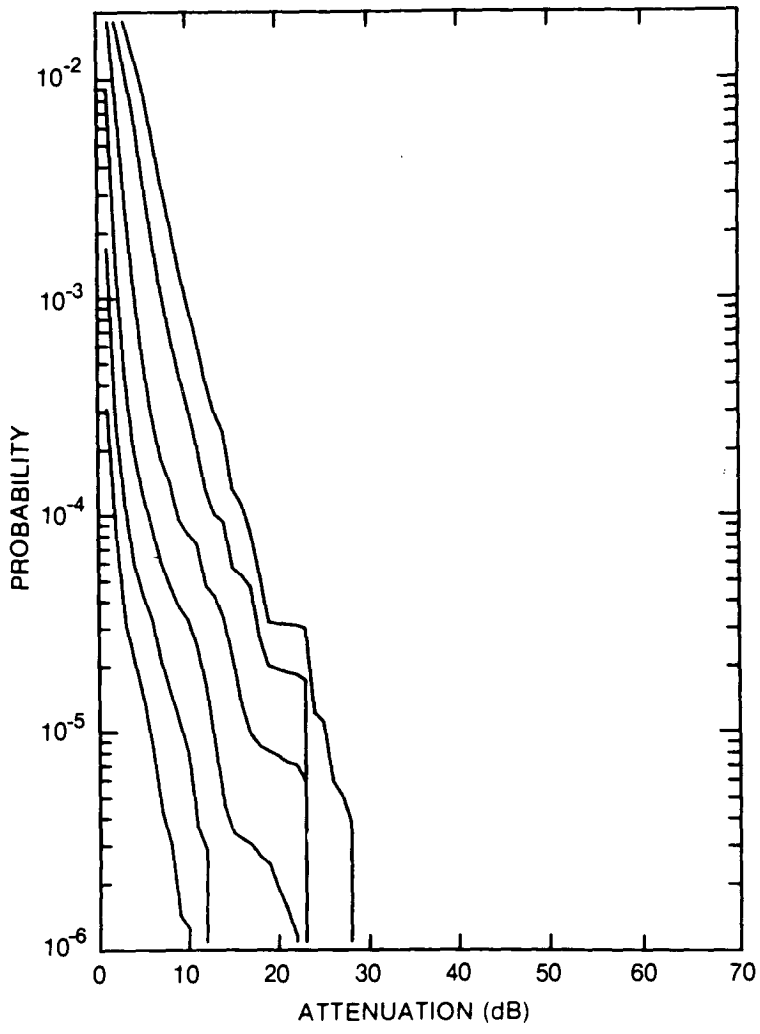

Figure 372. Cumulative distribution of rain attenuation for 12.8 GHz at Vancouver, BC. Curves, moving from lowest to highest, are for hop lengths of 5, 10, 20, 40, 80 and 120 km, respectively.

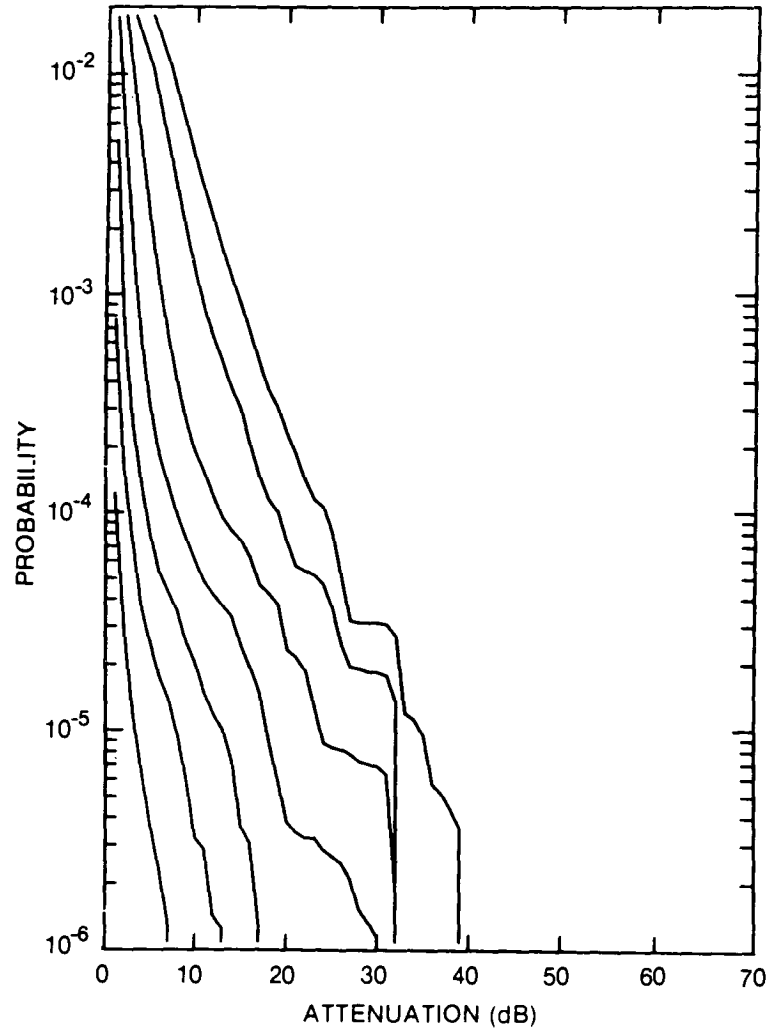

Figure 373. Cumulative distribution of rain attenuation for 15 GHz at Vancouver, BC. Curves, moving from lowest to highest, are for hop lengths of 2, 5, 10, 20, 40, 80 and 120 km, respectively.

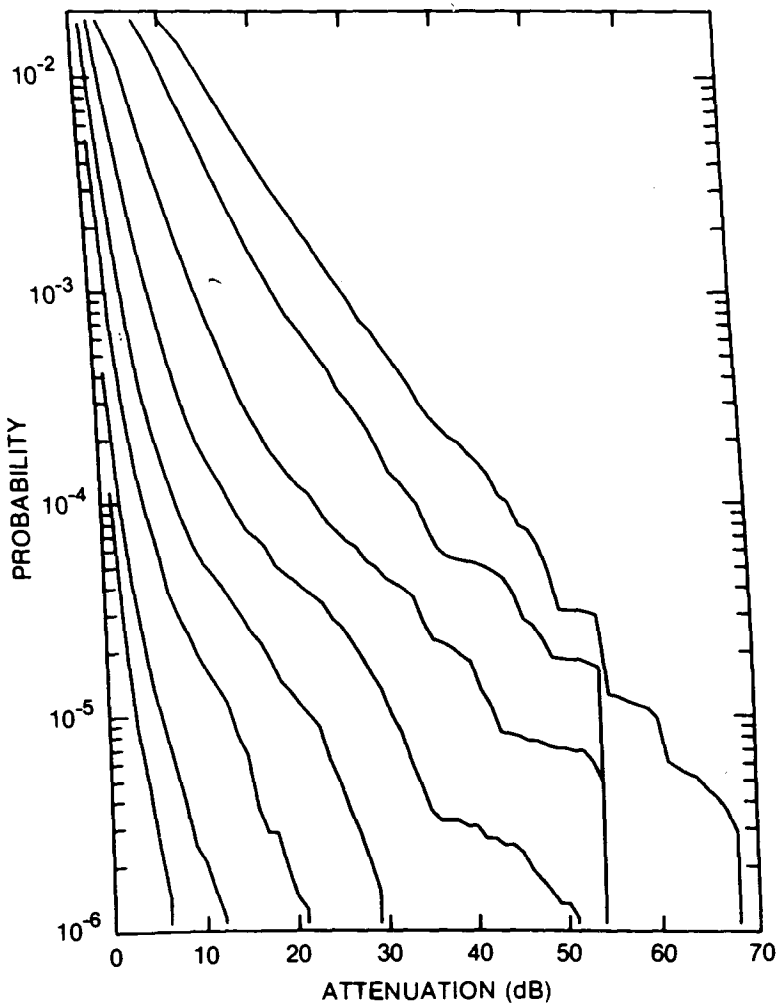

Figure 374. Cumulative distribution of rain attenuation for 20 GHz at Vancouver, BC. Curves, moving from lowest to highest, are for hop lengths of 1, 2, 5, 10, 20, 40, 80 and 120 km, respectively.

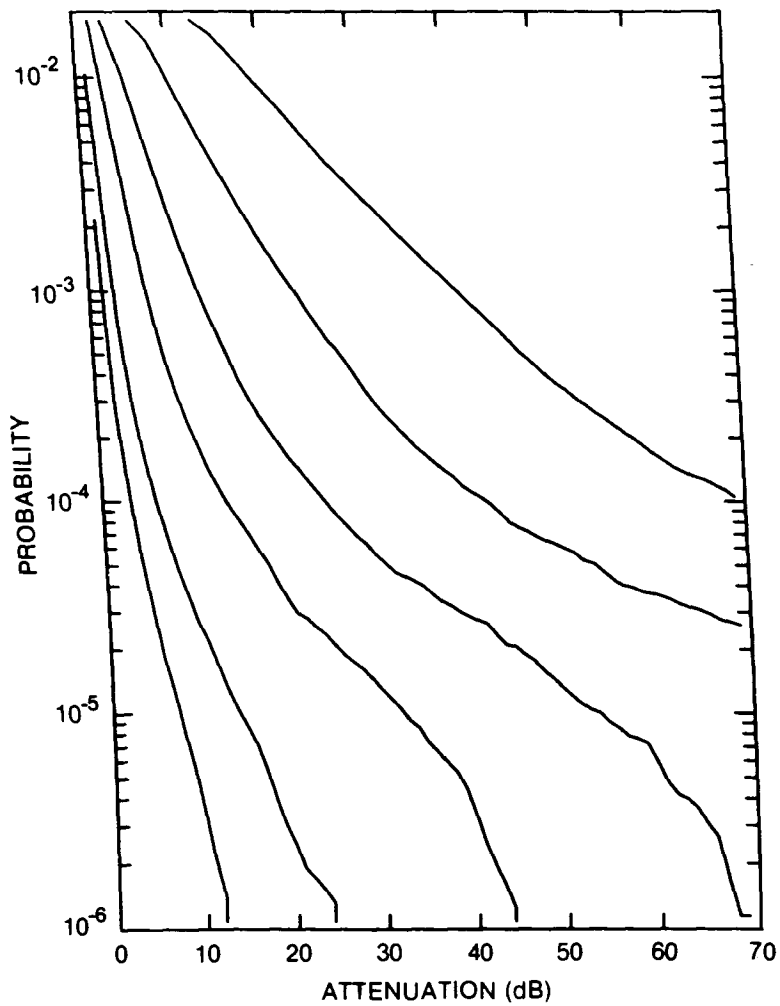

Figure 375. Cumulative distribution of rain attenuation for 35 GHz at Vancouver, BC. Curves, moving from lowest to highest, are for hop lengths of 1, 2, 5, 10, 20 and 40 km, respectively.

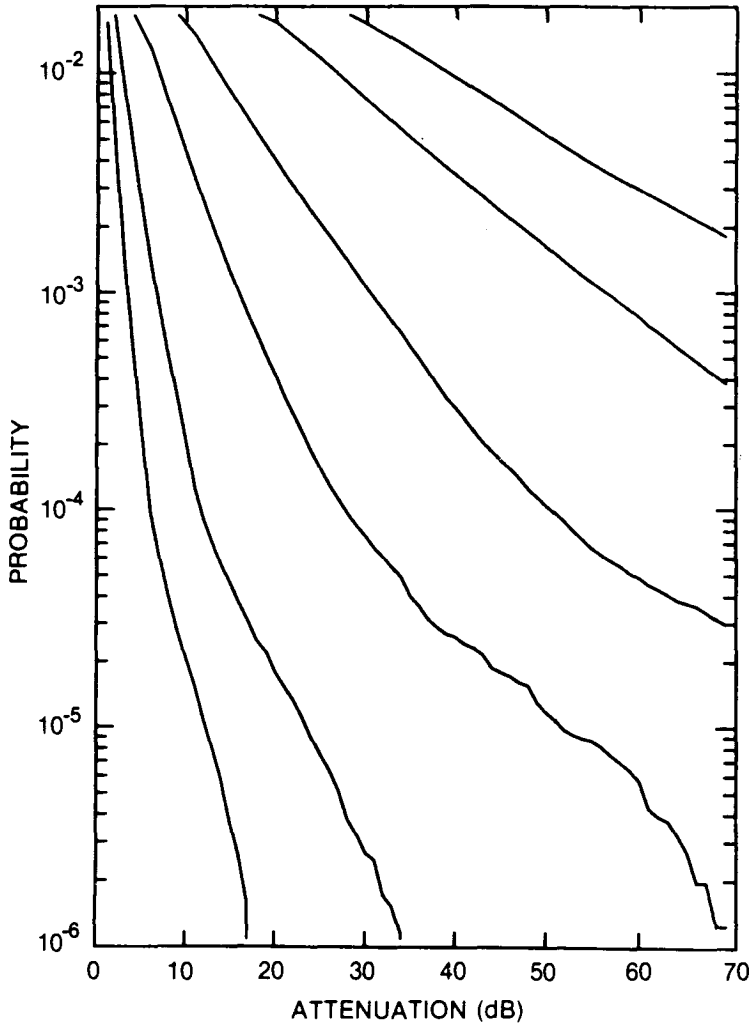

Figure 376. Cumulative distribution of rain attenuation for 56 GHz at Vancouver, BC. Curves, moving from lowest to highest, are for hop lengths of 1, 2, 5, 10, 20 and 30 km, respectively.

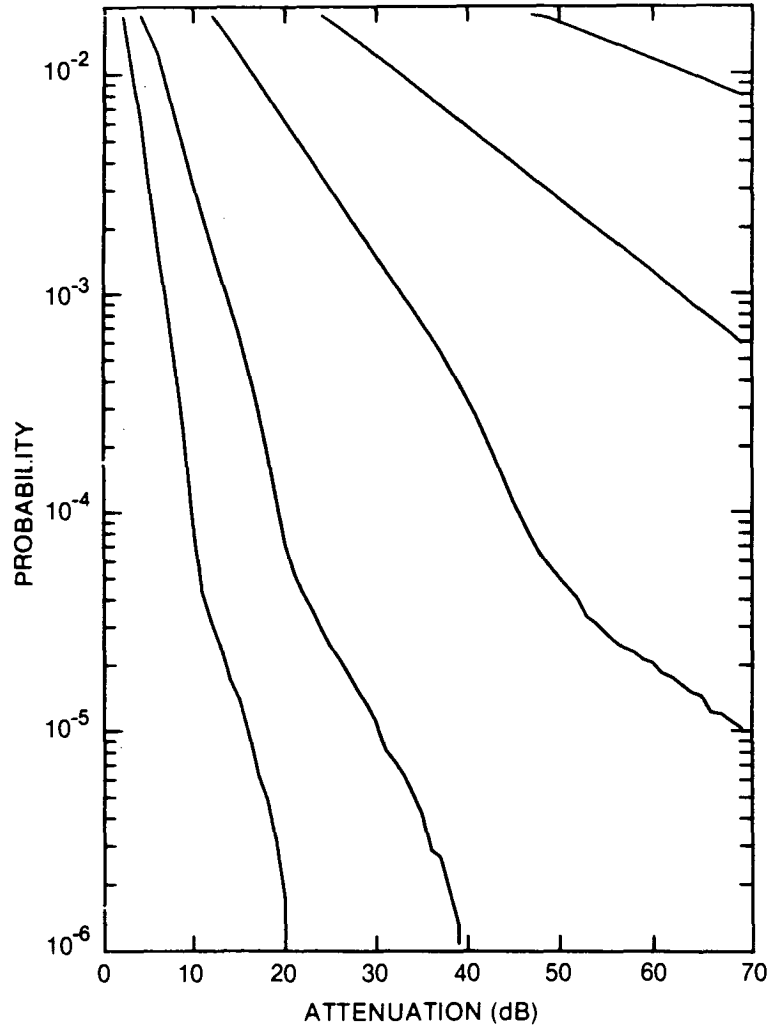

Figure 377. Cumulative distribution of rain attenuation for 100 GHz at Vancouver, BC. Curves, moving from lowest to highest, are for hop lengths of 1, 2, 5, 10 and 20 km, respectively.

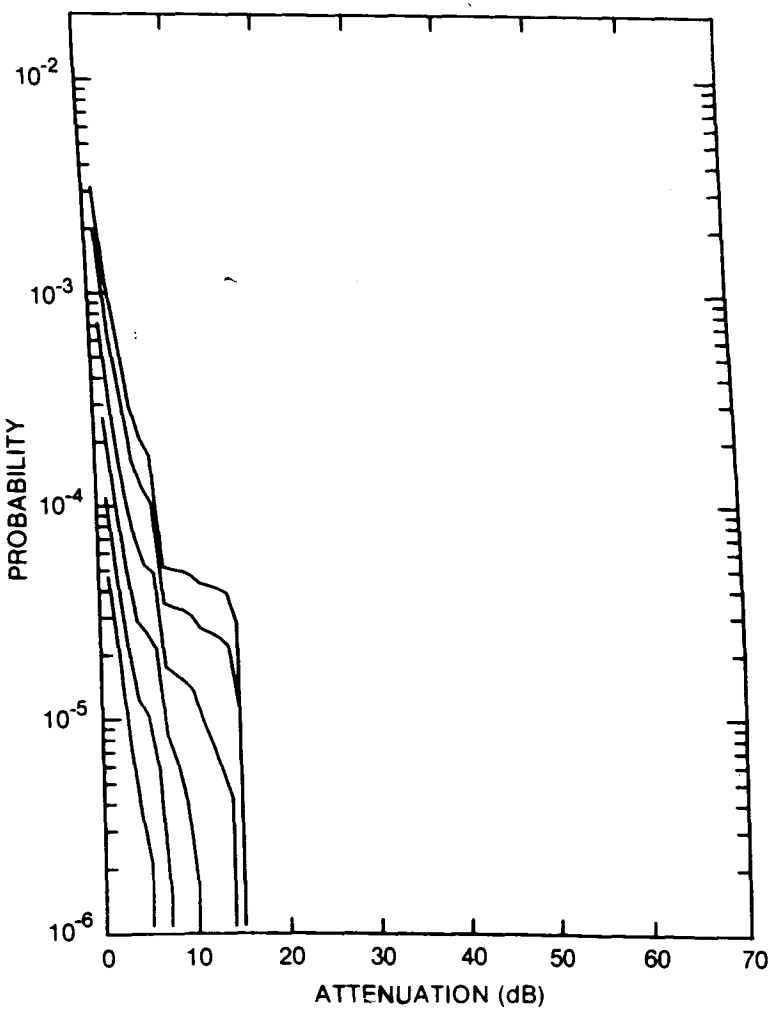

Figure 378. Cumulative distribution of rain attenuation for 8 GHz at Watino, ALTA. Curves, moving from lowest to highest, are for hop lengths of 5, 10, 20, 40, 80 and 120 km, respectively.

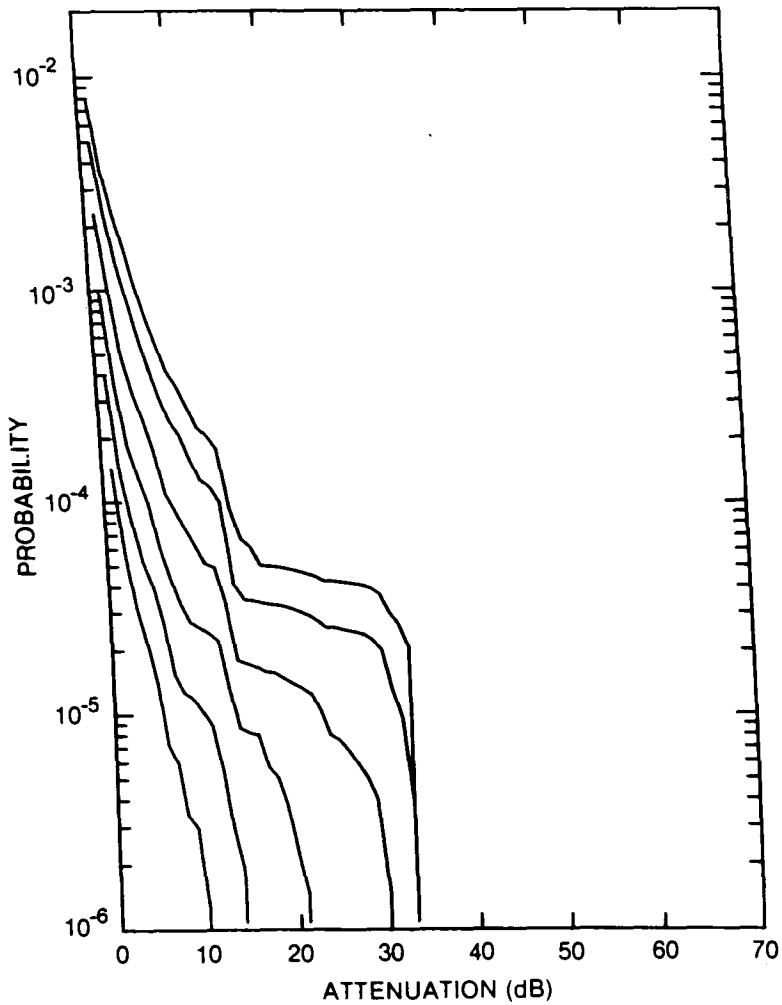

Figure 379. Cumulative distribution of rain attenuation for 11 GHz at Watino, ALTA. Curves, moving from lowest to highest, are for hop lengths of 5, 10, 20, 40, 80 and 120 km, respectively.

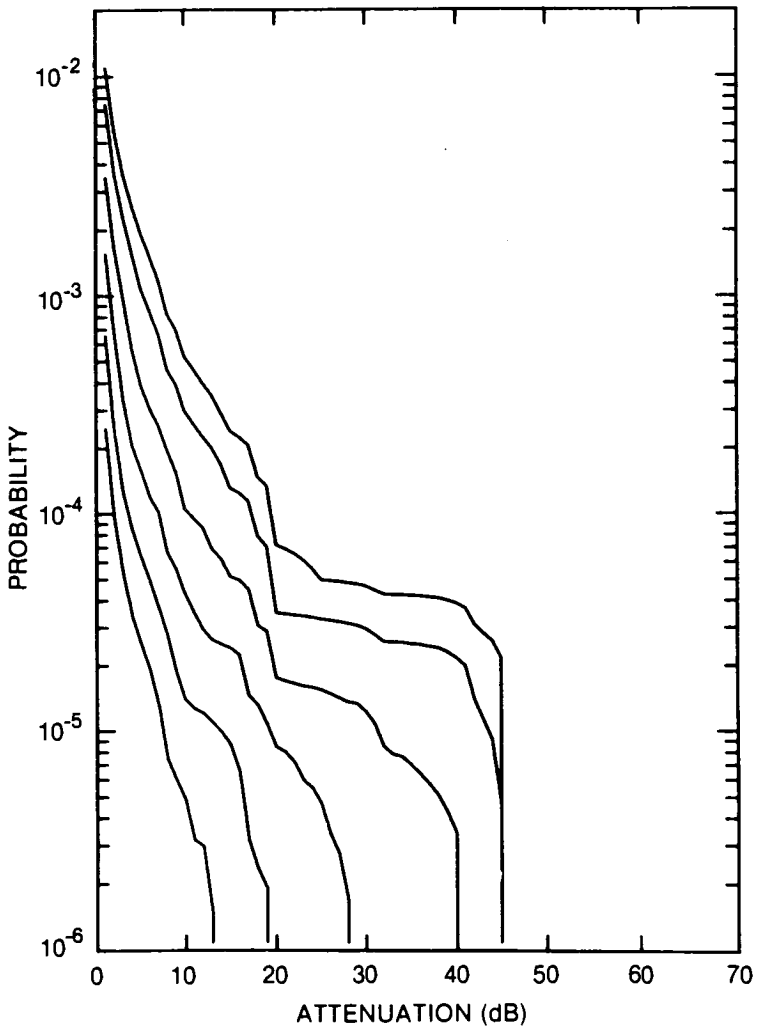

Figure 380. Cumulative distribution of rain attenuation for 12.8 GHz at Watino, ALTA. Curves, moving from lowest to highest, are for hop lengths of 5, 10, 20, 40, 80 and 120 km, respectively.

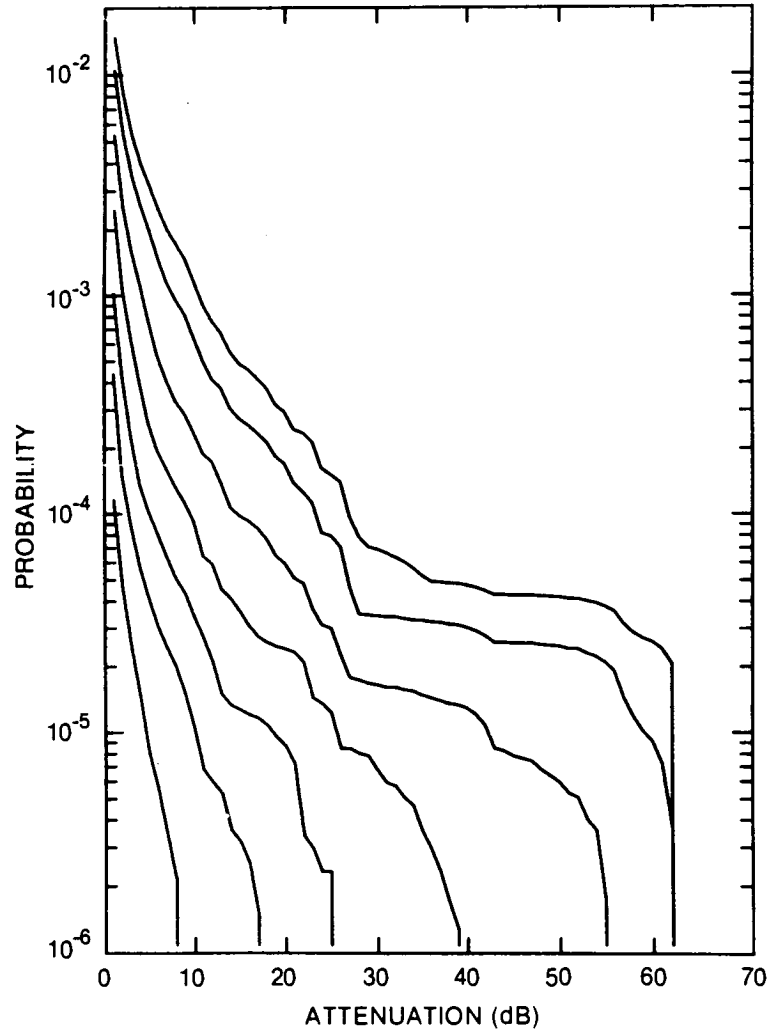

Figure 381. Cumulative distribution of rain attenuation for 15 GHz at Watino, ALTA. Curves, moving from lowest to highest, are for hop lengths of 2, 5, 10, 20, 40, 80 and 120 km, respectively.

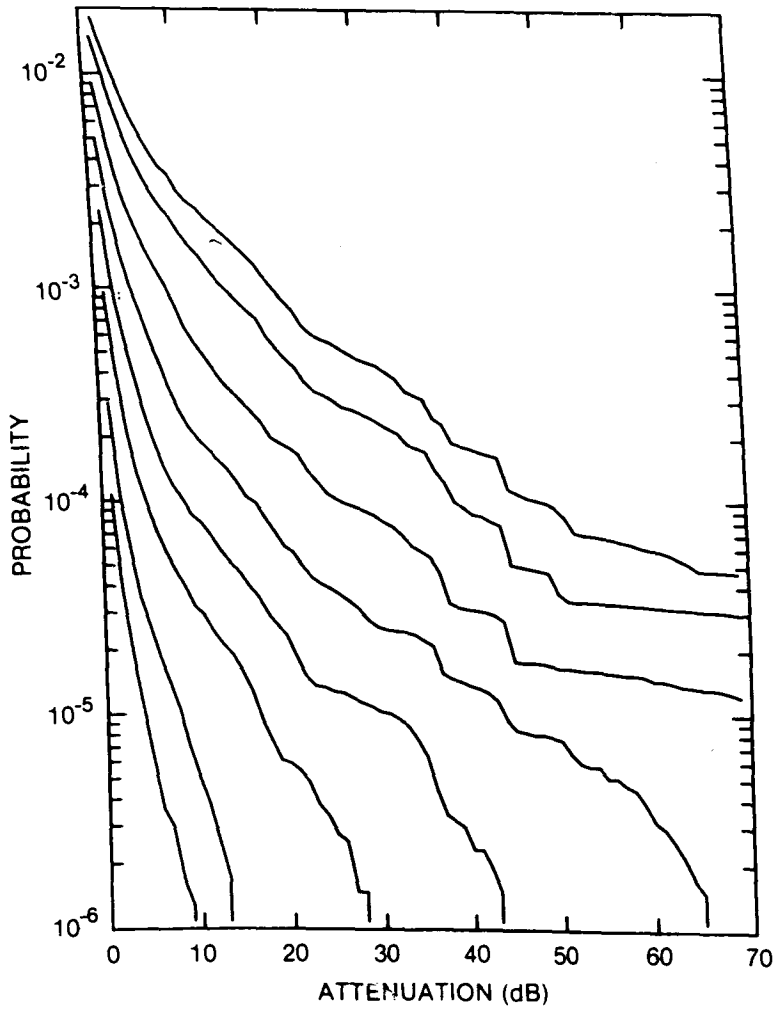

Figure 382. Cumulative distribution of rain attenuation for 20 GHz at Watino, ALTA. Curves, moving from lowest to highest, are for hop lengths of 1, 2, 5, 10, 20, 40, 80 and 120 km, respectively.

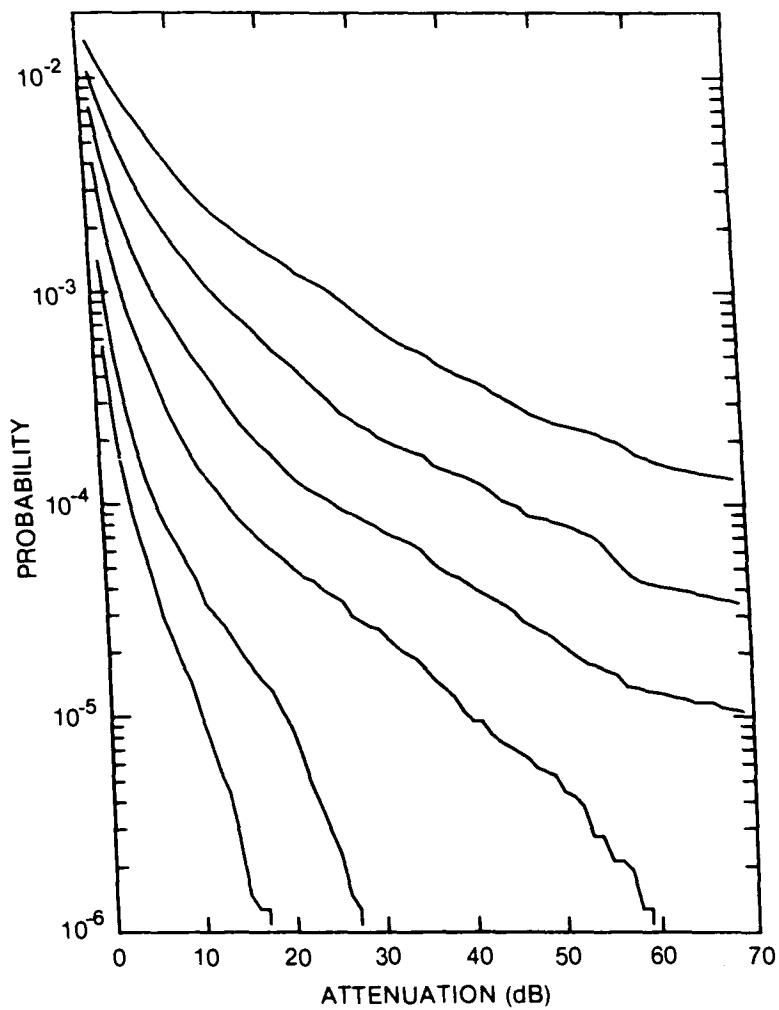

Figure 383. Cumulative distribution of rain attenuation for 35 GHz at Watino, ALTA. Curves, moving from lowest to highest, are for hop lengths of 1, 2, 5, 10, 20 and 40 km, respectively.

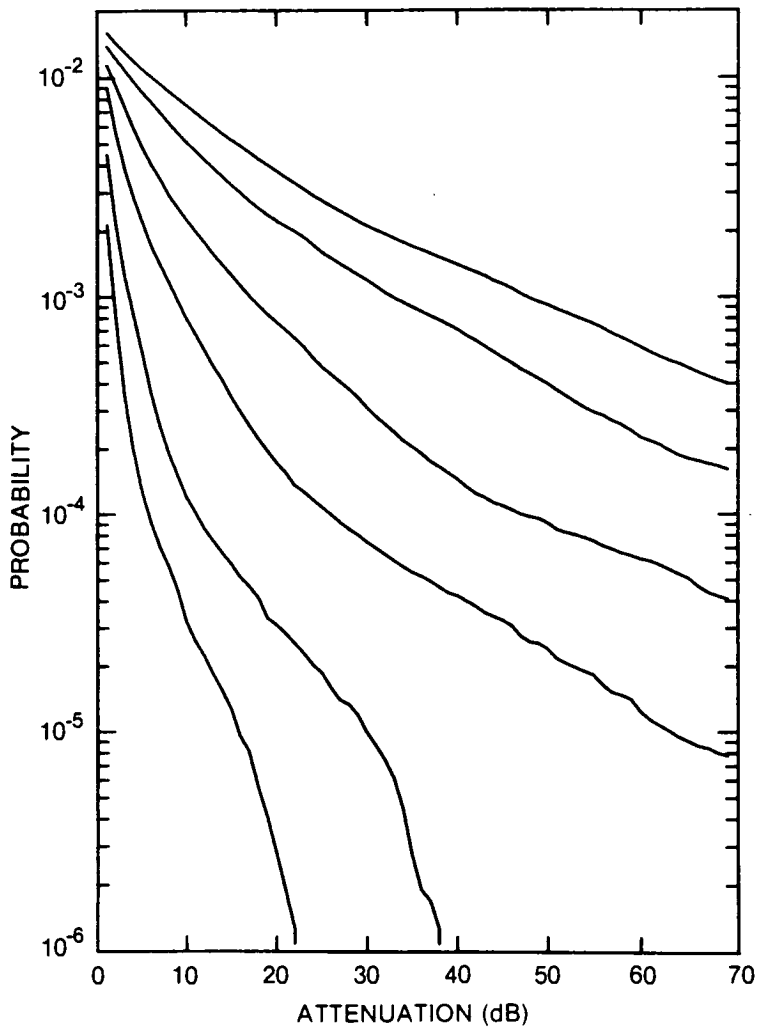

Figure 384. Cumulative distribution of rain attenuation for 56 GHz at Watino, ALTA. Curves, moving from lowest to highest, are for hop lengths of 1, 2, 5, 10, 20 and 30 km, respectively.

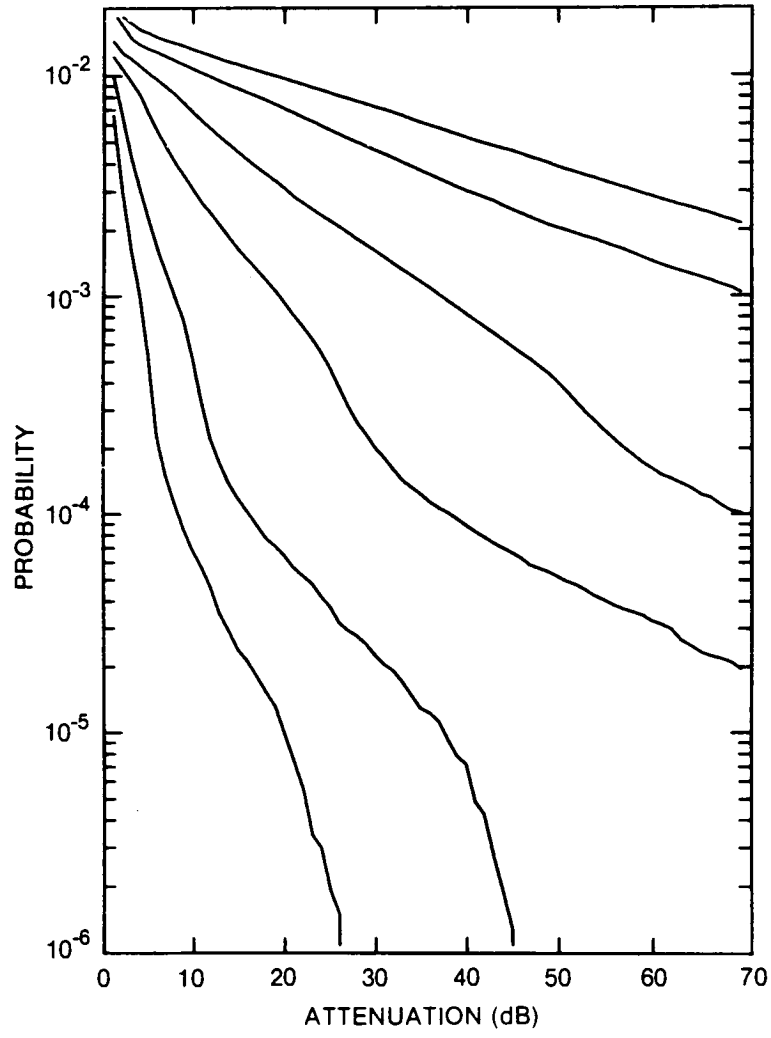

Figure 385. Cumulative distribution of rain attenuation for 100 GHz at Watino, ALTA. Curves, moving from lowest to highest, are for hop lengths of 1, 2, 5, 10, 20 and 30 km, respectively.

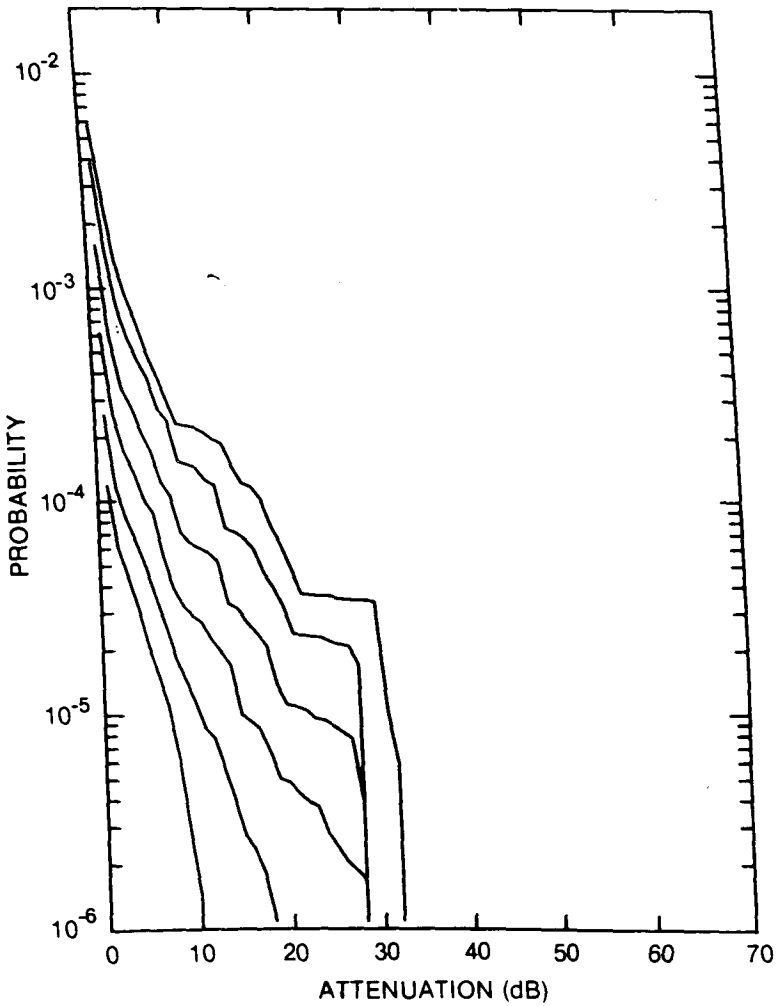

Figure 386. Cumulative distribution of rain attenuation for 8 GHz at Weyburn, SASK. Curves, moving from lowest to highest, are for hop lengths of 5, 10, 20, 40, 80 and 120 km, respectively.

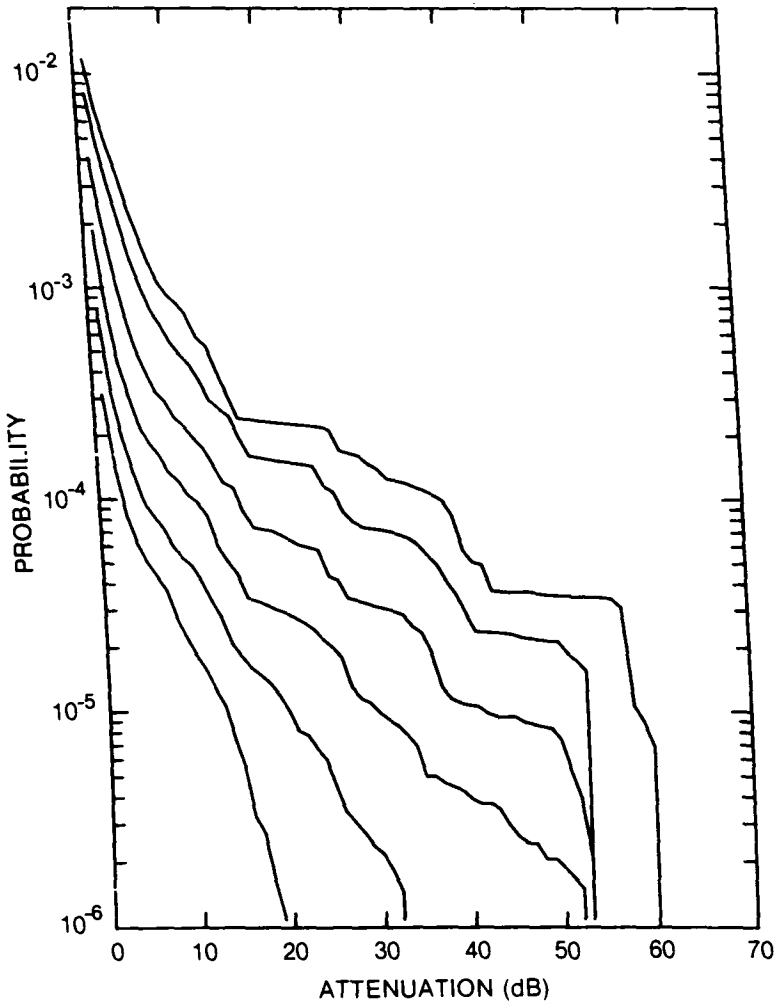

Figure 387. Cumulative distribution of rain attenuation for 11 GHz at Weyburn, SASK. Curves, moving from lowest to highest, are for hop lengths of 5, 10, 20, 40, 80 and 120 km, respectively.

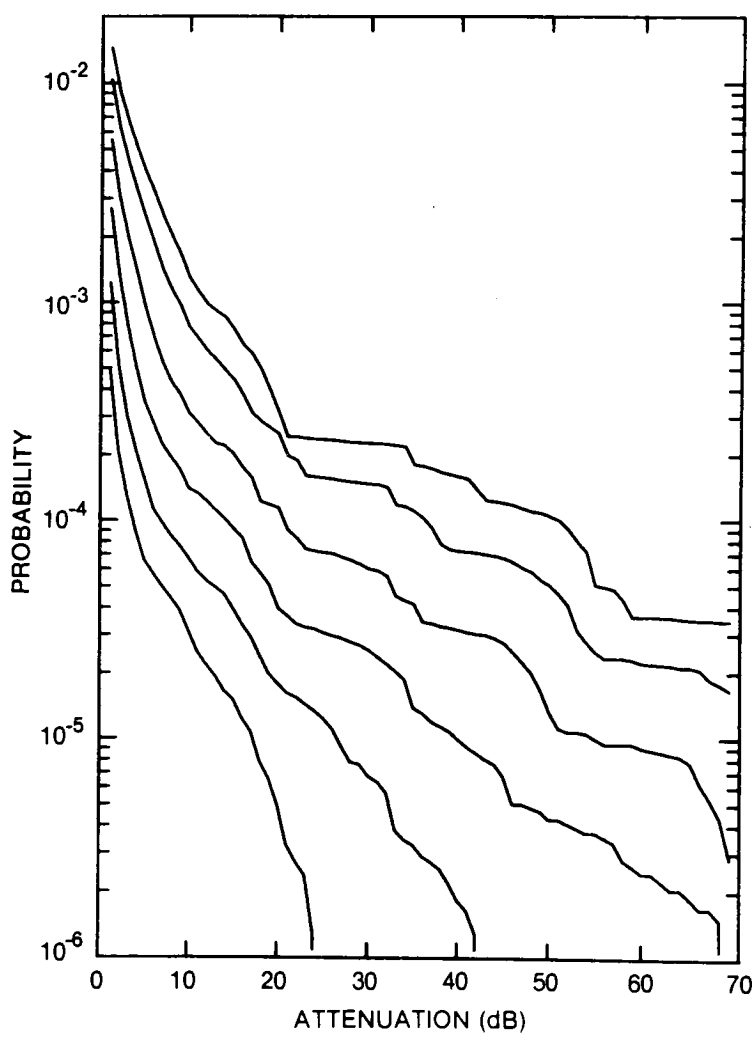

Figure 388. Cumulative distribution of rain attenuation for 12.8 GHz at Weyburn, SASK. Curves, moving from lowest to highest, are for hop lengths of 5, 10, 20, 40, 80 and 120 km, respectively.

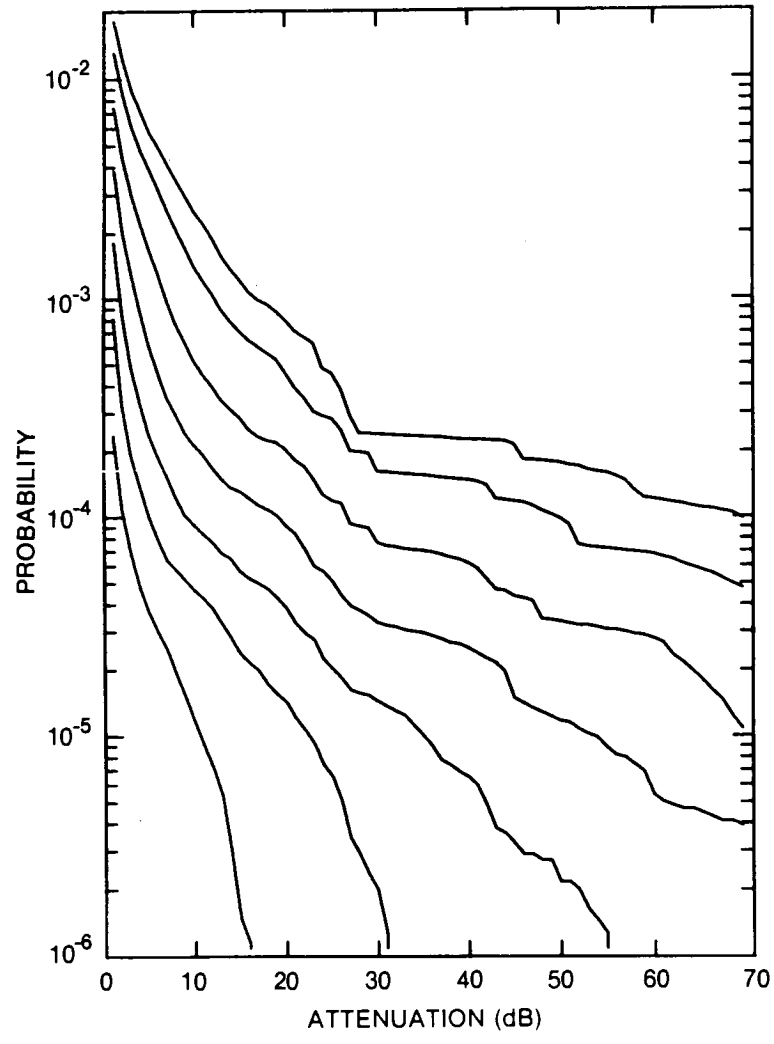

Figure 389. Cumulative distribution of rain attenuation for 15 GHz at Weyburn, SASK. Curves, moving from lowest to highest, are for hop lengths of 2, 5, 10, 20, 40, 80 and 120 km, respectively.

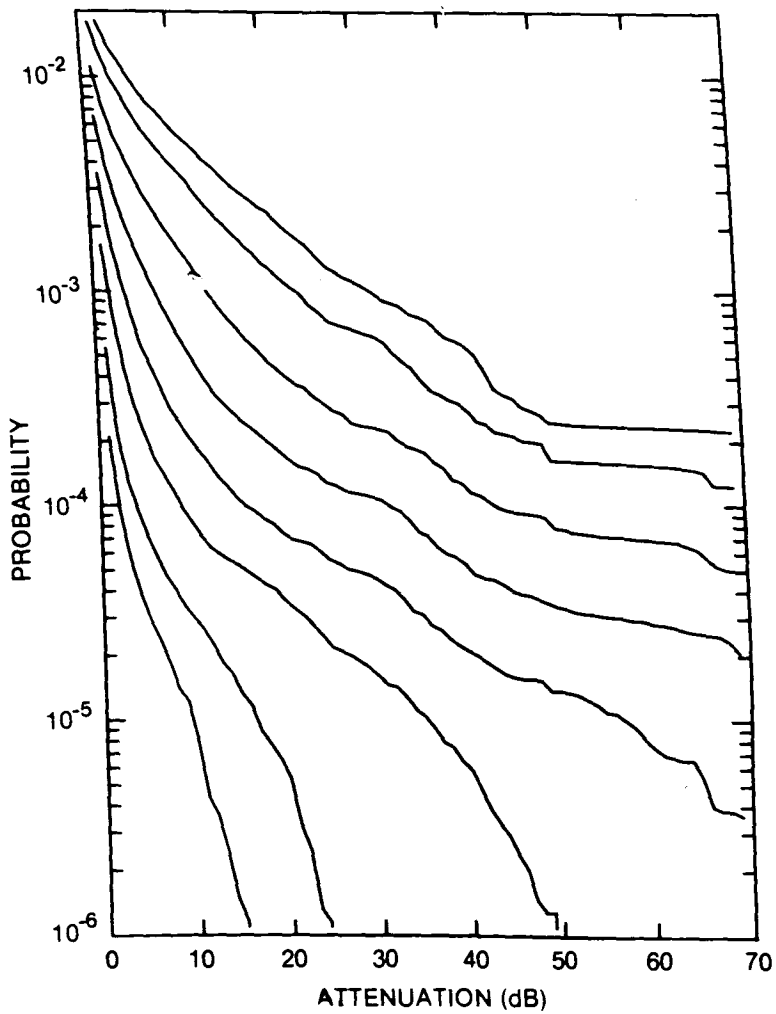

Figure 390. Cumulative distribution of rain attenuation for 20 GHz at Weyburn, SASK. Curves, moving from lowest to highest, are for hop lengths of 1, 2, 5, 10, 20, 40, 80 and 120 km, respectively.

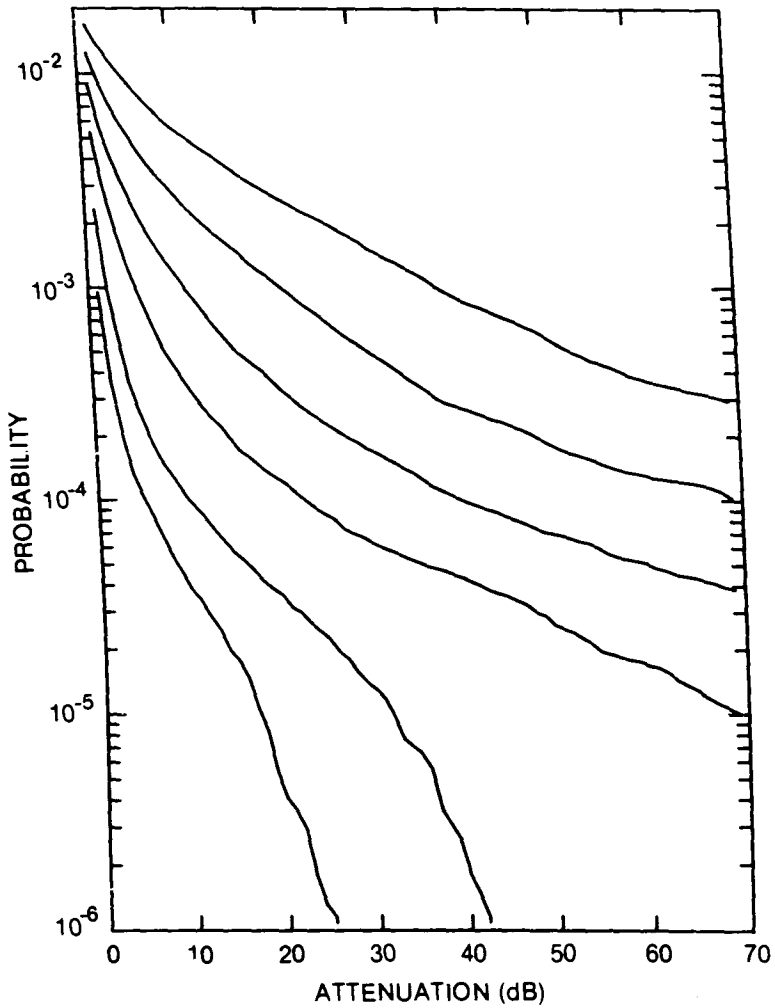

Figure 391. Cumulative distribution of rain attenuation for 35 GHz at Weyburn, SASK. Curves, moving from lowest to highest, are for hop lengths of 1, 2, 5, 10, 20 and 40 km, respectively.

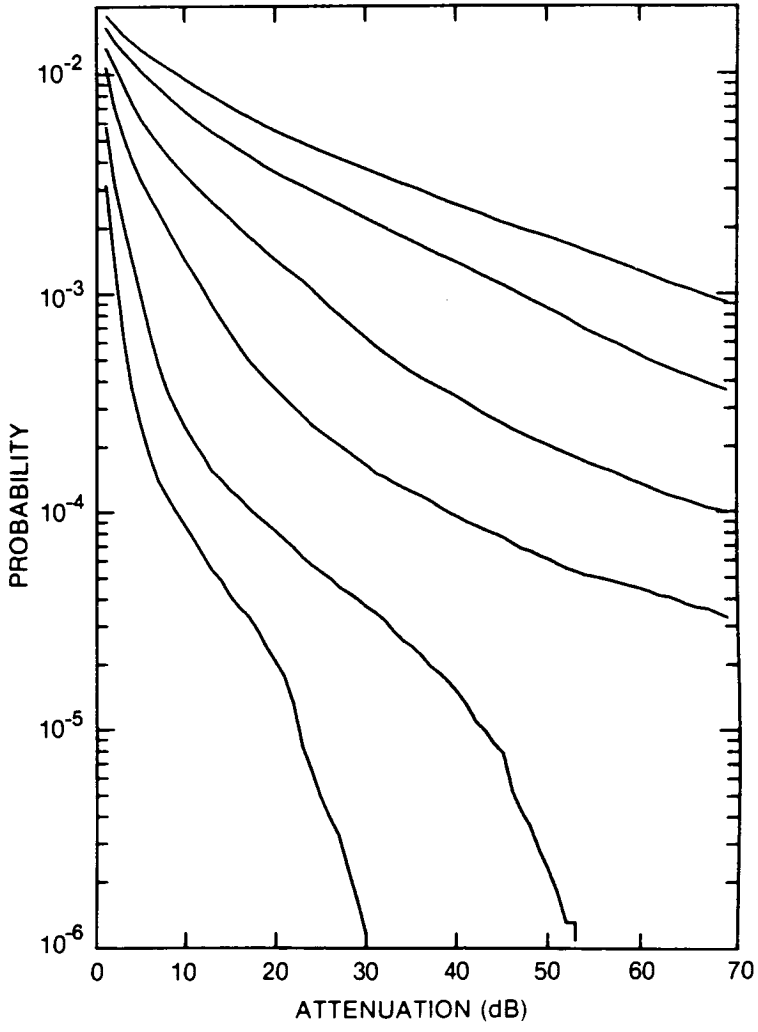

Figure 392. Cumulative distribution of rain attenuation for 56 GHz at Weyburn, SASK. Curves, moving from lowest to highest, are for hop lengths of 1, 2, 5, 10, 20 and 30 km, respectively.

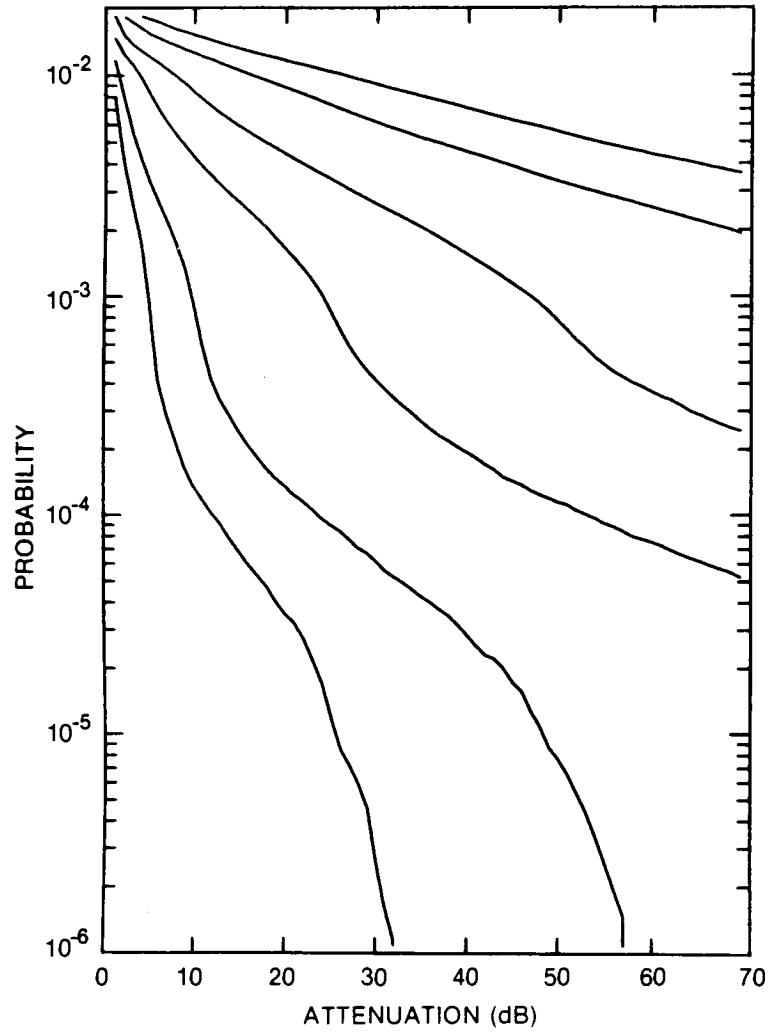

Figure 393. Cumulative distribution of rain attenuation for 100 GHZ at Weyburn, SASK. Curves, moving from lowest to highest, are for hop lengths of 1, 2, 5, 10, 20 and 30 km, respectively.

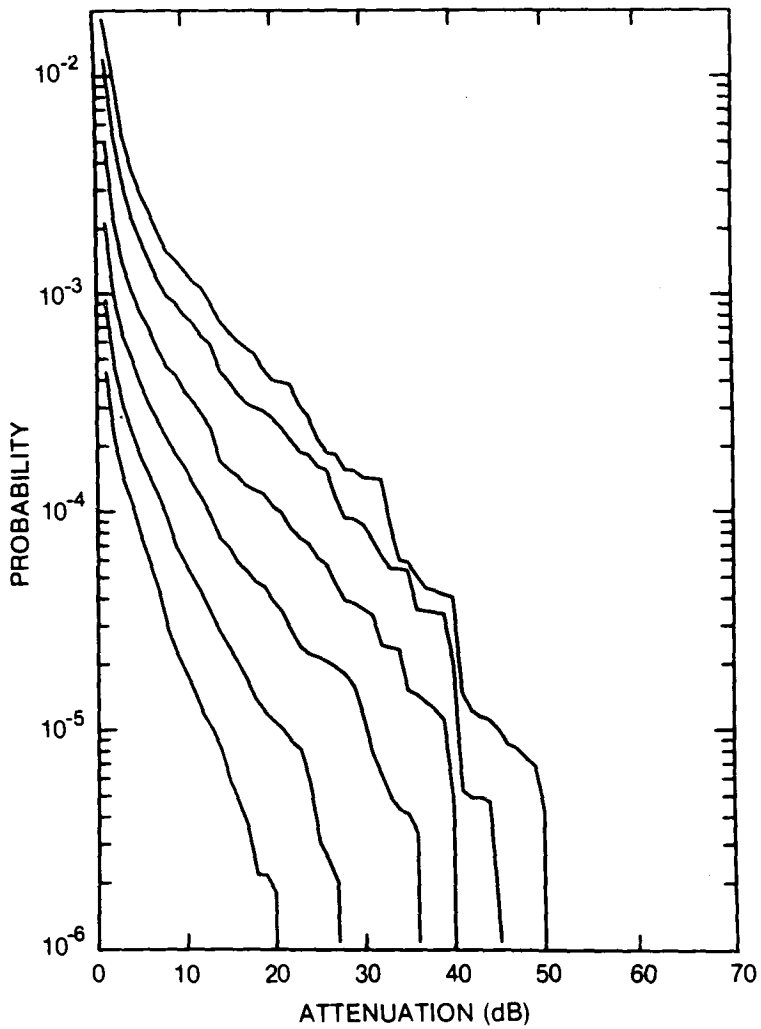

Figure 394. Cumulative distribution of rain attenuation for 8 GHz at Windsor, ONT. Curves, moving from lowest to highest, are for hop lengths of 5, 10, 20, 40, 80 and 120 km, respectively.

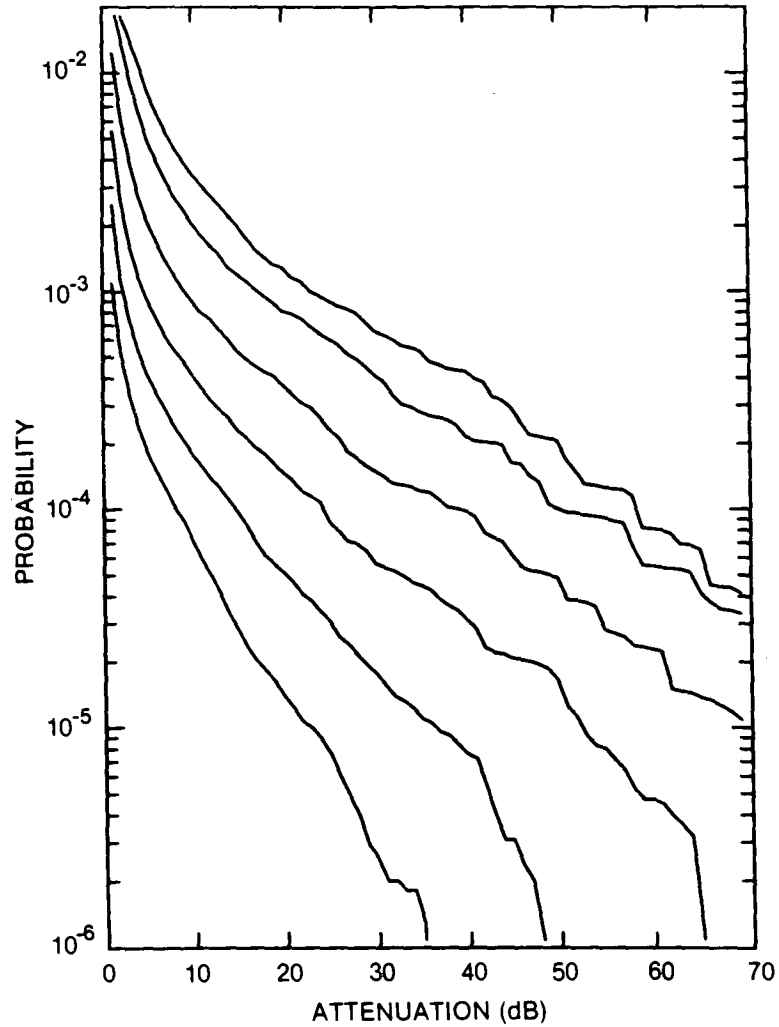

Figure 395. Cumulative distribution of rain attenuation for 11 GHz at Windsor, ONT. Curves, moving from lowest to highest, are for hop lengths of 5, 10, 20, 40, 80 and 120 km, respectively.

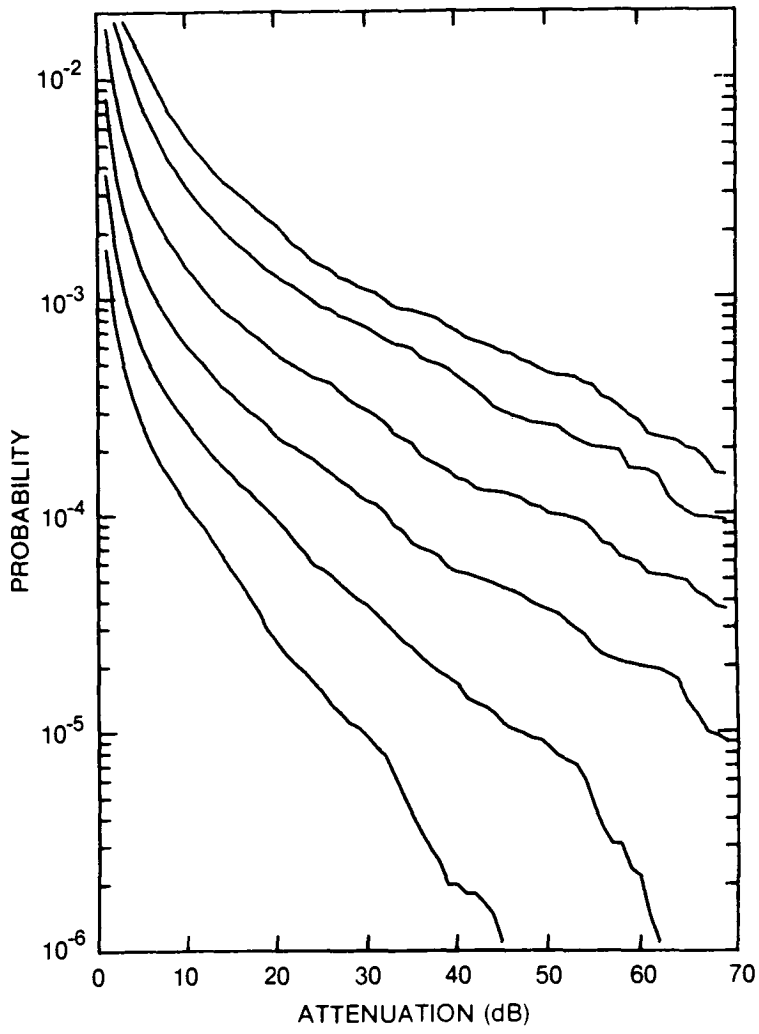

Figure 396. Cumulative distribution of rain attenuation for 12.8 GHz at Windsor, ONT. Curves, moving from lowest to highest, are for hop lengths of 5, 10, 20, 40, 80 and 120 km, respectively.

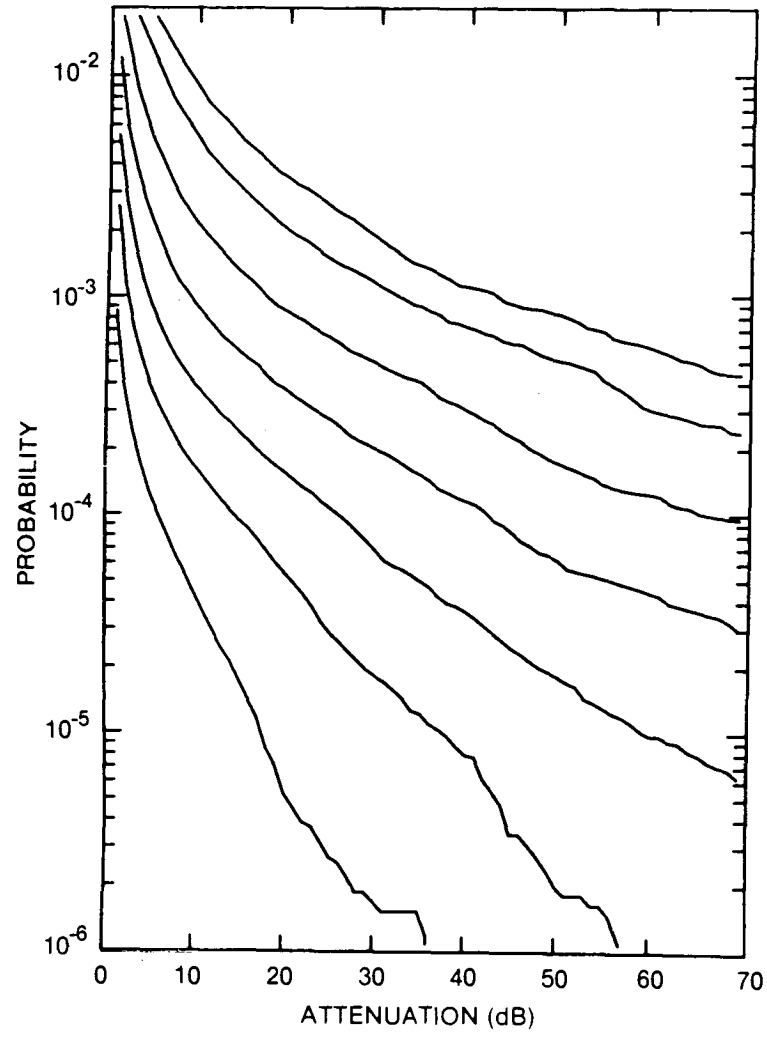

Figure 397. Cumulative distribution of rain attenuation for 15 GHz at Windsor, ONT. Curves, moving from lowest to highest, are for hop lengths of 2, 5, 10, 20, 40, 80 and 120 km, respectively.

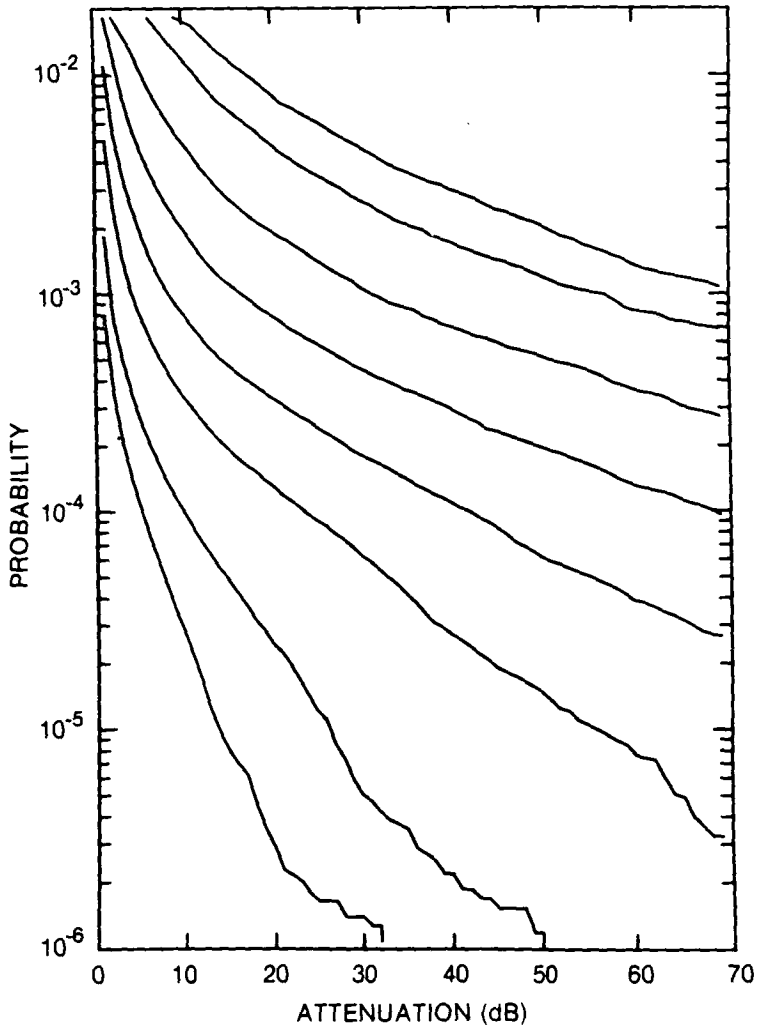

Figure 398. Cumulative distribution of rain attenuation for 20 GHz at Windsor, ONT. Curves, moving from lowest to highest, are for hop lengths of 1, 2, 5, 10, 20, 40, 80 and 120 km, respectively.

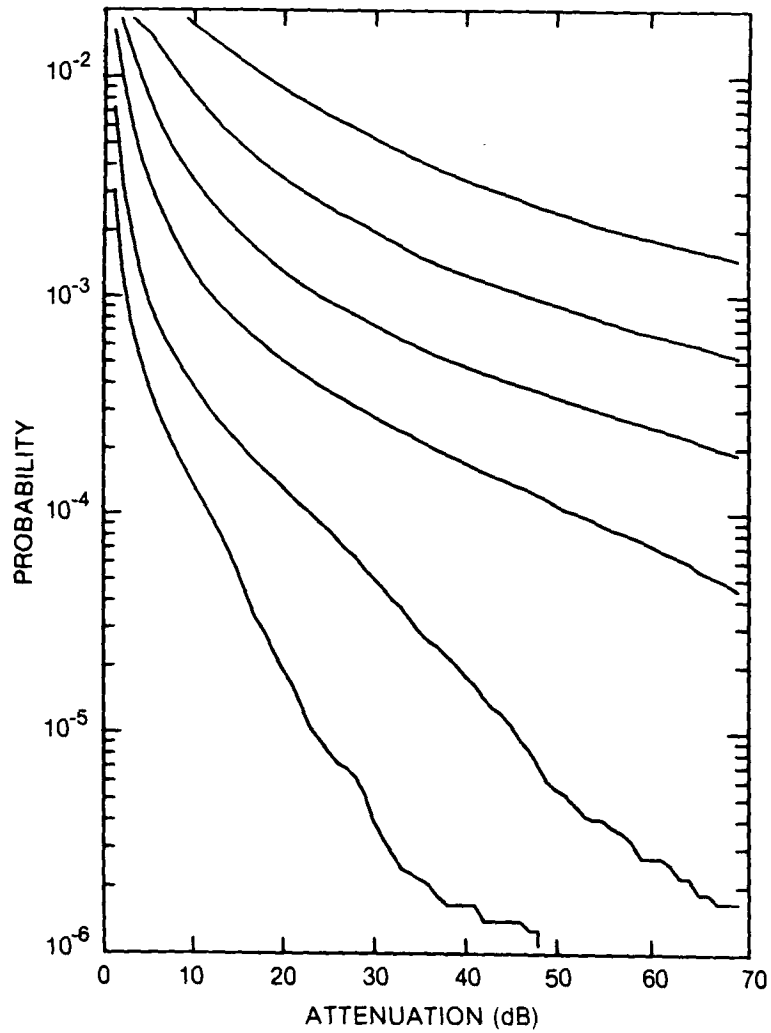

Figure 399. Cumulative distribution of rain attenuation for 35 GHz at Windsor, ONT. Curves, moving from lowest to highest, are for hop lengths of 1, 2, 5, 10, 20 and 40 km, respectively.

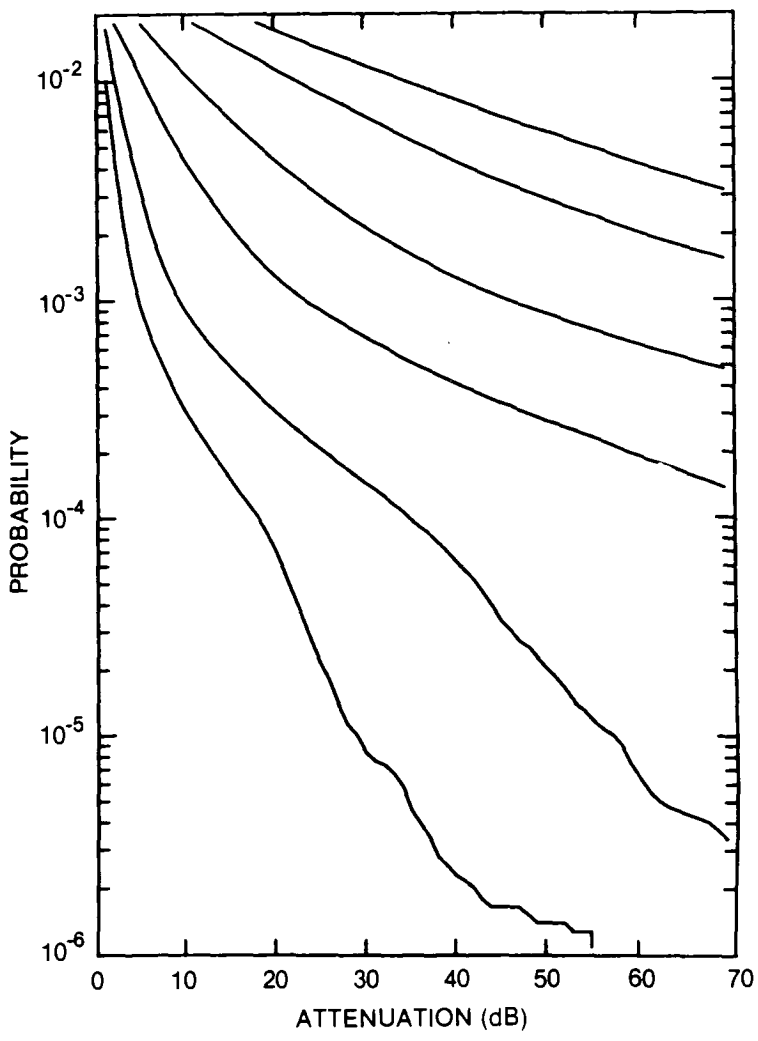

Figure 400. Cumulative distribution of rain attenuation for 56 GHz at Windsor, ONT. Curves, moving from lowest to highest, are for hop lengths of 1, 2, 5, 10, 20 and 30 km, respectively.

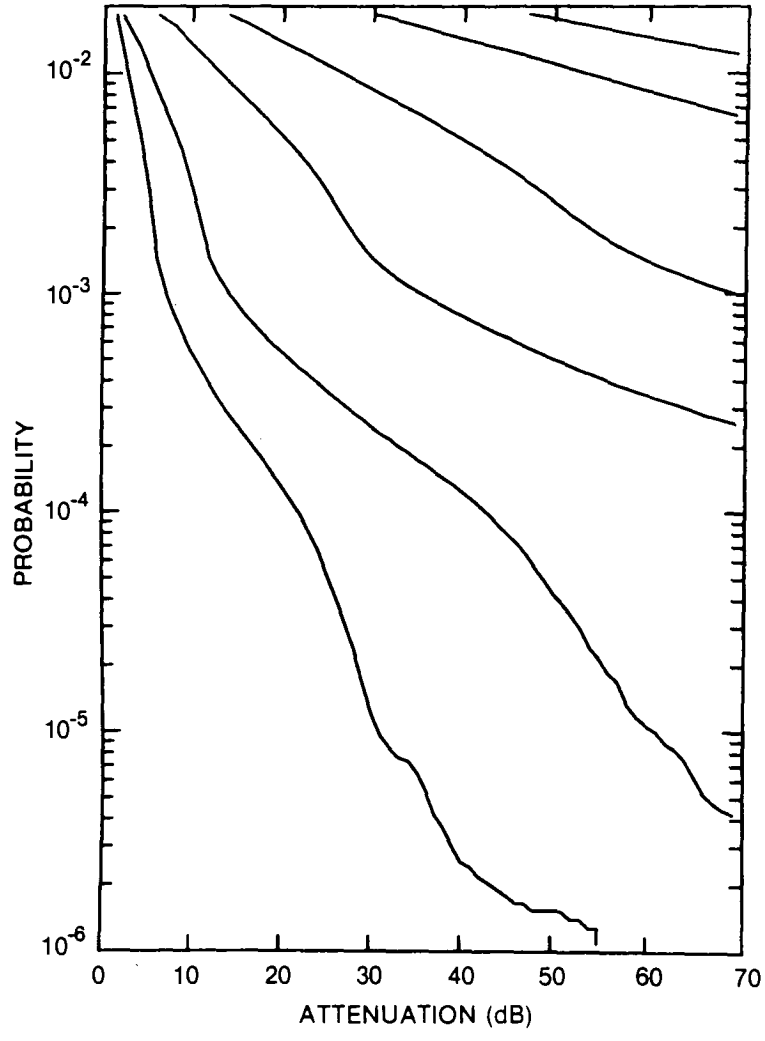

Figure 401. Cumulative distribution of rain attenuation for 100 GHz at Windsor, ONT. Curves, moving from lowest to highest, are for hop lengths of 1, 2, 5, 10, 20 and 30 km, respectively.

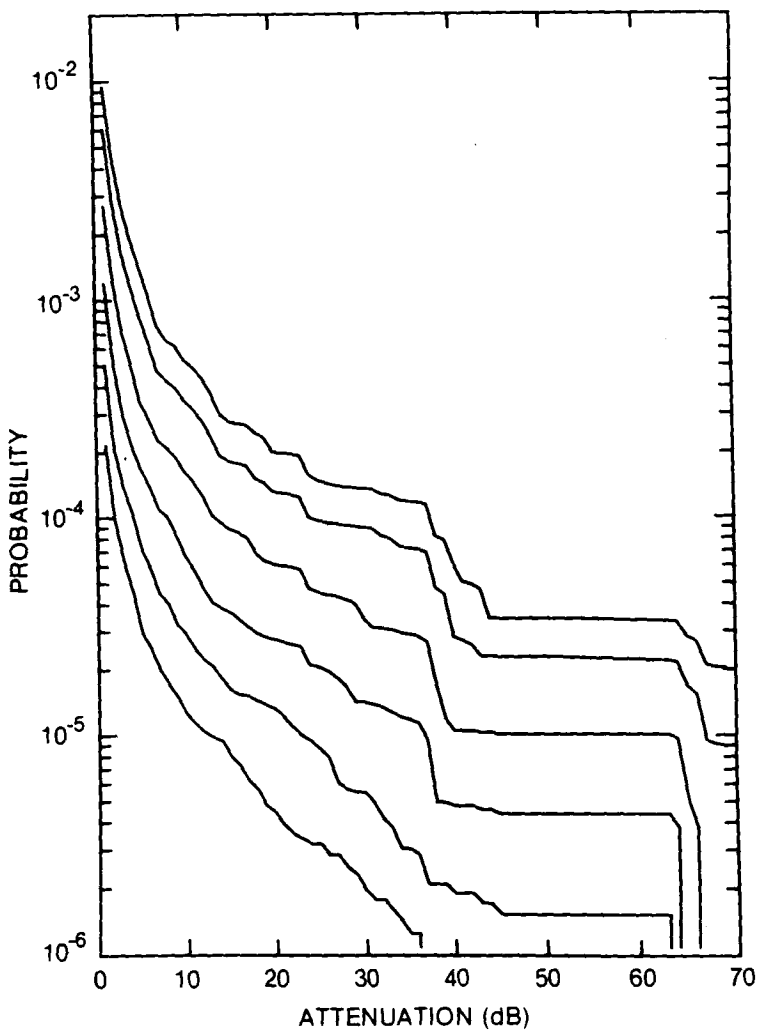

Figure 402. Cumulative distribution of rain attenuation for 8 GHz at Winnipeg, MAN. Curves, moving from lowest to highest, are for hop lengths of 5, 10, 20, 40, 80 and 120 km, respectively.

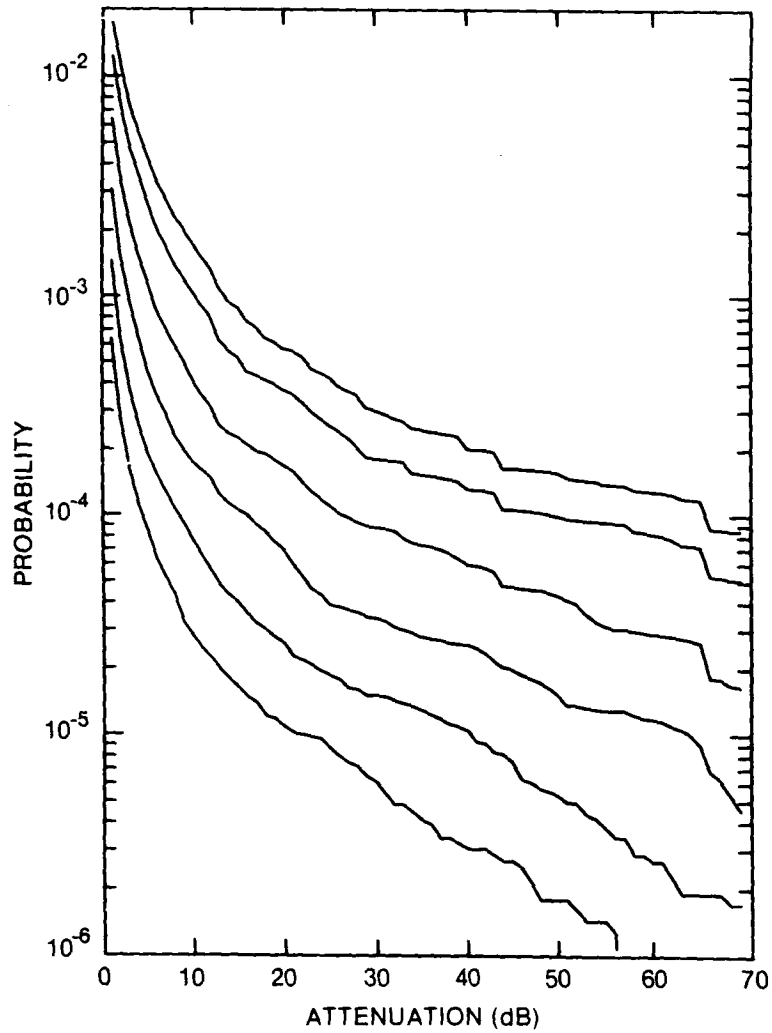

Figure 403. Cumulative distribution of rain attenuation for 11 GHz at Winnipeg, MAN. Curves, moving from lowest to highest, are for hop lengths of 5, 10, 20, 40, 80 and 120 km, respectively.

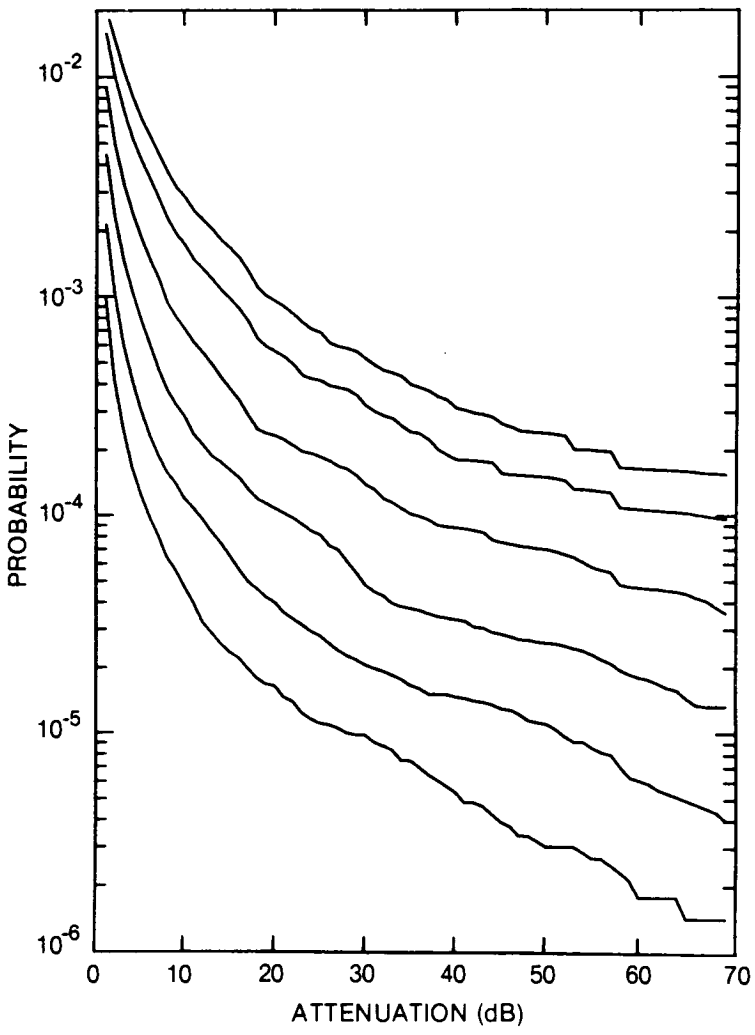

Figure 404. Cumulative distribution of rain attenuation for 12.8 GHz at Winnipeg, MAN. Curves, moving from lowest to highest, are for hop lengths of 5, 10, 20, 40, 80 and 120 km, respectively.

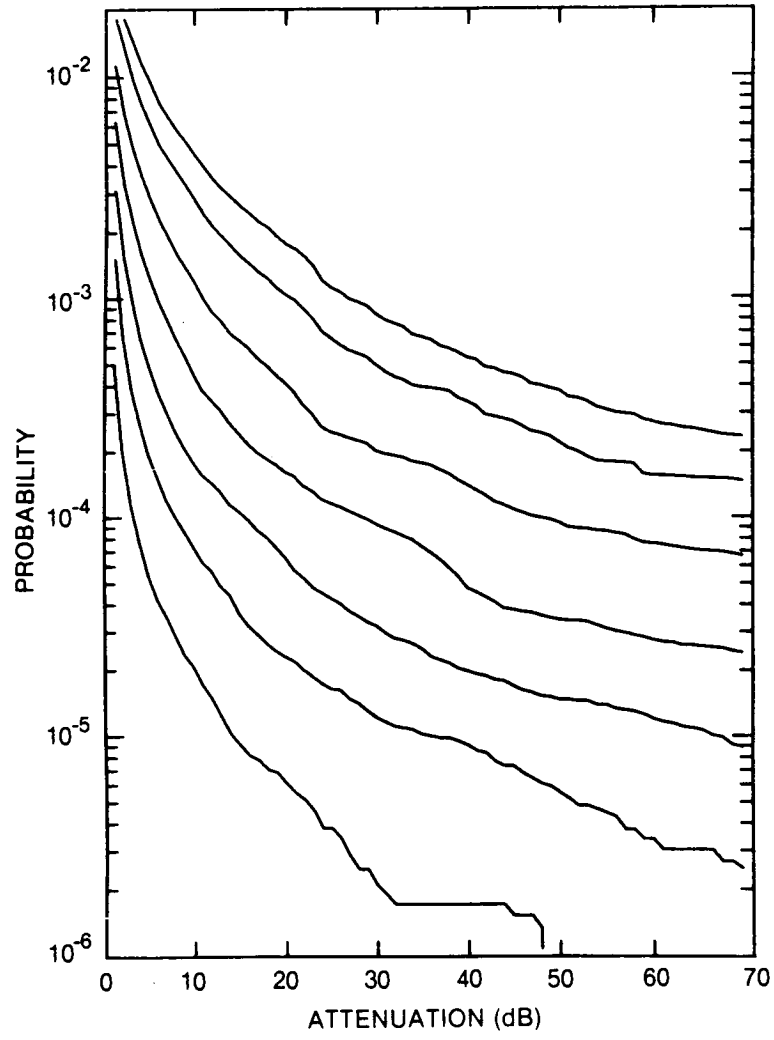

Figure 405. Cumulative distribution of rain attenuation for 15 GHz at Winnipeg, MAN. Curves, moving from lowest to highest, are for hop lengths of 2, 5, 10, 20, 40, 80 and 120 km, respectively.

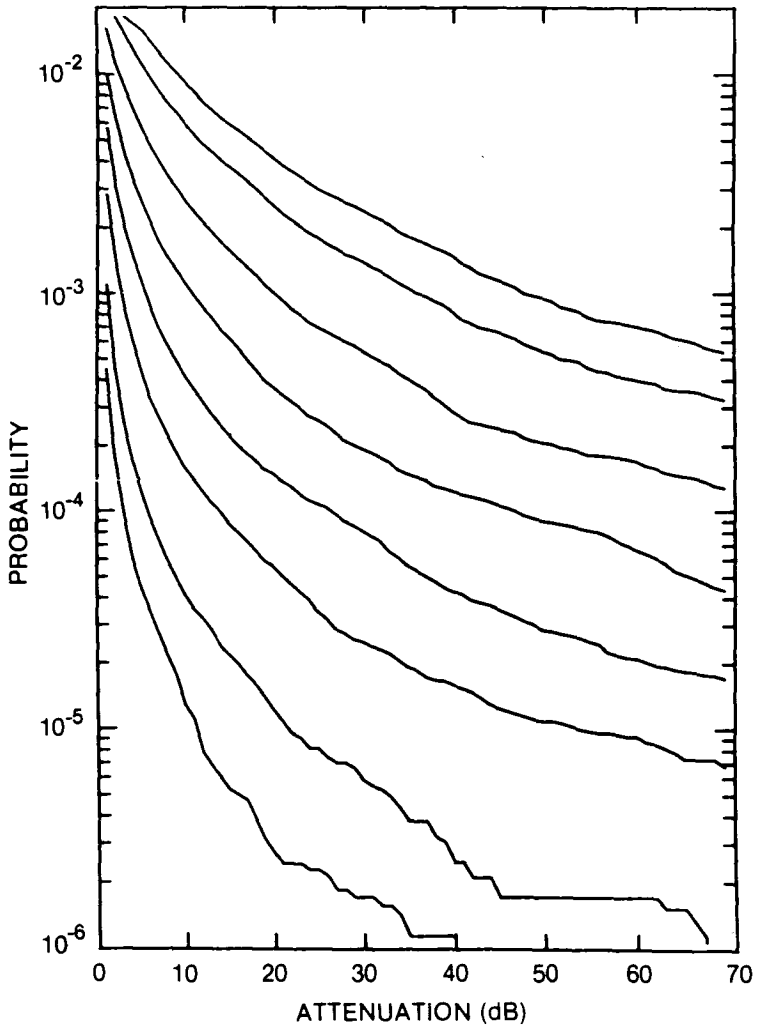

Figure 406. Cumulative distribution of rain attenuation for 20 GHz at Winnipeg, MAN. Curves, moving from lowest to highest, are for hop lengths of 1, 2, 5, 10, 20, 40, 80 and 120 km, respectively.

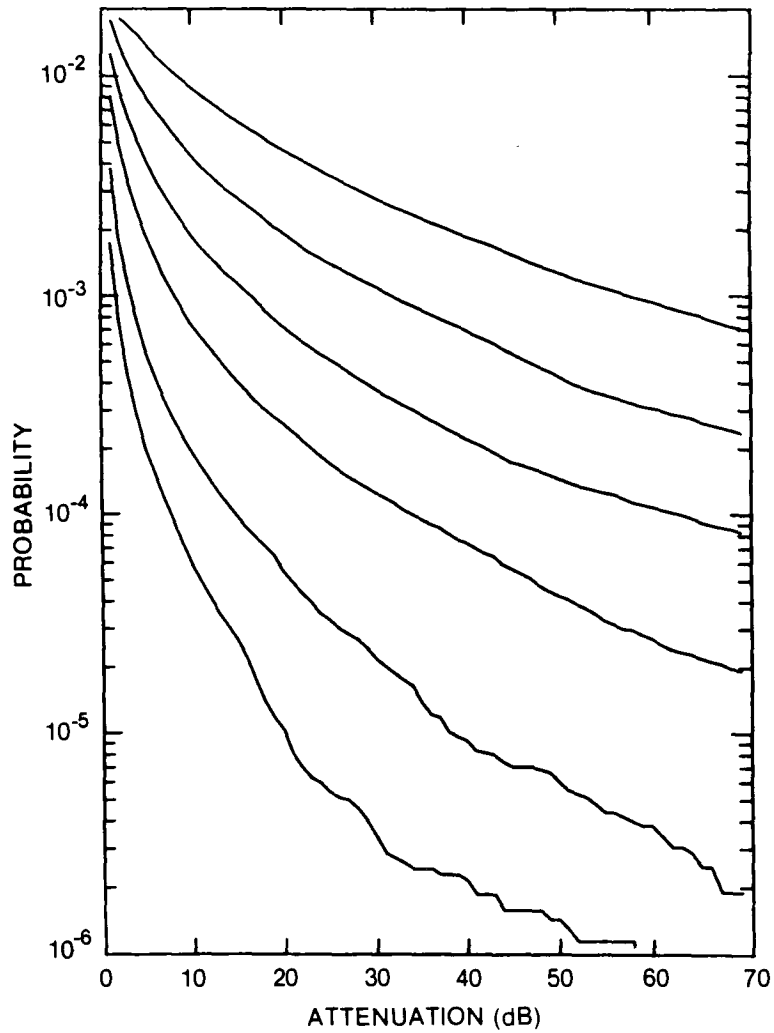

Figure 407. Cumulative distribution of rain attenuation for 35 GHz at Winnipeg, MAN. Curves, moving from lowest to highest, are for hop lengths of 1, 2, 5, 10, 20 and 40 km, respectively.

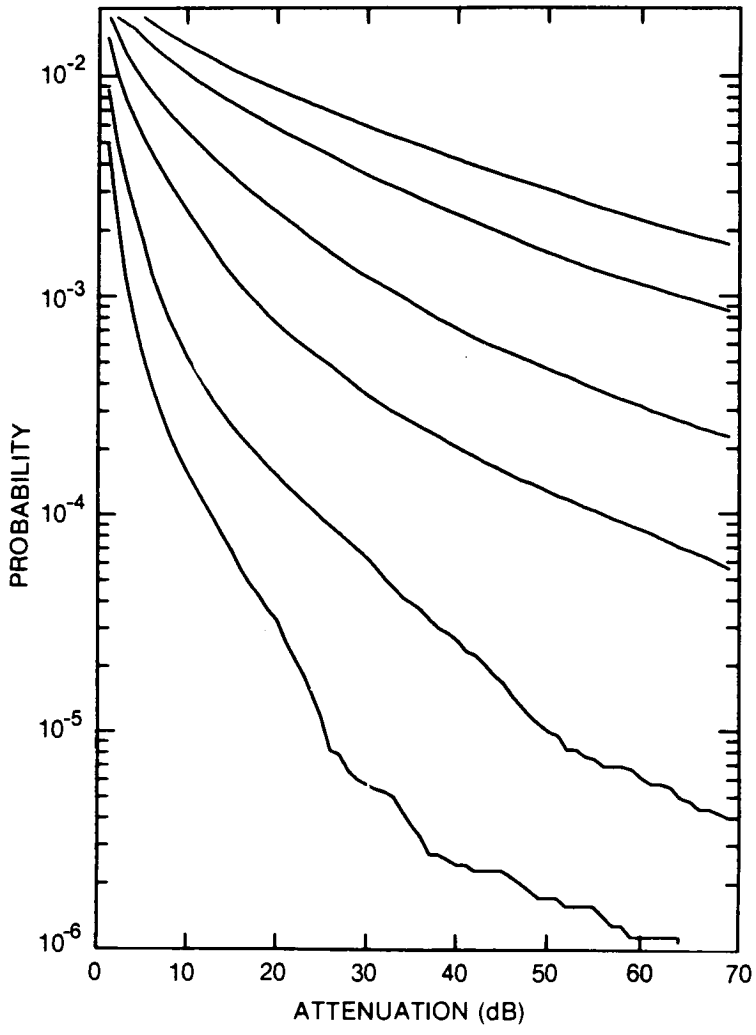

Figure 408. Cumulative distribution of rain attenuation for 56 GHz at Winnipeg, MAN. Curves, moving from lowest to highest, are for hop lengths of 1, 2, 5, 10, 20 and 30 km, respectively.

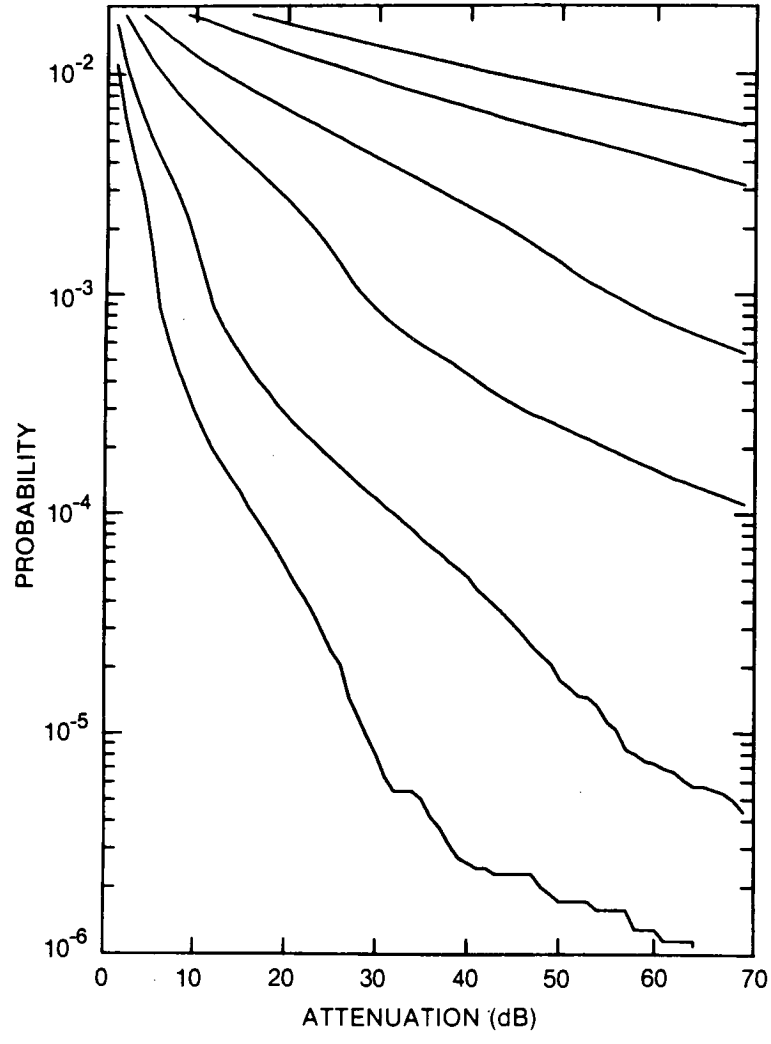

Figure 409. Cumulative distribution of rain attenuation for 100 GHz at Winnipeg, MAN. Curves, moving from lowest to highest, are for hop lengths of 1, 2, 5, 10, 20 and 30 km, respectively.

CRC DOCUMENT CONTROL DATA

1. **ORIGINATOR:** Department of Communications/Communications Research Centre

2. **DOCUMENT NO:** CRC Report No. 1351-E

3. **DOCUMENT DATE:** January 1982

4. **DOCUMENT TITLE:** Rain Attenuation Statistics
   For Terrestrial Microwave Links in Canada

5. **AUTHOR(s):** B. Segal

6. **KEYWORDS:**
   (1) Attenuation
   (2) Microwave Propagation
   (3) Atmospheric Precipitation

7. **SUBJECT CATEGORY (FIELD & GROUP: COSATI)**
   20 Physics
   20 14 Wave Propagation

8. **ABSTRACT:** Not applicable to this report.

9. **CITATION:**

RP&DS Rev. 1973

Government of Canada Gouvernement du Canada